NASA Conference Publication 2060

(NASA-CP-2060) THE 14TH ANNUAL CONFERENCE ON MANUAL CONTROL (NASA) 692 p HC A99/MF A01 CSCL 05H

N79-15588 THRU N79-15634 Unclas G3/54 42153

Fourteenth Annual Conference on Manual Control

April 25-27, 1978
University of Southern California
Los Angeles, California
and
Ames Research Center
Moffett Field, California

November 1978

National Aeronautics and
Space Administration

FOREWORD

This volume contains the proceedings of the Fourteenth Annual Conference on Manual Control held at the University of Southern California at Los Angeles from April 25 to 27, 1978. This report contains complete manuscripts of most of the papers presented at the meeting.

This was the fourteenth in a series of conferences dating back to December 1964. These earlier meetings and their proceedings are listed below:

First Annual NASA-University Conference on Manual Control, The University of Michigan, December 1964. (Proceedings not printed.)

Second Annual NASA-University Conference on Manual Control, MIT, February 28 to March 2, 1966, NASA SP-128.

Third Annual NASA-University Conference on Manual Control, University of Southern California, March 1-3, 1967, NASA SP-144.

Fourth Annual NASA-University Conference on Manual Control, The University of Michigan, March 21-23, 1968, NASA SP-192.

Fifth Annual NASA-University Conference on Manual Control, MIT, March 27-29, 1969, NASA SP-215.

Sixth Annual Conference on Manual Control, Wright-Patterson AFB, April 7-9, 1970.

Seventh Annual Conference on Manual Control, University of Southern California, June 2-4, 1971, NASA SP-281.

Eighth Annual Conference on Manual Control, University of Michigan, Ann Arbor, Michigan, May 17-19, 1972.

Ninth Annual Conference on Manual Control, Massachusetts Institute of Technology, May 23-25, 1973.

Tenth Annual Conference on Manual Control, Wright-Patterson AFB, April 9-11, 1974.

Eleventh Annual Conference on Manual Control, NASA-Ames Research Center, May 21-23, 1975, NASA TM X-62,464.

Twelfth Annual Conference on Manual Control, University of Illinois, May 25-27, 1976, NASA TM X-73,170

Thirteenth Annual Conference on Manual Control, Massachusetts Institute of Technology, June 15-17, 1977.

PRECEDING PAGE BLANK NOT FILMED

CONFERENCE CO-CHAIRMEN

George Bekey

University of Southern California

Duane McRuer

Systems Technology Incorporated

PUBLICATIONS COMMITTEE

Thomas Wempe

NASA-Ames Research Center

CONTENTS

Page

Foreword iii

Session A. Manual Tracking Experiments.
Chairman: D. Kleinman 1

1. *Directional Errors of Movements and Their Correction in a Discrete Tracking Task*, R. J. Jaeger, G. C. Agarwal, and G. L. Gottlieb 3

2. *Study of the Effect of Forcing Function Characteristics on Human Operator Dynamics in Manual Control*, K. Washizu, K. Tanaka, and T. Osawa 19

3. *An Extension of the Quickened Display for Manual Control*, M. Tomizuka and W. M. Tam 33

4. *Effect of Uncertainty on Manual Tracking Performance*, A. R. Ephrath and B. S. Chernoff 45

Session B. Human Operator Models: Identification and Conjecture
Chairman: S. Baron 53

1. *Modeling the Effects of High-G Stress on Pilots in a Tracking Task*, J. Korn and D. L. Kleinman 55

2. *AAA Gunner Model Based on Observer Theory*, R. S. Kou, B. C. Glass, C. N. Day, and M. M. Vikmanis 63

3. *Modeling the Human as a Controller in a Multitask Environment*, T. Govindaraj and W. B. Rouse 75

4. *The Internal Model: A Study of the Relative Contribution of Proprioception and Visual Information to Failure Detection in a Dynamic System*, C. Kessel and C. D. Wickens 85

Session C. Novel Modeling Concepts
Chairman: R. Hess 99

1. *A Comparison of Motor Submodels in the Optimal Control Model*, R. Lancraft and D. L. Kleinman 101

2. *Closed Loop Models for Analyzing the Effects of Simulator Characteristics*, S. Baron, R. Muralidharan, and D. Kleinman 113

3. *Prospects of a Mathematical Theory of Human Behavior in Complex Man-Machine Systems Tasks*, G. Johannsen and W. B. Rouse 137

CONTENTS (Continued) Page

4. *Petri Nets as a Modeling Tool for Discrete Concurrent Tasks of the Human Operator*, W. Schumacher and G. Geiser..... 161

5. *Discrete Time Pilot Model*, D. Cavalli..... 177

Session D. Flight Control and Pilot Dynamics
Chairman: I. Ashkenas..... 187

1. *Flight Experience with Manually Controlled Unconventional Aircraft Motions*, A. F. Barfield..... 189

2. *Pilot Optimal Augmentation Synthesis*, D. K. Schmidt..... 207

3. *Prediction, Evaluation, and Specification of Flying Qualities by Means of Step Target Tracking*, E. D. Onstott and W. H. Faulkner.. 221

4. *Analysis of a VTOL Hover Task with Predictor Displays Using the Optimal Control Model of the Human Operator*, G. Johannsen and T. Govindaraj..... 237

Session E. Ground Vehicle Control and Driver Behavior
Chairman: L. Summers..... 253

1. *Vehicle Steering Control: A Model of Learning*, A. Smiley, L. Reid, and M. Fraser..... 255

2. *Use of Reward/Penalty Structures in Car-Driving Research*, A. C. Stein, R. W. Allen, and S. H. Schwartz..... 267

3. *The Influence of Vehicle Aerodynamic and Control Response Characteristics on Driver-Vehicle Performance*, A. A. Alexandridis, B. S. Repa, and W. W. Wierwille..... 279

Session F. Manipulators and Remote Manipulation
Chairman: A. Freedy..... 295

1. *The Determination of the Operating Range of a Twin-Grip Control Yoke Through Biomechanical Means*, K. -P. Gärtner..... 297

2. *Event-Driven Displays for Manipulator Control*, A. K. Bejczy and G. Paine..... 307

3. *Manned Simulations of the SRMS in SIMFAC*, A. Lippay, G. Whitehead, and C. G. Wagner-Bartak..... 333

4. *Human/Computer Control of Undersea Teleoperators*, T. B. Sheridan, W. L. Verplank, and T. L. Brooks..... 343

CONTENTS (Continued) Page

Session G. Displays
Chairman: H. Jex 359

1. *Display Aids for Remote Control of Untethered Undersea Vehicles*, W. L. Verplank 361

2. *Safety Margin and Flight Reference System and Display for Powered Lift Aircraft*, R. K. Heffley and G. Hardy 371

3. *A Head-Up Display for Mid-Air Drone Recovery*, W. L. Augustine, E. L. Heft, T. G. Bowen, and R. L. Newman 381

4. *Evaluation of Display and Control Concepts for a Terminal Configured Vehicle in Final Approach in a Windshear Environment*, W. H. Levison 395

Session H. Eye/Head Tracking and Scanning
Chairman: K. Ziedman 417

1. *Two-Dimensional Eye Tracking: Sampling Rate of Forcing Function*, J. P. Hornseth, D. L. Monk, J. L. Porterfield, and R. L. McMurry 419

2. *Head Tracking at Large Angles from the Straight Ahead Position*, D. L. Monk, J. L. Porterfield, J. P. Hornseth, and R. L. McMurry 425

3. *Light Weight Helmet-Mounted Eye Movement Measurement System*, J. A. Barnes 437

Session I. Motion Simulation and Effects
Chairman: R. Stapleford 441

1. *The Effects of Closed Loop Tracking on a Subjective Tilt Threshold in the Roll Axis*, M. Roark and A. Junker 443

2. *Use of a Tilt Cue in a Simulated Heading Tracking Task*, W. H. Levison and A. M. Junker 451

3. *Roll Tracking Effects of G-Vector Tilt and Various Types of Motion Washout*, H. R. Jex, R. E. Magdaleno, and A. M. Junker 463

4. *A Method of Motion Simulator Design Based on Modeling Characteristics of the Human Operator*, D. W. Repperger and A. M. Junker 503

5. *Investigation of Nonlinear Motion Simulator Washout Schemes*, S. A. Riedel and L. G. Hoffmann 521

CONTENTS (Concluded) Page

Session J. Perception and Attention Allocation
Chairman: W. Rouse..... 533

1. *A Theoretical and Experimental Analyses of the Outside World Perception Process*, P. H. Wewerinke..... 535

2. *Linear Modeling of Attentional Resource Allocation*, B. J. Pierce and C. D. Wickens..... 557

3. *A Model for Dynamic Allocation of Human Attention Among Multiple Tasks*, T. B. Sheridan and M. K. Tulga..... 569

4. *Perceptual Factors and Performance of Air Traffic Controllers Using a Microwave Landing System*, G. Gershzohn..... 593

Session K. Decision-Making Behavior and Modeling
Chairman: R. Curry..... 607

1. *The Effects of Alcohol on Driver Performance in a Decision Making Situation*, R. W. Allen, S. H. Schwartz, A. C. Stein, and J. R. Hogge 609

2. *A Decision Model Applied to Alcohol Effects on Driver Signal Light Behavior*, S. H. Schwartz and R. W. Allen..... 631

3. *Combined Monitoring, Decision and Control Model for the Human Operator in a Command and Control Task*, R. Muralidharan and S. Baron..... 647

4. *A Model of Event Detection in Multiple Process Monitoring Situations*, J. S. Groenstein and W. B. Rouse..... 663

5. *Pilot Decision Making in a Computer-Aided Flight Management Situation*, Y. Chu and W. B. Rouse..... 677

Session L. Workload
Chairman: T. Sheridan..... 691

1. *Time Estimation as a Secondary Task to Measure Workload: Summary of Research*, S. G. Hart, D. McPherson, and L. L. Loomis..... 693

SESSION A: MANUAL TRACKING EXPERIMENTS

Chairman: D. Kleinman

N79-15589

DIRECTIONAL ERRORS OF MOVEMENTS AND THEIR CORRECTION IN A DISCRETE TRACKING TASK

Robert J. Jaeger
Gyan C. Agarwal
Gerald L. Gottlieb

College of Engineering
University of Illinois at Chicago Circle
Chicago, Illinois 60680

and

Rush Medical Center
Chicago, Illinois 60612

ABSTRACT

The human operator is prone to making errors in quick choice reaction time tasks. Many studies have shown that subjects can correct their own errors of movement more quickly than they can react to external stimuli. In the control of movements, three general categories of feedback have been defined as follows: 1) Knowledge of results, primarily visually mediated, 2) Proprioceptive or kinaesthetic such as from muscle spindles and joint receptors, and, 3) Corollary discharge or efference copy within the central nervous system.

Experiments were conducted on four normal human subjects to study the effects of these feedbacks on simple reaction time, choice reaction time, and error correction time. The movement used was plantarflexion and dorsiflexion of the ankle joint. The feedback loops were modified, 1) by changing the sign of the visual display to alter the subject's perception of results, and 2) by applying vibration at 100 Hz simultaneously to both the agonist and antagonist muscles of the ankle joint. The central processing was interfered with when the subjects were given moderate doses of alcohol (blood alcohol concentration levels of up to 0.07%).

Vibration and alcohol increase both the simple and choice reaction times. However, the error correction time is not influenced by either. This data reinforces the concept that there is a central pathway which can mediate error correcting responses.

INTRODUCTION

The human operator is prone to making errors in a quick choice reaction time (RT) task. The speed with which the operator can recognize errors and correct them is an important consideration in many industrial tasks. Many studies have shown that subjects can correct errors of movement more quickly

PAGE INTENTIONALLY

than they can react to external stimuli. (For a review of the literature see Schmidt, 1975, 1976; Angel, 1976; Schmidt & Gordon, 1977.)

In the control of movement by skeletal muscles, three general categories of feedback have been identified (Evarts, 1971). These feedbacks arise as follows: first, "knowledge of results" from the external environment is primarily visually mediated. Second, proprioception from internal receptors stimulated as a consequence of muscular contraction and joint rotation is primarily spindle and joint receptor mediated. Third, "efference copy" or "corollary discharge" (Von Holst, 1953) from structures and pathways within the central nervous system may operate before muscle contraction occurs.

Currently, the first and second categories of feedback are perhaps better understood than the third, although the role of efference copy in saccadic eye movements has received considerable attention (Robinson, 1971, 1976; Lehmann, 1971). These three categories of feedback may be anatomically interconnected, especially the proprioceptive and efference copy mechanisms (Oscarsson, 1970). It is postulated that the cerebellar anterior lobe is important for correcting errors in motor activity elicited from the cerebral cortex and carried out by command signals through pyramidal and extrapyramidal pathways.

Recent work of Angel and his colleagues (Angel & Higgins, 1969; Angel, 1976) has attempted to quantitatively approach efference copy by measuring RTs to correct movement errors and the accuracy of these corrections. It has also been noted (Poulton, 1974) that the many studies which have measured RTs for the correction of movements have found these times to range from essentially zero to in excess of 300 milliseconds.

Since a rather wide range of error correction times exists, it could be hypothesized that the three general categories of feedback each have their own range of operating times which together contribute to the overall wide range of these times. Under this hypothesis, if a sufficient number of measurements were made, a trimodal distribution might be found. The minimum duration for processing visual feedback from a movement appears to be over 190 msec (Keel & Posner, 1968). The kinaesthetic RT is of the order of 120 msec (Chernikoff & Taylor, 1952). This RT is of the same order as the time for "Functional Stretch Reflex" (Melville Jones & Watt, 1971; Evarts, 1973; Gottlieb & Agarwal, 1978). Dewhurst (1967) has reported values of kinaesthetic RT based on recordings of muscle activity in the biceps as short as 50 msec. However, he did not give any range for kinaesthetic RT or the mean value in his experiments.

The experiments of the present study were designed to enable comparison of correction times measured under normal conditions with those measured under conditions in which the proprioceptive mechanisms was interfered with. It was possible to do this by applying vibration to the tendons of the muscles involved. (Hagbarth & Eklund, 1966; Goodwin, McCloskey & Matthews, 1972; McCloskey, 1973; Craske, 1977). In some experiments, central processing was interfered with when the subjects were given moderate doses of alcohol (blood alcohol concentration (BAC) levels of up to 0.07%). Alcohol produces a depressive effect on the CNS much as a general anesthetic does and the degree of depression appears to be dose related (Wallgren & Barry, 1970.)

METHODS

Four subjects were used in the present study. Two of the subjects (GCA and GLG) had extensive previous experience with the experimental apparatus as subjects in other tracking type experiments, while the other two subjects had no such experience. Parts of these experiments were also done on several other subjects.

A schematic of the experimental apparatus is shown in Figure 1. (This apparatus has been used in several studies, for details see Agarwal & Gottlieb, 1977).

The subject sat in an adjustable height chair facing an oscilloscope display positioned at a slight angle in front of him, His right foot was strapped to a one degree of freedom foot pedal (rotation in plantar-dorsal directions) with velcro straps. Self adhesive surface electrodes were positioned over the soleus and anterior tibial muscles to record the electromyograms (EMGs) of these muscles. A ground electrode was placed on the thigh just proximal to the knee. The EMGs were full wave rectified and filtered before recording on the digital tape at a sampling rate of 500 per sec.

The oscilloscope display consisted of two dots. The first was the target dot which was under the control of the computer. It was defocussed to approximately 2 mm diameter. This dot assumed only one of three positions at any instant of time, either in the center of the screen or ±4.0 cm vertically away from the center. The second dot was the response dot which was under the control of the subject. It was focused to a sharp point approximately 0.5 mm in diameter. The subject could vary the position of the dot continuously along the vertical axis of the oscilloscope. The crucial part of the experiment was the "polarity" of the subjects' control of the response dot. This polarity was under the control of the computer. Normal or positive polarity meant that when the subject moved the pedal down (up) the response dot also moved down (up). Inverted or negative polarity meant that when the subject moved the pedan down (up), the response dot moved up (down). The purpose of this provision for polarity reversal was do decouple the proprioceptive feedback from the visual feedback and induce the subject to make errors in movement. The use of polarity reversal has been previously described by Gibbs (1965) and Angel and Higgins (1969).

The target dot was controlled by the computer as follows. The experiment began with the target dot in the center. After a random delay of 3 to 5 sec, the target dot stepped randomly up or down. The new position was maintained for a random period of 3 to 5 sec and then returned to center. Ten initial trials stepping out and returning to zero were performed at normal polarity. Following these ten initial trials, the computer reversed the polarity of the response dot. A random number (8 to 12) trials were performed at the reversed polarity, after which, the polarity again reversed for the next group of trials. The response immediately following a polarity reversal was always discarded, since it could be expected to contain a higher proportion of visually mediated error corrections than other responses.

This scheme of target dot movement also provided the opportunity to study simple and choice RTs, since the majority of responses were correct. When the target dot moved from the center, it moved randomly up or down, forcing the subject to choose before reacting. When the target dot next moved, it always

returned to zero, allowing the subject to make a simple reaction.

The subjects were instructed to make the response dot follow the movement of the target dot as quickly as possible with as much accuracy as possible, but to favor a fast response.

In the vibration experiments, two Hagbarth type vibrators (TVR vibrator - model #TMT-18, Heiwa Electronic Industrial Comp., Japan) were attached to the distal tendons of soleus and anterior tibial muscles (just above the ankle joint) with surgical tape. The vibrators were operated at 100 Hz continuously during the tracking task.

In the alcohol experiments, the subjects were given alcohol proportional to the body weight such that the ultimate BAC was in the range of 0.06 to 0.07%. The BAC was measured using a Mark II Intoximeter (Gas Chromatography Unit by Intoximeters, Inc.).

The measurement of the RTs were done off line by displaying the individual responses on a four channel oscilloscope using a cursor to indicate the time measurement after the input. The accuracy of these measurements is equal to the sampling interval, i.e., 2 msec. The RTs measured are indicated in Figures 2 and 3.

The statistical analysis included means and variances of the sample data and the t-test of equality of the means of two samples whose variances are assumed to be unequal (Sokal & Rohlf, 1969, Chapter 13).

RESULTS

Data were collected on separate days for each subject and for each experimental paradigm. The first day experiment was always under normal conditions. Typical responses are shown in Figure 2 for a correct response in a choice RT and for error response in Figure 3. The four traces are the angular rotation (θ), EMGs of the anterior tibial (AT) and gastrocnemius-soleus (GS) muscles and the angular velocity ($\dot{\theta}$). The angular velocity was obtained by digital differentiation of angular rotation. The simple and choice RTs (SRT & CRT), the error reaction time (ERT), and the error correction time (ECT) were measured using both the EMG and velocity data. In the following tables only the EMG related measurements are reported. The final conclusions would have been exactly the same using the velocity data.

Table I shows the simple and choice reaction times under normal conditions with positive and negative polarity movements. With the exception of subject GA, and GG's SRT, the RTs for the other three subjects with positive and negative polarity were not significantly different. In general there was a slight increase in the RTs with negative polarity. Since the RT differences with alcohol and vibration were more significant, the positive and negative polarity data was lumped together.

Table II shows SRTs for all subjects in three paradigm conditions. Note that in general, alcohol as well as vibration increased the SRT. This is also true for CRT shown in Table III. The t-test comparisons are made between the normal and altered conditions. In Table II, six out of eight t-test values are significant at $P < 0.01$ level. In Table III, seven out of eight t-test values are significant at $P < 0.01$ level.

Table IV shows the error reaction times in the three paradigm conditions.

Most errors occured in the choice reaction condition. There was a significantly larger number of errors with negative polarity than with positive polarity feedback. The error rates for the two conditions ranged between 16% and 33%. In these data, four out of eight t-test values show significant differences at $P < 0.01$ level.

Table V compares the data from Tables III and IV for choice RT and error RT under normal conditions. Note that error RTs are larger than the choice RTs and only one out of four t-test values show significant differences at $P < 0.01$ level.

Table VI shows the error correction times for the four subjects under our three paradigms. The error correction time is significantly less than the choice or error RT. None of the eight t-test values between normal and altered conditions show significance at $P < 0.01$ level.

Table VII shows the error rates for individual experiments as well as combined error rates for all subjects. The vibration input did not influence the error rates. Alcohol tended to increase the error rates in three out of four subjects but the t-test values do not indicate any significance. For $n = 4$ the t-test values are not very meaningful.

DISCUSSION

The paradigm of incompatible display has been used by Gibbs (1965), Angel & Higgins (1969), and Angel (1976). There is a clear increase in the SRT as well as CRT with negative polarity display (Table I). This increase was significant at $P < 0.01$ level for subjects GA and GG whose RTs were fastest. The significance of positive and negative polarity disappeared with increased RT of subject RJ and FM.

Vibration and alcohol increases both the SRT and CRT for correct movements as compared to the normal condition (Tables II and III). Carpenter (1962) has reviewed the literature on the effects of alcohol on psychological processes and concluded that in most studies, RT is lengthened at relatively low blood alcohol levels. Vibration of a tendon in humans causes a predictable increase in the contractile activity of the agonist, caused by autogenous reflex excitation of the alpha motoneuron (Hagbarth & Eklund, 1966). This leads to involuntary movements and illusion of movements (Goodwin et al 1972; McCloskey, 1973; Craske, 1977). In our experiments, vibrators were attached to both agonist-antagonist tendons and subjects reported numbness in the vibrated ankle joint. The significant increase in the SRT and CRT with vibration could indicate that large irrelevant position signals from the vibrated joint delays processing of visual information and command selection.

Tables IV and V show that the choice reaction time and the error reaction time (initial movement in the wrong direction) are not significantly different under normal conditions. This agrees with Gibbs (1965) findings that the response latencies of correct and incorrect responses were virtually equal on equiprobable steps. Although the response latencies for the four subjects are significantly different, there is no correlation between the response latencies and the errors of subjects (see Table VII), i.e., the subjects who responded most rapidly did not make the most errors (Gibbs, 1965). The ERT in most cases is longer than the CRT, suggesting that there was no temporal anticipa-

tion of the target (A paradigm which has been used by Schmidt and Gordon (1977) in their study).

The surprising result of this study is that whereas the SRT and CRT are influenced (increased) by vibration and alcohol, the error correction times are not significantly affected as given in Table VI. The average error correction time is shorter than the CRT for individual subjects. This is in agreement with findings by Gibbs (1965), Rabbitt (1966), and Angel and Higgins (1969), Megaw (1972), and Angel (1976).

The histograms of error correction times for the four subjects under three paradigm conditions are shown in Figure 4. For subjects GA and GG who had the most experience in tracking studies, most errors are corrected in less than 250 msec, i.e., less than their normal choice reaction times. For subject RJ a significant number of ECTs are larger than 250 msec. For subject FM, his RTs were the slowest and larger percentage of ECTs are above 250 msec.

The conclusion of Higgins & Angel (1970) and Angel (1976) that the origin of feedback from error responses is central rather than kinaesthetic is reinforced by the invariance of ECTs with vibration on the limb. The vibration increases the SRTs and CRTs which implies an influence of the peripheral input in motor command decision making.

Alcohol which is known to produce a depressive effect on the CNS also increases the SRTs and CRTs but does not significantly influence the ECTs with BAC levels of 0.07% or less used in these experiments.

ACKNOWLEDGEMENT

This work was supported by NSF grant ENG-7608754 and NIH grants NS-00196 and NS-12877. The alcohol experiments were supported by NIH grant AA02156 to Dr. Jeffrey Levett.

REFERENCES

Agarwal, G. C., & Gottlieb, G. L., Oscillation of the Human Ankle Joint in Response to Applied Sinusoidal Torque on the Foot. J. Physiology (London), vol. 268, pp. 151-176, 1977.

Angel, R. W., Efference Copy in the Control of Movement. Neurology, vol. 26, pp. 1164-1168, 1976.

Angel, R. W., & Higgins, J. R., Correction of False Moves in Pursuit Tracking. J. Expt. Psychology, vol. 82, pp. 185-187, 1969.

Carpenter, J. A., Effects of Alcohol on Some Psychological Processes. Quarterly J. Studies on Alcohol, vol. 23, pp. 274-314, 1962.

Chernikoff, R., & Taylor, F. V., Reaction Times to Kinaesthetic Stimulation Resulting from Sudden Arm Displacement. J. Experimental Psychology, vol. 43, pp. 1-8, 1952.

Craske, B., Perception of Impossible Limb Positions Induced by Tendon Vibration. Science, vol. 196, pp. 71-73, 1977.

Dewhurst, D. J., Neuromuscular Control System. IEEE Trans. Biomedical Eng., vol. BME-14, pp. 167-171, 1967.

Evarts, E. V., Central Control of Movement, Neuroscience Research Program, Bulletin, M.I.T. Press, vol. 9, 1971.

Evarts, E. V., Motor Cortex Reflexes Associated with Learned Movements, Science, vol. 179, pp. 501-503, 1973.

Gibbs, C. B., Probability Learning in Step-input Tracking. British J. Psychology, vol. 56, pp. 233-242, 1965.

Goodwin, G. M., McCloskey, D. I., & Matthews, P. B. C., The Contribution of Muscle Afferents to Kinaesthesia Shown by Vibration Induced Illusions of Movement and by the Effects of Paralysing Joint Afferents. Brain, vol. 95, pp. 705-748, 1972.

Gottlieb, G. L., & Agarwal, C. G., Stretch and Hoffmann Reflexes during Phasic Voluntary Contractions of the Human Soleus Muscle. Electroenceph. & Clinical Neurophysiology, 1978 (in press).

Hagbarth, K. E., & Eklund, G., Motor Effects of Vibratory Muscle Stimuli in Man. In Nobel Symposium I - Muscular Afferent and Motor Control, R. Granit (editor), Almquist and Wiksell, Stockholm, pp. 177-186, 1966.

Higgins, J. R., & Angel, R. W., Correction of Tracking Errors without Sensory Feedback. J. Experimental Psychology, vol. 84, pp. 412-416, 1970.

Keele, S. W., & Posner, M. J., Processing of Visual Feedback in Rapid Movements. J. Experimental Psychology, vol. 77, pp. 155-158, 1968.

Lehmann, D., EEG, Evoked Potentials, and Eye and Image Movements. In The Control of Eye Movements, P. Bach-y-rita (editor), Academic Press, N. Y., pp. 149-174, 1971.

McCloskey, D. I., Differences Between the Senses of Movement and Position Shown by the Effects of Loading and Vibration of Muscles in Man. Brain Research, vol. 63, pp. 119-131, 1973.

Megaw, E. D., Directional Errors and their Correction in a Discrete Tracking Task. Ergonomics, vol. 15, pp. 633-643, 1972.

Melville Jones, G., & Watt, D. G. D., Observations on the Control of Stepping and Hopping Movements in Man. J. Physiology (London), vol. 219, pp. 709-727, 1971.

Oscarsson, O., Functional Organization of Spinocerebellar Paths. In Handbook of Sensory Physiology, vol. II. Somatosensory System. A. Iggo (editor), Springer-Verlag, Berlin, pp. 121-127, 1970.

Poulton, E. C., Tracking Skill and Manual Control, Academic Press, N. Y., 1974.

Rabbit, P. M. A., Errors and Error Correction in Choice Response Tasks. J. Experimental Psychology, vol. 71, pp. 264-272, 1966.

Robinson, D. A., Models of Oculomotor Neural Organization. In The Control of Eye Movements, P. Bach-y-rita (editor), Academic Press, N. Y., pp. 519-538, 1971.

Robinson, D. L., & Wurtz, R. H., Use of an Extrarational Signal by Monkey Superior Colliculus to Distinguish Real from Self-Induced Stimulus Movement. J. Neurophysiology, vol. 39, pp. 852-870, 1976.

Schmidt, R. A., A Schema Theory of Discrete Motor Skill Learning, Psychological Review, vol. 82, pp. 225-260, 1975.

Schmidt, R. A., The Schema as a Solution to Some Persistent Problems in Motor Learning Theory. In G. E. Stelmach (editor), Motor Control: Issues and Trends, Academic Press, N. Y., pp. 41-65, 1976.

Schmidt, R. A., & Gordon, G. B., Errors in Motor Responding, "Rapid" Corrections, and False Anticipations. J. Motor Behavior, vol. 9, pp. 101-111, 1977.

Von Holst, E., Relations Between the Central Nervous System and the Peripheral Organs. British J. Animal Beh., vol. 3, pp. 89-94, 1954.

Wallgren, H., & Barry, H., Actions of Alcohol, vol. 1 & 2, Elsevier Publishing Comp., 1974.

TABLE 1: Effect of Display Polarity on Simple and Choice Reaction Times

SUBJ	Positive Polarity MEAN	SD	N	t	NEGATIVE POLARITY MEAN	SD	N
			Simple Reaction Times				
GA	216	32	113	-3.99*	248	78	110
GG	222	51	129	-2.52*	240	71	164
RJ	270	76	130	-1.42	283	78	156
FM	359	75	133	0.59	354	69	161
			Choice Reaction Times				
GA	235	57	98	-2.79*	272	102	73
GG	256	42	111	-2.00	271	70	122
RJ	268	80	83	-1.12	282	84	90
FM	338	76	112	-1.46	359	69	112

*P < 0.01

TABLE II: Simple Reaction Times

SUBJ	VIBRATION MEAN	SD	N	t	NORMAL MEAN	SD	N	t	ALCOHOL MEAN	SD	N
GA	246	45	150	-5.99*	219	39	233	-4.48*	235	42	297
RJ	316	92	156	-4.50*	277	77	286	-7.75*	333	96	269
FM	371	78	274	0.58	375	86	294	-5.68*	420	98	256
GG	311	84	164	-10.46*	232	64	293	-1.24	240	54	290

TABLE III: Choice Reaction Times

	VIBRATION				NORMAL				ALCOHOL		
SUBJ	MEAN	SD	N	t	MEAN	SD	N	t	MEAN	SD	N
GA	317	111	131	-5.58*	253	80	171	-0.64	258	59	152
RJ	333	83	98	-5.27*	277	86	173	-8.25*	355	88	166
FM	409	96	211	-7.43*	348	73	224	-11.28*	443	100	212
GG	330	85	136	-6.98*	272	61	233	-3.34*	288	61	230

TABLE IV: Error Reaction Times

	VIBRATION				NORMAL				ALCOHOL		
SUBJ	MEAN	SD	N	t	MEAN	SD	N	t	MEAN	SD	N
GA	274	60	19	-1.03	257	62	47	-0.56	263	59	104
RJ	342	65	55	-2.90*	311	55	80	-3.57*	343	69	111
FM	387	75	59	-1.83	363	72	68	-5.72*	443	70	41
GG	332	84	32	-2.42*	289	63	42	-0.08	290	60	45

TABLE V: Comparison of CRTS with ERTS under Normal Conditions

	CHOICE REACTION TIMES				ERROR REACTION TIMES		
SUBJ	MEAN	SD	N	t	MEAN	SD	N
GA	253	80	171	-0.37	257	62	47
RJ	277	86	173	-3.79*	311	55	80
FM	348	73	224	-1.50	363	72	68
GG	272	61	233	-1.62	289	63	42

TABLE VI: Error Correction Times

	VIBRATION				NORMAL				ALCOHOL		
SUBJ	MEAN	SD	N	t	MEAN	SD	N	t	MEAN	SD	N
GA	137	69	19	0.32	143	72	47	0.67	135	59	104
RJ	194	101	55	-1.71	166	81	80	-1.62	186	88	111
FM	259	72	59	2.18	293	103	68	2.23	251	90	41
GG	170	84	32	-0.05	169	72	42	-0.68	150	74	45

TABLE VII: Rate of Errors in Percent

SUBJ	VIBRATION	NORMAL	ALCOHOL
GA	0.063	0.107	0.188
RJ	0.178	0.148	0.203
FM	0.110	0.116	0.081
GG	0.096	0.074	0.080

	VIBRATION	t	NORMAL	t	ALCOHOL
MEAN	0.112	-0.04	0.111	-0.74	0.138
SD	0.048		0.030		0.067
N	4		4		4

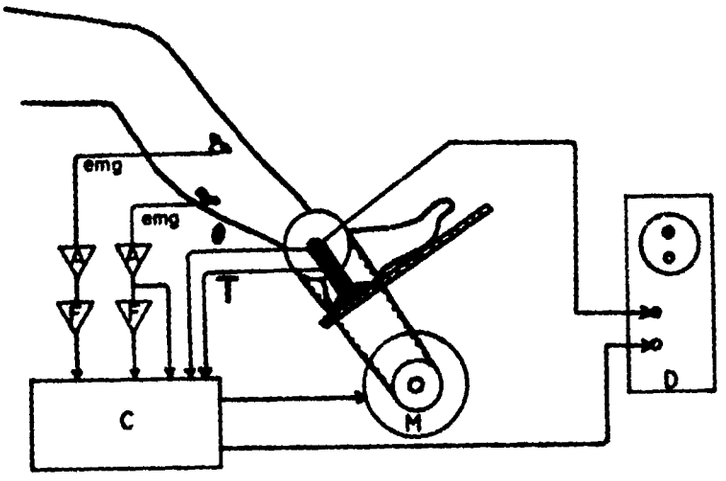

Figure 1

A schematic of the experimental apparatus. Electromyograms (EMGs) are measured using disk surface electrodes placed over the bellies of the gastrocnemius-soleus and anterior tibial muscles, EMG amplifiers (A) are differential amplifiers (bandwidth 60-600 Hz), filters (F) are third order averaging (10 msec averaging time), display oscilloscope (D) is a dual-beam Tektronix 502, digital computer (C) is a General Automation SPC016/65. The torque motor (M) and the torque measurements (τ) were not used in these experiments. The angular rotation (θ) is measured by a continuous transformer-type transducer, this signal is fed into the computer on an A/D input channel multiplied by +1 or -1 and outputed on D/A channel. This channel is operated independent of the data channels at a rate of 1 KHz.

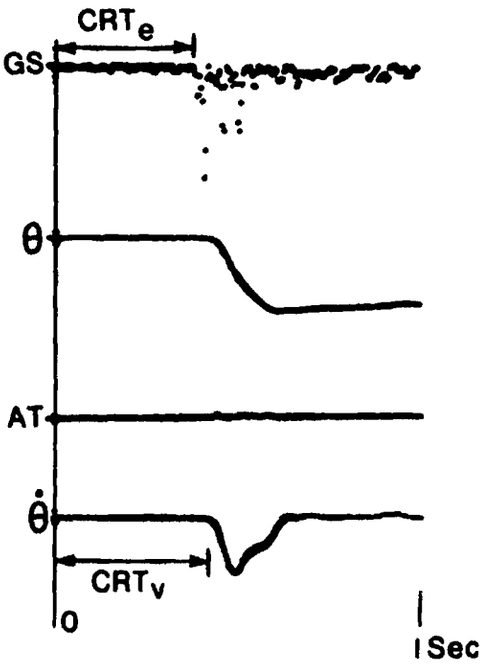

Figure 2

Typical response in a choice reaction with a display gain of +1 and a movement from central position to plantarflexion of the ankle joint. The choice reaction time (CRT) is measured from the jump of the target to the first EMG burst in gastrocnemius-soleus (GS) muscle. There is no EMG activity in the anterior tibial (AT) muscle. Total display time is 1 sec.

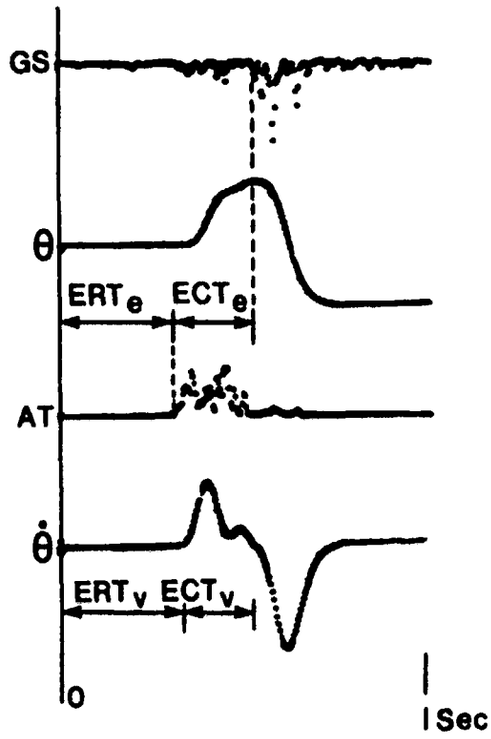

Figure 3

Typical response in error movement and subsequent correction. The display polarity is again +1. The error reaction time (ERT) and error correction time (ECT) are measured from the initial burst in the antagonist and agonist muscle EMGs. Total display time is 1 sec.

ORIGINAL PAGE IS
OF POOR QUALITY

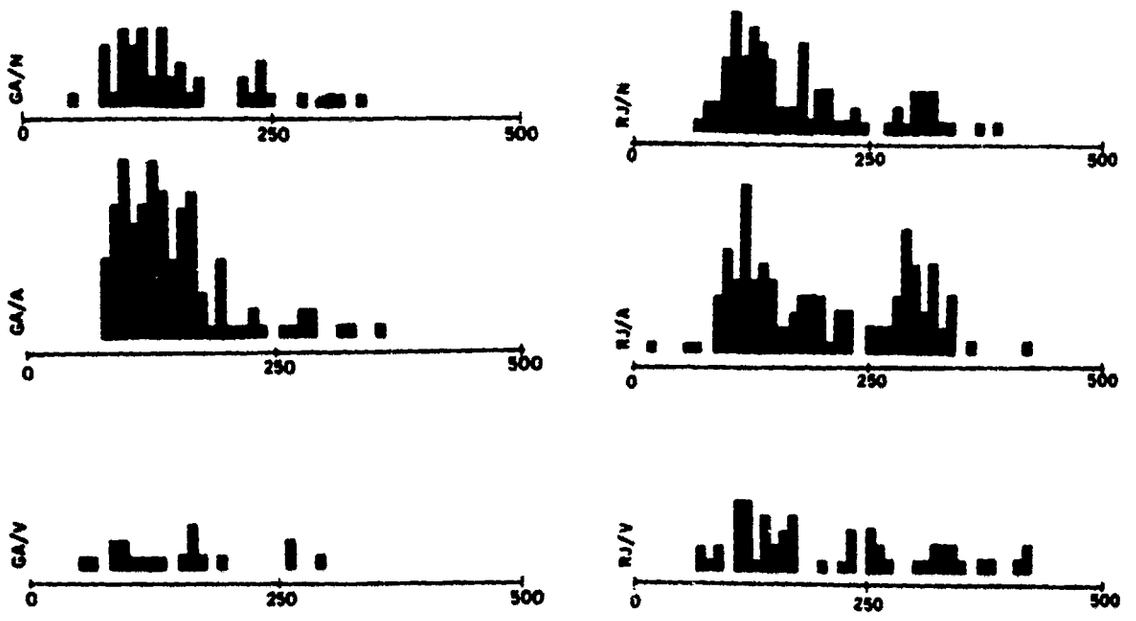

Figure 4

Histograms of the error correction times (ECTs) for the four subjects under normal (N), alcohol (A) and vibration (V) input paradigms. The time interval on abcissa is 500 msec. (continued on next page)

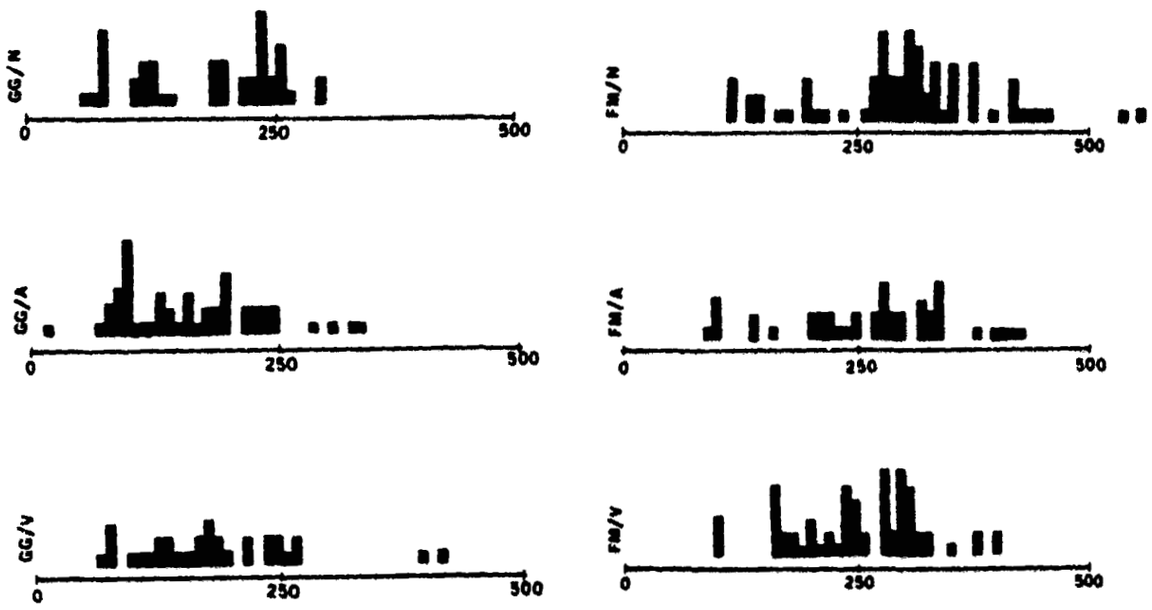

Figure 4 (continued)

D2

N79-15590

A STUDY OF THE EFFECT OF FORCING FUNCTION CHARACTERISTICS ON HUMAN OPERATOR DYNAMICS IN MANUAL CONTROL

by Kyuichiro Washizu*, Keiji Tanaka** and Tatsuo Osawa*

*Department of Aeronautics, University of Tokyo, Tokyo,
**Instrumentation and Control Division, National Aerospace Laboratory, Chofu, Tokyo

SUMMARY

This paper deals with the effect of the spectrum of the forcing function on the human pilot dynamics in manual control. A simple compensatory tracking experiment was conducted, where the controlled element was of a second-order dynamics and the forcing function was a random noise having a dominant frequency. The dominant frequency and the power of the forcing function were two variable parameters during our experiment.

The results show that the human pilot describing functions are dependent not only on the dynamics of the controlled element, but also on the characteristics of the forcing function. This suggests that the human pilot behavior should be expressed by the transfer function taking into consideration his ability to sense and predict the forcing function.

SYMBOLS

$A_{ij}(k)$	element of k-th autoregressive coefficient matrix
B	backward shift operator
c(t), c(n)	human pilot output
dB	decibel
e(t), e(n)	displayed error
i(t), i(n)	forcing function
K_f	static gain of forcing function filter

M	order of autoregressive model
$m(t)$, $m(n)$	controlled element output
s	variable of Laplace transform
$Y_c(j\omega)$	controlled element
$Y_f(j\omega)$	forcing function filter
$Yp(j\omega)$	human pilot describing function
Δ	sampling interval
ζ_f	damping of forcing function filter
ζ_n	damping of controlled element
σ_i^2	power of forcing function
ω_f	undamped natural frequency of forcing function
ω_n	undamped natural frequency of controlled element

INTRODUCTION

It is well known that when a human pilot controls the system, his control behavior depends on the characteristics of the forcing function to the system as well as of the controlled element itself. A great number of papers have been published on this problem.

Concerning the effect of the characteristics of the controlled element on pilot behavior, Washizu and Miyajima (reference 1), and Goto and Washizu (reference 2) pointed out in a series of study on manual control of a second-order system that the human pilot takes notice of the periodicity in the response of the controlled element, if any, and makes use of it to improve his control performance.

On the other hand, concerning the effect of the forcing function on pilot behavior, McRuer and Krendel (reference 3) pointed out that as the bandwidth of the forcing function increases, the effective time delay reduces probably due to the muscular reaction characteristics of the human pilot.

The purpose of the present paper is to investigate the effect of the forcing function spectrum on the human pilot dynamics in manual control. A simple compensatory tracking experiment was conducted, where the controlled element was of the second-order dynamics and the forcing function was a random noise having a dominant frequency. The dominant frequency and the power of the forcing function were two variable parameters during the experi-

ment. Pilot describing functions were derived from the autoregressive model coefficients identified using the Akaike's Final Prediction Error method.

EXPERIMENT

The system of our experiment was built up with an analogue computer, an oscilloscope and a control stick with a restoring spring. Its block diagram is as shown in figure 1. The error $e(t)$ was displayed on the oscilloscope by a line segment moving vertically. The pilot was requested to minimize the error to the best of his ability. The controlled element had a second-order stable dynamics, and its transfer function was of the form;

$$Y_c(s) = \frac{\omega_n^2}{s^2+2\zeta_n\omega_n s+\omega_n^2} \quad . \tag{1}$$

The damping ζ_n and undamped natural frequency ω_n of the controlled element were held fixed throughout our experiment such as,

$$\zeta_n = 0.1 \quad ,$$
$$\omega_n = \sqrt{20} = 4.47 \text{ (rad/sec)} \quad .$$

The shaping filter of the forcing function also had a second-order stable dynamics as,

$$Y_f(s) = \frac{K_f\omega_f^2}{s^2+2\zeta_f\omega_f s+\omega_f^2} \quad , \tag{2}$$

where the damping ζ_f was held fixed to 0.1 and the static gain K_f and the undamped natural frequency ω_f were two variable parameters. Thus, the white noise was transformed into a forcing function having a dominant frequency after passing the filter. The dominant frequency was varied by selecting the values of ω_f as,

$$\omega_f = 3.16,\ 2.24,\ 1.58 \text{ (rad/sec)} \quad .$$

We chose four levels for the power of the forcing function σ_i^2 by adjusting K_f of the equation,

$$\sigma_i^2 = \frac{\omega_f K_f^2}{4\zeta_f}\sigma_w^2 \qquad (3)$$

where σ_w^2 is the power of the noise source.

The experiment was of 12 cases, namely 3 kinds of frequencies and 4 power levels of the forcing function, and two runs of each case were performed. After sufficient excercise, the analog data of the length of 90 seconds for each runs were recorded. The data, i(t), e(t), c(t) and m(t) in figure 1 were transformed into digital data by use of the NOVA minicomputer system. The FACOM 230-75 computer was employed for numerical calculations of the following time series analysis.

ANALYSIS

By the use of the experimental data thus obtained, the human pilot describing functions were identified utilizing a time domain technique; that is, an autoregressive model was fitted to the data by using the Akaike's MFPE (Multiple Final Prediction Error) method. (reference 4)

In the first place, the data were sampled from the analog data of the pilot output c(t) and the error e(t) with the sampling interval Δ, which was set as 0.1 sec. The sampled data are denoted by c(n) and e(n). Then, the autoregressive model of the form;

$$\begin{bmatrix} c(n) \\ e(n) \end{bmatrix} = \begin{bmatrix} A_{11}(B) & A_{12}(B) \\ A_{21}(B) & A_{22}(B) \end{bmatrix} \begin{bmatrix} c(n) \\ e(n) \end{bmatrix} + \begin{bmatrix} \sigma_{11} & \sigma_{12} \\ \sigma_{21} & \sigma_{22} \end{bmatrix} \begin{bmatrix} \xi_1(n) \\ \xi_2(n) \end{bmatrix} \qquad (4)$$

$$A_{ij}(B) = a_{ij}(1)B + a_{ij}(2)B^2 + \cdots\cdots + a_{ij}(M)B^M \qquad (5)$$

$$Bx(n) = x(n-1) \qquad (6)$$

was fitted to the given data. B is the backward shift operator as shown in equation (6), and $A_{ij}(B)$'s in equation (4) are the power series in B that are made up of the autoregressive model coefficients $a_{ij}(k)$ with k going from 1 through M. The order of the model M is determined by the MFPE method. $\xi_i(n)$'s in equation (4) are mutually independent white noises.

Once we have succeeded in fitting the model to the given data, namely, $\sigma_{12} = \sigma_{21} \neq 0$, we can compute the pilot describing function using

$$\hat{Y}_p(j\omega) = \frac{A_{12}(j\omega)}{1 - A_{11}(j\omega)} \quad , \tag{7}$$

where $A_{11}(j\omega)$ and $A_{12}(j\omega)$ are obtained from $A_{11}(B)$ and $A_{12}(B)$ in equation (4) respectively, by replacing B with $\exp(-j\omega\Delta)$.

This method has recently been put into practical use, and our experience in using it has proved that it is quite efficient and powerful (reference 5). Application of this method to our data was also successful, as the estimated correlation coefficient of the noise sources, $\sigma_{12}/\sqrt{\sigma_{11}\sigma_{22}}$, was quite small.

RESULTS

Figures 2 and 3 are examples of the time histories of the records. Note that in figure 2, namely when the frequency of the forcing function ω_f was large, it is not evident that c(t) was affected by the forcing function periodicity. The pilot seemed to suppress only the controlled element periodicity.

On the other hand, figure 3 shows the time history of the case when ω_f was relatively small. In this case, it is evident that c(t) was made up of two main sinusoidals; one reflected the forcing function periodicity and the other reflected the pilot behavior which seemed to suppress the controlled element periodicity. This suggests that, when ω_f was relatively small, the human pilot behavior was affected by the forcing function.

Above tendencies can be seen more obviously in the power spectrum densities of the pilot output as shown in figure 4; namely in the vicinty of $\omega = \omega_f$, the power spectra were pulled up as σ_i^2 increased, and this phenomenon became more conspicuous when ω_f was relatively small.

Typical pilot describing functions are shown in figures 5 and 6. From these figures, the following tendencies have been observed;

1) If the power of the forcing function σ_i^2 is increased, while keeping the undamped natural frequency ω_f unchanged, the gain of the pilot describing function increases, but the phase lead becomes smaller in the frequency region below the undamped natural frequency of the controlled element ω_n.

2) If the frequency of the forcing function ω_f is decreased, while keeping the power σ_i^2 unchanged, the gain of the pilot describing function increases, but the phase lead becomes smaller in the low frequency range, especially in the neighbourhood of the undamped natural frequency of the forcing function.

Figure 7 shows the performance of the pilot control indicated by σ_e^2/σ_i^2. It is evident that the smaller the undamped natural frequency ω_f was, the better the performance became. This implies that when ω_f was small, the pilot could easily recongnize the forcing function periodicity, and his task became easier.

These results lead to the following consideration concerning the forcing function effects on human pilot control behavior.

The effect of the forcing function bandwidth on the pilot describing function is reported in reference 3. It is pointed out in the report that the effective time delay of the human pilot decreases as the bandwidth of the forcing function increases.

On the other hand, the present study put emphasis on the effect of the frequency ω_f and K_f of the forcing function shaping filter. It has been suggested that the increase in the power of the forcing function is likely to work so as to make the pilot employ the control that takes into account the dominant periodicity in the forcing function. The attempt to suppress the dominant frequency component may lead to the reduction of the power of the error. It has also been suggested from the present study that if the response of the controlled element and the forcing function have periodicities, the human pilot would try to augment the system stability by making use of the periodicity in the response of the controlled element, and then, try to make the performance as good as possible by making use of the periodicity of the forcing function. Especially, if the power of the forcing function is large and the two natural frequencies are separated, it would be easy for the pilot to notice these frequencies and to make use of these frequencies in the control.

The present study has shown that the human pilot dascribing functions are dependent not only on the natural frequency of the controlled element, but also on the frequency and the power of the forcing function. These results seem to suggest that the human pilot control behavior couldn't be expressed by a simple transfer function compensating the controlled element delay only, but should be expressed by the transfer function taking into consideration his ability to sense and predict the forcing function.

CONCLUDING REMARKS

The results show the effects of the forcing function on the human pilot such as;

1) If the power of the forcing function σ_i^2 increases, the gain of the human describing function $|\hat{Y}_p|$ increases, but the phase lead of $\hat{Y}_p$ becomes smaller at $\omega < \omega_n$.
2) If the undamped natural frequency of the forcing function ω_f decreases, the gain $|\hat{Y}_p|$ increases but the phase lead of $\hat{Y}_p$ becomes smaller especially in the vicinity of $\omega = \omega_f$.

3) The human pilot seems to try to augment the system stability and make the performance better by use of ω_n and ω_f, especially when σ_i^2 is large, and ω_n and ω_f are separated.

ACKNOWLEDGEMENT

The authors are deeply indebted to Mr. M. Okabe, Chief of Human Engineering Section of NAL, for his support on conducting the experiment.

REFERENCES

1. Washizu,K.; and Miyajima,K.: Some Consideration on the Controllability Limit of a Human Pilot. AIAA J., Vol.5, No.1, 1967, pp.151-155.

2. Goto,N.; and Wahizu,K.: On the Dynamics of Human Pilots in Marginally Controllable Systmes. AIAA J., Vol.12, No.3, 1974, pp.310-315.

3. McRuer,D.T.; and Krendel,E.S.: Mathematical Models of Human Pilot Behavior. AGARD-AG-188, 1974.

4. Akaike,H.: Statistical Predictor Identification. Ann. Inst. Statist. Math., Vol.22, 1970, pp.203-217.

5. Tanaka,K.; Goto,N.; and Wahizu,K.: A Comparison of Techniques for Identifying Human Operator Dynamics Utilizing Time Series Analysis. 12th Ann. Conf. on Manual Control, NASA TM X-73,170, 1976, pp. 673-685.

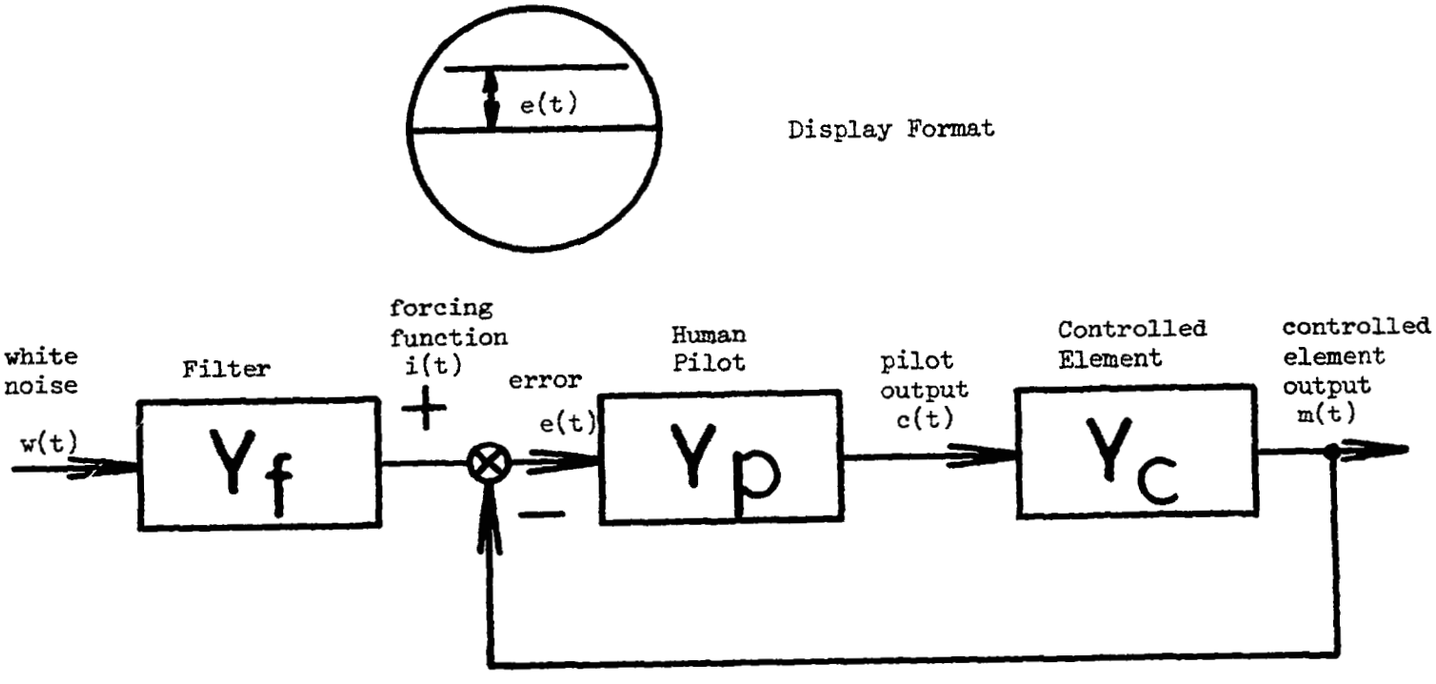

Figure 1. Block Diagram of the Experiment

ORIGINAL PAGE IS
OF POOR QUALITY

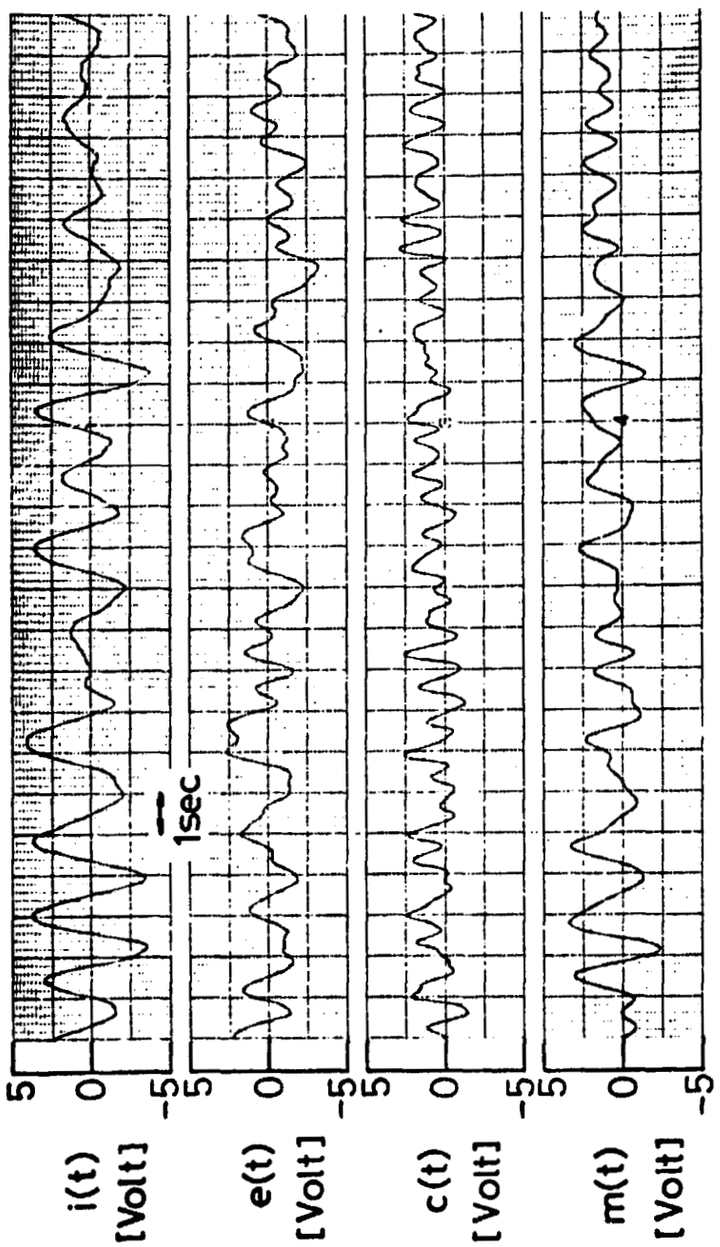

Forcing Function Periodic Time = $2\pi/\omega_f$ = 1.99 sec.
Controlled Element Periodic Time = $2\pi/\omega_n$ =1.40 sec.

Figure 2. An Example of the Time Histories of the Recorded Data
(ω_f = 3.16 rad/sec, and K_f = 1.41)

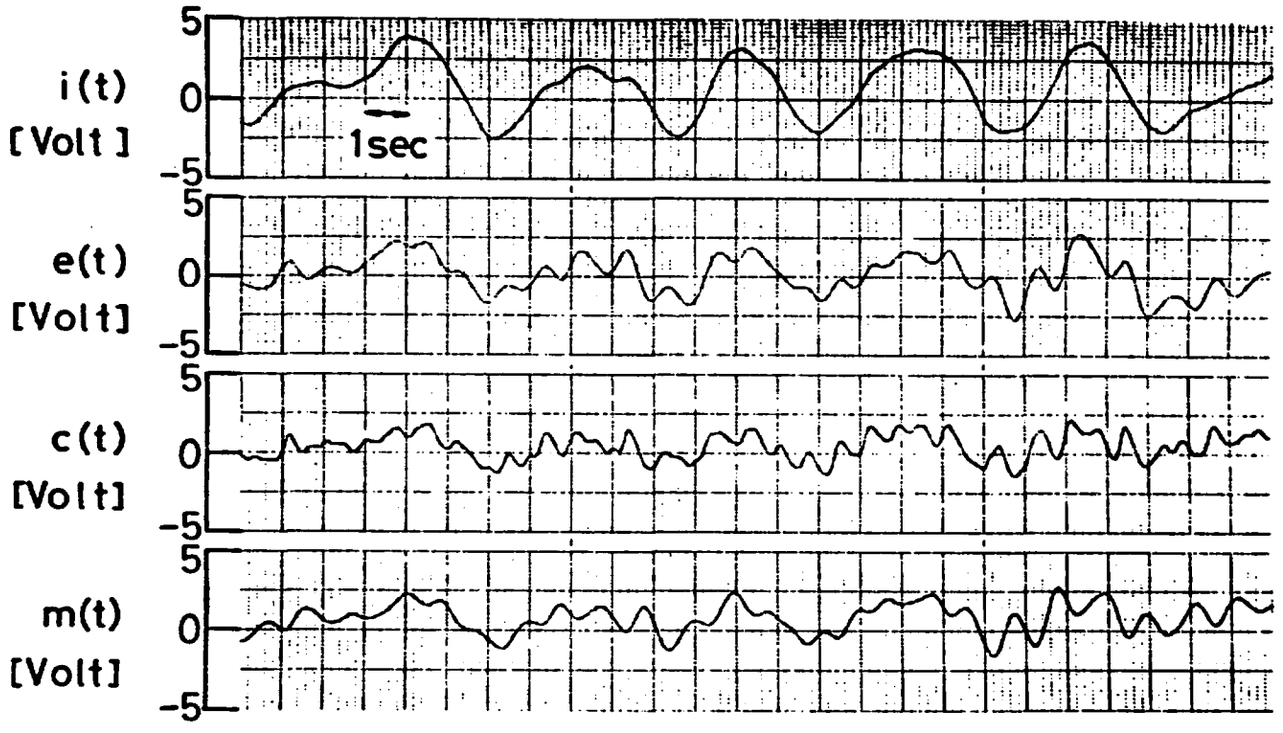

Forcing Function Periodic Time = $2\pi/\omega_f$ = 3.97 sec.
Controlled Element Periodic Time = $2\pi/\omega_n$=1.40 sec.

Figure 3. An Example of the Time Histories of the Recorded Data
(ω_f = 1.58 rad/sec, and K_f = 2.00)

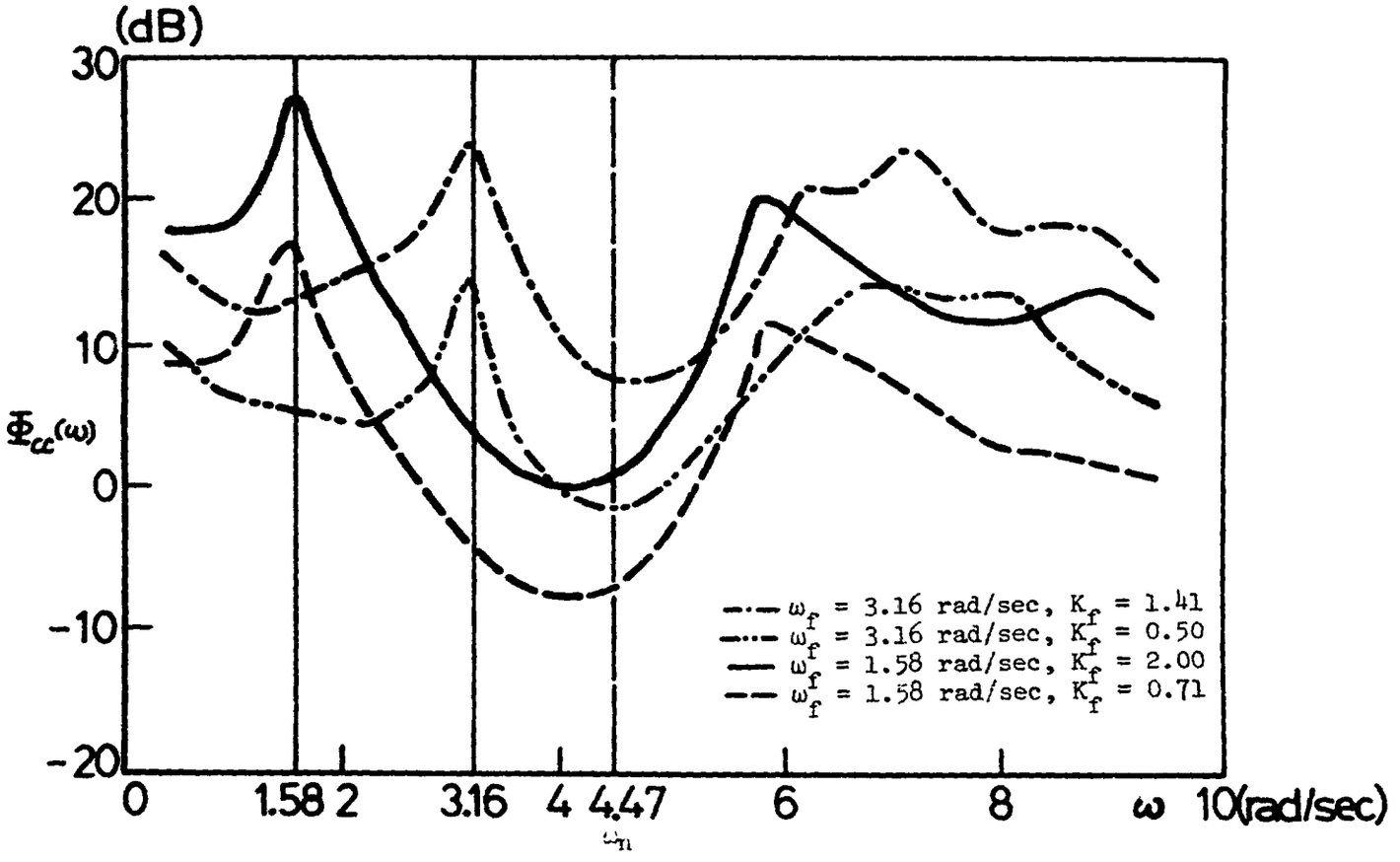

Figure 4. Examples of the Power Spectra of the Pilot Control Output

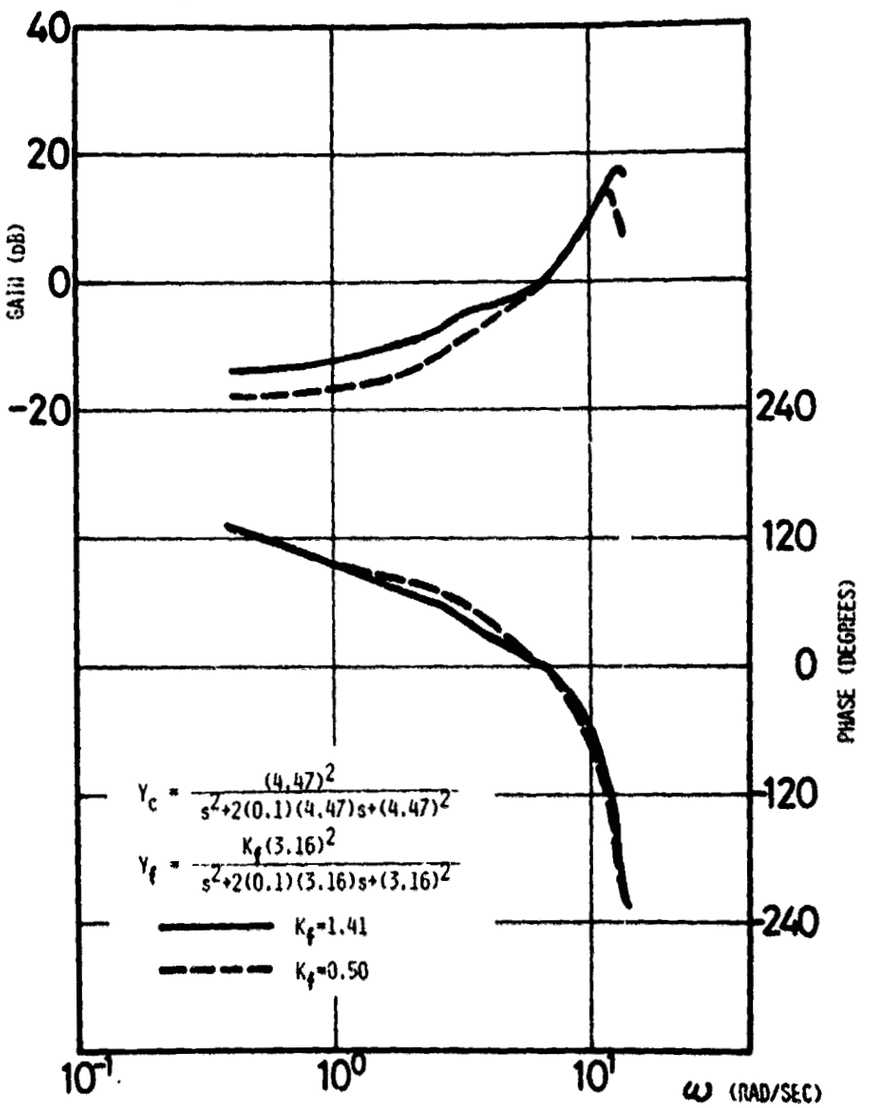

Figure 5. Comparison of Pilot Frequency Responses when ω_f=3.16 rad/sec.

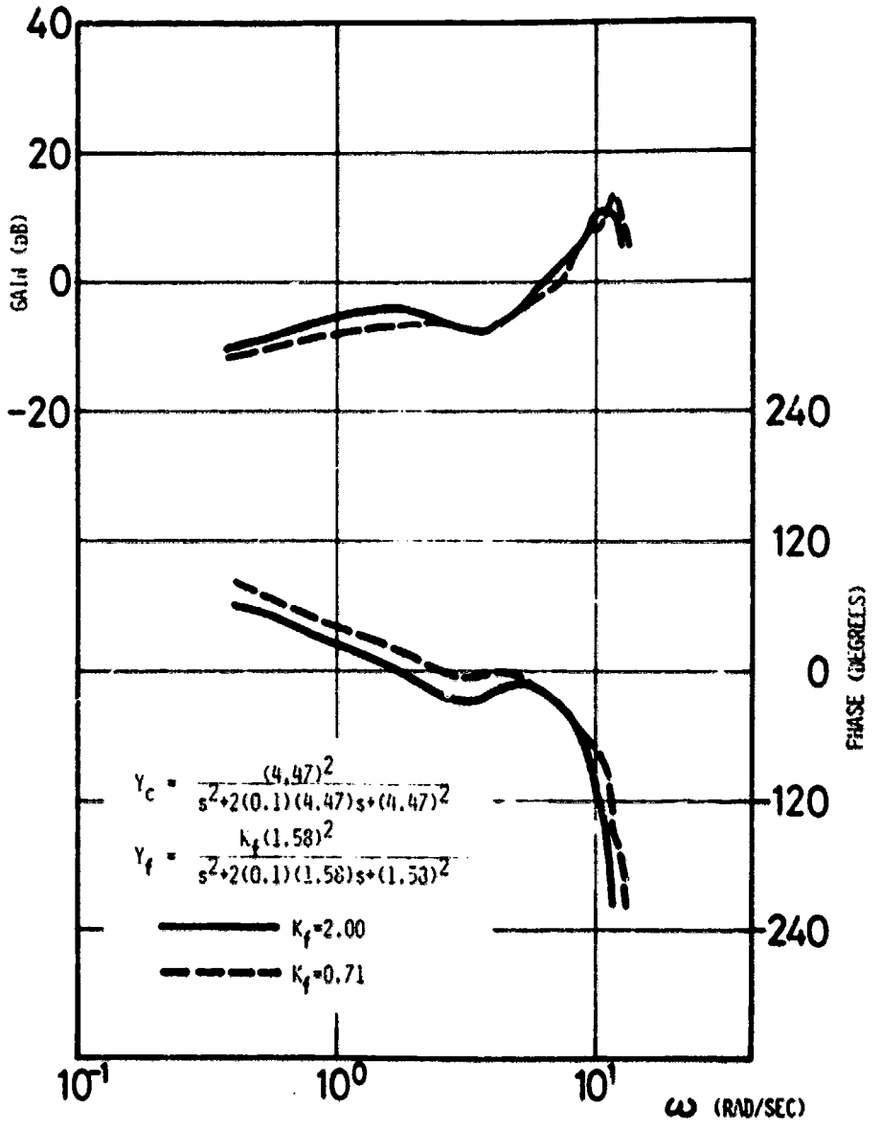

Figure 6. Comparison of Pilot Frequency Responses when ω_f=1.58 rad/sec.

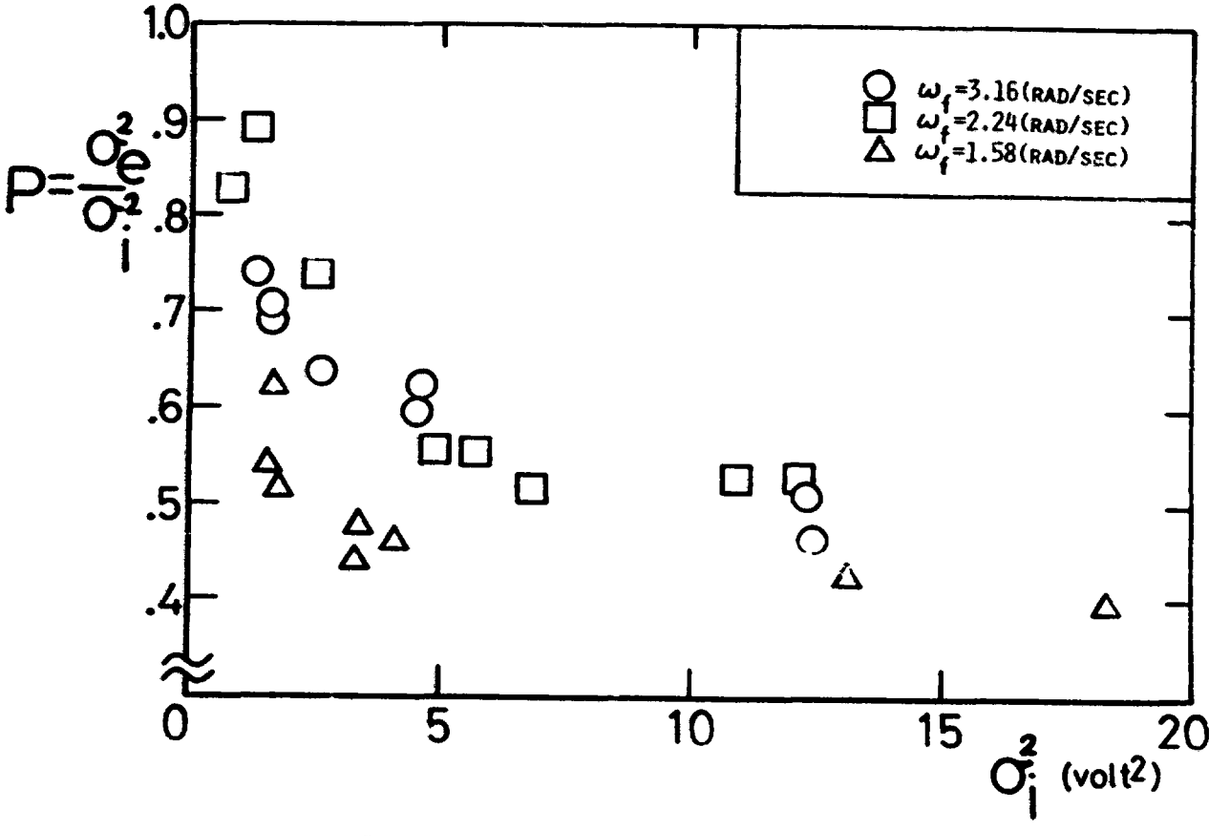

Figure 7. Effect of σ_i^2 and ω_f on Pilot Control Performance

N79-15591

AN EXTENSION OF THE QUICKENED DISPLAY FOR MANUAL CONTROL

By Masayoshi Tomizuka and Wai Ming Tam

Department of Mechanical Engineering
University of California, Berkeley

SUMMARY

It is very difficult (or even impossible) for a human to control plants of third order or more with little or no damping by just knowing the instantaneous error. It has been shown that adding first and/or higher order derivatives to the error signal and displaying the combined signal are effective in facilitating human control over such plants---signal quickening by Birmingham and Taylor. Their technique is further extended to incorporate the future trajectory variation into the displayed signal so as to minimize the tracking error. A method for tuning free parameters in ordinary and extended quickening is established by applying discrete-time optimal control. Experimental results for a triple integrator plant indicate the effectiveness of the proposed method to achieve high quality tracking.

INTRODUCTION

It is known to be very difficult for a human to control higher order plants with little or no damping with conventional compensatory or pursuit display (reference 1). To facilitate human control over such plants, Birmingham and Taylor (reference 2) proposed to incorporate the derivatives of the plant output into the displayed signal. The technique is called "signal quickening," and its effectiveness has been demonstrated. This can sometimes be done as shown in figure 1 for a triple integrator plant. When the reference trajectory, r(t), is constant, the quickened display makes it possible to achieve high quality regulation. However, if r(t) is time varying, it can not be expected that high quality tracking be achieved with the quickened display. This is because the human operator and plant introduce phase shifts between the reference trajectory and the plant output. To improve the tracking performance, more information on the reference trajectory, such as derivatives, future values, etc., is needed.

In many manual control situations, the reference trajectory is predetermined, or a portion of future reference trajectory can be detected in advance if not all future information is available. In such cases, the preview display in figure 2 has been shown to improve the tracking performance when the plant is relatively easy to control (references 3, 4 and 5). If the plant is higher order and weakly damped, preview information alone is not sufficient to achieve high quality tracking or even to stabilize the plant.

After noticing the limitations of quickened display and preview display, one may propose to combine those two and use a display as illustrated in figure 3. However, this scheme is not good for tracking since with such a dis-

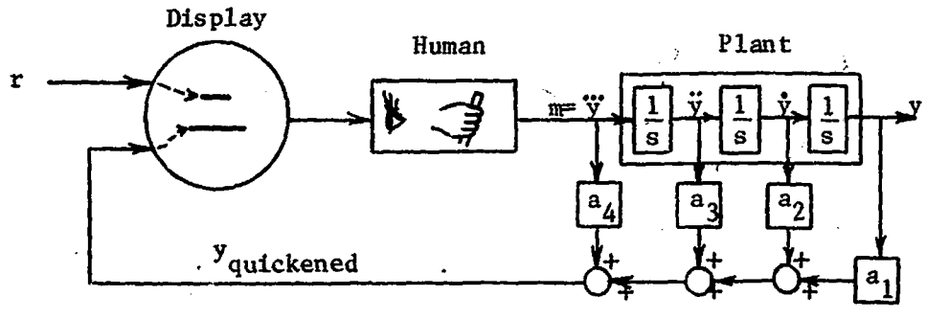

Fig. 1 Signal Quickening (Pursuit Type)

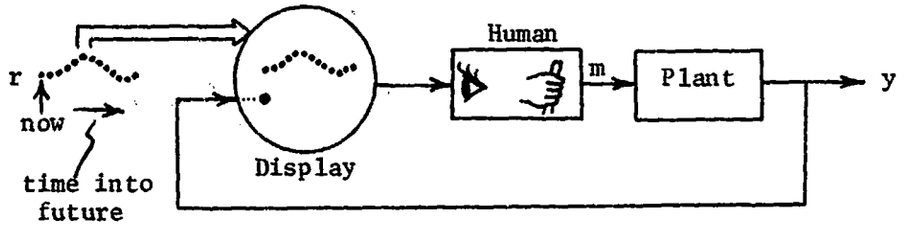

Fig. 2 Preview Tracking

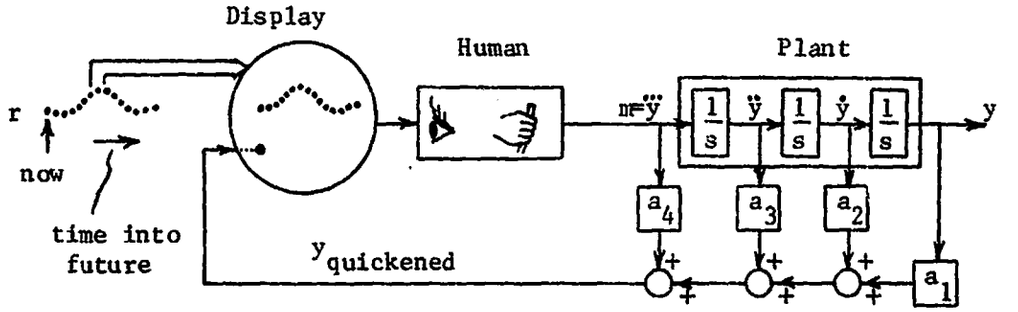

Fig. 3 Naive Combination of Quickened and Preview Displays

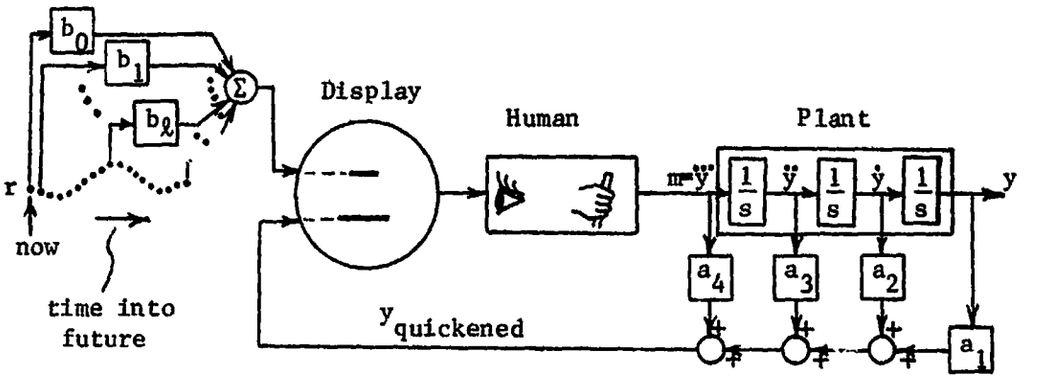

Fig. 4 Extended Quickening

play the human operator tries to match the distorted plant output with the reference trajectory. A better approach is to process future trajectory information by computer to generate a distorted reference signal which is compatible to the distorted plant output. This scheme is illustrated in figure 4 and is named "extended quickening". Due to innovations in microcomputer technology, this kind of digital data processing is not difficult nor expensive. The design of extended quickened displays involves the determination of the feedback (quickening) gains, a_i's, and feedforward or preview gains, b_ℓ's, such that high quality tracking is assured. A design method based on discrete-time optimal control is presented in the next section.

DESIGN OF EXTENDED QUICKENED DISPLAY

To simplify treatment, the design method is described for a triple integrator plant. However, the method applies equally to other kinds of plants.

Controlled Plant

A triple integrator plant can be represented by the following state and output equations.

$$\frac{d\underline{x}_p}{dt} = \underline{A}_p\underline{x}_p + \underline{B}_p m \tag{1}$$

$$y = x_{p1} \tag{2}$$

where

$$\underline{x}_p = \begin{bmatrix} x_{p1} \\ x_{p2} \\ x_{p3} \end{bmatrix} = \begin{bmatrix} y \\ \dot{y} \\ \ddot{y} \end{bmatrix}, \quad \underline{A}_p = \begin{bmatrix} 0 & 1 & 0 \\ 0 & 0 & 1 \\ 0 & 0 & 0 \end{bmatrix}, \quad \underline{B}_p = \begin{bmatrix} 0 \\ 0 \\ 1 \end{bmatrix},$$

$\cdot$ denotes the time derivative, m is the controlling input adjusted by the human operator and y is the plant output. Since extended quickening assumes the use of digital computers, equation (1) is approximated by the discrete state equation,

$$\underline{x}_p(k+1) = \underline{A}'\underline{x}_p(k) + \underline{B}'m(k) \tag{3}$$

where

$$\underline{A}' = e^{\underline{A}_p \cdot \Delta t} = \begin{bmatrix} 1 & \Delta t & (\Delta t)^2/2 \\ 0 & 1 & \Delta t \\ 0 & 0 & 1 \end{bmatrix}, \quad \underline{B}' = \int_0^{\Delta t} e^{\underline{A}_p \cdot \sigma} \underline{B}_p' d\sigma = \begin{bmatrix} (\Delta t)^3/6 \\ (\Delta t)^2/2 \\ \Delta t \end{bmatrix},$$

Δt is the sampling period and the index k denotes k-th sampling instance or time $k \cdot \Delta t$. The sampling period is selected to be 0.025 sec which is short enough to maintain small approximation error and yet is long enough for most microcomputers to implement extended quickening.

Human Operator

For design purposes, the human operator is first approximated by a simple time delay, e^{-sL}, where the delay time, L, is typically 0.1~0.2 sec. With a sampling period of Δt, the discrete-time model is a simple delay chain, z^{-d}, where d can be determined from $(0.1\sim0.2)/\Delta t$. In the following development, d is selected to be 6 which corresponds to 0.15 sec time delay with the selected Δt of 0.025 sec. The input to the human, u(k), is the displayed signal and the output of the human is the plant input, m(k). A state space model for the human operator is

$$\underline{x}_h(k+1) = \underline{A}_h \underline{x}_h(k) + \underline{B}_h u(k) \tag{4}$$

$$m(k) = x_{h1}(k) \tag{5}$$

where

$$\underline{x}_h = \begin{bmatrix} x_{h1} \\ x_{h2} \\ x_{h3} \\ x_{h4} \\ x_{h5} \\ x_{h6} \end{bmatrix}, \quad \underline{A}_h = \begin{bmatrix} 0 & 1 & 0 & 0 & 0 & 0 \\ 0 & 0 & 1 & 0 & 0 & 0 \\ 0 & 0 & 0 & 1 & 0 & 0 \\ 0 & 0 & 0 & 0 & 1 & 0 \\ 0 & 0 & 0 & 0 & 0 & 1 \\ 0 & 0 & 0 & 0 & 0 & 0 \end{bmatrix} \quad \text{and} \quad \underline{B}_h = \begin{bmatrix} 0 \\ 0 \\ 0 \\ 0 \\ 0 \\ 1 \end{bmatrix}.$$

Equations (3), (4) and (5) characterize the open loop human-plant dynamics.

Optimal Control Problem

The parameters, a_i's and b_ℓ's, in extended quickening can be found from the solution of an optimal control problem in which u(k) must be determined so as to minimize the cost functional given by

$$J = \sum_{i=k}^{\infty} \{(y(i) - r(i))^2 + w\cdot(\Delta u(i)/\Delta t)^2\} \tag{6}$$

where $\Delta u(i) = u(i) - u(i-1)$ $(=\Delta m(i+6))$, $\Delta u(i)/\Delta t \sim du/dt$, r is the reference trajectory and w is a positive constant. The first term in the cost functional penalizes the tracking error and the second term penalizes the jerky motion of the displayed signal.

The reference trajectory, r, is assumed to be previewable (by computer) in the sense that future information which includes the sampled values $\{r(k), r(k+1),\ldots,r(k+N_{\ell a})\}$ is avilable at time k where $N_{\ell a}$ is the preview (or look ahead) time. $N_{\ell a}$ is zero for conventional quickening. Preview information is not sufficient for finding the optimal control, u(k), since the cost functional includes r(i)'s from i=k to i=∞. Therefore, it is further assumed that the reference trajectory does not change from the time $i=k+N_{\ell a}$: i.e.

$$r(k+N_{\ell a}+i+1) = r(k+N_{\ell a}+i) \quad \text{for all } i>0 \tag{7}$$

Equation (7) applies for the determination of u(k) only. For determining u(k+1), updated preview information at time k+1 which includes the sampled value $r(k+1+N_{\ell a})$ is used, and the lower limit of the summation in the cost functional becomes k+1. If the statistical properties of the reference trajectory are known, they can be used in place of equation (7) (references 6,7). Figure 5 shows the assumptions made about the reference trajectory.

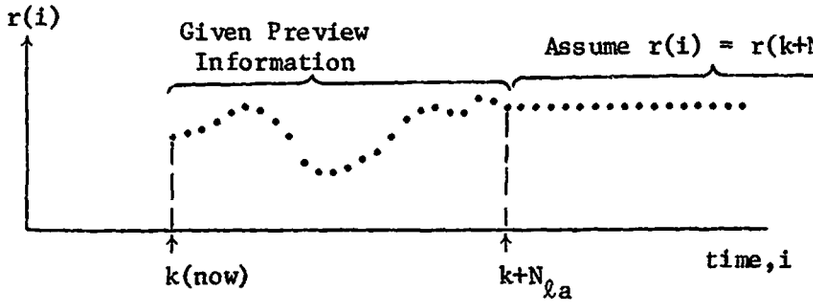

Fig. 5 Information on Future Reference Trajectory (at time k)

Equations (2)-(7) define an optimal control problem or more specifically a discrete time optimal preview control problem. This problem can be solved by dynamic programming or applying the results of linear quadratic (LQ) optimal control (reference 8).

Solution of the Optimal Control Problem

The optimal control, $u^{opt}(k)$, is

$$u^{opt}(k) = -\sum_{i=1}^{3} g_{pi}x_{pi}(k) - \sum_{i=1}^{6} g_{hi}x_{hi}(k) + \sum_{\ell=0}^{N_{\ell a}} g_{r\ell}r(k+\ell) \qquad (8)$$

where g_{pi}'s, g_{hi}'s and $g_{r\ell}$'s are all constant gains.

The feedback gains, g_{pi}'s and g_{hi}'s, are given by

$$\left[g_{p1}\ g_{p2}\ g_{p3}\ g_{h1}\ \cdots\ g_{h6}\right] = \left[R + \underline{B}^T\underline{K}\,\underline{B}\right]^{-1}\left[\underline{B}^T\underline{K}\,\underline{A} + \underline{P}\right] \qquad (9)$$

where

$$\underline{A} = \begin{bmatrix} \underline{A}_p' & \underline{B}_p' & \underline{0} \\ \underline{0} & & \underline{A}_h \end{bmatrix}, \quad \underline{B} = \begin{bmatrix} \underline{0} \\ \underline{B}_h \end{bmatrix}, \quad R = w/(\Delta t)^2, \quad \underline{P} = \left[0\ 0\ 0\ 0\ 0\ 0\ 0\ 0\ -R\right],$$

$\underline{K}$ is the steady state solution of the matrix Riccati equation,

$$\underline{K}(i) = \underline{A}^T\underline{K}(i+1)\underline{A} + \underline{Q} - \left[\underline{B}^T\underline{K}(i+1)\underline{A} + \underline{P}\right]^T\left[R + \underline{B}^T\underline{K}(i+1)\underline{B}\right]^{-1}\left[\underline{B}^T\underline{K}(i+1)\underline{A} + \underline{P}\right]$$
$$(\underline{K}(\infty) = \underline{Q}) \qquad (10)$$

and $\underline{Q}$ is a 9X9 matrix whose 1-1 element is 1, 9-9 element is R and all other elements are 0. Since $\underline{A}$, $\underline{B}$, $\underline{Q}$ and $\underline{P}$ are sparse, the Riccati equation can be efficiently solved by simple recursions. For example, it can be easily seen that $\underline{B}^T\underline{K} = \left[k_{91}\ k_{92}\ k_{93}\ \cdots\ k_{99}\right]$ and $\underline{B}^T\underline{K}\,\underline{B} = k_{99}$.

The feedforward or preview gains, $g_{r\ell}$'s, are given as follows:
For $N_{\ell a} = 0$ (no preview),

$$g_{r0} = g_{p1} \tag{11}$$

For $N_{\ell a} > 0$,

$$\left.\begin{aligned} g_{r0} &= 0, \quad g_{r\ell} = -\left[R + \underline{B}^T \underline{K}\, \underline{B}\right]^{-1} \alpha_{\ell-1}, \quad 1 \le \ell \le N_{\ell a} - 1 \\ g_{rN_{\ell a}} &= g_{p1} - \sum_{\ell=0}^{N_{\ell a}-1} g_{r\ell} \end{aligned}\right\} \tag{12}$$

where α_ℓ is the 1-9 element of the matrix

$$(\underline{A}_{closed})^{\ell} = (\underline{A} - \underline{B}[g_{p1}\ g_{p2}\ g_{p3}\ g_{h1}\ \cdots\ g_{h6}])^{\ell}. \tag{13}$$

Notice that the matrix $\underline{A}_{closed}$ characterizes the closed loop dynamics of the human-plant model plus feedback control law, and is normally asymptotically stable. Equations (12) and (13) indicate that the future values of the reference trajectory must be used in a way compatible to the closed loop dynamics and that $g_{r\ell}$'s with increasing ℓ are closely related to the unit pulse response of the closed loop system. The second expression in (12) implies that the summation of $g_{r\ell}$'s with respect to ℓ must be equal to g_{p1}, which assures zero steady state error for the step reference trajectory. For asymptotically stable $\underline{A}_{closed}$, α_ℓ approaches zero as ℓ increases, which implies that the future is less important to determine $u^{opt}(k)$ as it becomes further apart from the present time. This point has also been found in preview tracking (references 3, 4, 5)

Sturcture of Extended Quickening

The structure of extended quickening based on the optimal control result is depicted in figure 6.

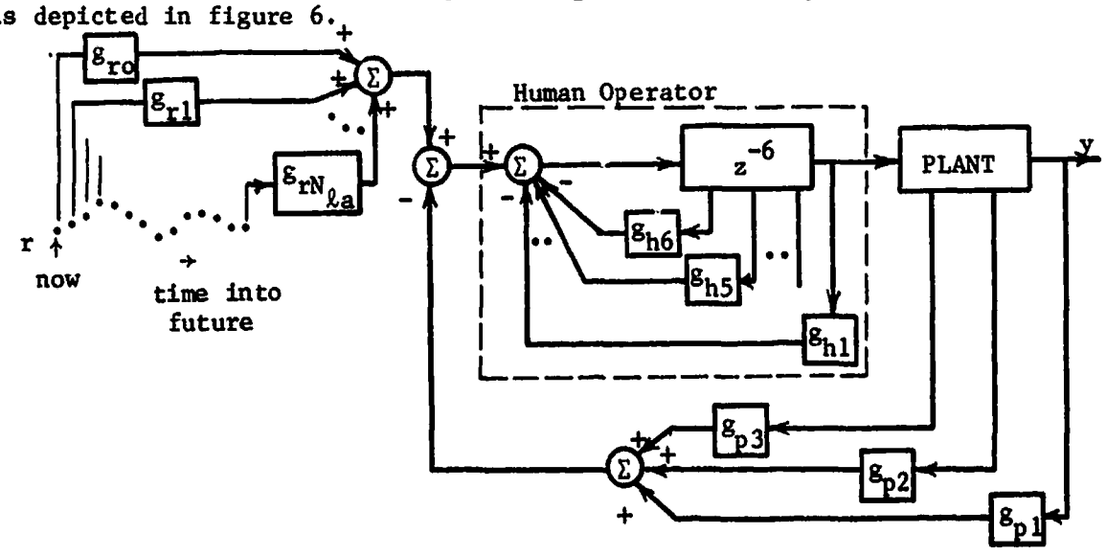

Fig. 6 Structure of Extended Quickening based on Optimal Control

The portion of the structure inside the dashed lines can be viewed as human operator. The reason for this will soon be explained.

For selected values of w over a wide range (w is defined in the cost functional (6)), the steady state solution of the Riccati equation (10) was computed and the feedback gains, g_{pi}'s and g_{hi}'s, were found. Results are summarized in the following table.

w	g_{p1}	g_{p2}	g_{p3}	g_{h1}	g_{h2}	g_{h3}	g_{h4}	g_{h5}	g_{h6}
1.0	0.0242	0.0669	0.0924	0.0023	0.0022	0.0022	0.0022	0.0021	-0.9347
0.1	0.0757	0.160	0.168	0.0042	0.0041	0.0040	0.0039	0.0038	-0.9129
0.01	0.236	0.382	0.309	0.0076	0.0074	0.0072	0.0069	0.0067	-0.884
0.001	0.730	0.914	0.573	0.014	0.013	0.013	0.012	0.012	-0.845
0.0001	2.255	2.20	1.076	0.026	0.025	0.024	0.022	0.021	-0.7935

Table 1 g_{pi}'s and g_{hi}'s for selected values of w

From Table 1, it is found that g_{h1}--g_{h5} are orders of magnitudes smaller than other feedback gains and that the values of g_{h6} is around -(0.8~0.9) regardless of the value of w. Hence it is possible to approximate the portion inside the dashed lines in figure 6 by

$$\frac{z^{-6}}{1 - (0.8\sim0.9)z^{-1}} . \qquad (14)$$

With our selection of Δt= 0.025 sec, the discrete transfer function (14) corresponds to

$$\frac{K e^{-0.15s}}{\tau_N s + 1} , \quad \tau_N = (0.125\sim0.25) \text{ sec} \qquad (15)$$

where the time constant, τ_N, was computed by $\tau_N \sim \Delta t/(1+ g_{h6})$. τ_N has a reasonable value as the human neromuscular lag constant (reference 1), which implies that the feedback effect via g_{h6} can be interpreted as a part of human dynamics. Therefore, the portion inside the dashed lines in figure 6 can be viewed as human operator, and the feedback gains to be externally furnished become g_{p1}, g_{p2} and g_{p3}. The feedforward and preview gains, $g_{r\ell}$'s, must also be externally furnished.

Determination of Parameters in Extended Quickening

In (extended) quickening (or more generally in manual tracking), the gain constants of the display and joystick are rather arbitrarily defined since their inputs and outputs are in different physical domains. It is also known that the human operator adjusts his gain so that the closed loop dynamics have reasonable response speed and adequate stability (reference 1). Therefore, for implementation of (extended) quickening the ratios among the feedback and feedforward gains (g_{pi}'s and $g_{r\ell}$'s) are more important than their values themselves. Based on this observation, we normalize the control gains with respect to g_{p1}. The normalized gains are the extended quickening parameters, a_i's and b_ℓ's, in figure 4, and they are

$$a_1 = 1, \; a_2 = g_{p2}/g_{p1}, \; a_3 = g_{p3}/g_{p1}, \; a_4 = 0 \text{ and } b_\ell = g_{r\ell}/g_{p1}. \qquad (16)$$

Using a_i's and b_ℓ's in (16), the signals to be displayed in extended quickening are, for pursuit type displays

$$s_p(k) = \sum_{i=1}^{3} a_i x_{pi}(k) \quad \text{and} \quad s_r(k) = \sum_{\ell=0}^{N_{\ell a}} b_\ell r(k+\ell) \tag{17}$$

and for compensatory type displays

$$s(k) = s_r(k) - s_p(k) \tag{18}$$

where s_p is the quickened plant output and s_r is the quickened reference trajectory. Final tuning of the parameters, a_i's and b_ℓ's, must be done by experiment.

EXPERIMENT

An experiment was conducted to examine the effect of different sets of feedback gains in Table 1 and to verify performance improvement that can be achieved by extended quickening. In the experiment, a triple integrator plant was implemented on an analog computer. An LSI-11 microcomputer was used for generating the reference trajectory, computing the extended quickening signals (s_p and s_r) and on-line data acquisition of experimental data. The display was of the pursuit type, and the two signals, s_p and s_r, were displayed by dots each with different intensity. Human subjects were asked to control the plant so that the quickened plant output, s_p, follow the quickened reference signal, s_r. Two kinds of reference trajectories were used in the experiment. One was a sequence of step changes with a 20 sec duration for each. The other was a Gauss-Markov random signal which was generated by a second order digital filter excited by a Gaussian white signal. The digital filter was an approximation of the continuous second order filter with the transfer function

$$G(s) = \frac{1}{s^2 + 2\zeta\omega_n s + \omega_n^2} \tag{19}$$

where ω_n and ζ were selected to be 1.5 rad/sec and 0.7. Selectable preview settings were provided which could be varied from $N_{\ell a} = 0$ (0 sec) to $N_{\ell a} = 200$ (5 sec). Evaluation of $s_r(k)$ with $N_{\ell a} = 200$ was not feasible in a 0.025 sec sampling period (cyclic time of computation). However, it was noted that the reference trajectory was smooth relative to a 0.025 sec sampling period (the approximate bandwidth of the filter (19) is 1.5 rad/sec ~ 0.25 Hz) and that a good approximation to $s_r(k)$ in (17) was

$$s_r(k) \simeq \sum_{\rho=0}^{N_{\ell a}/4} b'_\rho r(k+r\rho) \tag{20}$$

where $b'_\rho = b_{4\rho} + b_{4\rho+1} + b_{4\rho+2} + b_{4\rho+3}$. b'_ρ's were all precomputed, and (20) was used for on-line computation of $s_r(k)$.

Effect of Feedback Gains

The first set of experiment was conducted to examine the closed loop behavior with different combinations of feedback gains, g_{pi}'s (i.e. a_i's) in Table 1. In the experiment, the reference trajectory was a series of step changes and $N_{\ell a}$ was zero, i.e. conventional signal quickening. Time histories of the plant output (y's) for different values of w are shown in figure 7. It can be seen in the figure that the feedback gains obtained with the larger w make the closed loop relatively slow to respond while those obtained with the smaller w make the closed loop oscillatory and require more controlling effort of the human operator. It was concluded that the feedback gains obtained with w=0.01~0.1 were most suited for human control of the triple integrator plant.

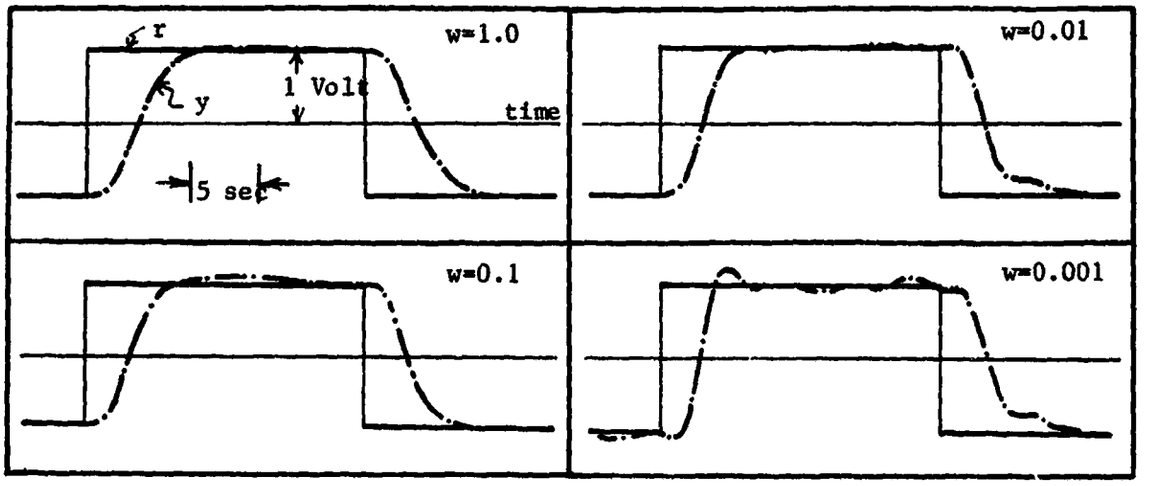

Fig. 7 Effect of Feedback Gains on Closed Loop Behavior

Extended Quickening

The extended quickening experiment was first conducted with the step reference trajectory. The parameters, a_i's and b_ℓ's, were selected to be those computed with w=0.1. This choice was based on the result of the first set of experiment, effect of feedback gains, described above. Time histories of the plant output for different values of preview time (or $N_{\ell a}$) are shown in figure 8. The inclusion of future values of the reference trajectory in the displayed signal, s_r, causes the plant output to respond prior to the step reference change. The maximum and RMS values of the tracking error were both improved by previewing the reference trajectory. A 4~5 second preview time ($N_{\ell a}$=160~200) was found to be sufficient to attain almost all the possible performance improvement relative

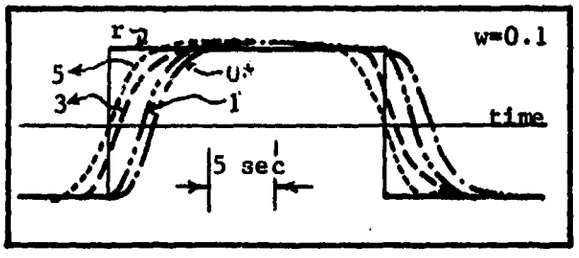

Fig. 8 Effect of Preview Time(* numbers indicate preview times in sec)

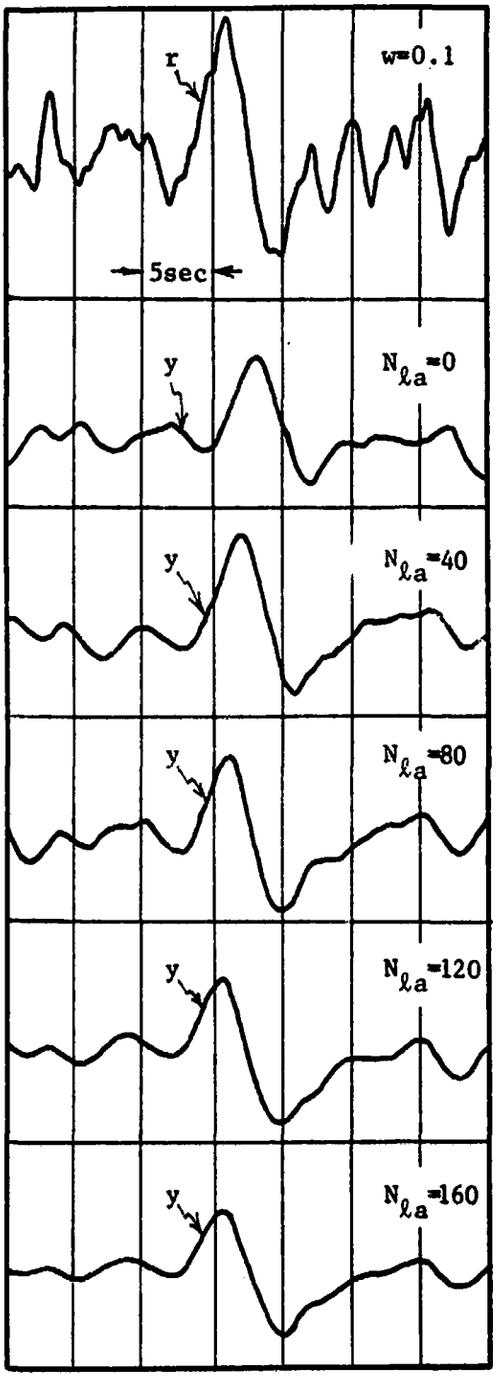

Fig. 9 Effect of Preview Time (random reference trajectory, Preview Time=0.025×$N_{\ell a}$ sec)

to the zero preview case which was about 50 % reduction of the maximum error (observed at the time of step reference change) and about 70 % reduction of the RMS error computed over 60 sec (i.e. 3 step changes of the reference trajectory). A similar improvement was also observed in the controlling input. Therefore, the difference among the four response curves in figure 8 is not simply a matter of translation.

The extended quickening experiment was also conducted with the random reference trajectory. Figure 9 shows the plant output for different values of $N_{\ell a}$. It can be seen in the figure that the phase shifts between the reference trajectory and the plant output gradually reduce as $N_{\ell a}$ increases. It was found that approximately a 2 second preview time ($N_{\ell a}$~80) was sufficient to achieve almost all the improvement in terms of the RMS tracking error, approximately 50 % reduction relative to the zero preview case. Further performance improvement beyond $N_{\ell a}$~80 was observed primarily in the controlling signal whose peak and RMS values were both continuously decreasing as $N_{\ell a}$ was increased from 80 to 200.

CONCLUSIONS

The signal quickening technique was extended to incorporate the future reference trajectory variation into the displayed signal so as to achieve high quality tracking in manual control of higher order plants with little or no damping. A design method for extended quickening systems was established based on the discrete time optimal control theory. The experiment for a triple integrator plant indicated that a drastic improvement of the closed loop performance can be obtained by extended quickening.

The extended quickening technique should be useful for various man-vehicle systems including airplane landing, maneuver, submarine control, etc. The main

motivation of (extended) quickening was to facilitate human control over high order plants with little or no damping. However, for the cases that plants are relatively easy to control, the technique should be still useful in various respects, e.g. for reducing the human work load.

The work reported in this paper is being continued to investigate the extended quickening technique in more realistic situations. Emphasis is placed on the following two points:

1. State Estimation: It was assumed that the derivatives of the plant output are directly measurable. Although the assumption holds in ideal situations such as the triple integrator plant on an analog computer in this paper, it is usually not possible to measure all derivatives directly. In such cases, one possibility is to include a Kalman filter or state observer in computer software.
2. Effect of Disturbance: In this paper, external disturbance inputs and/or noise were not considered. In practical situations, disturbance and noise can not be ignored, and their effect must be investigated.

REFERENCES

1. Sheridan, T. B. and Ferrell, W. R., Man-Machine Systems: Information, Control, and Decision Models of Human Performance, MIT Press, 1974.

2. Birmingham, H. P. and Taylor, F. V., "A Human Engineering Approach to the Design of Man-Operated Continuous Control Systems," Naval Res. Lab. Rep. 4333, April 1954.

3. Sheridan, T. B. et al., "Control Models of Creatures which Look Ahead," Proceedings of the 5th National Symposium on Human Factors in Electronics, 1964, pp. 229-240.

4. Reid, L. D. and Drewell, N. H., "A Pilot Model for Tracking with Preview," Proceedings of the 8th Annual Conference on Manual Control, AFFDL-TR-72-92, May 1972.

5. Tomizuka, M. and Whitney, D. E., "The Human Operator in Manual Preview Tracking (an Experiment and Its Modeling via Optimal Control)," Trans. of ASME, Journal of Dynamic Systems, Measurement, and Control, Vol. 98, No. 4, December 1976, pp. 407-413.

6. Tomizuka, M. and Whitney, D. E., "Optimal Discrete Finite Preview Problems (Why and How is Future Information Important?)," Trans. of ASME, Journal of Dynamic Systems, Measurement, and Control, Vol. 97, No. 4, Dec. 1975.

7. Tomizuka, M., "Optimum Linear Preview Control with Application to Vehicle-Suspension---Revisited," Trans. of ASME, Journal of Dynamic Systems, Measurement, and Control, Vol. 98, No. 3, September 1976.

8. Dorato, P. and Levis, A. H., "Optimal Linear Regulators: The Discrete-Time Case," IEEE Trans. on Automatic Control, Vol. AC-16, No. 6, Dec. 1971.

N79-15592

EFFECTS OF UNCERTAINTY ON MANUAL TRACKING PERFORMANCE

by Avi R. Ephrath & Barbara Chernoff

Department of Electrical Engineering & Computer Science
University of Connecticut
Storrs, Conn. 06268

SUMMARY

In this experimental study we investigated some transient phenomena and target acquisition modes associated with interrupted observations during ground-to-air AA tracking. Our subjects, using a two-axes control stick, tracked a computer-generated airplane image on a CRT display. The airplane image executed a low-level straight pass. At certain pseudo-random times during each 25-second run the screen was blanked for a period of one second (simulating a temporary loss of visual contact with the target due to clouds, fog or obstructions). When the target image reappeared the subjects reacquired it and continued tracking, attempting to minimize vector RMS error for the entire run (including the blanked period).

The results reveal an increase both in tracking error and in error variance during the blanked period, only when the target disappears while in the crossover region. Blanking at other times effected increased variance but had no effect on the mean error. Also, blanking before and after crossover had opposite effects: A blanking period just before crossover produced an increase lag while a blanking just after crossover resulted in a lead and thus made the error curve more symmetric.

INTRODUCTION

The problem of manual tracking performance with sampled observations has been studied before [e.g., Refs. 1, 2] from a "macroscopic" point of view. In these studies the overall control performance was investigated when the human was assumed to have access to periodic, frequent observations of the system outputs.

In the study reported here we intended to concentrate on the microscopic aspects of the tracking behavior. We were not interested in the operator's performance as a whole; rather, we set out to examine the details of the tracking behavior during periods when observations of the system outputs were not available to the human. Understanding the operator's behavior during such essentially open-loop tracking is of interest as these situations occur quite frequently in practice. Examples of operators subjected to this type of manual tracking may be the driver of a high-speed automobile during the first few seconds after entering a dark tunnel; a radar operator attempting to track a target with the aid of noisy position

44
PAGE INTENTIONALLY BLANK

data; or an anti-aircraft battery operating in an environment of electronic counter-measures, optical counter-measure or simple topographical and meteorelogical obstructions masking the target's image. Indeed, our experimental set-up simulated the situation of the latter, i.e., the AAA paradigm.

THE EXPERIMENT

Our experimental facility consisted of a PDP 11/20 computer, a CRT screen, and a two-axes control stick. The PDP 11/20 generated a delta-shaped airplane image used in the compensatory tracking, with the image displayed on the CRT screen (see Fig. 1).

Our subjects were instructed to manually track the delta-shaped image, both in elevation and in azimuth, as it passed across the CRT screen. Each target pass was a 25.6-seconds straight-and-level flyby. At predetermined times during the run the target disappeared from the screen for a period of one-second. This blanking simulated the temporary loss of visual contact with the target. Five experimental conditions were implemented.

Condition A: No blanking

Condition D: Blankings at -5 sec. and at +9 sec. (0. sec. = crossover)

Condition E: Blanking at -3 sec.

Condition F: Blanking at +1 sec.

Condition G: Blanking at +3 sec. and at +9 sec.

The purpose of two blanking periods (Conditions D and G) was twofold: In an attempt to prevent the subjects from relaxing their tracking effort after the first blank occured, the second blanking at +9 seconds was introduced. Also, this set of blanking periods enabled us to compare the transient tracking behavior of subjects during periods of good tracking (where the target angular velocity is small and the tracking error is also small) with the transient phenomena in the crossover region. Condition A - no blanking served as the control for the subjects' baseline tracking ability.

Six University of Connecitcut students, members of the University Air Force ROTC program, participated in thes experiment. They were trained extensively in this task by tracking a variety of flybys; however, they were not exposed to blankings until the formal experimentation commenced.

Each subject was presented with each of the five experimental conditions in randomized order and there were 7 replications, for a total of 35 runs per subject. The subjects were not informed as to the number of blanking periods in each run, nor were they told how many experimental conditions were to be presented. They were told, however, the total number of runs to be presented. The subjects were instructed to minimize their RMS tracking error for the entire run, including the blanked periods. Following each

run, each subject was informed of his RMS error score and was encouraged to keep it as low as possible.

Tracking errors in azimuth and elevation, and the control inputs in these axes were sampled by the PDP-11/20 at a rate of 40 Hz. Each 25.6-second run thus yielded 1024 datum points for each of these four dependent variables. The data were stored in real-time or secondary devices (discs and magtapes) for subsequent, off-line processing and analysis.

RESULTS AND DISCUSSION

Some results of this experiment are presented in Figures 2-6. Each figure is the summary azimuth data of the (6 subjects x 7 replications =) 42 runs per experimental condition. (In the interest of brevity, elevation data, which are completely analogous, were omitted here.) Figures 2a and 2b are the mean and standard deviation, respectively, of the angular tracking error under the baseline condition, Condition A (no blanking). Figure 2a exhibits the asymmetry (large lag just before crossover and smaller lead immediately after) characteristic of this tracking task [3]. Also, the tracking errors are quite small in the so-called "areas of good tracking" outside the crossover region.

Comparison of Figure 3 (standard deviation, Condition D) with Figure 2b reveals the two blanking periods which manifest themselves as spikes in Fig. 3. As expected, a blanking period just before crossover produces an increased lag (Fig. 5), while a blanking period just after crossover effects a lead and thus makes the error curve more symmetric (Fig. 6a).

These deviations from the baseline error curve were tested using a point-by-point t-test and were found to be significant, under Condition E and F, at the $P < 0.01$ level. During periods of good tracking, however, blanking had no effect on the tracking error mean. This was true not only with respect to the blanking period at +9 seconds but also with respect to the blankings at -5 seconds and at +3 seconds.

CONCLUSIONS

Increasing the operator's uncertainty of the target's position for short periods increases the lagging tendency before crossover and the leading tendency - when the instance of uncertainty occurs after crossover. Uncertainty on the operator's part of the target's motion always results in increased error variance; the error mean, however, is sensitive to uncertainty only when the tracking task is difficult. In periods of good tracking (and hence, small tracking error) uncertainty has little effect on the error mean.

REFERENCES

1. Senders, J.W., Ward, J.L., and Carbonell: Human Visual Sampling Processes. NASA CR-1258, 1969.

2. Senders, J.W. et al.: An Investigation of the Visual Sampling Behavior of Human Observers. NASA CR-434, 1966.

3. Kleinman, D.L. and Ephrath, A.R.: Effects of Target Motion and Image on AAA Tracking. Decision and Control Conference, New Orleans, La., Dec. 1977.

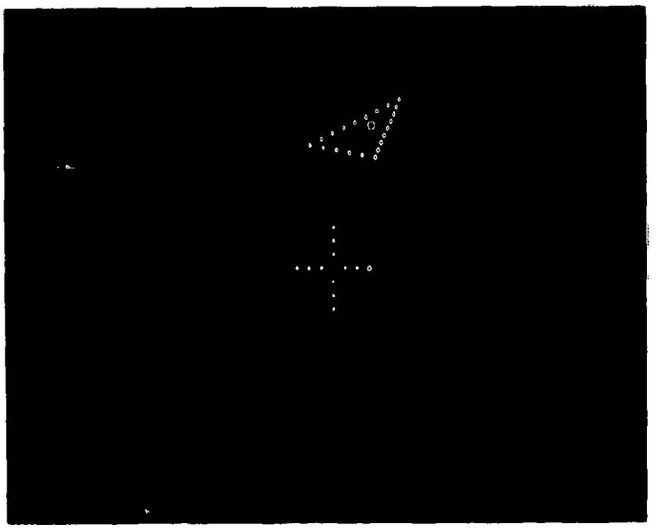

FIG. 1: CRT DISPLAY

ORIGINAL PAGE IS
OF POOR QUALITY

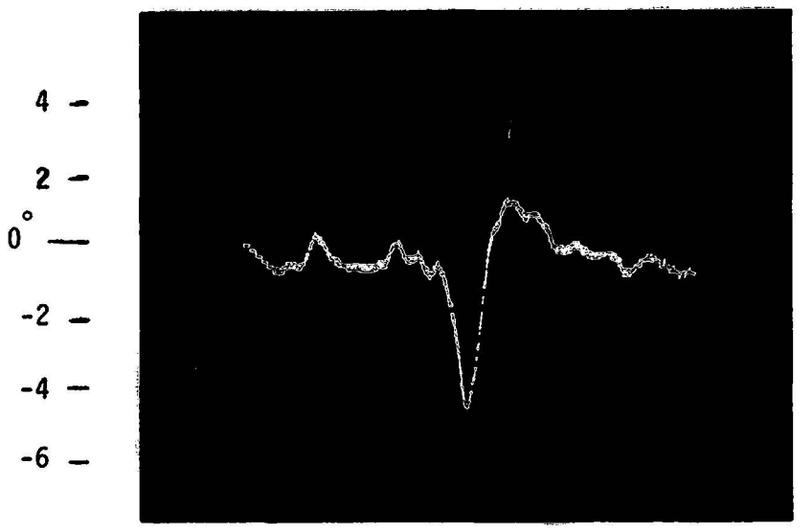

FIG. 2a: Azimuth Error Mean, No Blanking

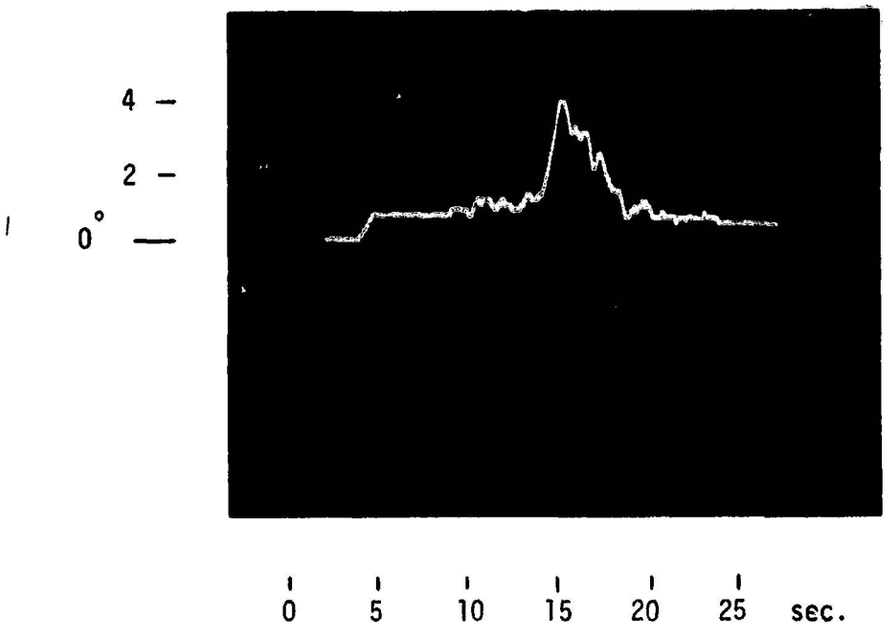

FIG. 2b: Azimuth Error S.D., No Blanking

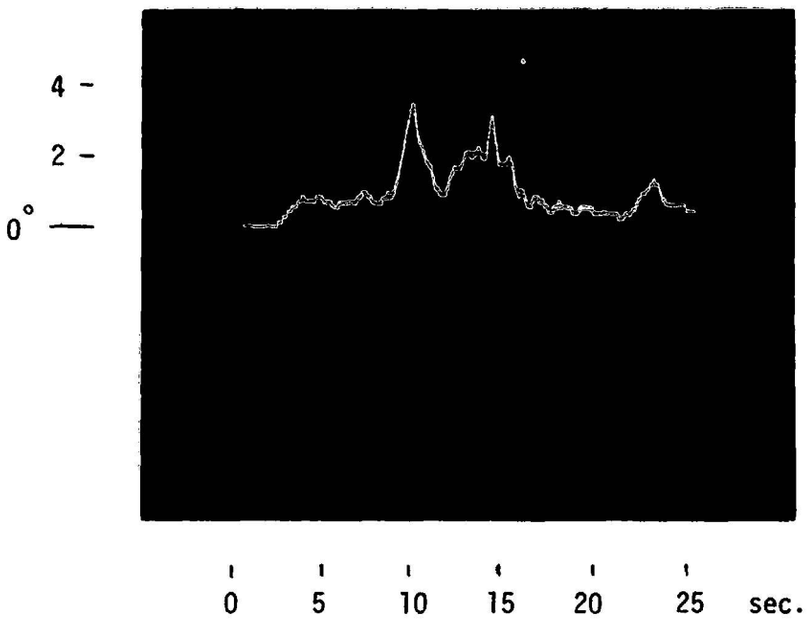

FIG. 3: Azimuth Error S.D., Blankings @ -5 & +9 sec

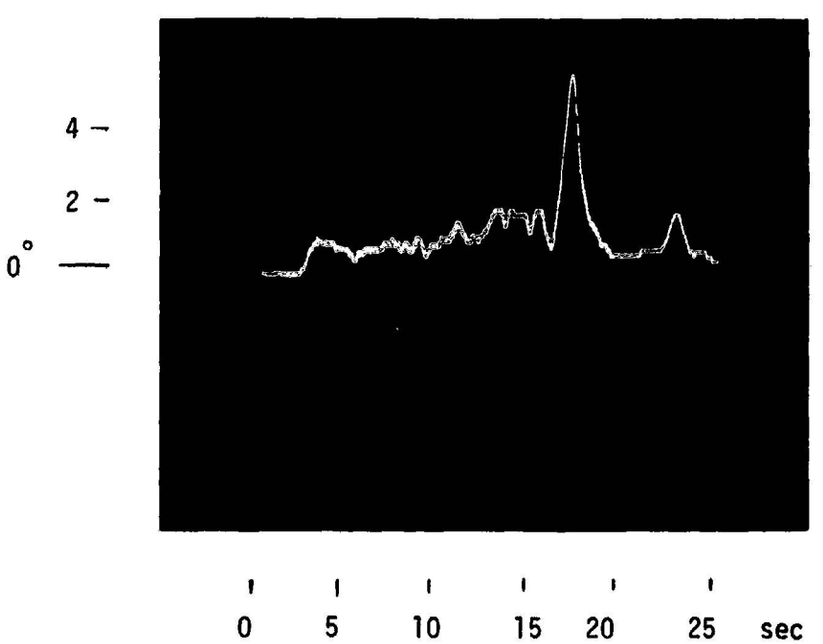

FIG. 4: Azimuth Error S.D., Blankings @ +3 & +9 sec.

ORIGINAL PAGE IS
OF POOR QUALITY

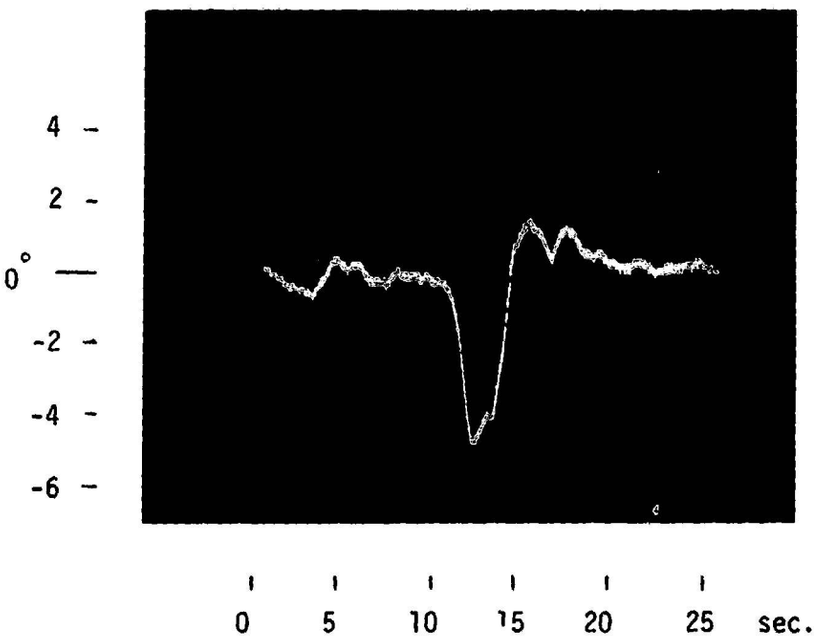

FIG. 5: Azimuth Error Mean, Blanking @ -3 sec.

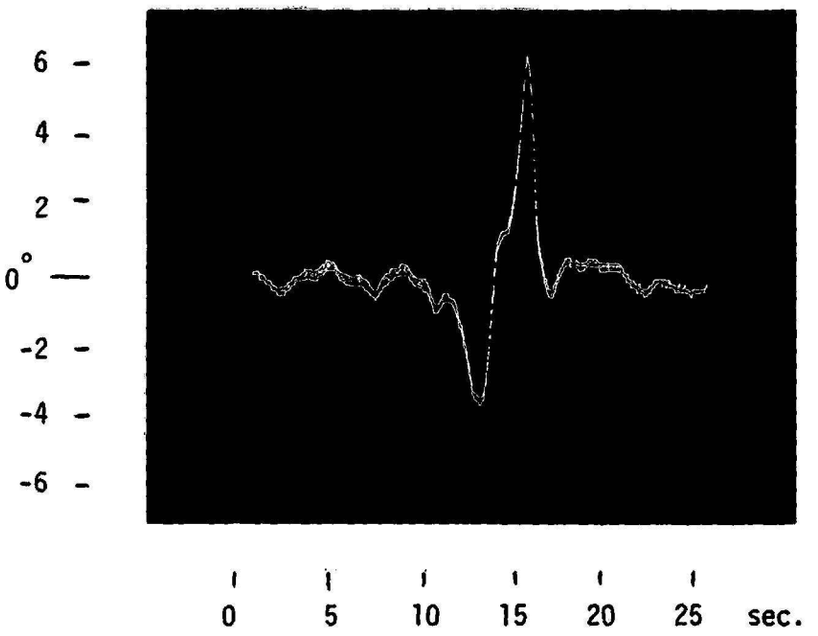

FIG. 6a: Azimuth Error Mean, Blanking @ +1 sec.

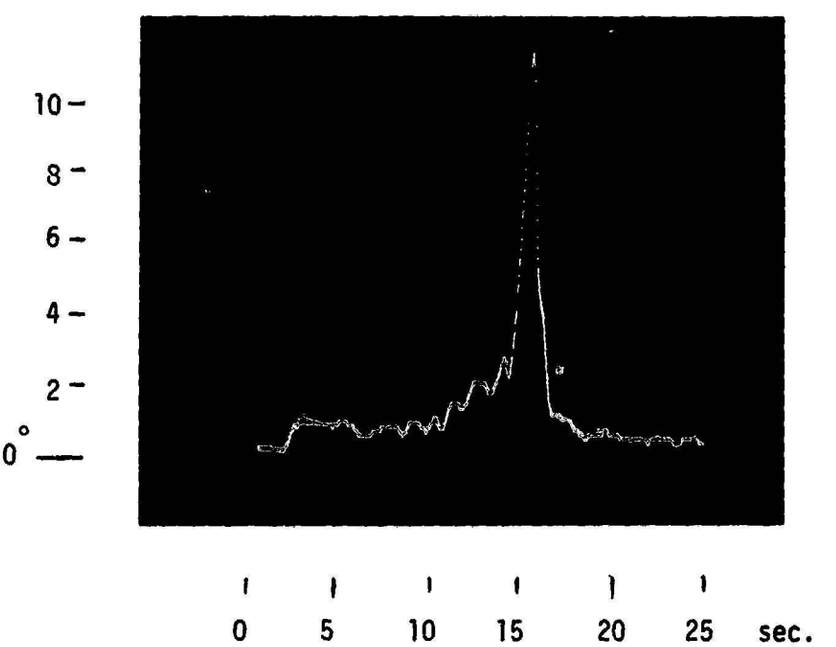

FIG. 6b: Azimuth Error S.D., Blanking @ +1 sec.

SESSION B: HUMAN OPERATOR MODELS: IDENTIFICATION AND CONJECTURE

Chairman: S. Baron

N79-15593

MODELING THE EFFECTS OF HIGH-G STRESS ON PILOTS IN A TRACKING TASK

by Jonathan Korn and David L. Kleinman

Department of Electrical Engineering & Computer Science
University of Connecticut
Storrs, Conn. 06268

SUMMARY

Air-to-Air tracking experiments have been conducted at the Aerospace Medical Research Laboratories (AMRL) using both fixed and moving base (Dynamic Environment Simulator-DES) simulators. The obtained data, which includes longitudinal error of a simulated air-to-air tracking task as well as other auxiliary variables, was analyzed using an ensemble averaging method.

In conjunction with these experiments, the Optimal Control Model (OCM) is applied to model a human operator under high-G stress.

INTRODUCTION

Recent efforts at Aerospace Medical Research Laboratories, WPAFB, have demonstrated initial feasibilities of applying the Optimal Control Model [1] of human response to the air-to-air tracking problem. The model has been able to generate predictions of ensemble mean and standard deviations of longitudinal tracking error, aircraft state variables and attained G_z forces corresponding to arbitrary target profiles. The preliminary modeling efforts were focused on two subproblems. First, effects that related cost functional weightings and internal model parameter changes to G-stress were considered. Second, a structural change of the model was suggested. The data for this model development and validation has been generated on the centrifuge (DES) facility at AMRL. The most recent data vs. model comparisons have shown excellent correspondance for tracking error ensemble statistics. Further model refinement efforts are now under investigation.

ENGAGEMENT SCENARIO

Figure 1 shows the geometry of the air-to-air tracking in the longitudinal plane [2]. In our modeling efforts we assumed no gunsight dynamics, i.e. the sight is fixed and aligned with the aircraft body axis. An additional simplification has been added by assuming that pitch angle equals the flight path angle.

PAGE 54 INTENTIONALLY BLANK

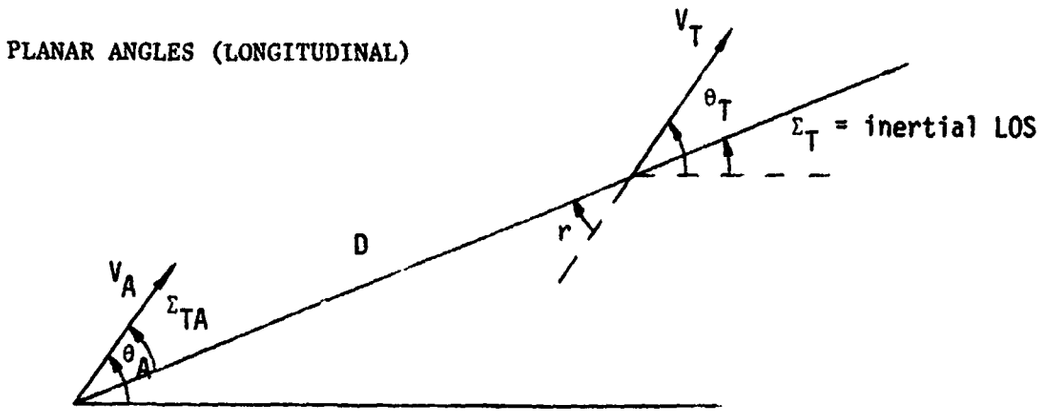

FIG. 1: TRACKING GEOMETRY

θ_A = pursuer fp angle θ_T = evader fp angle

Σ_T = inertial line of sight

$\Sigma_{TA} = \theta_A - \Sigma_T$ = relative line of sight

$r = \theta_T - \Sigma_T$ = aspect angle

OPTIMAL CONTROL MODEL FOR AIR-TO-AIR TRACKING

The OCM, modified to treat deterministic target motion assumes the system dynamics

$$\dot{\underline{x}}(t) = A_o \underline{x}(t) + \underline{b}_o u(t) + F_o z(t) \quad (1)$$

$$\underline{y}(t) = C_o \underline{x}(t) \quad (2)$$

where $u(t) \triangleq \delta_A$ is the elevator deflection and $z(t)$ is a function of the target motion. The state vector is

$$\underline{x}' = [q_T, q_A, \alpha_A, \theta_A - \theta_T, e]'$$

where $q_T(q_A)$ is the target (attacker) pitch rate, α_A is the attacker angle of attack and e is the tracking error. The observations are

$$\underline{y}' = [e, \dot{e}, r, \dot{r}]'$$

with correspondance to the OCM assumtion on observations. The human perceives only a delayed and noisy signal

$$\underline{y}_p(t) = \underline{y}(t-\tau) + \underline{v}_y(t) \tag{3}$$

where $\underline{v}_y(t)$ is a white observation noise with covariance

$$V_{y_i}(t) = \frac{\rho_y^\circ}{f_i(t)} \cdot \frac{(\bar{y}_i^2 + \sigma_i^2)}{N^2(a_i)} \qquad i = 1, \ldots, 4 \tag{4}$$

τ = operator time delay

ρ_y° = nominal noise to signal ratio

$f_i(t)$ = fractional attention allocation to the i-th observed variable

$N(a_i)$ = equivalent gain of the visual/indifference threshold a_i

$\bar{y}_i$ = mean of y_i

σ_i = standard deviation of y_i

The control input corresponds to the differential equation

$$\dot{u}(t) = -L_c \begin{bmatrix} \underline{\hat{x}}(t) \\ u(t) \end{bmatrix} + \frac{1}{\tau_N} v_u(t) \tag{5}$$

where L_c is the feedback gains vector, $\underline{\hat{x}}(t)$ is the estimated state, τ_N is the neuro-motor time constant and $v_u(t)$ is a white motor noise with covariance proportional to the covariance of $u(t)$

$$V_u(t) = \rho_u \, \mathrm{cov}[u(t)], \tag{6}$$

ρ_u being the motor noise ratio coefficient. The system matrices are

$$A_o = \begin{bmatrix} 0 & 0 & 0 & 0 & 0 \\ 0 & M_q & M_\alpha & 0 & 0 \\ 0 & 1 & Z_\alpha & 0 & 0 \\ -1 & 1 & 0 & 0 & 0 \\ 0 & 1 & 0 & V/D & 0 \end{bmatrix} \qquad \underline{b}_o = \begin{bmatrix} 0 \\ M_\delta \\ 0 \\ 0 \\ 0 \end{bmatrix}$$

$$C_o = \begin{bmatrix} 0 & 0 & 0 & 0 & 1 \\ 0 & 1 & 0 & V/D & 0 \\ 0 & 0 & 0 & -1 & 1 \\ 1 & 0 & 0 & V/D & 0 \end{bmatrix}$$

The vertical accelerations of the target, and those commanded by the attacker are respectively

$$G_T(t) = \frac{V}{g} \cdot x_1(t) + 1 \qquad (7a)$$

$$G_A(t) = \frac{V}{g} \cdot x_2(t) + 1 \qquad (7b)$$

The constants are

$M_\delta = 11$

$V = 1000$ ft/sec $D = 1000$ ft.

$g = 32.2$ ft/sec^2

$M_q = -7.63$ sec^{-1}

$M_\alpha = -20.66$ sec^{-1}

$Z_\alpha = -2.27$ sec^{-1}

A typical G_T time history, used in the present AMRL studies is shown in Fig. 2.

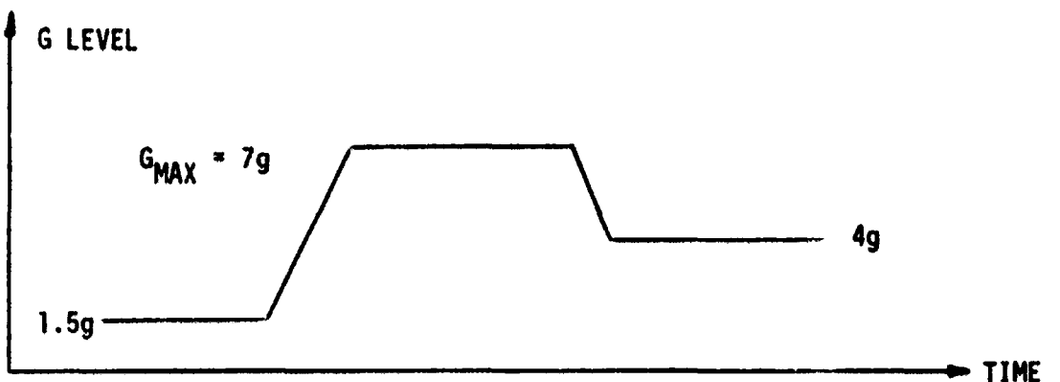

FIG. 2: TYPICAL G_T TIME-HISTORY

The internal model parameters were set to their nominal values $\tau = .2$ sec, $\rho_u = -20$ dB, $\rho_y = -14$ dB, $\tau_N = .1$ sec. Usually, the nominal value of ρ_y ($=\rho_y^\circ$) for a single observation channel would be -20 dB. In our case there are 4 observation channels which increase the nominal ρ_y to -14 dB.

PILOT MODEL REVISION AND RESULTS

Motivated by recent results in modeling AAA tracking under high uncertainty [3], we write the human's internal characterization of target motion ($x_1 = q_T$) as

$$\dot{x}_1(t) = -\alpha(t)\, x_1(t) + z_1(t) \tag{8}$$

rather than

$$\dot{x}_1(t) = z(t). \tag{9}$$

Now,

$$z_1(t) = z(t) + \alpha(t)\, x_1(t) = \frac{g}{V}\,[\dot{G}_T(t) + \alpha(t)\, G_T(t)] \tag{10}$$

Using this approach we note the following facts:

1. $\alpha(t)$ does not affect the system model.
2. $\alpha(t)$ does affect the Kalman filter submodel equation associated with this state,

$$\dot{x}_1(t) = -\alpha(t)\, x_1(t) + \xi(t)\ ;\ \xi(t) \text{ - white noise} \tag{11}$$

The target motion is perceived by the human operator as a Markov process as opposed to a random walk ($\alpha=0$). It reflects the pursuer's uncertainty in perceiving the target's motion. $\alpha(t)$ is chosen according to

$$\tau_L\, \dot{\alpha}(t) + \alpha(t) = \mathcal{N}(G_T) \cdot \sqrt{\Sigma_{11}} \tag{12}$$

where

$$\mathcal{N}(G_T) = 3 \cdot \left(\frac{G_T}{4}\right)^4 \tag{13}$$

The resulting model-vs-data comparisons for ensemble mean error ($\bar{e}(t)$) for dynamic and static-G cases (G-stress and no G-stress) are shown in Figures 3-4, respectively. The agreements are excellent through the transient G peak to recovery. Nominal parameters have been used for the basic OCM response parameters; the only change between static and dynamic cases is

$$\tau_L = \begin{cases} .53 & \text{static} \\ .97 & \text{dynamic} \end{cases} \tag{14}$$

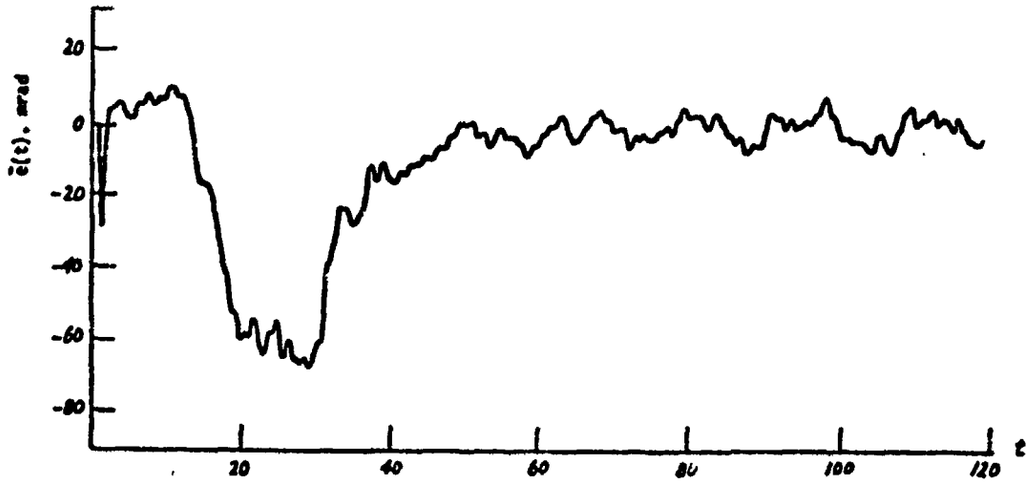

a) Experimental Data

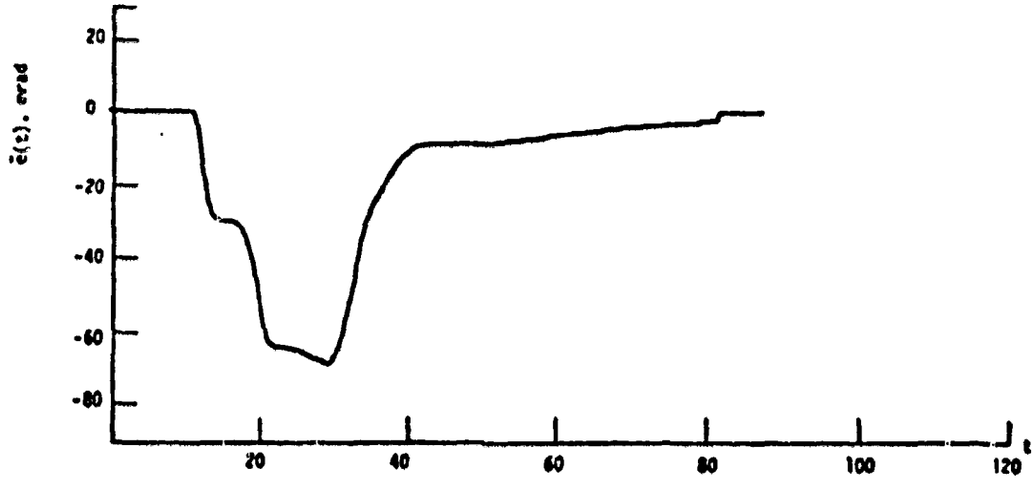

b) Model Predictions

FIG. 3: MEAN PITCH TRACKING ERROR, 1 PEAK, G STRESS

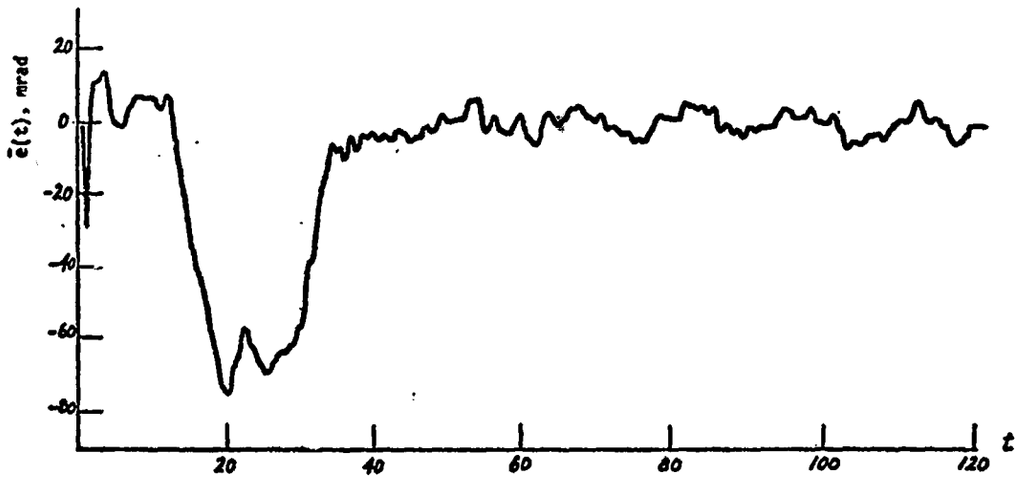

a) Experimental Data

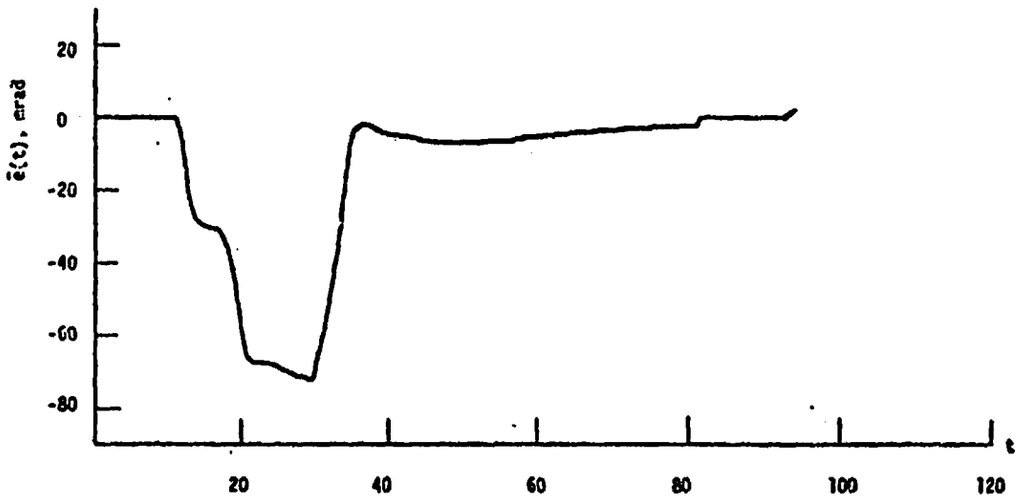

b) Model Predictions

FIG. 4: MEAN PITCH TRACKING ERROR, 1 PEAK, STATIC G

CONCLUDING REMARKS

A preliminary modeling work in the area of air-to-air tracking task has been conducted and the initial results have been extremely encouraging. However, further research is needed, and is presently continuing, to interpret these results and to match the standard deviation data.

For modeling work, a major concern is involved with the OCM internal parameters and their dependence on G_z and $\dot{G}_z$ levels. A set of new experiments will be conducted in the near future to enhance the observations of this dependence.

Also, the present model formulation does not include any motion-derived cues as G_z or $\dot{G}_z$; it merely regards these quantities as external stressors, and neglects any useful motion cues that they may provide. It is the feeling of the authors that this aspect of modeling work need to be considered in any future modeling efforts.

REFERENCES

1. Kleinman, D.L., Baron, S. and Levison, W.H.: A Control Theoretic Approach to Manned-Vehicle Systems Analysis. IEEE Trans. Autom. Control, Vol. AC-16, No. 6, 1971.

2. Harvey, T.R. and Dillow, J.D.: Application of an Optimal Control Pilot Model to Air-to-Air Combat. AIAA Guidance and Control Conference, August 1974.

3. Kleinman, D.L., Ephrath, A.R., and Rao, P. Krishna: Effects of Target Motion and Image on AAA Tracking. Univ. of Conn., Dept. of EECS, Tech. Report TR-77-7, Nov. 1977.

N79-15594

AAA GUNNER MODEL BASED ON OBSERVER THEORY

By R. S. Kou*, B. C. Glass*, C. N. Day** and M. M. Vikmanis*

*Systems Research Laboratories, Inc.
Dayton, Ohio 45440

**Aerospace Medical Research Laboratory
Wright-Patterson Air Force Base, Ohio 45433

SUMMARY

The Luenberger observer theory is used to develop a predictive model of a gunner's tracking response in antiaircraft artillery (AAA) systems. This model is composed of an observer, a feedback controller and a remnant element. An important feature of the model is that the structure is simple, hence a computer simulation requires only a short execution time. A parameter identification program based on the least squares curve fitting method and the Gauss Newton gradient algorithm is developed to determine the parameter values of the gunner model. Thus, a systematic procedure exists for identifying model parameters for a given antiaircraft tracking task. Model predictions of tracking errors are compared with human tracking data obtained from manned AAA simulation experiments conducted at the Aerospace Medical Research Laboratory, Wright-Patterson AFB, Ohio. Model predictions are in excellent agreement with the empirical data for several flyby and maneuvering target trajectories.

INTRODUCTION

A systematic study of threat effectiveness for antiaircraft artillery (AAA) systems requires the development of a mathematical model for the gunner's tracking response. The gunner model is then incorporated into computer simulation programs as shown in reference 1 for predicting aircraft attrition with respect to specific antiaircraft weapon systems. Two of the fundamental design requirements of a gunner model are simplicity in model structure and accuracy in the tracking error predictions. A simple gunner model structure will shorten computer simulation execution time. Obviously, accurate predictions of tracking error implies model fidelity with respect to describing the gunner's tracking performance. Then, the manned threat quantification in the threat analysis will be reliable.

An antiaircraft gunner model based on the Luenberger observer theory in references 2, 3 and 4, is developed in this paper. It satisfies both the design requirements mentioned above. The structure of the model is simple and its predictions of tracking errors are accurate. It is composed of three main parts - an observer, a feedback controller, and a remnant element. An observer is itself a dynamic system whose output can be used as an estimate of the state of a given system. The simplicity of the observer design makes the observer an attractive design method. The estimated state is then used to implement a linear state variable feedback controller which represents the gunner's control function in the compensatory tracking task. The effects of all the randomness sources due to human psychophysical limitations and of modelling errors are lumped into one random remnant element in this model design. Another important feature of this model is that its parameters can be determined systematically instead of by trial-and-error. A parameter identification program based on the least squares curve-fitting method in reference 5 and the Gauss-Newton gradient algorithm in reference 6 is developed for this purpose. This program iteratively adjusts the parameter values to minimize the least squares error between the model prediction of tracking error and actual human tracking data obtained from manned AAA simulation experiments conducted at the Aerospace Medical Research Laboratory, WPAFB, Ohio. Thus, it provides a convenient procedure for model validation. In addition, a computer simulation program is developed with the designed model describing the gunner's response for a given AAA tracking task. The program provides time functions of the ensemble mean and standard deviation for the model's tracking error predictions (azimuth and elevation). Computer simulation results are in excellent agreement with the empirical data for several aircraft flyby and maneuvering trajectories. This verifies that the model can predict tracking errors accurately and thus is a reliable description of the gunner's compensatory tracking characteristics.

A comparison between this model and the optimal control model in references 7, 8 and 9 (by Kleinman, Baron, Levison) is also given. It can be shown that the model based on observer theory is as accurate as the optimal control model in predicting tracking errors. In addition, the computer execution time of the AAA closed loop system simulation utilizing this model is less than 15% of that using the optimal control model. This is a primary advantage of a model with simple structure.

DESCRIPTION OF AN AAA GUN SYSTEM

The tracking task of an antiaircraft artillery (AAA) gun system can be described by a closed loop (single axis tracking loop) block diagram as shown in figure 1. Two gunners, one each for azimuth and

elevation axes, play the role of controller in this man-machine feedback control system. From his visual display, each gunner observes the tracking error, e_T (one for azimuth error and the other for elevation error), which is the difference between the target position angle θ_T and the gunsight line angle θ_g. Independently, the gunners operated the hand crank to control the gunsight system in order to align the gunsight line angle (output) with the target position angle (input). Therefore, the azimuth tracking task is decoupled from the elevation tracking task in this AAA system.

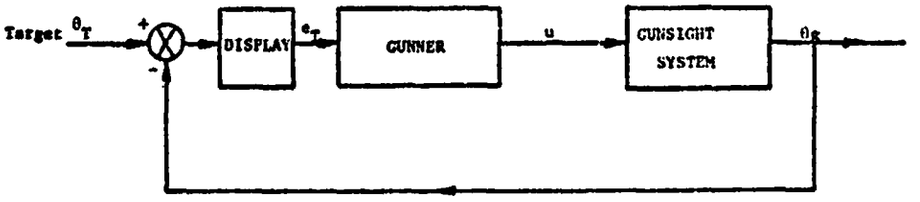

FIGURE 1: BLOCK DIAGRAM OF THE AAA CLOSED LOOP SYSTEM

The purpose of this paper is to develop a mathematical model of the response characteristics of a gunner in a compensatory tracking task. Therefore, in the following, we first describe the mathematical representation of the gunsight and rate-aided control dynamics (the gunsight system) and the target trajectories. In this paper the transfer function of the gunsight system considered is:

$$\frac{\Theta_g(s)}{U(s)} = \frac{1}{s} \tag{1}$$

for the azimuth angle tracking as well as the elevation angle tracking. ($\Theta_g(s)$ and U(s) are the Laplace transforms of $\theta_g(t)$ and u(t) respectively.) It can be shown that this transfer function is a valid representation of many practical gunsight systems. Several flyby and maneuvering trajectories in reference 10 of the target aircraft of 45 seconds duration were selected as input to the AAA system of figure 1. These trajectories are deterministic functions of time. (But their dynamic properties $\dot{\theta}_T$, $\ddot{\theta}_T$, etc., are not known precisely to trackers. The state space equation of the gunsight system and the target motion can be derived as follows.

$$\dot{\underline{x}} = A\underline{x} + Bu + F\ddot{\theta}_T \tag{2}$$

where $\underline{x}$ denotes the state vector having two components,

$$\underline{x} = \begin{bmatrix} x_1 \\ x_2 \end{bmatrix} = \begin{bmatrix} \theta_T - \theta_g \\ \dot{\theta}_T \end{bmatrix}$$

and A, B, and F matrices are

$$A = \begin{bmatrix} a_{11} & a_{12} \\ a_{21} & a_{22} \end{bmatrix} = \begin{bmatrix} 0 & 1 \\ 0 & 0 \end{bmatrix},$$

$$B = \begin{bmatrix} b_1 \\ b_2 \end{bmatrix} = \begin{bmatrix} -1 \\ 0 \end{bmatrix}, \quad F = \begin{bmatrix} f_1 \\ f_2 \end{bmatrix} = \begin{bmatrix} 0 \\ 1 \end{bmatrix},$$

and the scalars u and $\ddot{\theta}_T$ denote the control from the AAA gunner and the target acceleration. The tracking error e_T on the visual display is observed by the gunner and is expressed in the measurement equation:

$$y = C\underline{x} \tag{3}$$

where y is the observed tracking error and C is a row vector [1 0]. Equations (2) and (3) will be used in the next section to develop an AAA gunner model.

AAA GUNNER MODEL

This section presents a mathematical model of an antiaircraft gunner in the compensatory tracking task. The main design requirements for developing this model are:

- accurate model prediction of tracking errors
- simple model structure
- systematic determination of model parameters

In this paper, the Luenberger reduced order observer theory has been applied to design the gunner model which satisfies the above design requirements. Figure 2 shows the block diagram of this model consisting

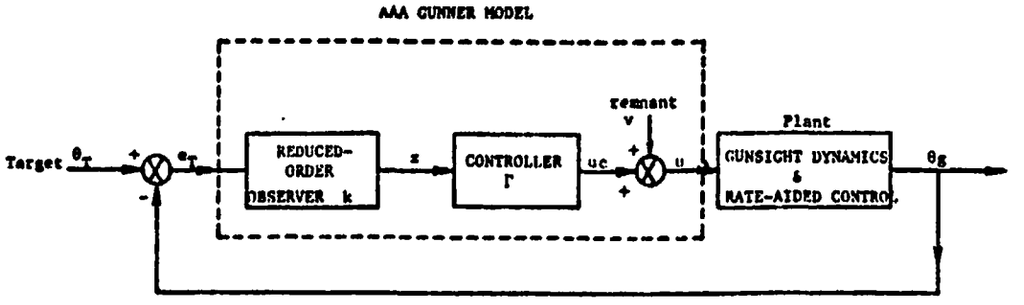

FIGURE 2: BLOCK DIAGRAM OF THE STRUCTURE OF THE AAA GUNNER MODEL

of three main elements: observer, controller, and remnant. The first element is a reduced-order observer which processes the gunner's observation from the visual display to provide an estimate of the states of the AAA system. It will be shown that the system equation (2) is a 2nd order system, but the reduced-order observer is only of the first order. Since some components of the state as given by the system outputs are already available by direct measurement. The estimation of these components of the state is not necessary and will cause a certain degree of redundancy. The use of a reduced-order observer eliminates this redundancy and still provides sufficient information to reconstruct (or estimate) the state of the observed system. The controller represents the gunner's tracking function by an estimated-state linear feedback control law. The observer and the controller consists of the deterministic part of the gunner model. The effects of the various randomness sources in the AAA man-machine closed loop system and of the modelling errors are lumped into one element called remnant which is the stochastic part of the gunner model. These randomness sources include the modelling error, the observation error, the neuromotor noise, etc. Mathematical equations of this model are given below.

Model Equations

System equations (2) and (3) are used in the design of the gunner model. However, the gunner doesn't have the precise information about the target dynamics, so the term representing target acceleration, $\ddot{\theta}_T$, in Eq. (2) will not be included in the design of the observer equation. The effect on the tracking error due to the modelling error of the gunner's uncertainty about target dynamics will be included in the remnant element. Now from Eq. (3),

$$y = C\underline{x} = x_1$$

the tracking error is available from direct observation. Thus, it is only necessary to estimate the second component x_2 of the state vector $\underline{x}$ in order to implement a state variable feedback control law. By the

reduced-order Luenberger observer theory in reference 4, an estimate $\hat{x}_2$ of the state variable x_2 can be obtained by

$$\dot{\hat{x}}_2 = (a_{22} - ka_{12})\,\hat{x}_2 + k\dot{y} + (a_{21} - ka_{11})\,y + (b_2 - kb_1)\,u_c \tag{4}$$

where a_{ij} and b_k are the elements of matrices A and B in Eq. (2), the scalar k is the observer gain, y and $\dot{y}$ are the observed tracking error and error rate respectively, and u_c is the linear feedback control law (the controller) with the form:

$$u_c = -[\gamma_1 \ \gamma_2] \begin{bmatrix} y \\ \hat{x}_2 \end{bmatrix}$$

where the feedback control gains γ_1 and γ_2 are two constants determined in reference 10. Note that the state feedback is composed of y (the observed variable which is x_1) and $\hat{x}_2$ (the estimated state of x_2). It can be shown that the system (2) and (3) is completely observable. (The definition of observability and the conditions of a system to be observable can be found in reference 11). Then, by the observer theory, there always exists an observer gain k to make the eigenvalue of the observer (Eq. (4)) negative. Thus, the output of the observer will be a good estimation to the state of the observed system. This shows the existence of proper observer gain k in Eq. (4). Actually, the value of observer gain k is determined by a curve-fitting identification program. The required differentiation of y in Equation (4) can be avoided by introducing the following variable:

$$z(t) = \hat{x}_2 - ky(t) \tag{5}$$

Hence the observer dynamics can be represented by

$$\dot{z} = (a_{22} - ka_{12})z + (a_{22} - ka_{12})ky + (a_{21} - ka_{11})y + (b_2 - kb_1)u_c \tag{6}$$

Next, the actual output of this model is expressed as the sum of the output u_c of the controller and the remnant element v.

$$\begin{aligned} u &= u_c + v \\ &= -[\gamma_1\gamma_2] \begin{bmatrix} y \\ \hat{x}_2 \end{bmatrix} + v \end{aligned} \tag{7}$$

where the remnant term v(t) is modeled as a white noise and its statistical properties are selected to be

$$\begin{aligned} &E\,[v(t)] = 0 \qquad\qquad \text{for all } t \\ &E\,[v(t)\,v(\tau)\,] = q(t)\,\delta(t - \tau) \quad \text{for all } t \text{ and } \tau \text{ where} \end{aligned} \tag{8}$$

E is the expectation operator, $\delta(t)$ is the Dirac delta function and the

covariance function q(t) is assumed as a function of estimated target dynamics,

$$q(t) = \alpha_1 + \alpha_2 \hat{\dot{\theta}}_T^2(t) + \alpha_3 \hat{\ddot{\theta}}_T^2(t) \tag{9}$$

where α_1, α_2, and α_3 are three nonnegative constants to be determined, and $\hat{\dot{\theta}}_T$ and $\hat{\ddot{\theta}}_T$ are estimated target angle rate and acceleration respectively.

Equations of the Closed-loop AAA System

In the previous section, the gunner model equations of the observer, the controller, and the remnant have been derived. These equations are combined with system equations (2) and (3) to obtain the mathematical model of the closed loop AAA system. Since $x_1 = y$, Eqs. (2) and (6) can be rewritten as follows:

$$\begin{aligned}
\dot{y} &= a_{11}y + a_{12}x_2 + b_1 u + f_1 \ddot{\theta}_T \\
\dot{x}_2 &= a_{21}y + a_{22}x_2 + b_2 u + f_2 \ddot{\theta}_T \\
\dot{z} &= (a_{22} - ka_{12})z + (a_{22} - ka_{12})ky + (a_{21} - ka_{11})y + (b_2 - kb_1)u_c \\
u &= u_c + v \\
u_c &= -[\gamma_1 \ \gamma_2] \begin{bmatrix} y \\ \hat{x}_2 \end{bmatrix}
\end{aligned} \tag{10}$$

By introducing new variables:

$$x_3 = x_2 - ky$$

and

$$e = x_3 - z \tag{11}$$

Eq. (10) can be rewritten as

$$\dot{X} = A_1 X + F_1 \ddot{\theta}_T + D_1 v \tag{12}$$

where X is the state vector of the overall system with components:

$$X = \begin{bmatrix} y \\ x_3 \\ e \end{bmatrix} = \begin{bmatrix} y \\ x_2 - ky \\ x_3 - z \end{bmatrix}$$

and A_1, F_1, and D_1 are matrices defined as follows:

$$A_1 = \begin{bmatrix} a_{11} + a_{12}k - b_1(\gamma_1 + k\gamma_2) & a_{12} - b_1\gamma_2 & b_1\gamma_2 \\ (a_{22}-ka_{12})k+a_{21}-ka_{11} & a_{22}-ka_{12}-(b_2-kb_1)\gamma_2 & (b_2-kb_1)\gamma_2 \\ -(b_2-kb_1)\ (\gamma_1+k\gamma_2) & & \\ 0 & 0 & a_{22} - ka_{12} \end{bmatrix}$$

$$F_1 = \begin{bmatrix} f_1 \\ f_2 - kf_1 \\ f_2 - kf_1 \end{bmatrix}, \qquad D_1 = \begin{bmatrix} b_1 \\ b_2 - kb_1 \\ b_2 - kb_1 \end{bmatrix}$$

Once the structure of the model is designed, the next step is to determine the parameters associated with this model (i.e. k, γ_1, γ_2, α_1, α_2, α_3 in Eqs. (6), (7) and (9)). It is important to have a systematic method to determine these parameters for a given AAA system. A parameter identification program based on the least squares curve-fitting method and the Gauss Newton gradient algorithm has been developed by the authors. This program can easily determine the parameters of the gunner model by minimizing the difference between the model prediction of the tracking error and the corresponding empirical data. The following equations (mean equation and covariance equation) are used in the curve-fitting program. Letting the expectation value of X be $\bar{X}$, then we have,

$$\dot{\bar{X}} = A_1\bar{X} + F_1\ddot{\theta}_T \tag{13}$$

and the covariance matrix of X (t) is $P(t) = E[\ (X(t) - \bar{X}(t))(X(t)-\bar{X}(t))^T]$; then it can be shown in reference 11 that the covariance matrix is governed by

$$\dot{P} = A_1P + PA_1{}^T + D_1\ q(t)\ D_1{}^T \tag{14}$$

Equations (13) and (14) are used in the paremeter identification program to fit the empirical data obtained from the manned AAA simulation experiments conducted at the Aerospace Medical Research Laboratory, Wright-Patterson AFB, Ohio. The detail of the identification program and the curve-fitting procedure can be found in reference 10. The results

of curve-fitting parameter identification program are shown in the following table:

	k	γ_1	γ_2	α_1	α_2	α_3
Azimuth Tracking	2.94	-2.87	-1.00	.0496	.0024	.103
Elevation Tracking	3.02	-3.01	-1.00	.0032	.00047	.259

SIMULATION RESULTS AND DISCUSSION

The numerical values of the parameters of this gunner model were determined in the previous section with respect to the gunsight dynamic system (Eq. (2)) and a specific target trajectory. The gunner model is now ready to be used for computer simulation. A computer simulation program of the AAA system with this model representing the gunner response was developed. The input to this program is the target motion trajectory. The outputs are the model predictions of the ensemble mean and standard deviation of the tracking error. A typical result is plotted in fig. 3 for a specific target trajectory. The solid line in fig. 3 denotes the

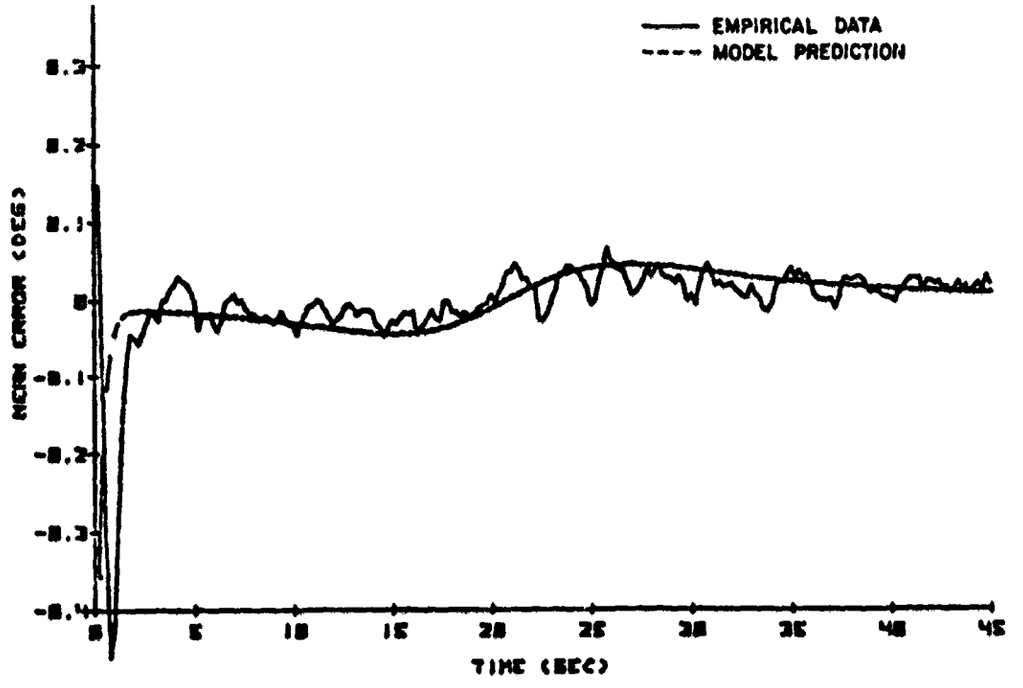

FIGURE 3. MEAN TRACKING ERROR

empirical data of the sample ensemble mean for azimuth tracking errors. The corresponding model prediction is denoted by the dotted line in fig 3. There is an excellent match between these two curves. Similar comparison between model predictions and empirical data for several other flyby and maneuvering target trajectories can be found in reference 10. All the simulation results show that this gunner model with the same parameter values can predict accurately the tracking errors for various target trajectories with similar frequency band widths. Therefore, it is a predictive model. The values of the model paremeters depends on the gun-sight dynamic system. Furthermore, this model is adaptive with respect to the target motion and this adaptive property is considered in the structure of the covariance function (Eq. (9)) of the remnant element.

A comparison of the model prediction accuracy between this model and the optimal control model in reference 7 has been done for several target trajectories. All the results show that both models give accurate predictions of tracking errors. A typical result is shown in fig. 4 for a flyby trajectory. It is obvious that the gunner model developed in

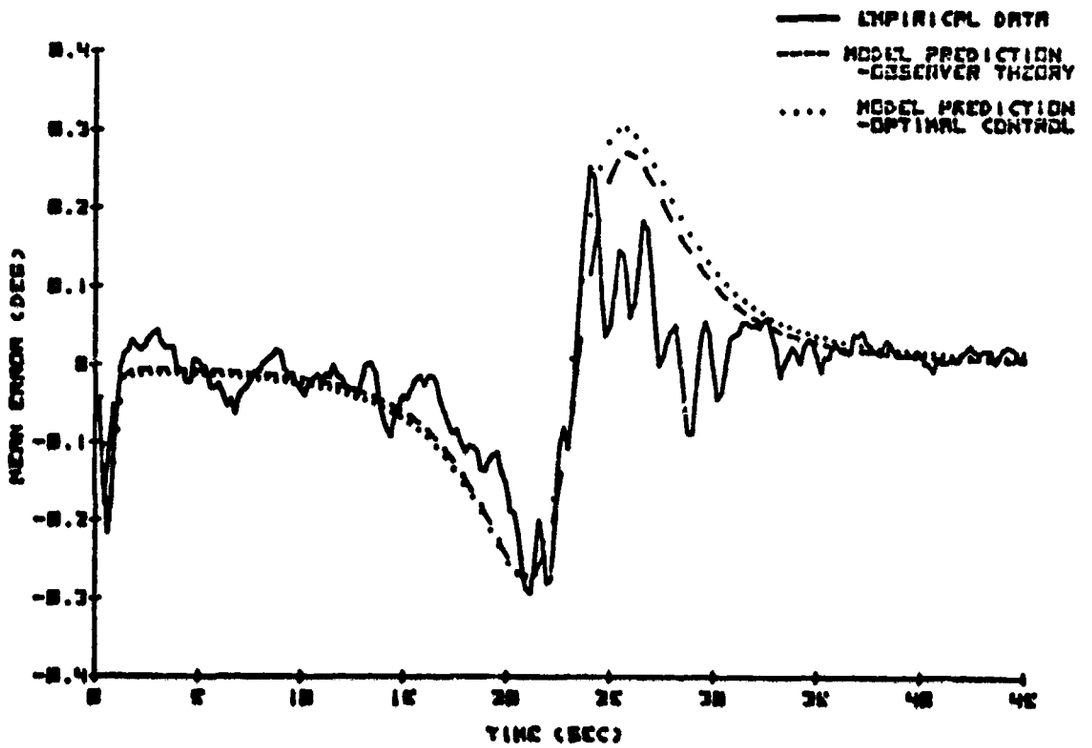

FIGURE 4. MEAN TRACKING ERROR
AZIMUTH

ORIGINAL PAGE IS
OF POOR QUALITY

this paper can predict the tracking errors as accurately as those obtained by the optimal control model. However the computer execution time of simulating the AAA gun system using the gunner model is less than 15% of that by the optimal control model. It is a primary advantage of a model with simple structure. It can be concluded that the gunner model based on observer theory is very useful in the analysis of the performance of the AAA gun system.

CONCLUSION

The Luenberger observer theory has been applied to design an antiaircraft gunner model which is composed of a reduced-order observer, a state variable feedback controller and a remnant element. The highlights of this model are simple in the structure and accurate in the model prediction of tracking errors. The key design requirement is to make the model structure simple so that it can shorten computer simulation time. It has also been shown in figures 3 and 4 that this model can predict the tracking errors accurately. In addition, a parameter identification program based on the least squares curve-fitting method and the Gauss Newton algorithm has been used to systematically determine the numerical values of the model parameters. This gunner model has been used to study the AAA effectiveness of several air defense weapon systems at the Aerospace Medical Research Laboratory, Wright-Patterson AFB. All the results show that it is an accurate and efficient antiaircraft gunner model.

REFERENCES

1. J. Severson and T. McMurchie, "Antiaircraft Artillery Simulation Computer Program - AFATL Program P001 - Vol I, User Manual", Developed by Air Force Armament Laboratory, Eglin AFB, Florida; Published under the auspices of the Joint Aircraft Attrition Program, Advanced Planning Group.

2. D. G. Luenberger, "Observing The State Of A Linear System", IEEE Transactions On Military Electronics, Vol. MIL-8, pp. 74-80, April 1964.

3. D. G. Luenberger, "Observers For Multivariable Systems," IEEE Transactions on Automatic Control, Vol. AC-11, pp. 190-197, April, 1966.

4. D. G. Luenberger, "An Introduction To Observers", IEEE Transactions On Automatic Control, Vol. AC-16, pp. 596-602, December 1971.

5. A. P. Sage and J. L. Melsa, System Identification, New York, Academic Press, 1971.

6. P. Eykhoff, System Identification. New York: John Wiley & Sons, 1974, p. 161.

7. D. L. Kleinman, S. Baron, and W. H. Levison, "A Control Theoretic Approach To Manned-Vehicle Systems Analysis", IEEE Transactions on Automatic Control. Vol. AC-16, No. 6, December 1971, pp. 824-832.

8. D. L. Kleinman and T. R. Perkins, "Modeling Human Performance in a Time-Varying Anti-Aircraft Tracking Loop", IEEE Trans. AC, Vol. AC19, No. 4, Aug. 1974.

9. D. L. Kleinman and B. Glass, "Modeling AAA Tracking Data Using The Optimal Control Model", 13th Annual Conference on Manual Control, MIT, June 1977.

10. R. S. Kou and B. C. Glass, "Development of Observer Model for AAA Tracker Response", Systems Research Laboratories, Inc., Report No. 6872-4. December 1977.

11. J. S. Meditch, Stochastic Optimal Linear Estimation and Control. New York: McGraw-Hill Book Company, 1969. P. 258.

N79-15595

MODELING THE HUMAN AS A CONTROLLER IN A MULTITASK ENVIRONMENT*

T. Govindaraj and William B. Rouse

Department of Mechanical and Industrial Engineering
Coordinated Science Laboratory
University of Illinois
Urbana, Illinois

SUMMARY

Modeling the human as a controller of slowly responding systems with preview is considered. Along with control tasks, discrete non-control tasks occur at irregular intervals. In multitask situations such as these, it has been observed that humans tend to apply piecewise constant controls. It is believed that the magnitude of controls and the durations for which they remain constant are dependent directly on the system bandwidth, preview distance, complexity of the trajectory to be followed, and nature of the non-control tasks. A simple heuristic model of human control behavior in this situation is presented. The results of a simulation study, whose purpose was determination of the sensitivity of the model to its parameters, are discussed.

INTRODUCTION

Although successful operation of an airliner is now possible from take-off to touchdown with minimum involvement of the human pilot [1] he must still perform various routine checks in the course of a normal flight. In addition, even when flying on autopilot, constant monitoring of various instruments is necessary to detect any out of tolerance signals and abnormal occurences of any events. Further, malfunctions or changes in atmospheric conditions, for example, might require that the pilot take over control and make course changes that are different from the preplanned trajectory. Thus, despite advances in automation, human control of aircraft is certainly still of interest.

When the human is controlling a plant, it has been observed that the controls applied are not always continuous. Continuous controls are necessary and are observed when the time constants involved are rather small and the deviations from some reference trajectory must be kept within some close tolerance. But when the time constants are relatively large, it is unnecessary and also difficult to apply the right amount of continuous control. For slowly responding processes it is often sufficient and desirable to apply step-like controls intermittently. This gives an opportunity to observe the actual behavior of the system, compare it with the

* This research was supported by the National Aeronautics and Space Administration under NASA-Ames Grant NSG-2119.

predicted behavior, and take corrective action. This usually prevails in a tracking situation where a certain length of the future command trajectory is available, along with the present required position. Further, applying the step-like controls also frees the human to engage in non-control tasks. In fact, this kind of behavior is common in process control situations and also has been observed in simulations of a flight management situation [2], [3].

When preview of the command trajectory for a certain distance into the future is available, it is likely that the human would apply step-like controls so as to minimize the future trajectory deviations rather than instantaneous deviations. A model which appears reasonable is one which updates the expected deviations of the cost over the length of the previewed trajectory and uses this information along with the knowledge that it "costs" to change control values. The cost to change control reflects the fact that non-control tasks must be attended to, though they may not be of primary importance. The "cost" is thus due to the feeling that the non-control tasks would "suffer" if attention is focused away from them and on the primary task alone. This cost may manifest itself as a tolerance threshold for error below which no action is taken. A measure for the cost of not attending to the subsystem tasks is available as a function of various probabilities and costs for delay of subsystem tasks [4].

BACKGROUND

Of the available models for manual control, the optimal control model would appear to be a suitable candidate. However, this model assumes that control remains non-zero at all times whereas in an intermittent control situation, control is zero for a significant portion of the time. Hence the mean fraction of time devoted solely to control, corresponding to non-zero control intervals, cannot be calculated with the optimal control model. For a given fraction of attention, the conventional optimal control model predicts only RMS errors and RMS control actions. While recent versions of the model do yield a measure of attention that should optimally be used for monitoring subsystems that dynamically relate to the control task, subsystem tasks that only remotely relate to the aircraft's dynamic response cannot be considered. Further, in multitask situations the optimal control model's performance criterion, which minimizes mean squared deviations, may not be appropriate. Finally, these approaches do not yield any predictions of the split of attention between control and non-control tasks or about the probability that the human is involved in the control of a continuous system at any particular instant.

The human in multitask situations has been modeled by Walden and Rouse [3] as a 'server' in a queue where 'customers' are the control and non-control tasks. The customers are assumed to arrive for service with exponentially distributed inter-arrival times (Poisson arrivals.) Service times are Erlang-k distributed. Some customers have a higher priority over others (e.g., control tasks over non-control tasks.) There are a total of N customers in the population (total number of possible tasks the human may be

called upon to attend), and N spaces are available in the queue (i.e., at worst all the N systems may require service simultaneously.) This situation can be modeled as a ($M/E_k/1$:PRP/N/N) queue. (See references [5] or [6] for details about the notation.) The queueing model predicts the fraction of time spent in each type of task (i.e., server utilization). The emphasis in this model is on the subsystem task performance. The control task is modeled in the sense that performing it consumes time. However, measures characterizing control performance (i.e., RMS errors) are not available.

AN INITIAL MODEL

Some success has been achieved using a heuristic model to describe control of an aircraft (with simplified dynamics) in a horizontal plane. Initial computer simulations indicate that this could be a fruitful approach. A piece-wise straight line map was created using uniformly distributed random variables for the length of straight line segments. The magnitudes for angle of turn between segments were chosen from nine values (10°-90°) with equal probability. The direction was chosen randomly. This type of map was designed because of the flexibility in determining the parameters. It is a simple matter to change the probability distributions of various parameters of the path, so that different conditions could be easily tested. It was assumed that the aircraft would be moving forward with constant speed. A point moved along the map corresponding to the desired aircraft position. A distance equivalent to two time constants ahead of the desired position on the map was shown as preview. Only lateral motion was considered. Control in the horizontal plane was achieved through use of the aileron to change the bank angle. The dynamics are shown in Figure 1.

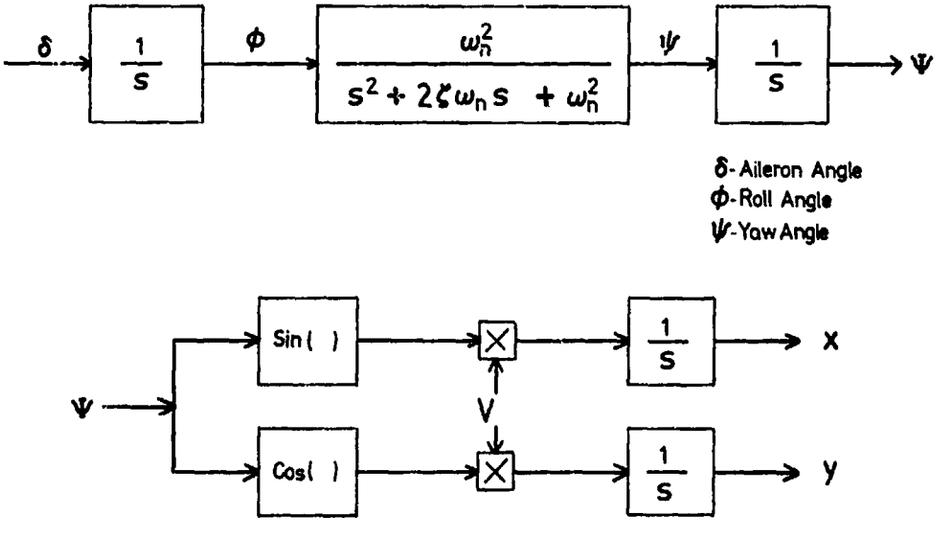

Fig. 1 Simplified Lateral Dynamics

The deviation from the desired position was constantly monitored. A perfect internal model of the aircraft was assumed. At every time instant, the model calculated the future positions for the entire preview length assuming that the roll angle would be zero. At any point, the error was calculated as the deviation from the commanded position, instead of the perpendicular distance to the map

It appears reasonable to expect that the importance given by the human operator to deviations from the desired trajectory will vary along the length of the trajectory. Deviations at the current time cannot be corrected or changed significantly due to the slow response of the system. Also, the expected deviations near the end of the previewed command trajectory need not be considered immediately, since enough time will be available in the future to correct these. Further, any changes "beyond the horizon" that would come into view soon can reasonably be ignored. Accordingly, the human might weight the mid-portion of the previewed command more than either end. So the weighting function for errors would increase to a maximum (from zero), about one time constant from the current position, and decrease again to a near zero value at the end of the trajectory.

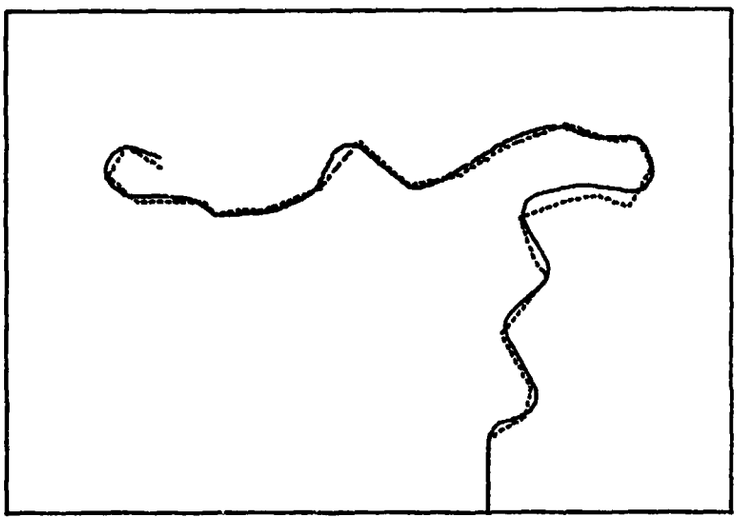

Fig. 2 Simulation Results : Heuristic Model

Weighted error is squared and summed over the preview length. If this predicted error function exceeds a certain threshold, 'aileron' is held at a maximum value until maximum bank angle is reached. If the error is within the threshold, the bank angle is made zero. Constant weights on errors were used for the simulation. The results are shown in Figures 2 and 3 and appear reasonable. The time intervals corresponding to non-zero

aileron action give a direct measure of fraction of time required for control which is proposed as a correlate of workload. Although the human must continuously monitor for cumulative error, workload due to this is assumed negligible compared to the workload involved in control where he must watch the effect of his actions more carefully.

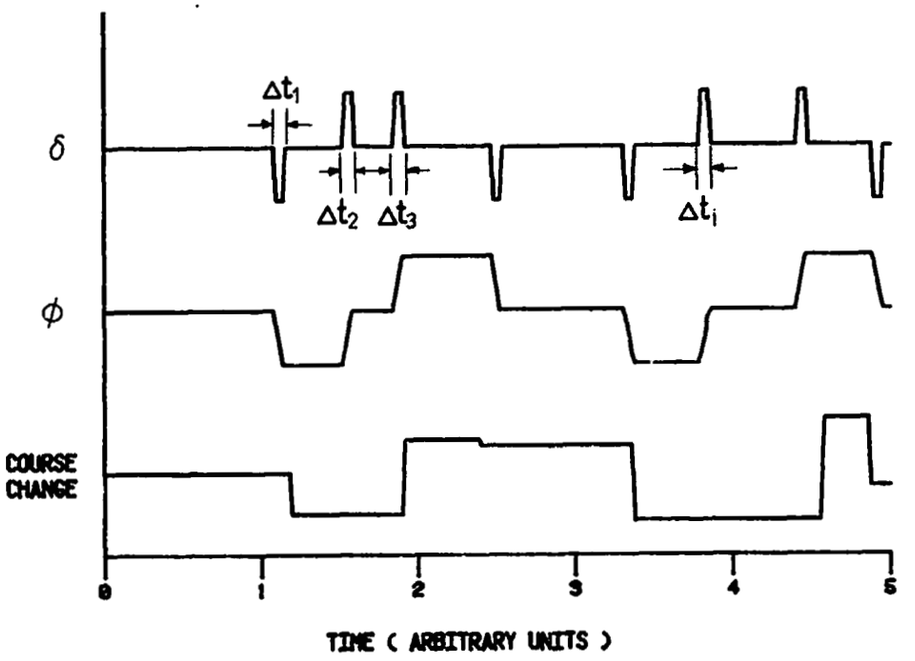

Fig.3 Control and Roll Angle History for a Given Course Change

Simulation experiments were conducted using a fractional factorial design to find out the sensitive/relevant parameters. A resolution VI design was used so that no main effect or two factor interaction is confounded with any other main effect, two factor interaction, or three factor interactions. The following parameters were assumed to affect performance:

1. Dynamics (τ of the process),	τ = 1,5
2 Average arrival rate of turns,	$1/\mu$ = $3\tau, 6\tau$
3 Standard deviation of course changes	σ = $10^\circ, 30^\circ$
4. Amount of preview	T_p = $2\tau, 4\tau$
5. Weighting function,	Rect. Triang.
6 Threshold on cumulative weighted error.	Low High

ORIGINAL PAGE IS OF POOR QUALITY

RMS errors and the fraction of time spent on control were used as performance measures. A constant function (rectangular) and a triangular function were used for weighting on errors. For other parameters, two extreme values were chosen, to obtain a total of 32 different conditions. Exponentially

distributed segment lengths and normally distributed angles of turn were used for the map. For each condition, two replications were run. The results are snown in Tables I and II.

Table I

Analysis for RMS Error

Factor	Effect	Sum of Squares	DOF	F Ratio	
1	4·433	314.409	1	131.037	P < 0.001
2	-0.671	7.206	1	3.003	
3	1.477	34.887	1	14.540	P < 0.001
4	4.087	267.247	1	111.381	P < 0.001
5	-1.397	31.219	1	13.011	P < 0.001
6	0.622	6.188	1	2·579	
12	-0.268	1.145	1	0.477	
13	1.108	19.653	1	8·191	P < 0.01
14	4.174	278.726	1	116.165	P < 0.001
15	-0.886	12.557	1	5.233	P < 0·05
16	-0.250	1.004	1	0.418	
23	-0.288	1.325	1	0.552	
24	0.049	0.038	1	0.016	
25	0.335	1.794	1	0.748	
26	1.315	27.676	1	11.535	P < 0.005
34	0.383	2.350	1	0.979	
35	1.295	26.822	1	11.179	P < 0.005
36	0.197	0.619	1	0.258	
45	-0.914	13.364	1	5.570	P < 0.025
46	0.258	1.062	1	0.443	
56	0.124	0.246	1	0.102	
Average Error	4.192	100.774	42		
Total		1150.313	63		

(1-Period, 2-Segment Length, 3-Angle of Turn, 4-Preview Length, 5-Weight, 6-Threshold)

Table II

Analysis for Fraction of Attention

Factor	Effect	Sum of Squares	DOF	F Ratio	
1	0·231	0.856	1	33·221	P < 0.001
2	-0.057	0·051	1	1.999	
3	0.017	0.005	1	0.181	
4	0.144	0.331	1	12.837	P < 0.001
5	-0.117	0.218	1	8.468	P < 0.01
6	-0.139	0·311	1	12.084	P < 0.005
12	0·004	0.000	1	0.011	
13	-0.018	0.005	1	0.206	
14	0.269	1.158	1	44.963	P < 0.001
15	0.000	0·000	1	0.000	
16	0.004	0.000	1	0.008	
23	0.067	0.072	1	2.783	
24	0.030	0.014	1	0·541	
25	0·005	0·000	1	0.017	
26	0.060	0.058	1	2·234	
34	-0.074	0·087	1	3·359	
35	0.047	0.035	1	1.374	
36	-0.043	0.030	1	1.155	
45	0.005	0 000	1	0·014	
46	0.048	0.037	1	1·435	
56	0.090	0.129	1	5.011	P < 0·05
Average	0·256				
Error		1.082	42		
Total		4·479	63		

(1-Period, 2-Segment Length, 3-Angle of Turn,
4-Preview Length 5-weight, 6-Threshold)

It can be seen that period, preview length and their interaction have the largest effect on performance. Different weighting functions also affect performance. In addition, RMS error is affected by the magnitude of turns and various interactions. Fraction of time spent on control is affected by the threshold. Higher threshold values reduce this fraction.

Though the interaction of mean segment length and threshold affects the RMS error, segment length alone does not affect either of the performance measures. This could be due to the constant forward speed in all cases, whereas the mean segment length is scaled by the time constant. For slower process, for a given threshold any error that may result takes a longer time to reduce to zero. Since the 'vehicle' would stay away from the

trajectory for a longer time, higher RMS error results.

Relatively high workload as well as higher RMS error is observed for the slower process with longer preview. Once the threshold is exceeded, the model applies an appropriate amount of control. However, due to the slow response, the magnitude of error remains near the threshold for some time. But, the error could change sign as new points come into view, and might call for a different control action. Due to longer preview the error changes sign quite frequently resulting in increased control action. This again results in the error remaining near the threshold. Thus, behavior similar to a limit cycle results which, interestingly, has been observed when naive subjects control slow processes. This could possibly be avoided by having one threshold above which control is actuated, and a lower threshold below which control is made zero.

CONCLUSIONS

The next phase of this work will involve development of an experimental situation for use with human subjects. Non-control tasks will be included to simulate a multitask environment. Simple arithmetic tasks may be used. Multiplication tasks with keyboard entry of results are a possibility. Complexity and the rate at which these are presented could be varied, so control task error criterion (i.e., the threshold) may perhaps be manipulated.

The possibility of developing analytical models using the min-max approach [7],[8],[9],[10], satisfaction approach [11], and fuzzy sets [12] will be pursued. An attempt will be made to cast our problem in a form suitable for analysis using the above methods, with possible modifications where necessary. Especially interesting in this regard is the satisfaction approach. It may be possible to formulate our problem in this framework, and obtain a heuristic-based solution with the addition of a few conditions related to the problem structure. With these models available, a more realistic experiment will be developed using the General Aviation Trainer II (GAT II). Along with the control task, the non-control tasks will be made more realistic.

In summary, a simple heuristic model for the control task was presented. Simulation results for a set of conditions describing various trajectories were given. The controller part assumes perfect internal model. Only the threshold must be determined to yield intermittent control. The period and the preview length were found to be the most important parameters affecting performance. This will form the basis for proposed experiments with humans. The model will be refined to take into account the results of these experiments and then, will be used along with a queueing model for non-control tasks, to model the overall multitask situation.

REFERENCES

1. Ropelewski, R. R.: "Air Inter's A-300 Autolandings Routine", Aviation Week and Space Technology, April 24,1978, pp.45-57.

2. Kok, J. J.; and van Wijk, R. A.: "A Model of the Human Supervisor", Proceedings of the Thirteenth Annual Conference on Manual Control, MIT, June 15-17, 1977.

3. Walden, R. S.; Rouse, W. B.: "A Queueing Model of Pilot Decision Making in a Multi-Task Flight Management Situation", Proceedings of the Thirteenth Annual Conference on Manual Control, MIT, June 15-17, 1977.

4 Rouse W. B.; and Greenstein, J. S.: "A Model of Human Decision Making in Multi-Task Situations: Implications for Computer Aiding", presented at the International Conference on Cybernetics and Society, Washington, D.C., 1976.

5. Allen, A. O.: "Elements of Queueing Theory for Systems Design", IBM Systems Journal, vol.14 no. 2, 1975, pp 161-187.

6. White, J. A.; Schmitt, J. W.; and Bennet, G. K.: ANALYSIS OF QUEUEING SYSTEMS, New York:Academic, 1975.

7. Witsenhausen, H. S.: "A Minimax Control Problem for Sampled Linear Systems", IEEE Trans. on Automatic Control, vol. AC-13, no. 1 February 1968.

8. Delfour, M. C.; and Mitter, S. K.: "Reachability of Perturbed Systems and Min Sup Problems", SIAM J. Control, vol. 7, no. 4, November 1969.

9. Bertsekas, D. P.; and Rhodes, I. B.: "On the Minimax Reachability of Target Sets and Target Tubes", Automatica, vol. 7, 1971, pp. 233-247.

10. Milanese, M.; and Negro, A.: "Min-max Control of Systems Approximated by Simple Models: L_1-Type Cost Functionals", Journal of Optimization Theory and Applications, vol 16, nos. 5/6, 1975, pp. 519-537.

11 Mesarovic, M. D.: "Satisfaction Approach to the Synthesis and Control of Systems", Proceedings of the Third Allerton Conference, 1965, pp. 930-942.

12 King P. J.; and Mamdani, E. H.: "The Application of Fuzzy Control Systems to Industrial Processes", Automatica, vol. 13, 1977, pp 235-242.

D8

N79-15596

THE INTERNAL MODEL: A STUDY OF THE RELATIVE CONTRIBUTION OF PROPRIOCEPTION AND VISUAL INFORMATION TO FAILURE DETECTION IN DYNAMIC SYSTEMS*

By Colin Kessel and Christopher D. Wickens

Department of Psychology, University of Illinois

SUMMARY

The development of the internal model as it pertains to the detection of step changes in the order of control dynamics is investigated for two modes of participation: whether the subjects are actively controlling those dynamics or are monitoring an autopilot controlling them. A transfer of training design was used to evaluate the relative contribution of proprioception and visual information to the overall accuracy of the internal model. Sixteen subjects either tracked or monitored the system dynamics as a 2-dimensional pursuit display under single task conditions and concurrently with a "sub-critical" tracking task at two difficulty levels. Detection performance was faster and more accurate in the manual as opposed to the autopilot mode. The concurrent tracking task produced a decrement in detection performance for all conditions though this was more marked for the manual mode. The development of an internal model in the manual mode transferred positively to the automatic mode producing enhanced detection performance. There was no transfer from the internal model developed in the automatic mode to the manual mode.

INTRODUCTION

Over the past few years there has been a great deal of research directed at the problem of determining the differences between operators and monitors of dynamic systems (References 1-7). While the conclusions reached by these authors do not always coincide, there is a general consensus that a greater understanding of the different processes operating in the two modes of participation is necessary for the successful integration of automated systems in the workplace.

We have provided a detailed theoretical analysis of the processes involved in the two modes of participation (Reference 7). Briefly, this analysis has argued that one way in which the differences between modes of participation can be studied is by determining the relative sensitivity of operators versus monitors in a failure detection task.

*This research was funded by the Life Sciences Program, Air Force Office of Scientific Research, Contract Number F44620-76-C-0009. Dr. Alfred Fregly was the scientific monitor of the contract.

PAGE INTENTIONALLY BLANK

Three attributes were identified that would seemingly facilitate failure detection in the controlling mode: (i) a smaller variability of the internal model of the system; (ii) the options of testing hypotheses about the nature of the dynamics by introducing signals into the system; and (iii) a greater number of information channels available upon which to base failure detection decisions. It was recognised however, that this latter advantage may be mitigated to the extent that: a) adaptation takes place reducing the strength of visual error information and, b) proprioceptive sensitivity is less than visual.

In comparison the monitoring mode was also characterised by two attributes that could facilitate detections: a greater "strength" of the visual signal (if adaptation by the autopilot does not take place) and a lower level of operator workload.

The study conducted (Reference 7) to test the above theoretical analysis found that detection performance in the manual mode was faster and only slightly less accurate than the autopilot mode. Furthermore the observed manual superiority was attributed to the additional proprioceptive information resulting from operator control adaptation to the system change. It is possible that some contribution to manual mode superiority in our prior study resulted from the greater internal model consistency in that mode. However this hypothesis was assumed to be doubtful because a within subjects design was employed, so that the same subjects participated in both automatic and manual conditions. Thus the internal model developed in manual conditions would presumably be available to facilitate detection in the automatic conditions as well.

In order to generate a greater distinction between the internal model employed in the two modes, the present study employed a between subject design using a transfer of training technique. This procedure enables an examination of the development of internal models, in the two modes of participation, and subsequently measures their impact upon transfer to the other mode.

It was hypothesized that this technique would increase the differential performance in detection between the two modes of participation while at the same time demonstrating that the internal model developed in the manual mode can subsequently be utilized to facilitate automatic mode failure detection performance.

METHOD

Subjects:

The subjects were 18 right-handed male university students. Subjects were paid a base rate of $2.50 per hour but could increase their average pay by maintaining a high level of detection performance.

C-2

Apparatus:

The basic experimental equipment included a 7.5 x 10 cm Hewlett Packard Model 1300 CRT display, a spring-centered, dual-axis tracking hand control with an index-finger trigger operated with the right hand, and a spring loaded finger controller operated with the left. A Raytheon 704 16-bit digital computer with 24k memory and A/D, D/A interfacing was used both to generate inputs to the tracking display and to process responses of the subject. The subject was seated on a chair with two arm rests, one for the tracking hand controller and one for the side-task finger controller. The subject's eyes were approximately 112 centimeters from the CRT display so that the display subtended a visual angle of 1.5°.

Tracking tasks. The primary pursuit-tracking task required the subject to match the position of a cursor with that of a target which followed a semi-predictable two-dimensional path across the display. The target's path was determined by the summation of two non-harmonically related sinusoids (.05 and .08 Hz) along each axis with a phase offset between the axes. The position of the following cursor was controlled jointly by the subject's control response and by a band-limited forcing function with a cutoff frequency of .32 Hz for both axes. Thus the two inputs to the system were well differentiated in terms of predictability, bandwidth, and locus of effect (target vs. cursor). The control dynamics of the tracking task were of the form $Y_c = \frac{1-\alpha}{s} + \frac{\alpha}{s^2}$ for each axis, where α was the variable parameter used to introduce changes in the system dynamics. These changes, or simulated failures, were introduced by step changes in the acceleration constant α from a normal value of .3, a mixed velocity and acceleration system, to α = .9, a system that approximates pure second order dynamics that requires the operator to generate considerable lead in order to maintain stable performance.

As the loading task, the Critical Task (Reference 8) was employed. This was displayed horizontally in the center of the screen and required the subject to apply force to the finger control in a left-right direction to maintain the unstable error cursor centered on the display. The value of the instability constant λ in the dynamics $Y_c = \frac{k\lambda}{s-\lambda}$ was set at a constant subcritical value. Two values (λ= 0.5 and λ= 1.0) were employed on different dual task trials.

Experimental Design and Task:

Three groups were used in the transfer of training design (see Figure 1). Group one transferred from manual (MA_I) on session one to automatic (AU_{II}) on session two; group two transferred from automatic (AU_I) to manual (MA_{II}) while group three was the control group for the automatic condition and monitored in the automatic mode in both sessions ($AU_{I(C)}$ and $AU_{II(C)}$). The control group for the manual group (MA_{II}) was MA_I. The various group comparisons are represented in Figure 1 by arrows and will be referred to at greater length in the results section.

Each group participated in six consecutive days of data collection. These were divided into two sessions; 3 days in each session with each session comprising 1 training day and two experimental days. Subjects in group one for example participated in 3 manual (MA_I) sessions and then transferred to 3 automatic (AU_{II}) sessions.

In the manual (MA) condition the subject performed the tracking manually while in the autopilot (AU) condition, his role in the control loop was replaced by simulated autopilot control dynamics consisting of pure gain, effective time delay, and a small added remnant. Each trial, MA or AU, lasted 150 seconds.

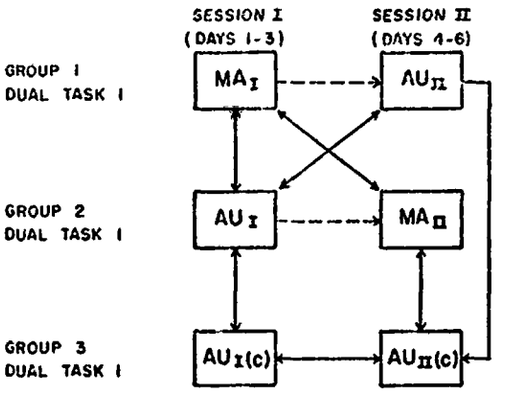

Figure 1: Experimental design and group comparisons

Training Day: The training day was designed to give the subject maximum experience and practice with the system. Subjects therefore received extensive practice tracking (or monitoring) with both prefailure and postfailure dynamics. Following this, they observed and then detected the step changes in dynamics. Practice with the critical side task was also included.

The presentation of the failure was generated by an algorithm that assured random intervals between presentations and allowed the subject sufficient time to establish baseline tracking performance before the onset of the next change. Task logic also ensured that changes would only be introduced when system error was below a criterion value. In the absence of this precaution, changes would sometimes introduce obvious "jumps" in cursor position.

During the detection trials, the detection decision was recorded by pressing the trigger on the control stick. This response presented a "T" on the screen and returned the system to normal operating conditions of the prefailure dynamics. If the subject failed to detect the change, the system returned to normal after six seconds via a 4 second ramp. On the basis of pretest data, it was assumed that six seconds was the interval within which overt responses would correspond to detected failures and not false alarms. The subjects were told to detect as many changes as possible as quickly as possible.

Experimental Days: The training day was followed by two consecutive experimental days. After four refresher trials in the AU or MA modes (depending upon the condition) with the side task, and a number of demonstrated failures, the subjects performed 15 experimental trials: 5 single task, tracking (or monitoring) only; 5 tracking with the easy critical task ($\lambda = 0.5$); and 5 tracking with the difficult critical task ($\lambda = 1.0$). The

order of presentation was randomized. Each trial contained an average of 5 failures per trial with a range of 4 to 6.

The subject was instructed to "do the side task as efficiently and accurately as possible," and told to maintain that task at a standard level of performance. After each trial the subject received feedback about both his side task and detection performance. The instructions, feedback and payoff schedule, therefore, clearly defined the side task as the loading task while allowing the tracking and detection tasks to fluctuate in response to covert changes in available attentional resources (Reference 9).

ANALYSIS

Detection performance was assessed in terms of the accuracy and latency of responses. In computing the accuracy measure, signal detection theory analysis based upon the method of free response was employed (Reference 10). This technique accounts for the presence of hits and false alarms in the data; and the semi random occurance of failures within a trial. The area under the ROC curve (A[ROC]) was employed as the final accuracy measure (Reference 11). Further details of this analysis procedure may be found in Wickens and Kessel (Reference 7, 12).

The A(ROC) measure and the latency measure were then plotted in the form of a joint speed-accuracy measure depicted in Figure 2. "Good" performance is represented by points lying on the upper left, in the region of fast accurate response. Performance was quantified by projecting the point locus obtained onto the positive diagonal performance axis. The performance scale is computed as (10 times A[ROC] - LATENCY) and will be called the "derived performance score." This procedure produces a performance index that ranges from 0 for chance level of accuracy with a latency of 5" to 10.0 for perfect detection with 0 second reaction time. The units assigned to this performance index are somewhat arbitrary but are based on the observation that the overall variability (standard deviation) of the raw latency scores were found to be roughly 10 times the variability of the A(ROC) measure.

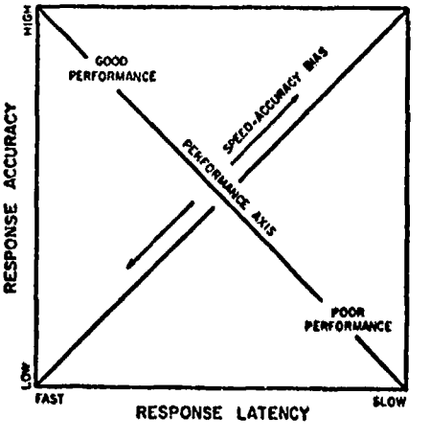

Figure 2: Speed-accuracy representation of detection performance

RESULTS

Averages and standard deviations were computed for the accuracy (A[ROC]), the latency and the derived performance measures following the rational and the procedures outlined in the preceding section.

The group averages for all three measures are presented graphically in Figures 3 and 4. Figure 3 represents the results for the single task condition while Figure 4 represents the dual task, workload condition collapsed over both levels of dual task difficulty (the rationale for this procedure is discussed below). The symbols in Figures 3 and 4 represent the group results in the speed-accuracy space, while the arrows and labels depict the derived performance scores for the various groups along the performance axis. In figures 5, 6, and 7 the experimental groups are plotted with the average derived performance score on the Y-axis.

The presentation of the results of the detection of failures will be divided into three sections. The first presents the results for each mode of participation, and represents a replication of the Wickens and Kessel (Reference 7) study with the between subjects design, the second examines the results of the loading task, while the third reports the results of the transfer of training experiment. Group differences were analyzed by means of a 3-way Analysis of Variance-ANOVA (groups x dual task x experimental days).

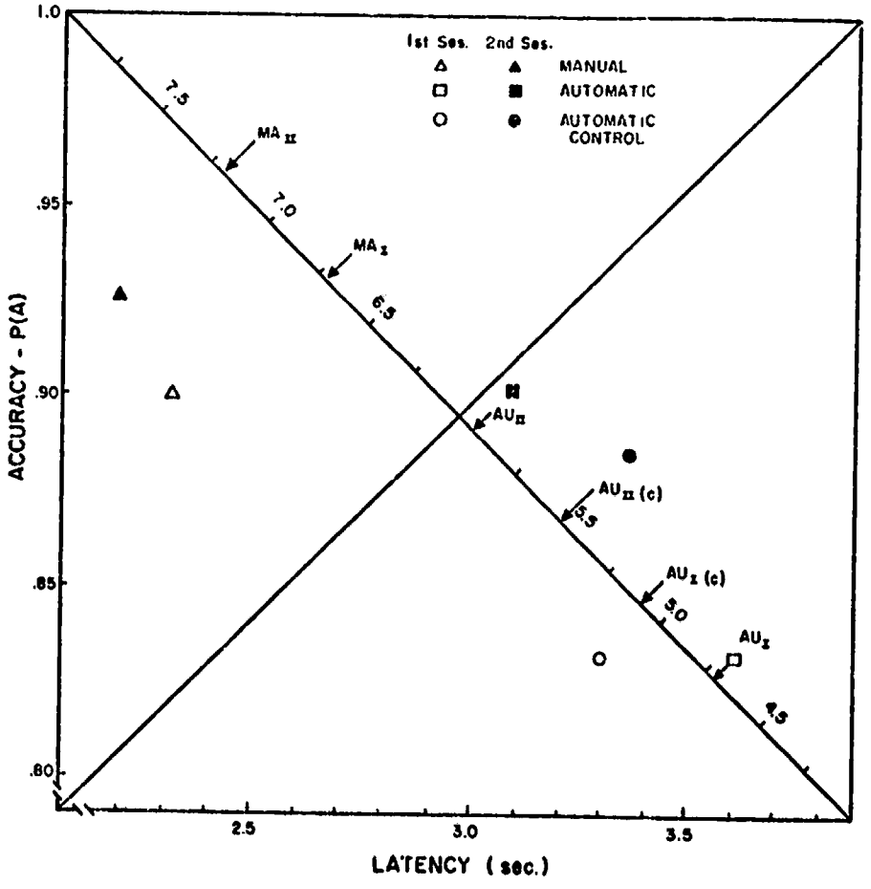

ORIGINAL PAGE IS OF POOR QUALITY

Figure 3: Effect of participatory mode and experimental condition on detection performance-Single Task

(a) Mode of Participation

The most pronounced effect in the experimental data is the consistent superiority of MA over AU detection. This statistically reliable effect is clearly evident in the derived performance score shown in Figures 5 and 6 and was tested by contrasting group AU_I with MA_I ($F_{1,10} = 18.4$ $p < .001$). Examination of Figures 3 and 4 reveals that the MA superiority is reflected in detection latency ($F_{1,10} = 13,66$, $p < .01$), as well as accuracy ($F_{1,10} = 15.55$, $p < .01$).

While these findings essentially replicate the Wickens and Kessel (Reference 7) study, it is important to note that the extent of MA superiority observed in the present results is greatly enhanced. In fact the magnitude of the MA-AU difference in the desired performance score is roughly five times its value obtained in the previous within-subject design. Contrasting the two studies, one finds that AU performance is unchanged, but MA performance in the present results is reliably superior to its level in the previous study ($t_9 = 2.18$, $p < .05$). These findings add strength to the argument

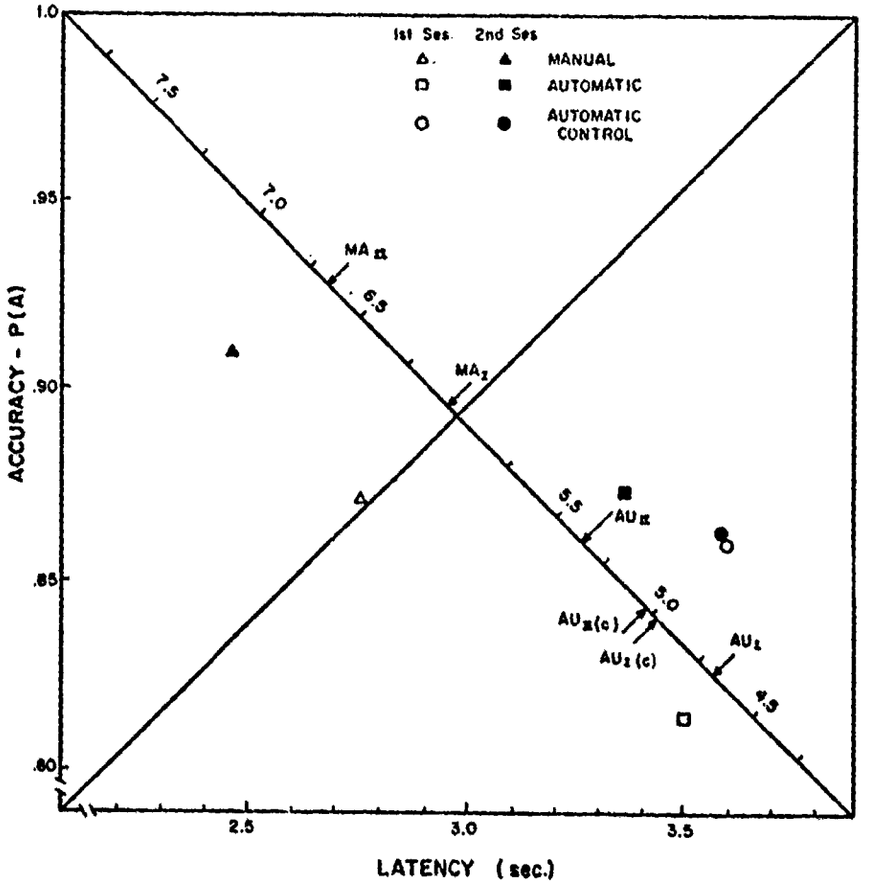

Figure 4: Effect of participatory mode and experimental condition on detection performance_Dual Task

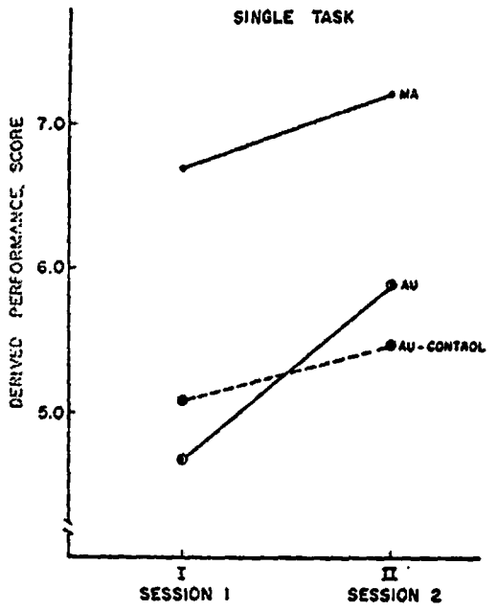

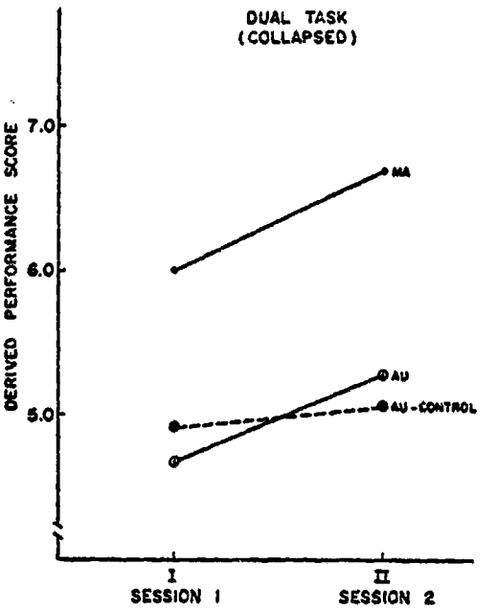

Figure 5 **Figure 6**
Detection performance as a function of experimental condition

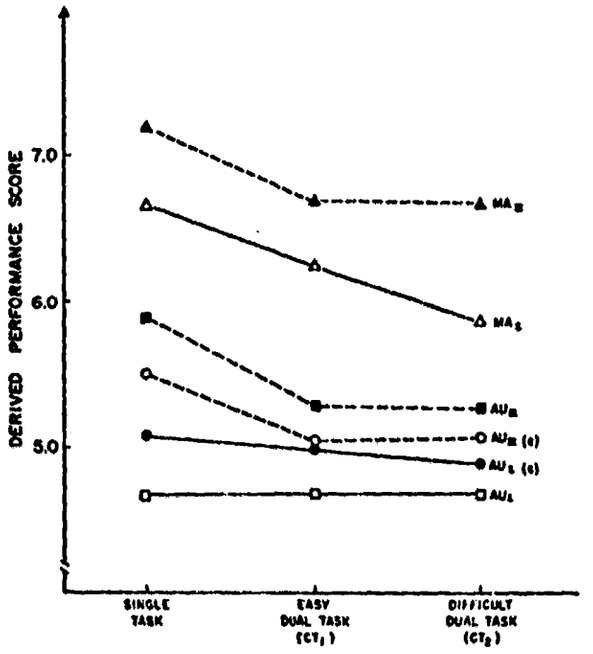

Figure 7: Effect of dual task on detection performance

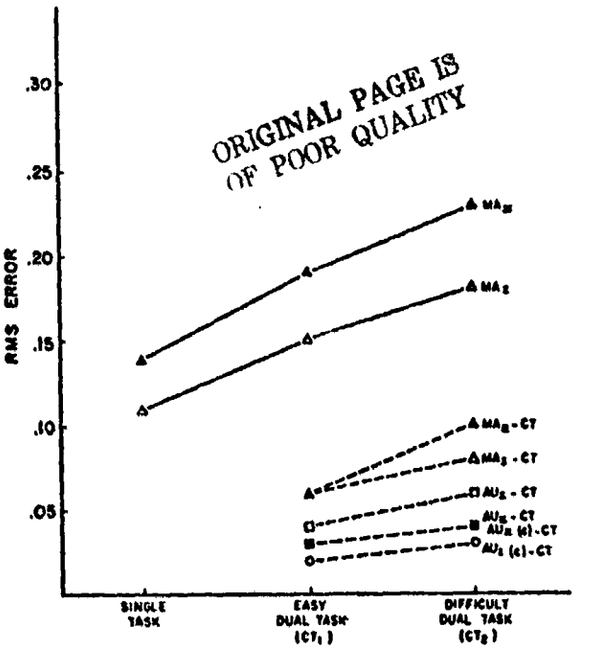

ORIGINAL PAGE IS
OF POOR QUALITY

Figure 8: Effects of dual task on manual tracking and critical task performance

ORIGINAL PAGE IS
OF POOR QUALITY

that internal models developed separately tend to be more consistent, less variable and more sensitive to system changes.

By comparing the single task performance in MA_{II} with AU_{II} (see Figures 3 and 5) it is possible to determine whether MA superiority is maintained after prior training in the other mode of participation. From Figures 3 and 5 we can see that while this difference has been reduced somewhat, the overall MA superiority remains intact. This MA_{II}-AU_{II} group difference is also statistically reliable ($F_{1,10} = 6.76$, $p < .05$).

(b) Critical Task

The impact of the critical tracking task may be evaluated both as it affected detection performance (Figure 7) and, in the MA mode, as it affects performance of the primary tracking task (Figure 8). From Figure 7, it is evident that the introduction of the CT produced a decrement in detection. As might be expected, the decrement in the MA mode was somewhat more pronounced. While there was no decrement for the AU_I groups there is a substantial decrement for the AU_{II} groups, equivalent to the decrement of both the MA groups. For both the MA_I-AU_I and the MA_{II}-AU_{II} analyses, task loading showed a statistically reliable effect ($F_{2,20} = 3.60$, $p < .05$; $F_{2,20} = 5.45$, $p < .025$ respectively). It should be noted however that the primary impact of this effect is localized in the introduction of the critical task, and not with the increase in its difficulty level, a point born out by further statistical analysis. (The near equivalence of the two dual task conditions was the justification for collapsing detection performance over the two conditions in further analysis.)

Figure 8 reveals that the critical task had a clear influence on MA tracking performance, both with its introduction, and with the increasing difficulty. Analysis performed on the MA_I and MA_{II} data alone[1] indicated that the effect was statistically reliable ($F_{2,20} = 45.97$, $p < .001$).

Finally, Figure 8 reveals slight, but consistent, decreases in critical tracking performance that occur as a result of increasing λ. These increases were found to be statistically reliable for all the groups. Since the subjects were all treating the critical task as a loading task it can be concluded that the increase in λ fact did serve to divert attentional resources from the primary tracking/detection process.

(c) Transfer of Training

Manual Mode. In determining the relative amount of transfer to the manual mode resulting from prior automatic training, the MA_{II} group is compared with its control group MA_I (Figure 1) which essentially had no prior experience in the failure detection task.

[1] Naturally AU "tracking" performance remains unaffected by critical task difficulty level.

From Figures 3 through 7 it can be seen that in general there is an overall MA_{II} superiority over MA_{I} for both single and dual task conditions. However the ANOVA failed to reveal these differences to be statistically reliable. Examination of the data on a day by day basis reveals that the overall MA_{I}-MA_{II} difference is due to large differences that exist on day 1 which appear to dissipate completely when the two groups are compared on day 2 performance. This finding can be seen as support for the basic hypothesis that exposure to prior AU tracking and the development of an internal model based on visual cues only, produces only a small and transient facilitation of subsequent development of the internal model based on MA tracking.

Automatic Mode. The degree of transfer resulting from prior MA training to the AU mode is reflected in the performance of subjects in condition AU_{II}, and the comparison of this performance with that of the control group ($AU_{I(C)}$-$AU_{II(C)}$). In Figures 5 and 6, it is evident that the latter group failed to benefit at all from prior AU training, an observation supported by the lack of statistical reliability of the main effect when $AU_{I(C)}$ and $AU_{II(C)}$ are compared. In marked contrast, Figures 5 and 6 suggest that the AU_{II} group in fact showed considerable benefit from their prior MA training when their performance is contrasted with that of the AU_{I} group. In Figure 5, the magnitude of this effect is seen to be considerably larger than the effect for the control group or for the MA_{I}-MA_{II} contrast discussed in the preceding section.

The statistical reliability of this improvement on the single task data was assessed by a groups (AU_{I} vs. AU_{II})x days (Day 1 vs. Day 2) 2 x 2 ANOVA.

Both main effects were statistically reliable. This indicates that (a) both groups improved with practice (over two days) in their respective AU conditions ($F_{1,10} = 14.77$, $p < .001$). (b) More crucially, from the viewpoint of the hypothesis under investigation, the AU_{II} group performed reliably better than did the AU_{I} group ($F_{1,10} = 5.19$, $p < .05$). It is of course possible to argue that this effect resulted from greater exposure to and familiarity with the overall experimental environment experienced by the AU_{II} group and not to transfer of the internal model. However this interpretation appears unlikely because the control group failed to show any such "generalized" transfer.

We can conclude that there is a transfer from MA to AU. The AU_{I}-AU_{II} differences are very large and statistically reliable and as such support the basic hypothesis that while there are different sets of cues operating, the MA condition produces an internal model of the system that can be utilized to advantage in subsequent automatic monitoring.

SUMMARY AND CONCLUSIONS

The major results can be summarized as follows:

1) Detection of step increases in system order when the operator remains in the control loop (MA mode) is considerably faster and more accurate than

when he is removed (AU mode). This finding is consistent with both the findings of Young (Reference 2) and of Wickens and Kessel (Reference 7).

2) The manual mode superiority was found to be more pronounced in this between subject design than the previous within subject study (Reference 7). This difference can be attributed to the fact that the subjects were allowed to develop separate internal models for either the manual or the automatic mode, thereby producing models that were always appropriate for the mode of participation employed.

What is interesting in contrasting the two studies is the fact that AU performance is virtually identical. The effect of the between-subjects manipulation instead seems to have been to produce a large improvement in MA detection.

This result suggests that in the previous experiment the AU internal model was developed unhindered by the concurrent development of the MA internal model while the reverse situation did not hold. It would appear that the development of the MA internal model in the previous experiment was somehow subject to interference from the AU model development, suggesting that subjects were paying attention to non-relevant, visual cues. It has been argued (Reference 7) that the sensitivity to proprioceptive information is reduced relative to visual information particularly when the two sources are available at the same time and are conveying conflicting information (References 13, 14, 15). In the AU mode the subjects have only visual cues as information while in the MA mode both visual and proprioceptive information is available. Thus in the previous study, during the development of the MA internal models there were times when these cues might be in conflict and subjects tended to fall back on the visual cues learned in the AU mode. This produced an over-emphasis on the visual cues and a subsequent degrading of the crucial proprioceptive information. The introduction of the between subject design forced subjects to develop separate internal models based upon the relevant cues available within each condition--a situation that has enhanced the MA-AU differences found in the previous experiment.

3) The overall MA superiority is evident in both single and dual task conditions. The effect of adding the Critical Task was to reduce the overall detection performance via a reduction in the accuracy of detections and an increase in response latencies. The impact of the second task was more marked for the MA condition than the AU condition. This result is consistent with the fact that the critical tracking task, placing heavy demands upon the subject's response mechanism, produced an increase in interference at the structural, motor level of performance in the MA mode that was not present in the AU mode of operation. Increasing the difficulty of the subcritical loading task appeared to have little effect on detection performance in either mode, although it did serve to disrupt tracking performance.

4) An analysis of the transfer of training experiment shows that there is very little transfer from the automatic mode to the manual mode. This fact adds further weight to the argument that the development of the internal model for the manual mode cannot utilize to advantage the internal model developed

ORIGINAL PAGE IS
OF POOR QUALITY

for the automatic mode. The addition of the proprioceptive channels and the interactive describing function in the manual mode appears to require the development of a separate and unique internal model.

5) There does appear to be positive transfer from the manual mode to the automatic, a finding that supports the basic hypothesis outlined above that while there are different sets of cues operating, the MA mode produces an internal model of the system that can be utilized to advantage in subsequent automatic monitoring.

6) Finally, the successful transfer from manual to automatic and the lack of transfer from the automatic to the manual modes tends to add weight to the basic hypothesis outlined above. This hypothesis states that the internal models developed in different modes of participation are relatively independent and therefore care must be exercised in extrapolating expected results in one mode of participation from performance in the other.

REFERENCES

1. Vreuls, D., et al. Pilot Failure Detection Performance with Three Levels of Fault Warning Information. Bunker-Ramo Corp., Report No. SRDS-RD-68-9, 1968.

2. Young, L.R. On Adaptive Manual Control. IEEE Transactions on Man-Machine Systems, Vol. MMS-10, pp. 292-331, 1969.

3. Ephrath, A.R. Detection of System Failures in Multi-axes Tasks. Proceedings of the 11th Annual NASA-University Conference on Manual Control. NASA TMX, 1975, 62, 464.

4. Curry, R.E. and Ephrath, A.R. Monitoring and Control of Unreliable Systems. T.B. Sheridan and G. Johannsen, Eds., Monitoring Behavior and Supervisory Control, New York: Plenum Press, 1976.

5. Johannsen, G., Pfendler, C. and Stein, W. Human Performance and Workload in Simulated Landing-approaches with Autopilot-failures. In T.B. Sheridan and G. Johannsen, Eds., Monitoring Behavior and Supervisory Control, New York: Plenum Press, 1976.

6. Ephrath, A.R. and Curry, R.E. Detection by Pilots of System Failures During Instrument Landings. IEEE Transactions on Systems Man & Cybernetics. Vol. SMC-7, No. 12, pp. 841-848, 1977.

7. Wickens, C.D. and Kessel, C. The Effects of Participatory Mode and Task Workload on the Detection of Dynamic System Failures. 13th NASA Conference on Manual Control, NASA, TMX-73, 170, 1977.

ORIGINAL PAGE IS
OF POOR QUALITY

8. Jex, R., McDonnell, J.D. and Phatak, A.V. A 'Critical" Tracking Task for Manual Control Research. IEEE Transactions on Human Factors in Electronics, Vol. HFE-7, pp. 138-144, 1966.

9. Wickens, C.D. In N. Moray, Ed., Mental Workload: Theory and Measurement. New York, Plenum Press, 1978, (in press).

10. Watson, C.S. and Nichols, T.L. Detectability of Auditory Signals Presented without Defined Observation Intervals. Journal of Acoustic Society of America, Vol. 59, pp. 655-668, 1976.

11. Green, D.M., and Swets, J.A. Signal Detection Theory and Psychophysics. New York: John Wiley and Sons, Inc., 1966.

12. Wickens, C.W. and Kessel, C. The Effects of Participatory Mode and Task Workload on the Detection of Dynamic System Failures. Institute of Aviation Tech. Report ARL-77-8/AFOSR-1977.

13. Posner, M.I. et al. Visual Dominance: An Information-processing Account of its Origins and Significance. Psychological Review, 1976, 83, No. 2, 157-171.

14. Klein, R.M. and Posner, M.I. Attention to Visual and Kinesthetic Components of Skills. Brain Research, Vol. 71, pp. 401-411, 1974.

15. Jordan, T.C. Characteristics of Visual and Proprioceptive Response Times in the Learning of a Motor Skill. Quarterly Journal of Experimental Psychology, Vol. 24, pp. 536-543, 1972.

SESSION C: NOVEL MODELING CONCEPTS

Chairman: R. Hess

98
PAGE INTENTIONALLY BLANK

N79-15597

A COMPARISON OF MOTOR SUBMODELS IN THE OPTIMAL CONTROL MODEL

by Roy E. Lancraft and David L. Kleinman

Department of Electrical Engineering & Computer Science
University of Connecticut
Storrs, Conn. 06268

ABSTRACT

Recent interest in the areas of modeling the effects of motion on human operators, and manual control of low bandwidth systems has led to the need for accurate submodels of the low frequency characteristics of the Human Operator (HO). Unfortunately, matching low frequency human response data has been a problem with almost all HO models, the well known Optimal Control Model (OCM) being no exception. This research is an attempt to better understand and hopefully eliminate these problems.

In this paper, properties of several structural variations in the neuromocor interface portion of the OCM are investigated. For example, it is known [1-2] that commanding control-rate introduces an open-loop pole at S=0 and will generate low frequency phase and magnitude characteristics similar to experimental data. However this gives rise to unusually high sensitivities with respect to motor and sensor noise-ratios, thereby reducing the models' predictive capabilities. Relationships for different motor submodels are discussed to show sources of these sensitivities. The models investigated include both pseudo motor-noise and actual (system driving) motor-noise characterizations. The effects of explicit priprioceptive feedback in the OCM is also examined. To show graphically the effects of each submodel on system outputs, sensitivity studies are included, and compared to data obtained from [1-2].

INTRODUCTION

Recently, motion studies [2,3] have shown the major effects of motion to be on low frequency ($\omega < 1$ rad/sec) HO magnitude and phase characteristics. This means that low frequency modeling errors present in the baseline implementation of the OCM must be minimized if the effects of including motion variables are to be felt. It is known [1,2] that changing the structure of the neuro-motor interface portion of the OCM will give the desired low frequency effects. Specifically if the HO commands control rate rather than control, the low frequency phase drooping occurs. However, in order to match human response data over simple vehicle dynamics, large deviations in the motor noise ratios were needed [2]. This clearly degrades the predictive

PAGE 100 INTENTIONALLY BLANK

power of the model. In this paper sub-models developed in [1,2] will be compared from a sensitivity point of view, in an attempt to better understand the limitations of each approach.

Problem Formulation

In this section structural changes will be made to the baseline OCM (for a more detailed description see Levison [2]). A general form will be developed first, with specific models introduced as special cases to it. In the development which follows, the time delay will be ignored since it has little bearing on our discussion.

The system being controlled is described by the state-space equation

$$\dot{x} = Ax + Bu + Ew \tag{1}$$

where:

x = "true" system state
u = "true" control input

and where displayed system variables are given by

$$y = Cx + Du \tag{2}$$

The system is assumed to be controlled to minimize (in steady-state) a quadratic cost functional

$$J = E\{y' Q_y y + g \dot{u}^2\} \tag{3}$$

based on the (delayed and) noisy information perceived by the HO. This information is assumed to consist of both displayed and proprioceptive variables, i.e.,

$$y_p = Cx + Du + v_y \tag{4a}$$

$$u_p = u + v_u \tag{4b}$$

where:

$$\text{cov}\{v_y\} = V_y + \rho_y E\{y^2\} \tag{5a}$$

$$\text{cov}\{v_u\} = V_u + \rho_u E\{u^2\} \tag{5b}$$

The control law that minimizes J is given by

$$\dot{u} = -[L_x \; L_u] \begin{bmatrix} \hat{x} \\ \hat{u} \end{bmatrix} \triangleq \dot{u}_c \tag{6}$$

where:

$\hat{x}$ = human's best internal estimate of x
$\hat{u}$ = " " " " $_u$

To model any actual noise at the motor end, a driving motor noise is added to (6). Notice control rate is generated rather than control. Thus,

$$\dot{u} = \dot{u}_c + v_{\dot{u}} \tag{7}$$

where:

$$\text{cov}\{v_{\dot{u}}\} = V_{\dot{u}} + \rho_{\dot{u}} E\{\dot{u}_c^2\} \tag{8}$$

However the human's internal representation of the neuromotor interface, Eq. (7), is:

$$\dot{u} = \dot{u}_c + v_p \tag{9}$$

where:

$$\text{cov}\{v_p\} = V_p + \rho_p E\{\dot{u}_c^2\} \tag{10}$$

and typically $\text{cov}\{v_p\} \neq \text{cov}\{v_{\dot{u}}\}$.

The pseudo motor noise v_p does not act as a driving noise to the system, but instead degrades performance by making estimation sub-optimal [2].

Implementing these changes gives rise to the structure shown in Fig. 1.

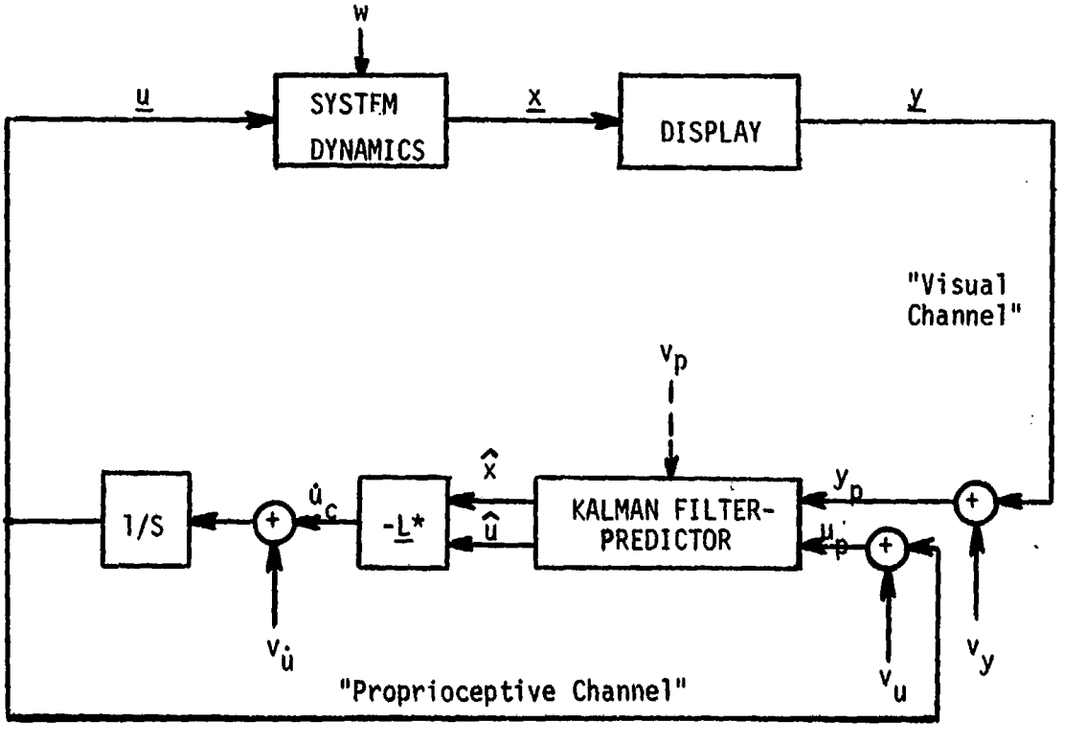

FIG.1 REVISED OPTIMAL CONTROL MODEL.

The particular submodels considered in this study are as follows:

Driving Noise Models:

1) $\mathrm{cov}\{v_p\} = \mathrm{cov}\{v_u\}$, i.e., optimal estimation occurs, driving motor noise equal to v_u
   - proprioceptive information available
2) Same as model (1), except no proprioceptive information available

Pseudo noise models:

3) $v_u = 0$, i.e., sub-optimal estimation occurs, only pseudo noise present
   - proprioceptive information available
4) Same as model (3) except no proprioceptive information available

SENSITIVITY RESULTS

Data from [1,2] was matched using each of the aforementioned models. Only K/S and K/S**2 dynamics were considered. The reader is referred to the sensitivity studies included in [1] so a comparison can be made to the baseline model.

K/S Dynamics

The following nominal parameters were found to give reasonable matches to the data, and will be used as a basis for the K/S sensitivity work. Notice that proprioceptive feedback is not needed for K/S dynamics; this agrees with findings in [1,2]. Therefore, for K/S dynamics we need only consider two models, driving noise and pseudo noise.

Model	SNR	SNR-u	MNR	TD	TN
1 & 3	-20	$-\infty$	-40	.17	.08
2 & 4	-20	--	-40	.17	.08

$\mathrm{SNR} \triangleq \rho_{y_\Delta}$

$\mathrm{SNR - u} \triangleq \rho_u$

$\mathrm{MNR} = \rho_u$ or ρ_p

$\mathrm{TD} = \tau$, $\mathrm{TN} = L_u^{-1}$

It was found that the trends discussed in [1] for SNR, TD and TN were the same for all the models considered. The only exception to this was for the driving noise models, where the low frequency remnant curves were slightly higher.

Effects of MNR

From Fig. 2 it is clear that motor noise mainly affects the low fre-

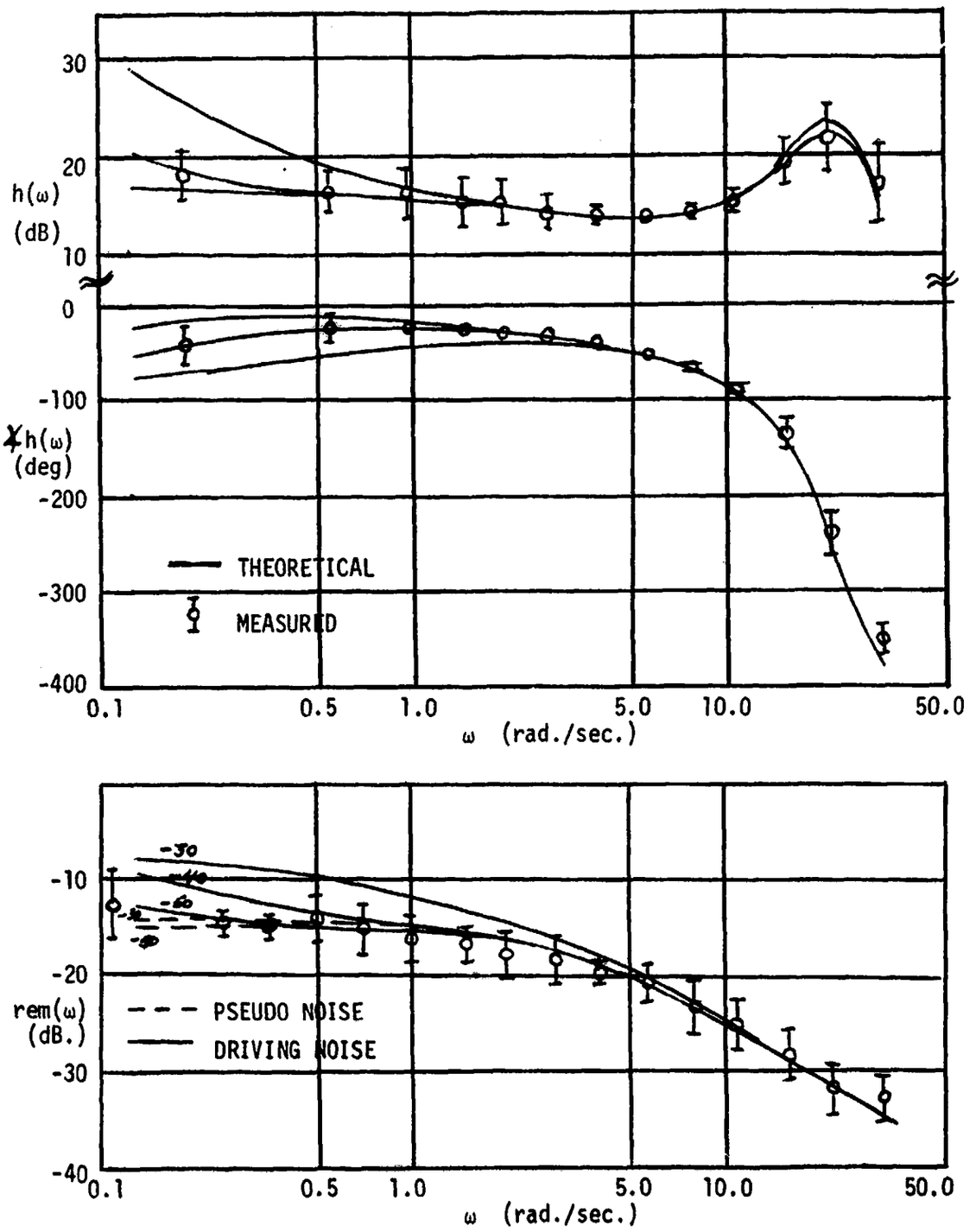

FIG.2 EFFECTS OF MNR ON K/S DYNAMICS.

quency portion of the magnitude, phase and remnant curves. There are basically two reasons for this. First,the shape of the low frequency portion is due to the integrator at the motor end (where in the baseline OCM, $1/(T_N S+1)$ was present). Secondly, the sensitivity is due to the degradation of estimation performance as the motor noise is increased. Because the level of the driving noise is so low, the linear part of the HO model (Bode plot) is the same whether pseudo noises or driving noises are used. Notice that the driving noise has a dominant affect only on the low frequency remnant.

All scores increase with increasing motor noise. Scores using the pseudo model are fairly insensitive to motor noise, since it is the degraded estimation which causes them to change. Scores using the driving model are much more sensitive to motor noise, since increasing the motor noise increases the remnant in the system.

K/S**2 Dynamics

The following is the nominal parameter set found for K/S**2 dynamics.

Model	SNR	SNR-u	MNR	TD	TN
1 & 3	-20	-25	-40	.21	.1
2 & 4	-20	---	-54	.21	.1

Here, as in K/S dynamics, trends discussed in [1] for SNR, TD, and TN also hold for our revised models. Below we discuss only the effects of MNR & SNR on control.

Effects of MNR

No Proprioceptive Information (models 2 & 4)

Looking at Figure 3 it is clear that the motor noise affects the low frequency Bode plots in a manner similar to that found for K/S dynamics. Again, more remnant power is shifted to the low frequencies for model 2 than for model 4.

Notice that model 4 matches the low frequency remnant very poorly (this could be improved slightly by increasing the noise on displayed error) and may be interpreted as a major shortcoming of this model since we desire a nominal set of parameters.

ORIGINAL PAGE IS
OF POOR QUALITY

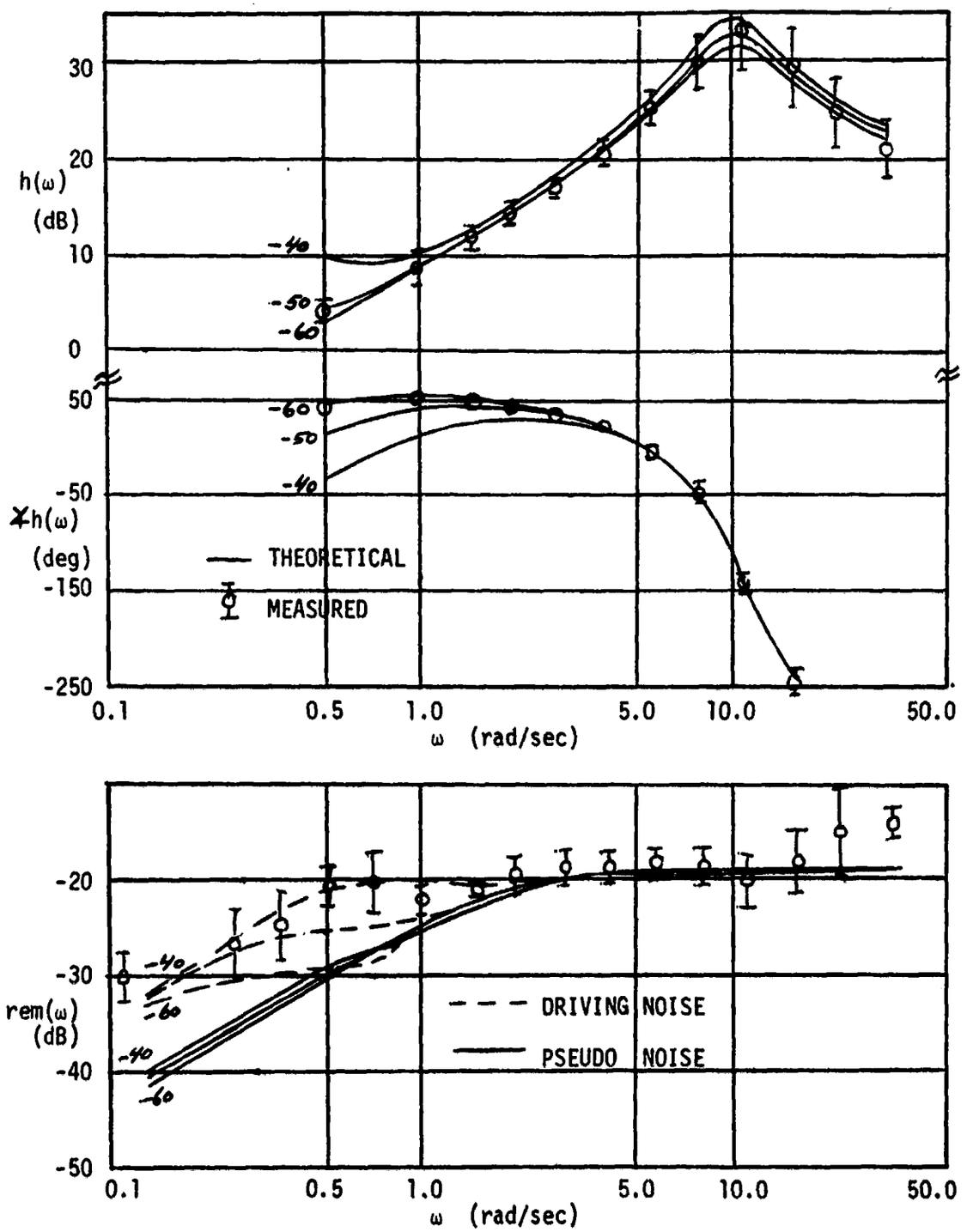

FIG.3 EFFECTS OF MNR ON K/S**2 DYNAMICS (MODELS 2 & 4).

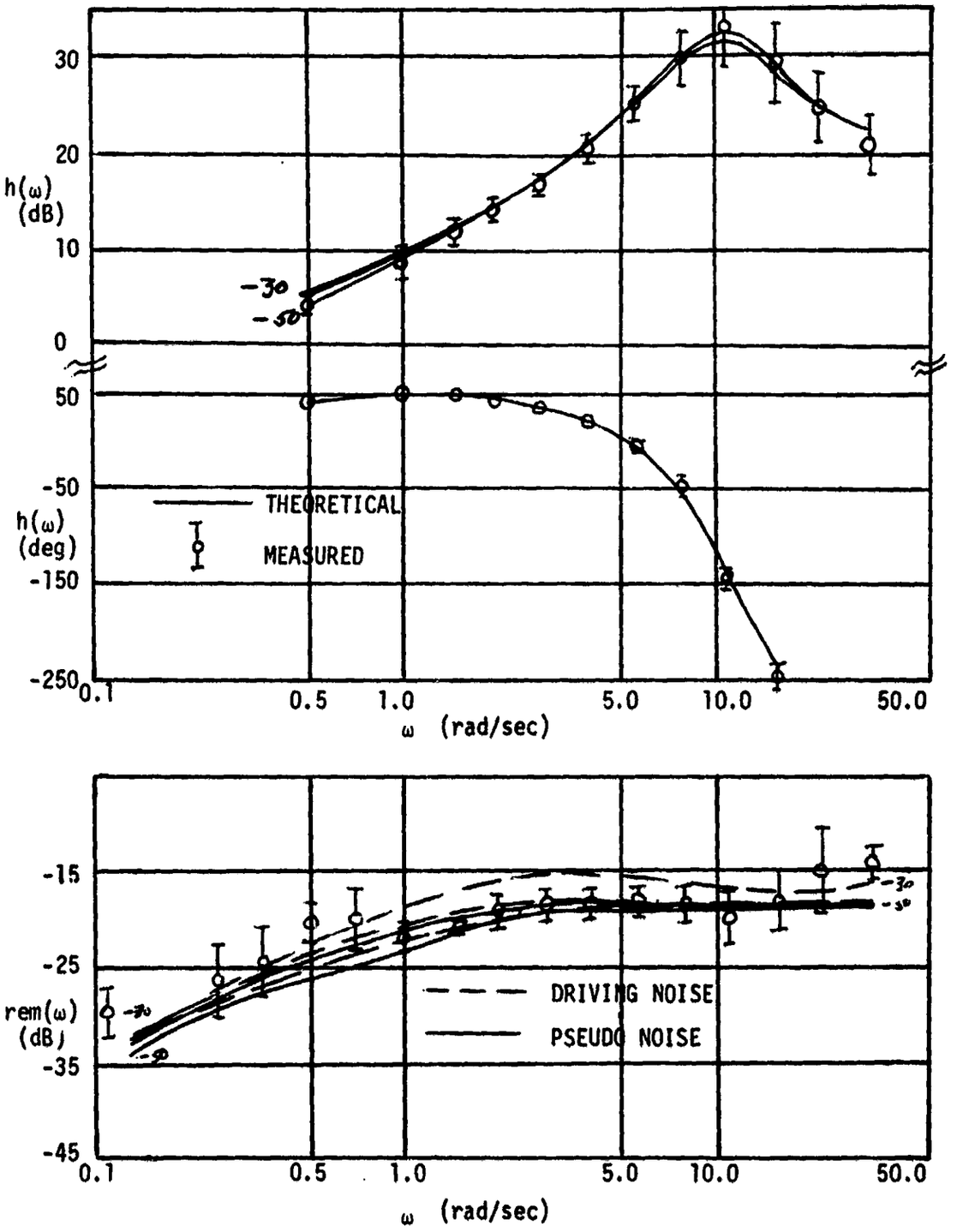

FIG.4 EFFECTS OF MNR ON K/S**2 DYNAMICS (MODELS 1 & 3).

With Propioceptive Information (Models 2 & 4)

The effects of including proprioceptive feedback can be seen by comparing Figs. 3 & 4. Again remnant is higher for driving motor noises, but it is spread out over a wider band of frequencies. This may be due to the circulation of remnant in the feedback loop. Although not shown, the scores for model 1 were always higher and more sensitive than those for model 3, and seemed to match the data better.

Notice that the sensitivity of the model to changes in the motor noise has been reduced dramatically by including proprioceptive feedback. Because the model now has observations of control and control rate to use in forming an estimate of control, estimation stabilizes and improves.

Effects of SNR (Models 1 & 3)

Figure 5 shows the low frequency remnant for model 3 much closer to that of model 1. Notice if the sensor noise is too large (>-15dB), the model ignores this observation and models 1 & 3 effectively become models 2 & 4. Since knowledge of the control signal is important in this task, it is clear that the model should be, and is, sensitive to the quality of this information. The low frequency effects result primarily from the movement of the estimator poles.

Sensitivity of Scores

Relative RMS error is plotted in Fig. 6 as a function of MNR. Because RMS error is the most sensitive score, Fig. 6 shows that including proprioceptive feedback reduces the sensitivity of all the scores.

Review

From the sensitivities studies it was seen that in general:

- All predicted scores were lower than measured ones for pseudo noise
- All system measures were more sensitive to driving motor noise than to pseudo noise
- This sensitivity can be reduced by including an observation of control
- The level of sensor noise on control induces the low frequency effects
- The integrator at the motor end confines the remnant power to the low frequencies

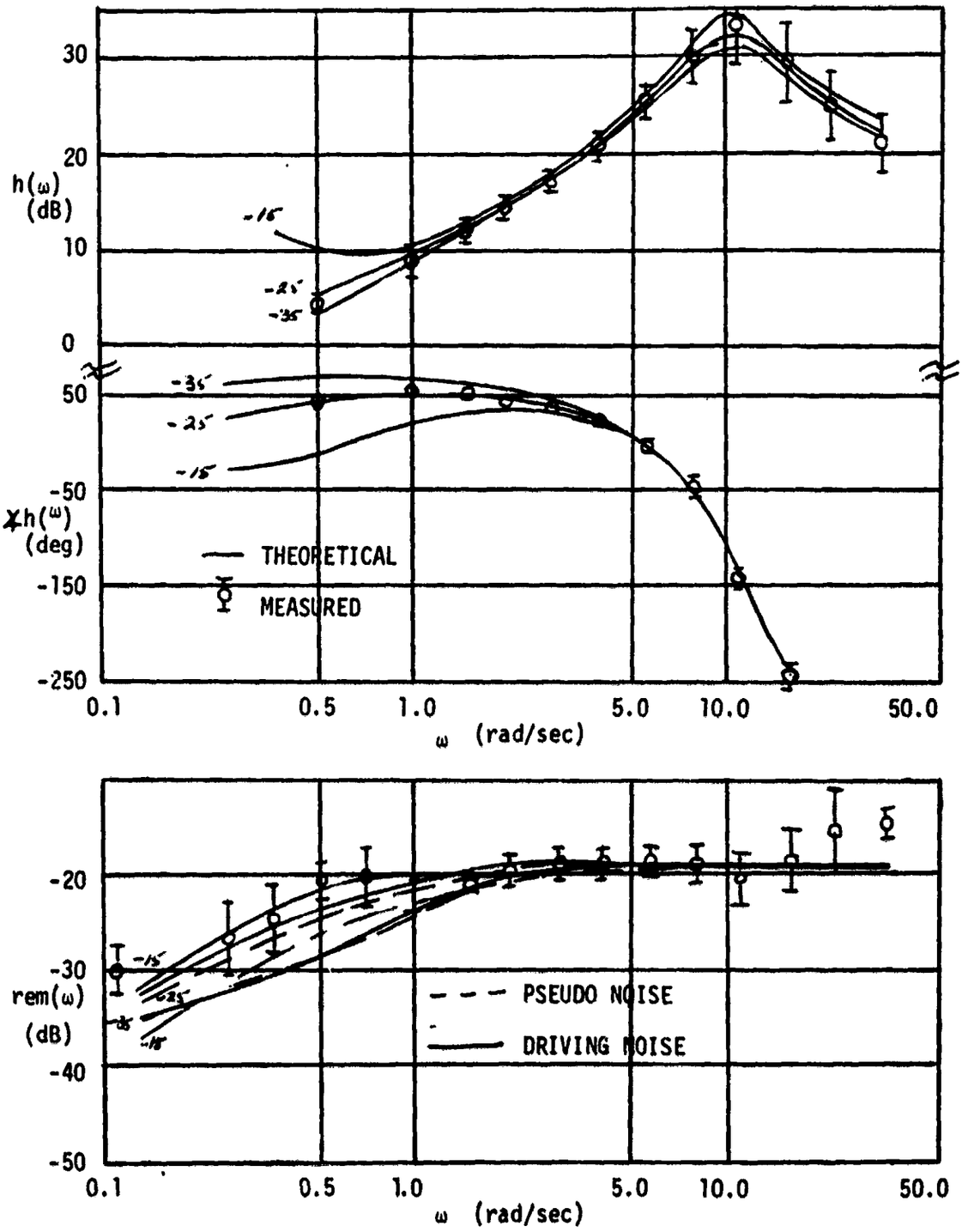

FIG.5 EFFECTS OF SNR-U ON K/S**2 DYNAMICS (MODEL 1 & 3).

ORIGINAL PAGE I
OF POOR QUALIT

ORIGINAL PAGE IS
OF POOR QUALITY

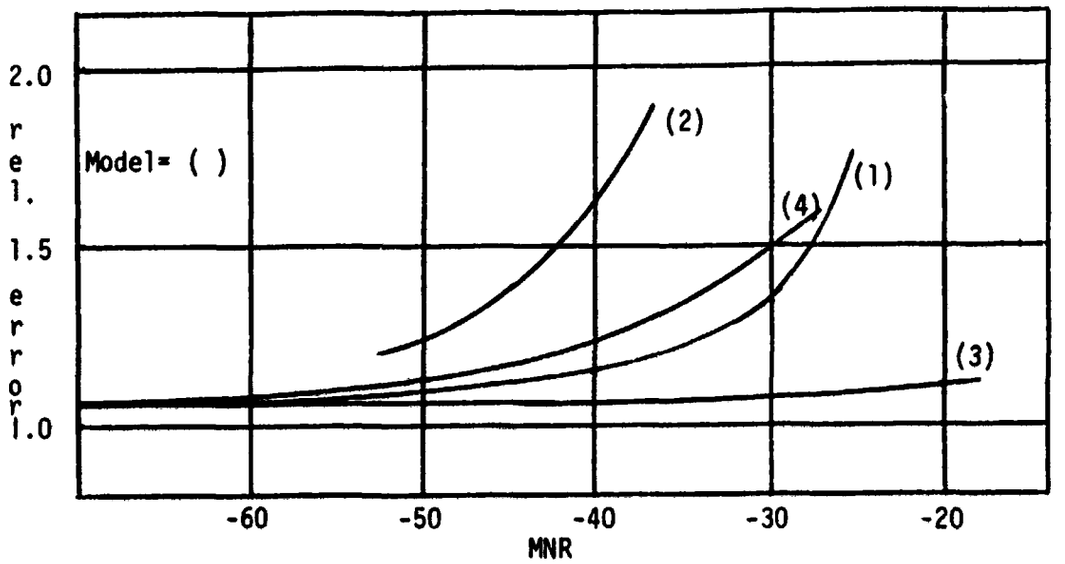

FIG. 6: SENSITIVITY OF RMS ERROR (K/S**2 TASK)

- It is difficult to match K/S**2 data, with a nominal set of parameters, using models 2 & 4

FINAL COMMENTS

Sensitivity studies have shown that including observations on control can reduce model sensitivity to driving motor noises. Also it was shown that a sensor noise added to control does not greatly affect the uncorrelated part of the model. Nominal parameters were found that could match K/S & K/S**2 dynamics, provided that observations on control are included for K/S**2 but not for K/S. If the model is allowed to allocate attention freely among all observed variables, this may provide a scheme for determining the sensor noises. One hypothesis is that this essentially forms a decision step (perhaps as part of the learning process) in the HO model, where it must evaluate the benefits of all the cues it has available to it and then decide on a subset which will be useful for control purposes.

More work needs to be done in order to find a good rule for picking the sensor noises. Testing models 1 and 3 over a wider set of system dynamics is also important to see if our findings are true in general or just a special case.

REFERENCES

1. Kleinman, D.L. & Baron, S.: Manned Vehicle Systems Analysis by Means of Modern Control Theory. NASA CR-1753, June 1971.

2. Levison, W.H., Baron, S., Junker, A.M.: Modeling the Effects of Environmental Factors on Human Control and Information Processing, AMRL-TR-76-74, Aug. 1976.

3. Levison, W.H. & Junker, A.M.: A Model for the Pilots Use of Motion Cues in Roll-Axis Tracking Tasks. AMRL-TR-77-40, June 1977.

N79-15598

CLOSED LOOP MODELS FOR ANALYZING THE EFFECTS OF SIMULATOR CHARACTERISTICS*

by

Sheldon Baron, Ramal Muralidharan, David Kleinman
Bolt Beranek and Newman Inc., Cambridge, MA

ABSTRACT

The optimal control model (OCM) of the human operator is used to develop closed-loop models for analyzing the effects of (digital) simulator characteristics on predicted performance and/or workload. Two approaches are considered: the first utilizes a continuous approximation to the discrete simulation in conjunction with the standard optimal control model; the second involves a more exact discrete description of the simulator in a closed-loop multi-rate simulation in which the optimal control model "simulates" the pilot. Both models predict that simulator characteristics can have significant effects on performance and workload.

1. INTRODUCTION

The development of engineering requirements for man-in-the-loop digital simulation is a complex task involving numerous trade-offs between simulation fidelity and costs, accuracy and speed, etc. The principal issues confronting the developer of a simulation involve the design of the cue (motion and visual) environment so as to meet simulation objectives and the design of the digital simulation model to fulfill the real-time requirements with adequate accuracy.

The design of the simulation model has become increasingly important and difficult as digital computers play a more central role in the simulations. For real-time digital simulation with a pilot in the loop the design problem involves specification of conversion equipment (A-D and D-A) as well as of the discrete model of the system dynamics. The design of an adequate discrete simulation is also related closely to the cue generation problem inasmuch as the errors and, in particular, the delays introduced by the simulation will be present in the information cues utilized by the pilot. The significance of this problem has been amply demonstrated.[1,2] Of course, human pilots can compensate for model shortcomings as well as for those of cue generation, with possible effects on the subjective evaluation of the simulation.

The objective of the work reported here was to develop a closed loop analytic model, incorporating a model for the human pilot (namely, the optimal control model), that would allow certain simulation design tradeoffs to be evaluated quantitatively and to apply this model to analyze a realistic flight control problem. The effort concentrated on the dynamic, closed loop aspects of

*The work described herein was performed under Contract No. NSA1-14449 for NASA - Langley Research Center. Mr. Russell Parrish was the Technical Monitor and contributed many helpful suggestions.

the simulation. Problems associated with perceptual issues in cue generation were not considered. However, the limitations imposed by the dynamics of visual cue generation equipment are considered and the model can be readily extended to incorporate the dynamics associated with motion simulation.

The optimal control model of the human operator[3,4] is central to the closed loop analysis techniques that have been employed. This model has been validated and applied extensively and has a structure that is well-suited to analysis of the simulation problems of interest. The model can be used to generate predictions of attentional workload as well as of closed-loop performance. This is significant because, as noted earlier, pilots may compensate for simulation shortcomings but with a workload penalty; such simulation-induced operator tradeoffs need to be explored.

Two approaches to closed-loop modelling are considered. The first employs a continuous approximation to the open-loop dynamics of the digital simulation in conjunction with the standard OCM. The second model attempts to represent the discrete simulation dynamics more exactly. It utilizes a simulation version of the OCM. This latter model is referred to as the hybrid model.

In the remainder of this paper, the closed loop models are described and some results of applying the models are presented and discussed. More extensive discussion and additional results may be found in Reference 5.

2. CONTINUOUS CLOSED LOOP MODEL

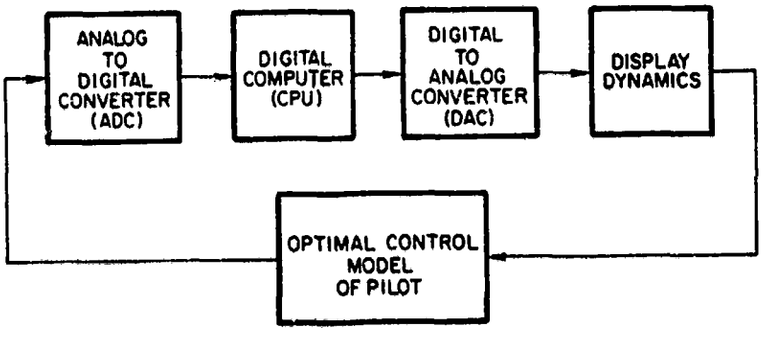

Figure 1. Simplified Model for Closed Loop Analysis of Digital Simulation

Figure 1 is a block diagram of a simplified closed-loop model for analyzing problems in digital, piloted simulation. The pilot model in Figure 1 is the OCM.[3,4] The elements corresponding to the simulator are an analog-to-digital converter (ADC), a digital computer (CPU), a digital-to-analog converter (DAC) and a visual display system. Briefly, the ADC is a sampler preceded by a

low-pass filter included to minimize aliasing effects, the CPU implements difference equations so as to simulate the vehicle's response to the pilot's (sampled) input, the DAC is a data-hold (either zero-order or first-order), and the visual display system is a servo-driven projector that continuously displays target position (relative to the aircraft) to the pilot. These elements will be discussed in more detail below.

2.1 Optimal Control Model for Pilot

Some of the features of the OCM that are particularly relevant to subsequent discussions are reviewed briefly here. Figure 2 illustrates the

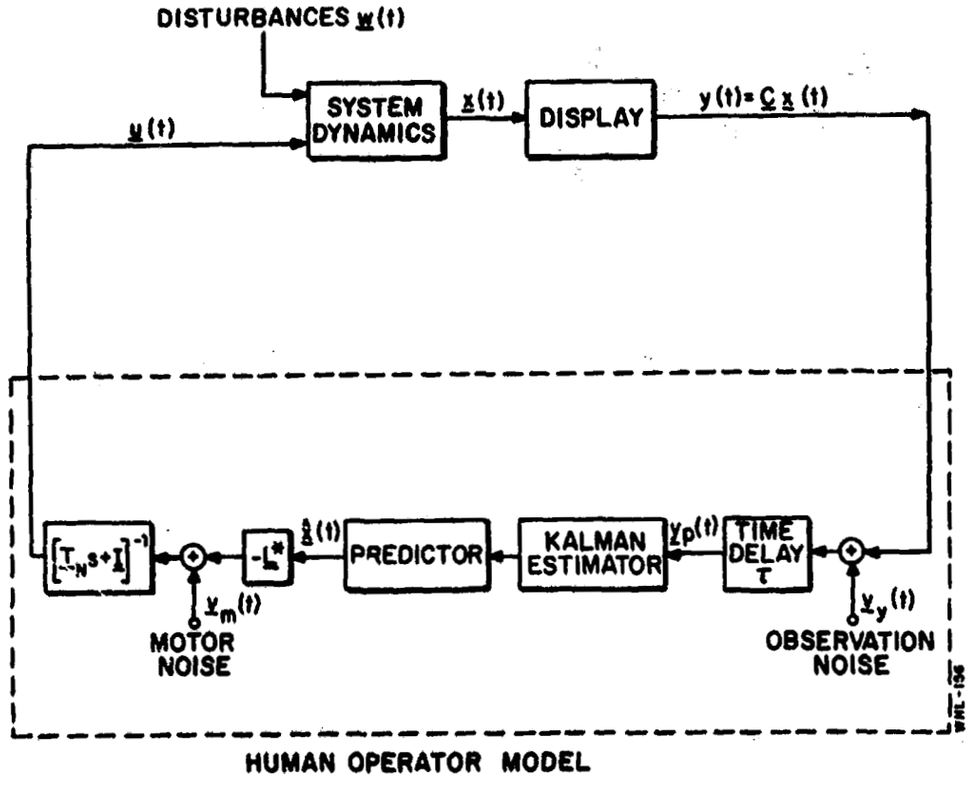

Figure 2. Structure of Optimal Control Model

structure of the OCM.

The OCM as originally conceived and developed presupposes that the system dynamics, corresponding to the element to be controlled, may be expressed in state variable format

$$\dot{\mathbf{x}}(t) = \mathbf{A}_c\mathbf{x}(t) + \mathbf{B}_c\mathbf{u}(t) + \mathbf{E}_c\,\mathbf{w}(t)$$
$$\mathbf{y}(t) = \mathbf{C}_c\mathbf{x}(t) + \mathbf{D}_c\mathbf{u}(t) \qquad (1)$$

where $\mathbf{x}$ is the n-dimensional state-vector, $\mathbf{y}$ is an m-dimensional vector of displayed outputs, $\mathbf{u}$ is the r-dimensional control input vector and $\mathbf{w}$ is a vector of disturbance and/or command inputs. The system matrices ($\mathbf{A}_c$, $\mathbf{B}_c$, $\mathbf{C}_c$, $\mathbf{D}_c$, $\mathbf{E}_c$) are generally assumed to be time-invariant, although this restriction can be relaxed. The above system dynamics include the linearized dynamics of the aircraft (or other controlled element) and any dynamics associated with measurement, control and display systems. The subscript c on the system matrices is included to emphasize that the dynamics are assumed to represent a continuous system.

For purposes of discussion it is convenient to consider the model for the pilot as being comprised of the following: (i) an "equivalent" perceptual model that translates displayed variables into noisy, delayed perceived variables denoted by $\mathbf{y}_p(t)$; (ii) an information processing model that attempts to estimate the system state from the perceived data. The information processor consists of an optimal (Kalman) estimator and predictor and it generates the minimum-variance estimate $\hat{\mathbf{x}}(t)$ of $\mathbf{x}(t)$; (iii) a set of "optimal gains", $\mathbf{L}^*$, chosen to minimize a quadratic cost functional that expresses task requirements; and (iv) an equivalent "motor" or output model that accounts for "bandwidth" limitations (frequently associated with neuromotor dynamics) of the human and an inability to generate noise-free control inputs.

The time delay or transport lag is intended to model delays associated with the human. All displayed variables are assumed to be delayed by the same amount, viz. τ seconds. However, delays introduced by the simulation can be added to the human's delay without any problem, so long as all outputs are delayed by the same amount. If such is not the case, then all outputs can be delayed by τ, where τ is now the sum of the minimal delay introduced by the simulation and the operator's delay, and additional delays for the outputs requiring them can be modeled via inclusion of Pade approximations in the output path.

The observation and motor noises model human controller remnant and involve injection of wide-band noise into the system. This noise is "filtered" by the other processes in the pilot model and by the system dynamics. It should be emphasized that the injected remnant is a legitimate (if unwanted) part of the pilot's input to the system and, therefore, significant amounts of remnant power should not be filtered out in the de-aliasing process of a valid simulation.

The neuro-motor lag matrix limits the bandwidth of the model response. Typically, for wide-band control tasks, involving a single control variable, a bandwidth limitation of about 10-12 rad/sec gives a good match to experimental results (i.e., a neuro-motor time constant of $T_N \simeq .08 - .10$). For many

aircraft control tasks there is no significant gain (i.e., reduction in error) to be obtained by operating at this bandwidth, and there can be some penalty in unnecessary control activity. For such tasks larger time constants (lower bandwidths) have been observed. In these cases, if the neuro-motor time constant is arbitrarily set at the human's limit (say $T_N \simeq .1$) good predictions of tracking or regulation performance are usually obtained; but the control activity and pilot bandwidth tend to be overestimated. Inasmuch as it may be useful to have more accurate estimates of pilot bandwidth for making decisions concerning approximations to the discrete simulations, T_N was chosen in this study on the basis of a model analysis of the tradeoff between error and control-rate scores. Essentially, this involves using the model to sweep out a curve of error-score versus control-rate score to find the value of T_n where marginal improvements in performance require substantial increases in rms control-rate (the "knee" of the curve). A value of approximately .15 sec (an operator bandwidth of about 1 Hz) was determined on the basis of this analysis.[5]

The optimal estimator, predictor and gain matrix represent the set of "adjustments" or "adaptations" by which the human attempts to optimize performance. The general expressions for these model elements depend on the system and task and are determined by solving an appropriate optimization problem according to well-defined rules. Of special interest here is that, in the basic continuous OCM, the estimator and predictor contain "internal models" of the system to be controlled and the control gains are computed based on knowledge of system dynamics. The assumption is that the operator learns these dynamics during training.*

The question arises as to the appropriate internal model when the human controls a discrete simulation of a nominally continuous system. It would appear that if the operator is trained on the simulation, then the appropriate model corresponds to the simulation model.** This will be the assumption employed with the continuous model.

Finally, it should be mentioned that the solution to the aforementioned optimization problem yields predictions of the complete closed-loop performance statistics of the system. Predictions of pilot describing functions and control and error spectra are also available. All statistical computations are performed using covariance propagation methods, thus avoiding costly Monte Carlo simulations. This is not the case for the hybrid model described later.

---

*This is generally more convenient than assuming that the external model differs from the true model and also leads to good performance prediction.[6]

**If the simulation model is poor, a control strategy that is inappropriate for the actual system could be learned with negative results in, say, transfer of training. This issue can be addressed with the hybrid model described later.

2.2 Open-Loop Simulator Dynamics

The application of the standard OCM to closed-loop analysis requires a continuous state representation of the complete controlled element. Since the human pilot in closed loop control will operate on essentially continuous outputs to generate continuous control inputs even when digital computers are used in the aircraft simulation, it is meaningful to consider a continuous transfer function approximation to the open loop simulation dynamics. Such an approximation is developed here. It consists of a rational transfer function multiplied by a transportation lag. The rational transfer function approximates the amplitude distortions introduced by discrete integration of the flight dynamics. The delay accounts for all the phase lags introduced by the simulator components. These phase lags are the major source of degraded performance and increased workload in closed loop tasks. However, the amplitude distortions can be significant for open-loop responses.

System Function From Stick Input to Displayed Output

Figure 3 is an elaborated diagram of the simulator portion of Figure 1.

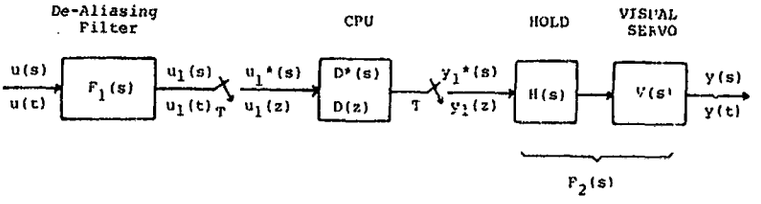

Figure 3. Open Loop Simulator Dynamics

Note that the output of the visual servo, y(t), is a continuous signal as is the input, u(t), to the A-D dealiasing pre-filter.* For analysis purposes we use the notation implied in Figure 3. Variables or functions with argument s represent Laplace transforms and those with argument z correspond to z-transforms. The starred quantities correspond to Laplace transforms of impulse sampled signals or of functions of z and are defined, e.g., by[7]

$$u_1^*(s) \triangleq u_1(z)\Big|_{z=e^{sT}} = \frac{1}{T}\sum_{n=-\infty}^{\infty} u_1(s+jn\Omega) \qquad (2)$$

or

*For simplicity, we consider single-input, single-output systems. The results obtained here can be generalized to more complex situations.

$$D^*(s) = D(z)\Big|_{z=e^{sT}} \tag{3}$$

where T is the sample period and

$$\Omega = \frac{2\pi}{T} = \text{sampling frequency} \tag{4}$$

From Figure 3, we obtain

$$\begin{aligned} y(s) &= F_2(s)y_1^*(s) = F_2(s)D^*(s)u_1^*(s) \\ &= F_2(s)D^*(s)\ \frac{1}{T}\sum_{n=-\infty}^{\infty} F_1(s+jn\Omega)u(s+jn\Omega) \end{aligned} \tag{5}$$

Equation (5) gives the exact transfer relation between u(s) and y(s). However, it is not a useful expression from the standpoint of closed-loop modeling because of the infinite summation.

The system function for a linear system (such as the simulation system under analysis) may be obtained by computing the steady-state response of the system to an input of the form exp(st). It is shown in Reference 5 that the system function from u(s) to y(s) (in steady-state) is periodic in time with a period equal to the sampling period. However, if the output y(t) is considered only at sampling instants, which amounts to introducing a "fictitious" sampler at the output, then the following time-independent transfer function is obtained.

$$G(s;t)\Big|_{\substack{\text{sample}\\ \text{times}}} = G(s) = F_2^*(s)D^*(s)F_1(s) \tag{6}$$

We shall consider G(s) defined in (6) to be the "exact" transfer function for the simulation. Note that $F_2^*(s) = (VH_1)^*(s)$.

Equation (6) is intractable for use with the continuous OCM. Therefore, it will be necessary to approximate (6) for closed-loop analysis. A straightforward approximation is to ignore all but the n=0 term in the expression for F_2^* which results in

$$G(s) \approx \frac{F_2(s)D^*(s)F_1(s)}{T} = \frac{V(s)H_i(s)D^*(s)F_1(s)}{T} \tag{7}$$

In utilizing (7) it will be necessary to approximate $D^*(s)$; the procedure for doing this will be discussed subsequently.

For the simulator of interest here,[8] the transfer functions for the de-aliasing filter and servo are, respectively,

$$F_1(s) = \frac{\omega_c^3}{s^3 + 2\omega_c s^2 + 2\omega_c^2 s + \omega_c^3} \tag{8}$$

$$V(s) = \frac{\omega_n^2}{s^2 + 2\zeta\omega_n s + \omega_n^2} \tag{9}$$

The hold transfer function is either

$$H_o(s) = \frac{1-e^{-sT}}{s} \tag{10}$$

or

$$H(s) = T(1+Ts)\left(\frac{1-e^{-Ts}}{Ts}\right)^2 \tag{11}$$

Sample periods, T, of 1/32, 1/16, 1/10 will be considered as these cover the likely range of interest for piloted simulation. Therefore, if the cutoff of the de-aliasing filter is chosen on the basis of the sampling theorem, $\omega_c >$ 5Hz. The visual servo dynamics of interest are characterized by ω_n = 25 rad/sec and ζ = .707.[8]

With these parameter values, each of the transfer functions of (8) - (11) may be approximated reasonably well by a pure transport lag in the frequency region of interest for manual control ($\omega <$ 10 rad/sec). That is,

$$
\begin{aligned}
F_1(s) &\approx e^{-\tau_F s} \\
V(s) &\approx e^{-\tau_V s} \\
H_o(s) &\approx e^{-\tau_o s} \\
H_1(s) &\approx e^{-\tau_1 s}
\end{aligned}
\tag{12}
$$

where

$$
\tau_F \approx \frac{2}{\omega_c} = \frac{2T}{\pi} \qquad \tau_o = T/2
$$

$$
\tau_V \approx (\zeta\omega_n)^{-1} = .057 \text{ sec} \qquad \tau_1 = T \tag{13}
$$

Substitution of (12) into (7) yields

$$
F_1(s)D^*(s)F_2(s) \approx D^*(s) \exp\left[-(\tau_F + \tau_V + \tau_i)s\right] \tag{14}
$$

where i = 0 or 1 for the zero-order or first-order hold, respectively.

2.3 Effects of Discrete Integration

In the previous section the transfer function D*(s) was left unspecified as was the manner in which it was to be approximated for continuous closed-loop analysis with the OCM. In general, D*(s) will be a "distorted" version of the continuous system dynamics that are to be simulated. Some general features of the distortions introduced by various integration schemes are analyzed and presented in Reference 5 along with results pertinent to the F-8 dynamics that are to be analyzed later. Here, we present a brief discussion of the general effects of discrete integration followed by a description of the method that will be used to approximate D*(s) in the continuous closed-loop analysis.

Consider the continuous vehicle-dynamics as described in the state-variable form of Equation (1). For constant system matrices, the transfer matrix between system outputs and control inputs is given by

$$
\begin{aligned}
\mathbf{y}(s) &= \mathbf{G}_c(s)\,\mathbf{u}(s) \\
\mathbf{G}_c(s) &= \mathbf{C}_c(s\mathbf{I}-\mathbf{A}_c)^{-1}\mathbf{B}_c + \mathbf{D}_c
\end{aligned}
\tag{15}
$$

When equations (1) are "integrated" digitally, they lead to a discrete approximation with the following transfer matrix[5]

$$
D^*(s) = \left\{\mathbf{C}_d[z\mathbf{I}-\mathbf{A}_d]^{-1}\,\mathbf{B}_d + \mathbf{D}_d\right\}\Big|_{z=e^{sT}} \tag{16}
$$

where the matrices in (16) depend on the particular integration scheme and sample period as well as on the corresponding continuous system matrices. Several points concerning Equation (16) are noteworthy. First, the elements of the discrete transfer matrix $D^*(s)$, cannot, in general, be expressed as the ratio of two polynomials in s of finite degree. Second, the Bode responses corresponding to (16) will differ from the continuous responses in both amplitude and phase; and, further, the responses for the discrete system are periodic in frequency with period equal to $2\pi/T$. Third, the poles and zeros of Equation (16) are infinite in number and are given by, for example,

$$P_i = \sigma_i + j(\omega_i + 2\pi k);\ k = 0, \pm 1, \pm 2, \ldots$$

Moreover, the principal values for the poles and zeros, i.e., those with $k = 0$, are not, in general, equal to the corresponding poles and zeros of the continuous system. Finally, simple integration schemes, such as Euler, will have the same number of principal poles as the continuous system, whereas multi-step integration schemes, like (Adams-Bashforth), will introduce principal roots that are spurious.

We now turn to the problem of approximating $D^*(s)$ so that the continuous representation of the simulator dynamics may be completed. Because of the restrictions imposed by the OCM, we restrict the possible approximations to the following form:

$$\frac{Y_i}{u_j} = D^*_{ij}(s) \approx \tilde{D}_{ij}(s)e^{-\tau_c s}$$

where $\tilde{D}(s)$ is a ratio of finite polynomials in s with numerator degree less than or equal to the degree of the denominator. Note that the same "computation" delay, τ_c is associated with each transfer function. This turns out to be a good approximation for the dynamics considered in Section 4. If different delays were needed, they would be included in $\tilde{D}$ via a rational Pade approximation.[5]

The simplest approach to selecting $\tilde{D}$ is to use (15) and let

$$\tilde{D}_{ij}(s) = \Phi_{c_{ij}}(s) \tag{17}$$

From the standpoint of the OCM, this means that the state equations for the original dynamics are used and discrete integration is modeled by adding a delay determined from the phase distortion. As has been stated earlier, such an approximation probably accounts for the major source of difficulty of discrete integration in closed-loop control. However, to employ it exclusively is to leave us somewhat uncertain as to the closed-loop significance of the amplitude distortions.

It was found[5] that very good approximations to discrete Bode responses could be obtained for the longitudinal control tasks that are to be analyzed later. These approximations involved perturbation of aircraft stability derivatives and CAS parameters to yield continuous modes that agreed with the discrete modes. In the case of A-B integration, it was also necessary to introduce a zero in the continuous vehicle transfer in order to reproduce the amplitude distortion introduced by this integration scheme.

When Equation (17) is substituted in (14), the basic result is that for the frequency range likely to be of interest in continuous aircraft control problems, the simulator transfer function can be modelled as

$$\frac{Y(s)}{u(s)} = \tilde{D}(s)e^{-\tau_s s} \tag{18}$$

where D(s) is an "approximation" to the Bode response for digital integration of the vehicle dynamics. The simulator delay, is given by

$$\tau_s = \tau_F + \tau_H + \tau_V + \tau_C \tag{19}$$

where τ_F, τ_H, τ_V and τ_C respectively, are the delays introduced by the de-aliasing filter, hold, visual servo and CPU (discrete integration).

The approximation of Equation (18) readily lends itself to efficient application of the OCM. The system matrices corresponding to a state representation of $\tilde{D}$ and the values for τ_s are easily obtained for different sample periods, etc. For each condition, a single run of the OCM is sufficient to predict the corresponding performance. Adjustment of pilot parameters, specifically observation noise levels, allows the sensitivity to pilot attention to be examined.[9]

3. THE HYBRID MODEL

There are shortcomings in the continuous model. For example, the effects of aliasing are not considered. Thus, the degrading effects of the de-aliasing filter are included in the continuous model but not its benefits. This means that decreasing the bandwidth, ω_c, of that filter can only lead to negative results, a situation that is not obviously true, in general. Similarly, because only the delays inherent in the data holds are considered, zero-order holds will always show less degradation than first-order holds. But, in some instances, the first order hold may provide advantages that outweigh the additional delay penalty. This type of trade-off cannot be explored with the continuous OCM without more sophisticated approximation to the simulator dynamics. Because of these and other potential shortcomings, it was decided to develop a hybrid model.

The approach to developing the hybrid model is to "simulate" the closed-loop simulation. A discrete simulation version of the OCM[10] was used in a closed-loop digital Monte Carlo type computation* in which "continuous" elements of the loop are updated at a rate significantly greater than discrete elements. In other words, the hybrid model is a multi-rate sampling system, rather than a true hybrid system. (Informal experimentation indicates that a sample rate five times that of the discrete elements is adequate to simulate continuity for the cases considered here.) In addition, to different sample rates for continuous and discrete elements, the updating of the discrete equations of the hybrid model is different for the two kinds of elements. In particular, discrete elements are updated by means of the integration scheme and time-step specified for the "true" simulation. The equations for continuous elements are updated at the faster rate via transition matrix methods.

The equations describing the hybrid model are quite complex and are described in detail in Reference 5. Here, we simply note two features of the model that are interesting and useful in subsequent analyses. First, the hybrid model was implemented so that the prediction time in the predictor of the OCM (See Figure 2) could be selected arbitrarily. This contrasts with the standard OCM in which the prediction time is always equal to the time delay. This additional freedom allows us to "sweep out" curves of performance versus prediction time. Theoretically, best performance should be obtained when the prediction time is equal to the sum of the human's delay and the simulator's delay, i.e. when the operator compensates optimally for both delays. Since the human's delay is an assumed parameter, the compensation time for best performance yields an independent measure of the simulator delay.

A second feature of the hybrid model is that the internal model for the OCM need not be the same as the system model.* This flexibility provides the hybrid model with a capability for examining transfer-of-training questions. In addition, since optimal performance should correspond to the operator's model being equivalent to the system model, the hybrid model can be used to evaluate different (internal) approximations to the discrete simulation.

A final point concerning the hybrid model is worth noting. Because it is a Monte Carlo model, it normally will require many computer solutions to obtain meaningful statistics. In the analyses to be performed here, however, we are interested in the steady-state response of stationary systems. Rather than average over many Monte Carlo solutions, we have assumed ergodicity of the processes and utilized time-averaging of a single response. Even with this simplification, it is fairly expensive computationally to obtain valid statistical results.[5]

---

*A truly hybrid (analog/digital) model is possible but would require a hybrid computer (which was not available).

*Indeed, the system model can even be nonlinear.

4. AN EXAMPLE

The models for closed-loop analysis of simulator effects have been applied to an "example" simulation involving air-to-air target tracking. Results have been obtained for both longitudinal and lateral control tasks, for augmented and unaugmented dynamics and for different target motions. In addition, the effects of changes in design parameters of each simulation component have been explored. The full range of results may be found in Reference 5. Here, a sample of the results is presented to show the extent of the simulation effects and the capabilities of the closed-loop models.

4.1 The Tracking Problem

Figure 4 shows the geometry of the air-to-air tracking in the longitudinal plane. The gunsight is assumed to be fixed and aligned with the aircraft body axis. For longitudinal tracking, we will assume that no information concerning the target's pitch angle, ϕ nor the relative aspect angle is available. The pilot's task is assumed to be that of minimizing the mean-squared, line-of-sight

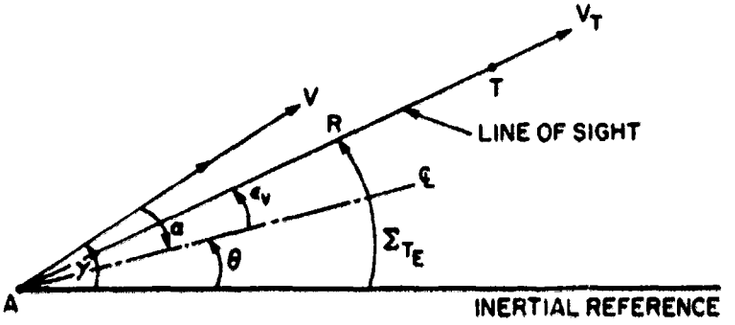

Σ_{T_E} = INERTIAL LINE-OF-SIGHT ANGLE (ELEVATION)
R = TARGET RANGE
ϵ_v = ELEVATION TRACKING ERROR = $\Sigma_{T_E} - \theta$

Figure 4. Target Geometry

tracking error ϵ_v.

The target is assumed to execute random vertical evasive maneuvers. In particular, target altitude variations are generated by passing white, gaussian noise through a third order filter as illustrated below.

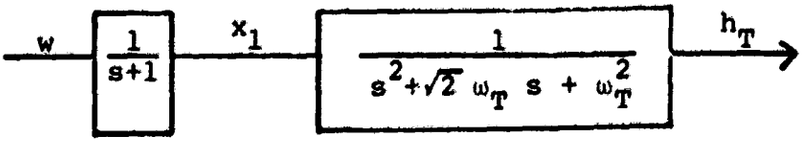

By selecting the covariance of the white noise and the cutoff frequency of the Butterworth filter, rms altitude variations and normal accelerations may be specified. Here, a cutoff frequency of $_t$ = .5 rad/sec was used and the noise covariance was chosen to give an rms altitude variation of 267 ft. and an rms acceleration of 3.1 g. Of course, the linearity of the problem allows us to scale the results to correspond to higher or lower accelerations.

The longitudinal short-period dynamics of the F8 without augmentation will be the baseline dynamics. The relevant equations may be found in Reference 5. The short period dynamics have a natural frequency of 2.28 rad/sec and a damping coefficient of .29; this represents poor short period handling qualities.[2] Because of this, and because we are interested in the effects of simulation parameters as a function aircraft dynamics, a set of augmented longitudinal dynamics will also be considered. A pitch command augmentation system (CAS) is used to modify the base airframe characteristics. The CAS design is a modified version of the design proposed in Reference 11.

The equations for the augmented dynamics are given in Reference 5. The F8 with the pitch CAS has short period roots with a natural frequency of 2.78 rad/sec and a damping coefficient of .64; this constitutes a significant improvement in the short period handling qualities.[2]

5. MODEL RESULTS

5.1 Continuous Model

The continuous model was used to analyze the effects of both simulation parameters and problem variables. With respect to the simulation, the effects of sample period and integration scheme are presented for the longitudinal CAS-OFF dynamics. Problem dependent effects are illustrated by comparing CAS-OFF and CAS-ON results.

We define a basic simulation configuration, corresponding to Figure 3, in which the cutoff of the de-aliasing filter is set at half the sample frequency, the visual servo has the DMS characteristics (ζ = .707, ω_n = 25 rad/sec), and a zero-order hold is used in data reconstruction.

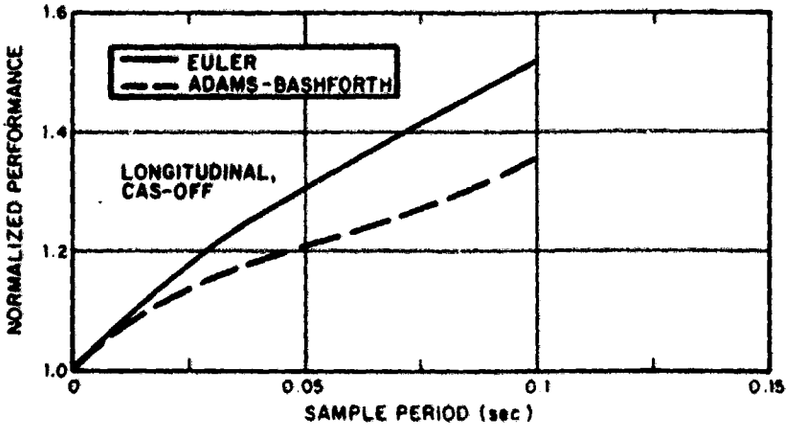

Figure 5. Effect of Discrete Simulation on Normalized Performance

Figure 5 gives normalized performance for the basic configuration as a function of sample period and integration scheme. Normalized performance is defined as the tracking error obtained for the simulation configuration divided by the tracking error that would be obtained in a continuous simulation with no delays (or in flight).* The normalization is determined by computing the performance utilizing the original, continuous state equations and assuming the only delay is that of the operator (.2 seconds).

Figure 5 shows substantial effects are introduced by the simulation, particularly at low sample rates. Even for the highest sample rate (T = .03125), there is a 16-20 percent performance degradation. A change of this magnitude exceeds the normal intra- and inter-subject variability in manual tracking tasks and would, therefore, be expected to be significant. For the lowest sample rates the performance degradation ranges from 35-50 percent, numbers that are clearly consequential. It is clear that, from a closed-loop tracking standpoint, A-B integration is superior to Euler integration.

The results in Figure 5 assume that the only adjustments in pilot strategy resulting from the simulation are an increase in prediction time to compensate for simulator delays and the adoption of an internal model that accounts for the amplitude distortions (and pole perturbations) introduced by the CPU. The results are based on the assumption of a fixed level of attention throughout. However, the pilot may choose to devote more attention to the task (work harder) and, thereby, reduce tracking error. A reasonable question to ask, then, is "How much more attention to the task would be required to achieve performance levels comparable to those that could be obtained in a continuous simulation?" This question can be addressed using the model for workload associated with the OCM.[9] The result of this analysis is shown in Figure 6.

*As might be the case in an all analog simulation with analog displays providing undelayed visual information.

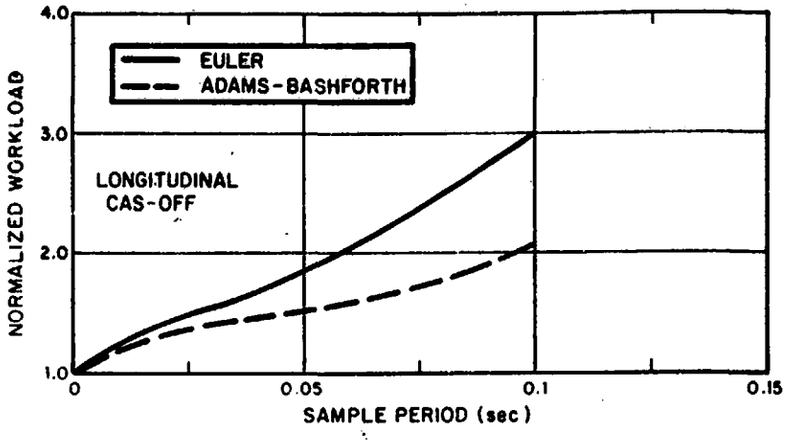

Figure 6. Simulation Workload Penalty

It can be seen from Figure 6 that to achieve the performance equivalent to that for continuous simulation, the pilot would have to increase his attentional workload by factors up to three for the conditions considered. There is a substantial workload penalty and it might be expected that a compromise between performance degradation and increased workload might evolve. This would be the case, especially if the pilot had not flown the vehicle or a continuous simulator in the same task so that there would be no basis for setting a criterion level of performance.

Before leaving the workload question, a further point is worth noting. In the describing function literature, it has been common practice to associate workload with the generation of lead. However, there has been no quantitative connection between the amount of lead and the increase in workload. In the present context, one can think of the increased prediction time necessary to compensate for simulator delays as imposing a (processing) workload analogous to that of lead generation. The measure of attentional workload given previously may then be thought of as an alternative means of quantifying the workload imposed by the requirement for additional prediction.

It was anticipated that there would be an interaction between the effects of simulation parameters and problem variables such as vehicle handling qualities. Thus, the above tracking task was analyzed for the CAS/ON configuration.

Figure 7 compares normalized longitudinal CAS-ON and CAS-OFF performance for the basic simulation. It can be seen that the CAS-ON performance is degraded more by the discrete simulation than the CAS-OFF performance. These results are explained by the fact that the delays introduced by digital integration are larger for CAS-ON dynamics than they are for CAS-OFF dynamics. The effects of longitudinal dynamics when viewed in terms of absolute performance are interesting and are also shown in Figure 7. The absolute performance for continuous simulation is better for CAS-ON than CAS-OFF (by about 3.5 percent) and the sensitivity to incremental computation delay is about

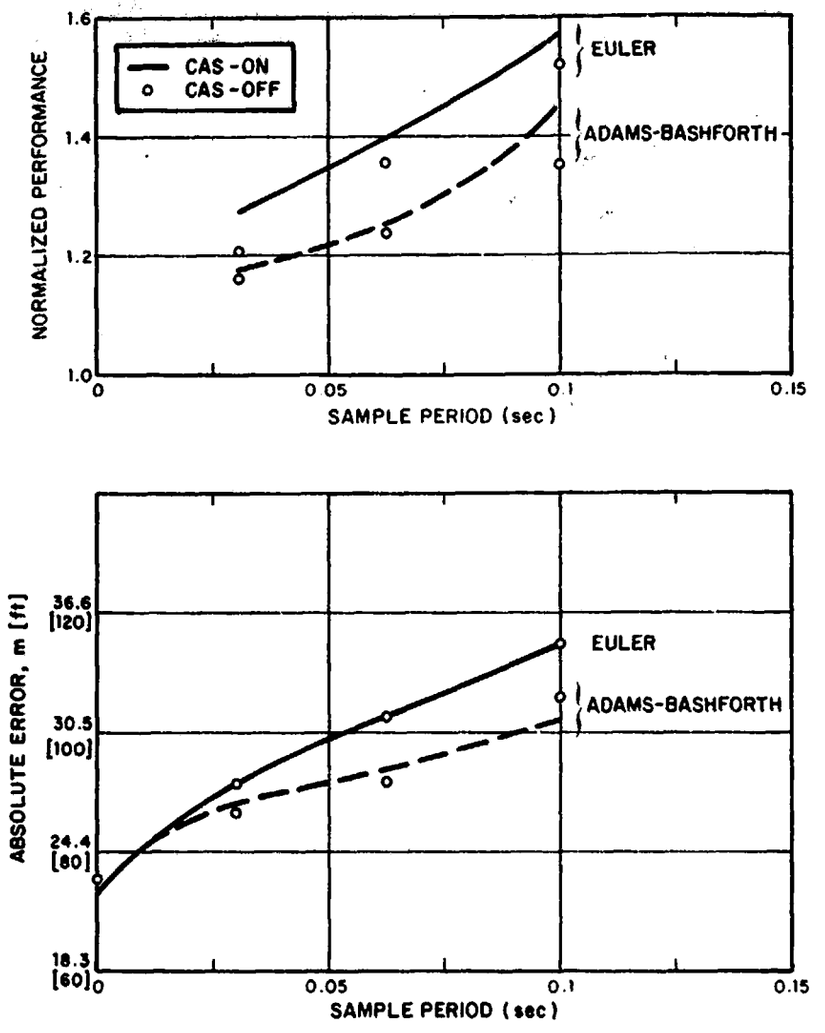

Figure 7. Effect of Vehicle Dynamics

the same for the two configurations. Thus, for a given simulation configuration, absolute performance for CAS-ON and CAS-OFF configurations will be about the same if Euler integration is used and the CAS-OFF configuration can give better performance if A-B integration is used. In other words, the discrete simulation washes out any improvement due to the CAS!

5.2 Hybrid Model

The hybrid model was used to investigate several issues that could not be examined readily in the continuous model context. Results were limited to the longitudinal unaugmented dynamics because of cost and time considerations

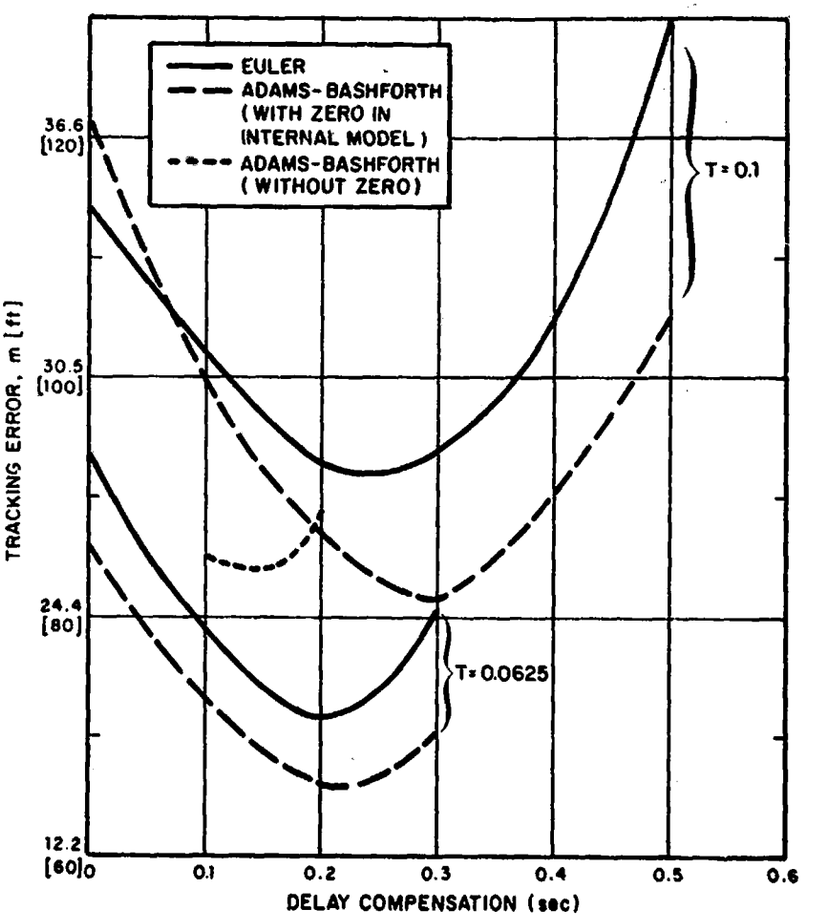

Figure 8. Effect of Operator Prediction Time

Figure 8 shows the sensitivity of performance to delay compensation time* for the basic simulation configurations with both Euler and A-B integration and

*The prediction time in excess of that needed to compensate for the operator's intrinsic delay of .2 sec.

for T = .1 and T = .0625. The "internal" models for the OCM in these cases are the continuous approximations to the discrete transfers that incorporate amplitude distortion effects; however, no delay is added to the human's delay of .2 seconds to account for the simulations delays. Thus, we expect the optimal prediction times to be approximately equal to the delay introduced by the simulation. This is indeed the case as can be seen in Figure 8. For Euler integration the minima occur at ~.26 sec and ~.2 sec. for T = .1 and .0625, respectively; the corresponding simulation delays are .27 and .19 .

For A-B integration the minima are at larger compensation times than for Euler. This is a result of the method used to account for amplitude distortion. (Recall that a zero was introduced in the transfer function and this necessitated an increased transport delay to match the phase lag at mid-frequencies.) With T = .1, the optimal prediction time is around .3 seconds and the simulation delay is ~.32 seconds. For T = .0625, performance does not appear to be very sensitive to prediction time in the neighborhood of the optimum. The simulation delay is ~.21 seconds and performance for this prediction time is indistinguishable from optimal performance. Figure 8 also shows a curve for the case where the operator's internal model does not include a zero to match the amplitude distortion of A-B integration. It can be seen that for this case a delay compensation of only ~.17 seconds is required. This corresponds to the delays introduced by the servo, pre-filter and zero-order hold. The optimal performance is marginally poorer than for the case with amplitude distortion included in the internal model. These results suggest that although including the zero provides a better model of the effect of A-B integration, the increased delay compensation needed to offset the extra lead should not be viewed here as a workload penalty.

These results confirm the estimates of simulation delay used in the continuous model. They also demonstrate implicitly how operators may adapt their behavior to compensate for simulator inadequacy. The added prediction required may impose a workload penalty as noted earlier.

Another form of adaptation to the simulation involves the pilots internal model. Two questions are of interest: 1.) What model will the trained operator adopt when "flying" the simulator?; and 2.) What is the "transfer" effect of a wrong model when transitioning from discrete simulator to continuous simulator (flight)? At least partial answers to these questions for the longitudinal dynamics and Euler integration are provided by the results shown in Figure 9.

Figure 9 gives performance vs. delay compensation for T = .1 and two internal models. One internal model is that derived to match the corresponding discrete transfer function while the other is the basic continuous model. It can be seen that better performance is obtained when the internal model corresponds to the approximate discrete model implying that this is a better model of the discrete simulation than is the original continuous model. Figure 9 also shows the effect of using the model corresponding to T = .1 seconds in a simulation where the actual sample period is .03125 seconds (i.e., nearly continuous) as compared to using the model for T = .03125 seconds (i.e., the correct one). If the operator optimizes delay compensation, performance will be degraded by about 10%. If, on the other hand, the delay compensation appropriate to T = .1 is used, a performance penalty of about 19% will be incurred. The effect is not substantial here but it might be in other tasks.

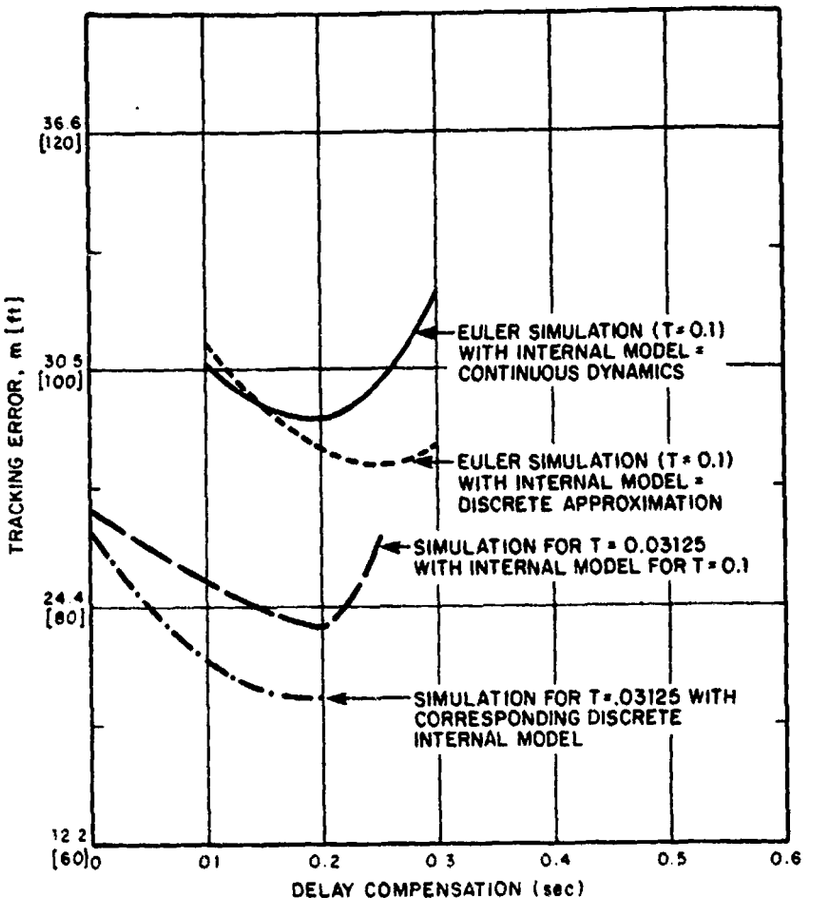

Figure 9. Effect of Internal Model

The effect of the cutoff frequency of the de-aliasing filter on performance is shown in Figure 10. Euler integration of the vehicle equations is used and other simulation parameters correspond to the basic configuration. The results are for a sample frequency of 10 Hz (T = .1) so a cutoff frequency of ω_c = 5 Hz satisfies the Nyquist requirement. Results are obtained for ω_c = 1, 5 and 20 Hz, respectively. The lowest value of ω_c = 20 Hz is based on the assumption that there is not significant signal power beyond 5 Hz so there is no need to set the filter break-point at that frequency and incur the delay penalty. The results in Figure 10 favor using the higher cutoff frequency, ω_c = 20 Hz, for this problem. Furthermore, there is a substantial penalty for using the low frequency cutoff. These two results imply that aliasing is not a problem here. We also note that the performance minima for ω_c = 20 Hz and 5 Hz occur at about the correct value of prediction time; the optimum prediction time for ω_c = 1 Hz

is much larger but not quite so large as the estimated total simulation delay of

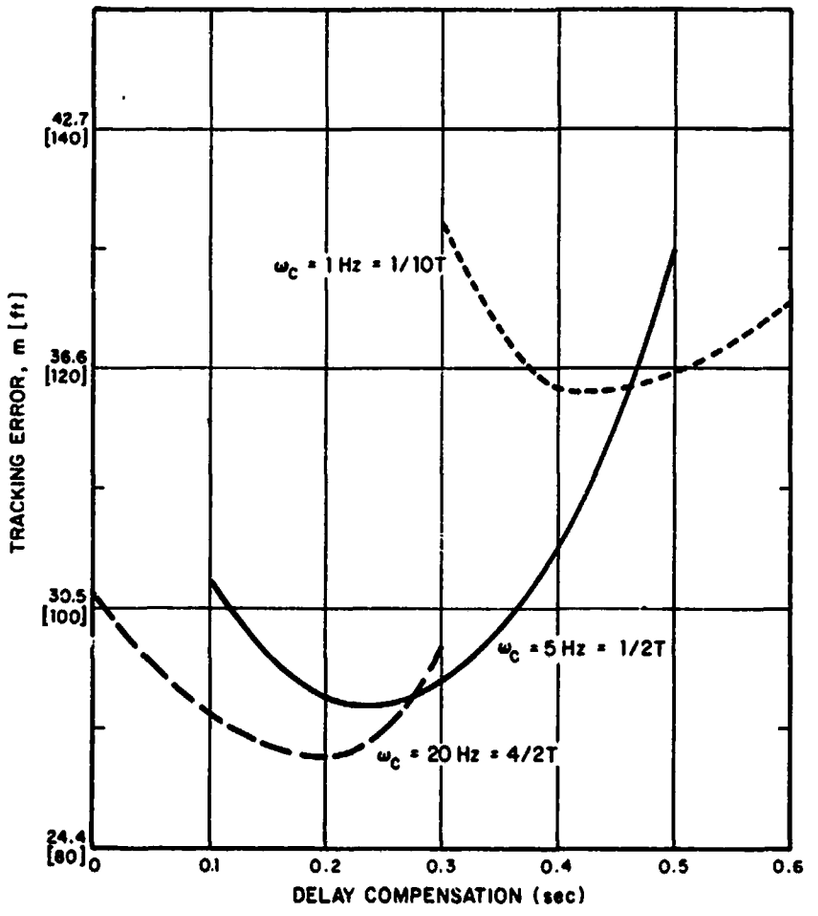

Figure 10. Effect of Dealiasing Filter Cutoff Frequency

.53 seconds.

The effects of using a first order hold instead of a zero order hold are shown in Figure 11 for both Euler and A-B integration at T = .1 and for Euler integration at T = .0625. The corresponding best zero order hold performance values are also shown for comparison purposes. At a sample period of .1 seconds, slightly lower tracking errors are obtained for Euler integration with a first order hold than with a zero order hold; in addition, the minimum performance is obtained with less delay compensation. The situation for A-B integration and a .1 second sample period is the reverse of that for Euler. That is, for A-B integration the first order hold degrades performance.

A possible explanation for these results is as follows. The first order hold uses intersample information which provides some lead. For long sample

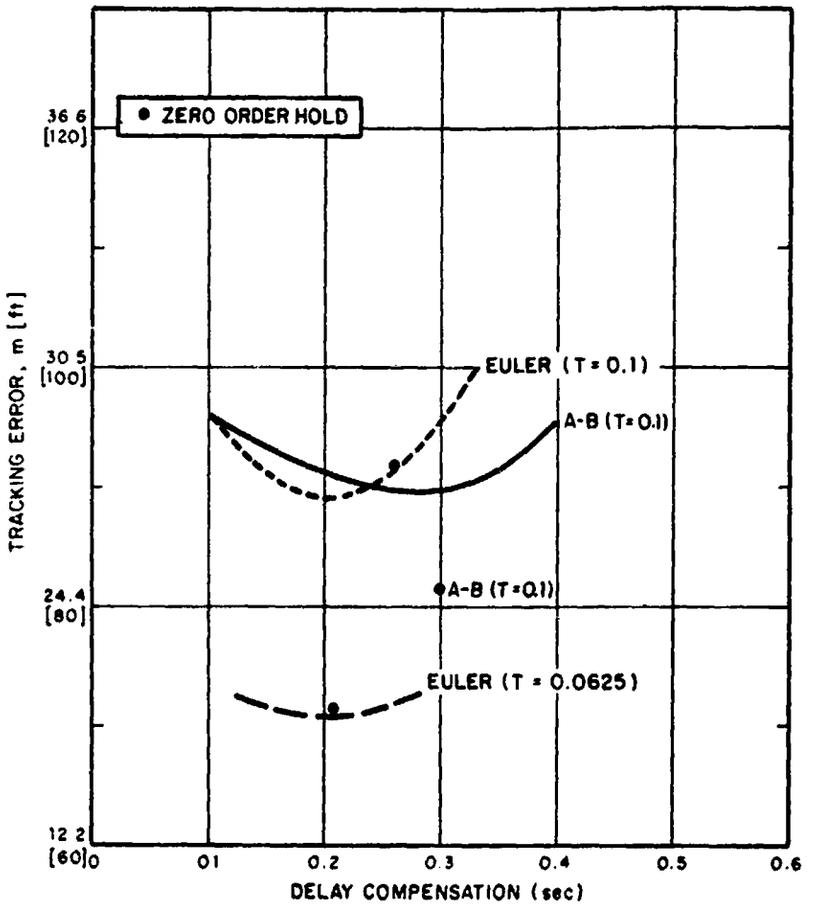

Figure 11. Effect of First Order Hold

periods and Euler integration, the effective lead provided is apparently more beneficial than the lag penalty associated with the higher order hold. The beneficial effects of a first order hold should decrease as the sample period decreases. This is supported by the results for T = .0625 which show no difference between the two holds. In the case of A-B integration the added delay of the first order hold dominates. This may be due to A-B integration having an implicit first order hold at the input, thereby reducing any advantage in adding such a hold at the output.

6. SUMMARY AND CONCLUSIONS

In this paper we have examined the effects of simulation parameters and components on simulator fidelity, particularly with regard to predicting operator performance and workload. Our focus has been on the dynamical aspects of simulator primarily as they relate to closed loop control. We have generally ignored questions that would necessitate inclusion of detailed models for cue perception leaving these to future study.

An approximate continuous model of the discrete simulation was incorporated in the standard optimal control model for the human operator. The resulting continuous closed-loop model was used to analyze both overall simulation effects and the effects of individual elements. The results showed that, as compared to an ideal continuous simulation, the discrete simulation could result in significant performance and/or workload penalties. The magnitude of the effects depended strongly on sample period as expected. From a closed-loop standpoint it seemed clear that A-B integration was much to be preferred. With respect to the other simulation components it can be said that any reduction in delay is desirable. Such reductions inevitably involve increased costs (hardware or software) which must be balanced against the expected improvements.

In addition to the continuous model, a hybrid model was developed to allow investigation of situations that could not be treated adequately with the continuous model. Several interesting results were obtained with this model. It was shown that for this (fairly typical) aircraft control problem signal bandwidths were such that the de-aliasing filter cutoff frequency could be set at a value greater than half the sample frequency. Also, there appeared to be a potential under certain conditions for improved simulator performance with a first order hold (rather than a zero order hold). The model was also used to show demonstrable effects for adopting the simulator dynamics as an internal model. The need to compensate for simulator delays via added prediction was also shown.

We believe the models developed here can be very useful in developing engineering requirements for flight simulators. These requirements will be problem dependent which is one reason why models are needed. As we see it now, the process for using the models would involve the following steps:

i) Use standard OCM to analyze ideal continuous simulation to develop baseline performance and to determine expected signal bandwidths.

ii) Analyze distortion introduced by discrete integration schemes and develop continuous models for discrete dynamics valid over the band of interest.

iii) Analyze effects of integration, cue dynamics etc. using continuous model.

iv) Use hybrid model to examine effects of data reconstruction, de-aliasing cutoff frequency etc.

Before this procedure could be used with complete confidence the models described herein need further validation and extension. It is especially important to collect data in a carefully controlled experiment to verify the individual simulation effects.

REFERENCES

1. Gum, D. R. and W. B. Albury, "Time-Delay Problems Encountered in Integrating the Advanced Simulator for Undergraduate Pilot Training," **Journal of Aircraft**, Vol. 14, No. 4, April 1977.

2. Queijo, M. J. and D. R. Riley, "Fixed-Base Simulator Study of the Effect of Time Delays in Visual Cues on Pilot Tracking Performance," NASA TN D-8001, October 1975.

3. Kleinman, D. L., S. Baron and W. H. Levison, "An Optimal Control Model of Human Response," **Automatica**, Vol. 6, No. 3, pp. 367-384, May 1970.

4. Baron, S., "A Model for Human control and Monitoring Based on Modern Control Theory", **Journal of Cybernetics and Information Science**, Vol. 1, No. 1, Spring 1976.

5. Baron, S., R. Muralidharan and D. L. Kleinman, "Closed Loop Models for Analyzing Engineering Requirements for Simulators", Bolt Beranek and Newman Inc., Report No. 3718, May 1978.

6. Baron, S. and J. Berliner, "The Effects of Deviate Internal Representations in the Optimal Model of the Human Operator," **Proceedings of Thirteenth Annual Conference on Manual Control**, M.I.T., Cambridge, Mass., June 1977.

7. Rosko, J.S., "Digital Simulation of Physical Systems" Addison-Wesley Publishing Co., Reading, Mass., 1972.

8. Ashworth, B.R. and W. M. Kahlbaum, Jr., "Description and Performance of the Langley Differential Maneuvering Simulator," NASA TN D-7304, NASA, Langley Research Center, June 1973.

9. Levison, W. H., J. I. Elkind and J. L. Ward, "Studies of Multi-Variable Manual Control Systems: A Model for Task Interference," NASA CR-1746, May 1971.

10. Kleinman, D. L., S. Baron and J. Berliner, "MCARLO: A Computer Program for Generating Monte-Carlo Trajectories in a Time-Varying Man-Machine Control Task," U.S. Army Missile Research and Development Command, Tech. Report TD-CR-77-2, Redstone Arsenal, Ala., June 1977.

11. Hartmann, G. L., J. A. Hauge and R. C. Hendrick, "F-8C Digital CCV Flight Control Laws," NASA CR-2629, February 1976.

N79-15599

PROSPECTS OF A MATHEMATICAL THEORY OF HUMAN BEHAVIOR IN COMPLEX MAN-MACHINE SYSTEMS TASKS*

Gunnar Johannsen** and William B. Rouse

Department of Mechanical and Industrial Engineering
Coordinated Science Laboratory
University of Illinois
Urbana, Illinois 61801

SUMMARY

Many useful mathematical models for manual control monitoring and decision-making tasks in man-machine systems have been designed and successfully applied. However, critical comments have occasionally been made, mainly by practitioners concerned with the design of complex man-machine systems. They blame especially models which seem to explain only data from abstract subtask experiments designed particularly for these models.

In this paper, an initial approach to bridging the gap between these two points of view is presented. From the manifold of possible human tasks, a very popular baseline scenario has been chosen, namely car driving. A hierarchy of human activities is derived by analyzing this task in general terms. A structural description leads to a block diagram and a time-sharing computer analogy.

The range of applicability of existing mathematical models is considered with respect to the hierarchy of human activities in real complex tasks. Also, other mathematical tools so far not often applied to man-machine systems are discussed. The mathematical descriptions at least briefly considered here include utility, estimation, control, queueing, and fuzzy set theory as well as artificial intelligence techniques. Some thoughts are given as to how these methods might be integrated and how further work might be pursued.

* This research was supported by the National Aeronautics and Space Administration under NASA-Ames Grant NSG-2119.

**Permanent address: Research Institute for Human Engineering (FAT) D-5309 Meckenheim, F.R. Germany

INTRODUCTION

When designing such systems as automobiles, aircraft, power plants, and management information systems, it is very important to understand the human's role in the system and design the man-machine interface appropriately. The engineering approach, which leads one to represent the machine in terms of differential equations, networks, etc. suggests that the human can also be represented as a set of mathematical equations for the purpose of systems analysis and design. Thus, considerable effort has been devoted to developing mathematical models of human behavior.

Despite the criticisms of those who find the analogy between humans and equations unpalatable, many models have been reasonably successful within the limited domains that they addressed. In fact, if we accept the premise that human behavior mainly reflects the external environment [1], then it is not surprising that man and machine can be described in similar terms. Quite simply, since the human adapts his behavior to the machine, his actions become somewhat machine-like. (Of course, from a design point of view, one tries to avoid requiring the human to adapt to the machine to any extreme extent.)

On the other hand, the success of models in limited domains has not had substantial impact in realistically complex domains. For example, manual control models are not everyday tools for the aircraft designer. Further, as the reader will see manual control models capture only a small portion of the total task of driving an automobile. For these reasons, designers have been known to claim that mathematical models of human behavior are not particularly useful. While the authors only partially agree with this opinion, even as it relates to currently available models, such statements have motivated the work upon which this paper is based.

Within this paper, the authors present a realistically complex task (i.e., automobile driving) and illustrate the various aspects of the task by using written protocols of subjects' behavior. A hierarchy of human activities is derived by analyzing this task in general terms. A time-sharing computer analogy and block diagram are presented. Numerous mathematical methodologies appropriate to representing such a model are discussed. Finally the state-of-the-art is summarized and the prospects are considered.

A REALISTIC TASK

In considering alternative realistic task domains, the authors discussed a variety of domains including aircraft piloting, industrial process monitoring, and automobile driving. After substantial discussion, it became quite clear that the domain to which both the authors and potential readers could most relate was automobile driving.

The "experiment" involved a hypothetical trip from the driveway of one author's house (GJ) to the home of the other author (WR). Two subjects participated (GJ and WR). Their task was to explain in detail what they would be doing throughout the hypothetical trip. Each subject independently generated a written protocol of the trip. The two resulting protocols were merged to produce Figure 1.

The activities in this figure can be categorized into several levels of behavior:

1. Reaching, twisting, and listening
2. Steering, accelerating, and braking
3. Looking around and estimating
4. Updating and evaluating
5. Planning
6. Reflecting and daydreaming

The authors would like to suggest that a theory of human behavior in realistic tasks should be able to model levels 1 through 5. In pursuit of this possibility, this list was somewhat compacted to yield the following aspects of behavior to be modeled:

1. Sensing and interpreting inputs
2. Planning
3. Implementing plans

To consider these three topics, an overall framework will be discussed in the next section and then, specific approaches to modeling will be considered in the subsequent section.

STRUCTURAL DESCRIPTION

Looking at the hierarchy of human activities discussed above as information processing activities, a time-sharing computer analogy seems to be a very appealing approach to understanding the structural interrelationships.

Figure 2 shows a sketch of such a time-sharing computer analogy. There are several possibilities for the central nervous system (CNS) to interact with the peripheral input and output devices (i.e., the sensory and the motor systems including speech generation). The CNS is viewed as being divided into an operating system and four classes of jobs," i.e., program/data files (see, e.g., [2], [3]). Hereby, a multi-processor system allowing a mixture of parallel and serial information processing is most likely to be a reasonable assumption for the human operator [4].

The operating system is responsible for scheduling the programs in a time-shared manner by using a priority interrupt policy. Conflicting criteria with respect to priority have to also be evaluated by the operating system. This might be a crucial task, especially in urgent situations.

Figure 1: Protocol for Typical City Trip

INSERT KEY IN IGNITION

PUT ON SEAT BELT

PRESS GAS PEDAL TO FLOOR AND ALMOST TOTALLY RELEASE

TURN KEY

LISTEN FOR ENGINE SOUND

IF SO, THEN GIVE GAS

ELSE, STOP AND GO BACK TO TURN KEY

WAIT FOR CAR TO WARM UP - DAYDREAM

LOOK AROUND - SEE IF I CAN BACK UP OKAY - INCLUDES USING MIRRORS

IF SO, THEN PUT CAR IN REVERSE

ELSE, WAIT FOR ALL CLEAR

PUT RIGHT ARM ON SEAT BACK SO AS TO SEE BETTER

STEER WITH LEFT ARM, ACCELERATE AND BACK ONTO STREET

DETERMINE WHEN CLEAR TO GO FORWARD - STOP BACKING UP - PRESS BRAKE

PUT CAR IN DRIVE

LOOK AROUND - SEE IF I CAN PROCEED

IF SO, ACCELERATE

ELSE, WAIT FOR ALL CLEAR

LIMIT SPEED SINCE STOP SIGN COMING UP - CONTINUE LOOKING AROUND

STEER SO AS TO STAY "SORT OF" IN LANE

ESTIMATE DISTANCE TO STOP SIGN - CHECK FOR TIME TO DECELERATE

IF SO, REMOVE FOOT FROM GAS AND OVER TO BRAKE

ELSE, UPDATE ESTIMATE OF DISTANCE - CONTINUE LOOKING AROUND/STEERING

TURN ON LEFT DIRECTIONAL

WHEN FAIRLY CLOSE TO STOP SIGN, PUSH BRAKE HARDER AND STOP

LOOK LEFT AND RIGHT FOR TRAFFIC

IF NONE TOO CLOSE (ESTIMATE IF I CAN MAKE IT). ACCELERATE, TURN LEFT

ELSE, WAIT FOR ALL CLEAR AND CONTINUE UPDATING ESTIMATES

STRAIGHTEN OUT SO AS TO KEEP "SORT OF" IN LANE

ACCELERATE, BUT NOT TOO MUCH BECAUSE STOP SIGN COMING UP

LOOK AROUND AT TRAFFIC - ALSO AT HOUSES AND YARDS - DAYDREAM

EXECUTE STOP SIGN ROUTINE - ONE FOR STOPPING - ONE FOR STARTING

- USE FOUR-WAY STOP SIGN ROUTINE

EXECUTE ENROUTE ROUTINE - INCLUDING TALKING, SIGHTSEEING, ETC.

•

•

PLAN ROUTE - WHAT STREETS TO TAKE

•

•

EXECUTE STOP SIGN/STOP LIGHT/TURNING/PASSING/LANE CHANGING ROUTINES

LOOK AROUND FOR APPROPRIATE PARKING SPACE

IF ONE FOUND, DETERMINE PLAN FOR GETTING INTO IT

ELSE, CONTINUE LOOKING - CONTINUE LOOKING AROUND AND STEERING

EXECUTE PLAN OPEN-LOOP, WITH FINAL UPDATES AS ERRORS CAN BE ESTIMATED

PUT CAR IN PARK

TURN OFF RADIO HEATER, ETC., IF APPROPRIATE

TURN OFF KEY

REMOVE KEY

The four classes of program/data files relate to a central-nervous representation of tasks the human operator has to perform. Each of these program classes is structured into main programs and interrelated subroutines.

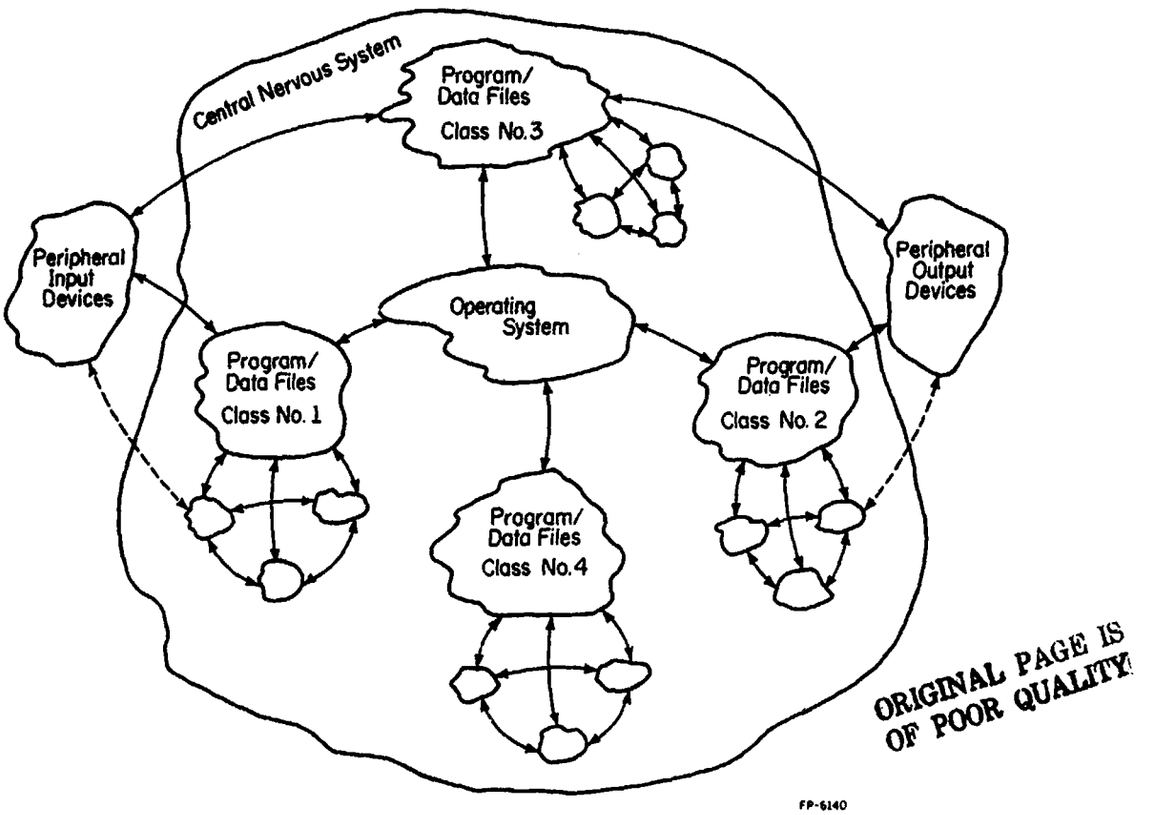

ORIGINAL PAGE IS
OF POOR QUALITY

Figure 2: Sketch of a Time-Sharing Computer Model of the Human Operator

Class No. 1 comprises input-related programs, e.g., human monitoring tasks and looking around procedures. Class No. 2 is similarly related to output activites, e.g., the structural organization of motion patterns (e.g., in reaching) and speech. Class No. 3 programs describe strict input-output relationships as in tracking-type control and choice-reaction tasks. All three classes contain programs with a high level of autonomy, perhaps carried out by peripheral processors. The operating system has to initiate and supervise these autonomous processes. Additionally, the adaptive control of the sampling process in parallel tasks has to be accomplished by the operating system.

Class No. 4 represents the long-term memory of the human which includes a knowledge base of facts, models, and procedures. The programs of class No. 4 are concerned with internal processes such as reflecting and planning which have access to the knowledge base, thereby occasionally

modifying it. The operating system is responsible for searching through the knowledge base (see, e.g., [5], [3]).

The time-sharing computer analogy outlined here is mainly assumed as a possible framework for future thinking about complex man-machine systems. To further illustrate the hierarchical multi-level structure of human activities within this framework, a block diagram is shown in Figure 3. Only the most important information flows between the different levels are outlined.

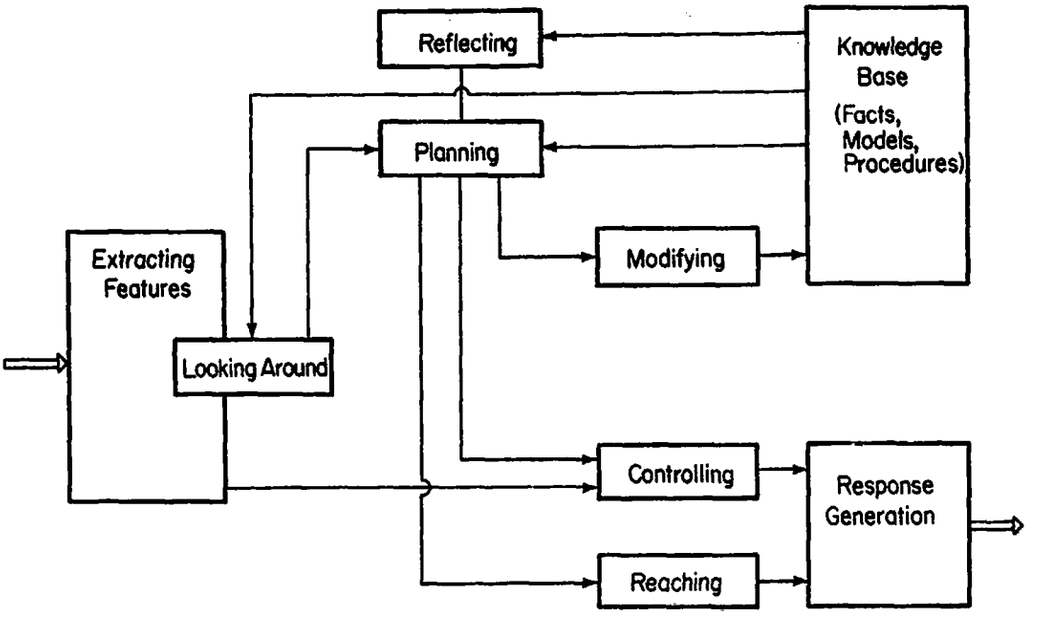

Figure 3: Hierarchical Multi-Level Structure of Human Activities

Lower level processes (bottom of Figure 3) are normally characterized by events occurring at a high frequency as compared to higher level processes (top of Figure 3). This refers to different time scales for different levels. However, because lower level processes may be autonomous, the difference in time scales does not mean that these processes have to be considered by the operating system more frequently.

In Figure 3, planning is denoted as a major activity. With data from the knowledge base and those from lower-level looking around procedures, sometimes influenced by higher-level reflecting, planning is the development of procedures to achieve overall goals and subgoals for lower-level processes. Modifying the knowledge base as well as goal-setting for controlling and reaching are shown as examples. Controlling itself is also best described as a multi-level structure, being a subset of the overall multi-level structure of Figure 3. Controlling and

reaching procedures result in output actions of the human operator via response generation which refers to the peripheral output devices in Figure 2. Correspondingly, the peripheral input devices of Figure 2 extract task-relevant features from sensory input information. This process is very closely linked with looking around procedures which are also indicated in Figure 3.

MATHEMATICAL MODELS

Sensing and Interpreting Inputs

Reconsidering the task analysis of car driving, how does the driver recognize stop signs, other cars, children, etc? Could one, at least in theory, develop an algorithm that successfully performs these aspects of driving?

To pursue this question, the literature of pattern recognition and artificial intelligence was considered. Fortunately, the literature in these areas has recently been summarized in the Systems, Man, and Cybernetics Review [6], by Sklansky [7], and in books by Winston [8], [9] for pattern recognition and artificial intelligence respectively.

Two approaches to pattern recognition have received particular attention: statistical methods and syntactical methods. The statistical methods use discriminant functions to classify patterns. This involves extracting a set of features from the pattern and statistically determining how close this feature set is to the a priori known features of candidate classes of patterns. The class whose features most closely match the measured features is chosen as the match to the pattern of interest, with of course some consideration given to the a priori probabilities of each class and the costs of errors.

The syntactic methods partition each pattern into subpatterns or pattern primitives. It is assumed that a known set of rules (a grammar) is used to compose primitives into a pattern. One approach to recognizing primitives is to use the statistical approach noted above.

Another aspect of pattern recognition involves image processing. here, each picture point (pixel) is classified according to gray level. Then, thresholds are used to segment the picture. More elaborate approaches use multi-dimensional classification of each pixel and then, use an appropriate multi-dimensional clustering of similar pixels.

Artificial intelligence researchers have devoted considerable effort to scene analysis. With emphasis on understanding scenes composed of somewhat arbitrary collections of blocks, methods have been developed to pick particular blocks out of scenes, even if the desired block is partially hidden.

Most of the methods discussed above have worked reasonably well within limited domains. When the context within which one is working is well-understood, it is often possible to successfully sense and interpret

inputs, although considerable computational power may be needed.

While the advent of inexpensive microelectronics might allow one to utilize large amounts of computational power in a model of human sensing and interpretation of data, there are bigger problems to be solved. Namely, it is difficult to deal with realistic contexts in a static manner. What a human sees depends on what he is looking for, what he expects to see, and the costs of not seeing it. These aspects of seeing cannot be considered out of context and without reference to the specific individual involved.

Several investigators have considered the issue of how the human allocates his attention among multiple displays [10], [11], [12], [13], [14]. However, these models have only been tested in fairly well-structured situations and thus, are as yet unproven in realistically complex tasks. Further, it is by no means obvious that these models will ever be able to handle looking around in the sense it appears in the driving scenario.

Thus, a general mathematical theory of human sensing and interpreting of inputs is far from available, especially if one would like to program this theory to drive a car. On the other hand, the disciplines of pattern recognition and artificial intelligence are beginning to succeed in specific applied domains such as industrial inspection [15], [16] and medical diagnosis [17]. Perhaps a concatenation of specific successes will lead to new insights into the problems of context and individual differences.

Planning

Studying the task analysis of car driving, it is readily apparent that much of the subjects' conscious activities were devoted to developing, initiating, and monitoring plans. This observation agrees with analyses of verbal protocols in several other task domains [1]. In fact, one might expect this result within any purposeful activity for which there are goals as yet unfulfilled.

To discuss planning, one first must emphasize the distinction between the process of developing plans and the process of executing plans [18]. Within this section only plan development will be considered, while the following section will discuss plan execution. One way to illustrate the difference between these two activities is to characterize plan development as a problem solving activity, while plan execution is looked at as a program execution activity [1].

One develops a plan in hopes that its execution will achieve some goals. While one usually accepts the overall goal as given (e.g., land the aircraft), the process of developing subgoals is often left to the human. The partitioning of goals into subgoals and then subgoals into lesser subgoals, etc. reflects a hierarchical mode of planning that has received considerable attention [19], [20].

The hierarchical approach allows one to develop plans that are broad and sketchy as opposed to detailed and concise. Thus, low level subgoals can be temporarily ignored until their immediacy demands attention. Similarly, future actions which require preconditions that are not as yet assured can perhaps be temporarily ignored if one feels that the environment is hospitable to one's goals [20].

On the other hand, low level subgoals must eventually be dealt with. Then, a concise system dynamics model such as Carbonell's probably provides a reasonable description of human behavior [21]. This model assumes that the human is dealing with a system describable by quantitative state transitions and amenable to quantitative control actions.

Such low level planning is probably unconscious. From the perspective of a computer analogy, one might say that high level conscious planning is like executing an interpreted program. (An interpreted program is one where the computer consciously has to interpret the meaning of each statement as it is executed.) On the other hand, low level unconscious planning is similar to executing a compiled program [1]. In fact, it might be claimed that low level planning cannot really be called planning. Instead, such activities are only the details of implementation, which are discussed later in this paper.

Planning appears to include the following aspects:

1. Generation of alternative plans,
2. Imagining of consequences,
3. Valuing of consequences,
4. Choosing and initiating plan,
5. Monitoring plan execution,
6. Debugging and updating plan,

where the latter three aspects deal with observing plan execution and subsequent replanning, but <u>not</u> with actual implementation.

How might one model the generation of alternative plans? One can look at a plan as a linked set of subplans [20]. However, at some level, subplans must be specific. In many tasks, the alternatives are clearly defined at the outset. On the other hand, there are many interesting tasks (e.g., engineering design) where the human must create alternatives. In such cases, humans usually first consider alternatives that have been successful in previous situations.

One might use Newell's pattern-evoked production systems as a model of how the human accomplishes this search for alternatives [1]. A production is a rule consisting of a situation recognition part that is a list of things to watch for, and an action part that is a list of things to do. (The word "production", as it is used here, has absolutely nothing to do with the manufacturing connotation of the word.)

As an alternative to production systems, the idea of scripts might provide a reasonable model, "A script is a structure that describes appropriate sequences of events in a particular context" [22].

The ideas of production systems and scripts are both related to the idea of the human having an internal model. However, as the reader will see, it is very different from the type of model assumed in the system dynamics domain. Namely, productions and scripts provide forecasts of typical consequences rather than models of internal state transitions.

Sometimes a new alternative is needed and it is very difficult to say how a totally new idea is generated. Linking the idea of associative memory [23], [24] with the idea of production systems or scripts, one can conjecture that new ideas are generated when the criterion for matching the new subgoal with past experiences is relaxed and/or non-standard features of the situation are emphasized.

Long-term plans that will not be immediately implemented are probably developed at the highest level in the goal hierarchy with only major goals considered. Such a plan might be a somewhat vague verbal statement or perhaps a sketch of activities and relationships. It is interesting to speculate upon (and perhaps research) what plans look like in the "mind's eye." For example, are plans list-like or are they more spatial, such as Warfield s interpretive structural models [25].

Short-term plans that will require immediate implementation cannot be quite so sketchy. In this case, the human has to consider specific actions. One would probably be reasonably successful in modeling this type of plan using production systems. In this case, specific features of the environment would automatically evoke particular responses. This type of behavior falls into the category of class No. 3 programs as defined in the time-sharing computer analogy introduced earlier. Realistic examples of application of this idea include aircraft attitude instrument flying [26] and air traffic control [27].

Given a set of candidate plans, the human must forecast or imagine the consequences of implementing each plan. One might assume that the human performs some type of mental simulation of the plan. For example, the human might use his current perception of the system dynamics to extrapolate the system s state as a function of planned control strategy. House has developed a model that describes this type of behavior. Succinctly, the model assumes that the human has both a long-term and short-term model of the system with which he is dealing and, that he uses a compromise between the two state predictions obtained from these models as a basis for decision making [28].

However, when plans are sketchy, at least in terms of intermediate preconditions, the human probably does not actually calculate consequences but instead simply maps plan features to previously experienced consequences. Then, until evidence forces him to reject the assumption, he assumes these previously experienced consequences will prevail. This type of behavior is represented quite nicely by the scripts concept [22].

Imagined consequences are then compared to goals. For low level plans, the comparison might be based on a well-defined criterion function. however, this is probably not the case for high level plans. Since high level goals and imagined consequences may be verbal and rather vague, it is likely that the human only tries to satisfice rather than optimize. One might represent this phenomenon using multi-attribute utility functions [29] that have broad optima. Alternatively, concepts from fuzzy set theory [30], [31] might be used to consider the membership of a set of consequences in the fuzzy set of acceptable consequences. The utility function approach is probably appropriate if one assumes that the human has a fairly precise knowledge of the possible consequences, and subsequently values some more than others. On the other hand, the fuzzy set approach would seem to be applicable to situations where the human s perception of the consequences is actually fuzzy.

The human chooses the most satisfactory plan and initiates its execution. If none of the available plans meets an acceptable level of satisfaction, the human either tries to debug the set of plans under consideration or perhaps tries to develop new plans. Debugging of partially failed plans may initially involve local experimentation to determine the cause of plan failure rather than a global reevaluation and complete replanning [32]. One approach to modeling debugging or trouble-shooting of plans is with fuzzy set theory [33].

Assuming that a plan has been initiated, the human monitors its execution and only becomes involved (in the sense of planning) if the unanticipated occurs or execution reaches the point that some phase of the plan must be more concisely defined. Monitoring for the unexpected might be modeled using production systems that trigger when the preconditions are not satisfied. Other approaches, based on filter theory [34] or pattern recognition methods [35], are also available but beyond the scope of the discussion here.

Once the unexpected has been detected, planning might shift into the above mentioned debugging mode. On the other hand, the need to shift from sketchy to concise planning may involve abandoning, for the moment, the broad hierarchical mode and shifting to a detailed partially pre-programmed mode.

How do all these bits and pieces fit into an overall model of planning? While it does seem that the hierarchical approach to planning combined with the production system and script ideas provide a reasonable framework, the state-of-the-art certainly does not allow one to construct a context-free planning model in the form of an executable computer program. This may be an inherent limitation if one accepts the premise that much of human behavior is merely a reflection of the task environment [1]. If this premise is true, then one should be very careful that laboratory abstractions capture a sufficient portion of the real world environment and thereby allow results to actually be transferable. Otherwise, one is only developing a theory of human behavior in laboratory games.

As a final comment on planning, a very important issue concerns the level at which one's study of planning behavior should be addressed. While an approach at the neuron level [36] may eventually lead to a successful model of human planning behavior, such an approach is unlikely to lead to success in the near future. Alternatively, one might try to develop models that explain or predict whether or not a plan will be successful. However, this type of model would yield little information about the planning process. It seems that one must approach studies on the conscious planning level using either verbal protocols [1], [37], [38] or at least methods that require plans to be explicitly measurable. Then, the variety of approaches to modeling discussed in this section can be applied to describing the planning process.

IMPLEMENTING PLANS

Implementing plans refers to human action, mainly controlling and reaching in the multi-level structure of Figure 3. Two basic approaches for mathematically describing these actions can be distinguished. The first approach includes time-line analysis, queueing theory, and simulation techniques, whereas the second includes the control theoretic approach in a more general sense.

In time-line analyses, the execution times of all particular task elements of a certain multi-task situation are assessed as well as the total task time needed [39], [40], [41], [42]. Available time margins or expected time pressure of the human operator can be calculated in order to estimate total task system performance and human operator workload. This method has been applied to evaluating rather complex man-machine systems by taking these apart in very much detail, e.g., to the level of reaching times for single switches.

A related but more analytical approach is the queueing theoretic one [11], [12], [43], [44], [45], [46], [47]. It is suitable not only for analysis but also for design purposes. The different tasks of a multi-task situation are considered as customers in a queue waiting to be serviced. Arrival and service rates as well as the waiting time for the tasks are characteristic measures. Service with a priority policy is possible. Also several servers (e.g., the human operator and a computer) may share responsibility for the total task.

Both approaches, time-line analysis and queueing theory, look at the implementation of actions in terms of time expenditure. If the accuracy of the actions is also to be taken into account, these methods have to be combined with others. Simulation techniques seem to be a reasonable approach where micro-subroutines simulate dynamically such human operator behaviors as short-term memory recall and movement of hands and feet [48]. This leads back to the time-sharing computer analogy. A goal-oriented priority interrupt structure for handling all tasks appropriately in a multi-task situation is most promising. However, this results in a more artificial-intelligence oriented simulation, using heuristics and data handling algorithms, rather than an analytical description.

A different approach for the description of human actions in man-machine systems applies control theory. Models for continuous manual control are well established. Numerous summaries in the forms of reports and books exist (e.g., [49], [50], [51]). Most popular are the quasi-linear and the optimal control models. The quasi-linear models describe the human control behavior by some task-specific modification of a generalized transfer function which is best satisfied in the crossover frequency region for many controlled element dynamics. In addition, an internal human noise source (the remnant) summarizes the portion of the human's output which cannot be explained linearly.

The optimal control model [52] includes two noise sources and also has a time delay and a neuromuscular lag term with a time constant similar to that of the quasi-linear model. A Kalman filter estimates the states of the controlled element, whereas a predictor compensates for the time delay. The optimal gains are calculated with respect to a criterion function which is a weighted sum of mean squared values of state and control variables.

The control theory models have been applied in several domains including aircraft piloting, automobile driving, ship piloting, and anti-aircraft artillery. Further, several display design methodologies have been developed. A recent special issue of Human Factors reviews many applications of control theory models [53].

With both the crossover model and the optimal control model, a stochastic reference input, either forcing function or disturbance, has been assumed. Therefore, these models are mostly applicable to the inner loops of manual vehicle guidance and control tasks. In the case of the optimal control model, key elements of this have also been applied to monitoring and decision-making tasks.

Many realistic tasks exist, however, in which deterministic inputs are dominant. Taking the baseline car driving scenario as an example, a more complicated deterministic input exists, i.e., the course of the street. For this task, a two-level model has been proposed which has a closed-loop stabilization controller and an anticipatory open-loop guidance controller working in parallel [54], [55]. The perceptual aspects of the anticipation of changes in the course of the street have been explained. However, it has been assumed that the driver tries to eliminate all deviations from the middle line of the street.

To overcome this simplification, the street might be viewed as a target tube in which the driver is allowed to move his car. Interestingly enough, many other human control tasks in vehicle guidance and industrial process control also require controlling the state of the system within a target tube rather than along a single reference line. Such a criterion makes these tasks much more relaxed than one often assumes in man-machine systems experiments.

Reviewing the control theory literature, some applicable methods for controlling within a target tube were found. They have never been used with man-machine systems problems. One approach assumes a criterion

ORIGINAL PAGE IS
OF POOR QUALITY

function which puts less weight on small errors by taking the fourth power of the error instead of the second power as in the optimal control model [56]. The other approach is called unknown-but-bounded control [57], [58], [59]. Figure 4 illustrates how the controller tries to keep the state (X) of the system always in an effective target tube to assure that it will never cross the boundaries of the outer target tube under all expected disturbances.

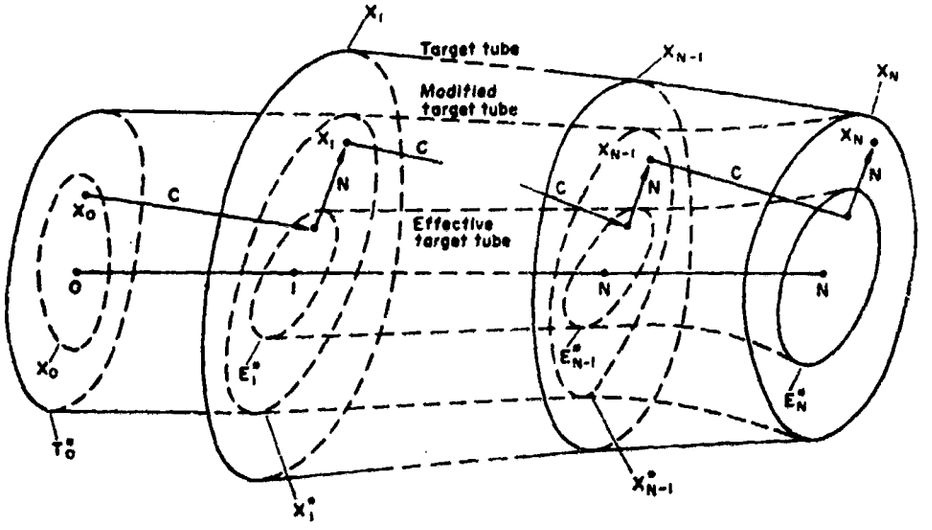

Figure 4: Schematic Presentation of the State of the System (X) as Affected by the Action of the Controller (C) to Counteract Disturbances (N) for Reachability of a Target Tube (from [57])

The unknown-but-bounded control approach combines state variable with set theoretic descriptions. Due to the higher mathematical effort, this approach has infrequently been applied in automatic control situations. However, it seems worthwhile to consider this approach in modeling biological or sociological systems. Human behavior in general is goal-oriented and the goal is very often defined as bringing or keeping some state variables within a certain target set or target tube.

In the baseline scenario, the target tube of Figure 4 would be the width of the street or one of its lanes. The effective target tube is planned by the driver as an area inside of which no control actions are necessary (see linear-plus-dead-band control laws in Glover and Schweppe [58]). Planning the effective target tube might also include some fuzziness. Whether the unknown-but-bounded control approach can be combined with fuzzy set theory which has recently been applied in industrial process control [60] has not as yet been investigated.

Another interesting issue is the notion of the internal model which has been considered to some extent in the discussion of the planning process. In modeling how the human chooses among alternative courses of action, an important issue concerns whether the human possesses a correct

internal model of his environment or, whether the model is incorrect as in learning situations or, very approximative as in large-scale systems (see, e.g., [61]). The process of building up an internal model during learning and how to use it by changing control laws or choosing among different kinds of control laws in time-varying systems, should be further investigated. The literature on adaptive manual control shows, for example, that the models assume a set of predetermined control laws matched with a set of different system dynamics (see e.g., [62]).

This leads to the idea of a memory for motor patterns. Instead of having an input-output transfer behavior, the human operator initializes predetermined motor patterns in many situations. These patterns are slightly corrected during their actual execution (see,e.g., [63]). Good examples are walking, bicycle riding, and piano playing. Also, the coordination and timing of a series of discrete manual control actions, e.g., in trouble-shooting tasks or in checking procedures of aircraft pilots or process operators, can be explained by predetermined motor patterns.

DISCUSSION AND CONCLUSIONS

In considering various approaches to tying all of the discussions in this paper together, the authors found the diagram in Figure 5 to be most useful. This diagram is a variation of a diagram discussed by Johannsen [64] for vehicle control tasks and Sheridan [1976] for human control of vehicles, chemical plants, and industrial robots.

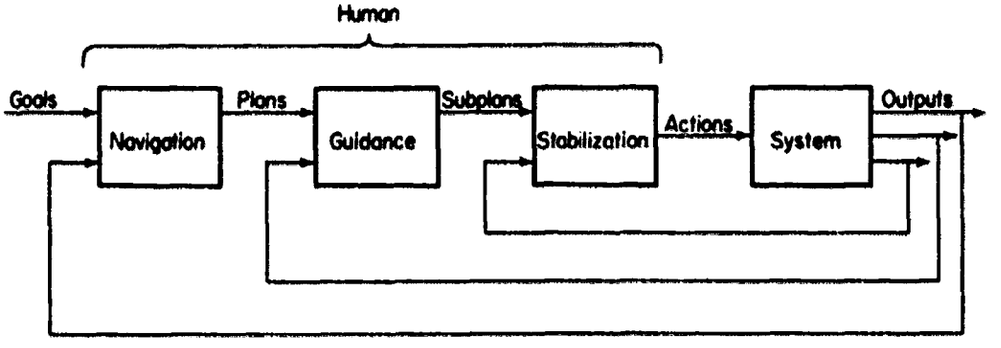

Figure 5: Hierarchy of Human Behavior

This diagram can be used to represent well-defined man-machine systems tasks such as those discussed by Johannsen [64] and Sheridan [65] as well as less well-structured tasks. For example, goals could mean success in life, plans could mean a career outline, subplans could mean a scheme to succeed in a specific job, and actions could mean one's daily activities. Thus, the diagram has broad applicability.

How can one analytically deal with such a general description? If one looks at control theory with a very general perspective that includes control with respect to continuous events as well as discrete events, then one can subsume most analytical methods (e.g., linear systems theory and queueing theory) within the category of control theory. This generalization, and willingness to expand the set of tools one utilizes, enables quantitative analysis of a larger portion of the hierarchy of behavior.

However, there are limits to context-free analytical modeling. First, there is the very important idea that human behavior mainly reflects the task environment. Thus, searching for a specific analytical model of general human behavior may only be fruitful to the extent that all task environments are common. Perhaps then, one should first search for commonality among environments rather than intrinsic human characteristics. In other words, a good model of the demands of the environment may allow a reasonable initial prediction of human performance. Thus, it is reasonable to initially assume that the human will adapt to the demands of the task and perform accordingly.

A second limitation to analytical modeling is due to the human's lack of analytical thinking, especially at upper levels of the hierarchy. First of all, the human is more of a satisficer than an optimizer. Thus, ideas such as a target tube within control tasks, fuzzy set theory, and some concepts from utility theory deserve more study and application within man-machine systems. What this means is that one should look at optimization with respect to broad criteria that allow multiple satisfactory solutions. An alternative approach to this issue is to discard optimization, but this would leave the modeler stripped of one of his most important tools and without a viable alternative.

Beyond the idea of satisficing, another important limitation to analytical modeling is that humans simply do not worry about details until it becomes necessary to do so. Thus, planning can be sketchy, perhaps in the form of scripts. Such sketchy planning can mean a drastic reduction in mental workload and also, that the human has the resources left to deal with more tasks as well as the flexibility to react to unforeseen events. These characteristics are precisely the reasons why humans are often included in systems.

However, the scripts idea presents a problem. While everyone might agree that humans use scripts to expedite performance of many tasks, knowledge of their existence is not sufficient to predict performance. One must know what the script specifically is. Thus, in complex tasks, one must measure not only performance (e.g., RMS error) but also the script.

This suggests that verbal protocols (perhaps analyzed by a computer that understands natural language) may be increasingly important research tools.

To conclude, this paper has presented a fairly general, but mainly verbal, model of human behavior in complex tasks. The ideas discussed have been based on analysis of a specific complex task (car driving) as well as a thorough review of the literature. Three very specific ideas have emerged. First, control should be looked at in a broad sense, incorporating a wide range of analytical methodologies. Second, the human satisfices rather than optimizes and criteria should reflect this. Third, higher-level activities such as planning require approaches that allow incompleteness, and approaches that capture the process of these activities and not just the results.

REFERENCES

1. Newell, A. and Simon, H.A., Human Problem Solving, Englewood Cliffs, N.J.: Prentice-Hall, 1972.

2. Tsichritzis, D.C. and Bernstein, P.A., Operating Systems. New York: Academic Press, 1974.

3. Habermann, A.N., Introduction to Operating System Design, Chicago: Science Research Associates, Inc., 1976.

4. Sanders, A.F., "Some Remarks on Mental Load," Moray, N. (Ed.). Mental Workload, New York: Plenum Press, 1978.

5. Atkinson, R.C. and Juola, J.F., "Search and Decision Processes in Recognition Memory," in: D.H. Krantz et al. (eds.): Contemporary Developments in Mathematical Psychology, Vol. I. San Francisco: W.H.Freeman and Company, 1974, pp. 243-293.

6. IEEE, "Current Perspectives in Pattern Recognition," Systems, Man, and Cybernetics Review, Vol. 6, No. 4, August 1977.

7. Sklansky J., "Image Segmentation and Feature Extraction," IEEE Transactions on Systems, Man. and Cybernetics, Vol. SMC-8, No. 4, April 1978, pp. 237-247.

8. Winston P.H. (Ed.), The Psychology of Computer Vision, New York: McGraw-Hill, 1975.

9. Winston, P.H., Artificial Intelligence, Reading, Mass.: Addison-Wesley, 1977.

10. Senders, J.W., "The Human Operator as a Monitor and Controller of Multidegree of Freedom Systems," IEEE Transactions on Human Factors in Electronics, Vol. HFE-5, No. 1, September 1964, pp. 2-5.

11. Carbonell, J.R., "A Queueing Model of Many-Instrument Visual Sampling," IEEE Transactions on Human Factors in Electronics, Vol. HFE-4, No. 4, December 1966 pp. 157-164.

12. Carbonell, J.R.; Ward, J.L.; and Senders, J.W., "A Queueing Model of Visual Sampling: Experimental Validation," IEEE Transactions on Man-Machine Systems, Vol. MMS-9, No. 3, September 1968, pp. 82-87.

13. Rouse, W.B. and Greenstein, J.S., "A Model of Human Decision Making in Multi-Task Situations: Implications for Computer Aiding," Proceedings of the 1976 International Conference on Cybernetics and Society, Washington, November 1976, pp. 425-433.

14. Sheridan, T.B. and Tulga, M.K., "A Model for Dynamic Allocation of Human Attention Among Multiple Tasks," to appear in the Proceedings of the Fourteenth Annual Conference on Manual Control, University of Southern California, April 1978.

15. Chien, R.T. and Snyder, W., "Visual Understanding of Hybrid Circuits via Procedural Models," Proceedings of the Fourth International Joint Conference on Artificial Intelligence, Tbilisi, USSR, September 1975 pp. 742-745.

16. Perkins W.A., "Model-Based Vision System for Scenes Containing Multiple Parts," Proceedings of the Fifth International Joint Conference on Artificial Intelligence, MIT, August 1977, pp. 678-684.

17. Wechsler, H. and Sklansky, J., "Automatic Detection of Rib Contours in Chest Radiographs," Proceedings of the Fourth International Joint Conference on Artificial Intelligence, Tbilisi, USSR, September 1975, pp. 688-694.

18. Martino, J.P., Technological Forecasting for Decision Making, New York: American Elsevier, 1972, Chap 10.

19 Sacerdoti, E.D., A Structure for Plans and Behavior, Ph.D. Dissertation, Stanford University, 1975.

20. Weissman, S.J., On a Computer System for Planning and Execution in Incompletely Specified Environments, Ph.D. Dissertation, University of Illinois at Urbana-Champaign, 1976.

21. Carbonell, J.R., "On Man-Computer Interaction: A Model and Some Related Issues," IEEE Transactions on Systems Science and Cybernetics Vol. SSC-5, No. 1, January 1969, pp. 16-26.

22. Schank, R.C. and Abelson R.P., Scripts, Plans, Goals, and Understanding, Hillsdale, N.J.: Lawrence Erlbaum, 1977.

23. Anderson, J.R. and Bower, G.H., Human Associative Memory, New York: Wiley, 1973.

24. Kohonen, T., Associative Memory, New York: Springer-Verlag, 1977.

25. Warfield, J.N., Societal Systems: Planning, Policy, and Complexity, New York: John Wiley, 1976.

26 Goldstein, I.P. and Grimson, E., "Annotated Production Systems: A Model for Skill Acquisition," Proceedings of the Fifth International Joint Conference on Artificial Intelligence, MIT, August 1977, pp. 311-317.

27. Wesson, R.B., "Planning in the World of the Air Traffic Controller," Proceedings of the Fifth International Joint Conference on Artificial Intelligence, MIT, August 1977, pp. 473-479.

28. Rouse, W.B., "A Theory of Human Decision Making in Stochastic Estimation Tasks," IEEE Transactions on Systems, Man, and Cybernetics, Vol. SMC-7, No. 4, April 1977, pp. 274-283.

29. Keeney, R.L. and Raiffa, H., Decision with Multiple Objectives, New York: Wiley, 1976.

30. Zadeh, L.A.; Fu, K.S.; Tanaka, K; and Shimura, M. (Eds.), Fuzzy Sets and Their Applications to Cognitive and Decision Processes, New York: Academic Press, 1975.

31. Kaufman A., Introduction to the Theory of Fuzzy Subsets, New York: Academic Press, 1975.

32. Davis, P.R., Using and Re-Using Partial Plans, Ph.D. Dissertation, University of Illinois at Urbana-Champaign, 1977.

33. Rouse, W.B., "A Model of Human Decision Making in a Fault Diagnosis Task," IEEE Transactions on Systems. Man, and Cybernetics Vol. SMC-8, No. 5, May 1978, pp. 357-361.

34. Gai E. and Curry, R.E., "A Model of the Human Observer in Failure Detection Tasks," IEEE Transactions on Systems, Man, and Cybernetics. Vol. SMC-6, No. 2, February 1976, pp. 95-94.

35 Greenstein, J.S. and Rouse, W.B.,"A Model of Human Event Detection in Multiple Process Monitoring Situations," to appear in the Proceedings of the Fourteenth Annual Conference on Manual Control, University of Southern California, April 1978.

36. Scott, A.C., Neurophysics, New York: Wiley, 1977.

37. Rasmussen, J. and Jensen, A., "Mental Procedures in Real-Life Tasks: A Case Study of Electronic Trouble Shooting," Ergonomics Vol. 17, No. 3, May 1974, pp.293-307.

38. Rasmussen, J., "Outlines of a Hybrid Model of the Process Plant Operator," in Sheridan, T.B. and Johannsen, G. (Eds.), Monitoring Behavior and Supervisory Control. New York: Plenum Press 1976, pp. 371-383.

39. Siegel, A.J. and Wolf, J.J., Man-Machine Simulation Models, New York: Wiley, 1969.

40 Linton, P.M.; Jahns, D.W.; and Chatelier, P.R., "Operator Workload Assessment Model: An Evaluation of a VF/VA-V/STOL System," Methods to Assess Workload, AGARD-CPP-216,1977.

41 Pew, R.W.; Baron, S; Feehrer, C.E.; and Miller, D.C., Critical Review and Analysis of Performance Models Applicable to Man-Machine Systems Evaluation, Bolt Beranek and Newman, Inc., Cambridge, Mass.: Rept. No. 3446, 1977.

42. Moray, N. (ed.), Mental Workload, New York: Plenum Press, 1978.

43. Senders, J.W. and Posner, M.J.M., "A Queueing Model of Monitoring and Supervisory Behavior," in T B. Sheridan and G. Johannsen, (Eds.), Monitoring Behavior and Supervisory Control, New York: Plenum Press 1976.

44. Rouse, W.B., "Human-Computer Interaction in Multi-Task Situations," IEEE Transactions on Systems, Man and Cybernetics, Vol. SMC-7, No. 5, May 1977, pp. 384-392.

45. Walden, R.S. and Rouse, W.B., "A Queueing Model of Pilot Decision Making in a Multi-Task Flight Management Situation," Proceedings of the Thirteenth Annual Conference on Manual Control, MIT, June 1977, pp. 222-236.

46. Chu, Y.Y. and Rouse, W.B., "Optimal Adaptive Allocation of Decision Making Responsibility Between Human and Computer in Multi-Task Situations," Proceedings of the 1977 International Conference on Cybernetics and Society, Washington, September 1977, pp. 168-185.

47. Chu, Y.Y. and Rouse, W.B., "Pilot Decision Making in a Computer-Aided Flight Management Situation," to appear in the Proceedings of the Fourteenth Annual Conference on Manual Control, University of Southern California, April 1978.

48. Wherry, R.J., Jr., "The Human Operator Simulator - HOS," Sheridan, T.B. and Johannsen, G. (Eds.) 1976, Monitoring Behavior and Supervisory Control, New York: Plenum Press, 1976, pp. 283-293.

49. McRuer, D.T. and Krendel, E.S., "Mathematical Models of Human Pilot Behavior," Advisory Group Aerospace Research Development, Neuilly sur Seine, France: AGARDograph No. 188, 1974.

50. Sheridan T.E. and Ferrell, W.R., Man-Machine Systems: Information, Control, and Decision Models of Human Performance, Cambridge, Mass.: MIT Press, 1974.

51. Johannsen, G., Boller H.E., Donges, E., and Stein, W., Der Mensch im Regelkreis, Lineare Modelle, Munchen: Oldenbourg, 1977.

52. Kleinman, D.L.; Baron, S.; and Levison, W.H., "An Optimal Control Model of Human Response. Part I: Theory and Validation," Automatica, Vol. 6, 1970, pp. 357-369.

53. Rouse, W.B. (Ed.), Special Issue on Applications of Control Theory in Human Factors, Human Factors, Vol. 19, Nos. 4 and 5, August and October 1977.

54. Donges, E., "Experimentelle Untersuchung des menschlichen Lenkverhaltens bei simulierter Strassenfahrt," Automobiltechnische Zeitschrift, Vol. 77, 1975 pp.141-146, 195-190.

55. Donges, E. "A Control Theoretic Model of Driver Steering Behavior," Proceedings of the 13th Annual Conference on Manual Control, MIT, Cambridge, Mass, 1977, pp. 165-171.

56. Galiana, F.D. and Glavitsch, H., "State Adaptation in Power Systems Control," Proceedings of the IEEE Power Engineering Society, Winter Meeting, New York, 1973.

57. Bertsekas, D.P. and Rhodes, I.B , "On the Minimax Reachability of Target Sets and Target Tubes," Automatica, Vol. 7, 1971, pp. 233-247.

58. Glover, J.D. and Schweppe, F.C., "Control of Linear Dynamic Systems with Set Constrained Disturbances," IEEE Transactions on Automatic Control Vol. AC-16, 1971, pp. 411-423.

59. Schweppe, F.C., Uncertain Dynamic Systems, Englewood Cliffs, N.J.: Prentice-Hall, 1973.

60. King, P.J. and Mamdani, E.H., "The Application of Fuzzy Control Systems to Industrial Processes," Automatica, Vol. 13, 1977, pp. 235-242.

61. Sheridan, T.B. and Johannsen, G. (Eds.), Monitoring Behavior and Supervisory Control, New York: Plenum Press, 1976.

62. Young, L.R., "On Adaptive Manual Control," Ergonomics, Vol. 12, 1969, pp.635-674.

63. Adams, J.A., "A Closed-Loop Theory of Motor Learning," J. Motor Behavior, Vol. 3, 1971, pp. 111-150.

64. Johannsen, G., "Preview of Man-Vehicle Control Session," in: Sheridan, T.B. and Johannsen, G. (eds), Monitoring Behavior and Supervisory Control, New York: Plenum Press, 1976, pp. 3-12

65. Sheridan, T.B., "Review of the International Symposium on Monitoring Behavior and Supervisory Control," Proceedings of the Twelfth Annual Conference on Manual Control, University of Illinois at Urbana-Champaign, May 1976, pp. 3-13.

ORIGINAL PAGE IS
OF POOR QUALITY

N79-15600

PETRI NETS AS A MODELING TOOL FOR DISCRETE CONCURRENT TASKS OF THE HUMAN OPERATOR

By W. Schumacher, G. Geiser

Fraunhofer-Gesellschaft e. V., Institut für Informationsverarbeitung in Technik und Biologie (IITB), Karlsruhe, F. R. of Germany

SUMMARY

Petri nets have been developed as a fundamental model of technical systems with concurrent discrete events. The major use of Petri nets has been the modeling of hardware systems and software concepts of computers. After a very brief introduction to their basic concepts, the use of Petri nets is proposed for modeling the human operator dealing with concurrent discrete tasks. Their properties useful in modeling the human operator are discussed and practical examples are given. By means of an experimental investigation of binary concurrent tasks which are presented in a serial manner it is shown how human behavior may be represented by Petri nets.

INTRODUCTION

In different application areas the human operator's role in man-machine systems is changing from that of a continuous controller to that of a monitor. This change is happening in control rooms of industrial plants and in aircraft piloting, where dispatching of concurrent demands becomes an essential feature of the human operator's task. Furthermore the multiple task situation is also given in automobile driving. Especially in high density traffic situations the driver has to deal with many concurrent demands originating from other road users, from traffic regulation, and from his own vehicle.

In general, concurrent tasks are imposed on the human operator by displays or by real events, their service requires a response from the human operator which is specified by the task. There are continuous demands like the control error of a continuous control loop or there are discrete events, which require continuous or discrete actions respectively. These demands compete for the human operator's attention, if they arrive in such an intensity, that the human operator's capacity is at least temporarily exceeded. In this case demands which cannot be dispatched immediately have to be stored in his memory, otherwise they are lost.

PAGE INTENTIONALLY BLANK

For the design of such man-machine systems, i. e. of their dynamic properties, displays, and controls, the human strategies in dispatching concurrent demands have to be described by means of experimental investigations and resulting quantitative models. Notions of queueing theory are suitable for the formulation of this task of the human operator (refs. 1, 2, 3), however instead of analytical solutions human behavior is often studied by simulation.

In this paper Petri nets are discussed as a modeling tool for the human operator dealing with concurrent demands. As a practical example the application of Petri nets for modeling human strategies is shown. These strategies have been evaluated by means of an experimental investigation of binary concurrent tasks displayed in a serial manner.

PETRI NETS

In the following a brief introduction to the Petri net is given; a more detailed presentation is contained in ref. 4.

A Petri net is an abstract, formal model of the information flow in systems with discrete sequential or parallel events. Its pictorial representation is a directed graph, for which an example is shown in Fig. 1. The graph consists of two types of nodes: places p_i (represented by circles) and transitions t_j (represented by bars). These nodes are connected by directed arcs from places to transitions and from transitions to places. If an arc is directed from node i to node j, then i is an input to j, and j is an output of i. In Fig. 1, e. g., place p_1 is an input to transition t_2, while places p_3 and p_4 are outputs of transition t_3. The nodes and arcs describe the static properties of a Petri net, its dynamic characteristics are represented by the movement of tokens (represented by black dots within the places). The distribution of tokens in a Petri net defines the state of the net and is called marking μ. For each marking μ a new marking μ' is defined by the following rules:

1. A transition is called enabled, if each of its input places has at least one token in it (e. g. transition t_2 in Fig. 1 is enabled).

2. Each transition which is enabled may fire.

3. A transition fires by removing one token from each of its input places and by adding one token to each of its output places (e. g. in Fig. 1, firing of transition t_2 results in two tokens in place p_1, zero token in p_4, and one token in place p_2).

The formal description of a Petri net is defined as a four-tupel of sets

$$C = (P, T, I, O) ,$$

with P as a set of places, T as a set of transitions, I as the input function, and O as the output function. The input function I defines for each transition t_j the set of input places $I(t_j)$. The output function $O(t_j)$ is defined correspondingly. For the example shown in Fig. 1 there are the following sets

$$P = \{p_1, p_2, p_3, p_4\} ,$$
$$T = \{t_1, t_2, t_3, t_4\} ,$$

$$I(t_2) = \{p_1, p_4\} , \qquad O(t_1) = \{p_1\} ,$$
$$I(t_3) = \{p_2\} , \qquad O(t_2) = \{p_2\} ,$$
$$I(t_4) = \{p_3\} , \qquad O(t_3) = \{p_3, p_4\} .$$

The vector $\mu = (\mu_1, \mu_2, \ldots, \mu_n)$ gives, for each of the n places in the net, the number of tokens in that place. A Petri net $C = (P, T, I, O)$ with the marking μ becomes the marked Petri net $C^* = (P, T, I, O, \mu)$.

An important tool for analysis of systems modelled by a Petri net is the reachability tree. It consists of a tree, whose nodes represent markings of the Petri net, and whose arcs represent the transitions which are enabled. The Petri net shown in Fig. 1 has the following degenerated reachability tree:

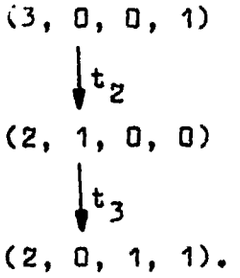

PROPERTIES OF PETRI NETS WITH REGARD TO THE DESCRIPTION OF THE HUMAN OPERATOR

In the following the properties of Petri nets are summarized with regard to the description of the human operator dealing with discrete concurrent demands (Table 1).

- Description of sequential and parallel processes
- Description of interactions between parallel processes
- Interpreted and uninterpreted modeling
- Hierarchical modeling
- Description of temporal order
- Description of deterministic and stochastic processes
- Modeling of priority systems
- Formal and graphic description

Table 1: Properties of Petri Nets with regard to the Modeling of the Human Operator

Petri nets are suitable for the description of sequential and parallel concurrent demands of the human operator as well. A net having only one token at the same time is describing a sequential process. The position of the token represents the state of the 'sequence control register' of the process. The graphic representation of such a net containing only transitions with one input and one output corresponds to the usual flow-chart. Fig. 2 shows as an example the observation of a traffic light represented by a flow-chart and by a Petri net.

A net having more than one token at any time describes a non-sequential process. Several tokens may result from a transition with several output places or they are an initial marking. Fig. 1 shows a Petri net with an initial marking of four tokens. Therefore it describes a system of partially parallel activities. It may be interpreted as a general model of the dispatching of concurrent demands, presented in a serial manner to the human operator. Concurrency is given by the fact, that during the service of one demand other demands are waiting or arriving. Then places p_1 to p_4 of Fig. 1 have the following interpretations:

p_1: number of demands waiting for service (represented by the corresponding number of tokens),

p_2: one demand is being served,

p_3: one demand has been served,

p_4: the human operator is ready for the next service.

The description of parallel activities by Petri nets can be applied to the modeling of interactions between different stages of human information processing and between the tasks of several operators as well. Fig. 3 shows as an example the crossing of two automobile drivers where two conflicting transitions without indication of priority exist. Modeling of priority systems is considered later on.

The interpretation of the Petri net shown in Fig. 1 may be specified with regard to practical applications. E. g. the demands may represent traffic signs which have to be observed by the driver or they are alarms of an industrial plant presented on displays in the control room. On the other hand Petri nets exist as uninterpreted models of which the abstract properties may be investigated.

Another valuable feature of Petri nets is their ability to model a system hierarchically. This means that parts of the human information processing may be represented by a single place or transition in order to have a more abstract model. Conversely places and transitions may be specified by subnets in order to get a more detailed description. The example of Fig. 1 is an extremely abstract model of the human operator, which will be specified by means of experimental results in chapter 4.

Petri nets describe the possible sequences of events, they do not reflect the variable amounts of time required by the different events. Because of this property Petri nets give no information about the duration of information processing of the human operator.

Petri nets are suitable for the modeling of deterministic and of stochastic sequences of events. Deterministic sequences ever have one transition being enabled, while stochastic sequences lead to situations in which more than one transition is enabled. The choice of the next transition to be fired occurs randomly. Fig. 4 shows two types of stochastic firing of transitions. Concurrent transitions may fire in either order whereas in conflicting transitions the firing of one will disable the other.

In order to model priority systems Petri nets were extended by inhibition arcs represented by an arc with a small circle instead of an arrowhead. An inhibition arc from place p_i to transition t_j enables the transition only to fire if the place p_i has zero token in it. Fig. 5 shows as an example the crossing of two drivers (compare Fig. 3) with priority of driver 1, described by an inhibition arc.

Furthermore Petri nets may be described in a formal as well as in a graphic manner. Especially the graphic representation seems to be a useful tool in describing complex information processing of the human operator.

MODELING OF HUMAN STRATEGIES IN DISPATCHING CONCURRENT DEMANDS BY PETRI NETS

Experimental Set-up

In order to investigate the human behavior in dispatching concurrent demands a simulator for the generation of the demands and for their service has been established. Fig. 6 shows the block diagram of the experimental set-up. There are 8 streams of binary demands presented by the numbers 1 to 8 on a common numeric display to the operator. The arrival pattern of each stream is given by the Poisson distribution. The service of each demand consists in pressing a corresponding push-button during a fixed lapse of time which is indicated by a service time lamp. The traffic intensity ρ, i. e. the ratio of the service time and the mean interarrival time of the demands, varied in the range $0.8 \leq \rho \leq 1.6$. The service of the demands had to be done in the order of arrival. The experimental sessions consisted of five trials of 200 s duration each. After each trial the traffic intensity was increased by an amount of 0.2, beginning with the value of $\rho = 0.8$. For $\rho \geq 1$ the human operator is unable to deal with the demands as fast as they arrive. Consequently the demands have to queue up in the operator's short term memory. Because of its limited capacity demands may be lost. By recording the service activities of the subjects the strategies in dealing with concurrent demands could be evaluated.

In the following the results from one experiment are presented, further investigations with this experimental set-up are described in ref. 5.

Experimental Results

In order to analyse the human strategies the contents of

the memory were evaluated; it is called waiting-room diagram. Fig. 7 shows a typical waiting-room diagram, where the number of demands in waiting-room 1, i. e. the length of the queue, is plotted as a function of time. At the arrival of a demand the length of the queue increases by one, at the beginning of a service the plot decreases by one. The upper plot shows the ideal waiting-room diagram, which is based on the assumption that there is an infinite waiting-room. All arriving demands are waiting for service, no demand is lost. The lower plot shows the minimal waiting-room diagram, with the assumption that lost demands did never enter the waiting-room. Demands which are not served are marked by a "N". By asking the subjects to communicate the contents of their memory at certain time instants, it could be shown that the real waiting-room diagram corresponds largely to the minimal waiting-room diagram.

By the analysis of the waiting-room diagram and supported by statements of the subjects two strategies for the service of the concurrent demands can be specified:

- Waiting-room with permanent access
  The demands enter into the waiting-room and queue up until a maximum length of the queue ($l_{max} \approx 3$) is reached. Then if one demand is served another may enter.

- Waiting-room with intermittent access
  The demands enter the waiting-room and queue up. By certain triggering events all arriving demands are rejected until the length of the queue is reduced to a low value. Triggering events are the reaching of a maximum length of the queue or the arrival of several demands with short interarrival times. In this case the maximum length of the queue is higher ($l_{max} \approx 5$) than with the strategy of permanent access.

The described strategies are extreme forms of behavior, in reality they occur in an approximate and mixed form. The strategy with intermittent access can be observed more often (factor 1.5) than the strategy with permanent access. Fig. 7 shows the waiting-room diagram in the case of intermittent access. This strategy is less efficient, because with permanent access there is a higher utilization of the waiting-room, i. e. the mean length of the queue is increased.

Modeling of the Human Strategies by Petri Nets

The human operator's activities in dealing with concurrent tasks are the input of information, the storage of information in his memory (waiting-room), and the service of demands by reactions. Fig. 8 shows the Petri net of the strategy with permanent access divided into these three parts. For simplicity the waiting-

room is assumed to have a capacity of three demands.

Complementary places are labelled by p and p'. For example the interpretation of place p_2 is "information input is idle" and of place p_2' "information input is busy". At the arrival of a demand it depends on the state of the information input whether the demand is lost (place p_2' marked) or not (place p_2 marked). In the latter case transition t_1 is fired and the demand is stored in that position of the waiting-room (p_4 ... p_6), which is free and has the lowest number. By the entrance of the demand into the waiting-room (firing of transition t_4, t_5 or t_6) the information input is reset by firing transition t_{11}. Demands arriving when the input is busy are lost by firing of transition t_2. Also if the waiting-room is completely occupied, i. e. the place p_6 is marked, the arriving demand is rejected and lost by firing of transition t_3.

If the waiting-room is empty, the arriving demand is stored in the first place of the waiting-room (marking of p_4'). If the service mechanism is idle (place p_7' marked), then the service of this demand may be carried out by firing of transition t_7 and by setting free the waiting-room place. If there are further demands in the waiting-room they advance one step by means of the transitions t_8 and t_9.

Fig. 9 shows the Petri net of the strategy with intermittent access. Compared with permanent access there are modifications especially in the input part of the model. The states of the places p_{12} and p_{12}' determine whether arriving demands are rejected or not. The rejection state (p_{12}' is marked) is triggered if the waiting-room is completely occupied, i. e. p_6' is marked. Then all demands are rejected and lost until the waiting-room is empty and the transition t_{12} is fired. Then arriving demands again have access to the waiting-room.

The strategies described have been simulated by means of a digital computer. Simulation data showed close agreement with experimental results. The description of the human strategies by means of Petri nets turned out to be a valuable tool for the analysis of human information processing.

This report was supported by the German Federal Ministry of Defense.

REFERENCES

1. Carbonell, J.R.: A Queueing Model of Many-Instrument Visual Sampling. IEEE Trans. on HFE-7 (1966), 157-164.

2. Chu, Y.Y.; Rouse, W.B.: Optimal Allocation of Decision Making Responsibility between Human and Computer in Multi-Task Situations. Proc. of the International Conference on Cybernetics and Society, Sept. 19-21, 1977, Washington, 168-175.

3. Tulga, M.K.; Sheridan, T.B.: Modeling human decision making behavior in supervisory control. Proc. of the International Conference on Cybernetics and Society, Sept. 19-21, 1977, Washington, 201-206.

4. Peterson, J.L.: Petri Nets. Computing Surveys, 9 (1977), 223-252.

5. Schumacher, W.: Human operator strategies in dispatching concurrent binary demands in man-machine systems. IITB-Mitteilungen 1978, Institut für Informationsverarbeitung in Technik und Biologie der Fraunhofer-Gesellschaft e. V., Karlsruhe, F.R. of Germany.

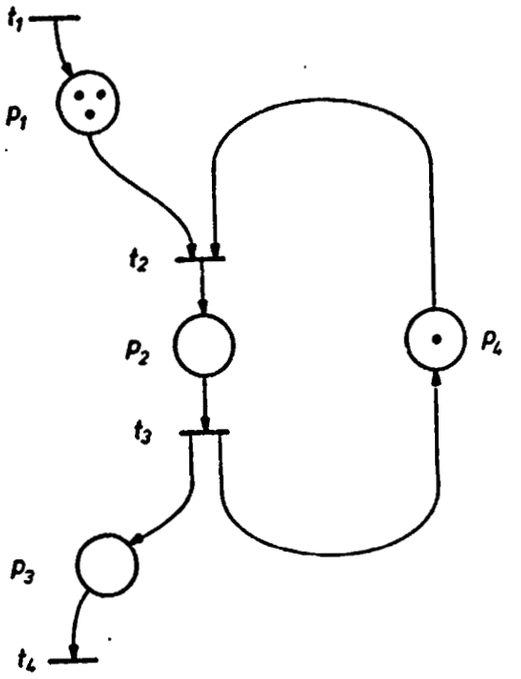

Fig. 1: A Petri net graph

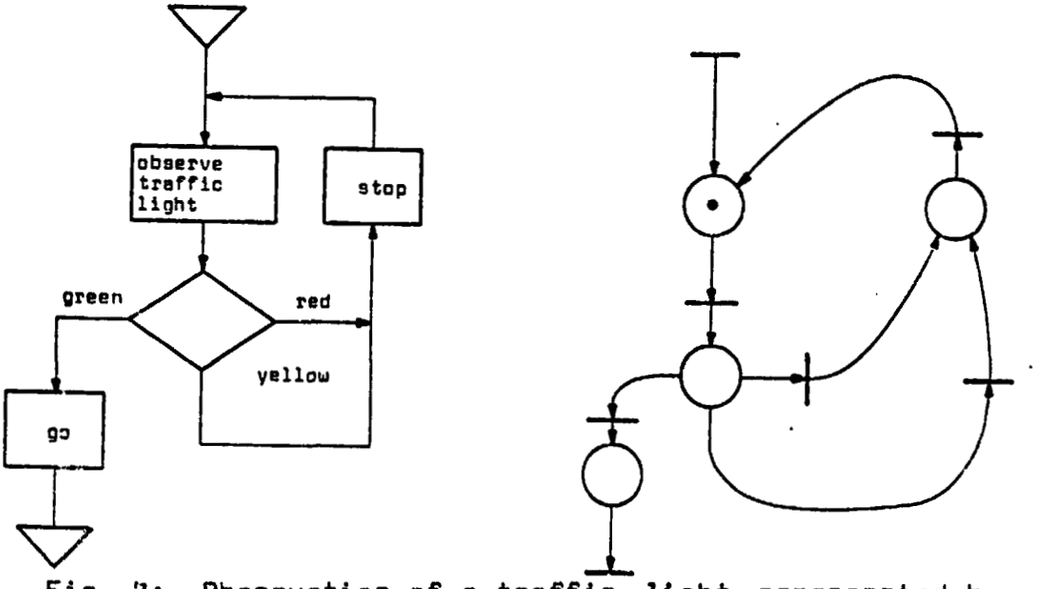

Fig. 2: Observation of a traffic light represented by a flow-chart and a Petri net

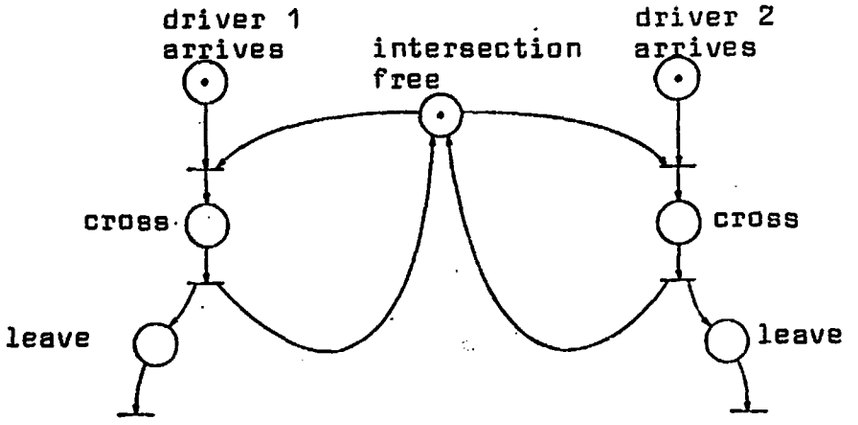

Fig. 3: Petri net of the crossing of two drivers

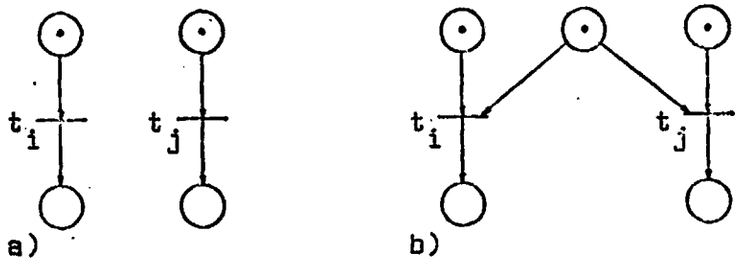

Fig. 4: a) Concurrent and b) conflicting transitions t_i and t_j

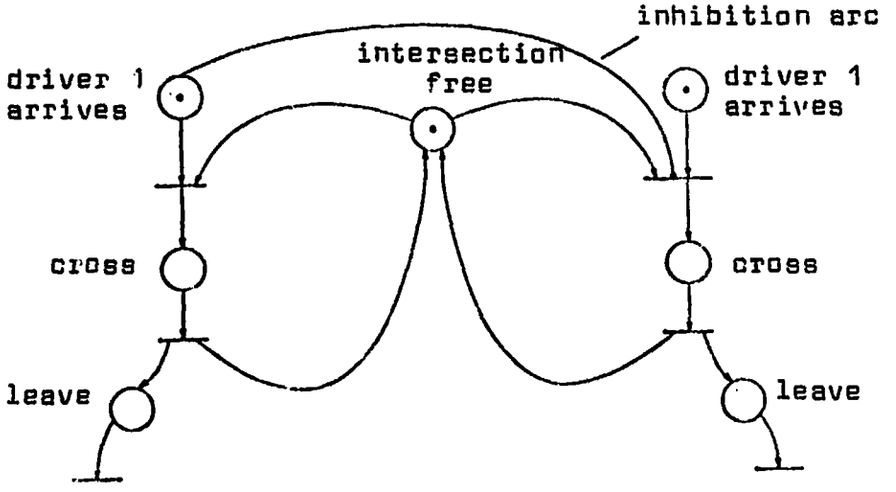

Fig. 5: Petri net of the crossing of two drivers with priority of driver 1

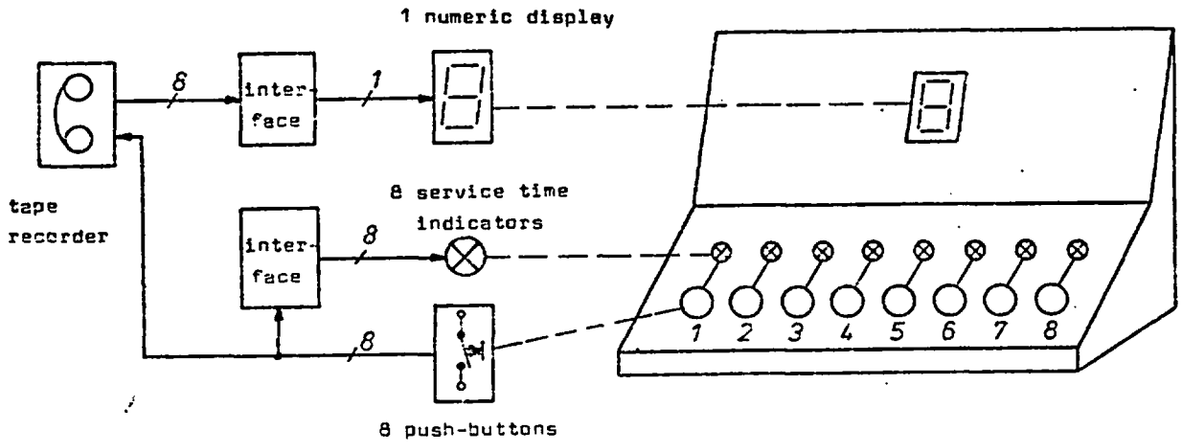

Fig. 6: Block diagram of the experimental set-up

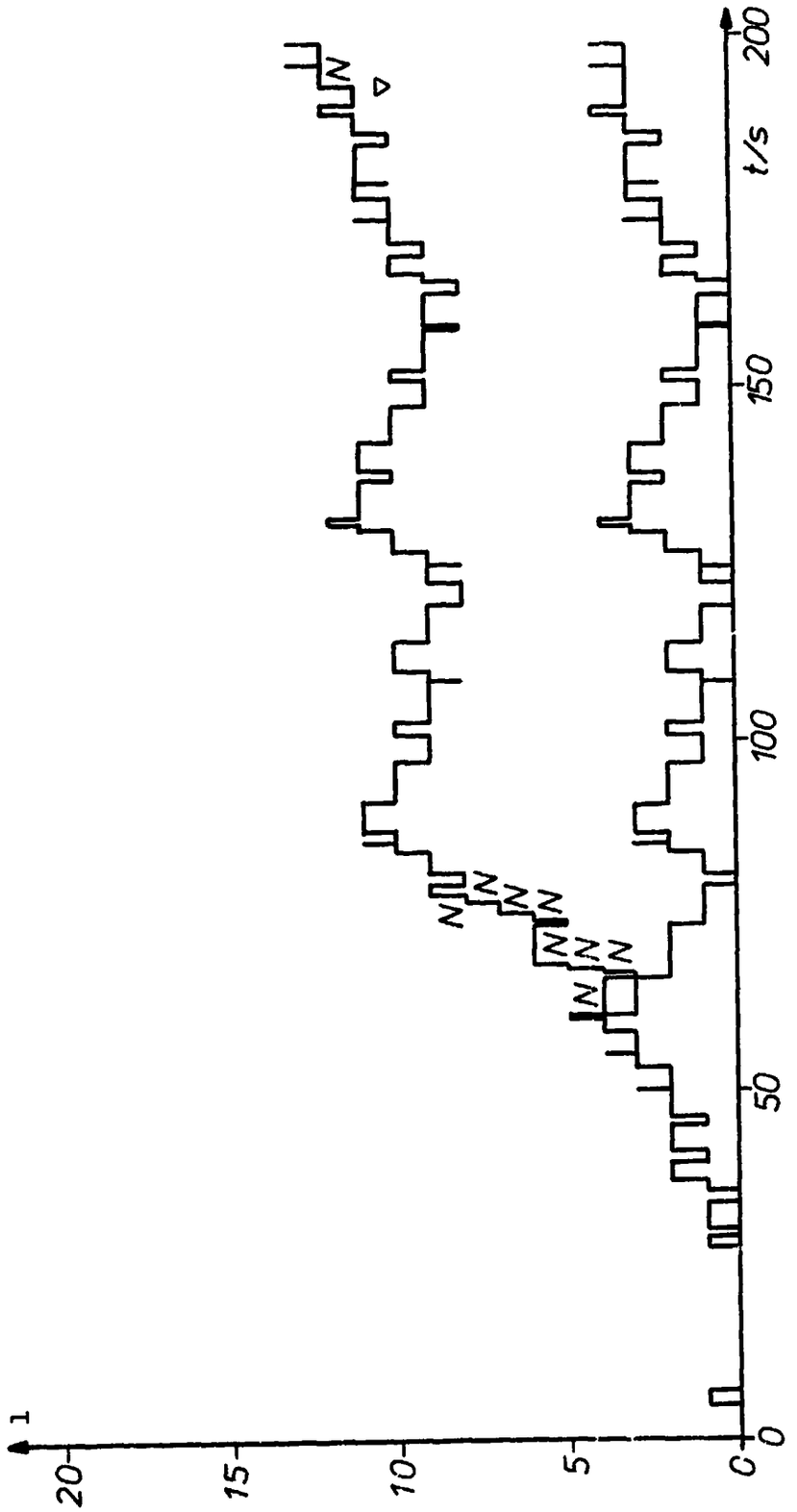

Fig. 7: Waiting-room diagram

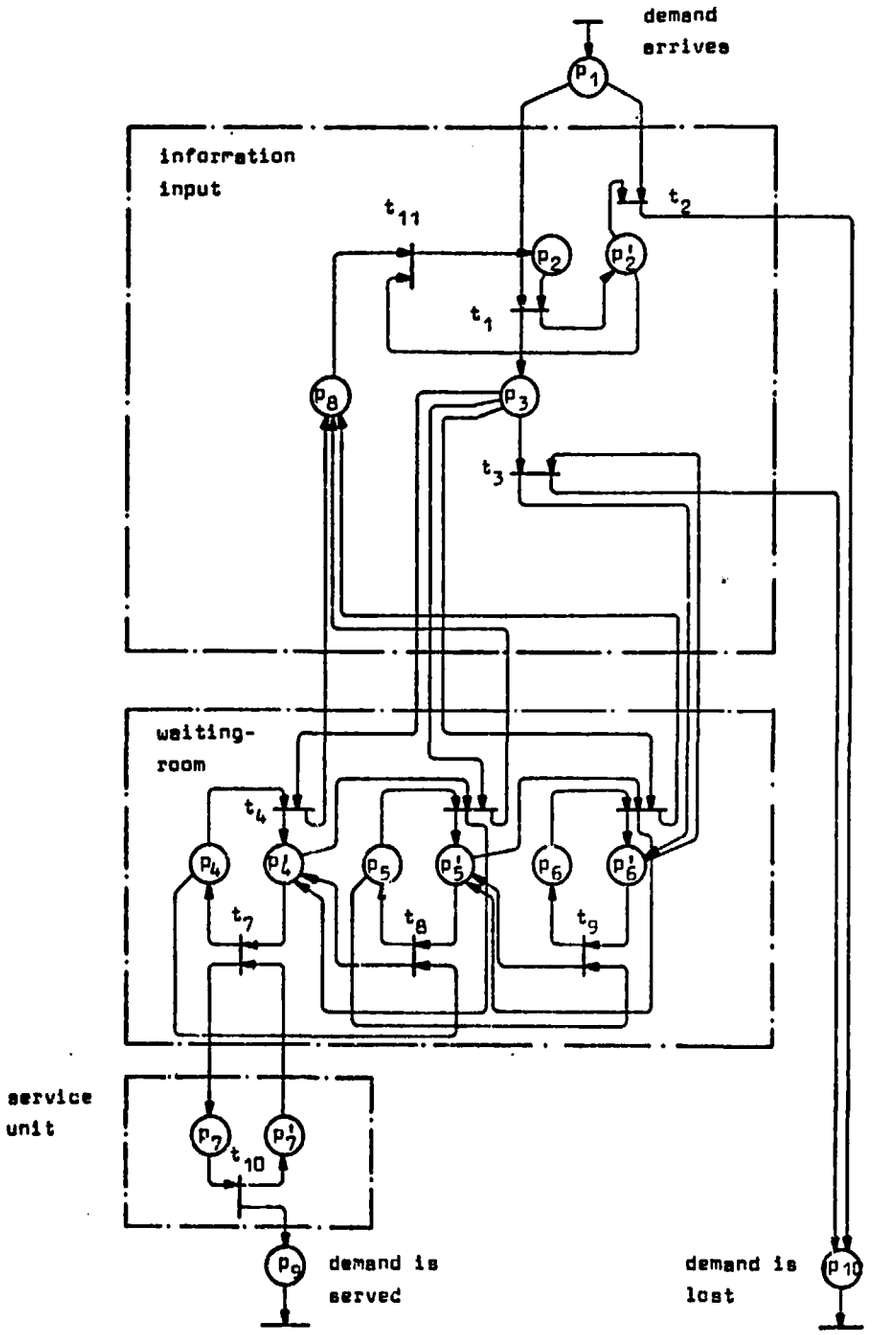

Fig. 8: Waiting-room with permanent access

ORIGINAL PAGE IS
OF POOR QUALITY

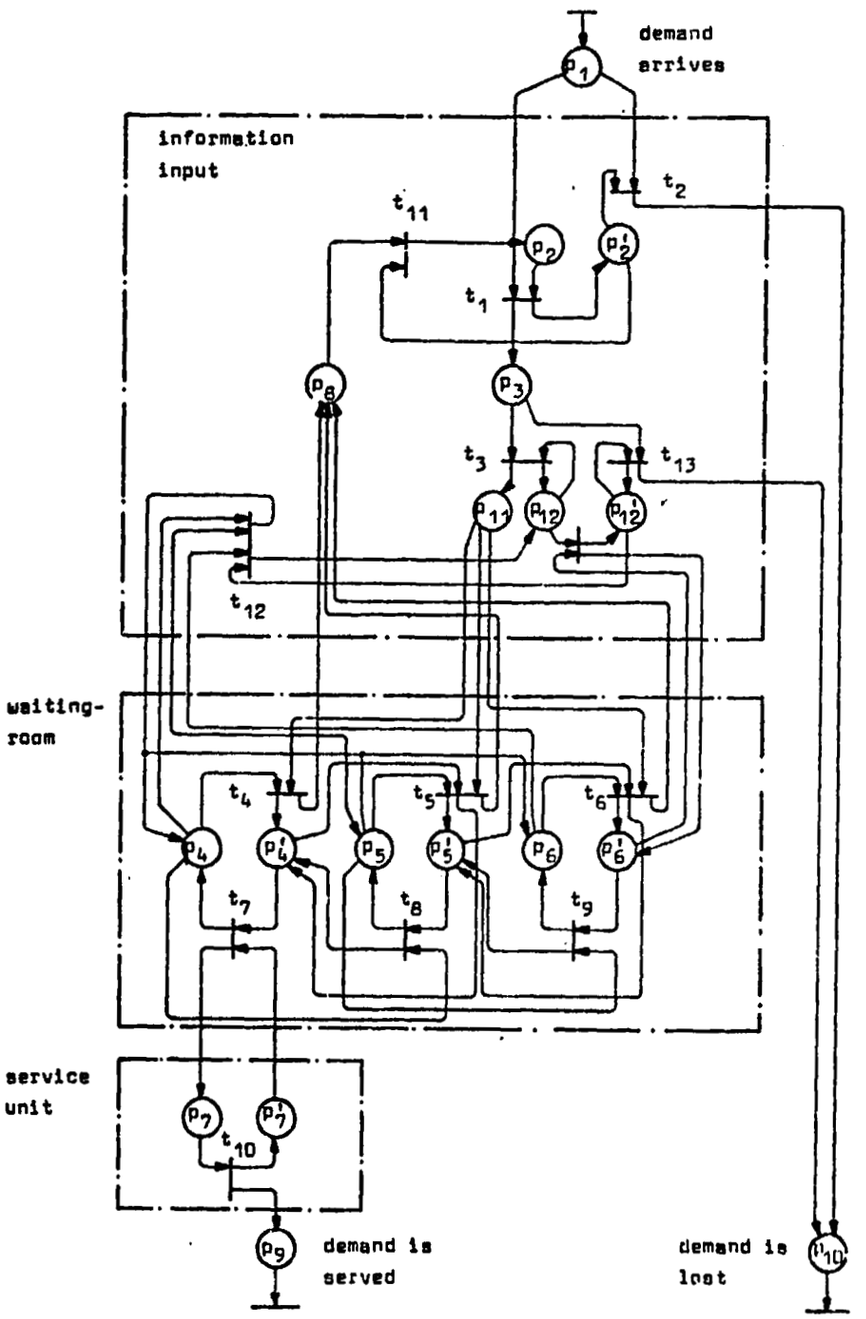

Fig. 9: Waiting-room with intermittent access

ORIGINAL PAGE IS
OF POOR QUALITY

N79-15601

DISCRETE-TIME PILOT MODEL

by Daniel CAVALLI

Office National d'Etudes et de Recherches Aérospatiales (ONERA)
92320 Châtillon (France)

SUMMARY

The objective of this paper is to demonstrate the originality of our approach with regards to already existing pilot models and to present recently obtained results.

We consider the pilot's behavior as a discrete-time process where the decision making has a sequential nature. This model contrasts very clearly with previous approaches namely the quasi-linear model which follows from classical control theory and the optimal control model which considers the human operator as a Kalman estimator-predictor. We also consider that the pilot's objective may not be adequately formulated as a quadratic cost functional to be minimized, but rather as a more fuzzy measure of the closeness with which the aircraft follows a reference trajectory.

All model parameters, in the digital program simulating the pilot's behavior, have been successfully compared in terms of standard-deviation and performance with those of professionnal pilots in IFR configuration. The first practical application of our pilot model has been the study of its performance degradation when the aircraft model static margin decreases.

I. INTRODUCTION

Research on human operator models and especially on models of spacecraft, aircraft and helicopter operators has often been influenced by the current state-of-the-art. Before further investigation, the human operator appears as highly adaptative, versatile, complex and sufficiently creative so that we can always recognize in the diversity of all strategies he may use, one we know well and want to find.

The first approach to the problem was from the control specialists of the 1950's, attempting, at the beginning age of servomechanisms, to apply their basic tool, namely the linear transfer function of a phase lead regulator (ref. 1). These studies relied heavily on simulation techniques using analog computers.

One of the most-commonly accepted representations is the quasi-linear model of McRuer (ref. 2, 3, 4) so named because it represents the human operator by a linear transfer function, plus a remnant to describe that part of the human response that is not predicted by the linear approximation. The transfer function is essentially the result of an approximation to the first harmonic and the remnant accounts for higher-order effects and for other modeling errors. The most celebrated result from the above study is probably the "cross over model" which is based on the fact that the human operator adjusts the parameters of his own transfer function so that his open-loop response satisfies the closed-loop stability conditions with a reasonable error.

At the same time sampled-data models have been proposed (ref. 5). This type of models is suitable for numerical computation on digital computers. However, the assumption of fixed-rate sampling appears as a weakness of this representation.

An alternative to the quasi-linear model has been developed by Kleinman, Baron and

PAGE INTENTIONALLY BLANK

Levison (ref. 6, 7, 8). This approach is based on advanced optimal control and estimation theory with the assumption that the well-trained human controller behaves in an optimal manner subject to his inherent limitations and contraints and the requirement of his task. However, is the human operator only a Kalman estimator whose objective may be formulated as the minimization of a given criterion ?

These modeling studies have advanced a great step forward when becoming interdisciplinary through the involvement of psychologists in the research teams. These scientists can probably be credited for the introduction of the concept of operating image (ref. 9, 10, 11, 12) which is an internal model of the vehicle allowing the human operator to predict its short-term response. The conventional approach and the purely psychological one are currently merging (ref. 13). Without repudiating previous philosophies, our current approach tries to make a synthesis of them and develop the model of a human operator based on a new and more accurate analysis of the aircraft pilot's behavior (ref. 14, 15, 16, 17).

II. ANALYSIS OF THE PILOT'S BEHAVIOR

Consider the behavior of the human operator in the case of aircraft control.

The aircraft position as sensed by the pilot from his instrument dials or outer sight is compared to the attitude required to follow the nominal flight path. As an example, if the horizontal bar of the ILS indicator lies above the central mark, the pilot analyzes this situation and selects the appropriate correction maneuver to carry out. Once the maneuver has been selected, the pilot's brain (i.e. the decision center) request from the eyes through an internal loop (fig. 1), to collect information relating to the longitudinal attitude. The difference between the actual attitude and the desired one is analyzed and the pilot selects the right control to actuate and determines the force to apply to it. In this example, the pilot pulls on the control stick with a force he judges as correct while requesting his arm, through another loop, to sense the applied force. Stick motion is stopped when the pilot feels that the desired force has been applied.

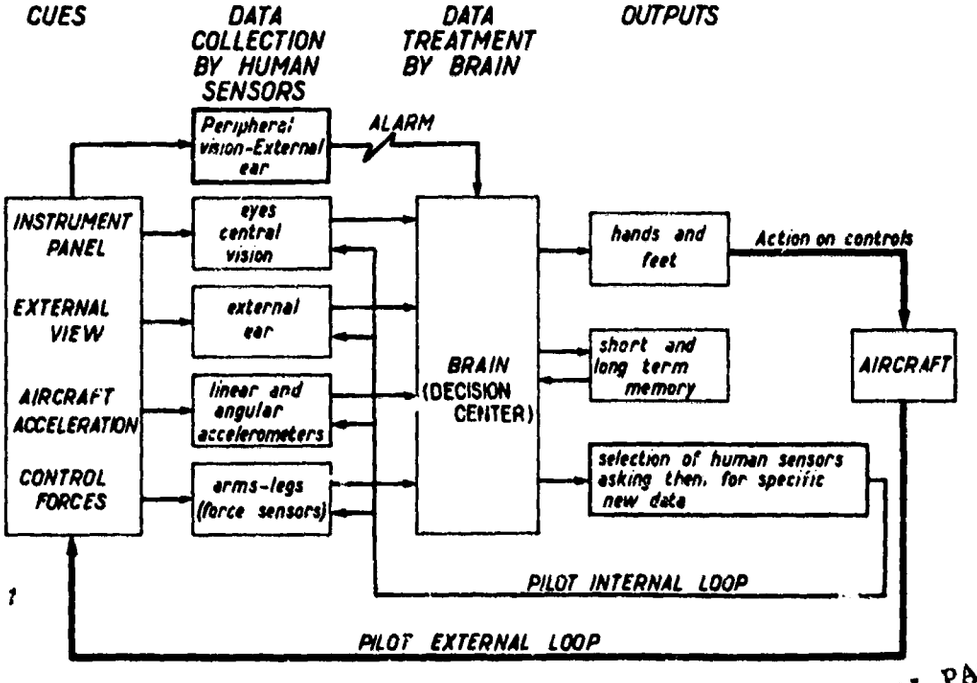

Fig. 1

ORIGINAL PAGE IS OF POOR QUALITY

Hence, the decision center (the brain) puts successively into action various loops while asking for further information from the human sensor. Three types of loops may be considered (fig. 2),

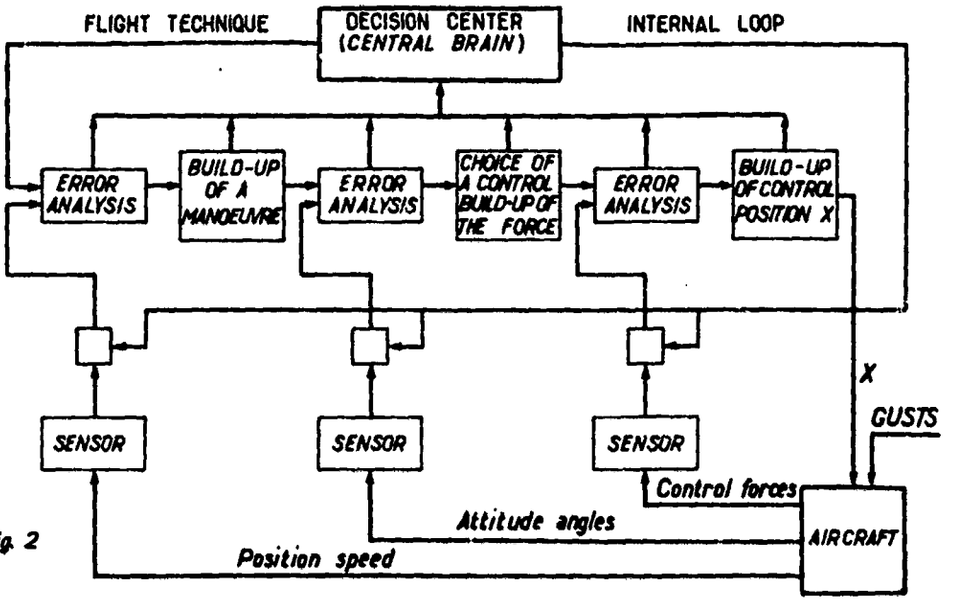

Fig. 2

– outer loops controlling the parameters related to the short-term safety, i.e. flight path, position and speed,

– loops controlling the parameters related to the immediate safety, i.e. the attitude angles, angle of attack, etc .... ,

– finally, the inner loops controlling the forces applied to the controls.

It should be noted that there is *only a single loop* in operation at a given time and this is one of the most fundamental differences between a human pilot and an autopilot. The selection of the currently operating loop is made by the decision center (brain) which designates the selected sensor to collect and transmit the necessary information through an internal loop (fig. 1).

An immediate consequence of this analysis is that it is impossible to determine directly the pilot's workload : at the present time, it seems virtually impossible to follow in detail the processing of data taking place within the brain.

Another consequence is that it is useless to determine experimentally a transfer function representing the pilot's behavior since there is not one, however complex, but a series of transfer functions used sequentially in an order determined by scanning of the various displays. This scanning itself depends on certain data, the environment, the pilot's training, etc... , that is partially on random phenomena. This random nature must be accounted for into some part of the pilot's behavior model.

III. RESPECT OF THE CONTROL LAW

The control law, which is the keeping of permissible deviations of the controlled parameters with respect to the nominal flight path, ensures the immediate safety as well as the short-term safety. This law is used by the pilot as a guideline, it depends on the objective

set by the pilot and on his ability to adapt himself to the conditions of the flight phase execution.

First, the objective set by the pilot may not be formulated in the form of a criterion to be minimized (as proposed by Kleinman, Baron and Levison (ref. 6, 7, 8)). The pilot is neither a perfect being, nor a well-trained monkey who as it is well known, does a better work than a human operator when his task is that of a robot. The human brain can collect a great number of quantitative and qualitative data, some of them being only sensations. The brain is able to built a model of the situation, to compare it with typical situations held in memory, and decide upon an action even if the case has not been foreseen. Then, the objective is much fuzzier : it consists on controlling the plane to reference flight path as close as possible to the nominal flight path. This reference corresponds to the pilot's learning and his know ledge of the plane.

The pilot possesses rather remarkable capabilities of adaptation which are evidenced by the nature of his control commands. An interpretation of this adaptability is the concept of operating image or internal model. The pilot possesses a probably very simplified model of the aircraft which permits him to predict its short-term response given his previous actions.

This concept of internal model permit us to account for the predictive nature of a human pilot's control, as opposed to conventional autopilots.

IV. CHOICE OF A MULTILOOP SEQUENTIAL MODEL

Taking into account the above considerations, a mathematical model must satisfy the following conditions to be as close as possible to the human pilot's behavior (ref. 15).

a) The elementary activities of data collection, development of correction procedures and actuation of controls occur sequencially and not simultaneously as in continuous type models.

b) The various control loops must be identified according to the type of aircraft as well as the nature and number of observed parameters. The type of each loop must be defined, namely as flight path loop relating to short-term safety, attitude loop relating to immediate safety, or loop relating to the control action (see fig. 2).

c) The instants of time when the various loops are activated are not defined in a deterministic manner but are partially random (Poisson process). *Only a single loop* can be in operation at a given time and the pilot applies rules based on his proficiency and personal experience from one loop to another or to monitor the instrument panel. These rules are not strict and depend on the pilot's judgment. Definition of a precise model for the process of selecting among the various loops is one of the most difficult problems to solve and is fully ignored in single loop models.

d) The model must be conceived in such a way that its various characteristic parameters be adjustable from one model of aircraft to another within a given type of aircraft. Obviously, the model for a Mach-2 fighter is necessarily different from that of a conventional subsonic aircraft.

e) Finally, the model must provide a good evaluation of the pilot's workload.

Research on such a multiloop model called "discrete-time model" because of its sequential nature, has been carried out in France, at ONERA (Office National d'Etudes et de Recherches Aérospatiales – French National Aerospace Agency) since 1973. These studies (ref. 16, 17) have led to the development of a computer program simulating the behavior of a pilot of a heavy transport plane (Airbus A300B) and capable to perform a particular flight path (final descent of an ILS approach). The model will soon be extended to make it adapt to various aircrafts of the same type (this version is currently being tested with a model of the Dassault Falcon 20).

ORIGINAL PAGE IS
OF POOR QUALITY

V. DESCRIPTION OF THE DISCRETE-TIME PILOT MODEL

In this model, it is assumed that, at a given time, the pilot can either make a decision or carry out one of the following three elementary actions :

- actuate a control,
- read an information on the instrument panel,
- monitor a given parameter displayed on a dial.

It is assumed that the pilot's strategy, that is the process of selecting among the various procedures of parameter correction, has a sequential nature and is a function of the flight situation defined by the aircraft type and condition, the flight phase and atmospheric conditions.

Experimental data have led to distinguish between three levels of activity in the pilot's operating mode (fig. 3). This classification is only an assumption, but seems to be close to reality and corresponds to the three types of loops discussed above.

LEVEL	*DEFINITION*	*OBJECTIVE*	*COST*
STRATEGY	*Choice of correction procedures*	*Short - term safety*	*Mental load (decision)*
CORRECTION PROCEDURE	*Algorithmic sequence of elementary actions*	*Immediate safety*	*Mental load (memorization)*
ELEMENTARY ACTION	*• Read indicator • Act on one control • Monitor one dial*		*Physical load*

Fig. 3 – Levels in operating mode.

The model selects the correction procedure to be used as a function of the followed strategy. This procedure is further divided into a sequence of elementary actions (instrument reading, monitoring of a parameter, action on a control) which are successively taken.

A dual integration is performed at each time in the model, namely the integration of the equations of motion and the integration of the equations describing the operating image of the situation as memorized by the model.

In the proposed strategy, care has been exercised to make a clear distinction between the selection of dials monitoring (a strategy with Markovian readings is used) and the selection of parameter correction procedures (a strategy with short term evaluation is used). The differenciation between these two strategies is based on the concept of seriousness of the instantaneous situation as perceived by the pilot's model and defined by :

$$G(O) = \text{Max. on the main parameters} \left| \frac{\text{estimated deviation}}{\text{permissible deviation}} \right|$$

This is the maximum ratio, over the flight path main parameters, between the estimated deviation (as memorized or predicted by the internal model) of a given parameter and its permissible deviation. The permissible deviations are determined experimentally. If $G(O)$ is under a given minimum threshold of seriousness, the situation is evaluated as safe and the model adopts the dial monitoring strategy ; if $G(O)$ is above his threshold, the situation is evaluated as serious and the model applies the strategy of parameter correction procedures (fig. 4).

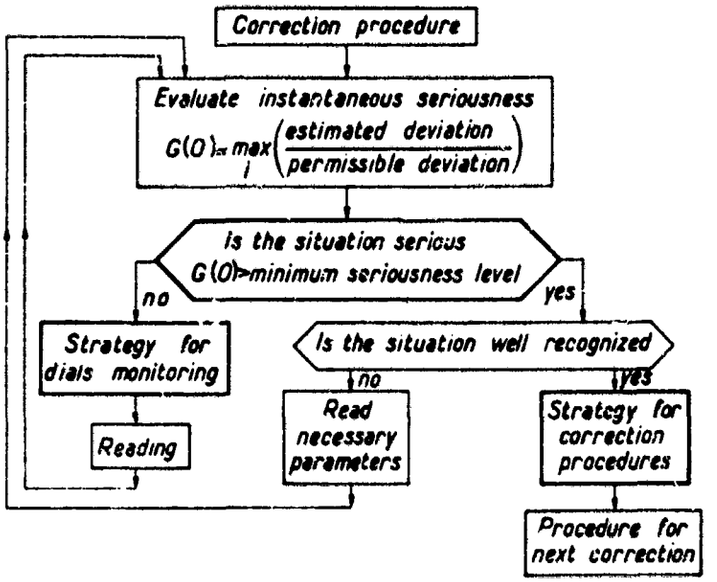

Fig. 4 – Overall strategy.

As far as the strategy of dials monitoring is concerned, the sequence of observed dials is governed by a matrix of conditional probabilities of reading each instrument after another one. This matrix is called "switching matrix". After each instrument reading, the value of a random variable determines which dial will be read next, depending on the switching matrix. The sequence of reading times is regarded as a Poisson process. Figure 5 gives an example of switching matrix in the case of the ILS approach phase of an Airbus A-300B. This matrix has been determined experimentally by means of an electro-oculometer. In retrospect, were observed in this matrix the features of elementary monitoring rules during IFR flight. For instance, the artificial horizon was mostly observed.

SWITCHING MATRIX

	ε GL	ε LOC	ż	Φ	Θ	Ψ	F	z	V
ε GL	0.03	0.10	0.11	0.04	0.15	0.03	0.06	0.21	0.20
ε LOC	0.28	0.15	0.05	0.21	0.06	0.23	0.05	0.05	0.08
ż	0	0.03	0.06	0.07	0.10	0.05	0.06	0.11	0
Φ	0.10	0.39	0.12	0.29	0.18	0.28	0.17	0.09	0.10
Θ	0.40	0.14	0.20	0.16	0.29	0.13	0.19	0.31	0.18
Ψ	0.06	0.12	0.16	0.13	0.13	0.10	0	0.16	0.07
F	0	0.01	0.10	0.01	0	0.05	0.11	0	0.09
z	0.03	0.04	0.13	0.07	0.07	0.11	0.12	0.12	0.08
V	0.08	0.02	0.07	0.02	0.02	0.02	0.24	0.05	0.20
Σ	=1	=1	=1	=1	=1	=1	=1	=1	=1

MATRIX OBTAINED WITH EOM EQUIPMENT

- ALL PARAMETERS $x_i < L_i$ ⇒ INSTRUMENT READINGS ARE GOVERNED BY THE SWITCHING MATRIX
- ONE PARAMETER $x_i \geq L_i$ ⇒ READING OF x_i
- SEVERAL PARAMETERS $x_i \geq L_i$ ⇒ READING OF x WHICH HAS THE GREATEST PROBABILITY IN THE SWITCHING MATRIX

L_i LEVEL GIVEN IN ADVANCE FOR EACH PARAMETER x_i

Fig. 5 – Strategy for dials monitoring.

C-3

ORIGINAL PAGE IS
OF POOR QUALITY

The strategy of the correction procedures is based on the fact that the human pilot makes decisions depending on the short-term predicted evolution of the situation while taking into account all previous actions.

The model has no access to the equations governing the aircraft dynamics but, by using its operating image, it can predict approximately the short-term situation. This prediction capability is used by the model to select the best correction procedure to implement, each time it is necessary. This choice is made by developping a logical tree (fig. 6) in which,

- the root is the memorized situation (So) ;
- branches are the correction procedures whose implementation is considered ;
- nodes other than the root are situation predicted from the root by means of the operating image while taking into account the intented correction procedures.

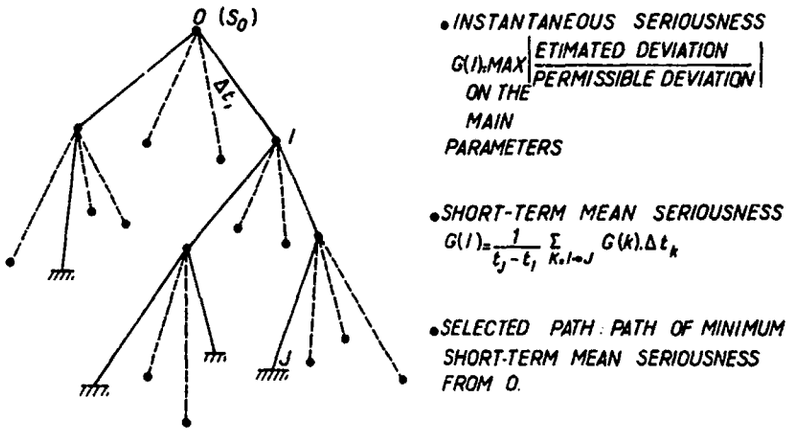

Fig. 6 – Strategy for correction procedures.

The instantaneous seriousness G(K) is computed at each node K. Considering that it remains constant during the time Δtl elapsed from the previous node to the node I, the model computes a short-term mean seriousness $G(I)$ on each path leading to a terminal node. To that end, the instantaneous seriousness is weighted by the time elapsed on each branch and the result is divided by the total time elapsed on the path. The short-term mean seriousness of a path (I, J) is then expressed by

$$G([I, J]) = \frac{1}{t_J - t_I} \sum_{K = I \rightarrow J} G(K) \cdot \Delta tk$$

The mean seriousness of the best path $G([I, J])$ chosen at I is denoted $G(I)$. This choice is simply made by taking among all possible paths from I the one with the minimum mean seriousness.

The path from the root with the minimum mean seriousness is then chosen and the implementation of the correction procedure corresponding to its first branch can be initiated.

VI. PROGRAM APPLICATIONS

Two applications have been made to validate this program. Both apply to the simu-

lation of the final descent of the ILS approach phase for an Airbus A-300B. First, a statistical comparison has been made between the performances of the model and those of professionnal pilots. Secondly, the performance loss of the model when the static margin of the simulated aircraft is decreased has been investigated.

VI,1. Comparison between the model and professionnal pilots

It is meaningless to compare the time responses obtained from the model and from human pilots. As good as it may be, the match between the curves cannot be perfect. A statistical comparison would be more meaningful. We have therefore chosen a comparison between the standard deviation and the performance, which are defined below for the various flight parameters.

$$\text{Standard deviation } \sigma x = \sqrt{\frac{\int_0^t x^2\,dt}{t}}$$

$$\text{Performance } \quad Px = \sqrt{\frac{t}{\int_0^t |x|\,dt}}$$

where t is the duration of the final descent of the ILS approach phase.

The results from the model have been compared to those of five professionnal pilots performing final descents in IFR conditions on a flight simulator representing the heavy transport plane considered in this study. The comparison is illustrated in figure 7 ; it can be seen that the model exhibits a behavior close to the pilot's as far as the above defined standard deviations and performances are concerned.

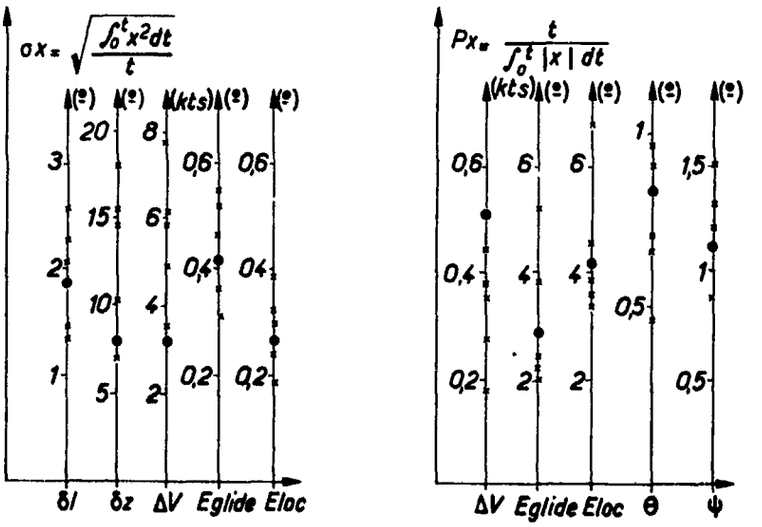

Model-pilot initial deviations at 1900 feet

x human pilot

● model

Localizer deviation : − 0,6°
Glide path deviation : 0,65°
ΔV = + 8 kts (Va = 137 kts)

Fig. 7 – Standard-deviations and performances.

ORIGINAL PAGE IS
OF POOR QUALITY

VI,2. Application of the model to flight control with reduced static margin

One of the first practical applications of the model has been the study of its performance loss when the static margin of the simulated aircraft decreases, i.e. when the center of gravity moves backward, progressively destabilizing the plane. It appears that the performance of the model decreases when the static margin is reduced, which seems realistic. The loss of control occurs suddenly (fig. 8) when the workload resulting from a decrease in static margin becomes excessive. The most interesting result of this study is that, whenever control difficulties appear on the pitch axis, the overall aircraft control is impaired ; for most of the cases losses of control occur on the transversal axis.

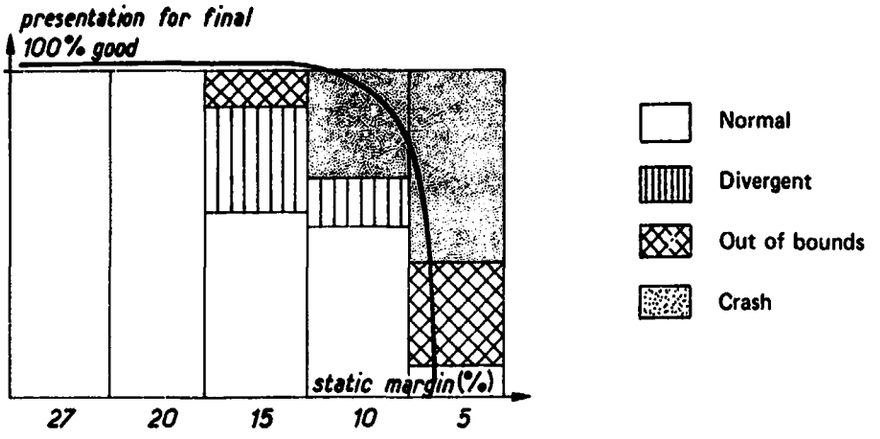

Fig. 8 – Basic ILS approaches with reduced static margins.

VII. CONCLUSION

The model described in this paper is expected to be more conform to the actual pilot's behavior than those of previous studies. It tries to make a synthesis between the mathematical approach and the psychological approach through the introduction of the aircraft internal model.

In the future, studies will attempt to introduce the concept of pilot adaptativity to a new type of aircraft as well as the concept of learning which could take into account the degree of professionnal development of individual pilots.

REFERENCES

1. Goodyear Aircraft Corporation – Final Report : Human Dynamics Study – Report GER-4750, April 1952.

2. McRuer D., Graham D., Krendel E., Reisener W. – Human pilot dynamics in compensatory systems. USAF Tech., Report AFFDL TR-65-15, July 1965.

3. McRuer D., Jex H. – A review of quasi linear pilot models. IEEE Transactions on Human Factors in Electronics, vol. 8, No. 3, pp. 231-249, September 1967.

4. McRuer D.T., Krendel E.S. – Mathematical Models of Human Pilot Behavior. AGARDograph No. 188, January 1974.

5. Bekey G.A., Meissinger H.F., Rose R.E. – Mathematical models of human operators in simple two-axis manual control systems. IEEE Transactions on Human Factors in Electronics, vol. 6, pp. 42-52, 1965.

6. Kleinman D.L., Baron S., Levison W.H. – An Optimal Control Model of Human Response – Part I, pp. 357-369, Part. 2, pp. 370-383, Automatica, vol. 6, No. 3, May 1970.

7. Kleinman D.L., Baron S. – Manned Vehicle Systems Analysis by Means of Modern Control Theory. NASA CR-1753, June 1971.

8. Kleinman D.L., Baron S., Levison W.H. – A Control Theoretic Approach to Manned-Vehicle Systems Analysis. IEEE Trans., vol. AC-16, No. 6, pp. 824-832, December 1971.

9. Piaget J., Inhelder B. – Mémoire et Intelligence. Col. BSI-PUF-1968.

10. Bisseret A. – Mémoire opérationnelle et structure du travail. Bulletin de Psychologie XXVI, 1972-1973.

11. Sperandio J.C. – Compléments à l'étude de la mémoire opérationnelle. Deux expériences sur les contrôleurs de la navigation aérienne. Le Travail Humain, vol. 38, 1975.

12. Veldhuyzen W., Stassen H.G. – The Internal Model - What does it mean in Human Control ? - International Symposium NATO "Monitoring Behavior and Supervisory Control", Published in NATO Conference Series III, vol. 1 by Plenum Press, 1976.

13. Phatak A.V. – Formulation and Validation of Optimal Control Theoretic Model for Human Operator. IEEE Systems Man and Cybernetics Newsletters, vol. 2, June 1976.

14. Wanner J.C. – General guideline for the design of manned aerospace vehicles - Automation on Manned Aerospace System. AGARD Conf. Proc. No. 114 (1973).

15. Wanner J.C. – The multiloop concept of the pilot workload as a basis of future experiments and studies. T.P. ONERA No. 1978-10.

16. Cavalli D., Soulatges D. – Discrete-time modelization of human pilot behavior. Proceedings of the 11th Annual Conference on Manual Control. NASA Ames Research Center, Ca. May 1975, NASA TM X-62, 464, pp. 119-129.

17. Cavalli D. – Discrete-time modeling of heavy transport plane pilot behavior. Proceedings of the 13th Annual Conference on Manual Control, MIT, Cambridge, Mass., June 1977, pp. 321-328.

SESSION D: FLIGHT CONTROL AND PILOT DYNAMICS

Chairman: I. Ashkenas

D14

N79-15602

FLIGHT EXPERIENCE WITH MANUALLY CONTROLLED UNCONVENTIONAL AIRCRAFT MOTIONS

BY

A. FINLEY BARFIELD

AIR FORCE FLIGHT DYNAMICS LABORATORY

WRIGHT-PATTERSON AFB, OHIO

ABSTRACT

During 1976 and 1977, a modified YF-16 aircraft was used to flight demonstrate decoupled control modes under the USAF Fighter Control Configured Vehicle (CCV) Program. Higher levels of direct force control were achieved by the aircraft than had previously been flight tested. The direct force capabilities were used to implement seven manually controlled unconventional modes on the aircraft, allowing flat turns, decoupled normal acceleration control, independent longitudinal and lateral translations, uncoupled elevation and azimuth aiming, and blended direct lift. A miniature two-axis force controller was installed on top of the YF-16 sidestick controller for commanding the decoupled modes. At the pilot's discretion, the directional modes could also be commanded using rudder pedals.

The unconventional control modes were flight evaluated during simulated operational tasks, such as air-to-ground bombing and strafing, and air-to-air tracking and defensive maneuvering. The flight testing identified many actual and potential uses for these control modes, but also identified areas where refinements are needed to arrive at operationally suitable implementations. This paper describes the design, development, and flight testing of these new control modes. It includes lessons learned in the areas of unconventional control law implementation and controller design. The need for task-tailored mode authorities, gain-scheduling and selected closed-loop design is discussed.

INTRODUCTION

The Air Force Flight Dynamics Laboratory's Fighter CCV Advanced Development Program was conducted to develop and evaluate advanced control concepts for improving fighter aircraft mission effectiveness. Specific new control degrees of freedom were provided in an existing high-performance fighter. Control modes selected for implementation had been identified by previous research efforts as possessing the potential for significantly improving fighter aircraft performance. Use of these unconventional control modes provided the pilot with unique aircraft maneuvering capabilities. This program provided the first true test of

188

PAGE INTENTIONALLY BLANK

the utility of these new capabilities. Design, modification and flight testing were conducted under contract to General Dynamics/Fort Worth.

The YF-16 shown in Figure 1 was uniquely suited as a testbed for the program. It served as a state-of-the-art baseline configuration with its full authority quad redundant analog Fly-by-Wire control system, sidestick controller, and advanced aerodynamic design employing vortex lift and leading edge maneuvering flaps. The aircraft was designed to be statically unstable longitudinally in subsonic flight with artificial stability being provided by the control system. Angle of attack and "g" limiting allowed full maneuvering without reliance on stall warning or cockpit instruments and provided maximum use of the airframe load factor capability throughout the flight envelope. This advanced control system design facilitated implementation of the new CCV control modes.

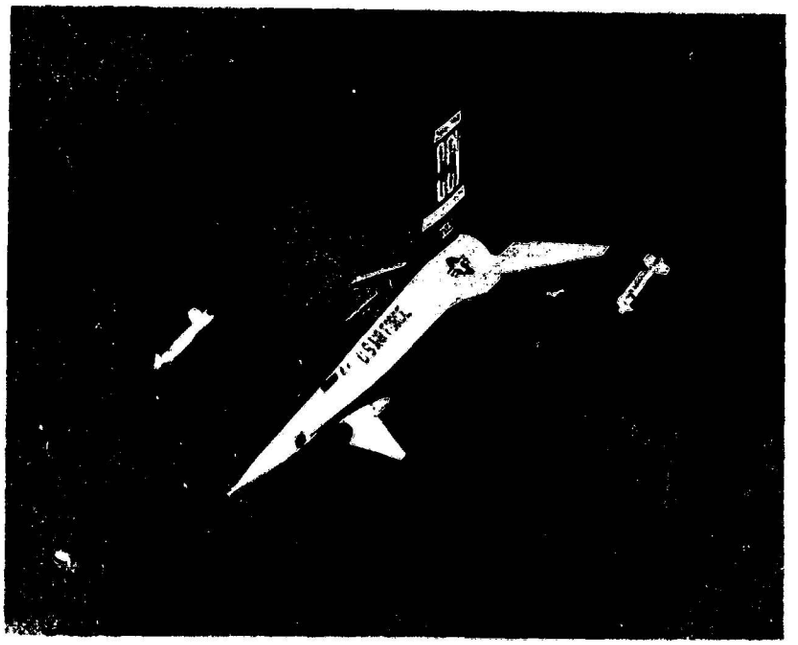

Fig 1 Fighter CCV Test Aircraft

ORIGINAL PAGE IS
OF POOR QUALITY

DESIGN APPROACH

Cost effectiveness and safety considerations were major driving factors in the configuration selection and design. In this light only minor modifications were made to the YF-16 aircraft. Although providing a means of assessing the new control capability, this approach prevented overall control and aerodynamic design optimization. Exterior changes to the aircraft consisted of the addition of twin all-movable vertical canards. The new surfaces, canted outward 30 degrees from vertical, were

attached at the engine inlet. The installation was accomplished without altering the external or internal mold lines of the inlet. Although separately actuated, the canards are deflected together by the same pilot-generated command signal. Use of the canards in conjunction with the rudder enabled direct sideforce to be developed by the aircraft. The flaperons were modified to allow both up and down symmetric deflections. Operation of the flaperons with the horizontal tail provided a direct lift capability.

An auxiliary analog computer was added to allow implementation of the new control laws. A fail-safe design was required. Additionally, the CCV modifications were not to result in degradation of the operational reliability of the basic YF-16 control system. That system was retained intact to provide suitable control and stability augmentation. The conventional YF-16 control system formed the baseline configuration for the program. It also served as the reversion configuration should problems cause CCV system disengagement. The addition of CCV signal interfaces was the only change to that system. Control reconfiguration was achieved by injection of bias signals and crossfeeds to alter the normal pilot commands or system feedbacks. Operation throughout the aircraft's envelope was needed for a valid evaluation of the unconventional modes. Gain scheduling was extensively employed to provide proper response as flight conditions varied. Emphasis was placed on obtaining maximum CCV mode capability across the mach-altitude range without creating adverse transients.

Crew station changes involved the addition of instruments such as sideslip, side acceleration, canard and flaperon position indicators to allow evaluation of CCV responses by the pilot. A CCV control panel was installed to enable mode selection, and modifications were made to the trim button on the sidestick controller to provide a means of commanding the open-loop CCV modes.

UNCONVENTIONAL CONTROL MODES

At the pilot's command were six open-loop modes illustrated in Figures 2 and 3. Direct control of the aircraft's flight path in two axes was provided by the A_n and A_y modes. The aircraft rotated in pitch and yaw with the velocity vector. In pitch, α was held constant while direct lift was generated on the aircraft. Sideslip remained zero during use of the sideforce mode as side acceleration was generated allowing turning of the aircraft without banking. Attitude control at constant flight path angle was available with the α_1 and β_1 modes resulting in independent fuselage pointing in either axis. Vertical and lateral translations were provided by the α_2 and β_2 modes. In this case vertical velocity and side velocity were the controlled parameters at constant aircraft attitude. Thus the aircraft could effectively elevate or side step.

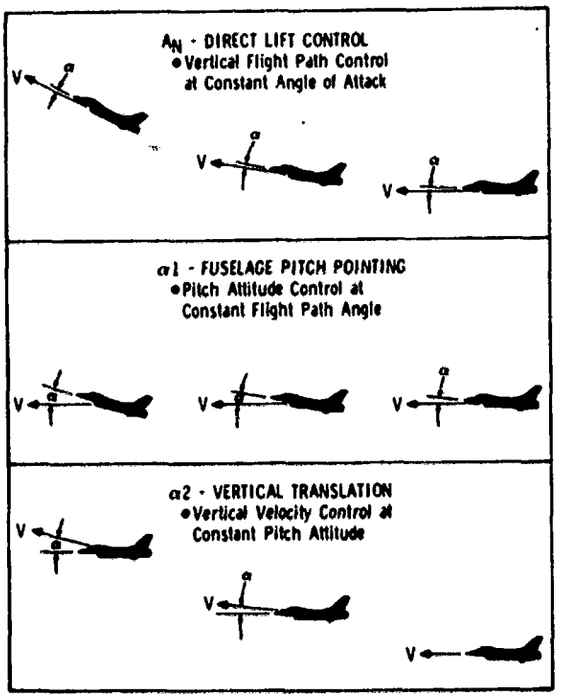

Fig 2 Open-Loop Longitudinal CCV Modes

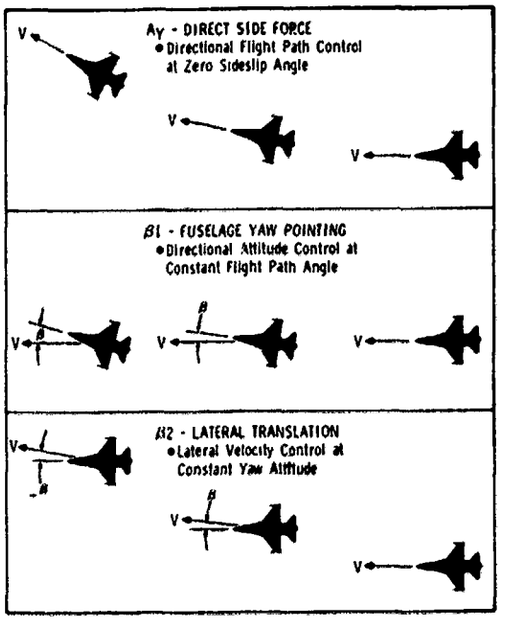

Fig 3 Open-Loop Directional CCV Modes

One closed-loop mode, Maneuver Enhancement (ME), was also available to the pilot. Direct lift was blended with basic aircraft pitch control in this mode. It provided an initial direct lift during a maneuver which was washed out as the commanded aircraft normal acceleration was obtained. Use of this capability resulted in maneuver quickening. Due to the use of normal acceleration feedback, a level of gust alleviation was also provided as illustrated in Figure 4.

Implementation in accordance with the approach of an "add on" design is illustrated with the simplified block diagrams in Figures 5, 6 and 7. The conventional YF-16 control system is shown in solid black in the figures. Dashed lines indicate the CCV modes. For the three open-loop longitudinal modes, the pilot commands flaperon deflection directly with the elevator being driven through a scheduled crossfeed gain. Biases to prevent opposition of the CCV commands are computed and introduced into the YF-16 control system. In the case of the A_n mode, Figure 5, stick command and pitch rate paths are modified by the bias signals. CCV system gains were determined using wind tunnel data and digitally predicted aircraft responses.

ORIGINAL PAGE IS
OF POOR QUALITY

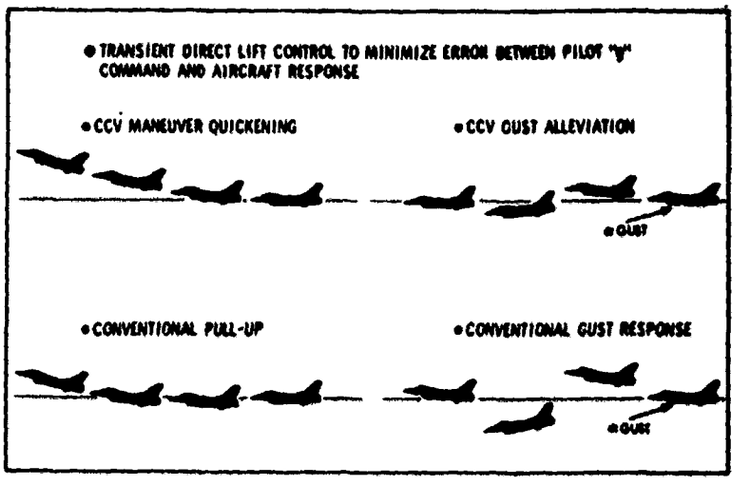

Fig 4 Maneuver Enhancement Mode

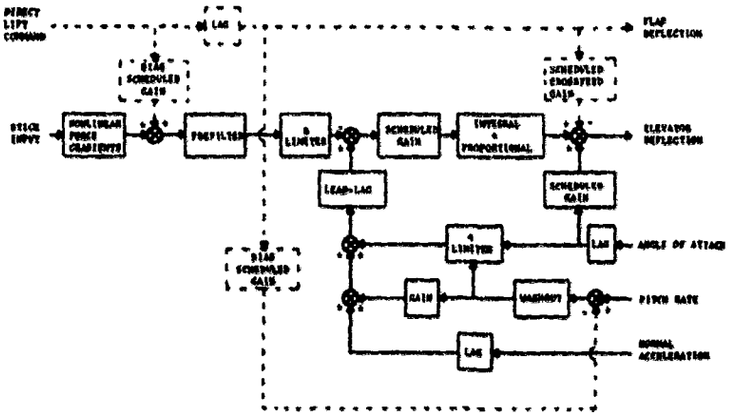

Fig 5 Simplified Functional Block Diagram of the A_n Mode

The directional modes are structured in much the same manner. The pilot commands a canard deflection with an appropriate crossfeed to the rudder as shown for the direct sideforce mode in Figure 6. In this case a gain scheduled crossfeed to the flaperons is needed to counter rolling moments from the canard-rudder deflections. Biases are also added to the yaw rate and lateral acceleration feedbacks of the basic control system.

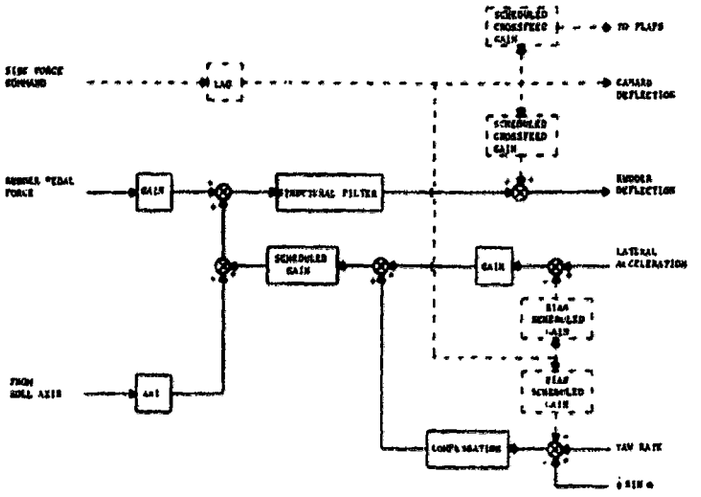

Fig 6 Simplified Function Block Diagram of the A_y Mode

The one exception to this type of implementation is Maneuver Enhancement. As shown in Figure 7, the error between pilot command and aircraft normal acceleration drives the flaperons and horizontal tail. A washout in the pitch rate feedback path, and integral plus proportional control in the forward path, provides a "g" command response in steady state. Thus as the aircraft attains the commanded "g" level, the direct lift flaperons return to zero deflection. The technique provides an instantaneous direct lift for maneuver quickening. Gust alleviation is obtained when the normal accelerometer feedback senses gust induced aircraft response and drives the flaperons to counter it.

Minor modifications to the YF-16 cockpit were made to allow use of the CCV modes. Specific modes are selected by the pilot using the CCV control panel shown in Figure 8. Any of the three open-loop longitudinal modes can be commanded by fore or aft force on the CCV controller installed on the YF-16 sidestick, Figure 9. The trim switch was replaced with the two-axis CCV force controller, and the normal "coolie hat" thumb button was retained. The three open-loop directional modes can be selected for operation through either rudder pedal inputs or left/right force on the CCV controller. Besides mode selection the control panel also provides the pilot with pitch and roll autopilot

functions as well as mode purification capability. Purification was designed to allow engineering evaluation of the modes by enabling various feedbacks to force "pure" steady state uncoupled aircraft motion. In this way the adequacy of interconnect and bias gain schedules based on predicted CCV responses could be ascertained. The control panel also provides a means of removing side acceleration, A_y, feedback to the rudder in the basic control system. Various self-test functions were also included for system checkout and diagnosis on the ground.

ORIGINAL PAGE IS
OF POOR QUALITY

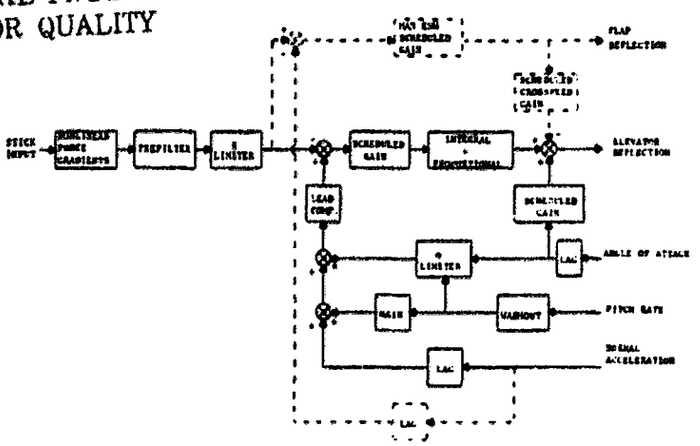

Fig 7 Simplified Functional Block Diagram of Maneuver Enhancement

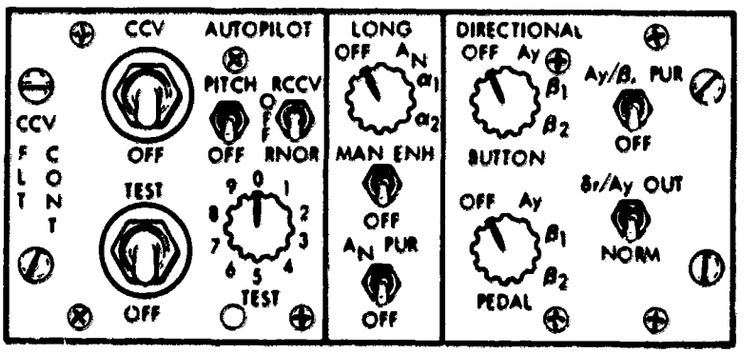

Fig 8 CCV Control Panel

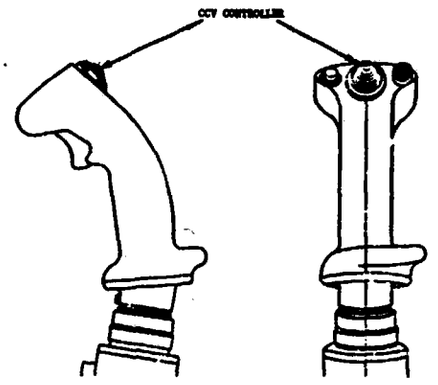

Fig 9 CCV Controller Installation on Sidestick

The basic airplane sidestick controller is essentially a force stick although the sensors employed are Linear Variable Differential Transformers which measure a very small displacement of the stick resulting from forces applied by the pilot. Maximum command in pitch requires 31 lbs.,and maximum roll requires a little more than 15 lbs. Both axes have parabolic stick force versus command gradients. The CCV button has a 0.1 lb. deadzone with a linear force versus command gradient up to a maximum of 3.1 lbs.

FLIGHT TESTING

The flight test program consisting of 87 flights and totalling over 125 flight hours was conducted at Edwards AFB in California. Figure 10 presents the range of flight conditions over which testing was performed. Initially the flight envelope was cleared in tests to identify flutter, aeroservoelastic instabilities, or stability and control problems. The effect of the canards addition on inlet/engine operation and the aerodynamic destabilizing effects were also evaluated during the initial tests. Preliminary checks were performed to verify proper functioning of the CCV control system. Engineering evaluations were then conducted to ascertain the functional adequacy of the CCV control system design and to obtain data for detailed evaluation of the various mode characteristics. Figure 10 also indicates test conditions for evaluating predicted performance improvements with Relaxed Static Stability (RSS). Although not covered in this paper, the aircraft's fuel system was modified to allow a wide range of center-of-gravity locations to be evaluated during the later portion of the test program. Finally quasi-operational tasks were conducted simulating air-to-air gunnery, formation, refueling, air-to-ground bombing and air-to-ground strafing.

ORIGINAL PAGE IS
OF POOR QUALITY

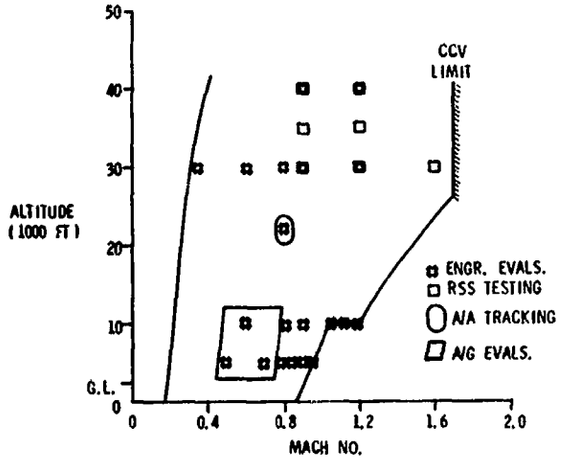

Fig 10 Primary Test Points

The CCV modes produced responses as predicted, and the modified aircraft was found to be free of instabilities. It also possessed adequate handling qualities throughout the flight envelope up to its angle of attack and sideslip limits. No adverse effects of the canards on inlet or propulsion system performance were detected. Although the canards were destabilizing both longitudinally and directionally, the YF-16 control system provided stability augmentation that effectively compensated for the change. The engineering evaluations provided data to allow refining of the CCV control system gain schedules which had been selected originally on the basis of wind tunnel information. The evaluations also verified the available CCV mode authorities. Direct lift levels of up to $\pm$ 1.5 g's and side force levels of 0.9 g were obtained. These capabilities varied considerably with flight conditions since the design was to obtain maximum capability, and not to provide uniform authority. Yaw pointing levels approaching $\pm$ 5 degrees and pitch pointing of approximately $\pm$ 2 degrees were realized. Translation authorities of 1500 fpm rate of climb for the α_2 mode and 40 kts side velocity for the β_2 mode were demonstrated.

The Handling Qualities During Tracking (HQDT) technique developed at the NASA Dryden Flight Research Center and the Air Force Flight Test Center was used for engineering analysis of the CCV modes during tracking. For this technique, scored gun camera film is used to obtain a quantitative measure of handling qualities, control system characteristics, and precision controllability during high-gain tracking tasks. A fixed depressed reticle is used in a preplanned tracking task employing in this case an F-4 or T-38 target aircraft. The air-to-air tracking maneuver

consisted of windup turns (WUT) to 4.5 g's and 3g constant turns. The technique was also applied to air-to-ground runs with limited success. Unfortunately, the technique does not resemble most air-to-ground delivery techniques. RMS, mean, and median tracking errors along with time histories of pipper position relative to the target are provided by the technique. This data was used in connection with pilot ratings and comments to evaluate the CCV modes' usefulness. Ordnance was not actually delivered because the YF-16 testbed did not have a weapon delivery capability.

Early in the evaluations, results from tracking with Maneuver Enhancement indicated the usefulness of this mode. Figure 11 is a longitudinal parameters comparison of the aircraft with and without ME during a windup turn tracking task. The reduction in magnitude of pitch rate perturbations and pilot inputs indicates a useful mode for precise tracking. Tighter "g" control was available to the pilot, and small corrections could be made without causing large rotational rates. This preliminary assessment proved to be correct when pilots from the F-16 Joint Test Force evaluated the modes in simulated air-to-air gunnery.

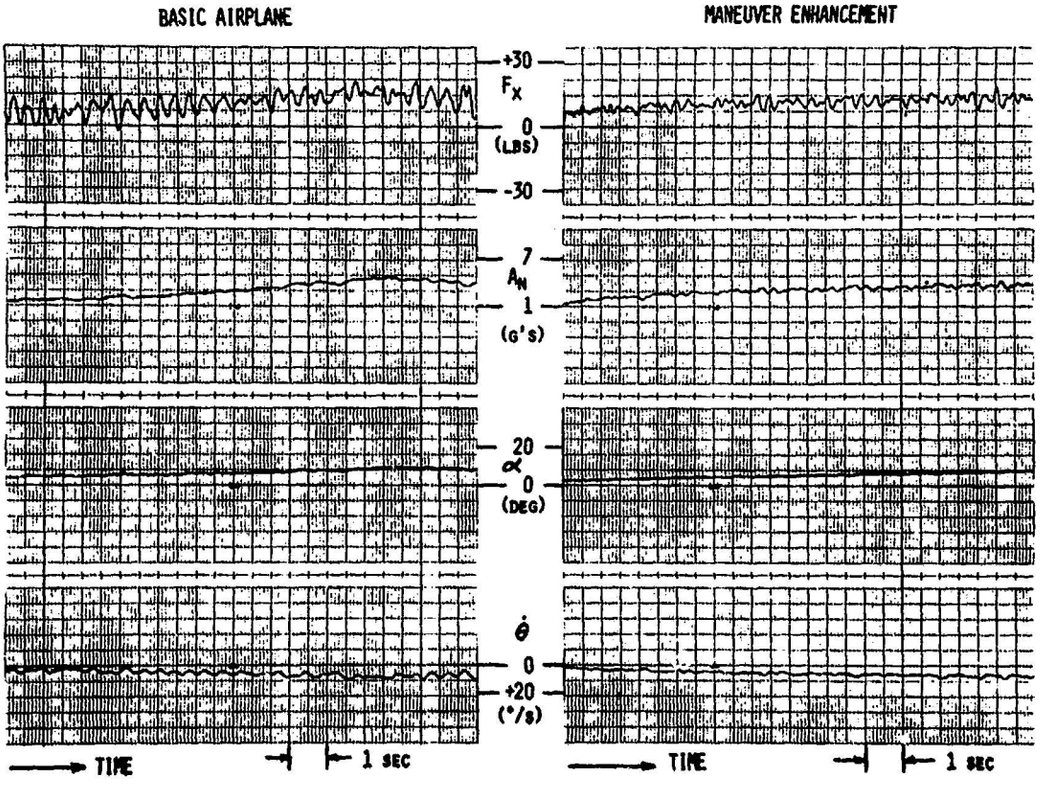

Fig 11 Windup Turn Tracking

ORIGINAL PAGE IS
OF POOR QUALITY

Overall assessment of the CCV modes for various operational tasks are shown in Figure 12. This is a consensus of pilot opinion on the potential improvement these modes could provide. A "G" or green rating indicates that the mode is either preferred or has the potential for improvement over conventional controls. The "Y" or yellow rating is used to denote that the mode did not show a potential improvement over conventional controls or that pilot ratings and comments were inconclusive.

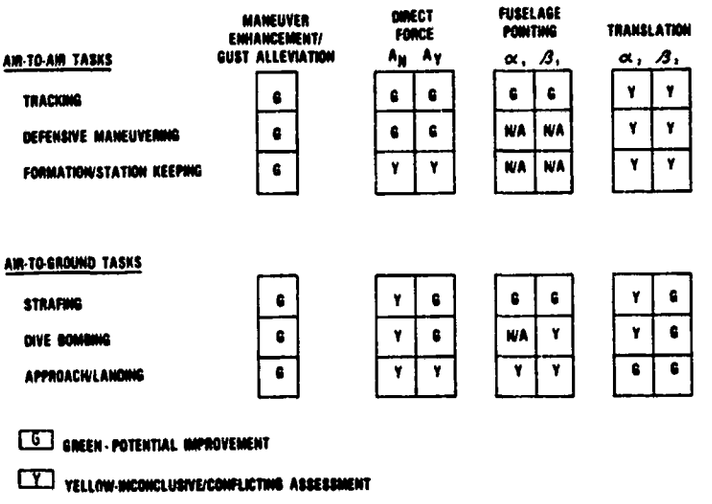

Fig 12 CCV Mode Assessment

Maneuver Enhancement was considered an improvement as it was implemented on the test aircraft in all air-to-air tasks. It provided tighter control in a tracking situation without the usual rotational perturbation. Pilot control was not complicated by an additional controller since this was a blended mode on the normal sidestick. Washout of flaperon deflections prevented saturation problems of the limited authority direct lift capability.

The direct force modes, A_n and A_y,were preferred over pointing or translation for precise tracking. The mechanization allowed pilots to "beep" CCV commands using the button controller in much the same manner as a trim switch. It provided an immediate precise change in flight path. Such a "beep" technique was realizable because command and release cause no objectionable pipper transients. The direct force modes were also considered to hold promise for some unusual and effective defensive maneuvering capabilities, but larger authority levels than obtainable on the CCV YF-16 were desired by most of the pilots.

The pointing modes were difficult for manual pilot control. Although providing reasonable authority and precise fuselage pointing, the command had to be held in continuously. Upon release of the CCV controller, the pipper moved sharply away from the target as the aircraft returned to align with the velocity vector. This proportional input on the CCV controller,while trying to keep the basic tracking solution through changing forces on the sidestick,resulted in what one pilot referred to as a hand conflict. A tendency existed to rapidly reach and hold full pointing capability as the maneuver changed. The pilot had to immediately realize when maximum capability had been reached and revert to basic aircraft control for further error reductions. This would result in maneuvering the aircraft with full pointing capability being commanded and at times introduced unwanted lags in tracking. Even with these drawbacks, the mode was rated highly as far as its potential for improvement. Most pilots commented that an automatic tie-in with the fire control system would make a very effective gunnery system.

The translation modes were implemented with slow onset rates and low steady state authorities which made them unsuitable for air-to-air combat maneuvering. Due to the open-loop design, the aircraft had a tendency to coast after a translation command had been removed. This was bothersome to the pilot as he tried to close on another aircraft since exact final position was not easily predicted. The translation modes could be used for formation/station keeping; however, the task was adequately handled with the basic aircraft controls. Thus, a clear need for improved means of accomplishing the task did not exist. The one exception was application in refueling operation. The CCV modes were believed to offer significant advantages in this case. Unfortunately, due to the limited redundancy in the mechanization and safety considerations, such applications could not be evaluated. Refueling with CCV modes engaged was prohibited.

For the air-to-ground work, Maneuver Enhancement again demonstrated an improvement as implemented on the test aircraft (Figure 12). This was primarily due to: 1) the gust alleviation capability it provided; and, 2) the increased response when pulling out of a dive. The manual control task was not significantly changed with the blended implementation on the sidestick. Normal piloting techniques could be used for task accomplishment.

Direct side force, A_y, received favorable pilot rating for both strafing and dive bombing. The primary advantage was elimination of having to roll-pull-roll back to make directional corrections. The effect of each correction could be immediately and easily determined since the basic sight picture remained unchanged. Rudder pedals for A_y commands were well liked,and the pilots easily adapted to their use. The authority provided appeared excessive for terminal tracking. The A_n mode found only sparing application in the air-to-ground tasks because longitudinal control posed no specific problem and was easily accomplished with the normal stick commands. Use of the force button was not natural

for the pilot in these tasks, and cross-talk between button and stick existed.

Pointing capability in both axes was found useful for strafing runs. Two techniques were used with pitch pointing. In the first method the pipper was allowed to walk up to the target and was then held on the target with the pointing capability to provide a longer firing opportunity. The second technique involved using full nose down pointing throughout the run. This allowed considerably more ground clearance during low-level passes. For bombing, the pointing modes were not appropriate since the velocity vector was not being changed. There was one exception. It was possible to use the mode to mimic the translation mode's crosswind cancelling capability with higher responsiveness. This was accomplished by establishing a crab in the normal manner to counter the crosswind and allow the flight path to cross the target. Then yaw pointing was used to align the nose with the resultant velocity vector giving the pilot a good HUD sight-target picture.

Longitudinal translation was useful in the power approach for maintaining a desired glide path. However, due to the limited authority and slow response, it was not satisfactory for strafing or bombing. In addition, the normal longitudinal command provided adequate control for these tasks. The lateral translation capability was useful for crosswind corrections during both landing approach and dive bombing. It could also be used to attack moving targets from an approach perpendicular to the target's motion. Slowness of response and the requirement to hold a constant button force during mode usage were considered drawbacks of these two modes.

SIMULATION INVESTIGATION

Results of the flight testing showed the need for additional unconventional control mode studies. Pilot comments clearly indicated the capability provided by the unconventional modes had the potential for improving the aircraft's effectiveness, but some aspects of the particular implementation on the test vehicle were unsatisfactory. The two-axis force button selected after evaluation of several types of controllers in a fixed-base simulation at General Dynamics provided adequate for engineering evaluations but lacking for operational usage. Various mode authorities, responses and mechanizations were found to be inadequate for tracking and weapon delivery tasks. The flight test effort had been extremely ambitious in terms of flight rate. This restricted modifications from being accomplished to the CCV hardware except to satisfy safety-of-flight requirements. As a result of these findings, the Flight Control Division of the Flight Dynamics Laboratory initiated an extensive simulation investigation to be conducted on the Large Amplitude Multi-mode Aerospace Research Simulator (LAMARS) shown in Figure 13. LAMARS comprises part of the Flight Dynamics Laboratory's Engineering Flight Simulation Facility at Wright-Patterson. The sphere, containing a single place cockpit, and the 30 ft. support beam are computer controlled to provide realistic cockpit motion cues. The pilot's visual display is

projected on the interior of the 20 ft. sphere. It can be either a simple sky/earth image or projection of terrain features from one of two 15 ft. by 48 ft. terrain boards. An air-to-air target aircraft projector is also included for combat simulations. The spherical contour provides a maximum 266 degree horizontal and 108 degree vertical field of view. Motion capability of the simulator is listed in Figure 14. A hybrid computing system forms the core of the simulation facility. Nonlinear aerodynamics and the complete YF-16 and auxiliary CCV control system have been modeled on the computers.

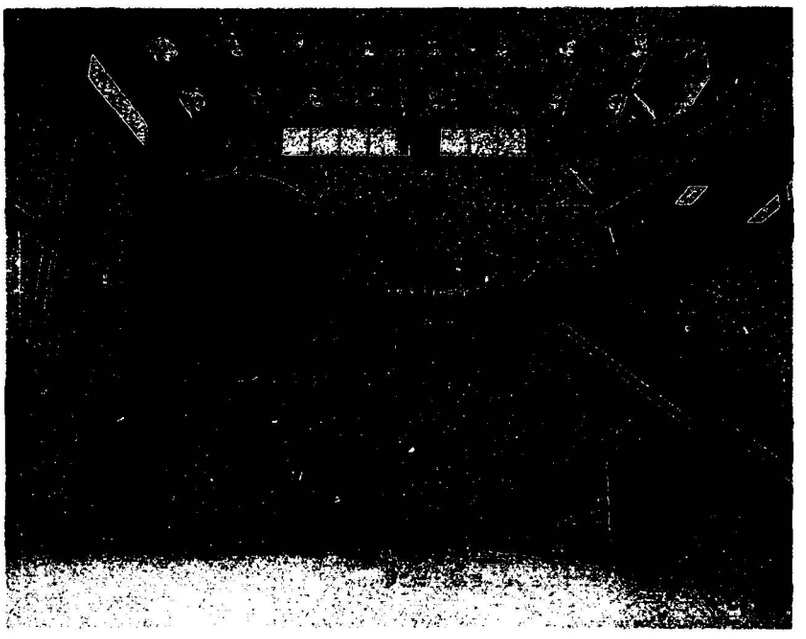

Fig 13 LAMARS Facility

Major emphasis of the simulation program will be the development of Task-Oriented CCV control modes. The LAMARS effort will pursue two different approaches in the investigation of unconventional aircraft maneuvering capabilities. The first will be concerned with minor modifications to the CCV modes as they were implemented on the YF-16. This approach is aimed at resolving basic problems/shortcomings highlighted during the flight test program. Candidate changes are listed below:

- CCV controller gradient variations
- Alternate gain scheduling
- Integral command of pointing and translation modes
- Elimination of operating restrictions

ORIGINAL PAGE IS
OF POOR QUALITY

° Mode authority matching and tailoring

	DISPLACEMENT	NO-LOAD VELOCITY	STALL ACCELERATION
BEAM-VERTICAL	± 10 FT	13 FT/SEC	± 3 G
BEAM-LATERAL	± 10 FT	10 FT/SEC	± 1 65 G
SPHERE-PITCH	± 25 DEG	60 DEG/SEC	± 400 DEG/SEC^2
SPHERE-YAW	± 25 DEG	50 DEG/SEC	± 200 DEG/SEC^2
SPHERE-ROLL	± 25 DEG	60 DEG/SEC	± 460 DEG/SEC^2

Fig 14 LAMARS Motion Capability

The gradient variations and gain scheduling are both intended to reduce mode sensitivity evident in the air-to-ground tasks. An integral mechanization would allow "pulse" type inputs without requiring the pilot to hold CCV commands during a tracking task. Unfortunately, this quickly results in mode authority saturation. A trim type follow-up technique is needed in which adverse pipper motion does not result. In order to develop "pure" CCV modes and insure safety from failures with the limited redundancy employed in flight test, rather severe restrictions were placed on several modes. The emphasis will now be on obtaining "useful" modes by reducing these restrictions such as bank angle and α limits and accepting impure responses. In the interest of providing the pilot with a useful tool, authority of the modes will be tailored to the operational task and matched in both axes for control harmony. In addition, the CCV modes will be evaluated with several HUD gun-sight systems to ascertain the benefits and problems associated with such use.

The second approach involves alternate methods of providing the CCV capabilities to the pilot and new control law structures. It includes consideration of the following techniques:

° Blended modes using only the YF-16 sidestick

° Weapon-line stabilization and improved gust alleviation

° Closed-loop velocity command

Based on the acceptance by the pilot of the maneuver enhancement mechanization and the fact that pilot workload was actually increased with the addition of another controller in the cockpit, blending of CCV

modes with the basic aircraft controls is needed. Such blending must not result in adverse transients on initial command or when reaching maximum CCV authority. In addition, a means must be provided to washout CCV inputs to prevent combat maneuvering with residual canard or flaperon deflections. The mode to be blended will be selected based on its usefulness in the particular mission phase being flown. The techniques being considered included frequency selective separation of CCV versus conventional stick inputs using filter techniques and separation based on detected command magnitude and rate. In both cases gradual removal of the CCV mode in steady state is required. A recentering technique allowing placement of CCV command gradient within the basic control system stick force gradient is also being examined. Such a technique would provide the CCV capability as a vernier control for the pilot while allowing normal aircraft maneuvering for large inputs. Such a recentering scheme must allow full aircraft capability to be commanded and must not produce an unacceptable stick force per "g" relationship.

Work is being conducted to arrive at an optimum design of maneuver enhancement to provide weapon-line stabilization for improved gunnery. In this application the primary design objective is faster acquisition and better tracking as opposed to simply quickened maneuvering response. Changes to improve the gust alleviation capability are also being studied, but the focus is on reducing pipper disturbance rather than improving ride quality.

Closed-loop design providing a velocity command system for the translation modes is aimed at faster mode response and the elimination of coasting. With such a design, the pilot would command vertical or side velocity instead of flaperon or canard deflection. The control system positions the surfaces as needed to develop or cancel independent translations. This would improve mode usefulness in tasks requiring precise positioning and possibly allow application to combat maneuvering.

The flight test also accented the need for more operationally oriented evaluation techniques. The HQDT constant "g" and WUT tracking maneuvers for 20 to 30 seconds are not reasonable for representation of the air-to-air combat situation. Although providing useful information on basic control characteristics in a tracking task, it is not well suited for task-oriented design. In an effort to solve this problem, the LAMARS simulation will be using various weapon delivery scoring techniques based on aircraft position, target location and munition ballistics. However, HQDT type data will be taken for correlative purposes. Target aircraft combat algorithms to allow realistic operational task evaluation of the CCV modes have also been developed.

CONCLUSIONS

Flight testing of the Fighter CCV has provided valuable insight into the implications to manual control of uncoupled aircraft motions. A pronounced learning curve was encountered due to the very unusual maneuvers possible with the CCV modes in the flight evaluation. While

ORIGINAL PAGE IS
OF POOR QUALITY

providing additional capability, the open-loop modes sometimes resulted in an increase in pilot workload with the addition of another controller. Use of rudder pedals for A_y command was natural for the pilot. The one blended closed-loop mode, Maneuver Enhancement, was found to be beneficial during all evaluation tasks. Although requiring optimization, the blending technique was readily accepted by the pilot. The flight test program demonstrated the feasibility of decoupled aircraft control and verified predicted performance levels. It also provided an indication of the usefulness of these new control modes in operational tasks.

The urgent need for task-oriented control mode investigations was clearly indicated during the test program. The CCV modes were implemented from an engineering standpoint of obtaining "pure" motion with well-behaved responses and maximum capability throughout the flight envelope. Emphasis must now be placed on designing to the specific task application. Through the use of AFFDL's large moving-base simulator and lessons learned from flight testing, engineering efforts are underway to provide CCV capabilities to the pilot in a manner that will significantly improve fighter aircraft effectiveness. Prior to adaptation in future designs, these capabilities must be provided in ways which do not complicate the manual control task. A multimode approach is indicated in which the pilot is provided with various predetermined combinations of conventional and CCV control tailored to the specific mission phase.

N79-15603

PILOT-OPTIMAL AUGMENTATION SYNTHESIS

by

David K. Schmidt

School of Aeronautics and Astronautics
Purdue University
West Lafayette, Indiana 47907

Abstract

Given adequate open-loop specifications, for example, aircraft handling qualities criteria, design techniques, particularly modern control approaches, are available to the system designer for synthesizing even the most complex flight control systems. Unfortunately, however, weaknesses exist in the handling qualities areas, particularly for "non-conventional" aircraft such as V/STOL and control configured vehicles (CCV's). In this paper, an augmentation synthesis method usable in the absence of quantitative handling qualities specifications, and yet explicitly including design objectives based on pilot-rating concepts, will be presented. The algorithm involves the unique approach of simultaneously solving for the stability augmentation system (SAS) gains, pilot equalization and pilot rating prediction via optimal control techniques. Simultaneous solution is required in this case since the pilot model (gains, etc.) depends upon the augmented plant dynamics, and the augmentation is obviously not a priori known. Another special feature is the use of the pilot's objective function (from which the pilot model evolves) to design the SAS.

Introduction

Given adequate design specifications, or aircraft handling qualities criteria, and a valid system model, design techniques, particularly modern control approaches, are available to the system designer for synthesizing even the most complex flight control systems. Unfortunately, however, weaknesses exist in the design specification area for non-conventional aircraft such as V/STOL and control configured vehicles (CCV's). The assertion here is that due to the "non-conventional," multi-variable nature of the vehicle (and the piloting task in the case of V/STOL), and due to the anticipated complexity of the systems involved, a "non-conventional" approach to the control design problem is worthy of investigation.

Since pilot acceptance is the ultimate criteria, in the absence of prior pilot opinion we must predict pilot rating. This is in contrast to design methods which attempt to a priori define "good" dynamics, and then use a model-following design technique[1], that is, design the augmentation so the augmented system will behave like the "good" model. One major drawback to this approach is that one is never sure that the pilot will agree with the

206
PAGE INTENTIONALLY BLANK

designers choice of "good" dynamics.

To predict pilot rating, some form of pilot model is required and two types of pilot models exist. Each have been used extensively; they include describing-function models[2] and optimal control models[3]. It is felt that for the problem at hand the optimal-control pilot model is ideal. It is more compatible with the multi-variable aspects of the problem and the advanced control design techniques already existing. Also, the form of the pilots equalization network is automatically determined, a very important property in this case.

Both pilot modeling approaches have been used primarily to study closed-loop system performance. Recent application areas for the optimal control model include low-visability landing of CTOL[4] and STOL aircraft[5] and the stability of the pilot aircraft system in maneuvering flight[6]. However, any stability augmentation systems in these studies were designed initially, from handling criteria for example, then the system performance evaluated as a separate step. That is, the SAS was designed first using the conventional approaches (e.g., pole placement), then the pilot model was added around the augmented system to evaluate "piloted" system performance.

Alternate approaches include the pilot as part of the plant[7], then the SAS design proceeds for the "pilot-augmented" plant. Buy the form of the pilot model must be assumed before beginning this design process, an undesirable situation for systems with non-conventional plant dynamics. The pilot is known to adapt his gain and form of equalization to the plant and task, but selecting the pilot model a priori would tend to imply knowledge of and invariance of the form of pilot model. Hence, the form of the pilot model should be determined as an integrated part of the system design. As stated previously, this is naturally accomplished with the optimal-control pilot model.

An analytical pilot model has also been used, although not as frequently, to predict pilot opinion. The most notable of these techniques, applied to the VTOL hover task, was the "paper pilot" developed by Anderson[8,9]. In this approach, parameters in the pilot describing function of assumed form are chosen such that a pilot-rating metric is minimized. This metric consists of a measure of performance (e.g., rms tracking error), and a measure of pilot workload (e.g., the amount of lead the pilot must introduce). In an assessment of this technique[10] it was found that a pilot rating functional based on easily measured motion quantities was adequate for pilot opinion prediction. However, the proposed pilot model was found to require some additions for better system performance predictions. Notably, these improvements included modification in form (describing function) and the addition of the pilot's remnant (or the "random" portion of the pilot's control input.) Hence, again we see the problems created by imposing an assumed form of the pilot's describing function.

This problem would appear to be alleviated by the use of the optimal pilot model. In fact, Hess[11] has found that the optimal control model can be used equally well for predicting pilot opinion, and has used this approach

in analytical display design for helicopters[12,13]. Use of the optimal pilot model for pilot rating allows for a natural pilot-rating metric via the pilot model objective function. Proper selection, based on the task, of the state and control weights in the objective function provides for the determination of the pilot gains, equalization, and pilot rating prediction simultaneously. As we have mentioned previously, this is a very important point in dealing with systems with non-conventional dynamics for which the pilot's describing function may not be known. If this approach is now integrated with the SAS design problem, a proposed design procedure results.

The Pilot Model

As presented in Reference 3, the optimal pilot model evolves from the assumption that the well-trained, well-motivated pilot selects his control input(s), $\bar{u}_p$, subject to human limitations, such that the following objective is minimized,

$$J_p = E\left\{\lim_{T\to\infty} \frac{1}{T} \int_0^T (\bar{y}'Q\bar{y} + \bar{u}_p'R\bar{u}_p + \dot{\bar{u}}_p'G\dot{\bar{u}}_p)dt\right\}$$

The dynamic system being controlled by the pilot is described by the familiar linear relation

$$\dot{\bar{x}} = A_p\bar{x} + B_p\bar{u}_p + \bar{w}$$

$$\bar{y} = C\bar{x} \qquad (1)$$

where $\bar{x}$ is the system state vector, $\bar{u}_p$ the pilot control vector, $\bar{y}$ the output vector, and $\bar{w}$ is the vector of zero-mean external disturbances with covariance

$$E[\bar{w}(t)\bar{w}'(t+\sigma)] = W\delta(\sigma)$$

Included as human limitations are observation delay, τ, and observation noise, $\bar{v}_y$. So the pilot actually perceives the noise-contaminated, delayed states, or

$$\bar{y}_p = C_p\bar{x}(t-\tau) + \bar{v}_y(t-\tau)$$

The covariance of the zero-mean observation noise may include the effects of perception thresholds and attention allocation, and is denoted

$$E[\bar{v}_y(t)\bar{v}_y'(t+\sigma)] = V_y\delta(\sigma)$$

Defining the augmented state vector, $\bar{\bar{x}} = \text{col}[\dot{\bar{x}},\bar{u}_p]$, the solution to the problem, or the pilot's control is given as

$$\dot{\bar{u}}_p^* = -G^{-1}[0\,|\,I]K_p\bar{x}$$

where K_p is the positive definite solution to the Riccati equation

$$-\left[\begin{array}{c|c} A_p & B_p \\ \hline 0 & 0 \end{array}\right]' K_p - K_p \left[\begin{array}{c|c} A_p & B_p \\ \hline 0 & 0 \end{array}\right] - \left[\begin{array}{c|c} C_p' QC_p & 0 \\ \hline 0 & R \end{array}\right]$$

$$+ K_p B_o G^{-1} B_o' K_p = \dot{K}_p \qquad (2)$$

It will be convenient to partition K_p such that

$$K_p = \left[\begin{array}{c|c} K_{p_1} & K_{p_2} \\ \hline K_{p_3} & K_{p_4} \end{array}\right]$$

and note that now the equations for the optimal control $\bar{u}_p^*$ is

$$\dot{\bar{u}}_p^* = -G^{-1}K_{p_3}\hat{\bar{x}} - G^{-1}K_{p_4}\bar{u}_p^{*\dagger}$$

or a linear feedback of the best estimate of the state, $\hat{\bar{x}}$, and some control dynamics. (These control dynamics have been shown to be equivalent to the pilot's neuro-muscular lag.)

Now, the state estimator consists of a Kalman filter and a least-mean square predictor, or

$$\dot{\hat{\bar{x}}}(t-\tau) = A_p\hat{\bar{x}}(t-\tau) + \Sigma C_p' V_y^{-1}[\bar{Y}_p(t) - C_p\hat{\bar{x}}(t-\tau)] + B_p\bar{u}_p^*(t-\tau)$$

$$\hat{\bar{x}}(t) = \bar{\beta}(t) + \ell^{A_p\tau}[\hat{\bar{x}}(t-\tau) - \bar{\beta}(t-\tau)]$$

---

†To model the pilot's remnant, motor noise is usually added to the control equation. The final pilot's control is represented by

$$\dot{\bar{u}}_p^* = -G^{-1}K_{p_3}\hat{\bar{x}} - G^{-1}K_{p_4}\bar{u}_p^* + G^{-1}K_{p_4}\bar{v}_m$$

where

$$E[\bar{v}_m(t)\bar{v}_m'(t+\sigma)] = V_M\delta(\sigma)$$

with $\dot{\bar{\beta}} = A_p\bar{\beta} + B_p\bar{u}_p^*$

and the estimation error covariance matrix Σ is the solution of the Riccati equation

$$A_p\Sigma + \Sigma A_p' + W - \Sigma C_p' V_y^{-1} C_p \Sigma = [0]$$

This system of equations, when solved, determines the optimal-control pilot model.

Finally, as noted previously, Hess has found that when the weightings on the state and control (i.e., Q anf R) in the pilot's objective function are appropriately selected, the resulting magnitude of the pilots objective function, after solving for the pilot model, is strongly correlated with the pilot's rating of the vehicle and task. If the pilot rating is given in the Cooper-Harper system, the relation is

Pilot Rating (PR) = 2.53 in (10 Jp) + 0.28

Now, through this relation and the solution of the pilot model above, we now have not only a pilot-control model but a prediction of the pilot's rating of the dynamic system.

Augmentation Synthesis Method

In the determination of the pilot model parameters above, we have expressed the system dynamics in terms of the matrices A_p and B_p. However, since the augmentation has not been defined, the augmented plant, A_p and B_p is as yet unknown.

Consider the un-augmented plant dynamics to be described by

$$\dot{\bar{x}} = A\bar{x} + B\bar{u} + \bar{w}$$

where, as before, $\bar{x}$ is the system state vector and $\bar{w}$ is the same disturbance vector. However, A and B are now the un-augmented system matrices, and $\bar{u}$ is the control input vector. Now, the total control input to the plant will include pilot input, $\bar{u}_p$, plus augmentation input, $\bar{u}_{SAS}$, or

$$\bar{u} = \bar{u}_p + \bar{u}_{SAS}$$

Further, from the pilot model, we know that although the feedback gains (e.g., $G^{-1}K_{p_3}$, $G^{-1}K_{p_4}$) have not been determined, the pilot's control input in expressible as

$$\dot{\bar{u}}_p = -G^{-1}K_{p_3}\dot{\hat{\bar{x}}} - G^{-1}K_{p_4}\bar{u}_p \qquad (3)$$

Now, the estimate of the state, $\hat{\bar{x}}$, can be expressed in terms of the true state plus some estimation error, $\bar{\varepsilon}$, or

$$\hat{\bar{x}} = \bar{x} + \bar{\varepsilon}$$

By treating this error as another disturbance, $\bar{w}_p$, we can write the pilot's control equation as

$$\dot{\bar{u}}_p = -G^{-1}K_{p_3}\bar{x} - G^{-1}K_{p_4}\bar{u}_p + \bar{w}_p$$

(Note, the disturbance term, $\bar{w}_p$, can also include the pilot's remnant as well.) Combining this relation with the plant dynamic and pilot equations we have

$$\dot{\bar{x}} = \left[\begin{array}{c|c} A & B \\ \hline -G^{-1}K_{p_3} & -G^{-1}K_{p_4} \end{array}\right]\bar{x} + \left[\begin{array}{c} B \\ \hline 0 \end{array}\right]\bar{u}_{SAS} + \left[\begin{array}{c} \bar{w} \\ \hline \bar{w}_p \end{array}\right] \qquad (4)$$

where $\bar{x} = \text{col}[\bar{x}, \bar{u}_p]$.

We now may proceed to determine an objective function for determining $\bar{u}_{SAS}$.

From the correlation between pilot rating and the pilot's objective function we clearly see that the best (i.e., lowest) pilot rating implies the lowest pilot objective function. Therefore, for optimum pilot rating, the control $\bar{u}_{SAS}$ should be chosen to minimize J_p as defined in the pilot rating method. (This method defines the state and control weights, Q and R, as the inverse of the maximum allowable deviations in the variables as perceived by the pilot.) Finally, to preclude infinite augmentation gains, we must also penalize augmentation control energy. Therefore, the augmentation is chosen to minimize

$$J_{SAS} = J_p + E\left\{\lim_{T\to\infty}\frac{1}{T}\int_0^T \bar{u}'_{SAS}\, F\, \bar{u}_{SAS}\, dt\right\}$$

or

$$J_{SAS} = E\left\{\lim_{T\to\infty}\frac{1}{T}\int_0^T (\bar{y}'Q\bar{y} + \bar{u}_p'R\bar{u}_p + \dot{\bar{u}}_p'G\dot{\bar{u}}_p + \bar{u}'_{SAS}F\bar{u}_{SAS})dt\right\}$$

and Q, R, and G are as chosen in the pilot's objective function, J_p.

This may be written as

$$J_{SAS} = E\left\{\lim_{T\to\infty} \frac{1}{T} \int_0^T (\bar{x}'P\bar{x} + \bar{u}'_{SAS}F\bar{u}_{SAS})dt\right\}$$

where

$$P = \left[\begin{array}{c|c} C_p'QC_p + K_{P_3}'G^{-1}K_{P_3} & K_{P_3}'G^{-1}K_{P_4} \\ \hline K_{P_4}'G^{-1}K_{P_3} & R+K_{P_4}'G^{-1}K_{P_4} \end{array}\right]$$

and instead of Equation 3 being substituted for $\dot{\bar{u}}_p$ in the above J_{SAS}, we have invoked a sort of separation principle and substituted the relation

$$\dot{\bar{u}}_p = -G^{-1}K_{P_3}\bar{x} - G^{-1}K_{P_4}\bar{u}_p$$

The justification for this relation being used lies in the fact that we wish to synthesize the augmentation based on how the pilot is <u>trying</u> to perform the control function rather than on how the pilot is capable of doing so.

With this objective function and the system dynamics given in Equation 4, the problem is now stated in conventional form, except K_{P_3} and K_{P_4} are as yet undetermined of course. If we assume, for example, full state feedback, the solution of this problem is known to be

$$\bar{u}^*_{SAS} = -F^{-1}[B' \,\vdots\, 0]K_{SAS}\bar{x}$$

or

$$\bar{u}^*_{SAS} = -F^{-1}B'K_{SAS_1}\bar{x} - F^{-1}B'K_{SAS_2}\bar{u}_p$$

where

$$K_{SAS} = \left[\begin{array}{c|c} K_{SAS_1} & K_{SAS_2} \\ \hline K_{SAS_3} & K_{SAS_4} \end{array}\right]$$

is the solution to the Riccati equation

$$-\left[\begin{array}{c|c} A & B \\ \hline -G^{-1}K_{P_3} & -G^{-1}K_{P_4} \end{array}\right]' K_{SAS} - K_{SAS}\left[\begin{array}{c|c} A & B \\ \hline -G^{-1}K_{P_3} & -G^{-1}K_{P_4} \end{array}\right]$$

$$- P + K_{SAS}\left[\begin{array}{c} B \\ \hline 0 \end{array}\right]F^{-1}[B' \,\vdots\, 0]K_{SAS} = \dot{K}_{SAS} \qquad (5)$$

We see in this expression that the solution for K_{SAS} obviously depends on K_p (or K_{p_3} and K_{p_4}). Returning to the Riccati equation for the pilot gain (Equation 2), we also see that that equation depends in turn on the SAS gains (or K_{SAS}) since the pilot Riccati equation involves the augmented plant matrices A_p and B_p. As a result of the SAS design procedure just presented, we now know, however, the SAS structure. Returning to the pilot model, we may now include this SAS structure specifically, so that A_p and B_p (as in Equation 1) may in fact be expressed as

$$A_p = A - BF^{-1}B'K_{SAS_1}$$

and $$B_p = B(I - F^{-1}B'K_{SAS_2})$$

Substituting these expressions in the pilot Riccati equation yields two coupled Riccati equations, one for the pilot gains, Equation 2, and one for the SAS gains, Equation 5. These may be solved simultaneously for K_{SAS} and K_p by integrating both equations backward. Note that this solution does not involve a two-point-boundary-value problem. The system is represented in Figure 1.

A Simple Numerical Example

Consider a simple tracking task with the controlled element (plant) dynamics considered in Ref. 11,

$$\theta(s)/\delta(s) = K/s^2, \quad K = 11.7$$

The command signal, θ_c, is white noise, w, passed through the filter

$$\theta_c(s)/w(s) = 3.67/(s^2 + 3s + 2.25)$$

and $$E(w) = 0, \quad \sigma_w^2 = 1.0$$

If we define the state vector as $\bar{x} = \text{col}(\theta_c, \dot{\theta}_c, \theta, \dot{\theta})$, we have the plant

$$\dot{\bar{x}} = A\bar{x} + B\delta + 3.67\bar{w}$$

where

$$A = \begin{bmatrix} 0 & 1 & 0 & 0 \\ -2.25 & -3. & 0 & 0 \\ 0 & 0 & 0 & 1 \\ 0 & 0 & 0 & 0 \end{bmatrix}$$

$$B' = [0,0,0,11.7]$$

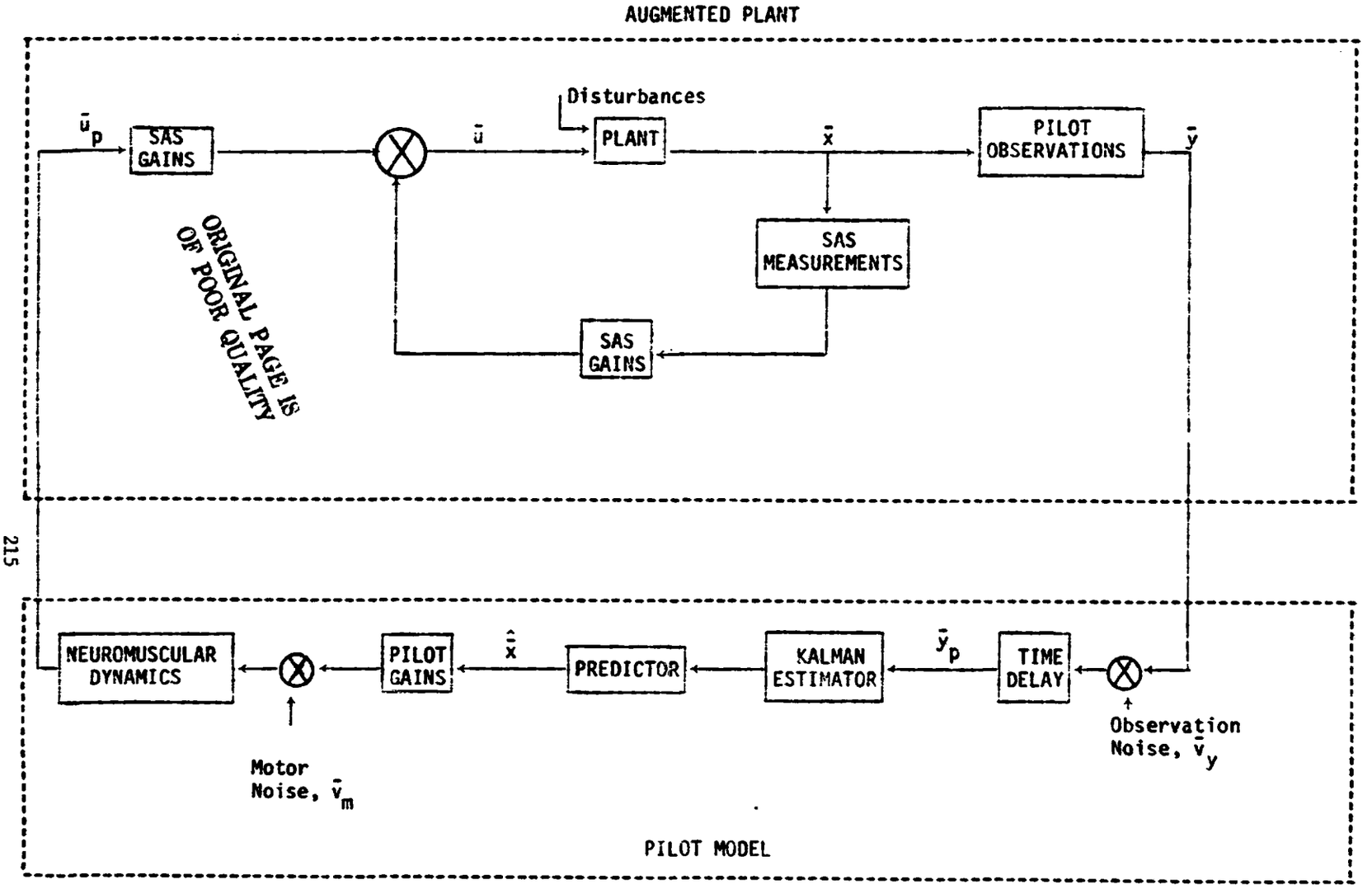

Figure 1 Piloted Vehicle Schematic

For this system, error and error rate are perceived by the pilot or

$$\bar{y}_p = \begin{bmatrix} \theta_c - \theta \\ \dot{\theta}_c - \dot{\theta} \end{bmatrix} = \begin{bmatrix} 1. & 0 & -1. & 0 \\ 0 & 1. & 0. & -1. \end{bmatrix} \bar{x}$$

The performance index, chosen consistent with Hess's rating hypothesis is

$$J_p = E\left\{\lim_{T\to\infty} \frac{1}{T} \int_0^T [(\theta_c - \theta)^2 + .01\delta_p^2 + g\dot{\delta}_p^2]dt\right\}$$

and g is chosen to yield a neuromuscular lag, $1/\tau_N = G^{-1}K_{p_4} = 10.$, or $\tau_N = 0.1$ seconds. Unagumented, the pilot Riccati equations are solved with the following noise statistics (human limitations)

1) Equal attention allocation between error and error rate.
2) Observation thresholds on error and error rate = 0.5(units of display displacement.)
3) Sensor noise, $(V_y)_{ii}/E(y_i^2) = -20dB \quad i=1,2$
4) Motor noise, $(Vu)/E(u_c^2) = -20db$, where $u_c = -G^{-1}K_{p_3}\hat{x}$
5) Observation delay, $\tau = 0.1$ seconds

The "piloted" system performance is given in the following table.

Table 1, Un-augmented System Performance

$(\theta_c - \theta)$ rms	δ_p rms	J_p	P.R.
1.17	1.00	1.39	6.9*

* This pilot rating has been verified by experiment

Assuming full-state feedback, the augmentation control law is

$$\delta_{SAS} = -K_1\theta_c - K_2\dot{\theta}_c - K_3\theta - K_4\dot{\theta} - K_\delta\delta_p$$

The SAS objective function is

$$J_{SAS} = J_p + E\left\{\lim_{T\to\infty} \frac{1}{T} \int_0^T f\delta_{SAS}^2 \, dt\right\}$$

so the piloted plant, including augmentation will be

$$\dot{\bar{x}} = A_p\bar{x} + B_p\delta_p + 3.67\bar{w}$$

where

$$A_p = \begin{bmatrix} 0 & 1. & 0 & 0 \\ -2.25 & -3. & 0 & 0 \\ 0 & 0 & 0 & 1. \\ -11.7K_1 & -11.7K_2 & -11.7K_3 & -11.7K_4 \end{bmatrix}$$

$$B_p' = [0,0,0,11.7(1-K_\delta)]$$

Solving the pilot and SAS Riccati equations simultaneously, and then determining piloted system performance as before yields the results given in the following table.

Table 2 Augmented System Performance

f	$(\theta_c - \theta)$ rms	δ_p rms	J_p *	P.R.**
100.0	1.10	0.89	1.21	6.6
10.0	0.79	0.61	0.62	4.9
1.0	0.38	0.35	0.15	1.3

* Note this is the numerical value of the pilot's objective function, J_p, not J_{SAS}.
** Predicted pilot rating based on J_p.

The augmentation gains, K_1 - K_4 and K_δ, for the three cases above are given in Table 3, along with the augmented plant eigenvalues.

Table 3 Augmentation Gains

f	K_1	K_2	K_3	K_4	K_5	Plant Eigenvalues*
100.0	-.009	-.002	.009	.003	.004	$-.017 \pm .331j$
10.	-.078	-.016	.084	.024	.036	$-.142 \pm .982j$
1.	-.513	-.090	.542	.130	.155	$-.758 \pm 2.40j$

* Not including noise filter eigenvalues of course.

Summary

In summary, we have cited the flight-dynamic and control problems of non-conventional flight vehicles (V/STOL and CCV) due to the complexity of augmentation required and the lack of handling qualities objectives. We have presented a methodology intended to be suitable for this type of problem. The method uses an optimal control pilot model, not only to predict

piloted performance but pilot rating as well. With the optimal-control model structure, we were able to formulate the augmentation synthesis problem as an optimal control problem with the parameters in plant matrices depending on the pilot model, and vice versa. This necessitates simultaneous solution of the two (pilot and augmentation) problems. We have included the form of the solution under the assumption of full-state variable feedback and no measurement noise, and a simple numerical example.

The first extension to be addressed will be the solution for the case of limited state feedback. This case is actually closer to pure plant augmentation than the case addressed here. In our solution, and in the example, we have closed the tracking loop, and pure plant augmentation would only feed back plant states. However, the primary purpose of our discussion here was to provide the problem structure which would be unchanged regardless of augmentation approach.

Further extensions will also include the cases with state estimation, with and without measurement noise. Also, the necessity of pre-tuning the pilot model will be investigated.

References

1. Kriechbaum, G., K.L. and R.W. Stineman, "Design of Desirable Airplane Handling Qualities via Optimal Control," Journ. of Aircraft, Vol. 9, No. 5, May, 1972.

2. McRuer, D.T. and E.S. Krendel, Mathematical Models of Human Pilot Behavior, AGARD-AG-188, AGARD, NATO, Jan., 1974.

3. Kleinman, D.L., S. Baron, and W.H. Levison, "An Optimal Control Model of Human Response, Part I: Theory and Validation," and Part II: Prediction of Human Performance in a Complex Task," Automatica, Vol. 6, 1970, pp. 357-383.

4. Harrington, W.W. Capt., "The Application of Pilot Modeling to the Study of Low Visibility Landing," NASA-TMX-73, 170, Proceedings of the Twelfth Annual Conf. on Manual Control, May, 1976.

5. Porter, M.B. Jr., "The Effects of Stability Augmentation on the Gust Response of a STOL Aircraft During a Curved Manual Approach" Ph.D. Dissertation, School of Aeronautics and Astronautics, Purdue University, West Lafayette, IND., May, 1975.

6. Broussard, J.R. and R.F. Stengel, "Stability of the Pilot-Aircraft System in Maneuvering Flight," NASA-TMX-73,170, Proc. of the Twelfth Annual Conf. on Manual Control, May, 1976.

7. Cunningham, T.B., "The Design of a Pilot Augmented Landing Approach Control System," Ph.D. Dissertation, School of Aeronautics and Astronautics, Purdue Univ., W. Lafayette, IND., May, 1973.

8. Anderson, R.,"A New Approach to the Specification and Evaluation of Flying Qualities," AFFDL-TR-69-120, USAF Flight Dynamics Laboratory, 1969.

9. Dillow, J.D., Major, The "Paper Pilot" - A Digital Computer Program to Predict Pilot Rating for the Hover Task, AFFDL-TR-70-40, USAF Flight Dynamics Laboratory, March, 1971.

10. Teper, G.L. An Assessment of the "Paper Pilot" - An Analytical Approach to the Specification and Evaluation of Flying Qualities, AFFDL-TR-71-174, USAF Flight Dynamics Laboratory, June, 1972.

11. Hess, R.A., A Method for Generating Numerical Pilot Opinion Ratings Using the Optimal Pilot Model, NASA-TMX-73, 101, Feb., 1976.

12. Hess, R.A., "Analytical Display Design for Flight Tasks Conducted Under Instrument Meteorological Conditions,"IEEE Trans. on Systems, Man and Cybernetics, Vol. SMC-7, No. 6, June, 1977.

13. Hess, R.A., "Application of a Model-Based Flight Director Design Technique to a Longitudinal Hover Task," Journ. of Aircraft, Vol. 14, No. 3, March, 1977.

D16

N79-15604

PREDICTION, EVALUATION, AND SPECIFICATION OF FLYING QUALITIES BY MEANS OF STEP TARGET TRACKING

E. D. Onstott
W. H. Faulkner

Northrop Corporation
Aircraft Group
Hawthorne, California

ABSTRACT

A new approach to flying qualities specification and evaluation is presented which coordinates current research in the areas of pilot ratings, pilot-aircraft modeling techniques, and simulation and flight test procedures. A time-domain pilot model is described which can model discontinuous and nonlinear pilot behavior in conjunction with completely general time-varying nonlinear aircraft models to simulate discrete manuevers. This pilot-aircraft model is applied to an existing set of in-flight simulation data, and calculates tracking error and time-on-target statistics for step target tracking that directly relate to the reported pilot comments and ratings. Predicted step target tracking data for eighteen F-5E flight conditions are presented, and the use of the method for control system design is demonstrated using the YF-17.

INTRODUCTION

Pilot ratings and pilot comments often refer to two basic kinds of evaluation:

1) How well can the aircraft be made to perform?
2) How hard is the task to carry out?

Since these two questions are asked simultaneously by the Cooper-Harper decision tree employed by the pilot in assigning a rating, performance and pilot workload are combined into a single scalar quantity, the rating. Pilot rating prediction formulas have been developed that weight normalized statistical performance, usually an rms tracking error, along with an assumed correlate of pilot workload, such as the pilot lead compensation constant. Although these methods have correlated well with steady state tracking data, the predictive and practical aspects of this approach have yet to be demonstrated, especially in view of the simplifications required in task descriptions and system models. One basic problem with these approaches is that pilot model parameters of lead, reserve attention as defined by additional task

220

requirements on the pilot, or other identifiable pilot characteristics are difficult to relate quantitatively to pilot comments. Furthermore, the limitation of pilot model analysis to steady state statistics of a linearized pilot-aircraft model precludes analysis of discrete flight test maneuvers such as wind-up turns and step target tracking.

Furthermore, as the control characteristics of advanced tactical aircraft depend increasingly less on the dynamics of the bare unaugmented airframe, the existing relations of handling qualities evaluation parameters to airframe dynamics become less reliable. Since most flying qualities evaluation and specification methods depend upon this correlation between airframe parameters and pilot ratings, there are now serious deficiencies in existing design criteria. MIL-F-8785B, Military Specification, Flying Qualities of Piloted Airplanes, Reference 1, presents boundaries of acceptance in terms of such quantities as short period frequency and damping. These criteria have been obtained through operational experience with large numbers of past and current aircraft, and present values of airframe parameters that correlate with pilot ratings.

References 2 and 3 present a simple and direct method for evaluating the performance of a tactical aircraft performing a discrete step target tracking maneuver. This approach calculates tracking error and time-on-target statistics for step target tracking in a way that is directly related to both pilot ratings and comments. As an illustration of this technique, the definitive in-flight simulation study of longitudinal flying qualities, performed by Neal and Smith, Reference 4, was analyzed in terms of step target tracking.

The objective of this paper is to summarize References 2 and 3 and to present further details and applications of this flying qualities prediction and evaluation method by demonstrating YF-17 control system design improvement.

DISCRETE AND STEADY-STATE TRACKING

Much analysis of closed loop piloted tracking has been published for random steady-state tracking tasks. These studies, References 5 and 6, for example, have demonstrated that pilot models are useful in the prediction of tracking performance of continuous random tracking tasks, and success has been achieved in correlating model parameters with pilot opinion ratings obtained from flight simulations, Reference 7.

However, in actual flight situations, the pilot is also faced with the task of performing quick corrections to flight path or attitude errors. The ability of an aircraft

to respond well to such discrete corrections in a short tracking time is therefore of great importance to flying qualities analysis. This is particularly true in target tracking where the target must first be acquired and then precisely tracked.

It is clear that the objectives of quick initial response and precise tracking once the target is acquired are to some degree opposed. If the pilot pulls the airplane toward the target too rapidly, unwanted overshoot and oscillation about the target may result. On the other hand, pulling too slowly to the target may lead to steady tracking but with a penalty of unacceptably slow target acquisition. The ability to investigate this compromise and predict how well the overall task can be achieved for a given aircraft is the primary advantage of using time-domain pilot models to investigate step target tracking.

Consider a target that suddenly appears above steady-state trim pitch for the tracking aircraft. The pilot sees the target and initiates a pull-up. At some point, say D seconds into the maneuver, he will possibly change the nature of his control to initiate precision tracking and reduce steady-state errors. By repeatedly flying this maneuver, he will learn just how much he can force a quick initial response without producing overshoot and oscillation. The performance of this step target tracking task can then be measured by rms tracking error and time-on-target for a given pipper size and total tracking time.

The Northrop time-domain pilot model, Reference 3, is set up to perform this tracking task in just the way the pilot does it as described above. This is shown in Figure 1. There will be two forms for the pilot compensation elevator command δ_e: one which provides the initial target acquisition, and the other after time D has passed which controls final precision tracking and eliminates steady state errors. These are of the form:

ACQUISITION

$$\text{time} < D, \quad \delta e_I = (\text{Delay } \tau) \left\{ K_{p_I} \left(\theta_e(t) + T_{l_I} \dot{\theta}_e(t) \right) \right\}$$

TRACKING

$$\text{time} > D, \quad \delta e_P = (\text{Delay } \tau) \left\{ K_{p_P} \left(\theta_e(t) + T_{l_P} \dot{\theta}_e(t) + K_{IC} \int_0^t \theta_e(s)\, ds \right) \right\}$$

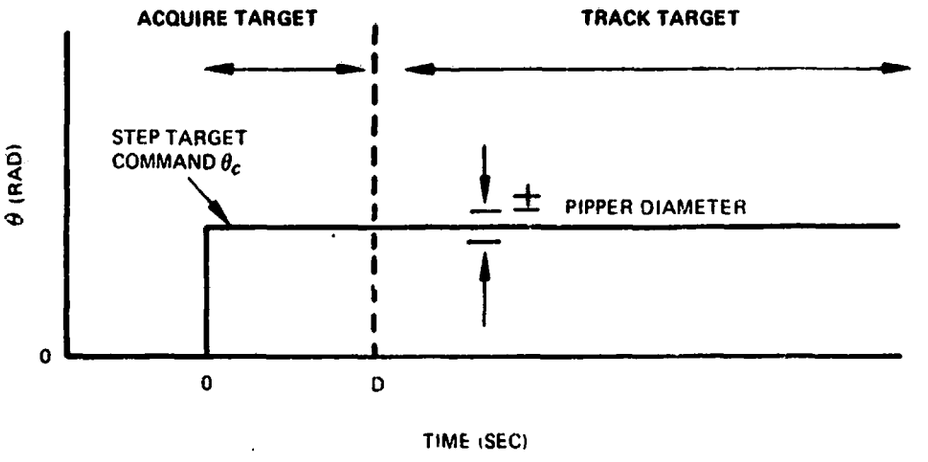

Figure 1. Definition of Step Target Tracking Task

where θ_e is pitch angle tracking error and the subscripts I and F refer to initial acquisition and final tracking, respectively. The K_{IC} term represents a pilot's avoidance of steady state error by means of integral control. A pilot delay of $\tau = 0.3$ sec will be used.

The following quantities must be adjusted in order to perform a simulation of this step tracking task for the evaluation of a given aircraft configuration:

$$K_{P_I},\ T_{L_I},\ D,\ K_{P_F},\ T_{L_F},\ K_{IC}$$

This adjustment is performed using an optimization principle. For the analysis of step target tracking, it will be assumed that the pilot optimizes time-on-target and that this leads to the best compromise of rapid target acquisition and steadiness of target tracking. The adjustment rule for the pilot model is thus: choose the parameters any way that leads to maximum time-on-target.

PILOT — AIRCRAFT ANALYSIS OF LONGITUDINAL STEP TARGET TRACKING

One of the most familiar and widely employed guides to longitudinal flying qualities is the data obtained by Neal and Smith of Cornell Aeronautical Laboratory during an in-flight simulation sponsored by the Air Force Flight Dynamics Laboratory in 1970. The test matrix included variations in short period frequency, damping, and control

system parameters. Flight test evaluation included pitch angle tracking of both random and step commands. The reported pilot ratings and pilot comments cover stick forces, predictability of response, attitude control/tracking capability, normal acceleration control, effects of random disturbances, and IFR problems. Most pilot comments deal with initial response ("predictability of response") or precision attitude tracking control ("attitude control/tracking capability").

Forty-two configurations, Series 1 through 7, were calculated and presented in Reference 3. A pipper diameter of 0.005 radian, a step size of 0.2 radian, and a total tracking time of 5 seconds were adopted. Since the system was linear, any choice of step and pipper size that preserves the 40 to 1 ratio will lead to the same time-on-target and normalized rms θ_e statistics.

Figure 2 shows the calculated step tracking response of one of the better configurations surveyed, 7C, which was given a rating of PR = 1.5. In this case, the rapid acquisition of the target leads to low rms θ_e, while the steadiness of the precision tracking results in large time-on-target. On the other hand, Figure 3 shows a poor configuration, 1F (PR = 8), that has sluggish response indicated by high rms θ_e. Even worse is the inability of this configuration to settle out on the target, so that time-on-target is mostly achieved during target crossings. Other configurations show a wide

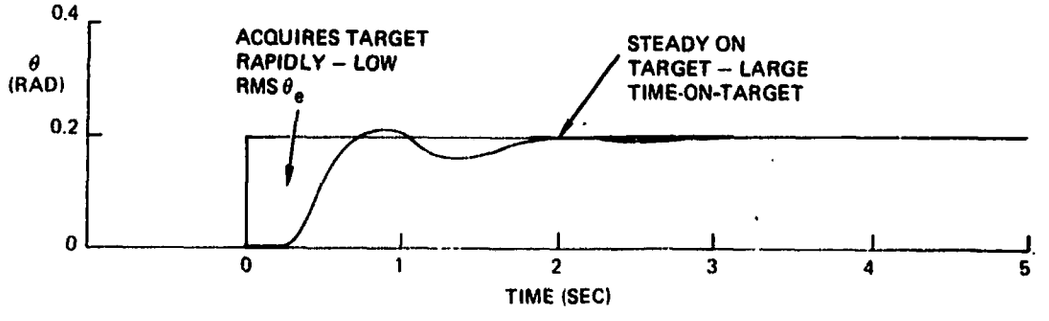

K_{PI}	= 70.0	K_{PF}	= 65.0	TOT	= 2.80
T_{LI}	-.05	T_{LF}	= 0	RMSθ_e	= .32
D	.5	K_{IC}	= 0	PR	= 1.5

Figure 2. Configuration 7C Step Tracking Response

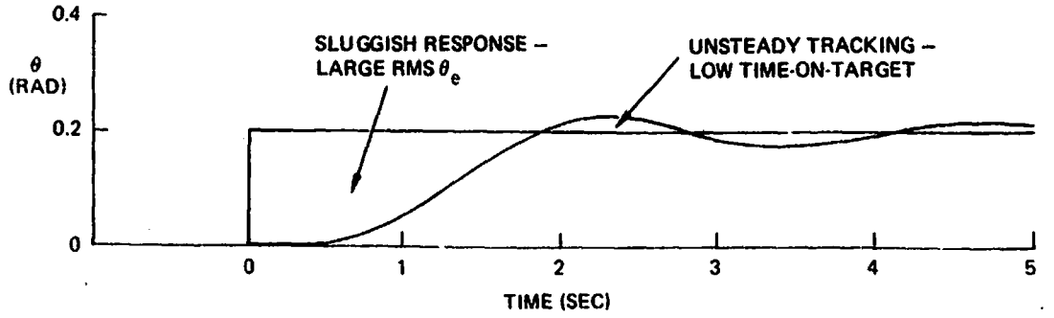

K_{PI}	= 4.6	K_{PF}	= 7.0	TOT	= .4
T_{LI}	= .2	T_{LF}	= .5	RMSθ_e	= .47
D	= 1.5	K_{IC}	= 0	PR	= 8.0

Figure 3. Configuration 1F Step Tracking Response

range of specific handling qualities problems; aircraft that exhibit great overshoot and others whose steady-state error is difficult to overcome, even with the use of the integral control compensation.

The primary objective of the flying qualities specifications, called out in MIL-F-8785B, is to establish numerical criteria that define levels of performance in terms of pilot ratings: Level 1 — PR 1-3.5, Level 2 — PR 3.5-6.5, and Level 3 — PR 6.5-9.5.

It is useful to examine the correlations of the rms θ_e and time-on-target data calculated for the Neal and Smith configurations with pilot ratings. The rms θ_e data are presented in Figure 4. The expected result of increasing pilot rating number with increasing rms θ_e is clearly shown. However, if an attempt is made to draw specification boundary as a vertical line at some rms θ_e value, in order to specify the performance in Level 1 or 2, the result is that no lines can be drawn that do not also include many points from the wrong levels. This failure of rms θ_e to correlate with pilot ratings sufficiently well for specification purposes has been frequently noted. From the description of the piloted task, it is clear that the rms θ_e statistic is incidental, time-on-target being the primary performance measure. If calculated time-on-target is plotted against pilot ratings, there is again a strong correlation, as shown in Figure 5. Unfortunately, this correlation is even less able to furnish specification boundaries than the rms θ_e vs pilot rating data.

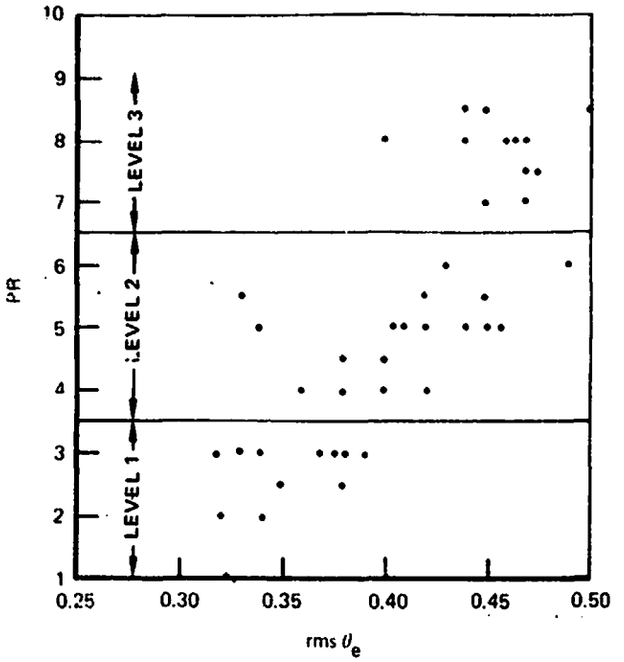

Figure 4. Correlation of rms θ_e with Pilot Ratings

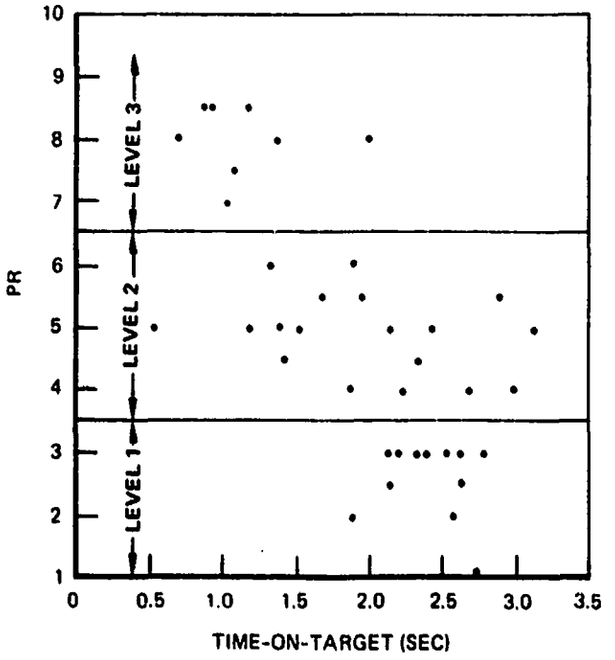

Figure 5. Correlation of Time-On-Target with Pilot Ratings

CORRELATION OF STEP TARGET DATA WITH NEAL-SMITH PILOT RATINGS

From the above it is clear that the single performance parameters rms θ_e or time-on-target are not sufficient to specify acceptable performance of the Neal and Smith configurations. If one considers that the pilot might trade rms θ_e and time-on-target against one another in generating his pilot rating, these statistics become more useful. To see how this trade-off may take place, normalized rms θ_e is plotted versus time-on-target with the point indicated by the minimum pilot rating given by a test pilot during the in-flight simulation. This is shown in Figure 6 along with apparent boundaries that neatly separate the regions of Levels 1, 2, and 3. With the exception of seven points out of forty-two, all configurations lie in regions bounded by apparent curves that illustrate the trade-off between the two performance measures. These curves show, for example, that a pilot will tolerate more sluggish response in a given

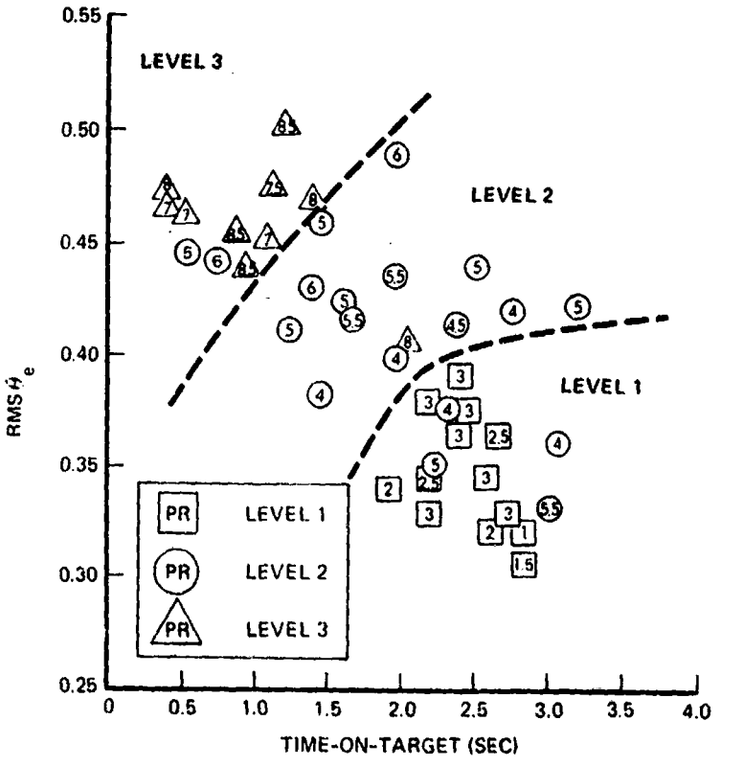

Figure 6. Pilot Ratings as Functions of rms θ_e and Time-On-Target

ORIGINAL PAGE IS
OF POOR QUALITY

Level if the resulting time-on-target is especially good, and conversely. Since the parameters rms θ_e and time-on-target correlate with pilot ratings obtained during a flight test program that examined various tracking tasks, the representation of target tracking by the step target appears to be justified.

VALIDATION OF THE STEP TARGET METHOD USING THE F-5E AIRCRAFT

Further validation of the method was obtained by comparing F-5E aircraft with and without control augmentation at nine flight conditions representative of the primary maneuvering envelope. Full data is given in Reference 3 from which the examples shown in Figures 7 and 8 are drawn.

Comparison in Reference 3 of the step tracking responses for each flight condition with and without augmenter shows the importance of proper augmentation for good tracking response. In the augmented cases, the initial response is faster as reflected in the rms tracking error statistic, while the better damped dynamics lead to larger time-on-target values. To demonstrate the validity of the boundaries shown in Figure 6 based on the Neal-Smith data, the F-5E response data is plotted on these boundaries in Figure 9. Since the augmented F-5E has good Level 1 flying qualities, while the unaugmented aircraft may or may not meet Level 1 criteria, the Level 1-Level 2 boundary is consistent with the F-5E data. In this way, not only do the data of Figure 9 show the gradient direction of improving performance which characterized the Neal-Smith data, but the actual suggested boundary position is consistent as well.

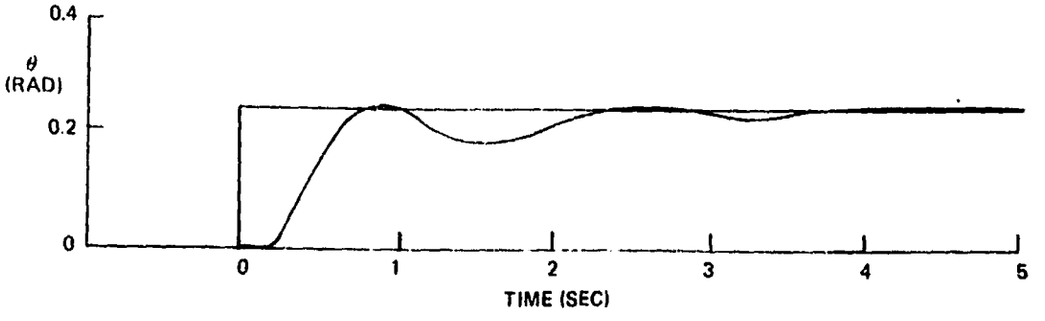

K_{PI}	= - .49	K_{PF}	= - .6	TOT	= 2.26
T_{LI}	= .3	T_{LF}	= .2	RMSθ_e	= .31
D	= .8	K_{IC}	= .06	AUGMENTER	

Figure 7. F-5E Case 4 Step Target Tracking Response

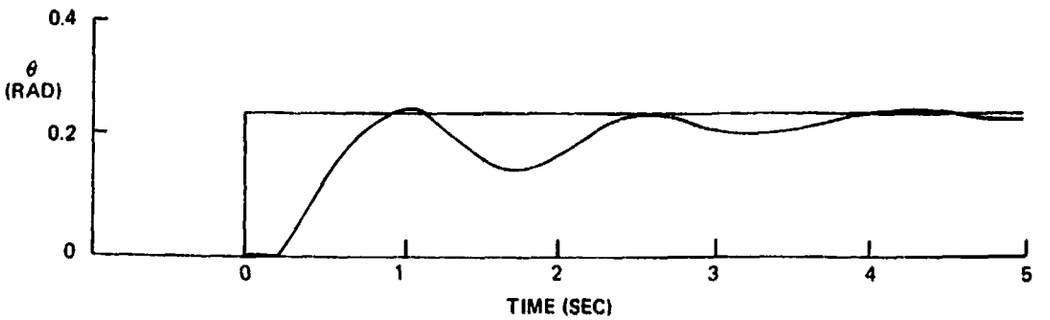

K_{PI}	= - .23	K_{PF}	= - .3	TOT	= 1.50
T_{LI}	= .5	T_{LF}	= .7	RMSθ_e	= .34
D	= .8	K_{IC}	= .09	NO AUGMENTER	

Figure 8. F-5E Case 4 Step Target Tracking Response

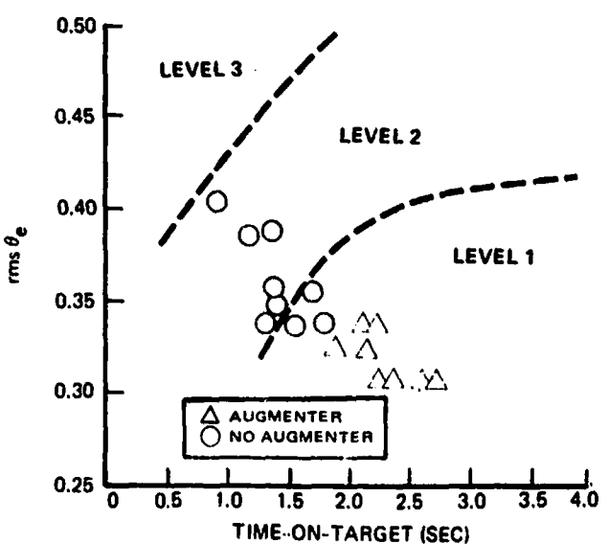

Figure 9. F-5E Validation of Step Target Prediction Method

YF-17 CONTROL IMPROVEMENT DESIGN EXAMPLE

Recently, the step target method was used to evaluate and study possible control configuration improvement of the YF-17 aircraft. The baseline aircraft was designed to meet the Neal-Smith flight control criteria, but a multi-parameter perturbation of control constants has led to improvements in predicted tracking performance. Flight simulations are now planned to verify these predictions, which involved only small changes in control parameters.

The predicted improvements are shown for a number of flight conditions in Figure 10. Time-on-target and rms tracking error are plotted against the boundaries shown in Figures 6 and 9. The tail of each arrow represents the baseline YF-17 as flight tested, and the head shows the predicted response of the aircraft with the modified control design. It is clear that these small changes in the control parameters have produced substantial improvements in the predicted tracking performance. It should also be pointed out that these calculations were performed using the full nonlinear YF-17 aircraft and control descriptions.

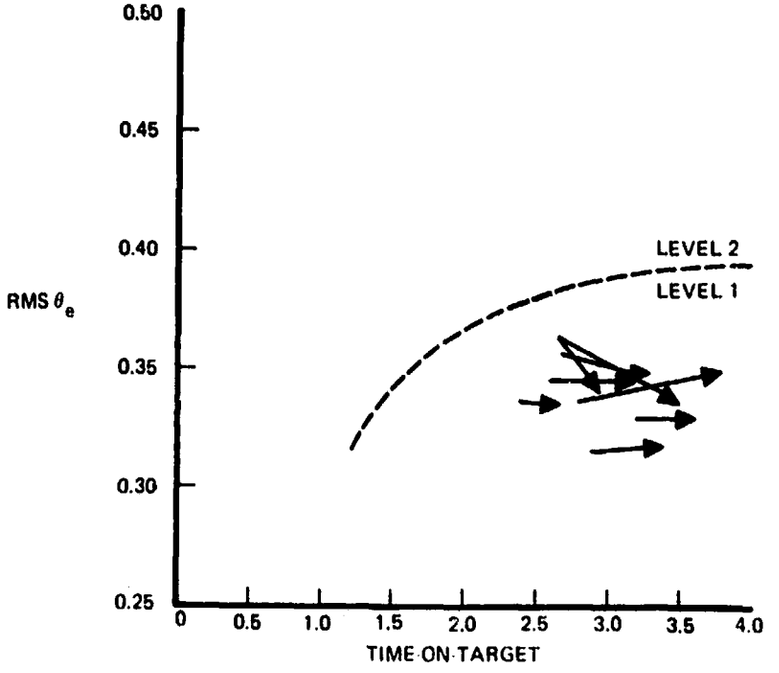

Figure 10. Predicted Improvement of Baseline YF-17 Step Target Tracking

The tracking improvements shown in Figure 10 were calculated using the same modified control parameters in each case. The most striking of the time-on-target improvements is seen by comparing the baseline step response shown in Figure 11 with the modified performance shown in Figure 12. The flight condition for this case is Mach 0.6 at sea level.

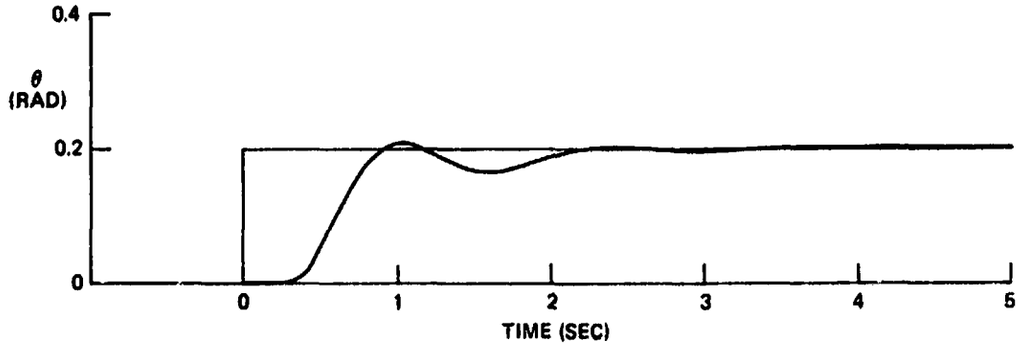

Figure 11. Step Target Tracking Response of Baseline YF-17

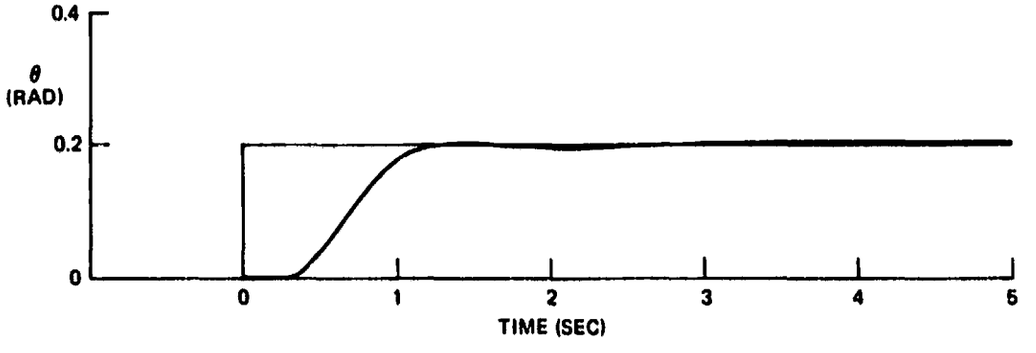

Figure 12. Step Target Tracking Response of Modified YF-17

SPECIFICATION OF AIR-TO-AIR TRACKING PERFORMANCE

The success of the step target tracking prediction method allows the following suggestions for tracking performance specification. For a specification to be a useful, discriminating, and fair criterion for tactical aircraft procurement, the following items must be satisfied:

1) The specification item must be numerical.

2) The specification item must correlate with pilot comments and pilot ratings.

3) The specification item must be easily measured in flight test or flight simulation.

4) The specification item must be reliably predictable by analytical means for use in early design and development evaluation.

5) The method that predicts the specification item must be applicable in a completely standardized form that evaluates the most general models of the candidate aircraft available.

6) The specification item must be valid for all current acceptable aircraft, and must exclude poor or unacceptable aircraft.

Unfortunately, these six requirements for military specification criteria have not all been met by any steady-state approach to the precision tracking problem. However, the transient method of step target tracking potentially satisfies these items. In particular, the step target method has the following characteristics that correspond to the requirements listed above:

1) The step target method is based on the numerical measures of rms tracking error and time-on-target as shown in Figure 6.

2) The two measures correspond with pilot comments in the following way:

rms tracking error:	Quickness of response and overshoot characteristics
time-on-target:	Steadiness on target and precision tracking characteristics

In addition, these two measures strongly correlate with pilot ratings obtained by Neal and Smith.

3) The use of step target tracking is already an established flight test procedure. It is completely standardized and easily tested.

4) The step target response is easily predicted for longitudinal step target tracking, and the extension to multiaxis target tracking is straightforward.

5) The method can be used with all representations of candidate aircraft from linear to full nonlinear equations.

6) The method clearly establishes performance boundaries for the Neal-Smith and F-5E aircraft. The only remaining requirement for MIL-F-8785B inclusion is further validation by current advanced tactical aircraft.

FINAL REMARKS

Pilot ratings have been successfully correlated with regions in the two-dimensional space having calculated rms tracking error and time-on-target coordinates for the in-flight simulation data obtained by Neal and Smith. This shows the generality, versatility, and practicality of time-domain pilot models. By demonstrating analytically the tradeoff between target acquisition and precise tracking for a short tracking period, the interrelationships of pilot ratings, the dynamics of pilot control compensation, and discrete maneuver flight test procedures are made clear. Validation by F-5E aircraft and a control improvement design study of the YF-17 further demonstrate the use and practicality of the method. It is expected that future research into multiaxis step target tracking will yield similar correlations with flight test data. In the meantime, the time-domain pilot model can be readily used to evaluate a wide variety of continuous and discrete tasks encountered in the flying qualities of modern high performance aircraft.

ACKNOWLEDGMENT

This work was partially performed under Contract 33615-77-C-3008 for the U.S. Air Force Flight Dynamics Laboratory, FGC, Wright-Patterson AFB, Ohio.

REFERENCES

1. "Military Specification, Flying Qualities of Piloted Airplanes," MIL-F-8785B, August 1969.

2. Onstott, E.D. and Faulkner, W.H., "Discrete Maneuver Pilot Models for Flying Qualities Evaluation," Journal of Guidance and Control, Vol. 1, No. 2, March-April 1978.

3. Onstott, E.D. and Faulkner, W.H., "Prediction, Evaluation, and Specification of Closed Loop and Multiaxis Flying Qualities," AFFDL-TR-78-3, Air Force Flight Dynamics Laboratory, February 1978.

4. Neal, T.P. and Smith, R.E., "An In-Flight Investigation to Develop Control System Design Criteria for Fighter Airplanes," Vols. I and II, AFFDL-TR-70-74, Air Force Flight Dynamics Laboratory, December 1970.

5. McRuer, D.T. and Krendel, E.S., "Mathematical Models of Human Pilot Behavior," AGARDograph No. 188, Advisory Group for Aerospace Research and Development, January 1974.

6. Faulkner, W.H. and Onstott, E.D., "Error Rate Information in Attention Allocation Pilot Models," Proceedings of the Thirteenth Annual Conference on Manual Control, June 1977.

7. Anderson, R.O., "A New Approach to the Specification and Evaluation of Flying Qualities," AFFDL-TR-69-120, Air Force Flight Dynamics Laboratory, May 1970.

D17

N79-15605

ANALYSIS OF A VTOL HOVER TASK WITH PREDICTOR DISPLAYS USING AN OPTIMAL CONTROL MODEL OF THE HUMAN OPERATOR*

Gunnar Johannsen** and T. Govindaraj

Department of Mechanical and Industrial Engineering
Coordinated Science Laboratory
University of Illinois
Urbana Illinois 61801

SUMMARY

The influence of different types of predictor displays in a longitudinal VTOL hover task is analyzed in a theoretical study. It has been assumed that pitch angle and position will be presented to the pilot in separate displays namely the artificial horizon and a position display. The predictive information is calculated by means of a Taylor series. The future pitch angle is extrapolated 0.7s ahead and displayed as an additional bar, whereas the position is displayed as an extrapolated path element. This path element is approximated by three straight line segments, i.e., three future position values are calculated with the end point being 2.0s ahead.

From earlier experimental studies it is well known that predictor displays improve human and system performance and result in reduced human workload. In this study, the optimal control model is used to prove this effect theoretically. The status and predictive quantities are considered as separate observed variables. The Taylor series coefficients are incorporated in the observation matrix. Also, rate information included in the movement of the position and pitch angle indication is represented.

Several cases with differing amounts of predictive and rate information are compared. The results show the expected improvements in human and system performance in terms of RMS-values. The strongest influence is caused by the indication of the extrapolated path element, especially the end point. Computed cost gradients and fractions of attention show the relative importance of the individual pieces of displayed information. An optimization of the attention allocation shows a further improvement in system performance in all cases.

* This work was supported in part by the National Aeronautics and Space Administration under NASA-Ames Grant NSG-2119.

** Permanent Address: Research Institute for Human Engineering(FAT)
D-5309 Meckenheim, F. R. Germany

PAGE 236 INTENTIONALLY BLANK

I Introduction

Predictor displays have been investigated intensively in laboratory simulations [1]-[5]. It has been found that they improve human and system performance and result in reduced human workload. More recently, predictor displays have been receiving increasing attention (see, e.g., [6]) because the technology of computer graphics has reached a high standard [7] which allows one to implement these displays more easily in real man-machine systems.

During the last few years, an optimal control model of the human operator (see, e g., [8], [9]) has been applied as a unified methodology for analytical display design and evaluation [10]-[13]. Attitude/director indicator and flight director displays have been considered as examples.

This paper is a contribution to such an analytical display design and evaluation procedure. Different types of predictor displays in a longitudinal VTOL hover task are analyzed theoretically by means of the optimal control model of the human operator. Rather than fitting experimental data, the purpose here is to calculate the expected human and system performance with different display designs. These results are validated by intuitive reasoning by considering earlier experimental results

In the next section, the VTOL hover task is described. The assumed predictor-display layout is explained in Section III. Section IV gives a brief overview of the optimal control model and emphasizes specific considerations for applying this model to the utilization of predictor displays. Finally, the results of a case study are discussed in Section V

II Description of the VTOL Hover Task

The task chosen in this paper concerns the longitudinal motion of a hovering VTOL aircraft. For comparison purposes the task is the same as that in [14] which since then has also been considered in other papers, e.g.,[15], [16].

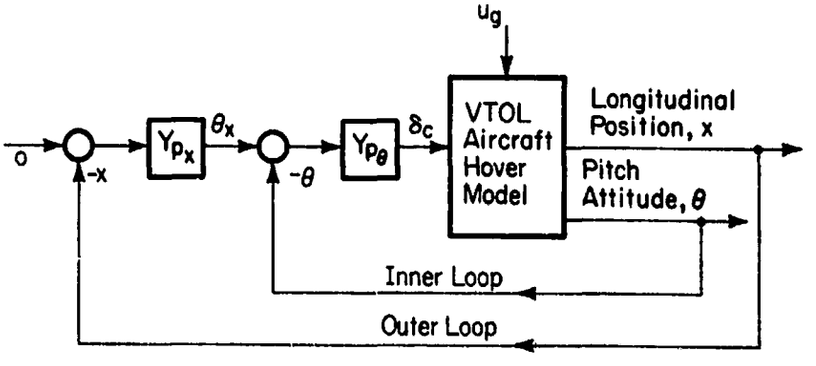

Figure 1: Series Loop Model for Pilot Longitudinal Control in Hover (after [15])

Figure 1 shows a possible structure of this man-machine system, assuming a series loop model for the pilot in which his behavior is represented by the two transfer functions Y_{px} and $Y_{p\theta}$.

The system dynamics of the aircraft are described by the following equation (see also Figure 2):

$$\begin{bmatrix} \dot{u}_g \\ \dot{x} \\ \dot{u} \\ \dot{\theta} \\ \dot{q} \\ \dot{\delta} \end{bmatrix} = \underbrace{\begin{bmatrix} -\omega_b & 0 & 0 & 0 & 0 & 0 \\ 0 & 0 & 1 & 0 & 0 & 0 \\ X_u & 0 & X_u & -g & 0 & 0 \\ 0 & 0 & 0 & 0 & 1 & 0 \\ M_u & 0 & M_u & 0 & M_q & M_\delta \\ 0 & 0 & 0 & 0 & 0 & -100 \end{bmatrix}}_{\underline{A}} \begin{bmatrix} u_g \\ x \\ u \\ \theta \\ q \\ \delta \end{bmatrix} + \begin{bmatrix} 0 \\ 0 \\ 0 \\ 0 \\ 0 \\ 100 \end{bmatrix} \delta_c + \begin{bmatrix} w_1 \\ 0 \\ 0 \\ 0 \\ 0 \\ 0 \end{bmatrix} \qquad (1)$$

$$\dot{\underline{x}} = \underline{A} \cdot \underline{x} + \underline{b} \cdot u + \underline{w}$$

Equation (1) includes a first order lag filter for deriving the longitudinal gust u_g from a white noise source w_1 as well as a first order lag with time constant T_δ = 0.01s limiting the control rate of the actuator. The main reason for the second lag is to extend the state vector in such a way that the second derivative of the pitch angle is also a component of the state vector. This is needed for the predictor display as will be shown later.

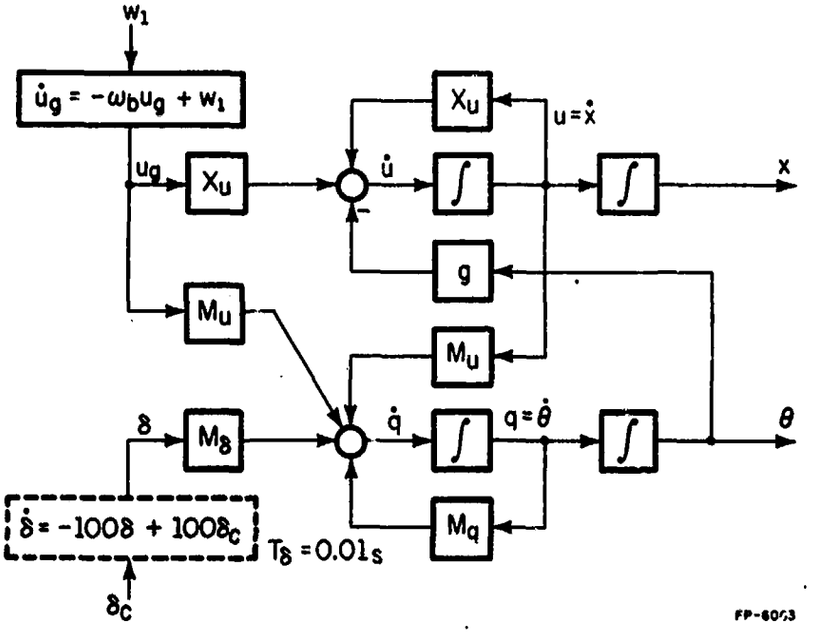

Figure 2: Block Diagram of the Aircraft Dynamics

In Equation (1) and Figure 2, g is the gravitational constant and X_u, M_u, M_q, M_δ are aircraft stability derivatives. Their values are chosen to be the same as in the nominal case in [15], namely

$X_u = 0.1 s^{-1}$, $M_u = 0.0207\ ft^{-1}s^{-1}$, $M_q = -3.0 s^{-1}$, $M_\delta = 0.431 s^{-2}$.

Also, the simulated gust is the same as in [15]. The bandwidth of the gust filter is $\omega_b = 0.314\ rad.s^{-1}$ and the rms-value of the gust is $u_{g_{rms}} = 5.14$ $ft.s^{-1}$, i.e., the variance of the driving white noise is $W_{11} = 16.59$.

III Layout of Assumed Predictor Displays

Two main techniques have been used for generating predictor displays. One is the fast-time model technique [3], [4]; the other one is the extrapolation technique [2], [5]. In this paper, the extrapolation technique is applied. Its advantage is that no model of the aircraft needs to be implemented and run repetitively, faster than real time, to generate predictions on the basis of expected control inputs. Instead, the predictions are calculated by means of a Taylor series on the basis of present measurable position, rate, and acceleration. The only disadvantage of this technique is that it might be difficult to generate noise-free acceleration information, if this is not measurable.

The extrapolation technique is used in the present study to predict extrapolated longitudinal position x as well as pitch angle θ. For position x the predicted value is calculated as follows:

$$x_{PD}(t) = x(t + \tau_x) = x(t) + \tau_x \dot{x}(t) + \frac{\tau_x^2}{2} \ddot{x}(t) \qquad (2)$$

The corresponding Taylor series expression for the pitch angle θ reads:

$$\theta_{PD}(t) = \theta(t + \tau_\theta) = \theta(t) + \tau_\theta \dot{\theta}(t) + \frac{\tau_\theta^2}{2} \ddot{\theta}(t) \qquad (3)$$

The Taylor series expressions of Equations (2) and (3) are truncated after the second derivative terms. This has been found in earlier experimental studies (see [5]) to be a reasonably good approximation.

It has been assumed, for the longitudinal hover task studied here, that the pilot would view displays with predictive information like those shown in Figure 3. The pitch angle and position information is separately indicated in two displays. The one for the pitch angle or inner loop of Figure 1 is like one dimension of an artificial horizon, whereas the one for the position or outer loop of Figure 1 is presented as a function of time. Similar displays have been studied experimentally in [5] with similar system dynamics, which allows for adopting the following data. A prediction span of

τ_θ = 0.7s seems to be appropriate for pitch. For the position, the indication of an extrapolated path element with a prediction span showing the range between the actual value and the end point (see Figure 3), i e., τ_x = 0...2s, has been chosen. The curved extrapolated path element can be approximated by, e.g., three straight lines as shown in Figure 3. This reduces the calculation of the path element to that of three points in the future i.e., (1/3, 2/3, and 1) τ_x ahead.

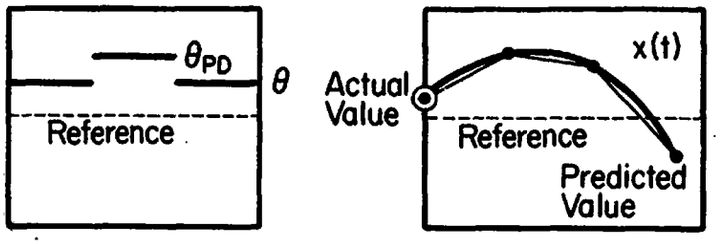

Figure 3: Displays with Predictive Information for Indications of Pitch Angle (left) and Position (right)

IV. Application of the Optimal Control Model

In this paper the same optimal control model for the human operator has been applied as in [15]. In the block diagram of Figure 4, a distinction has been made, however, between influences of display parameters and human perceptual abilities on the observation vector y(t). The human perceptual abilities include (1) estimation in the sense of extracting the first derivative of a displayed variable from its movement as well as (2) perceptual thresholds for the position and rate of displayed variables. For this study all thresholds have been assumed to be zero.

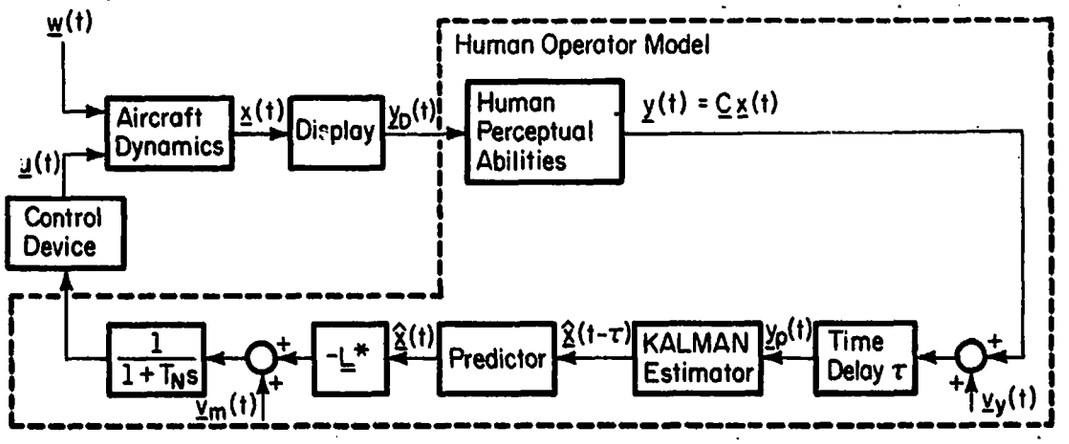

Figure 4: Optimal Control Model for the Human Operator (after [15] and [9])

For reasons of comparing the results of this paper with those of [15], the same parameters of the human operator model and the cost functional have been adopted, whereas the aircraft dynamics are those described by Equation

(1), i.e., having only the very slight change mentioned before. The cost functional for optimal control is

$$J = \overline{x^2} + 400\ \overline{q^2} + \tilde{g}\ \overline{\dot{\delta}_c^2} \tag{4}$$

i.e., a weighted sum of the mean squared values of the position x, the pitch rate $q = \dot{\theta}$, and the control rate $\dot{\delta}_c$. The time delay of the human operator model is $\tau = 0.15$s, and the lag time constant of the neuromuscular system is adjusted to $T_N \simeq 0.1$s by an appropriate choice of $\tilde{g}$ in Equation (4), i.e., $\tilde{g} = 0.03$. The noise-to-signal ratio of the motor noise is $\rho_m = -25$dB. The noise-to-signal ratios of the observation noises change in this study. However for the baseline display format with the same observation vector $\underline{y} = [x,u,\theta,q]^T$ as in [15], they are adopted as $\rho_1 = \rho_2 = \rho_3 = \rho_4 = -20$dB.

The described optimal control model should be able to explain the improvements of human and system performance which occur when predictor displays are used. Looking at Figure 3, one can see that all status and predictive information can be described by the following observation vector:

$$\underline{y} = \begin{bmatrix} x \\ u \\ x_{1/3PD} \\ x_{2/3PD} \\ x_{PD} \\ \theta \\ q \\ \theta_{PD} \end{bmatrix} = \underbrace{\begin{bmatrix} 1 & 0 & 0 & 0 & 0 & 0 \\ 0 & 1 & 0 & 0 & 0 & 0 \\ 1 & 1/3\tau_x & 1/18\tau_x^2 & 0 & 0 & 0 \\ 1 & 2/3\tau_x & 2/9\tau_x^2 & 0 & 0 & 0 \\ 1 & \tau_x & 1/2\tau_x^2 & 0 & 0 & 0 \\ 0 & 0 & 0 & 1 & 0 & 0 \\ 0 & 0 & 0 & 0 & 1 & 0 \\ 0 & 0 & 0 & 1 & \tau_\theta & 1/2\tau_\theta^2 \end{bmatrix}}_{\underline{P}} \begin{bmatrix} \\ x \\ \dot{x} \\ \ddot{x} \\ \theta \\ \dot{\theta} \\ \ddot{\theta} \\ \end{bmatrix} \tag{5}$$

which can be expressed in terms of position x and pitch angle θ as well as the first and second derivatives of both variables by applying Equations (2) and (3). The observation vector in Equation (5) considers also rate information, namely $u = \dot{x}$ and $q = \dot{\theta}$ as in the baseline display format, thereby combining the two influences of display parameters and human perceptual abilities of Figure 4.

As the observation vector is normally derived from the state vector, the vector on the right side of Equation (5) composed of position x, pitch angle θ and its first and second derivatives has to be expressed in terms of the state vector. All these components appear in the systems equation (1) and in Figure 2. The mathematical description is:

$$\begin{bmatrix} x \\ \dot{x} \\ \ddot{x} \\ \theta \\ \dot{\theta} \\ \ddot{\theta} \end{bmatrix} = \begin{bmatrix} x \\ \dot{x} \\ \dot{u} \\ \theta \\ \dot{\theta} \\ \dot{q} \end{bmatrix} = \underbrace{\begin{bmatrix} 0 & 1 & 0 & 0 & 0 & 0 \\ 0 & 0 & 1 & 0 & 0 & 0 \\ X_u & 0 & X_u & -g & 0 & 0 \\ 0 & 0 & 0 & 1 & 0 & 0 \\ 0 & 0 & 0 & 0 & 1 & 0 \\ M_u & 0 & M_u & 0 & M_q & M_\delta \end{bmatrix}}_{\underline{T}} \underbrace{\begin{bmatrix} u_g \\ x \\ u \\ \theta \\ q \\ \delta \end{bmatrix}}_{\underline{x}} \qquad (6)$$

Taking Equations (5) and (6) together results in the following equation for the observation vector:

$$\underline{y} = \underline{P} \cdot \underline{T} \cdot \underline{x} = \underline{C} \cdot \underline{x} \qquad (7)$$

Equation (7) shows that a matrix multiplication is necessary to find the observation matrix $\underline{C}$. One of the two matrices being multiplied, i.e., $\underline{P}$, reflects the display format and the human perceptual abilities, whereas the other one, i.e., $\underline{T}$ contains mainly components of the systems matrix $\underline{A}$.

In order to investigate the influence of different amount of predictive and rate information, a theoretical case study with the optimal control model has been run. The 13 cases studied differ only in their observation vectors which are chosen as shown in Table I. Available information is denoted by a "1" whereas a "0" means that this component of the observation vector is not present in the corresponding case.

Table I
Composition of the Observation Vectors for the Case Study

	A	B	C	D	E	F	G	H	I	J	K	L	M
x	1	1	1	1	1	1	1	1	1	1	1	1	1
u	1	0	0	1	1	0	0	1	0	0	1	1	0
$x_{1/3PD}$	0	0	0	0	0	0	0	0	0	1	1	1	1
$x_{2/3PD}$	0	0	0	0	0	0	0	0	0	1	1	1	1
x_{PD}	0	0	0	0	0	0	0	1	1	1	1	1	1
θ	1	1	1	1	1	1	1	1	1	1	1	1	1
q	1	1	0	0	1	1	0	1	0	0	1	1	0
θ_{PD}	0	0	0	0	1	1	1	0	0	0	0	1	1

Case L is identical with Equation (5). From this, all others have been derived by omitting a certain amount of information, i.e., deleting the corresponding rows in the observation vector and observation matrix.

Cases A, B, C, and D are concerned with the influence of rate information which has also been investigated in [17]. Case A is the baseline display format of this study and is the same as in [15]. Cases E, F, and G consider only predictive pitch information, whereas cases H, I, J, and K assume only predictive position information, being either only the end point (H,I) or the complete extrapolated path element (J,K). Finally, cases L, M include both predictive pitch and position information.

The case study is carried out using the version of the optimal control model which is described in [18].* This includes an optimization of the fractions of attention the pilot devotes to the individual pieces of displayed information. The optimization technique based on the cost gradients of all pieces of information is described in more detail in [19]. The observation noise-to-signal ratio P_i of the ith observed variable is related to its fraction of attention f_i by

$$P_i = P_o \frac{1}{f_i} \qquad (8)$$

$$\text{with} \quad \sum_i f_i = f_{\text{total}}$$

where P_0 is the full attention noise-to-signal ratio, normally -20 db [10]. Thus the above mentioned noise-to-signal ratios of -20dB for all four

* The authors are grateful to Aerospace Systems, Inc., Burlington, Mass., and William C. Hoffman in particular for furnishing the optimal control model software.

observed variables in the baseline display format correspond to a total attention of 4. The value of 4 is the baseline for full attention and should not be interpreted as the human operator devoting 4 times his full attention to the task.

V Results

Performance scores have been shown in Figures 5 and 6 for all 13 cases. These correspond to a total attention of 4, with attention allocation optimized. RMS-longitudinal and pitch errors have been plotted. They are discussed in some detail here. For both variables, position x and pitch angle θ certain trends are apparent. The error is reduced in all cases when prediction information is presented (cases E-M). There is an increase in RMS-errors when the rate information is not available (without prediction ; see cases A-D).

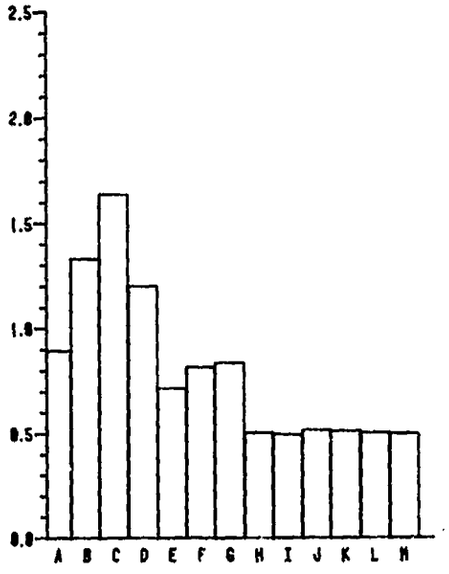

Figure 5: RMS-Longitudinal Errors

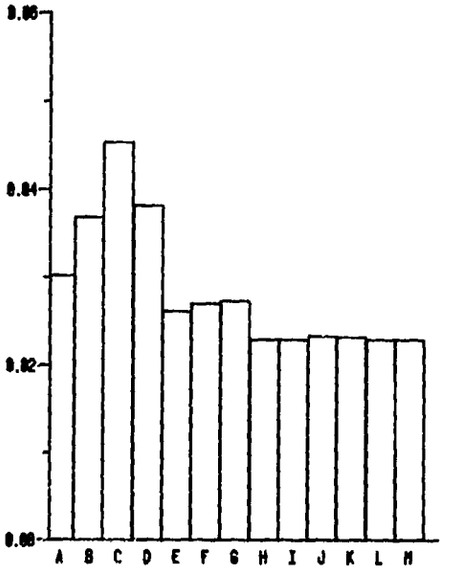

Figure 6: RMS-Pitch Errors

(for all 13 Cases with Optimized Attention Allocation)

For the longitudinal position, the absence of derivative information for position and pitch (C) results in about 80% increase in RMS-error. When only rate u is removed (B), the error increases by about 50%, whereas the increase is only about 33% when the pitch rate is absent (D). Therefore, it is very important that the displays are designed to easily allow the human operator to make good rate estimates.

Compared with the base line performance (A), the reduction in RMS-error is rather small when only the pitch angle predictor is available (E). The error is reduced by about 20%. With predictor information, lack of pitch

rate does not have much effect (see G vs. F), presumably due to the rate information contained implicitly. When rate u is not available (F,G), the RMS-error is reduced only slightly compared with A even when prediction is available for pitch. However, when B and C are compared to F and G respectively, the error is reduced by 35 to 50% with the addition of predictor information.

It is significant to observe that the lack of rate information does not affect the results when the position predictor display is available. This is seen in H and I having nearly equal performance scores. From the baseline performance (A), a reduction in RMS-error of about 45% is observed. It is also important to note that compared to C, the addition of position prediction alone reduces the error to less than 1/3 of its original value. This is validated by intuitive reasoning based on earlier experimental results [5]. With the predictor for a two-dimensional map display, it was found that the lap time, i.e., for one circuit of the map, was reduced by 32%.

When the position predictor is available, all the cases (H-M) result in about the same RMS-errors. This happens irrespective of whether the position and pitch rates and the attitude predictor information are available. This confirms our belief that it is more important to employ predictor display aiding for the slower time constant outer loop. An unexpected result, however, is the fact that additional intermediate points of the extrapolated path element (J-M) do not further improve performance. The most important predictive information seems to be the indication of the end point of the extrapolated path element.

The trends for the pitch angle error are similar to the longitudinal position error. When all derivative information is removed (C), the error increases by about 50%. Absence of u (B) results in a 23% increase, whereas for the pitch rate (D) the corresponding increase is about 30%. The order of B and D is reversed with respect to position error, as could be expected. The pitch angle predictor reduces the error by about 10% (E). Loss of pitch rate information is not important when the predictor is available (G vs. F). These results are in qualitative agreement with earlier experimental results [5] , where RMS-errors have been improved by a factor of 2-4 with the addition of a predictor for an artificial horizon in a pure attitude control task. Further reduction in RMS-pitch error, by 23%, occurs when the position predictor display is added (H-M). This is a 50% reduction compared to the no-derivative case (C). As before, no substantial difference occurs if the rate information or intermediate points are removed when the position predictor display is available.

ORIGINAL PAGE IS
OF POOR QUALITY

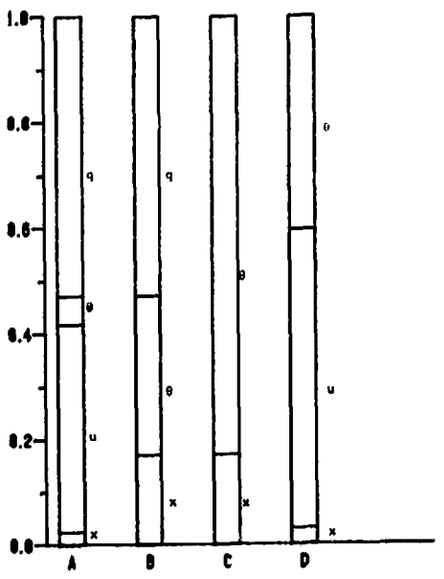

Figure 7: Optimized Fractions of Attention for Cases A B C D

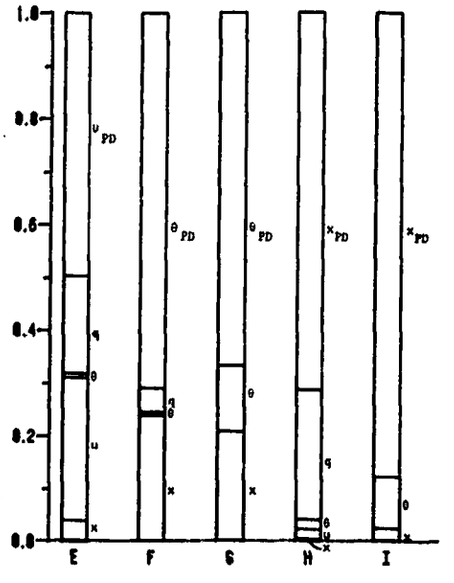

Figure 8: Optimized Fractions of Attention for Cases E F,G H,I

For all 13 cases, the optimized fractions of attention are plotted in Figures 7,8,and 9. The total attention is constant at 4 for all cases, normalized to 1 in the figure, assuming that the human operator will not increase his effort with additionally displayed information. For each displayed variable fractions of attention are shown which result in minimum total cost. When rate information is available, the optimum fraction of attention required is more (mostly by about 8 to 10 times) for the rate than for the corresponding displayed variable itself, i.e., position or pitch angle (Figure 7).

With no predictor, the inner loop (see Figure 1) demands more attention (by about 4 times more than the outer loop), when rate u is not available (cases B C). With the addition of the predictor, position or pitch or their derivatives require comparatively less attention than the predicted variables. The predictor requires 3 to 15 times more attention.

Total attention for the position predictor is about 2 to 3 times greater than that for the pitch predictor (Figure 9). From this and the discussions for RMS-errors, the importance of the position predictor information is obvious.

It should be pointed out that for constant total attention, the RMS-errors are still small even when the information available is limited (e g., only 3 variables in case I compared to 8 in case L), as long as the position predictor is available. This could be due to less noise in observing what is available and, hence the possibility for better state estimation. From the foregoing discussions it is clear that the rate

information is highly useful when a predictor is not available. Having a predictor for the low speed outer loop is more important for performance since it reduces the RMS-errors more effectively.

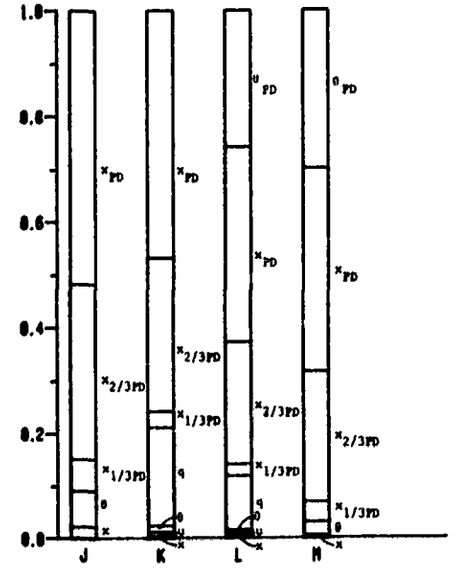

Figure 9: Optimized Fractions of Attention for Cases J,K,L,M

In Figure 10, the RMS-values of position, pitch angle, and control for different cases with and without rate and predictor information are plotted corresponding to optimized attention allocation. These cases have been chosen because the additional indication of the end point of the extrapolated path element (H) compared with the baseline display format (A) results in the simplest predictor display design with the maximum performance improvement. Compared with these two cases, C and I show the influence of the omitted rate information. The trends discussed earlier are seen again in Figure 10.

The effects of varying the total attention and optimizing the attention allocation are illustrated for RMS-longitudinal errors for the cases A,C,H, and I (Figure 11). The first bar in each case corresponds to variable total attention split equally among displays (1 for each observed variable). For the second bar, total attention is 4, split equally between the inner loop and the outer loop, and equally among displays in any particular loop. The remaining bar corresponds to a total attention of 4, split optimally. The errors are reduced by 18% for case A. For case C, a reduction of about 30% occurs when total attention changes from 2 to 4. Optimization reduces this further by only 8%. The slight increase of RMS-error in case H is due to a decrease in total attention from 5 to 4. However, in case I, the increase in total attention from 3 to 4 does not change the RMS-value. When attention is optimized, up to 30% reduction in error is obtained.

ORIGINAL PAGE IS
OF POOR QUALITY

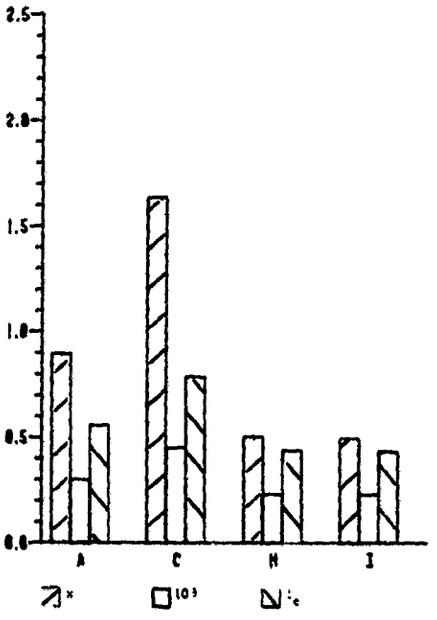

Figure 10: RMS-values of Position x, Pitch Angle θ, and Control δ_Q for Cases A,C,H,I with Optimized Attention Allocation.

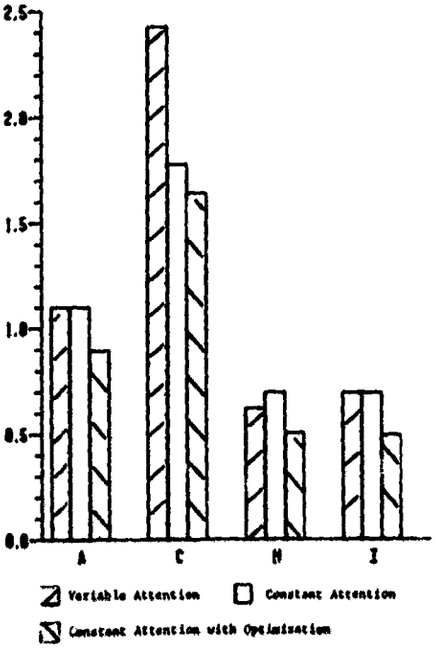

Figure 11: RMS-Longitudinal Errors For Cases A,C,H,I with Variable and Constant Total Attention.

It is necessary to point out that the fractions of attention obtained may not be the globally optimum values. Due to the coupling between inner and outer loop and the interdependence of prediction and rate information (see Figure 2 and Equations 2 and 3), different combinations of initial conditions lead to different optimal attention allocations with similar total cost values. This corresponds, however, to the freedom the human operator has also in choosing between equally appropriate combinations of interrelated information. The optimized fractions of attention shown in this paper seem to be typical values found with different initial conditions.

VI Conclusions

Predictors improve man-machine system performance as shown by the model results of this study. This is consistent with the results obtained e g., in [5]. The position predictor display is more useful in reducing the RMS-errors. Especially, the end point of the extrapolated path element has the strongest influence. Due to slower dynamics, it is possible that the human finds it difficult to infer the longitudinal position rate compared to pitch rate.

The addition of a predictor might result in reduced workload as evidenced by the smaller RMS-control movements. The control actions by the pilot are guided by the predictor. This could also have an effect on the internal model because estimation of the states is aided by the predictor display. The accuracy requirements of the state predictor implicitly included in the optimal control model of the human operator might be relaxed. The improvement of state estimation with an even inaccurate internal model might also be important for monitoring and supervisory control tasks. Separate studies are needed to evaluate this effect.

The study shows that the optimal control model is suitable for analytical predictor display designs. Using this methodology it is possible to investigate the effects of certain display parameters, e.g., to find the optimal length of the prediction span. This may allow one to avoid expensive man-in-the-loop simulation studies.

VII References

1 Wierwille, W.W.; "Improvement of the Human Operator's Tracking Performance by Means of Optimum Filtering and Prediction," IEEE Trans. Human Factors in Electronics, Vol. HFE-5, 1964, pp. 20-24.

2 Bernotat, R.: "Das Prinzip der Voranzeige und seine Anwendung in der Flugführung." Z. Flugwiss., Vol. 13, 1965, pp. 373-377.

3 Kelley, C.R ; Manual and Automatic Control, New York: Wiley, 1968.

4. Warner, J.D.S.; "A Fundamental Study of Predictive Display Systems," NASA CR-1274, 1969.

5 Dey, D.; and Johannsen, G.: "Anthropotechnische Untersuchung einer Übergrundanzeige und eines künstlichen Horizonts mit Voranzeige zur manuellen Regelung von VTOL-Flugzeugen," Z. Flugwiss., Vol. 21, 1973, pp. 140-145.

6. Roscoe, S.N.; and Eisele, J.E.: "Integrated Computer-Generated Cockpit Displays," In: Sheridan, T.B., Johannsen, G. (Eds.) Monitoring Behavior and Supervisory Control, New York: Plenum Press, 1976, pp. 39-49.

7 Machover, C ; Neighbors, M.; and Stuart, C.: "Graphics Displays," IEEE Spectrum, Vol. 14, 1977, pp. 24-32.

8 Kleinman, D.L.; Baron, S; and Levison, W.H.: "An Optimal Control Model of Human Response. Part I: Theory and Validation," Automatica, Vol. 6. 1970, pp. 357-369.

9 Johannsen, G.; Boller, H.E.; Donges, E.; and Stein, W: Der Mensch im Regelkreis - Lineare Modelle, München: Oldenbourg. 1977.

10 Baron, S.; and Levison W.H.; "An Optimal Control Methodology for Analyzing the Effects of Display Parameters on Peformance and Workload in Manual Flight Control", IEEE Trans. Syst. Man Cybern., Vol. SMC-5, 1975, pp. 423-430.

11 Baron, S.; and Levison, W.H.; "Display Analysis with the Optimal Control Model of the Human Operator," Human Factors, Vol. 19, 1977, pp. 437-457.

12 Hess, R.A.; "Analytical Display Design for Flight Tasks Conducted Under Instrument Meteorological Conditions," IEEE Trans. Syst. Man Cybern. Vol. SMC-7, 1977, pp. 453-462.

13 Curry, R.E.; Kleinman, D.L.; and Hoffman, W.C : "A Design Procedure for Control/Display Systems," Human Factors, Vol. 19, 1977, pp. 421-436.

14 Miller, D.P.; and Vinje, E.W.; "Fixed-Base Flight Simulator Studies of VTOL Aircraft Handling Qualities in Hovering and Low-Speed Flight," Wright-Patterson AFB, Ohio: AFFDL-TR-67-152, 1968.

15. Baron, S.; and Kleinman, D.L.: "Prediction and Analysis of Human Performance in a VTOL Hover Task," Proc. 7th Annual Conf. on Manual Control, NASA SP-281, 1972, pp. 247-256.

16 Hess R.A., "Prediction of Pilot Opinion Ratings Using an Optimal Pilot Model," Human Factors, Vol. 19, 1977, pp. 459-476.

17 Baron, S.; and Berliner, J.E.; "The Effects of Deviate Internal Representations in the Optimal Model of the Human Operator." U.S. Army Missile Research and Development Command, Alabama: Tech. Rept. TD-CR-77-3, 1977.

18 Curry, R.E.; Hoffman, W.C.; and Young, L.R.; "Pilot Modeling for Manned Simulation," Vol. I; Doyle K M and Hoffman W C ,...., Vol. II (Program User's Manual), Wright-Patterson AFB, Ohio: AFFDL-TR-76-124, 1976.

19. Hoffman, W.C.; Curry, R.E.; Kleinman, D.L.; Hollister, W.M.; and Young, L R.; "Display/Control Requirements for VTOL Aircraft," Aerospace Systems, Inc. Burlington, Mass : ASI-TR-75-26 (NASA CR-145026), 1975.

SESSION E: GROUND VEHICLE CONTROL AND DRIVER BEHAVIOR

Chairman: L. Summers

PRECEDING PAGE BLANK NOT FILMED

N79-15606

VEHICLE STEERING CONTROL: A MODEL OF LEARNING

Alison Smiley, Ph.D.*
Southern California Research Institute
Los Angeles, California
and
Lloyd Reid, Ph.D.
Institute of Aerospace Studies
University of Toronto
Ontario, Canada
and
Morris Fraser, M.D.
Department of Systems Design
University of Waterloo
Ontario, Canada

SUMMARY

A hierarchy of strategies were postulated to describe the process of learning steering control. Vehicle motion and steering control data were recorded for twelve novices who drove an instrumented car twice a week during and after a driver training course. Car-driver describing functions were calculated, the probable control structure determined, and the driver-alone transfer function modelled. The data suggested that the largest changes in steering control with learning were in the way the driver used the lateral position cue.

INTRODUCTION

Various aspects of driver behavior have been studied using manual control theory. To date, most, if not all, of this research has used experienced drivers. The research to be described in this paper used inexperienced drivers in order to study the changes in the driver describing function as a novice learns to steer a car.

The mathematical model used to describe the driver is the crossover model, described in Reference 1. Though the model was developed using single-loop, compensatory tracking tasks, it has been successfully used to describe car driving where two loops are involved. The basic tenet of the crossover model is that the human adapts to each controlled element so that the open loop man-machine transfer function always has the form:

$$Y_p(jw)Y_c(jw) = \frac{w_c e^{-jw\tau}}{jw} \qquad (1)$$

*Work sponsored by the National Research Council of Canada and drawn from principal author's Ph.D. dissertation completed at the U. of Waterloo, Canada.

PAGE INTENTIONALLY BLANK

where w_c is the system crossover frequency, and τ is the effective time delay (incorporating delays due both to the operator and the control device), Y_p is the operator describing function, Y_c is the transfer function describing the control device dynamics, and jw is the complex frequency variable.

Weir and McRuer (Reference 2) applied this model to automobile lane-keeping steering tasks in order to determine which of the available visual cues would yield good performance without great effort on the part of the driver. From previous studies with the crossover model it has been shown that the human operator selects from the possible cues or feedbacks those that minimize his/her equalization requirements. In other words, the operator prefers to act as a simple gain and time delay rather than as a single or double differentiator, and selects cues so that s/he can do this. The car dynamics in lateral position are such that the use of lateral error as a cue would require the operator to act as a differentiator. ($Y_p(jw) = jwKe^{-jw\tau}$ from the crossover model.) This eliminates lateral error as a dominant cue for the experienced driver. Heading angle and rate, path angle and rate, and time-advanced lateral deviation were studied (Reference 2) as possible cues. As heading rate control allows a fairly large lag and produces a high crossover frequency, it appears to be the best cue to use. As its use is associated with high frequency control movements, heading angle (an intermediate frequency cue) is a more probable cue in less demanding situations. Control is unlikely to be purely directional since drifts in lateral position will occur which, if uncorrected, may result in the car going out of the lane. Therefore, it was suggested that a probable structure for an experienced driver is an outer loop controlling lateral position and an inner loop controlling heading angle or rate. The heading angle inner loop provides the path damping necessary for a stable, well-behaved closed loop system - and thereby avoids the necessity of the operator differentiating the input (which would difficult because it must be done at low frequencies as well as high) which would be needed to stabilize the outer loop, if it were the only loop closed. Though a single loop structure of time advanced lateral deviation had also been suggested in Reference 2, the time advance (preview time) necessary for such a control loop to work was in the order of 5 to 10 seconds. Below these values the lead generated by using predicted future lateral deviation 'would not compensate sufficiently for the inherent lags in the driver/vehicle system'. In Reference 3 a survey is presented of the research on estimated preview times used by experienced drivers. Only when the driver viewed the road through a narrow slit were preview times in the range needed for good use of time advanced lateral deviation as a control loop. This suggests that such a control loop is an unlikely possibility under normal driving conditions. The reader must be cautioned at this point that statements about which cues are used in driving in no way imply that these cues are directly perceived by the driver. For example, the driver may perceive heading angle directly or may perceive some function of heading angle. The mathematical analysis cannot differentiate between two such dependent variables.

Hypotheses About Learning Steering Control

Perceptual-motor learning studies, eye movement studies of novice drivers and anecdotal information obtained from driver instructors were used to generate hypotheses about the stages in the learning of steering control. In the first stage it was postulated that the driver controls lateral position (y), the most obvious cue. In reference 4 it was shown through a study of the eye movements of novice drivers that novices tended to look closer in front of the vehicle than experienced drivers, suggesting they were looking for lateral position cues. As was pointed out earlier, lateral position is a difficult cue to control so this stage was not expected to last long (see Fig. 1).

With experience the novice begins to look further ahead of the car. This is necessary in order to better monitor the environment but also allows the driver to pick up heading angle (ψ) movements more easily. The car's dynamics in heading angle ($G^{\psi}_{\delta w}$) are rate dynamics, so that the driver's control may be modelled by a simple gain and time delay. Thus the second stage is that the driver will use heading angle as the dominant cue, but will still control lateral position directly (as in the first structure), with corrections being made when a significant lateral position error has accumulated. An analogous strategy was used by subjects in an experiment described in reference 5, where subjects using an oscilloscope centered a target on crosshairs by sequentially pressing two keys, one causing target acceleration to the right and the other, to the left. The response pattern suggested that some subjects modified their responses on the basis of feedback i.e. after drifting off target they made a single, long duration corrective movement, while other subjects, who maintained a higher rate of responding and were consistently better in overall performance, used a more efficient strategy. These latter subjects 'when the target drifted off center to the left...maintained a high rate of responding but at the same time gradually increased the length of time the right key was active relative to the left key, so that over a series of responses the target was made to drift back towards the center'. It was postulated that at an intermediate stage, learning drivers would be using a strategy similar to Pew's first group of subjects, which would be represented by an alternating operation on lateral position and heading angle as shown in Fig. 2.

In the final stage of learning, it was postulated that the driver would begin to use dual loop control, where heading angle is the dominant cue, controlled by an inner loop, and lateral position is controlled with an outer loop. In this way lateral position may be controlled by heading angle corrections i.e. using a simple gain ($Y'_y = K_y$) rather than having to estimate rate of change of lateral position. The operators control of heading angle was modelled by a gain, $K\psi$, a lead term ($1 + T'_r jw$), and a time delay ($e^{-jw\tau}$). (i.e. $Y_{\psi} = K_{\psi}(1 + T'_r\, jw)e^{-jw\tau}$). The lead term is needed to offset a lag in vehicle response at higher frequencies. For the experimental car the break frequency of this lag occurred at $T_r = 9.4$ rad./sec., therefore the same value was assumed for T'_r when the driver-alone transfer function was modelled. In reference 6 it was shown that this structure satisfied the crossover model

and appeared to provide a reasonable fit to experimental data. Such a form of control is analogous to that used by the subjects using the more efficient strategy in the experiment described in reference 5.

Theoretical Analysis

The driver-car transfer function for the control structures postulated as stages in the learning process will now be derived.

. Using Fig. 1, the following relationship may be obtained:

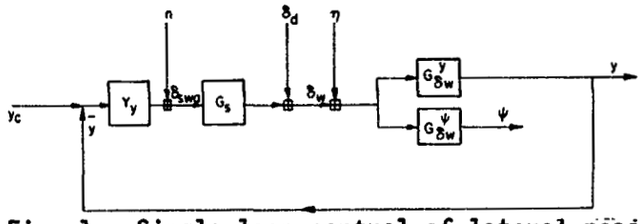

$$\delta_w = \delta_d + nG_s - \varepsilon_w G^y_{\delta w} Y_y G_s - nG^y_{\delta w} Y_y G_s \quad (2)$$

Fig. 1. Single-loop control of lateral position (δswa-steering wheel angle, δw-front tire angle, Gs-steering gain, other definitions in text)

If each variable is cross-correlated (see reference 7 for a description of these techniques) with the input disturbance, δ_d, the following is obtained:

$$\phi_{\delta_d\delta_w} = \phi_{\delta_d\delta_d} + \phi_{\delta_d n} G_s - \phi_{\delta_d\delta_w} G^y_{\delta_w} Y_y G_s - \phi_{\delta_d n} G^y_{\delta} Y_y G_s \quad (3)$$

The remnant, n, is by definition that part of the drivers output which is uncorrelated with the input, so that $\phi_{\delta_d n}$ may be considered to be zero. Because δ_d is such designed so that it is much larger than n, $\phi_{\delta_d n}$ will be negligible in comparison with $\phi_{\delta_d\delta_w}$ and $\phi_{\delta_d\delta_d}$. Equation (3) is then reduced to:

$$\frac{\phi_{\delta_d\delta_d} - \phi_{\delta_d\delta_w}}{\phi_{\delta_d\delta_d}} = Y_y G_s G^y_{\delta_w} \quad (4)$$

For structure 2 this expression is equal to $Y_\psi G_s G^\psi_{\delta_w}$ or $Y_y G_s G^y_{\delta_w}$ depending on which loop is in use. For the dual-loop structure 3 this expression becomes:

$$\frac{\phi_{\delta_d\delta_d} - \phi_{\delta_d\delta_w}}{\phi_{\delta_d\delta_d}} = Y_\psi \left[1 + \frac{Y'_y G^y_{\delta_w}}{G^\psi_{\delta_w}}\right] G^\psi_{\delta_w} G_s \quad (5)$$

ORIGINAL PAGE IS
OF POOR QUALITY

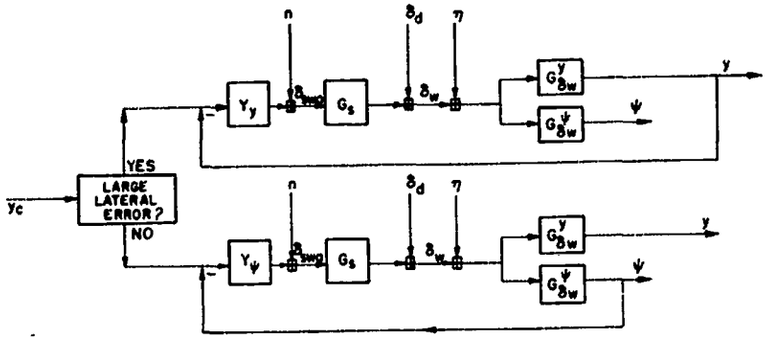

Fig. 2. Parallel loop control of heading angle and lateral position

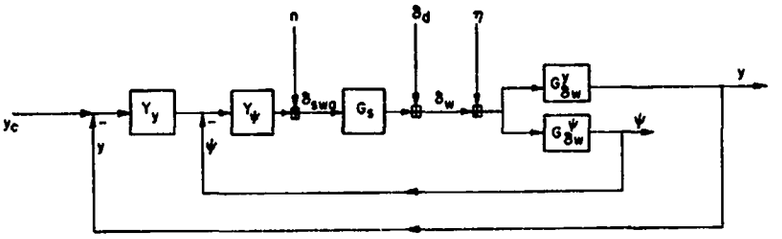

Fig. 3. Dual loop control of heading angle and lateral position

Thus, no matter which structure the driver is using, the same cross spectral expression is calculated to obtain the car-driver transfer function. However, as will now be shown, the form of the transfer function obtained differs depending on which structure is in use.

In the first two structures, either heading angle or lateral position is being controlled at any one time. Thus the first two structures are single control loops which, in the frequency range used in this study, may be expected to conform closely to the crossover model. Therefore, using equation (1), the car-driver transfer will have the form $w_c e^{-jw\tau}/jw$. When this function is plotted on a Bode plot (amplitude and phase vs. frequency) the amplitude slope is 20db per frequency decade (see Fig. 4).

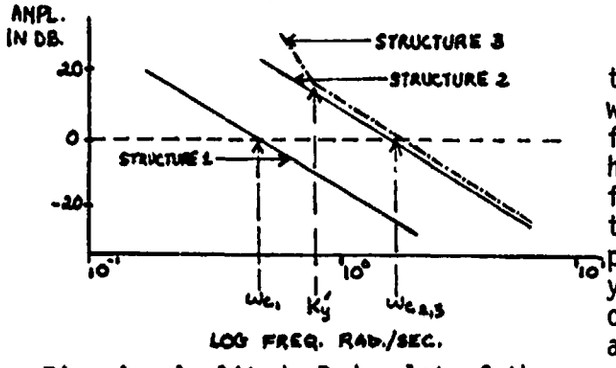

Fig. 4. Amplitude Bode plot of the car-driver transfer function for structures 1, 2, 3

The values assumed for the driver's transfer functions in the third structure were such that the car-driver transfer function could be modelled at mid- and high frequencies (i.e., near crossover frequency) by the crossover model, as in the first two structures. However, the presence of the outer loop operating on y, affects the expected amplitude slope of the Bode plot. Using equation (5), as frequency increases, the ratio $G^{y}_{\delta_w}/G^{\psi}_{\delta_w}$ decreases rapidly so that the main effect of the Y'_y term is at low

frequencies, where it causes an increase in the amplitude slope as seen in Figure 4. Thus structure 3 may be distinguished from structures 1 and 2 by the presence of an increased slope in the Bode amplitude plot of the car-driver transfer function. Structures 1 and 2 must be distinguished from each other by more subtle cues, however. Because of the change in operator requirements, a change from control of lateral position to dominant control of heading angle would result in a jump in crossover freqeuncy and an increased phase angle at low frequencies. (The difficulty of generating the low frequency lead needed for lateral position control results in a pronounced phase droop at low frequencies and a lower crossover frequency.)

The considerations discussed above were used to help determine the control structure used by the subjects.

EXPERIMENTAL PROCEDURE

Subjects

To test the hypothses about changes in steering control with learning, twelve novice drivers participated in an experiment using an instrumented car over a five week period. The subjects were all high school students who at the start of the experimental test period were beginning a three week intensive driver training program. They were selected on the basis of having had minimal experience of driving. Three subjects had never driven a car before being recorded driving the instrumented car and the other subjects had driven on at most five previous occasions. The subjects were tested on nine separate occasions over the five week period.

Equipment

The instrumented car driven by the subjects was capable of recording driver control measures, vehicle motion variables and vehicle lane position, and was built by Systems Technology Inc., Los Angeles, and lent to this author by the U.S. National Highway Traffic Safety Administration. The car is described in detail in an STI technical manual (Klein et al, 1976). Two features of particular interest, though, are the lateral position detector and the servo control.

The lateral position detector was developed by the Institute for Perception in the Netherlands. It consists of a position transducer and a control unit. The position tranducer uses a rotating prism to scan the intenstiy of reflected light in a lateral plan across the road and reflect the light in a photoamplifier. Any marker which sufficiently contrasts with its surroundings is taken as being part of the reference line by the lane tracker. For the experiment a 2.5 inch wide strip was laid down as a center lane marker to be picked up by the position detector.

The servo control allows for application of steering inputs to the front wheels independently of the driver's steering inputs. This is accomplished by

hooking up an analogue tape recorder containing a taped disturbance which is played back and passed by means of an electro-mechanical device through the steering linkage to the front wheels. This provides a means of measuring the closed loop dynamic behavior of the driver by insertion of a known input or disturbance function into the loop. The disturbance function used in the experiment was a sum of nine sinusoids - .377, .503, .754, 1.257, 1.634, 2.765, 4.271, 5.781 and 10.801 rad./sec. Each of these input frequencies has an integral number of cycles in a 50 second run length. The advantage of using a sum of sines input is that while the remnant is spread out over many frequencies, the input is concentrated at discrete frequencies. Thus, at these discete frequencies, where the driver car-driver transfer function is measured, the remnant is swamped by that part of the output signal which is correlated with the input, so that relatively clean estimates of the correlated output are obtained.

The variables recorded during the subject runs were: steering wheel angle, front tire angle, heading angle, lateral acceleration, lateral position, forward velocity and the disturbance signal input.

Procedure

Each of the twelve subjects came to the test site twice a week for five weeks. On the first test day it was determined from the first two subjects that the novices could manage a speed of 40 k.p.h. This determined the speed which was used for all the test runs. Runs were made up and down two marked lanes on a half mile stretch of an unused runway. In total 200 seconds of data were collected for each subject on each day.

RESULTS

Changes in the Car-Driver Transfer Function with Learning

Table 1 summarizes the one factor, repeated measures, analyses of variance which were carried out for the amplitude and phase angle values in the car-driver transfer function, using twelve subjects and nine (treatment) days. Analysis of the power spectrum of steering wheel angle showed that the driver's input at frequencies above 2.765 rad./sec. was negligible (< 1% of total input). Also, at these frequencies the signal to noise ratio is high and therefore the estimates are less reliable. Consequently changes at the first six frequency points (in the disturbance signal car-driver transfer function) are of greatest interest.

Table 1 and Figure 5 show that a significant increase in amplitude of the car-driver transfer function occurred over the test period at the first four freqeuncy points. However, the amplitude at the first frequency point showed the most dramatic change. While the means of the first two days were approximately equal, the mean increased by 40% on the third day and fluctuated about this value for the last six days. As this large increase did not occur at frequency points adjoining .377 rad./sec., a change in slope of the amplitude plot of the car-driver tansfer function is indicated. When individual subject

TABLE 1
Summary Anova Results: Amplitude and
Phase of the Car Driver Transfer Function
Nine (treatment) Days: 12 Subjects

	Amplitude		Phase	
Frequency rad./sec.	$F_{8,88}$	Differences Between Days (.05 Level)	$F_{8,88}$	Differences Between Days (.05 level)
.377	2.242^{+}	Day 1 < 3-9	1.622	
.503	3.158^{++}	Day 1 < 5,6,9: Day 2 < 9	1.550	
.754	4.725^{+++}	Day 1 < 3-9; Day 2 < 4,9	0.930^{++}	
1.257	2.651^{++}	Day 1 < 3-9	4.216^{+++}	Day 2>5; Day 8>5; Day 9>5-7
1.634	0.845		8.646^{+++}	Day 1-6 < 8,9
2.765	1.607		21.234^{+++}	Day 1,2<4-9; Day 3-6<7-9

level of significance: + .05, ++ .01, +++ .001

plots were examined it was found that, for half of the subjects, the amplitude of the .377 rad./sec. point showed a sharper increase over the first three days than did the amplitudes at other frequencies, while, for the other half, the whole amplitude slope increased. As will be shown in the section on modelling, an increase in the amplitude slope, particularly at low frequencies, is a result of the way subjects used the lateral position cue.

When the phase angle (of the car-driver transfer function) drops below -180^{0}, the car-driver system becomes unstable so that an input generates an exponentially increasing output. Therefore, large phase angles ($> -180^{0}$) are to be desired around crossover. (Phase angles at frequencies further from crossover have little effect on system stability.) Figure 6 shows that at the frequencies surrounding the crossover the phase angle increases gradually, though a little erratically, between days one and nine, indicating that the subjects improved their stability of control.

The changes in amplitude and phase angle of the car-driver transfer function over the test period were reflected in improved tracking performance, with the largest improvements occurring during the first three days.

For all the variables studied, the changes that took place over the last six days were much less dramatic, and much more erratic, than those that occurred over the first three days. If measures on day 3 are compared with those for days 8 and 9, no changes are significant, but the following trends were noted: an increase in the amplitude of the car-driver transfer function at .503, .754, and 1.275 rad./sec., an increase in phase margin, and reduced heading angle deviation.

Modelling the Driver-Alone Describing Function

In the first two structures postulated, the driver adapts to each set of controlled mechanics in such a manner that the overall car-driver transfer function has the same form (see Fig. 4). However, as was noted previously,

ORIGINAL PAGE IS
OF POOR QUALITY

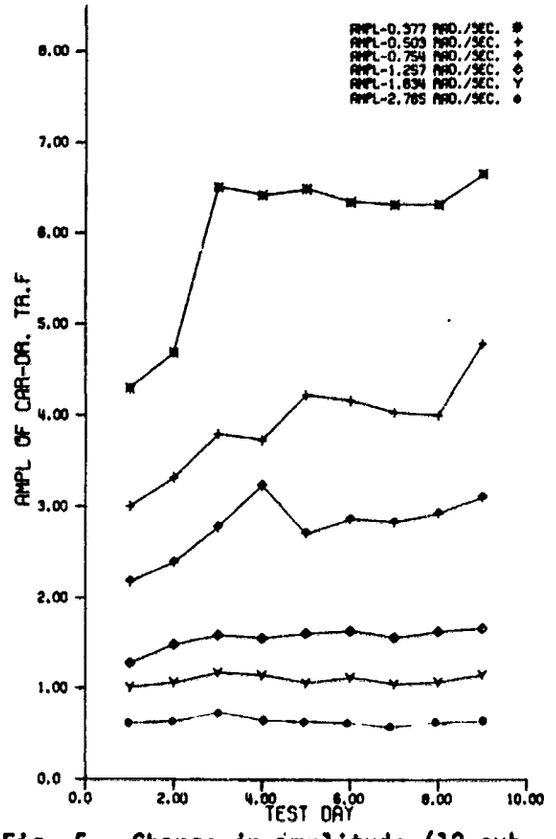

Fig. 5. Change in amplitude (12 subjects)

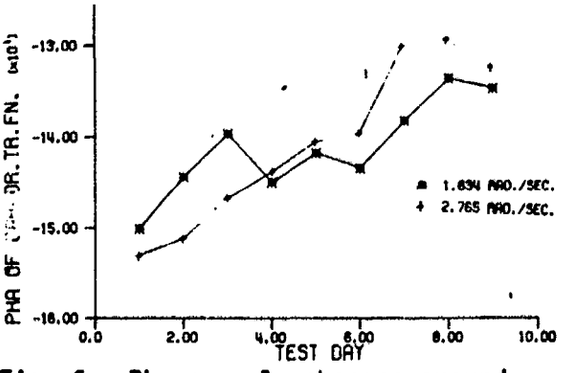

Fig. 6. Phase angle changes around crossover (12 subjects)

experimental data shows that a switch from proportional control (i.e., control of lateral position) to rate control (i.e., control of heading angle) results in a large improvement in crossover frequency. Although there was mean increase in crossover frequency in this study, from 1.696 to 1.929 rad./sec., the increase was small, occurred gradually, and was statistically insignificant. Only two of the twelve subjects showed large changes in crossover frequency. Further examination of the data suggested that reasons other than a change in control structure were responsible for the increase.

Another factor which aids in deciding upon the control structure in use is the percent of high frequency area (%HFA) in the power spectrum of the steering wheel angle. A car's dynamics are such that at the higher frequencies it shows a greater response in heading angle than it does in lateral position. Therefore, a driver who controls lateral position most use lower frequency inputs to get a reasonable response from the car. Consequently, one would expect that %HFA would be lower for a driver controlling lateral position than it would be for a driver controlling heading angle. The data showed that the %HFA was higher rather than lower, though not significantly so, in the first days of the experiment than in the last. This is another indication that the subjects were probably not using the first postulated structure where lateral position was the primary cue for control.

Though this assumption will be used in determining how the driver transfer functions will be modelled, it must be stressed that the structure of a system with only one input, with which to identify two operator transfer functions, can only be inferred; it cannot be known with certainty.

If the first structure can be eliminated as a mode of control, the modelling of the driver-alone transfer function is simplified.

Let us consider the third control structure. As was discussed previously, the form used for Y_y, the driver's operation on functions of lateral position, was to be a simple gain K_y. If the data are fitted to this third structure, but have, in fact, been generated by the subject's using the second structure, the term K_y will be zero. Consequently, equation (5) will reduce to an equation which describes the second control structure. Consequently the value of K_y will indicate which structure was probably in use.

The effective driver-alone transfer function for the third structure was derived by removing $G^{\psi}_{\delta_w}$, the car's dynamics in heading, and modelled using:

$$Y_p = \underbrace{K_\psi(1 + T'_{rjw})e^{-jw\tau}}_{Y_\psi}\left[1 + \underbrace{K_y}_{Y_y}\frac{G^y_w(jw)}{G^{\psi}_{\delta_w}(jw)}\right] \qquad (5)$$

Table 2 shows the values derived for K_ψ, τ, T'_r, and K_y for selected test days, averaged over twelve novice drivers (see also Figure 7).

TABLE 2
Parameters for the Averaged
Effective Driver Transfer Function

Day	K_ψ deg./deg.	K'_y rad./sec.	τ sec.
1	0.590	0.20	.42
2	0.655	0.20	.42
3	0.595	0.44	.36
6	0.615	0.71	.37
9	0.630	0.82	.25

(since $T'_r \simeq T_r$ (= 9.4 rad./sec. for the test car), $T'_r = T_r$ was assumed), $K'_y = K_y U_o$ where U_o is the forward velocity

Discussion of Modelling Results

Data, from experienced drivers, that (in reference 8) was fitted to the third control structure show the amplitude fit to be good across all frequencies measured and the phase fit to be best nearest the crossover frequency. This same type of model fit was obtained with the experimental data. Goodness of fit parameters were calculated using the distance from the modelled to the actual data point, relative to the standard deviation at that point. For the experimental car, the response lag which is offset by the driver's use of heading rate (vs. heading angle) begins to have effect at 9.4 rad./sec. (the break frequency). Though $1/T'_r$ is expected to be approximately equal to 9.4 rad./sec., and because this value is far enough outside the measurement frequency range to have little effect on the model anyway, 9.4 rad./sec. was used for the value of $1/T'_r$ for all days. It is evident from the fit parameters

ORIGINAL PAGE IS
OF POOR QUALITY

in Table 2 that the largest changes occured in the value of K'_y. The smaller changes in the K_ψ parameter indicate that heading angle was controlled in much the same way on the first day as on the last. In contrast, the value of K'_y doubled between days two and three, moving within the measurement frequency range (i.e., > .377 rad./sec.), and doubled again between days three and nine. This change reflects the large increase in the amplitude of the car driver transfer function at .377 rad./sec. between days two and three. The increases in the value of K'_y point to the increased control of lateral position as defined in the third structure. The phase fits were so poor that very little faith can be placed in the time delay values. However, they do conform to the findings of other reasearchers that the time delay decreases with learning (Reference 1). A large improvement in the model fit to the phase data occurred over the learning period as the low frequency phase droop became less noticeable (as illustrated in Fig. 7).

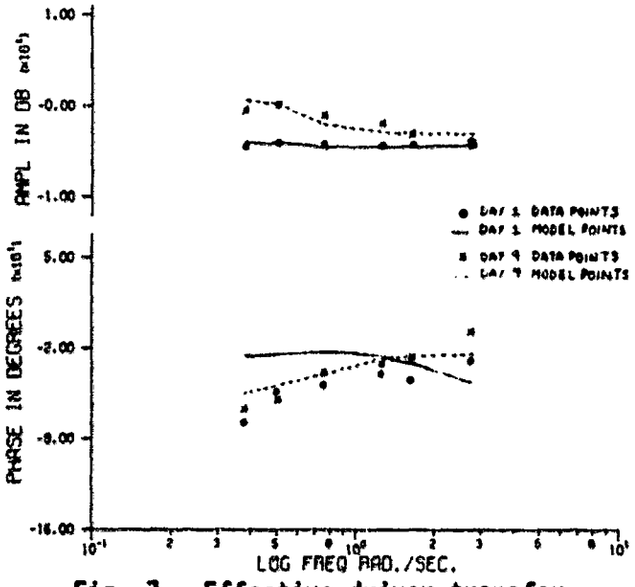

Fig. 7. Effective driver transfer function, averaged over 12 subjects, days 1 and 9

CONCLUSIONS

In summary, though the fit parameters do not indicate a sharp division between days one and two and day three, enough of a change in K'_y is indicated to suggest that on day three and thereafter the drivers' control structure bore more resemblance to structure three, where an outer loop controlled lateral position, than to structure two, while on days one and two, the reverse was true.

Other experimenters, using laboratory tracking tasks (Reference 9) have not found changes in strategy with the learning of tracking control but did note improvements in gain and crossover frequency. Using a more complex tracking task, steering a car, such a change in strategy was found to occur, as well as the previously noted change in gain. Phase margin rather than crossover frequency was found to improve with learning indicating that the subjects opted for an improvement in stability of control over improved system response.

REFERENCES

1. McRuer, D.T. and Krendel, E.S. Mathematical models of human pilot behavior. AGARD Report #Ag-188, 1974.

2. Weir, D.H. and McRuer, D.T. A theory for driver steering control of motor vehicles. Highway Research Record, No. 247, 1968.

3. McLean, J.R. and Hoffman, E.R. The effects of restricted preview on driver steering control and performance. Human Factors, 15(4), 1973.

4. Mourant, R.R. and Rockwell, T.H. Strategies of visual search by novice and experienced drivers. Human Factors, 14(4), 1972.

5. Pew, R.W. Acquisition of hierarchical control over the temporal organization of a skill. Journal of Exper. Psych., 71(5), 1966.

6. Weir, D.H. and McRuer, D.T. Measurement and interpretation of driver steering behavior and performance. SAE Paper No. 730098, 1973.

7. Bendat, J.S. and Piersol, A.G. Random data: Analysis and measurement procedures. Wiley-Interscience, 1971.

8. McRuer, D.T. and Klein, R.H. Automobile controllability - driver/vehicle response for steering control. Systems Technology Inc., Los Angeles, California, November, 1974.

9. Reid, L.D. An investigation into pursuit tracking in the presence of a disturbance signal. Procedures of the Fifth Annual NASA-University Conference on Manual Control, 1970.

49

N79-15607

USE OF REWARD-PENALTY STRUCTURES IN HUMAN EXPERIMENTATION

Anthony C. Stein, R. Wade Allen, and Stephen H. Schwartz

Systems Technology, Inc.
Hawthorne, California

SUMMARY

This paper reviews the use of motivational techniques in human performance research and presents an example study employing a reward-penalty structure to simulate the motivations inherent in a real-world situation. The influence of motivation on human performance has been an issue since the beginning of behavioral science. Most often, motivation is controlled through procedures designed to minimize its influence as an uncontrolled variable. Driver behavior in a decision-making driving scenario was studied.

The task involved control of an instrumented car on a cooperative test course. Subjects were penalized monetarily for tickets and accidents and rewarded for saving driving time. Two groups were assigned different ticket penalties. The group with the highest penalties tended to drive more conservatively. However, the average total payoff to each group was the same, as the conservative drivers traded off slower driving times with lower ticket penalties.

INTRODUCTION

Reward-penalty structures have existed since the beginning of experimentation, and the effects of such structures have evolved into a separate area of research. As early as 1922, A. M. Johanson observed the effects of rewards and penalties on reaction times. These classic results (cited in Ref. 1) are shown in Fig. 1. Researchers have examined the motivational aspects (Refs. 2-6), looked at rewards' distracting effects (Refs. 7-10), and looked at the positive effects of rewards (Refs 11 and 12). What does this experimentation mean, and how can the researcher of today utilize the efforts of others?

Subject motivation is a primary concern in any experiment. "We want the subject motivated to come back for 12 experimental sessions;" or "we want the subject motivated to respond as quickly as possible;" or "we want the subject motivated to respond in a manner consistent with his or her normal behavior." Rewards and penalties play an important part in this motivation.

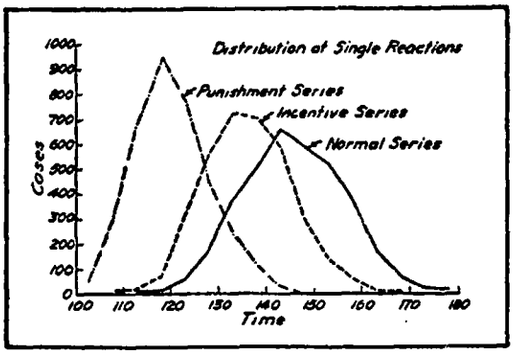

Figure 1. Change in the Distribution of Reaction Time Under the Influence of Incentives. Auditory stimulus. In the "incentive series" O was informed of his last RT; in the "punishment series" he received a shock in the finger when the reaction was at all slow. Each curve shows the distribution of 3600 single reactions obtained from three Os whose times were nearly the same. (Adapted from Ref. 1)

To assess reward-penalty structures with regard to their consequences, and to develop a structure for a given experiment, requires a basic knowledge of the literature, terminology, and present methodologies. This paper is a review of the present body of knowledge with an emphasis on reward-penalty design consequences for human performance research.

PREVIOUS RESEARCH

Definitions

The distinction between intrinsic and extrinsic motivation should be an important consideration when designing a reward-penalty structure. If a person chooses to work a series of complex mathematical problems because of personal enjoyment, then the "perceived locus of causality" (Ref. 6) is internal, and the task is intrinsically motivating. If, however, the person chooses to work the problems to gain an external reward, and the "perceived locus of causality" is external, then the task is extrinsically motivating (Refs. 3, 4, 6, 13-15).

Deci (Refs. 2 and 3), Deci, Benware, and Landy (Ref. 4), and Edwards (Ref. 16), all point out that reward-penalty structures can be designed to be either extrinsically motivating or neutral. If the experimenter chooses to have the structure of neutral influence on the subject, and at the same

time achieve high subject motivation, it becomes necessary to use a task that has been, or can be, shown to be intrinsically interesting to the subject population. If the choice is to have a structure that makes the reward or penalty contingent on performance, or in some other way extrinsically motivating, then the choice of experimental task is of secondary consideration. It has been shown by Lepper and others (Refs. 3, 4, 13, and 14) that subjects performing tasks of high intrinsic motivation, receiving extrinsic rewards, perceive the locus of causality to be external, and show low intrinsic motivation.

Purpose of Rewards and Penalties

As pointed out by Edwards (Ref. 16), rewards and penalties can serve three purposes: 1) motivators, 2) information givers, and 3) instructions. If the subject is rewarded only for participation in an experiment, then the reward serves as a motivator; the subject will perceive the locus of causality as internal, and the experimental task will be intrinsically motivating. If the reward-penalty structure is changed, and task performance is rewarded the reward or penalty will serve as information, in addition to any motivating influence it has. If the experimental task is solving complex mathematical problems, and the subject is paid hourly for experimental participation, then task performance is unrelated to the reward, and the reward's purpose is that of a motivator. If the reward is increased as a function of problem completion time, or number of problems solved, the reward takes on the additional quality of an information giver. In this case it is important to note that correct response is not required.

If correct response is required for a reward increase, or incorrect response is punished, the reward also serves as an instruction. In this case the reward not only provides motivation and information, it now tells the subject the relative desirability of a specific response. Withholding the reward until the completion of the experiment does not alter its motivational or instructional qualities. Because the reward is performance related, withholding payment (or information about the reward "earned") only eliminates the informational feedback quality.

Form of Rewards and Penalties

Rewards and penalties can take many forms, and the type of reward or penalty chosen by the experimenter should be an important part of the reward-penalty design. The overall effect of the reward or penalty needs to be assessed prior to its introduction in the experiment. For example, Deci (Ref. 2) found that monetary rewards caused a decrease in intrinsic motivation, while rewards by use of verbal reinforcement caused an increase. McCloskey (Ref. 17), in her work with staff turnover rates, found that psychological rewards such as recognition, help from peers, and educational opportunities were more important in keeping an employee than salary or job

ORIGINAL PAGE IS
OF POOR QUALITY

benefits; and that money alone would not keep an employee. Viesti (Ref. 18) found that on an insightful learning task pay made no difference in performance.

One of the most commonly used rewards is money. Many researchers have examined the advantages and pitfalls of this reward form, and their findings can be of great assistance in developing a reward-penalty structure.

Money seems to provide the best balance between response and error rate. Daniels, et al.(Ref. 11), found that response speed remained constant, but a drastic reduction in error rate was observed when real instead of imaginary money was used. Slovic, Lichtenstein, and Edwards (Ref. 19) found that subjects employed simpler decision strategies in an imaginary incentive design than with real payoffs. Also Slovic (Ref. 20) found that when subjects made hypothetical choices, they maximized gain and discounted losses; however, when their choices had real consequences, the subjects were considerably more cautious.

The researcher should be cautioned by the work of Greenberg (Ref. 21) and Leventhal and Whiteside (Ref. 22), however. They have shown that monetary reward can be used to motivate performance, but that overreward is frequently employed. In some cases the overrewarding tendency was so strong that higher rewards were given to lower performing workers. Furthermore, Spence (Refs. 8 and 9), Miller and Estes (Ref. 10), and McGraw and McCullers (Ref. 7) point out that increased rewards may draw attention from the experimental task.

EXPERIMENTAL STUDY

The above research findings clearly show the need for appropriate reward-penalty designs, both in form and magnitude. The following examples, part of a study on alcohol-driver interaction, show how this information can be used to create a reward-penalty structure.

In a study concerning the effects of alcohol on drivers' decision making behavior, two separate experiments were conducted. The first was run in our fixed-base driving simulator (Ref. 23) and the second in an instrumented vehicle designed for the National Highway Traffic Safety Administration (Ref. 24).

In both experiments the subject was required to complete a driving scenario in both sober and intoxicated states. The following is a brief discussion of the requirements, design, and effects of variations in a motivational reward-penalty structure.

ORIGINAL PAGE IS
OF POOR QUALITY

Reward-Penalty Structure

Driving in the real world is motivated by a variety of counteracting incentives. Drivers wish to minimize trip time but avoid tickets and accidents. Driving behavior is influenced by these motivations, particularly in risk-taking/decision-making tasks. In order to encourage real-world-like behavior we must attempt to simulate the real-world incentives. The problem with simulating typical driving incentives is that they include some difficult-to-quantify variables, such as the subjective value of time gained by driving faster and the subjective fear of low probability events such as auto crashes. Negative reinforcement with electric shock is a classical experimental technique and might serve to simulate the pain of an accident, but this technique is difficult to quantify and recent subject welfare guidelines make it unattractive. In a recent aircraft landing experiment involving pilot decision making (Ref. 25), the experimenters went so far as to inform their pilot subjects that they would be eliminated from the experiment in the event they crashed in order to make them as averse to crashes as they would be in real life. However, this approach would be logically awkward in this study because we would lose selected and trained subjects and, furthermore, the majority of driving accidents do not involve fatalities.

The traditional method of quantifying incentives for experimental control is to relate them to some well-defined variable with interval properties by measuring indifference curves (Refs. 26 and 27). The most well-defined, widely studied, and widely used norm is money, primarily because of its interval properties and interchangeability. Money has some limitations; for example, the decision-making behavior has been shown to be confounded by the subject's financial status. However, this can be experimentally controlled by controlling the knowledge of results (Ref. 28). In general, the additional experimental effort required to scale other disincentives (e.g., shock, loud noises, etc.) has led to widespread use of money for rewards and punishments in decision-making experiments.

In both experiments the reward-penalty structures had multiple requirements. A major concern was that the subject complete the driving scenario in a normal manner, with a reasonable motivation for timely progress and a desire to avoid tickets and accidents; that is, we wanted the subject to drive as if the driving situation were being experienced in the real world. A second requirement was that the subjects return for participation in six full-day experimental sessions. Finally, we chose to alter the penalty structure in the experiment to determine the behavioral effects of increased ticket penalty on the driver.

With the exception of ticket penalties, the reward-penalty structure for both experiments was the same. In order to provide a basic motivation to remain in the study, the subjects were paid an hourly wage. This payment was received by the subject irrespective of performance. To facilitate completion of the driving scenario, and to encourage normal driving behavior, we used an additional reward-penalty structure scaled to real world occurrences.

Rewards consisted of $10.00 for completing the driving scenario, and $2.00 for every minute of total elapsed driving time under 20 minutes. Assuming a real world situation of leaving a bar intoxicated,. this rewarded the subject for making it home and for driving with the flow of traffic, thus avoiding detection.

In both experiments, crashes (i.e., hitting an obstacle or adjacent car, or running off the roadway) were penalized $2.00.

Tickets were given for running a red light or for speeding. Again to simulate a real world driving experience, the traffic police were present only 30% of the time. In experiment 1 (the simulation), tickets were either $1.00 or $2.00, depending on the group to which the subject was assigned. In experiment 2 (full-scale), tickets were either $1.00 or $4.00.

Subjects received immediate feedback if they crashed (buzzer), or received a ticket (siren and red lights), but total rewards and penalties were withheld until the completion of the experimental day. Again this simulates the real world, because the cost of a ticket or crash is rarely known when the incident occurs.

RESULTS AND DISCUSSION

To determine the suitability of our reward-penalty structure to the experiment, two criteria can be used. First, did all the subjects complete the experiments? In both experiment 1 and experiment 2 the answer was yes, indicating that we were able to keep the subjects sufficiently motivated to return. Second, to correlate our results with real world driving statistics, we compared our simulator and field test results with epidemiological data of over 7000 alcohol related traffic accidents. As evidenced in Fig. 2, the simulator results and the field results compare favorably with the actual accident data, thus indicating drivers motivated to take comparable risks.

Finally, in our investigation of the behavioral effects of a change in penalty structure, we found in experiment 1 no significant difference between the $1.00 ticket group and the $2.00 ticket group. Experiment 2, however, did show a significant difference between the $1.00 ticket group and the $4.00 ticket group.

In Fig. 3 we see that the high penalty group in the field study had on the average of one-third less tickets, with speeding tickets showing a greater sensitivity than signal light tickets. These results are statistically significant as shown in Table 1. Driving time differences between the two penalty groups were marginally significant (Table 1) and consistent with the ticket results, e.g, larger time and fewer tickets. Payoff was <u>not</u> significantly different between the penalty groups, however (Table 1), which indicates a compensatory tradeoff between driving time and ticket rate.

TABLE 1. ANALYSIS OF VARIANCE SUMMARY FOR OVERALL SCENARIO PERFORMANCE IN THE FIELD VALIDATION STUDY

SOURCE	ERROR TERM[a]	DEGREES OF FREEDOM	F RATIOS					
			PAYOFF	DRIVING TIME	ACCI-DENTS	SIGNAL TICKETS	SPEEDING TICKETS	ROUTE ERRORS
Day	DS(P)	1	19.33***	2.92	12.71**	2.09	13.96**	1.50
Penalty	S(P)	1	2.37	4.20†	1.92	10.80**	5.47*	1.33
Trial	TS(P)	2	10.44**	2.27	13.56**	4.72*	3.71*	1.41
DP	DS(P)	1	0.33	0.42	1.08	0.52	2.67	1.50
DT	DTS(P)	2	13.71***	1.0	11.55**	2.16	4.10*	1.26
PT	TS(P)	2	0.59	2.02	0.40	1.13	0.53	1.33
DPT	DTS(P)	2	1.40	1.65	1.27	2.08	0.90	1.49

Level of Significance: †$p < 0.10$; *$p < 0.05$; **$p < 0.01$; ***$p < 0.001$.

[a]Error term degrees of freedom: S(P) - 12, DS(P) - 12, TS(P) - 24, DTS(P) - 24.

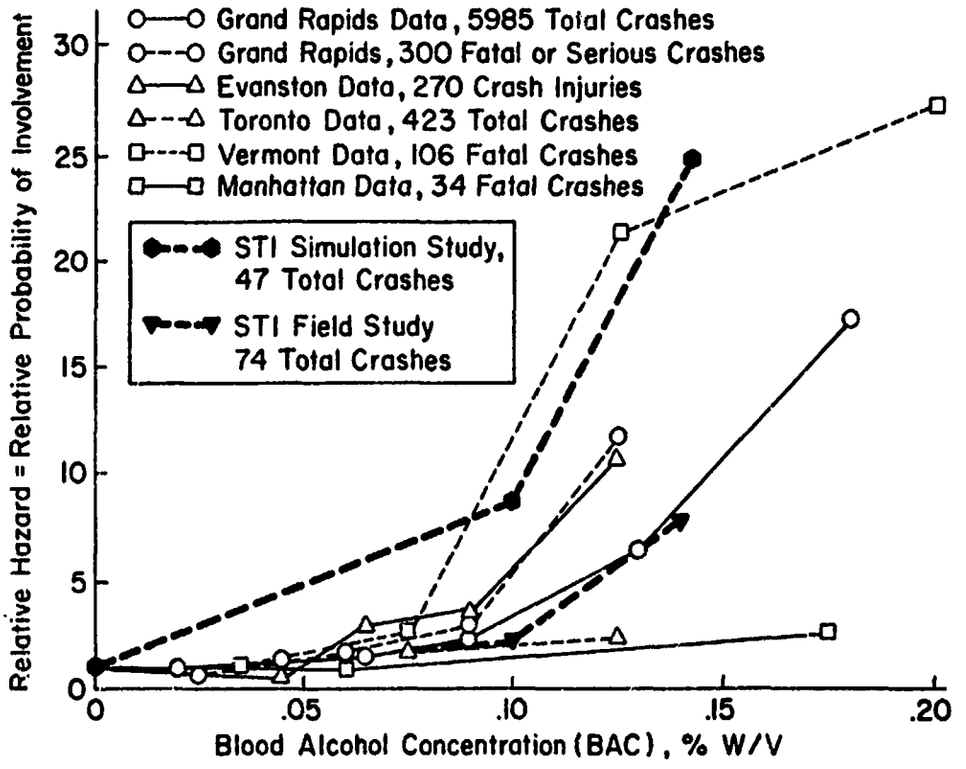

Figure 2. Relative Probability of Crash Involvement as a Function of BAC Where 1.0 = Relative Probability at Zero Alcohol (Adapted from Ref. 29)

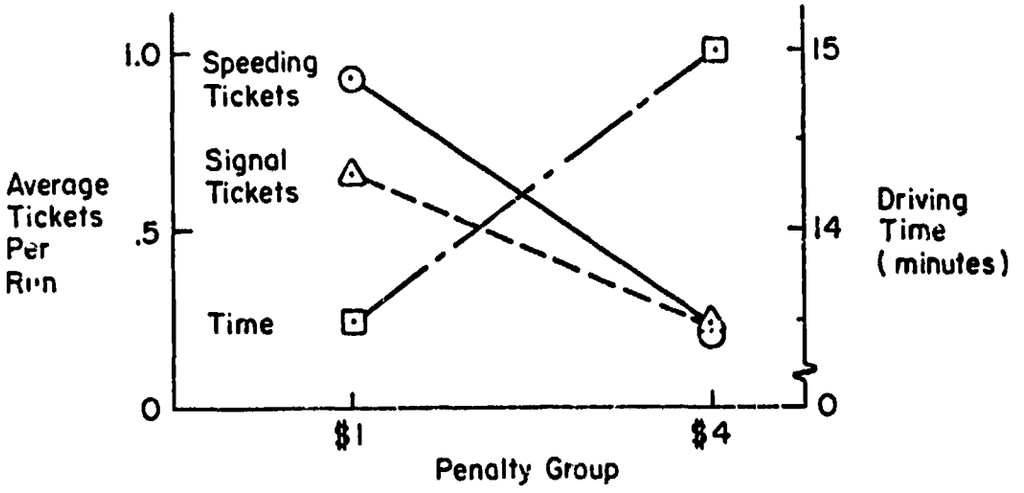

Figure 3. Penalty Effect on Ticket Rate and Total Time to Complete the Driving Scenario

Some insight into the ticket reduction with increased penalty can be gained from the signal light risk acceptance plot shown in Fig. 4 (Ref. 30). Here we see that the high penalty group perceived higher risks in signal failures (i.e., running the red light) and was willing to go less often. The combined effect was much more conservative behavior for the high penalty group, leading to better driving performance. The P(G) and SP(F/G) differences in Fig. 4 were statistically significant, but the SP_c difference was not. No group differences were observed for accident data in the experiment, and because of the magnitude of the ticket and P(G) group differences it is assumed that these are true penalty effects and not just between-group differences.

CONCLUDING REMARKS

The following conclusions were drawn with respect to the reward-penalty structure in our experiments:

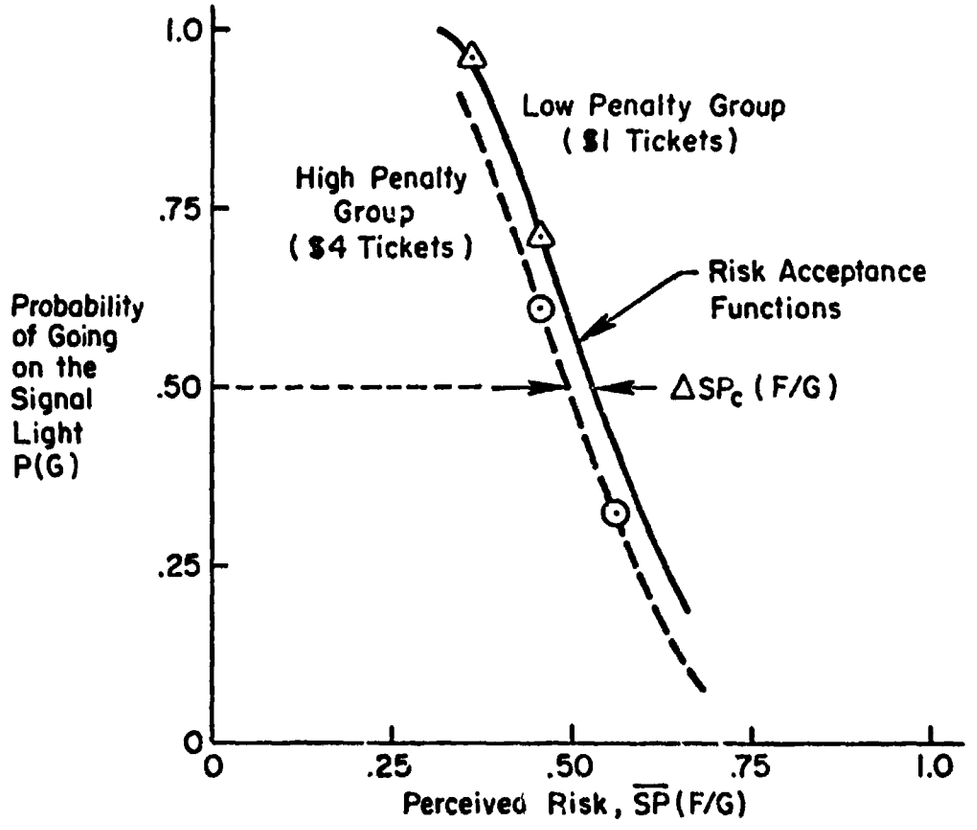

Figure 4. Mean Subjective Probability of Failure to Make It Through the Light If It Were Attempted

* Driving is not intrinsically motivating to the majority of the population, and in experimental tasks is even less so. Real-world Motivation incentives such as accidents, tickets, and desire to safe time, are extrinsic.

* Rewards and penalties must be tangible. Imaginary rewards and/or verbal reinforcement are not sufficient.

* Rewards and penalties should serve as general motivation, but not direct feedback in the driving scenario.

* Between runs in an experimental session, overall performance payoffs should be withheld in order to avoid feedback or reinforcement which might modify behavior on subsequent runs.

* Our results show that employing a specifically designed monetary reward-penalty structure provides sufficient extrinsic motivation to duplicate a "real world" driving situation.

These results on reward/penalty effects on driver risk taking might be extrapolated to real-world driving behavior. Perhaps drivers would drive more conservatively with increased and more evenly applied penalties for traffic violations.

REFERENCES

1. Woodworth, R. S.; and Schlosberg, H.: Experimental Psychology. Holt, Rinehart and Winston, 1964, p. 28.

2. Deci, Edward L.: Effects of Externally Mediated Rewards on Intrinsic Motivation. J. Personality and Soc. Psych., vol. 18, no. 1, 1979, pp. 105-115.

3. Deci, Edward L.: Work. Who Does Not Like It, and Why. Psych. Today, vol. 6, no. 3, Aug. 1972, pp. 57-58.

4. Deci, Edward [illegible].; Benware, Carl; and Landy, David: The Attribution of Motivation as a Function of Output and Rewards. J. Personality, vol. 42, no. 4, 1974, pp. 652-667.

5. Lepper, Mark R.; and Greene, David: Turning Play Into Work: Effects of Adult Surveillance and Extrinsic Rewards on Children's Intrinsic Motivation. J. Personality and Soc. Psych., vol. 31, no. 3, pp. 479-486.

6. Heidler, F.: The Psychology of Interpersonal Relations. Wiley, 1958.

7. McGraw, Kenneth O.; and McCullers, John C.: The Distracting Effect of Material Rewards: An Alternative Explanation for the Superior Performance of Reward Groups in Probability Learning. J. Experimental Child Psych., 1974, pp. 149-158.

8. Spence, Janet T.: The Distracting Effects of Material Reinforcers in the Discrimination Learning of Lower- and Middle-Class Children. Child Development, vol. 41, 1970, pp. 103-111.

9. Spence, Janet T.: Do Material Rewards Enhance the Performance of Lower Class Children. Child Development, vol. 42, no. 5, 1971, pp. 1461-1470.

10. Miller, L. B.; and Estes, B. W.: Monetary Reward and Motivation in Discrimination Learning. J. Experimental Psych., vol. 61, 1969, pp. 501-504.

11. Daniels, E. B.; Kobas, G. B.; and Drury, C. G.: Monetary and Non-Monetary Incentives in Motor Performance. Ergonomics, vol. 19, no. 1, 1976, pp. 61-68.

12. Estes, W. K.: Reinforcement in Human Behavior. Am. Scientist, vol. 60, no. 6, Nov.-Dec. 1972, pp. 723-729.

13. Bem, D. J.: Self Perception Theory. Vol 6 of Advances in Experimental Social Psychology, L. Berkowitz, ed., Academic Press, 1972.

14. Lepper, Mark R.; and Greene, David: Turning Play Into Work: Effects of Adult Surveillance and Extrinsic Rewards on Children's Intrinsic Motivation. J. Personality and Soc. Psych., vol. 31, no. 3, 1975, pp. 479-486.

15. Strickland, L. H.: Surveillance and Trust. J. Personality, vol. 26, 1958, pp. 200-215.

16. Edwards, Ward: Cost and Payoffs Are Instructions. Psych. Review, vol. 68, no. 4, 1961, pp. 275-284.

17. McCloskey, Joanne: Influence of Rewards and Incentives on Staff Nurse Turnover Rate. Nursing Research, vol. 23, no. 3, May-June 1974, pp. 239-247.

18. Viesti, Carl R., Jr.: Effective Monetary Rewards on an Insight Learning Task. Psychonomics Sci., vol. 23, no. 3, 1971, pp. 181-184.

19. Slovic, P.; Lichtenstein, S.; and Edwards, W.: Boredom-Induced Changes in Preferences Among Bets. Am. J. Psych. vol. 78, 1965, pp. 208-217.

20. Slovic, Paul: Differential Effects of Real Vs. Hypothetical Payoffs on Choices Among Gambles. J. Exp. Psych., vol. 80, 1969, pp. 434-437.

21. Greenberg, Jerald: Equity and the Use of Over Reward to Motivate Performance. J. Personality and Soc. Psych., vol. 34, no. 2, 1976, pp. 179-190.

22. Leventhal, Gerald S., and Harold D. Whiteside. Equity and the Use of Reward to Elicit High Performance. J. Personality and Soc. Psych., vol. 25, no. 1, 1973, pp. 75-83.

23. Allen, R. Wade; Hogge, Jeffrey R.; and Schwartz, Stephen S.: An Interactive Driving Simulator for Driver Control and Decision-Making Research. Proceedings of the Eleventh Annual Conference on Manual Control, NASA TM X-62,464, May 1975, pp. 396-407.

24. McRuer, Duane T.; Peters, Richard A.; Ringland, R. F.; Allen, R. Wade; et al.: Driver Performance Measurement and Analysis System (DPMAS). Task I: Requirements and Plans for Prototype Equipment. DOT HS-801 234, Oct. 1974.

25. Curry, R. E.; Lauber, J. K.; and Billings, C. E.: Experiments in Pilot Decision-Making During Simulated Low Visibility Approaches. Proceedings of the Eleventh Annual Conference on Manual Control. NASA TM X-62,464, May 1975, pp. 19-23.

26. Raiffa, Howard: Decision Analysis: Introductory Lectures on Choices Under Uncertainty. Addison Wesley, Reading, Mass., 1968.

27. Fischer, Gregory W.: Multi-Dimensional Value Assessment for Decision Making. University of Michigan, Dept. of Psych., Rept. 037230-2-T, June 1972.

28. Rapoport, Amnon; and Wallsten, Thomas S.: Individual Decision Behavior. Ann. Review of Psych., vol. 23, 1972, pp. 131-176.

29. Hurst, P. M. Epidemiological Aspects of Alcohol in Driver Crashes and Citations. Chap. 6 of Alcohol, Drugs and Driving. DOT HS-801 096, Mar. 1974, pp. 131-171.

30. Schwartz, Stephen H.; and Allen, R. Wade: A Decision Model Applied to Alcohol Effects on Driver Signal Light Behavior. Presented at the 14th Annual Conference on Manual Control, published in this volume.

C-4 N79-15608

THE INFLUENCE OF VEHICLE AERODYNAMIC AND CONTROL RESPONSE CHARACTERISTICS ON DRIVER-VEHICLE PERFORMANCE

by

Alexander A. Alexandridis
Brian S. Repa
Engineering Mechanics Department
General Motors Research Laboratories
Warren, Michigan 48090

Walter W. Wierwille
Virginia Polytechnic Institute and State University
Blacksburg, Virginia 24061

SUMMARY

The effects of changes in understeer, control sensitivity, and location of the lateral aerodynamic center of pressure (c.p.) of a typical passenger car on the driver's opinion and on the performance of the driver-vehicle system were studied in the moving-base driving simulator at Virginia Polytechnic Institute and State University. Twelve subjects with no prior experience on the simulator and no special driving skills performed regulation tasks in the presence of both random and step wind gusts.

INTRODUCTION

The performance of the driver-vehicle system in the presence of cross-wind disturbances is influenced by the location of the lateral aerodynamic center of pressure (c.p.) of the vehicle.

The extent to which changes in c.p. location are discernible and/or objectionable to ordinary drivers has up to this time been unknown. Most of the previous studies on wind gust disturbance regulation tasks have concentrated on a single c.p. location with the c.p. most frequently placed at the front wheels (references 1-5). Also, although the influence of changes in design parameters, such as understeer and control sensitivity, have been studied previously (references 3, 4), the interaction of these parameters with the location of the c.p. in a closed-loop task is unknown.

The present study examines the influence of various combinations of understeer, control sensitivity, and c.p. location on the performance of twelve ordinary drivers in the presence of wind gust disturbances.

The Virginia Polytechnic Institute and State University (VPI&SU) moving-base driving simulator was chosen for the tests because of the control it offers over the parameters of interest and because of the success of previous research performed with the facility (reference 1). The following sections

describe the simulation facility, the experimental design and procedure employed, the performance measures utilized, and the results obtained.

THE VPI&SU DRIVING SIMULATOR

This experimental facility provides the subject with an on-line, computer-generated, television-type display of the roadway in coordination with the motion cues of yaw and roll, as well as lateral and longitudinal translation. In addition, four channels of sound along with vibration are provided for the enhancement of the simulation realism.

Three separate inputs were provided to the vehicle model used for the simulation; namely, steering wheel displacement, accelerator/brake displacement, and aerodynamic force (wind gust). The model consisted of a set of transfer functions relating the three inputs to the vehicle motion components.

References 1, 6, and 7 contain a detailed description of the driving simulator and related equipment; figure 1 shows the simulator motion platform.

DEFINITIONS AND EXPERIMENTAL PROCEDURE

Definitions

The three experimental variables are defined briefly as follows:

1. C.p. location, x_a : The distance between the front-wheel axis and the point of action of the lateral aerodynamic force F_a (see figure 2).

This variable is expressed as a percentage of the vehicle wheelbase (x_a = 0.0% corresponds to a c.p. location at the front wheels).

2. Understeer, K : The numerical difference between the sideslip angles developed at the front and rear wheels during a 1-g lateral acceleration.

Understeer is conventionally measured in deg/g. A more detailed description of this concept is given in reference 8. Figure 2 shows the paths that vehicles with understeer ($K > 0$), neutral steer ($K = 0$), and oversteer ($K < 0$) would follow under the influence of an external side force acting at the center of gravity.

3. Control sensitivity, C.S. : The steady-state lateral acceleration (in g's) developed by a vehicle following a steering wheel displacement of 1.75 rad (100.0 deg).

Experimental Design

A mixed between-subjects and within-subjects factorial design was used, containing two levels of understeer (K = 3.0, 5.0 deg/g), two levels of control sensitivity (C.S. = 0.8, 1.2 g/100 deg), and three c.p. locations (x_a = 0%, 19%, 37% of wheelbase) for a total of twelve vehicle configurations. Six male and six female college students without any previous simulator experience were used as subjects. Three male and three female subjects were randomly assigned to each of the two understeer conditions (understeer was a between-subjects variable). The other two variables were factorially complete and equally likely for all subjects. The subjects were given a 1.5 min period of practice following which they were required to maintain a constant speed of 97 km/h (60 mph) while keeping their normal lane position in the presence of random wind disturbances. Data were collected for a period of 2.0 min. Following the random wind disturbances, a series of step gusts were presented for an additional 2.0 min period. At the end of each run, the subjects rated the disturbances they encountered, taking into account the vehicle path deviations and the amount of steering activity needed to maintain course.

Data Collection

The time histories of the vehicle lateral position and yaw heading deviations, as well as the driver's steering wheel inputs were recorded on an F.M. tape recorder. The objective measures of performance were the root-mean-square (rms) values of these time histories, together with the peak lane overshoots during the step gusts.

RESULTS

Subjective Ratings

Figure 3 shows that the subjective ratings improve as the c.p. moves rearward. The other two variables had no significant effect on the ratings.

Random Disturbance Performance

Significant differences in lane-keeping performance occurred as a result of changes in C.S. and x_a . There is a strong indication of an

effect on lateral position deviation due to an interaction between understeer and c.p. location and a significant effect from this interaction on yaw deviations.

Figure 4 shows that increases in both C.S. and x_a result in decreases in lateral position deviations. The nature of the interaction between K and x_a that approached significance in shown in figure 5. The higher value of understeer has a beneficial effect on lateral position deviations only when the c.p. is located close to the front wheels. Figures 6 and 7 show similar effects for yaw angle deviations.

Steering wheel deviations were significantly affected by all three vehicle parameters. Furthermore, there were significant effects due to interactions between c.p. location and understeer and between c.p. location and control sensitivity.

Figure 8 shows that increases in K, C.S., and x_a all have a similar effect; namely, to decrease steering deviations. Figure 9 reveals that increases in both K and C.S. result in greater decreases in steering deviations the closer the center of pressure is to the front wheels.

Step Disturbance Performance

The peak lane position overshoot was measured from the actual vehicle position prior to the gust onset and not from the center of the lane.

Figure 10 shows that increases in x_a and in C.S. reduce peak lane position overshoot. The effects of understeer were accentuated as the c.p. location moved forward, with the lower level of understeer resulting in the largest lane position overshoot.

DISCUSSION

The subjective and objective measures used in the present study indicate that c.p. location is an extremely important parameter for wind gust regulation performance. Scores on the 0-10 Rating Scale, maximum lane deviations following a step wind gust, and steering wheel deviations during presentation of the random wind gust were all highly significantly affected by changes in c.p. location. Actual lane position deviations during the random wind gust task were only slightly less sensitive to changes in c.p. location than these other measures.

In spite of its great importance, however, c.p. location is difficult to control in practice (reference 9). For this reason, other means for improving disturbance responses of the closed-loop driver-vehicle system were explored; namely, through changes in understeer and control sensitivity. Both parameters were found to have a significant effect on wind gust regula-

tion performance, although subjective opinion data failed to detect this effect. Increased levels of understeer (K = 5.0 deg/g vs. 3.0 deg/g) and control sensitivity (C.S. = 1.2 g/100 deg vs 0.8 g/100 deg) both had a beneficial effect on measures of path control and driver steering wheel deviations. These beneficial effects were accentuated where they were needed the most; namely, at forward c.p. locations.

CONCLUSIONS

The following conclusions were reached:

- Driver opinion ratings were significantly influenced by c.p. location only, with rearward locations rated the most favorable.
- Lane-keeping accuracy improved as the c.p. moved rearward and as control sensitivity increased.
- For the forward c.p. locations, lane-keeping performance improved with increased understeer.
- Steering wheel activity required for control was reduced by increased understeer and control sensitivity and by rearward movement of the c.p., with the effects of understeer and control sensitivity accentuated at forward c.p. locations.

Overall, the location of the aerodynamic center of pressure was the predominant vehicle characteristic with an influence that could only partially be offset by changes in understeer and control sensitivity.

REFERENCES

1. Repa, B. S.; and Wierwille, W. W.: Driver Performance in Controlling a Driving Simulator with Varying Vehicle Response Characteristics. SAE Paper No. 760779, 1976.

2. Repa, B. S.; Zucker, R. S.; and Wierwille, W. W.: The Application of Integral Performance Criteria to the Analysis of Discrete Maneuvers in a Driving Simulator. Proc. Thirteenth Annual Conference on Manual Control, 1977.

3. Repa, B. S.; Alexandridis, A. A.; Howell, L. J.; and Wierwille, W. W.: Study of Vehicle Steering and Response Characteristics in Simulated and Actual Driving. SAE Paper No. 780011, 1977.

4. McRuer, D. T.; and Klein, R. H.: Automobile Controllability -- Driver/Vehicle Response for Steering Control. Systems Technology, Inc., Vol. I, Summary Report, Contract No. DOT-HS-359-3-762, 1975.

5. Crossman, E.; and Szostak, H.: Man-Machine Models for Car Steering. Fourth NASA-University Conference on Manual Control, NASA SP-214, 1968.

6. Wierwille, W. W.: A Part-Task Driving Simulator for Teaching and Research. Computers in Education for ASEE Transactions, December 1973.

7. Wierwille, W. W.: Driving Simulator Design for Realistic Handling. Proc. Third International Conference on Vehicle System Dynamics. Swets and Zeitlinger, B. V., Amsterdam, 1975.

8. Bundorf, R. T.; and Leffert, R. L.: The Cornering Compliance Concept for Description of Vehicle Directional Control Properties. SAE Paper No. 760713, 1976.

9. Bundorf, R. T.; Pollock, D. E.; and Hardin, M. C.: Vehicle Handling Response to Aerodynamic Inputs. SAE Paper No. 716B, 1963.

ORIGINAL PAGE IS
OF POOR QUALITY

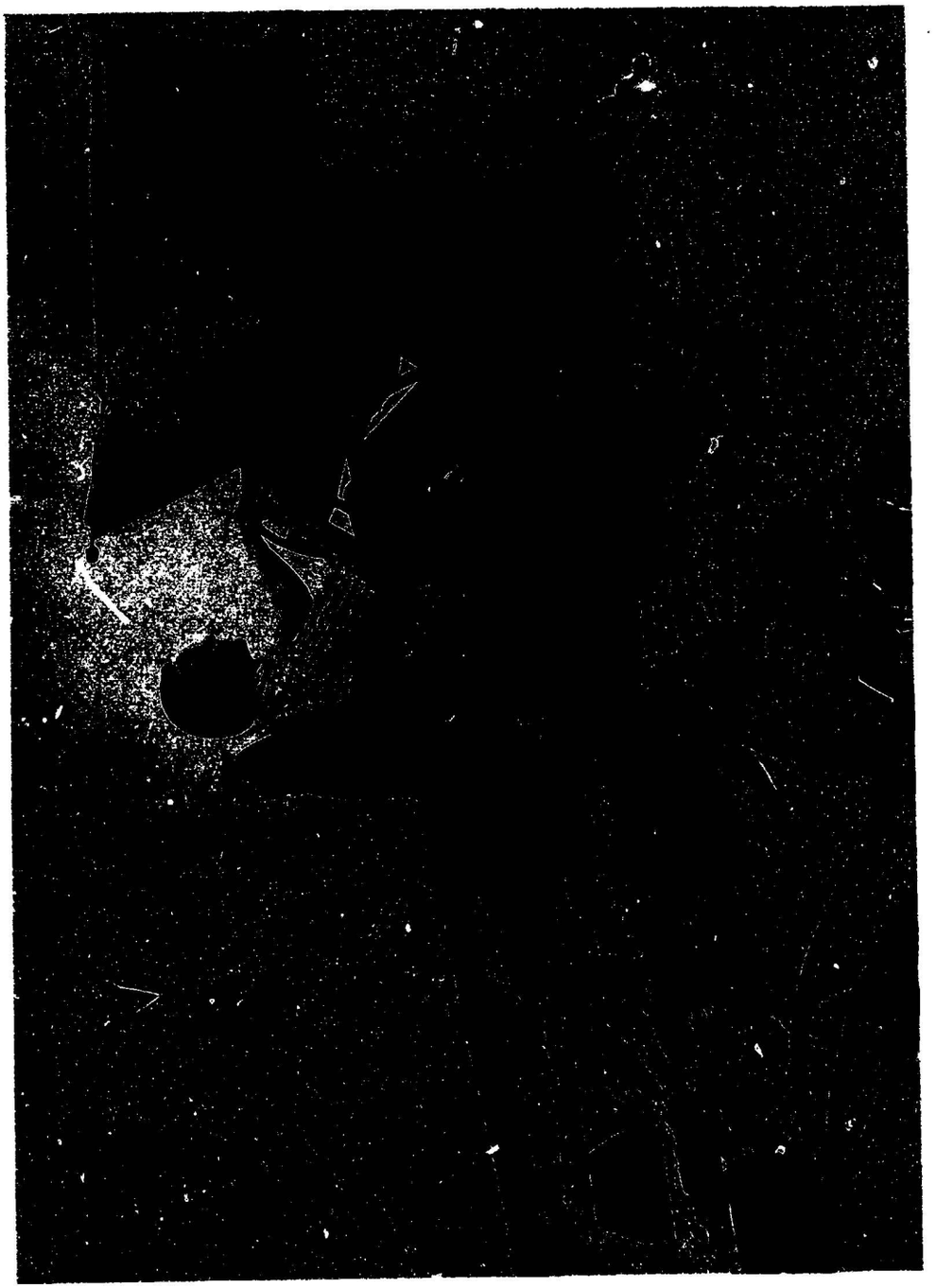

FIG. 1 DRIVING SIMULATOR MOTION PLATFORM

C. P. LOCATION

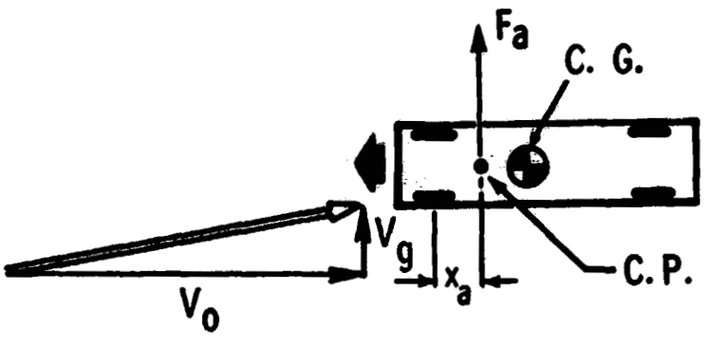

UNDERSTEER

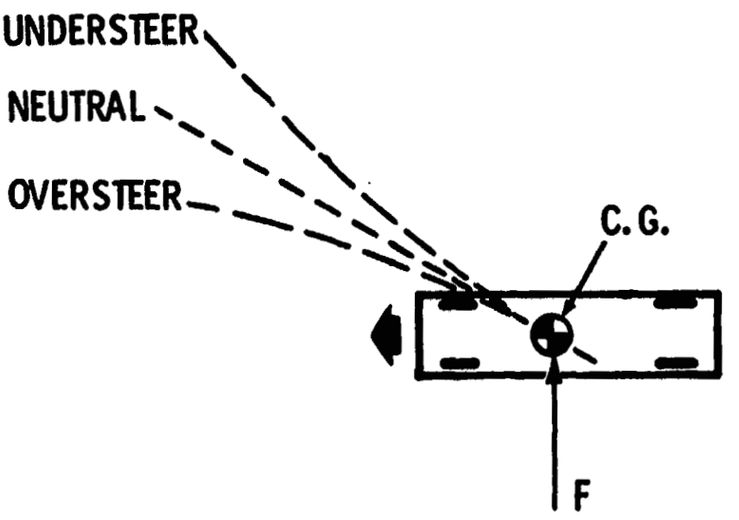

FIG. 2 DEFINITIONS

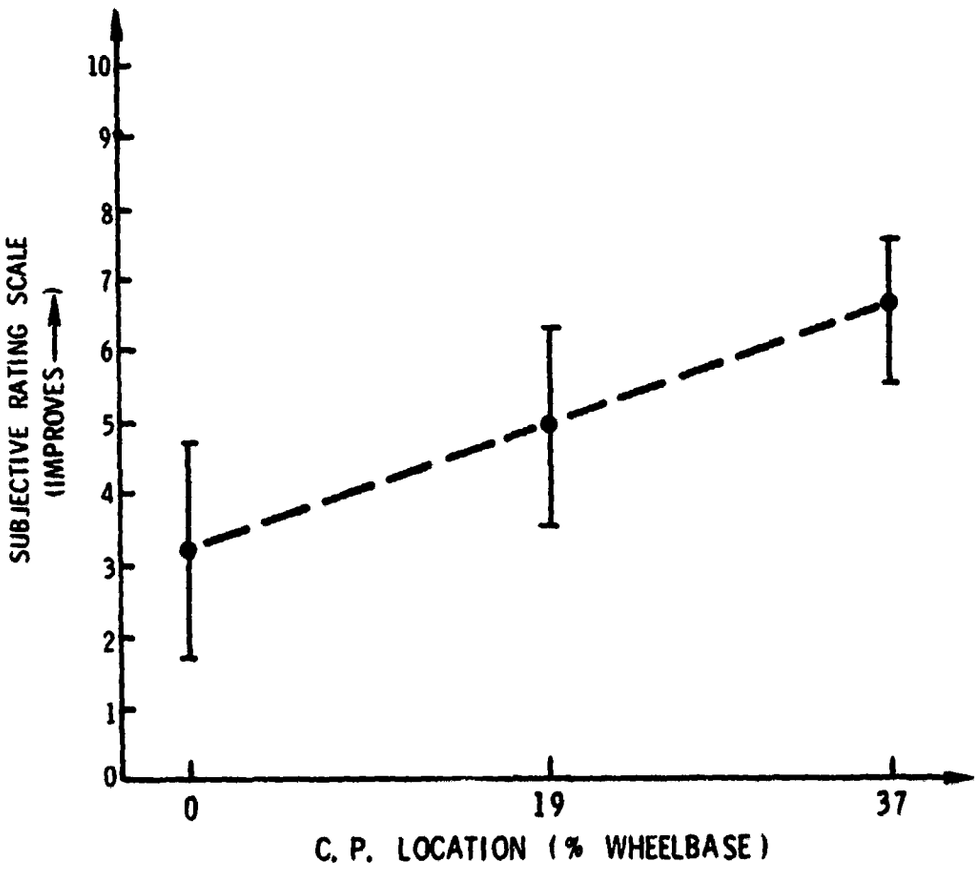

FIG. 3 DEPENDENCE OF SUBJECTIVE RATINGS OF VEHICLE CONFIGURATIONS ON C.P. LOCATION

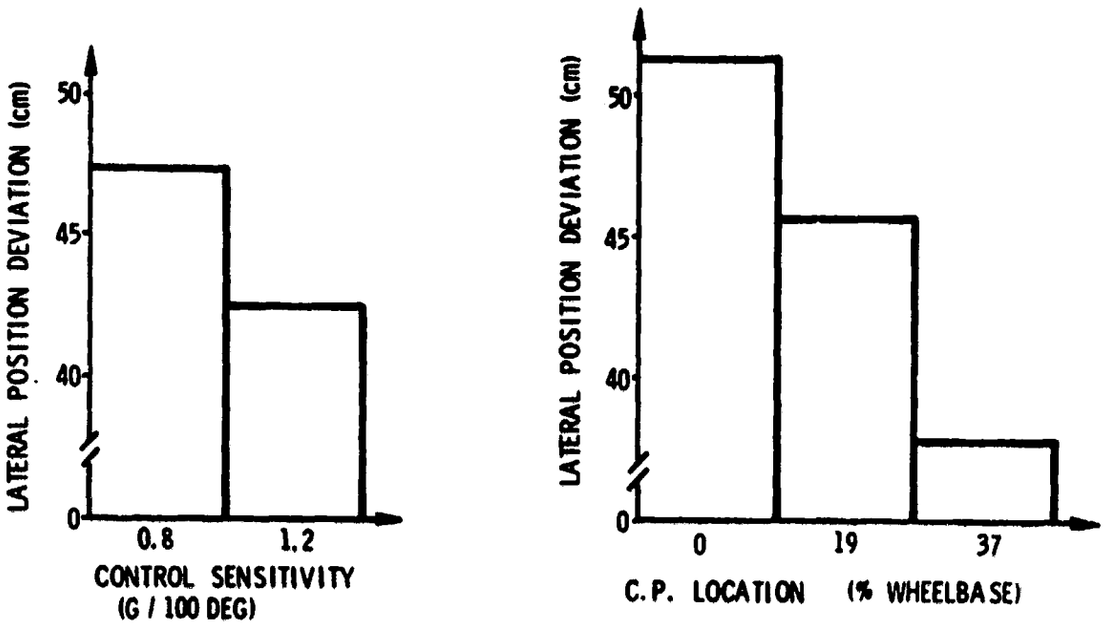

FIG. 4 EFFECTS OF CONTROL SENSITIVITY AND C.P. LOCATION ON LATERAL POSITION DEVIATION (RANDOM WIND GUST)

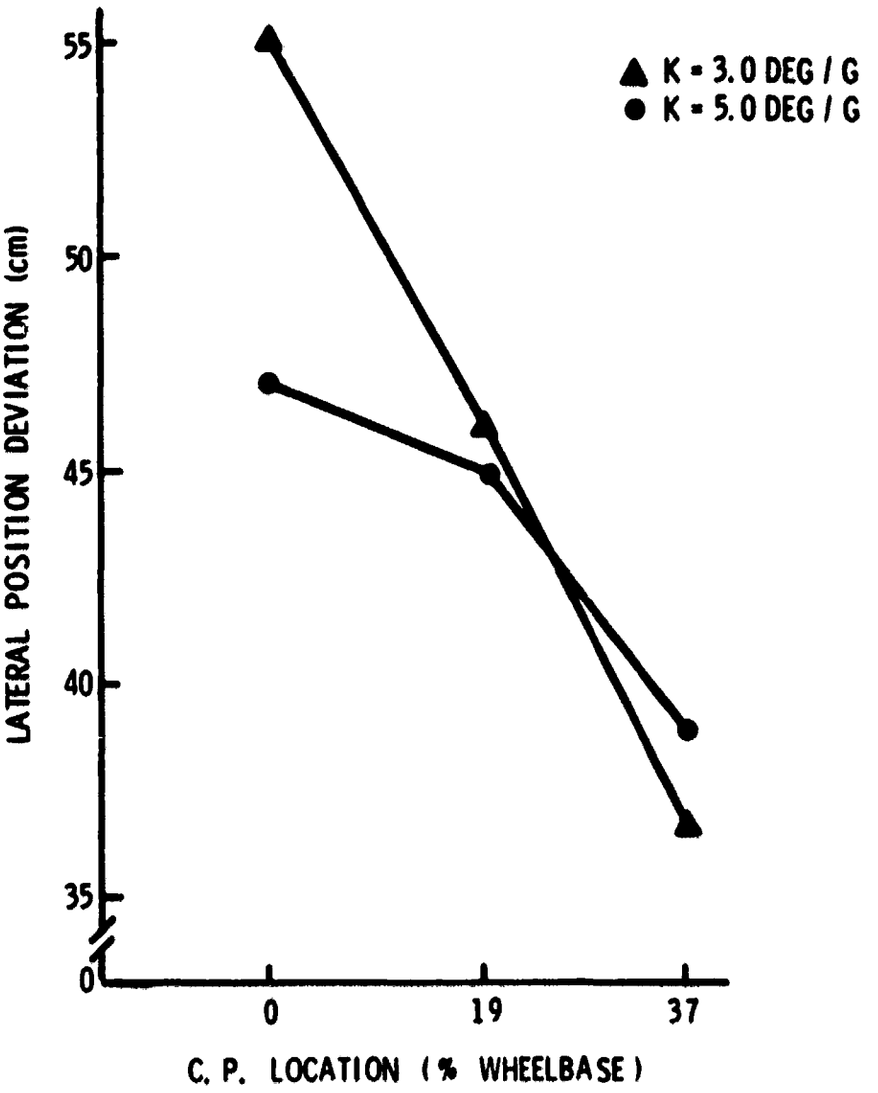

FIG. 5 COMBINED EFFECTS OF UNDERSTEER AND C.P. LOCATION ON LATERAL POSITION DEVIATION (RANDOM WIND GUST)

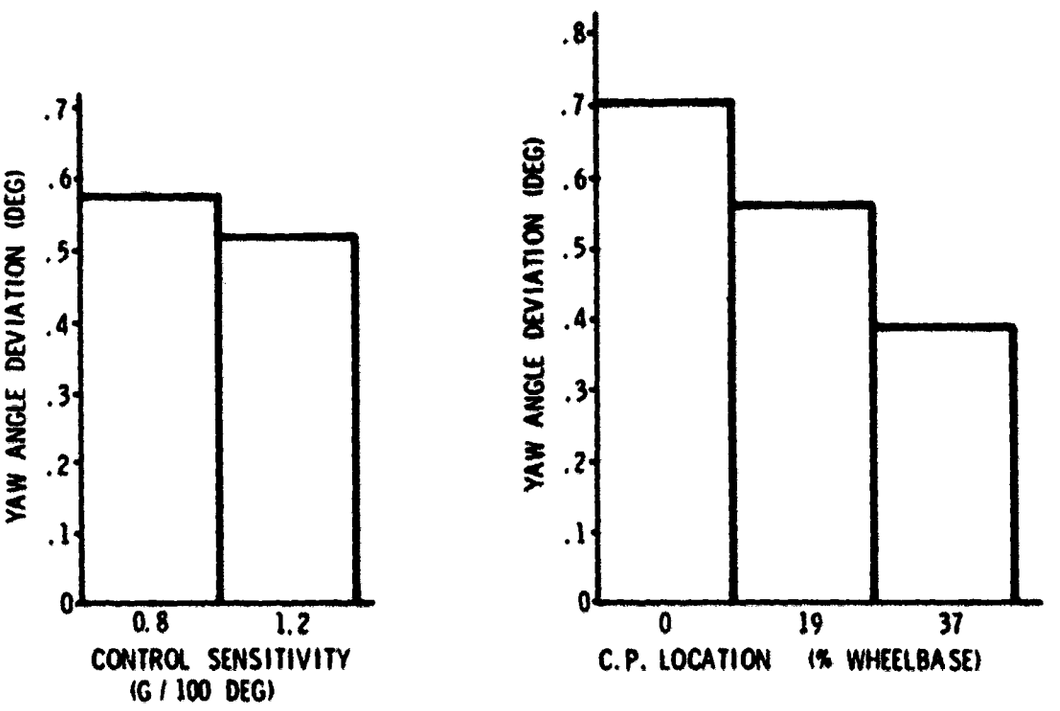

FIG. 6 EFFECTS OF CONTROL SENSITIVITY AND C.P. LOCATION ON YAW ANGLE DEVIATION (RANDOM WIND GUST)

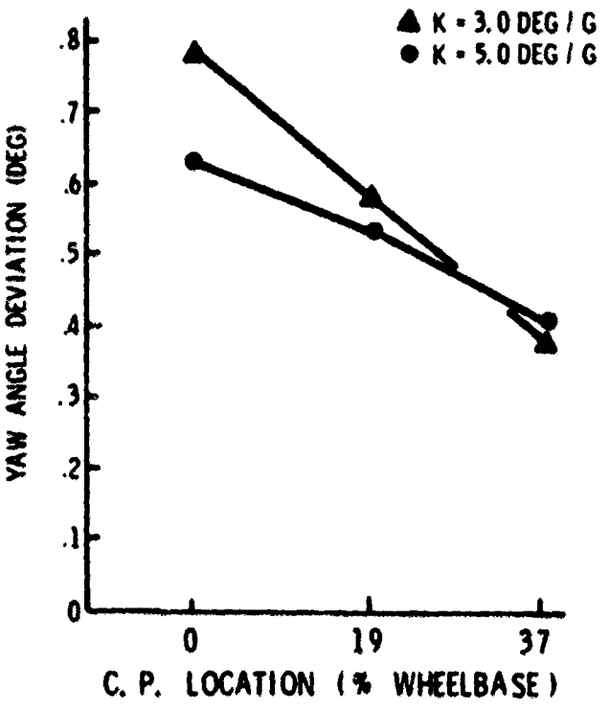

FIG. 7 COMBINED EFFECTS OF UNDERSTEER AND C.P. LOCATION ON YAW ANGLE DEVIATION (RANDOM WIND GUST)

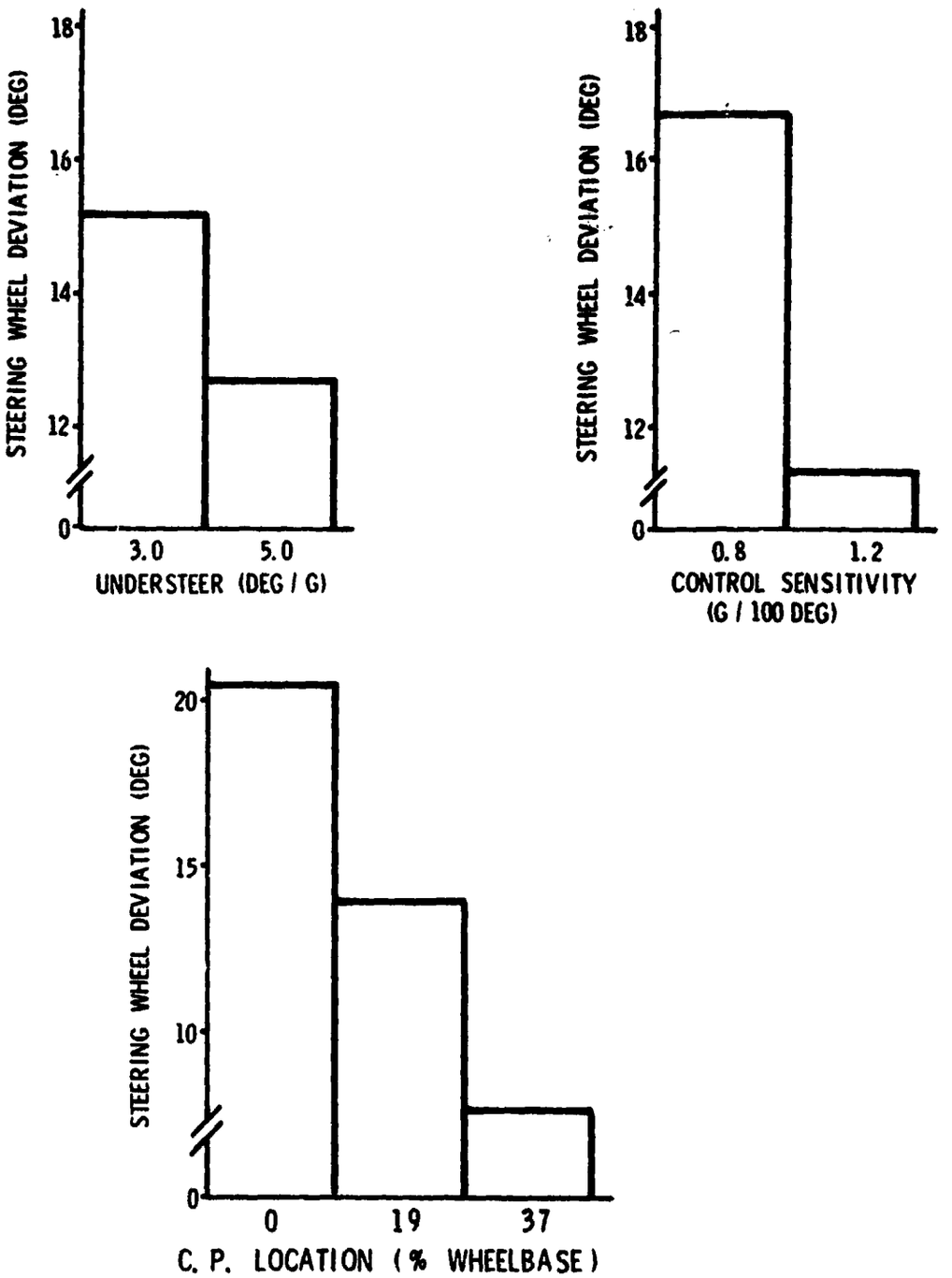

FIG. 8 EFFECTS OF UNDERSTEER, CONTROL SENSITIVITY, AND C.P. LOCATION ON STEERING WHEEL DEVIATION (RANDOM WIND GUST)

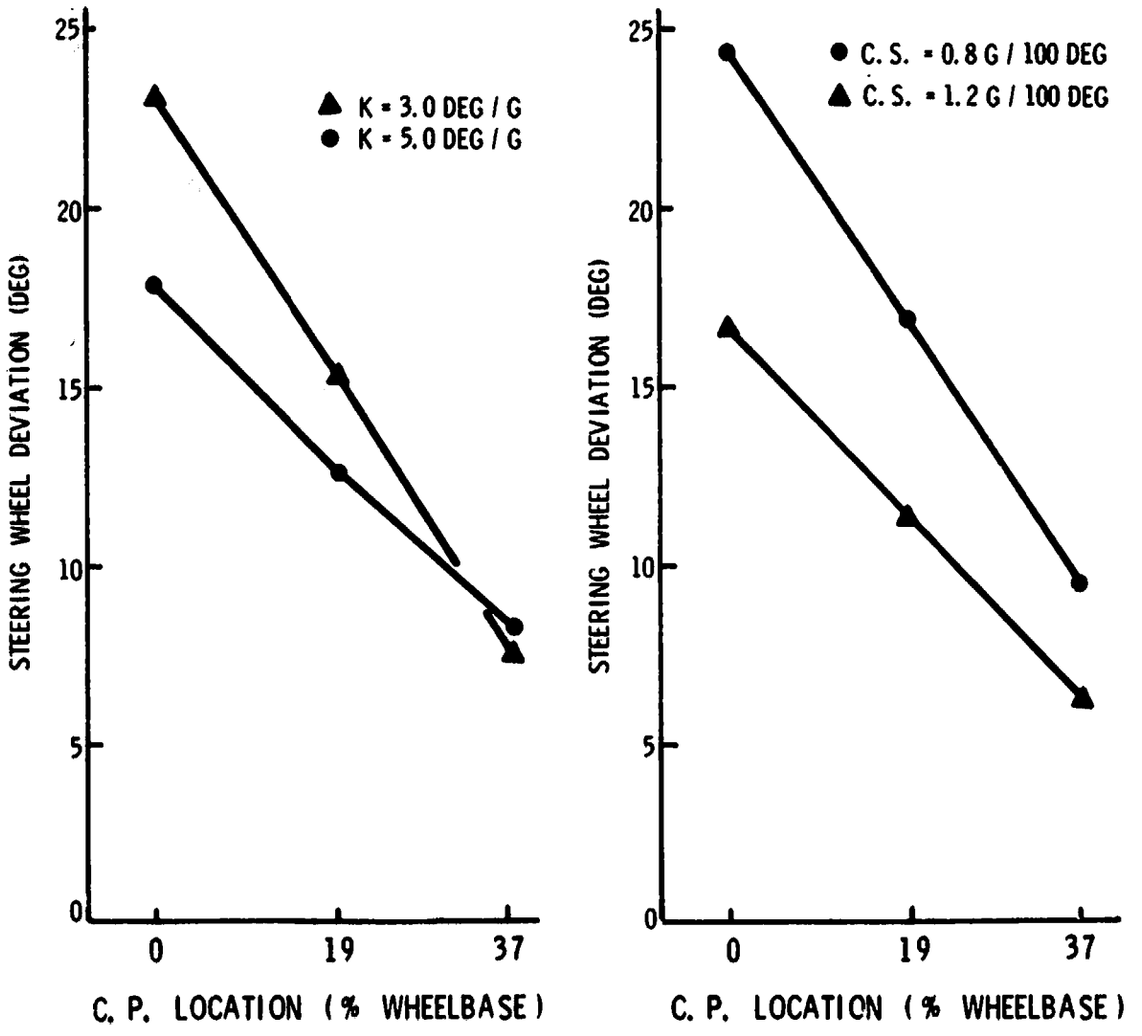

FIG. 9 COMBINED EFFECTS OF UNDERSTEER AND C.P. LOCATION AND OF CONTROL SENSITIVITY AND C.P. LOCATION ON STEERING WHEEL DEVIATION (RANDOM WIND GUST)

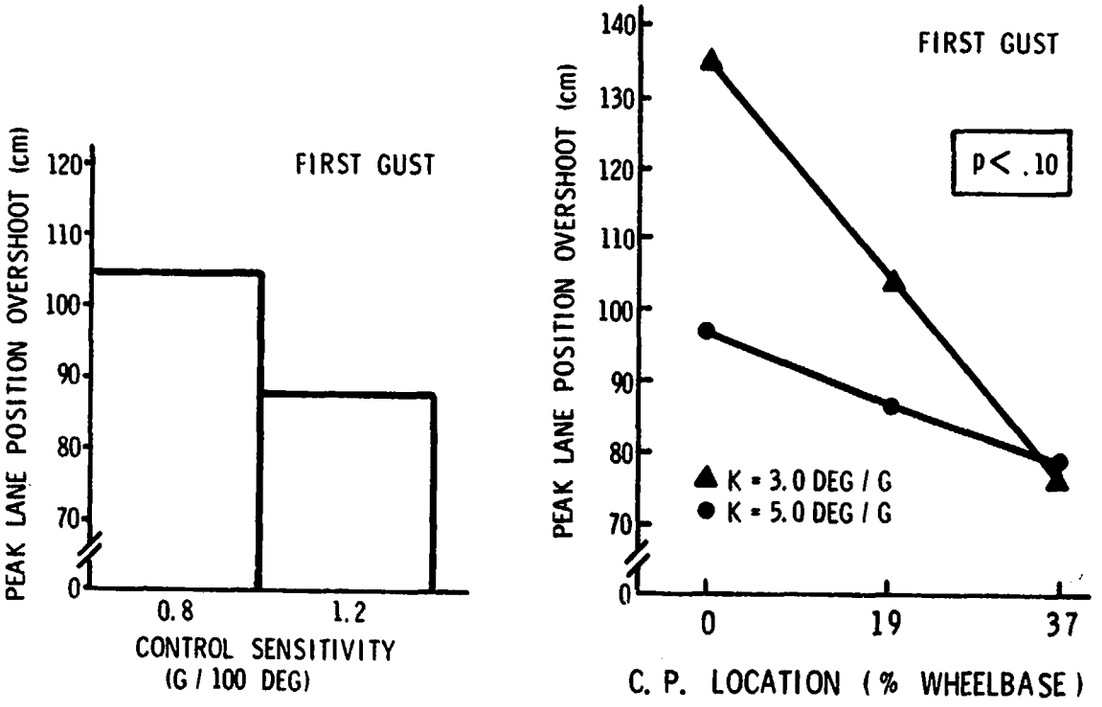

FIG. 10 EFFECTS OF C.P. LOCATION, CONTROL SENSITIVITY, AND UNDERSTEER ON PEAK LANE POSITION OVERSHOOT (STEP WIND GUST)

SESSION F: MANIPULATORS AND REMOTE MANIPULATION

Chairman: A. Freedy

D21

N79-15609

THE DETERMINATION OF THE OPERATING RANGE OF A TWIN-GRIP CONTROL YOKE THROUGH BIOMECHANICAL MEANS

by Klaus-Peter Gärtner
Forschungsinstitut für Anthropotechnik (FAT)
(Research Institute for Human Engineering)
Meckenheim, F.R. Germany

Summary

A twin-grip control yoke was designed as an ergonomic case study that allows dual axis control inputs, both axes being rotational. Inputs are effected by rotating the grips. It will be reported how the handles were designed with respect to their shape and size and how the angular range of the control yoke in both rotational axes was evaluated.

The hand grip design is based on the anthropometric data of the hand. The main parameters for the layout are the breadth of the hand, the grip circumference, and the thumb length. The steering task for which the control yoke is designed requires that the grip shape takes into account task relevant grip characteristics, such as a rest for hand and thumb as well as a thumb operated switch button. One of the design requirements is the full use of the available motion range for steering inputs in the two rotational axes which is limited by the human arm-hand-system.

Using EMG activities, which were measured at the forearm, the permissible pitch and roll angles of the control yoke were evaluated to be $\pm 30^{\circ}$. The limitation stems exclusively from the combined limits of the radial and ulnar ranges of abduction of the human wrist joint. It should be pointed out that in this study the control range was not limited by muscle fatigue which is also measurable with EMG but rather by EMG levels which avoid painful loads on tendon and ligament structures. The experimental series is based on an isotonic rotation in both axes. EMG activities were only measurable under extreme angles of deflection. If the operator has to deflect the control element from its neutral position against a spring resistance a further reduction of the operational range will be expected.

Introduction

In this study, a control yoke which requires two-hand operation was tested to determine its operating ranges. The intention of this investigation was to find out the optimal form of the control yoke and the maximum permissible operating range in both rotating axes. In these experiments controls had no spring resistance. Future studies will involve controls with spring resistance.

296

PAGE INTENTIONALLY BLANK

The control yoke has two rotating axes. Vehicle direction changes to the left or right are accomplished by turning the yoke as with a steering wheel of an automobile, called here roll motion. Vertical vehicle direction changes are accomplished by rotating the yoke handles towards or away from the operator which will be called pitch motion.

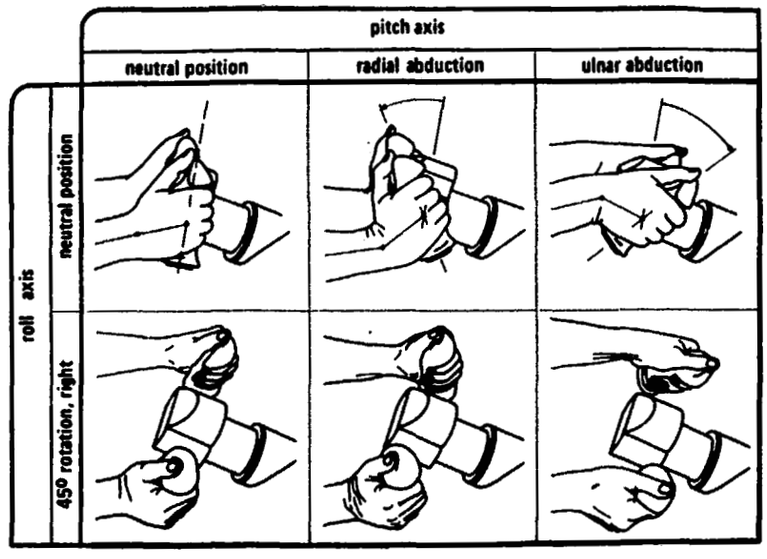

Figure 1 : Influence of roll axis rotation of a twin grip control yoke on radial and ulnar abduction angles of both hands

In the left of the upper row of figure 1 is to be seen the neutral position and in the middle and right pictures of this row the extreme excursion during the pitch movement. These two pictures illustrate the biomechanical position limits of the hand when rotating the yoke towards and away from the operator. The pitch motion of the hand towards the operator is accomplished by radial abduction ; pitch motion away from the operator is accomplished by ulnar abduction. Similar hand positions are shown in the lower row of pictures with a 45° roll angle position coupled with neutral, radial and ulnar pitch abduction.

With 0° pitch angle and roll motion to the right, radial pre-abduction will have occured in the right hand and some ulnar pre-abduction in the left hand, thereby restricting the available amount of further abduction for pitch command purposes. It can be shown that with increases in roll motion to the right pre-abduction will increase until biomechanical limitations make pitch commands impossible or very difficult. Similar pre-abduction occurs with left roll motions.

ORIGINAL PAGE IS
OF POOR QUALITY

ORIGINAL PAGE IS
OF POOR QUALITY

Biomechanical consideration of the arm-hand-system

Figure 2 illustrates the abduction range of the hand. In the left part of the picture there is shown a hand in two positions holding a stick. The hand rotates by an assumed axis of rotation through the wrist joint, as indicated by a small circle. This hand, turned 8 to 12°, corresponds to the normal resting position of the human hand.

If the prolonged center line of the forearm is considered as the reference line a natural pre-abduction of the hand can be noticed. The values given in the literature [e.g. 1] for the ulnar and radial abduction of the hand are based on this resting position. There is obviously no relationship between the angle at which the hand is in the natural resting position and the maximum range of abduction of the 5th to 95th percentile. On the right part of the figure the angle range is shown for the radial abduction with 35° and for the ulnar abduction with 53° measured from the resting position of the hand. This abduction angle of 88° is equivalent to the 90th percentile.

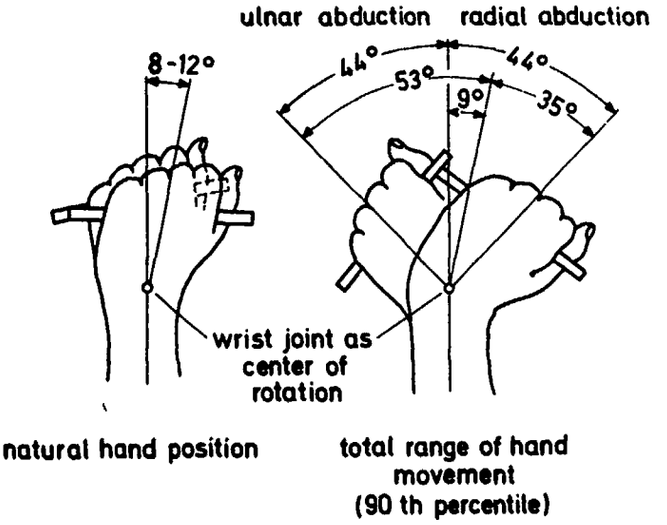

Figure 2 : Abduction range of the hand

If 9° is subtracted , which corresponds to the natural pre-abduction from the range of the ulnar abduction, a value of 44° both for the ulnar and for the radial angular range will be obtained. This consideration is important for practical applications in so far as there should be the same angular range in radial as in ulnar direction for the pitch movement, i.e. the up and down maneuver of the vehicle. If the total abduction ability of the hand is used for turning a control yoke, two

rotational axes can be selected. These two rotational axes of the control yoke cross in the steering column. In figure 3 the case is shown where the rotational axis of the wrist joint is equal to the axis of the control element. Consequently, there is hardly any motion of the forearm. The total range of abduction is used as pitch angle range, that is for radial abduction of 35° and for ulnar abduction of 53°, measured from the resting position. There is a light disadvantage of forearm movement when the rotational axis of the wrist joint does not correspond with the rotational axis of the hand grip for small and large hands. This effect does not occur if the rotational

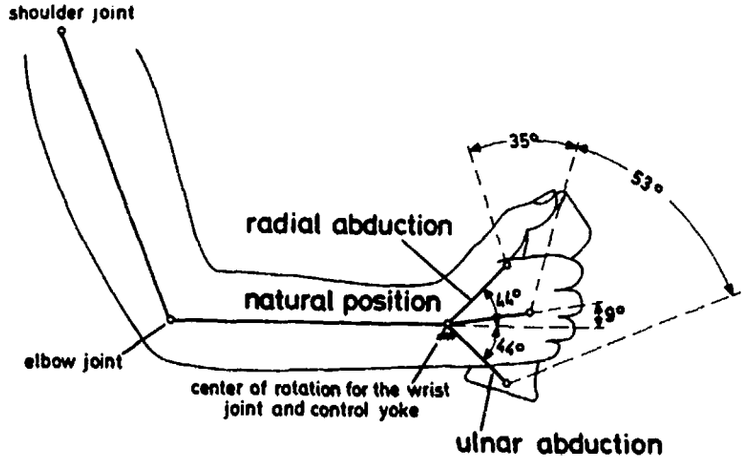

a) rotational axis through the wrist joint

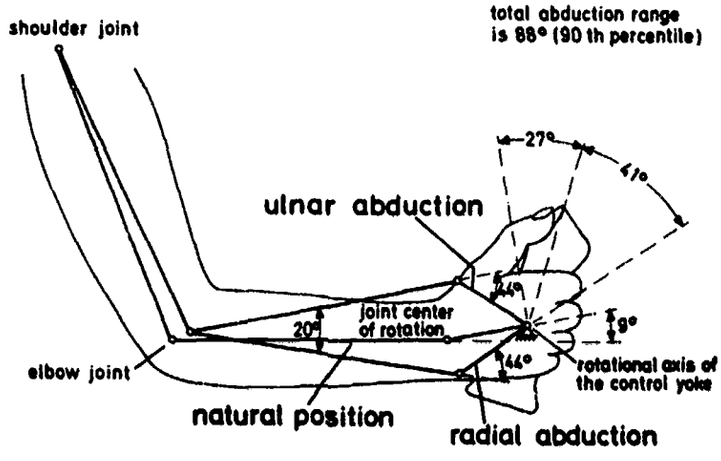

b) rotational axis through the volar hand

Figure 3 : The range of forearm motion for different rotational axes of the control yoke

ORIGINAL PAGE IS OF POOR QUALITY

axis of the hand grip corresponds with the center of the hand volar or palm as shown in the picture below. A pronounced up and down movement of the forearm which results during ulnar and radial abduction is illustrated in figure 3. Though, radial and ulnar abduction come to their limits at 88° for the maximal abduction of the 90th percentile, the maneuvering pitch angle range only reaches 68°, e.g. 27° for radial and 41° for ulnar abductions from the resting position.

Anthropometrical Design of the control grip

Figure 4 shows the operator sitting in front of the control console. The angle of inclination with respect to the body will be selected in a way so that the arm-hand-system of a 50th percentile operator measured from the shoulder reference point is in a position to turn the control yoke with the same angular values in ulnar and radial direction. A control yoke is shown, the rotational axis of which goes through the volar hand.

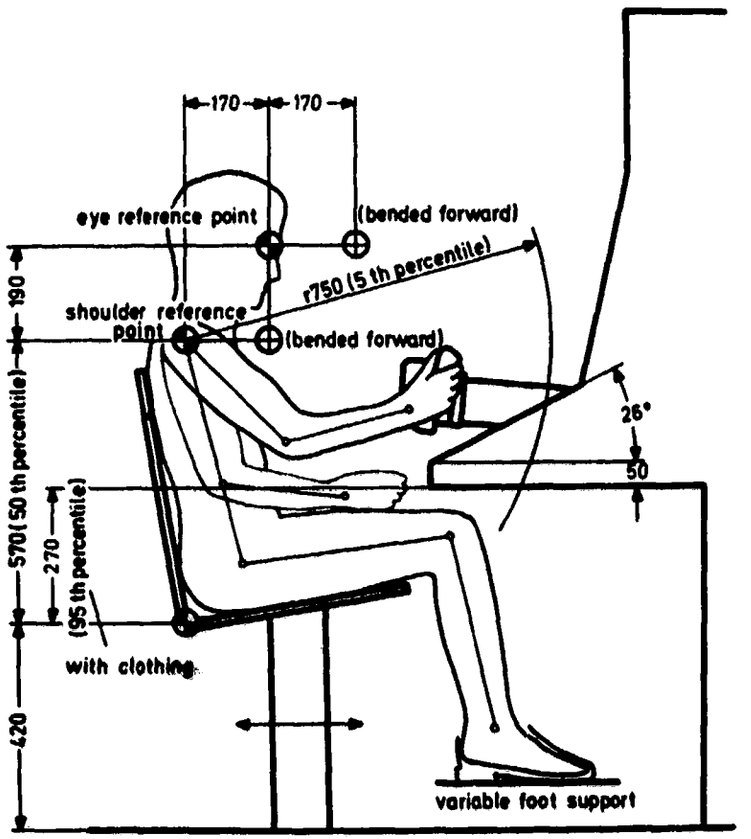

Figure 4 : Suggested anthropometric parameters for seated operator console

The control task for which the control yoke was designed requires a specially shaped grip which takes into account task relevant grip characteristics, such as a hand and a thumb rest and a switch button that is thumb operated (figure 5). The design of the grip was based on the 95th percentile hand. The dimension A of the palm was based on hand width. The hand fits between the hand rest and the top section of the grip. The fingers span the grip slantwise to the longitudinal axis of the grip and not in parallel fashion as they would with a cone.

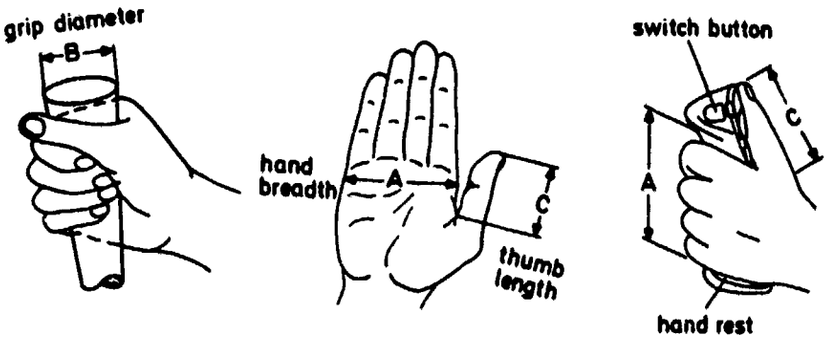

Figure 5 : Anthropometric parameters for designing a handgrip

So long as the switch button is not used, the operator can smoothly move his hands with the control yoke and follows its motions. Under these working conditions the hand of the 95th percentile man is resting on the hand support and the thumb is on its thumb rest. Smaller hands such as the 50th or 5th percentile hands can use either the hand rest or the thumb rest as a basic working position during the control task.

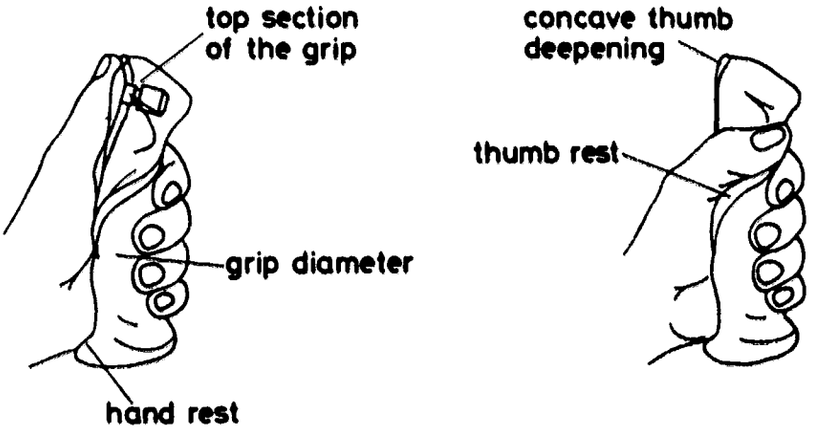

Figure 6 : Anthropometric parameters for designing a handgrip

The basic dimensions of the grip are the dimensions of an ideal conical bar which was first used by Henning. Henning suggests an increase in radius by 5 mm for each 80 mm in length. The grip is finger parallel and the forearm axis is vertical to the cone axis.The circumference is about 150 mm for a 95th percentile hand. As can be seen from the left picture of figure 6 the finger tips touch lightly the opposite part of the hand and the thumb rests on parts of the pointing finger. If the cone is closed the fingers are inclined to the longitudinal axis of the cone. A grip was designed using finger indentation and an appropriate deviation of the cone shape as may be seen in figure 5.

With this grip the finger tips of the 95th percentile hand are at small but constant distance from the opposite part of the hand. For the smaller hands like 50th or 5th percentile hands this distance becomes larger but still guaranties a good form closure. With this design a larger thumb rest was used which results in a separation of the possible touch between the thumb and the fingers. The location of a switch button in the grip head was based on the thumb length of the 50th percentile hand. Thumbs which are longer and shorter than 50th percentile are still in position to operate the switch button by use of lower or upper parts of the thumb respectively.A concave depression in the top section of the grip allows sufficient motion for larger thumbs when pressing the switch.

Biomechanical determination of the operating range of the twin-grip control yoke

For the layout of a control yoke both anthropometric and biomechanic qualities of the human hand-arm system must be considered. A method is proposed in this paper which permits a determination of a biomechanical range on the basis of surface electromyography activities which are involved in movement and force exertion. At the limits of movement, rather high EMG activity occurs together with such consequences as muscle, tendon, or ligament strain and/or pain.

For EMG measurements, subjects were instructed to grip the yoke lightly with both hands so that no forearm muscles were contracted. For each selected roll angle position of the yoke, the control was then slowly moved through both pitch directions. Raw EMG signals were processed with a double wave rectifier and a special averaging filter [2, 3, 4] .

EMG activity for the right hand in a number of different roll angle positions are illustrated in figure 7 as a function of pitch angles for roll angles in the right direction. The curves illustrated are only for EMG values recorded during increasing pitch angles as these represent the worst case for control evaluation.

The upper EMG value of "1" unit was arbitrarily given to the EMG level obtained when wrist joint pain was experienced after repeatedly holding an angle position for a few seconds. The maximum value of the curves (approx. .75 units) is obtained at the maximum pitch angle which was measured. The maximum pitch angle

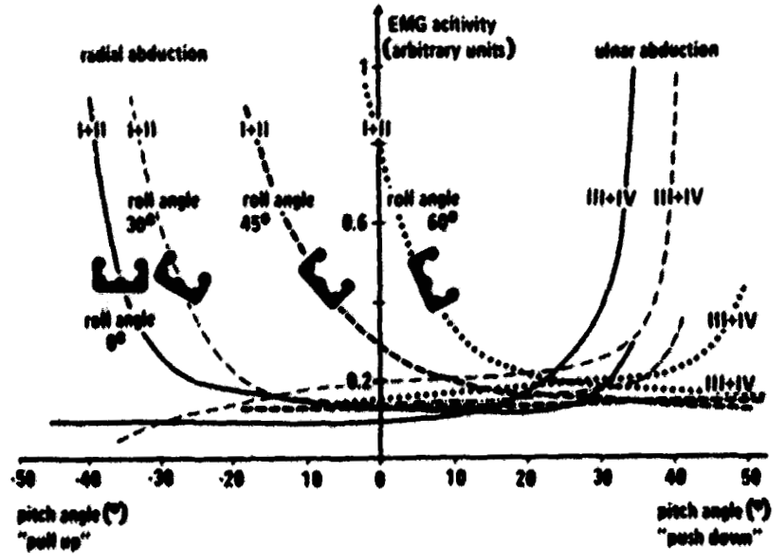

Figure 7 : EMG activities of radial and ulnar abductors of a right hand with 90th percentile wrist movement range as a function of pitch angle for various roll angles. Roll movement is in right

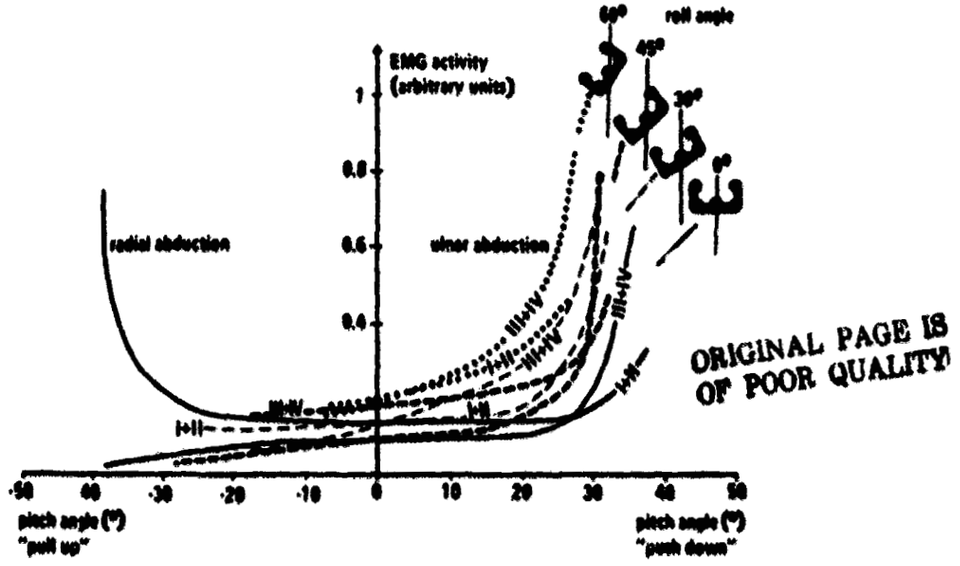

ORIGINAL PAGE IS
OF POOR QUALITY

Figure 8 : EMG activities of radial and ulnar abductors of a right hand with 90th percentile wrist movement range as a function of pitch angle for various roll angles. Roll movement is in left

measured was selected after experimentally determining the maximum pitch angle at which no wrist pain build-up occured during fairly long measuring sessions. For any given pitch angle there is a tendency for pre-abduction to be larger with larger constant roll angles. It can be seen that at 0° roll angle the full range of possible wirst movement of the subject can be used for pitch commands in both directions because there is no pre-abduction. At 60° roll angle to the right, radial pre-abduction is so large that no pitch angle movement in this "pull up" direction is possible. In the right side of the figure the EMG curves for ulnar abduction i.e. in the "push down" direction is illustrated. The 45° and 60° roll angle permit relatively large "pull up" commands although the curves do not rise as high as those for radial abduction on the left side of the figure. The reason for this is that ulnar abduction of the left hand, which is not illustrated, reaches a limit at these pitch angles before the right hand, thereby preventing further ulnar abduction of the right hand. Of course, release of the control by the left hand would have permitted further movement.

EMG values for ulnar and radial abduction of the right hand is shown in figure 8 for left roll at various roll angles. As can be seen on the left side of the figure for left roll, right hand "pull-up" pitch commands or radial abduction movement is so severely limited by radial pre-abduction of the left hand in all roll angle positions except 0° that further movements are not possible. The range of ulnar abduction or "push-down" commands illustrated on the right side of the figure is slightly reduced by ulnar pre-abduction thereby allowing considerable movement before the ulnar abduction limits are reached.

Discussion of the EMG-measurements

In designing a range for this control device the following points are the most important to consider. 1. It should permit the largest possible pitch angle in both directions for each of the largest possible roll angles for subjects with 5th percentile wrist movement ranges. 2. Only lower levels of EMG activity should occur most of the time during control operations. Moderate EMG activity levels should occur very briefly and no high EMG activity at all.

As can be noticed in the figure 7 and 8 these requirements can be satisfied for the subject tested with roll and pitch angle ranges of approx. $\pm 30^{\circ}$ each (at which no more than 0,5 units of EMG activity are reached). It should be pointed out that in this study the control range was not determined by muscle fatigue limits which are also measurable with EMG but rather by EMG levels which avoid painful loads on tendon and ligament structures. The EMG measuring method presented proved to be a valuable objective aid for determining an advantageous control range.

References

[1] Damon, A., H.W. Stoudt, R.A. McFarland. 1966. The Human Body in Equipment Design. Havard University Press, Cambridge.

[2] Kreifeldt, J.G. 1971. Signal versus noise characteristics of filtered EMG used as a control source. IEEE Trans. Biomed. Eng. 18: 16 - 22.

[3] Rau, G. 1973. Ein verbessertes Meßsystem zur quantitativen Oberflächenmyographie (An improved measuring system for quantification of surface electromyography). Anthropotechnische Mitteilung No. 2/73. Forschungsinstitut für Anthropotechnik, Buschstraße, 5309 Meckenheim, Germany.

[4] Rau, G. 1974. Improved EMG quantification through suppression of skin impedance influences. In : Richard C. Nelson and Chauncey A. Morehouse (eds.) Biomechanics IV, pp. 322 - 327. University Park Press, Baltimore.

D22

N79-15610

EVENT-DRIVEN DISPLAYS FOR MANIPULATOR CONTROL *)

A. K. Bejczy
Member of Technical Staff

G. Paine
Member of Technical Staff

Jet Propulsion Laboratory
California Institute of Technology
Pasadena, California 91103

SUMMARY

This paper considers the problem of constructing event-related information displays from multidimensional data generated by proximity, force-torque and tactile sensors integrated with the terminal device of a remotely controlled manipulator. Event-driven displays are constructed by using appropriate algorithms acting on sensory data in real time. The purpose of event-driven information displays is to lessen the operator's workload and to improve control performance. The paper describes and discusses several event-driven display examples that have been implemented in the JPL teleoperator project, including a brief outline of the data handling system which drives the graphics display in real time. One application shows the integration of a set of four proximity sensors with a JSC four-claw end effector for the shuttle manipulator training facility of JSC. The paper concludes with a discussion of future plans to integrate event-driven displays with visual (TV) information.

I. INTRODUCTION

The objective of this paper is to show and discuss display techniques aimed at reducing the dimensionality of proximity, force-torque and tactile sensor data, and conveying the sensory information to the operator of a remote manipulator in terms of significant events related to the control task. An event-driven display is a display which shows whether or not some desired state of the teleoperator effectors/sensors has been achieved. It may or may not show the details of the state itself, rather it displays the occurrence of the event. Hence, event-driven displays compress and explicitly indicate sensory data in terms of control goals or subgoals which require specific control decisions and actions.

The general problem of displaying information generated by proximity, force-torque, tactile and slippage sensors integrated with the terminal device of a mechanical arm has been treated in a previous paper (see Reference 1).

*) This work represents one phase of research carried out at the Jet Propulsion Laboratory, California Institute of Technology, under Contract No. NAS7-100, sponsored by the National Aeronautics and Space Administration.

The information generated by these sensors is basically non-visual: short (few centimeters) distances in given direction between terminal device and object; amount of force and/or torque exerted by the terminal device on objects along three orthogonal axes referenced to the terminal device; distribution and amount of contact area pressure between terminal device and object; or slip of an object in some direction on the inner surface of mechanical "fingers". Hence, the general problem and objective of displaying this type of information to the operator of a remote manipulator are to make non-visible events visible or, alternatively, to make non-visible events easily perceivable by using some appropriate means (e.g., audio tones).

The information generated by proximity, force-torque, tactile and slippage sensors has two specific features: it is multidimensional, and it requires quick (sometimes split-second) decision or control response. It is noted that, in general, the required decision or control response is also multidimensional. The use of multidimensional data with quick response requirements in a real time manual or computer control environment is a demanding perceptual and cognitive workload for the operator of a remote manipulator. It is a major source of errors, and can result in a general degradation of control performance. The purpose of event-driven sensory information displays is to lessen the operator's workload and to improve overall control performance of remote manipulators.

The concept of sensory information "events" is discussed in Section II. The general features of "event-driven displays" are briefly discussed in Section III. Section IV describes several event-driven display examples that have been implemented in the JPL teleoperator project. These include two uses of four proximity sensors and a single use of a six-dimensional force-torque sensor integrated with manipulator end effectors employing both audio and graphic display techniques. One application shows a set of four proximity sensors integrated with a JSC four-claw end effector to be used at the JSC Manipulator Development Facility. A simple touch sensor example is also described. The concluding Section V summarizes the results and outlines future plans to integrate event-driven displays with visual (TV) information. A brief description of the data handling system which drives the graphics displays in real time is presented in the Appendix.

II. SENSORY INFORMATION "EVENTS"

Proximity, force-torque and touch sensor data are inherently multidimensional. A six-dimensional force-torque sensor outputs the time trajectories of three orthogonal force and three orthogonal torque components normally referenced to a hand coordinate frame. The hand coordinate frame itself is a variable (i.e., has time trajectories) relative to a fixed "base" reference frame. A multipoint proportional touch sensor measures the area distribution and amount of contact pressure over a fixed surface. A single proximity sensor measures short (few centimeters) distances in a given direction relative to a hand coordinate frame. Several proximity sensors in a given emplacement geometry on the hand can measure several or all six position and orientation variables of the hand relative to objects.

A sensor-referenced or sensor-guided manipulator control task contains a goal or a set of subgoals. The control goal or subgoals are expressed as a combination of various sensory data. The simultaneous occurrence of time trajectories of various sensory data at a single point or within a given subvolume of a multidimensional data space can be called a sensory information "event". Hence, sensory information "event" is the projection or mapping of the control goal or subgoals into a multidimensional data space.

Figure 1 gives simple illustrations for the concept of sensory information "event". Equal length of two proximity sensor beams can be an "event" in the sense that it may signify, e.g., the roll, yaw or pitch alignment of a mechanical hand relative to an object. Equal magnitude of two orthogonal force components can be an "event" in the sense that it may signify, e.g., the push or pull of an object by a mechanical hand in a given direction. Or, for instance, half contact coverage of a touch-sensitive area on a mechanical finger can be an "event" in the sense that it may signify, e.g., that there is sufficient contact between hand and object for successful grasp.

The operator's attention in both manual and computer control is normally focused at the control goals or subgoals, that is, at the sensory information "events". Typically, when such "events" occur, some control action must be taken. It is to the operator's advantage to have these sensory "events" displayed in easily perceivable and unmistakably unique forms. In the absence of such "event" displays, the operator must determine the occurrence of the "event" by following and evaluating a multidimensional set of data in real time. This is not only a demanding task and heavy workload for the operator, but also a common source of errors.

III. DISPLAY OF "EVENTS"

Event-driven displays can be implemented by developing and/or employing appropriate real-time algorithms which (a) coordinate and evaluate sensor data in terms of predefined "events" and, (b) drive some appropriate information display in real time. Manipulator control tasks can be subdivided into a multitude of sensory "events", and each event may have a variety of characteristic parameters. Thus, the development of fairly general purpose event-driven displays requires that the logic/parametric structure of the algorithms be flexible in the sense that changing control goals or subgoals can be accommodated by simple call-changes in the algorithms in a given control/operation environment.

The actual event display can be implemented by alternative means, the selection of which depends on the application environment. For event displays, both audio and visual display techniques are suitable. An important consideration for selecting or designing event displays is the "warning effect" the display can or shall impose on the operator. By definition, the occurrence of a sensory event should call the operator's attention to some appropriate control decision or control action, without disturbing his normal visual attention directed toward the overall control task. Note that the control can require split-second decisions. Another important consideration

is related to the selection of the content of the display format. How much and what kind of detailed information the operator should be exposed to in addition to the "event information" within the same general frame of information? Too much information can be disturbing. Too little information can defy the purpose. The display of uncorrelated data, or the display of correlated data in uncorrelated form, may impose heavy cognitive load on the operator.

Properly designed event-driven displays are expected to have a number of benefits: (a) simplify on-line control decisions; (b) reduce errors caused by human factors; (c) reduce perceptual/cognitive workload on human operator in a real-time control environment; (d) improve overall control performance in control situations which many times require split-second type control decisions.

IV. EXAMPLES

A. Event-Driven Proximity Displays

Event-driven displays have been constructed for proximity sensors on two arms in the JPL teleoperator project, and also for a proximity sensor system developed at JPL and integrated with the four-claw end effector of JSC to be used at their shuttle manipulator training facility.

1. JPL Teleoperator Arms

Both the JPL/CURV and JPL/Ames arms are equipped with four proximity sensors, and the event-driven display developed recently is applicable to both sensor systems. Although the sensor hardware is quite different on the two arms, the sensor display drive software is common except for the routines that get the data. Similarly, the event logic is common. The details of the computer hardware and software are described in the Appendix.

The general format of graphics display of four proximity sensors data is shown in Figure 2. The display shows a view of the "bone" of a parallel jaw hand and four beams emanating from the hand, two from each jaw. The beam lengths are proportional to the sensitive length of the sensor beams. Each beam length is bound to 10 cm (4 in.).

Figure 3 summarizes the proximity events together with the event logic and event parameters that have been implemented. In the present implementation the parameter D is fixed at 5 cm. D is always defined parallel to and halfway in between the two beams which measure roll and yaw alignments, respectively, and relative to the line connecting the two fingertips. The tolerance, T, can be set by switch inputs on the computer's front panel. Values from 0.5 to 7.5 cm are allowed. Any combination of the four event logic equations may be selected to control the event success blinker. The success may be defined as X alignment with a tolerance, say, of 1 cm (corresponding to about 5 degrees when the hand is fully open). Or, the success may

be defined as Y range of 5 cm together with X alignment to within 0.5 cm tolerance (corresponding to about 2.5 degrees when the hand is fully open). This latter "success case" would be useful in moving the hand over a table to a wall while holding an object vertical. With this event logic, the hand roll angle would be small as the range measurement is made on both sensors and the object would be held with the hand 5 cm above the table. The final approach to the wall would be reached with the hand perpendicular to the wall.

The event indicator blinker has initially been placed in the top left hand corner of the monitor screen. Though all four sensor beams are shown on the monitor, the operator does not have to evaluate the four beams quantitatively in terms of a predefined event. This is done for him by the display drive logic automatically and in real time. He can take a more qualitative look at the four beams to determine, e.g., why the success blinker is "off"; that is, what to do in order to get the success blinker "on".

Figure 4 shows two uses of the event-driven proximity display. The first pair of photographs (Figure 4A) shows the hand above a table and skewed to a block. The task is to achieve alignment with the table and the block. The display shows the operator how to bring the hand perpendicular to the block while maintaining the hand level at 5 cm above the table. The second pair of photographs (Figure 4B) shows that this has occurred and the event blinker has come on. The third pair of photographs (Figure 4C) shows a different alignment problem. Here, it is desired to bring the hand in level over the plate on the table. There are no forward references. Following the required corrections as indicated by the display, the desired level state is achieved, and the event blinker comes on as shown in the fourth pair of photographs (Figure 4D).

While the two uses of the event-driven display shown in Figure 4 are simple, they do demonstrate the usefulness of the concept. As more complex tasks are performed and analyzed, a detailed examination of the benefits can be made. Future improvements in implementation are also planned to enable a broader variety of events to be defined. Ranges, alignment angles and tolerances could be individually defined rather than being commonly constrained as at present.

2. JSC Four-Claw End Effector

A proximity sensor has been developed for and integrated with a four-claw end effector of JSC. The purpose of this sensor system is to aid the operator to find the proper final depth positioning and pitch and yaw alignments of the four-claw end effector on a 16-m long manipulator relative to the grapple fixture of a large payload. The overall control is visually guided.

The sensor system, together with the grasp envelope and measurement definitions are shown in Figure 5. The use of the sensor system is presently restricted to the verification of a "successful grasp state" before grasp action is initiated. The "successful grasp state" is defined by the dimensions of the grasp envelope (see Figure 5) and by the dynamics of grasp.

When a "successful grasp state" has been reached, the data processing electronics automatically turns on a simple "success display" (a buzzer or a green light, or both), indicating to the operator that he is ready to grasp.

The data processing required to drive the "success display" has two modes: analog and digital. The analog drive logic implementation is quite simple as indicated in Figure 6. In fact, with this simple analog implementation the full capabilities of the sensor system cannot be utilized to account for all physically possible combinations of depth, pitch and yaw error states which, due to the dimensions of the end effector's grasp envelope, still would allow successful grasp. To achieve a full utilization of the sensor system capabilities versus all allowable depth, pitch and yaw error combinations, "success algorithms" have been developed and implemented using an Intel 80/20-4 single-board microcomputer together with an Intel single-board A/D converter.

For the purpose of experimentation, several "success algorithms" have been implemented in the digital computer to drive the displays. The algorithms are simple, and account for all (or for almost all) allowable error states combinations for successful grasp. Algorithms have also been implemented which utilize the outputs of any three out of the four sensors to indicate the "success states". This is useful if one sensor eventually fails, or if one sensor eventually misses the top (reference) surface of the grapple fixture due to allowable lateral alignment errors. (Note that the four-sensor configuration is redundant to define and compute depth, pitch and yaw errors. A triangular configuration of three sensors would be sufficient for that purpose.)

For the sake of brevity, only one "success algorithm" is shown in this paper, summarized in Figure 7. It is called "conic algorithm" since it condenses the individually allowable pitch and yaw errors into a simple allowable cone angle error condition. (See Condition 2 in Figure 7.) Three kinds of "success definitions" have been developed, each with three sets of "success parameters". All nine variations have been implemented for "all four" and for "three-out-of-four" sensors. All together 18 algorithms are stored in EPROM in the microcomputer. Any one of the 18 algorithms are easily callable by dialing the appropriate number between 1 and 18 on a BCD switch integrated with the microcomputer.

Very successful operational ground tests have been conducted with the sensor and simple display system at JSC using the 16-m long arm of the JSC Manipulator Development Facility in realistic large payload handling experiments. Fig. 8 shows a floor set-up scene (direct visual contact with target) for capturing a moving target. All together 112 test runs have been performed by 4 operators. The final result is that, when the "success display" (tone or green light) was on, the operators got a capture every time. There were no operator mistakes under sensor-indicated grasping conditions, and the sensors never indicated wrong conditions for grasping. Three of the four operators favored the buzzer for "success display". The utility of the display increased with task difficulty. The display was required to aid the operator to successfully complete the most difficult tasks without error.

The simple success display (tone or green light) does not show the details of the three-dimensional (depth, pitch and yaw) error states. Advanced graphics display concepts have been developed and implemented recently using the JPL teleoperator breadboard system to experiment with various formats. The advanced formats have been designed to convey to the operator not only the "success" information but also the details of the three (depth, pitch and yaw) errors so that the operator will know from the sensors "what to do" in order to get to the "success" state or to fine-control the grasp. Fig. 9 shows an advanced "success display" concept implemented in color graphics. Success is indicated here by all error bars turning green. The unsuccessful error combinations are indicated by all error bars turning red. The length of the error bars is proportional to the respective errors under both "green" or "red" conditions.

B. Event-Driven Force-Torque Display

Fig. 10 shows a six-dimensional force-torque sensor integrated with the JPL/CURV arm. The sensor mechanism has been built by Vicarm Inc. The sensor electronics and data handling have been developed at JPL. More details of this sensor system can be found in Ref. 2. Fig. 10 also shows a graphics display format: each force and torque component is displayed both numerically and graphically. The length of the bars is proportional to the value of the respective force or torque components. The bars originate from the center vertical line on the screen. To the left from this center line the force-torque field is negative, to the right it is positive. The force-torque components are referenced to a hand-based coordinate frame. The force-torque distribution seen on the graphics display of Fig. 10 actually shows the forces and torques felt at the hand base while the hand is pushing the object as indicated on the same figure. As seen, a simple push scene can generate a rather complex force-torque relation felt at the hand base.

The application of event-driven displays to force-torque sensor data will significantly enhance the use of that data type under manual or computer aided control. The events marked can show complex relationships between forces and torques alone or in combination. Further, when the desired force-torque events are not existing, the display format can be changed to show the operator what has to be done to reach the desired state. A simple example can best illustrate the concept.

Consider the task of sliding a block in a groove across a table by pushing it. (See Fig. 11) The applied forces must be in the direction of the groove if the block is to be moved efficiently and safely. Fig. 11 also shows an appropriate "event-driven" display. When the forces are applied correctly, the operator will know it by the event indicator. If not, the operator will see the force errors and be able to apply the needed corrections. Practical application and demonstration are needed before the benefits of this display concept can be fully documented.

An interesting use of even-driven displays is to signal the operator to switch displays. Say, for example, it is necessary to move a manipulator to an object and then move the manipulator into contact with the object without knowing the exact position of the object beforehand, or having specially positioned TV's showing all the necessary views.

With event-driven displays, the task could be performed as follows: using a proximity event display set in a position sensing mode, the operator moves the manipulator rapidly towards the object. When signalled that the manipulator is near the object, the operator slows its motion and switches the display to a force/torque even mode. When contact has been achieved, the operator is again signalled before the forces reach an unacceptable level. Thus, event-driven displays used in combination hold great promise for even greater benefits in that tasks can be performed more rapidly, more reliably and with lower expenditure of resources.

C. Event-Driven Touch Display

The touch sensor unit being used here has two 4 by 8 matrices of points that can sense applied pressures. These matrices, or perhaps some with higher point density, can be mounted on the inside of mechanical fingers (jaws) and used to sense contact areas or the location of points of contact between finger and object. Similar units could be mounted on other surfaces to sense other contact forces or patterns of contact areas. At each point of the sensor matrix the pressures applied locally are sensed by measuring the conductivity of a pressure sensitive plastic. The measurement concept and the actual sensing elements are shown in Fig. 12.

Fig. 12 also shows the basic touch sensor displays. The numeric representation of the sensor output gives a more quantitative impression of the applied forces distribution and is particularly useful for diagnostic work. The color or B/W shades displays are more graphic and are easier to understand at a glance although less information is presented.

A particular event-driven touch sensor display is planned to be implemented to further enhance the control context of data presented to the operator. The display concept (shown in Fig. 13) is aimed to give a quantitative indication to the operator when the contact area increases by predefined amount. While the pressures applied will still be shown as dark or light shades of a color, the color itself will be changed to reflect the total applied pressure over a given area. The matrix displayed may be red, if less than half the sensitive points have made contact; orange, if between 1/2 and 3/4 have; or green, if more than 3/4 have. Thus, a green condition will signify a safe grasp.

V. CONCLUSIONS

1) Performance tests conducted at JSC with a three-dimensional proximity sensor system and "go-no go" display have shown the basic utility of a simple event-driven display which conveys critical control information to the operator based on real-time algorithmic evaluation of multidimensional data.

2) In general, event-driven displays enhance the control context of sensory information since events can be defined with respect to critical control decisions or control actions.

3) Preliminary experiments strongly indicate the need of integrating visual and non-visual sensory information within a single perception format. This may require the development of TV monitors with sensory information overlayed to or cut into the camera information.

4) Extensive experimentation is needed with a multitude of event-driven display formats in order to develop a reliable rating of the different formats. The experimentation will by necessity encounter questions in human factors engineering. Presently it is not clear what kind of objective measures would be suitable to meet the challenges in the performance evaluation of event-related human factors.

ACKNOWLEDGEMENT

The contributions of Mr. E Shalom and Mr. K. W. Rudd to the software development is gratefully acknowledged.

REFERENCES

1. Bejczy, A. K., and Paine, G., "Displays for Supervisory Control of Manipulators," Proceedings of the 13th Annual Conference on Manual Control, Massachusetts Institute of Technology, Cambridge, MA., June 15 - 17, 1977.

2. Bejczy, A. K., "Issues in Advanced Automation of Manipulator Control," Proceedings of the 1976 Joint Automatic Control Conference, Purdue University, West Lafayette, Indiana, July 27 - 30, 1976.

APPENDIX

1. Computer System

A single computer system is used for software development and display driving. Its principal elements are shown in Fig. 14. The signals to be displayed can come from any of five sources: JPL/AMES arm proximity sensors, JPL/CURV arm proximity and force-torque sensors, touch sensors, or the JSC four-claw proximity sensors. (These last signals come through an Intel 80/20 processor.) The display computer processes these signals into the desired display format so that they may be seen in color or in B/W, with or without alpha-numeric text.

The display computer is an S100 bus based system and employes a Z80 based processor operating with a 4 MHZ clock. The computer communicates to the outside world through a 7 channel 8 bit A/D converter, 2 serial ports, 8 bit parallel ports, a dual floppy disk, and, of course, a graphics color/BW TV display. The operator interface is through an ADM-3A terminal, a TTY and the dual disk.

The graphics display is performed by DMA on a memory map. That is, the display driver circuitry timing operates independently from the main program and shares the memory storing to the screen image. Various display parameters are under program control: display on/off, point density, B/W or color, etc. The graphics densities employed are: 64 by 64 color and 128 by 128 B/W for the touch sensor; 128 by 128 B/W for the proximity sensors on the JPL/CURV and Ames arms and for the force-torque sensor on the JPL/CURV arm; and 64 by 64 color for the JSC four claw proximity sensors.

The signals from the JPL/Ames arm proximity sensor electronics are sent to the display computer on 4 analog lines. The A/D conversion is done inside the display computer by an 8 bit successive approximation converter. Each conversion takes about 5 μs.

The signals from both sensors (proximity and force-torque) on the JPL/CURV arm are converted to 12 bit digital words in the CURV vehicle electronics and then stored in a buffer memory associated with the Interdata M70 minicomputer which performs control and supervisory functions. The data is transferred in parallel to the display computer as two 8 bit words. The data to be transferred is specified by the address sent to the buffer memory from the display computer.

The signals from the touch sensor are converted to 12 bit digital words by the touch sensor electronics. The point of the sensor matrix to be sampled is under control of the display computer. An address is sent to the touch sensor electronics, the point is sampled, and the data is sent to the display computer as two 8 bit words. Due to the handshaking signals which are under software control, the whole process takes about 100 μs.

The signals from the JSC four-claw proximity sensors are processed by the Intel SBC 80/20-4 computer. Only the pitch, yaw, and range error signals and the "event" signal are passed over to the display computer. These signals are

encoded into three 8 bit parallel words. The two computers run asynchronously since the TV graphics display process is much slower than the event indication bulb and tone process (about 16 times per second versus about 100 times per second.)

2. Software System

The software for the display programs has been written in assembly language to maximize the signal processing and display formatting rate. This has been an effective approach since the processing and formatting are logically and mathematically simple. Typically, the symbolic language version of a program takes 10-15K bytes to store, and the machine language version 1-2K bytes.

The programs have been written in a structured subroutine format. The top level is a sequence of calls to subroutines. The first calls are to routines which initialize constants and set up the displays. These are followed by the main program loop which calls routines: to see if the display program should be exited, change parameters based on switch or keyboard inputs, input data, calibration of data, perform logic tests, format the data for the displays, etc. Each of these subroutines is a complete logical entity, so that new functions may be added by simply inserting new calls. A similar approach has been taken for the lower levels of subroutines. The program data structures have been designed so that they allow an EPROM version of the programs. Thus to perform tests only a small fraction of the computer system is needed. Further the operation of the system for demonstrations is simplified.

The program for displaying proximity sensor data from the sensors on the JPL/CURV arm and performing event logic is typical of the display computer programs. The first level structure is shown in part A of Fig. 15. The actual process for getting the data, processing and displaying it are shown in part B of Fig. 15. The modularity of the structure was a significant help in adding the event logic and display to the prior programs. All that was necessary was to add the two blocks which perform the event logic tests and which time and display the event blinker. Likewise, when changing the JPL/Ames arm proximity sensor program to accept data from the JPL/CURV arm proximity sensors all that was necessary was to change the "Read Sensor Data" subroutine. The subroutines, incidentally, were taken from a previous force-torque sensor program.

ORIGINAL PAGE IS
OF POOR QUALITY

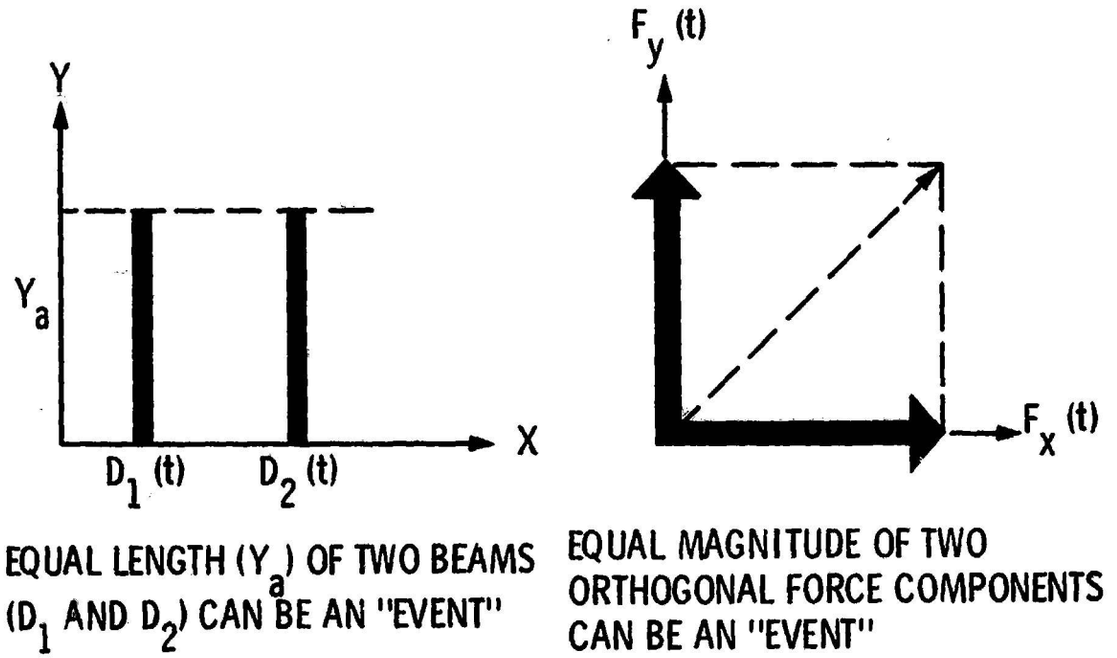

Figure 1. Examples for Event Definition

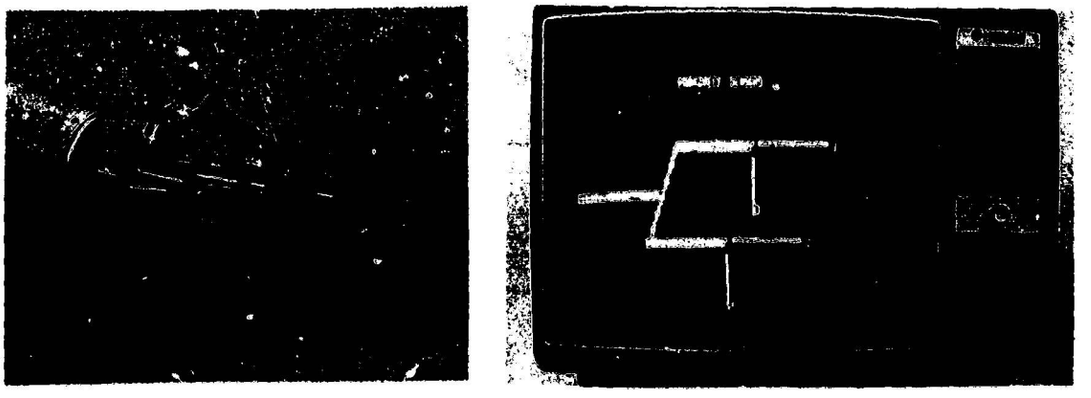

Figure 2. General Graphics Display of Proximity Sensor Beams

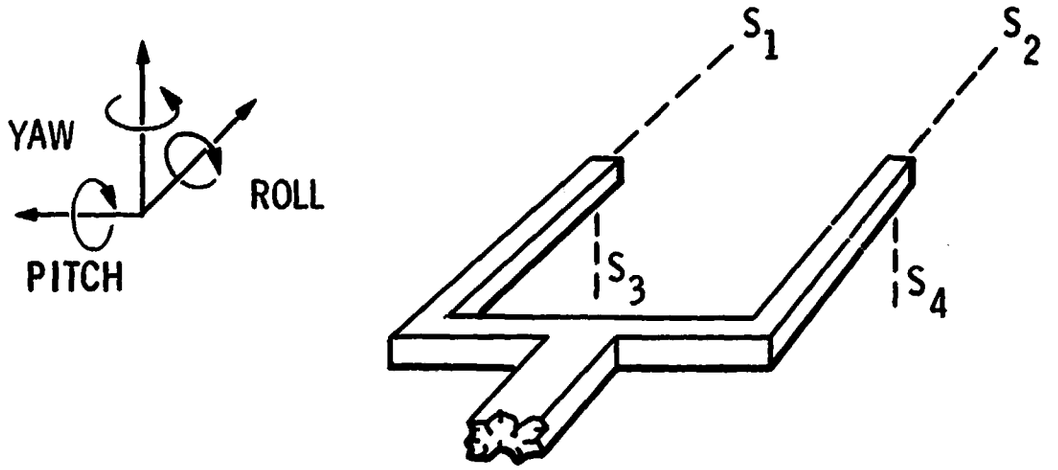

S_i = RANGE MEASURED BY SENSOR "i", i = 1,2,3,4

D = DISTANCE

T = TOLERANCE

} PRESET PARAMETERS

LOGIC DEFINITIONS FOR EVENT E_i = {K}

E_i = 0 FOR $K \geq 0$: EVENT ISN'T THERE, BLINKER "OFF"

E_i = 1 FOR $K < 0$: EVENT OCCURED, BLINKER "ON"

EVENTS	LOGIC EQUATIONS
1. YAW ALIGNMENT AT "D" WITH "T" TOLERANCE	$E_1 = \{\|S_1 - D\| - T > 0\} \bullet \{\|S_2 - D\| - T > 0\}$
2. YAW ALIGNMENT ONLY WITH "T" TOLERANCE	$E_2 = \{\|S_1 - S_2\| - T > 0\}$
3. ROLL ALIGNMENT AT "D" WITH "T" TOLERANCE	$E_3 = \{\|S_3 - D\| - T > 0\} \bullet \{\|S_4 - D\| - T > 0\}$
4. ROLL ALIGNMENT ONLY WITH "T" TOLERANCE	$E_4 = \{\|S_3 - S_4\| - T > 0\}$

Figure 3. Proximity Sensing Events Example

ORIGINAL PAGE IS
OF POOR QUALITY

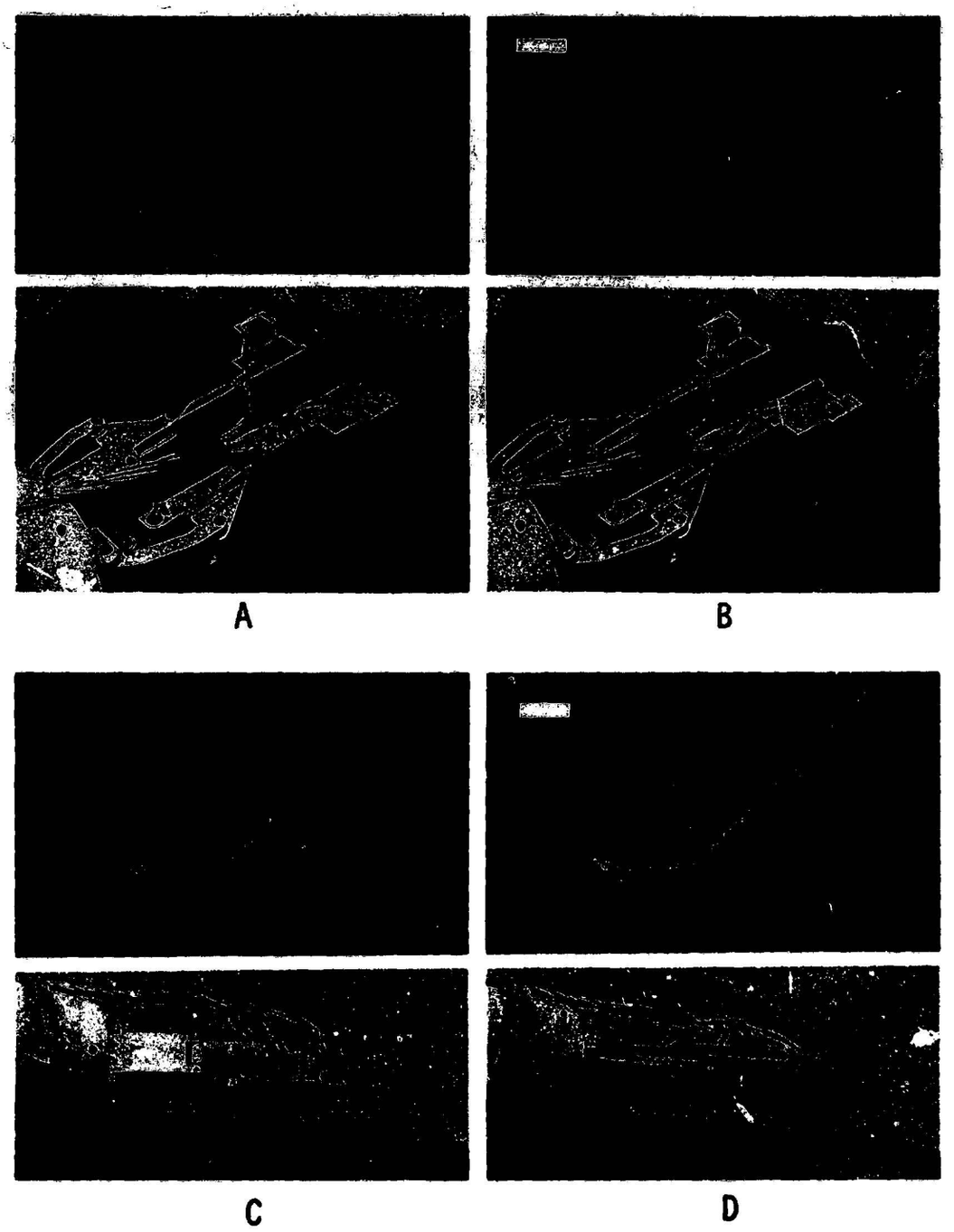

Figure 4. Proximity Sensing Events Graphics Display

ORIGINAL PAGE IS
OF POOR QUALITY

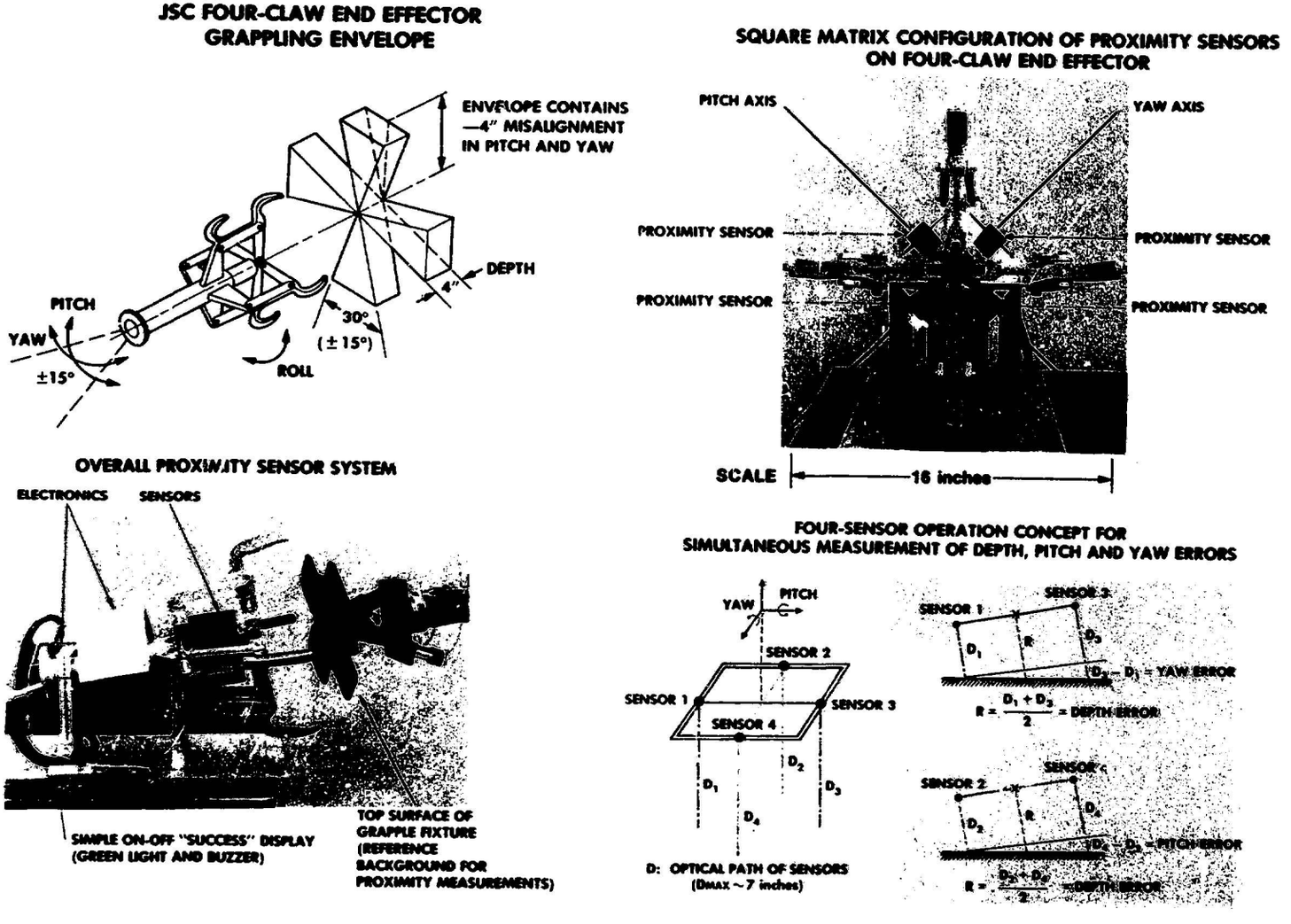

Figure 5. Four Proximity Sensors on JSC Four-Claw End Effector

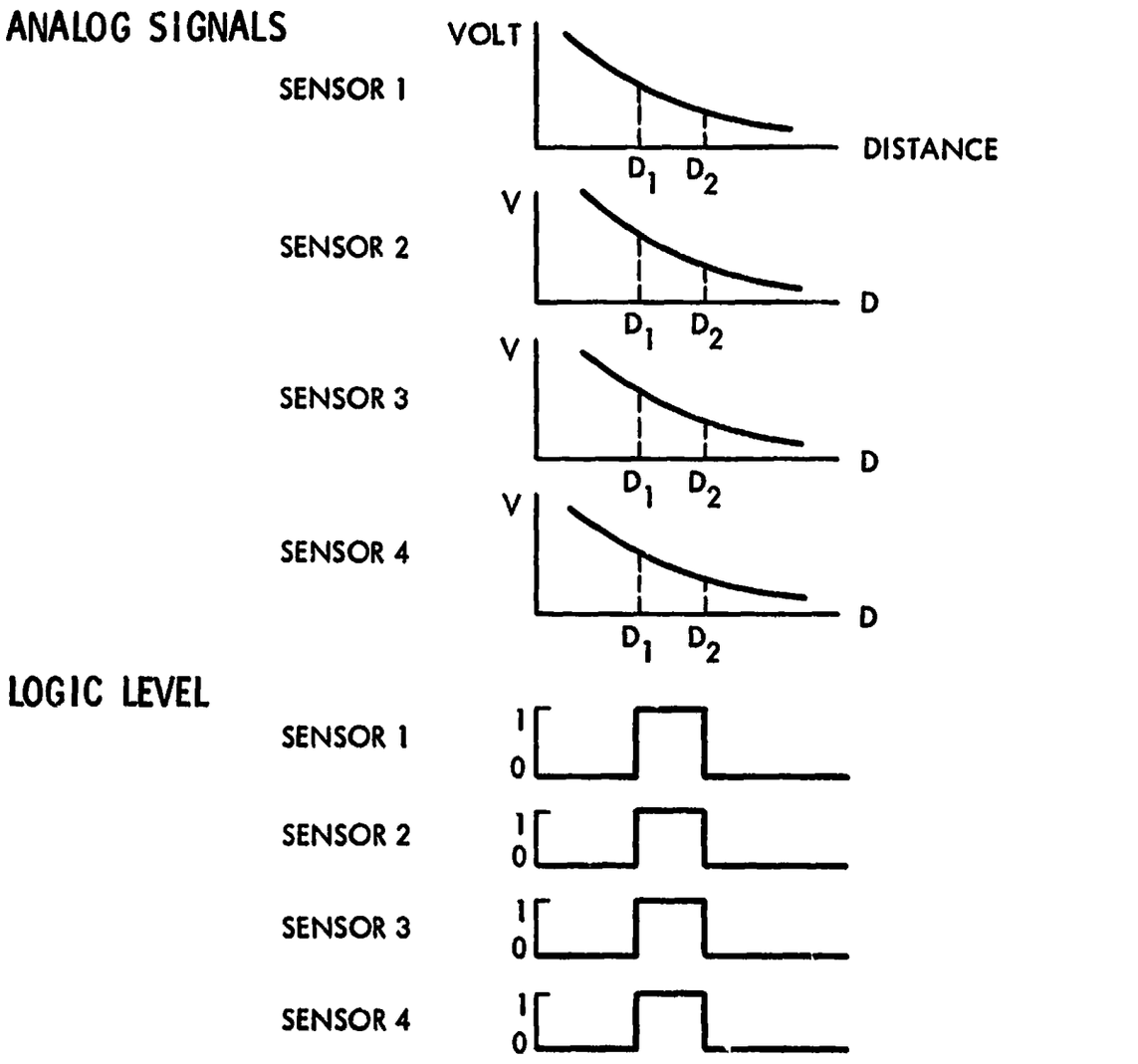

SUCCESS: EACH OF THE FOUR SENSORS OUTPUT IS IN LOGIC STATE "1" (THEN TONE AND/OR GREEN LIGHT ARE AUTOMATICALLY TURNED ON INDICATING TO OPERATOR THAT DEPTH POSITION AND PITCH AND YAW ALIGNMENTS OF END EFFECTOR ARE OK FOR SUCCESSFUL GRASP OF TARGET)

Figure 6. Analog "Event Logic" Indicating Acceptable Combinations of Range, Pitch and Yaw Errors for Successful Grasp Using Four Proximity Sensors Integrated with JSC Four-Claw End Effector

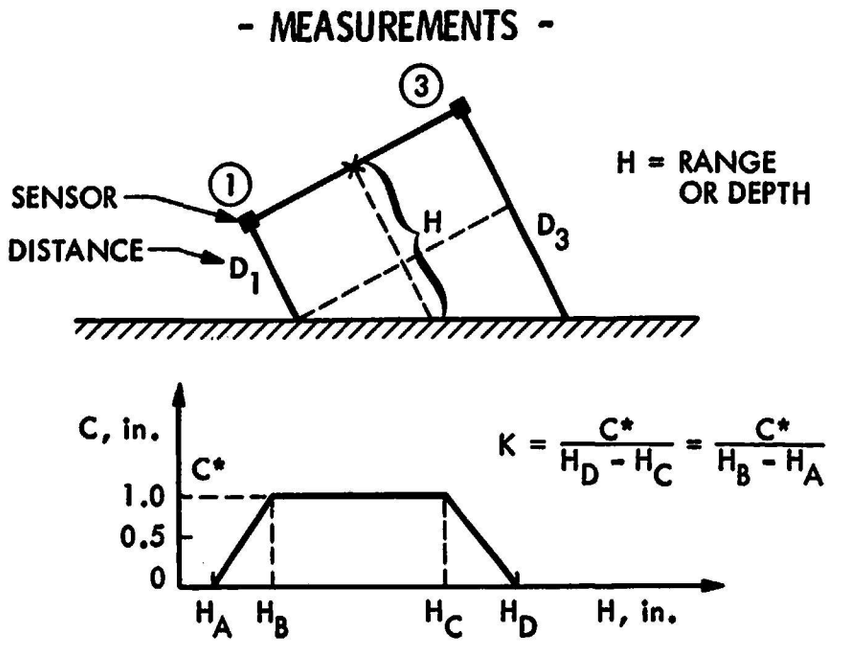

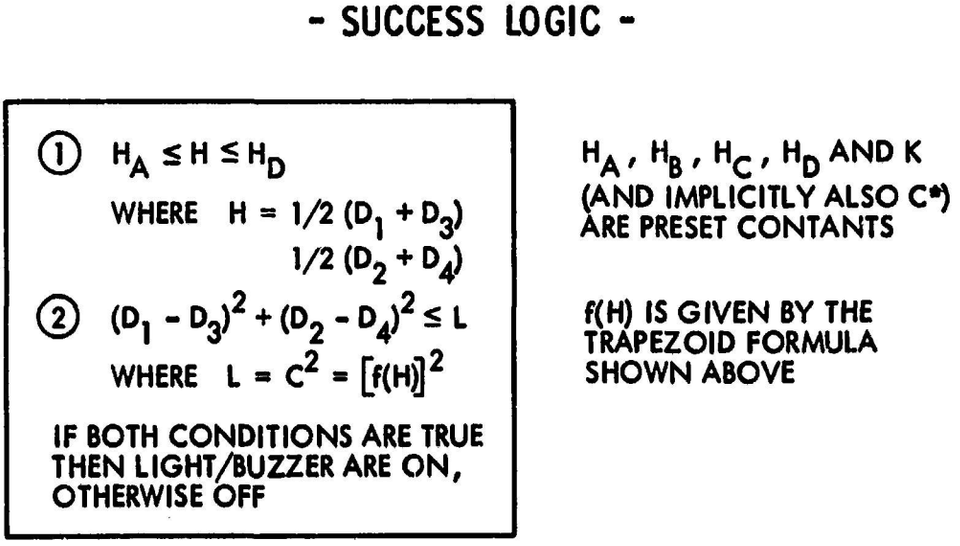

Figure 7. Conic Algorithm Indicating Acceptable Combinations of Range, Pitch and Yaw Errors for Successful Grasp Using Four Proximity Sensors Integrated with JSC Four-Claw End Effector

ORIGINAL PAGE IS
OF POOR QUALITY

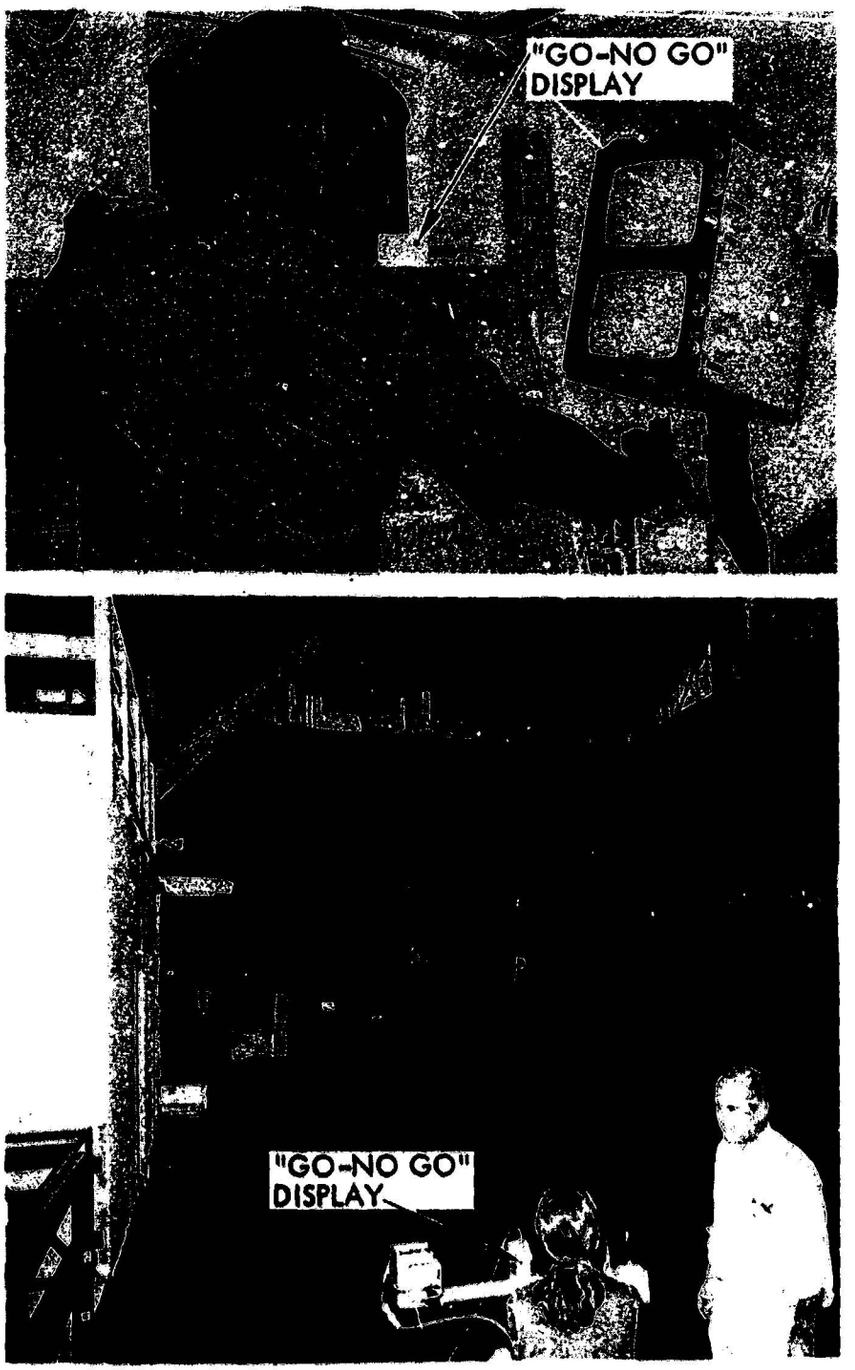

Figure 8. Test Scenes at the JSC Manipulator Development Facility Using Four Proximity Sensors Integrated with JSC Four-Claw End Effector and Simple "Go-No Go" Event Display

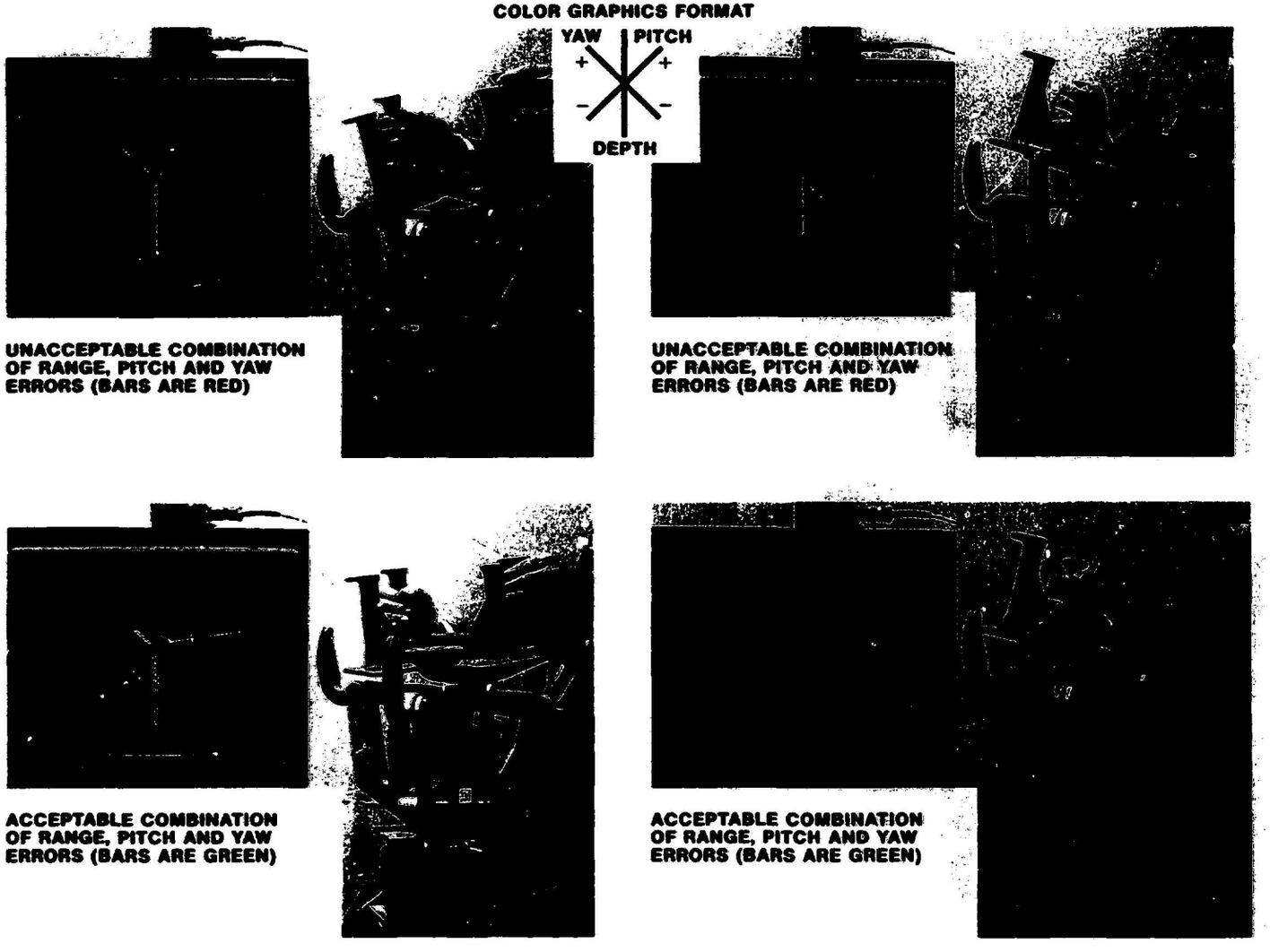

Figure 9. Graphics Display Concept Indicating Both Success and Details of Error States

ORIGINAL PAGE IS
OF POOR QUALITY

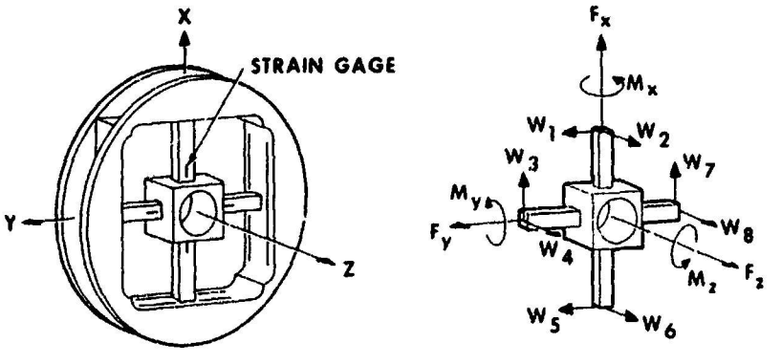

TRANSFORMATION MATRIX
UNDER IDEAL CONDITIONS

FORCES AND TORQUES REFERENCED TO X-Y-Z SENSOR COORDINATES

$$\begin{bmatrix} F_x \\ F_y \\ F_z \\ M_x \\ M_y \\ M_z \end{bmatrix} = \begin{bmatrix} 0 & 0 & k_{13} & 0 & 0 & 0 & k_{17} & 0 \\ k_{21} & 0 & 0 & 0 & k_{25} & 0 & 0 & 0 \\ 0 & k_{32} & 0 & k_{34} & 0 & k_{36} & 0 & k_{38} \\ 0 & 0 & 0 & k_{44} & 0 & 0 & 0 & k_{48} \\ 0 & k_{52} & 0 & 0 & 0 & k_{56} & 0 & 0 \\ k_{61} & 0 & k_{63} & 0 & k_{65} & 0 & k_{67} & 0 \end{bmatrix} \begin{bmatrix} W_1 \\ W_2 \\ W_3 \\ W_4 \\ W_5 \\ W_6 \\ W_7 \\ W_8 \end{bmatrix}$$

FORCES SENSED AT SPOKE ELEMENTS

Figure 10. Force-Torque Sensor Measurement Transformation and Graphics Display

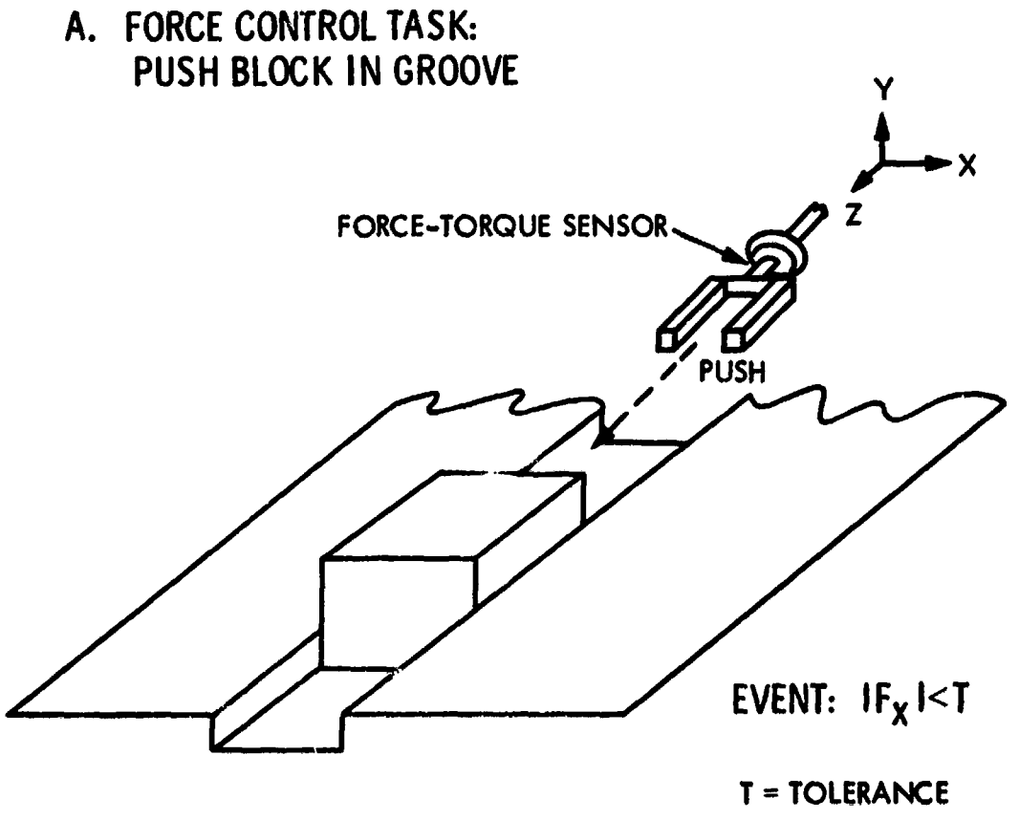

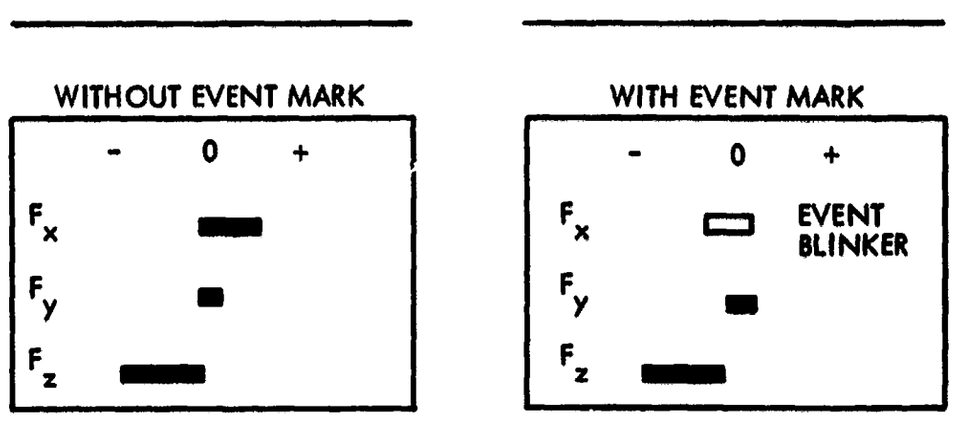

Figure 11. Force-Torque Sensing Event Example

ORIGINAL PAGE IS
OF POOR QUALITY

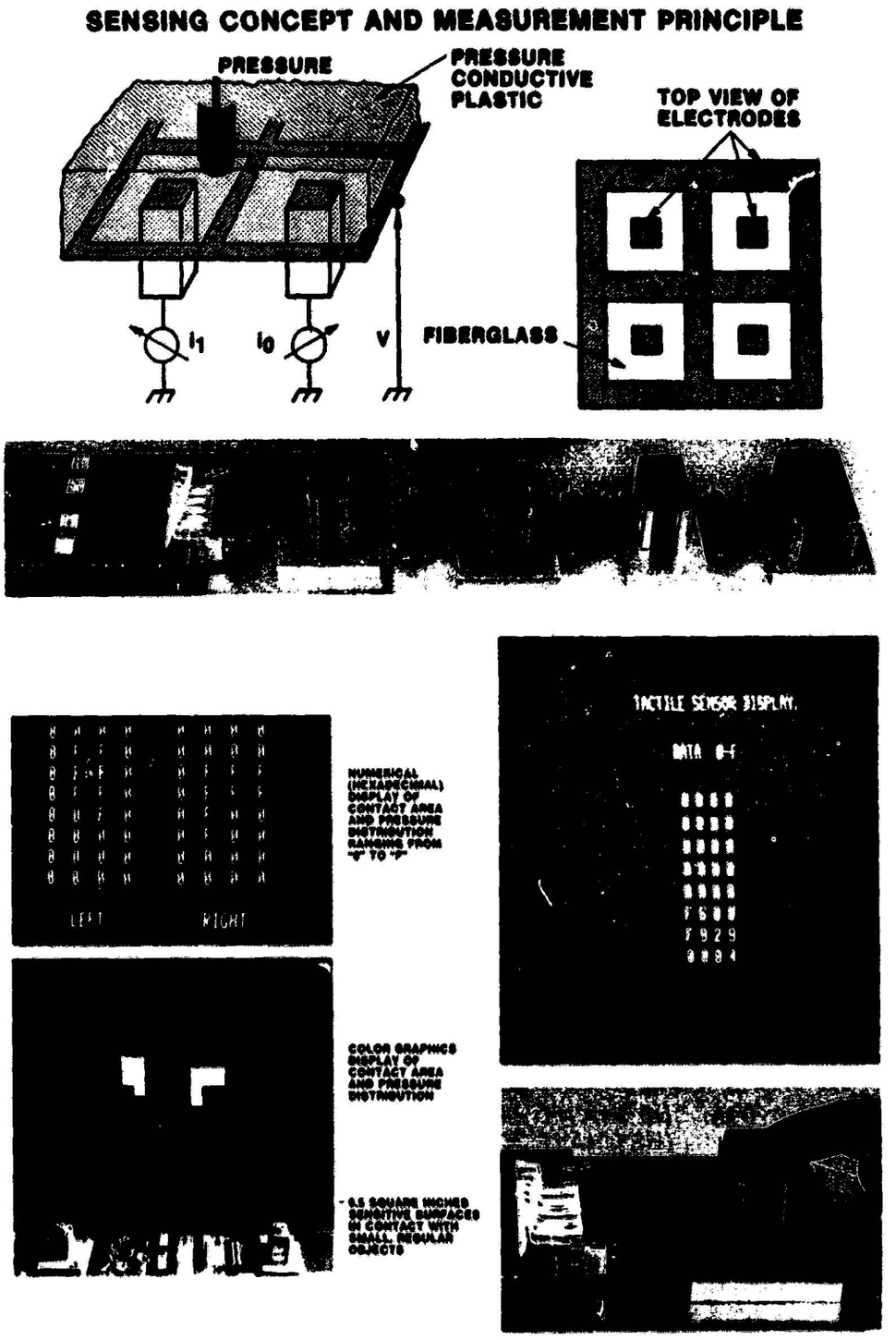

Figure 12. Multipoint Proportional Touch Sensors with Numeric and Color Graphics Displays

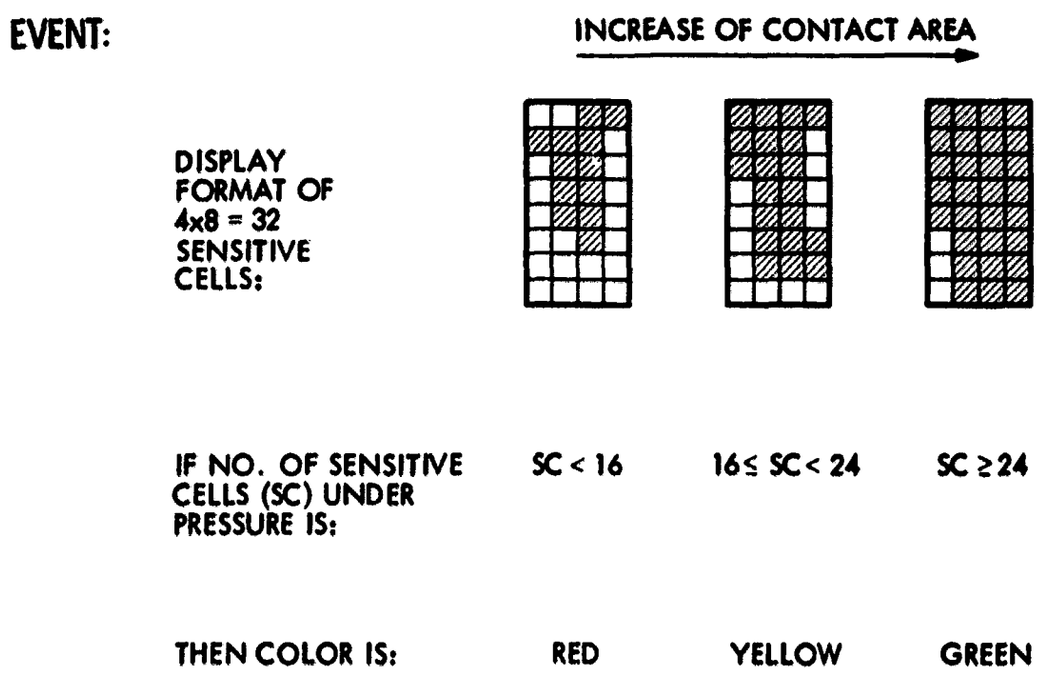

(NB: THE SHADED CELLS ARE THOSE UNDER PRESSURE. THEY HAVE TONES IN THE RESPECTIVE COLORS DARKER THAN THE UNSHADED CELLS.)

Figure 13. Touch Sensing Event Example

ORIGINAL PAGE IS
OF POOR QUALITY

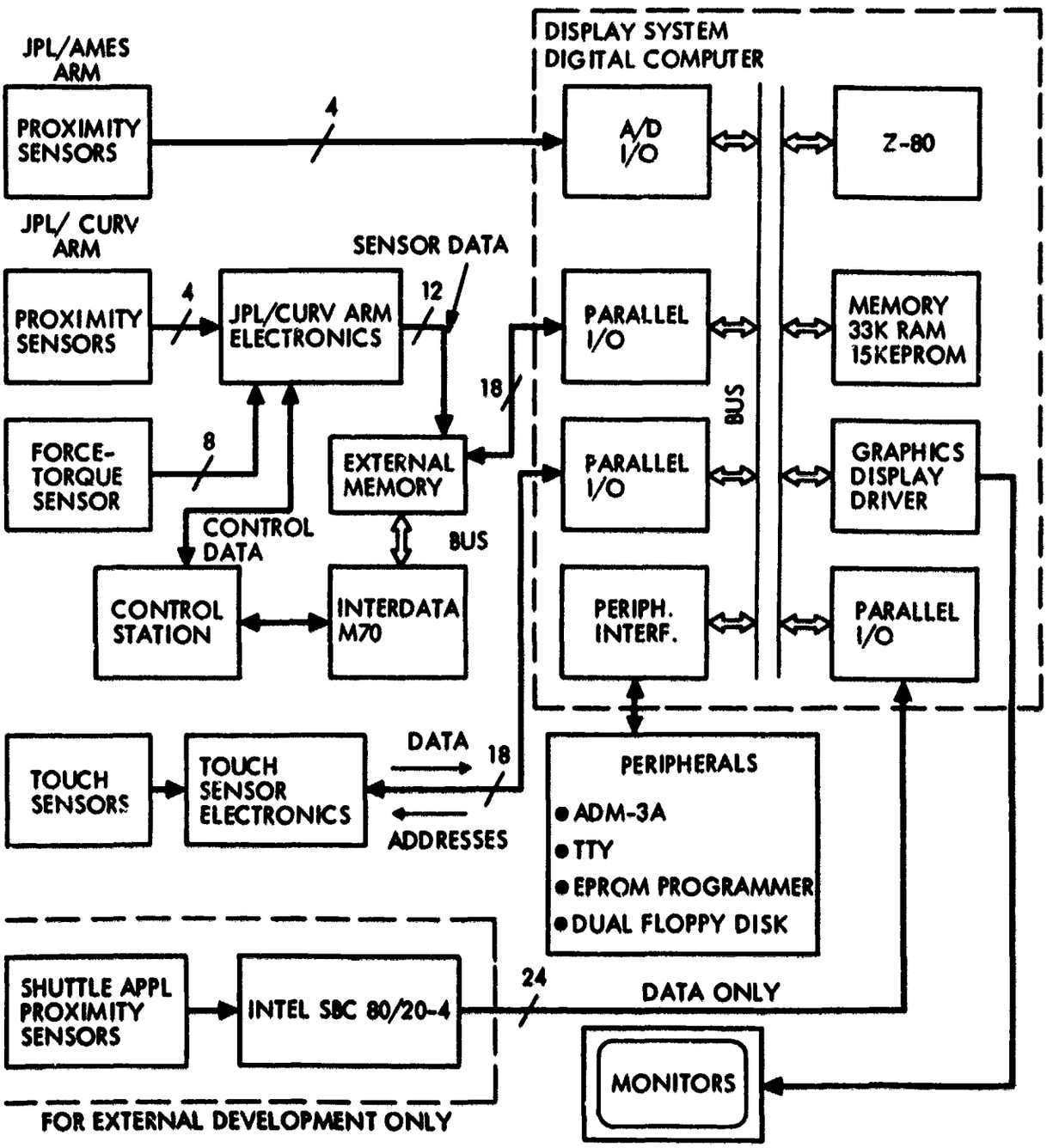

Figure 14. Computer System for Sensor Data Graphics Displays in the JPL Teleoperator Project

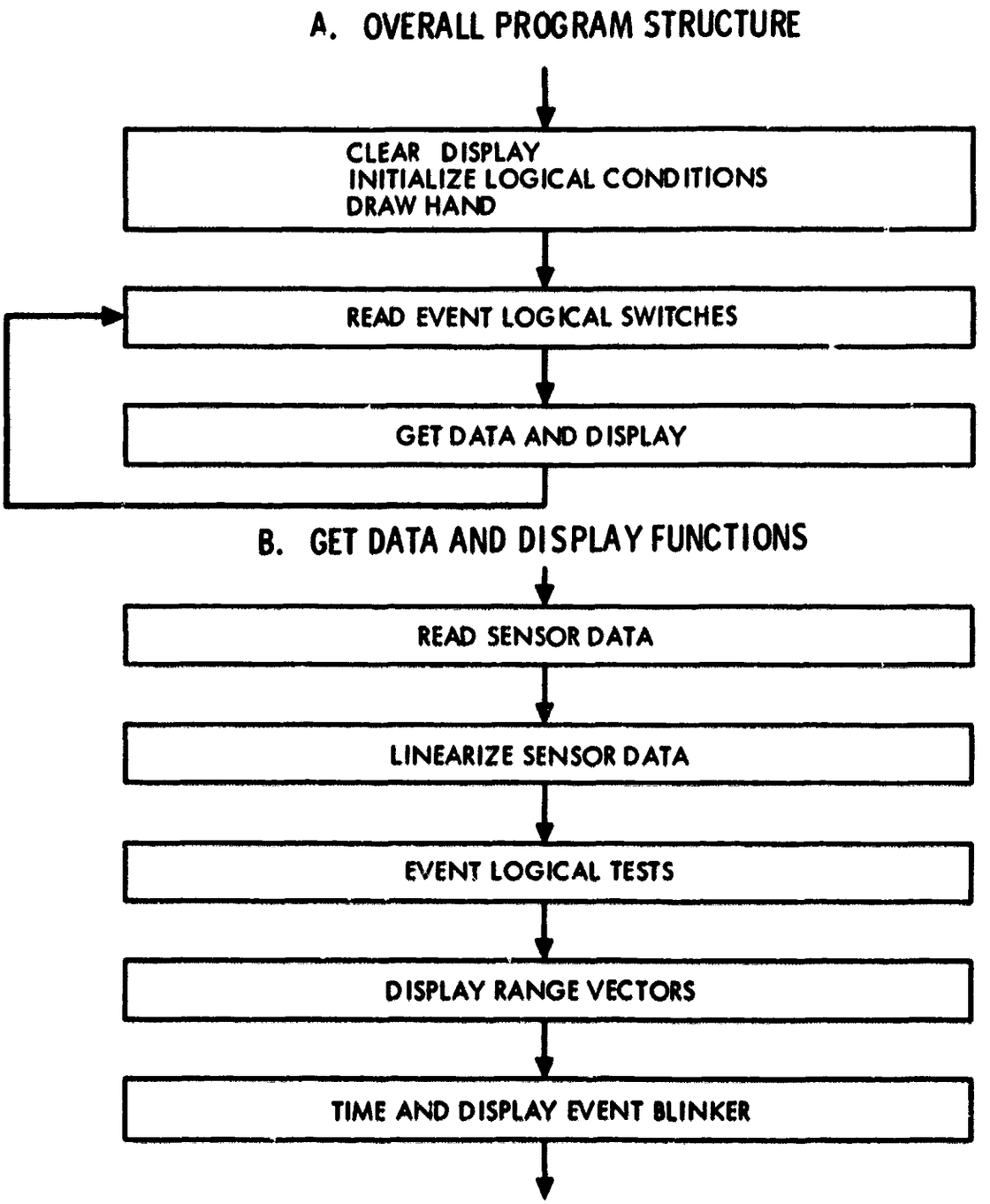

Figure 15. Software System Structure for Proximity Sensor Data Graphics Display in the JPL Teleoperator Project

N79-15611

MANNED SIMULATIONS OF THE SRMS IN SIMFAC

by

Andrew L. LIPPAY, Staff Engineer, Human Engineering, CAE Electronics, Montreal, Quebec, Canada

and

Graham D. WHITEHEAD, Ph.D. Engineering Specialist,

Dr. Claus G. WAGNER-BARTAK, Deputy Program Manager, RMS Division, SPAR Aerospace Products, Ltd, Toronto

INTRODUCTION

SIMFAC is a general-purpose real-time simulation facility currently configured with an Orbiter-like Crew Compartment and a Displays & Controls (D&C) Subsystem to support the engineering development of the Space Shuttle Remote Manipulator (SRMS).

The simulation consists of a software model of the anthropomorphic SRMS manipulator arm including the characteristics of its control system and joint drive modules. Structural flexibility is modelled by presenting the principal modes in six degrees of freedom.

The SRMS control system is normally operated in a Resolved Motion Rate Common mode, commonly known as the Manual Augmented or simply Manual mode. The point of resolution if just inside the tip of the End Effector of the arm, where the head of the Payload Grapple Fixture would fall when in the nominal position for legal capture. A Single mode is also available for selection, whereby the Operator individually commands each joint in turn. In both of these modes a Coarse/Vernier range may be selected, and Rate Hold function may be applied in the Manual mode.

Four coordinate systems may be selected which define the point of resolution and the spatial system response to hand controller inputs. The principal reason for this is to enable the Operator to move the End Effector (and the Payload when attached) in the most direct way possible and reduce the amount of mental transformation required.

Automatic sequences are available to manoeuvre the arm between fixed points. A terminal position and attitude may be determined by pre-programming or by detailed Operator input via a keyboard. The system will move in an optimized path to the terminal point, provided the initial conditions have been fulfilled.

SIMULATION & SCENE GENERATION SUBSYSTEMS

A master/slave computer pair (TI 980B), an Array Processor and floating-point hardware complex execute all computations under a simulator-oriented multi-task operating system (SIMTOS), driving a multi-process interface to which all displays, instruments and other input/output circuitry are connected. An extensive set of peripherals perform data gathering and software development/maintenance tasks.

Displays in SIMFAC are driven by a set of three Varian computers (V73), an array processor and picture generation hardware. An Aft and an Overhead out-the-window scene are presented on two large CRT screens equipped with pancake windows to approximate infinity optics. Two smaller monitors simulate CCTV scenes from six possible camera

positions in selected pairs. Of these the camera mounted on the wrist of the arm seems to carry the greatest impact and will be discussed in detail below.

The visual presentation is driven by a serial data link output from the simulation subsystem, delivered every 50 msec, the pictures are refreshed three times between the frame updates. Camera controls enable the Operator to zoom all cameras, and to pan and tilt all except the End Effector (Wrist) Camera.

Cockpit displays and controls resemble the Manipulator Station of the Orbiter. Mode selector switches, digital position/attitude/rate readouts and a comprehensive Caution & Warning annunciator panel are mechanized and driven by the main model outputs.

A Translational (THC) and a Rotational Hand Controller (RHC) are mounted to the left and right of the D&C panel. The THC has one linear and two pivoted axes in a package representing the flight article. It controls the rates of movement in the X, Y and Z freedoms of the point of resolution in the coordinates selected. The RHC has three pivoted axes and controls the attitude (angular) rates about the point of resolution. It also carries the Rate Hold, Capture/Release and Coarse/Vernier auxiliary controls. The THC has rate-dependent damping, both have spring return and breakout forces.

Caution/Warning annunciators include a Master Alarm coupled with an audio tone, and a lighted annunciator panel. The two most frequently activated are the Reach Limit Alarm, indicating that one of the joints is too close to its angular limit, and the Singularity alarm signalling a limited arm geometry such as that of the arm at rest in its latches, fully extended and unable to accommodate an applied load by yielding to excessive forces.

The manual control problem can be appreciated by considering that the design load limit of the arm is a deflection of 25.4 mm (1.0") under a lateral force of 4536 g (10) lbs, with the not-to-exceed limit being 4763 g 15 lbs. Software stops provide protection by refusing to drive a joint into its hard stops and arm movement ceases completely if the Reach Limit alarm does not result in the reversion of the manual inputs.

THE SRMS TASK IN SIMFAC

The principal task of the SRMS Operator is to manoeuvre the arm and its End Effector into a precise position and attitude with respect to the Payload in order to establish a rigid contact with the Grapple Fixture, and thence manoeuvre the Payload into the desired position and attitude with respect to the appropriate coordinate references, with zero residual energy remaining in the total system. In real life, the End Effector must not contact the Payload until the

latter has been secured against escape, and must not touch any other part except the grapple fixture. The Payload may initially be moving with respect to the Orbiter or it may be docked and secured in the Cargo Bay of the Orbiter. Relative velocity in excess of 0.061 m/s (0.2 fps) constitutes an illegal capture condition where contact must not be attempted. The arm must arrest the Payload within 608 mm (2.0 feet) after Capture. The positioning accuracy must be such that the maximum size Payload 18.24m long, 4.56 m dia (or 60 feet long x 15 feet diameter) can be placed into the Cargo Bay with an all-around clearance of 76.2 mm (3.0 ins).

In the case of the simulated moving Payload, the Operator must establish stable tracking with the End Effector before attempting to grapple, in approx. 80 secs. from the time the Payload enters the effective reach envelope of the arm. This phase is the most dynamic of the entire control task and will be the principal subject of discussion from here on. The tracking and eventual capture are based almost exclusively on the visual information provided by the CCTV camera carried by the arm. This scene is presented on a small CCTV monitor to the right of the Operator with a reticule applied to the glass envelope. This "gunsight" scene has a significant impact on the Operator; any high rate of movement or oscillatory behaviour generates a high gain condition in the external man-machine loop, increases the workload and may lead to PIO (Operation-Induced Oscillations). Among other things, it encourages capture attempts "on risk", i.e. without the assurance of being within legal limits. Since the camera is simulated as mounted on the wrist, a less than stable platform, arm flexibility effects generate just such visual dynamics, in addition to those produced by the real movement of the Payload with respect to the End Effector. Furthermore, the Operator is not positioned on the same platform, hence he will not receive motion cues to help him compensate for the lively visual scene.

A less dynamic but equally difficult situation ensues when the principal axes of the Payload or the End Effector are displaced from being parallel to those of the Orbiter. The four available coordinate systems recognized by the control algorithm are referenced to the End Effector, the Orbiter, and the Payload, respectively, and the fourth is divided between the Payload for attitudes and the Orbiter for translations. Euler sequences destroy the spatial correspondence between the hand controllers and system response where the coordinate system in use moves with the Payload or End Effector, but the Operator remains "frozen" to the Orbiter. Furthermore, a coordinate system, consistent in the engineering sense, will generate contradictory display increments and cause wrong-sign inputs unless its sign

convention is duly adjusted to conform with the aeronautical "positive" and "negative" in terms of switch or stick movements.

In summary, the SRMS command task is somewhat similar to flying a airplane by remote control, rather than that of piloting an aircraft.

OPERATOR TACTICS AND OPTIONS

Successful Operators in the SIMFAC simulations have quickly learned to accommodate the basic system responses and developed individual but similar command techniques. In the capture task they eliminate attitude errors first, in Coarse mode at a safe distance from the Payload, then use long, smooth approaches, maintain tracking. They apply ramped, well-damped command inputs to avoid flexibility effects and to reduce the image displacement rate on the End Effector gunsight scene. One attitude and one translational correction is applied as a pair to avoid roll-pitch cross-coupling and to minimize target displacement on the CCTV scene. Trained Operators maintain a good inner image of the arm geometry and are able to avoid joint angle limits, estimate the total arm performance available and even trade-off rotational vs. translational corrections for a smooth and efficient approach. The SIMFAC hand controller characteristics are said to make a significant difference against earlier models which had no damping and generally poor engineering quality.

Operator options such as Vernier selection which reduces the command authority to 10%, and Rate Hold, are used by all Operators, the former mostly to reduce the liveliness of the gunsight scene and to increase precision as required. The system applies Vernier automatically on Capture, i.e. during the transition between unloaded and loaded arm, and a manual selection reduces the Loaded Vernier velocity to 50%.

WORKLOAD

A peak is reached during the Track and Capture task. Arm flexibility effects appear in the CCTV reticule as elliptical oscillations, easily excited with high visual effects especially at close range. However, they damp out if not further excited and true PIO does not develop. The spare Operator capacity is significantly reduced, the gunsight scene is the focus of intense concentration. The selection of Vernier is easily predictable for most Operators, as a function of range from the Grapple Fixture, since it is determined by their acceptance of activity on the CCTV scene.

Other sources of increased workload include the necessity to make ramped inputs to command precision movements, to perform mental transformations in Payload manoeuvering and the management of the D&C subsystem, especially while operating in the Single mode, controlling each joint individually. Ramped inputs require high concentration over

many seconds; well-balanced and damped hand controller characteristics are essential. Coordinate transformations also require high mental effort during the final phases of Payload positioning, since a wrong-sign input will not only disturb a near-perfect deployment condition, but many cause collisions during the berthing task, with the Payload in close proximity with the Orbiter.

Displays and Controls Management involves mode selection and display selection, since all parameters cannot be simultaneously displayed; XYZ position and pitch-yaw-roll attitude must be selected for digital display readout. Mode selection must be followed by an Enter command to be accepted by the system. The Single mode involves not only display selection (associated with the tasks the mode is normally used) but also the selection of each of the six joints followed by the operation of a double-throw switch for positive or negative input.

In summary, the Resolved-Motion Rate Control system provides adequate means to control the manipulator arm by one Operator as specified for the SRMS tasks. Research work at MIT, NASA/JSC, NASA/Ames and NASA/Marshall have been compared with some experimental setups at Martin-Marietta, as well as Honeywell and CAE experience in fly-by-wire applications, and command philosophies such as the replica arm and force-stick controllers have been considered but later rejected in favour of the displacement stick and rate command with resolved-motion augmentation. A six degree-of-freedom controller would have been favoured for a single/command/input point but had to be abandoned for lack of cockpit space and because of higher design risk.

OPERATOR ERRORS AND SOURCES

Up to the time of this writing, the main SIMFAC effort was directed to validate the flexible arm and SRMS subsystems simulation, and to establish basic controllability and operability for the tasks specified. Initial work has been completed to simulate malfunctions and off-nominal conditions to verify procedures and indicate parameter sensitivities. No attempts have been made to simulate side-tasks, Orbiter environment and on-orbit workload. However, comments of Operators have been carefully recorded and analyzed, and their assessment of their own performance was elicited whenever practicable, both in terms of the simulation and the simulated SRMS tasks.

Short of malfunctions, the reference coordinate systems and sign conventions presented the greatest single problem as soon as human operators were inserted in the control loop.

The End-Effector CCTV scene with its reticule is essentially a fly-to display. One of the Alignment Aids (Payload target) resembled the

small aircraft symbol usually found on artificial horizons and flight directors. An Operator with long flying experience promptly reverted to the fly-from technique associated with that type of instruments and has had considerable trouble in readjusting his thinking during the demanding Track and Capture task. With a different target he had no difficulty.

Arm geometry causes non-linear responses due to limitations in the individual joint drives, necessary to ensure that the End Effector does not exceed certain velocity limits. Finite joint ranges and arm singularities also cause uncommanded stoppages. While most of these effects can be avoided or accommodated by trained Operators, the visual conditions in SIMFAC do not provide texture, hardware markings, shadows and other assistive side effects.

Visual conditions in the Space Shuttle are expected to vary between extremes, from sunshafting and specular reflections to near-total darkness. Wide variations in illumination will occur with every adjustment of the Orbiter attitude or Payload position. Judgement of depth or X-ranging is expected to be poor in real life as it is in SIMFAC, with its two-dimensional visual displays.

The dynamic aspects of the SIMFAC visual presentation are quite adequate. However, the SRMS task itself produces low-key visual cues with low dynamics, difficult to detect and monitor. A 18.24m (60 ft.) long Payload suspended say 15.2m (50 ft.) away from the Operator may have a very low yaw rate but its end bulkheads move with relatively high speed, and may contain great energy with the maximum Payload mass of 29,484 Kg (65,000 lbs). Furthermore, arm flexibility effects and control system responses are very similar in their visual aspects under certain circumstances near the Cargo Bay, potentially inducing the Operator into erroneous corrective action.

The SIMFAC Displays and Controls Subsystem resembles the Orbiter complement but is not completely representative of it and lacks some of the visual impact of the flight article. The hand controllers are engineering model quality but well engineered and have acceptable force characteristics and feel.

The harmony of manual input to system response is generally good, the controllers providing a one-to-one relationship with the desired Payload or End Effector movement. The displays follow the system responses adequately and present necessary and useful task information. However, the harmony between the command inputs and the display responses is not optimized in that the position and attitude information is referred to the Orbiter, while the command axes may be transferred to the End Effector or Payload. Hence, the same manual input will drive one display window or

another, depending on the Euler angles. The Operator then has to compensate with mental transformations and therefore is prone to errors and incorrect inputs. This effect is most noticeable in precision manoeuvres during Berthing and Payload Deployment, when the Operator is "flying the Payload on instruments", i.e. making final adjustments by the digital displays. This observation on SIMFAC resulted in a change of SRMS coordinate systems and displayed values.

The management of displays and controls is a significant side task with some peak workloads occurring in parallel with other high-activity periods.

AREAS FOR FURTHER WORK

Visual improvements are being planned for SIMFAC. Full hidden line removal and additional scene contents are considered. As noted above, the dynamics of the visual scenes are largely satisfactory and carry a high impact.

Orbiter-SRMS interaction, namely reactive forces and the operation of the Orbiter attitude control systems, have not been fully simulated in SIMFAC.

Man-machine integration and rigorous Operator modelling work would be most desirable from the resarch point of view, since these are outside the scope of an industrial development. Multi-axis hand controllers, computer-driven active force feel systems, integrated displays may be needed for future generations of Remote Manipulators. The loop dynamics exhibited by the wrist camera in this simulation in connection with the human visual and neuromotor channels is peculiar to large manipulators and presents a set of interesting modelling tasks in itself.

GENERAL OBSERVATIONS

The simulation as a whole is considered successful, judging from the reaction of Operators to computer glitches and malfunctions. These indicate that the experienced Operator is very much in the simulation picture and is using his best efforts to perform the task.

Learning curve effects are readily visible and repeatable, well documented. The task presented in SIMFAC, that of capturing a free-flying satellite and berthing it into the Cargo Bay is deemed equivalent to the worst case task expected to be attempted in real life.

Quick setup and initialization capability of SIMFAC facilities manned simulation under reasonably consistent conditions.

The observed command strategy and Operator behaviour, as well as individual performances, clearly indicate not only the existence of an "inner model" but the necessity of one even in the static sense, whereby some Operators manage to maintain a picture of arm configuration regardless of arm visibility, and avoid potential

joint limits, singularities and collisions.

Some Operators perform equally well in dynamic and precision manoeuvres, others exhibit a distinct preference and success in one or the other. No explanation is offered at this time except the possibility that the force characteristics of the hand controllers may have enhanced competence in some cases by matching the individual neuromotor systems.

The flexibility of the dynamic arm presented a distinct increase of task difficulty compared to the kinematic arm model, but all operators managed to adapt their input rates and control strategies to overcome these effects. It may be noted that both the increased dynamics in the wrist camera scene due to flexibility, and the absence of an alignment aid target, led to attempts to capture with less than proper alignment or at a questionable capture distance.

Simulated malfunctions presented in SIMFAC generated three distinct phases of response in each Operator participating in the tests. At first, a malfunction was immediately considered on the SIMFAC system, i.e. a simulation error. No corrective action was attempted. In the next phase, most Operators blamed themselves, claimed Crew Error and tried to rectify it until they realized that the corrective commands were ineffective. Finally, absolutely everything out of line was suspect, and immediately questioned as to which malfunction is being presented.

From the point of view of man-machine integration, the external loop composed of the Operator, the Wrist Camera display and the behaviour of the End Effector due to flexibility effects and arm geometry present a intricate problem. It is impossible to analyze these relationships on paper and understand the wide range of factors involved, many of which are intangible, such as the aeronautical control conventions ingrained in Operators with piloting experience. SIMFAC has some shortcomings; to be sure; the visual scenes lack texture, reflections and shadows, contrast and similar effects, but the dynamics of the presentation are sufficiently convincing to point out flaws in the man-machine interface and to validate system stability and operability with man in the loop.

N79-15612

HUMAN/COMPUTER CONTROL OF UNDERSEA TELEOPERATORS+

T.B. Sheridan, W.L. Verplank and T.L. Brooks

Man-Machine Systems Laboratory
Department of Mechanical Engineering
Massachusetts Institute of Technology
Cambridge, Massachusetts 02139

Abstract

This paper discusses the potential of supervisory controlled teleoperators for accomplishment of manipulation and sensory tasks in deep ocean environments, and discusses one such system. Teleoperators and supervisory control are defined, the current problems of human divers are reviewed, and some assertions are made about why supervisory control has potential use to replace and extend human diver capabilities. The relative roles of man and computer and the variables involved in man-computer interaction are next discussed. Finally, a detailed description of a supervisory controlled teleoperator system, SUPERMAN, is presented.

1. Teleoperators and Supervisory Control

Many future undersea tasks may be accomplished by "teleoperators". We define teleoperators to be general purpose submersible work vehicles controlled remotely by human operators and with video and/or other sensors, power and propulsive actuators for mobility, with mechanical hands and arms for manipulation and possibly a computer for a limited degree of control autonomy. A manned submersible is not a teleoperator vehicle, but its attached manipulators are certainly teleoperators, requiring control through a viewing port or through closed-circuit video. Sometimes the term "teleoperator" is restricted to telemanipulator, excluding the system for remotely positioning and orienting a sensor, but for the sake of generality we include this important function.

This paper focuses on those aspects of undersea teleoperation which concern the human operator and the man-machine interface, and within this still relatively broad domain, it concentrates on the prospects for utilization of "supervisory control". Supervisory control is a hierarchical control scheme whereby a system (which could be a teleoperator, but could also be an aircraft, power plant, etc.) having sensors, actuators and a computer, and capable of autonomous decision-making and control over short periods and in restricted conditions, is remotely monitored and intermittently operated directly or reprogrammed by a person.

The distinction between direct human control of a teleoperator and supervisory control of a teleoperator is made graphically in Figure 1. In

+ This work was supported by Office of Naval Research (Contract N00014-77-C-0256) and by the MIT Office of Sea Grant (National Oceanographic and Atmospheric Administration).

PAGE INTENTIONALLY BLANK

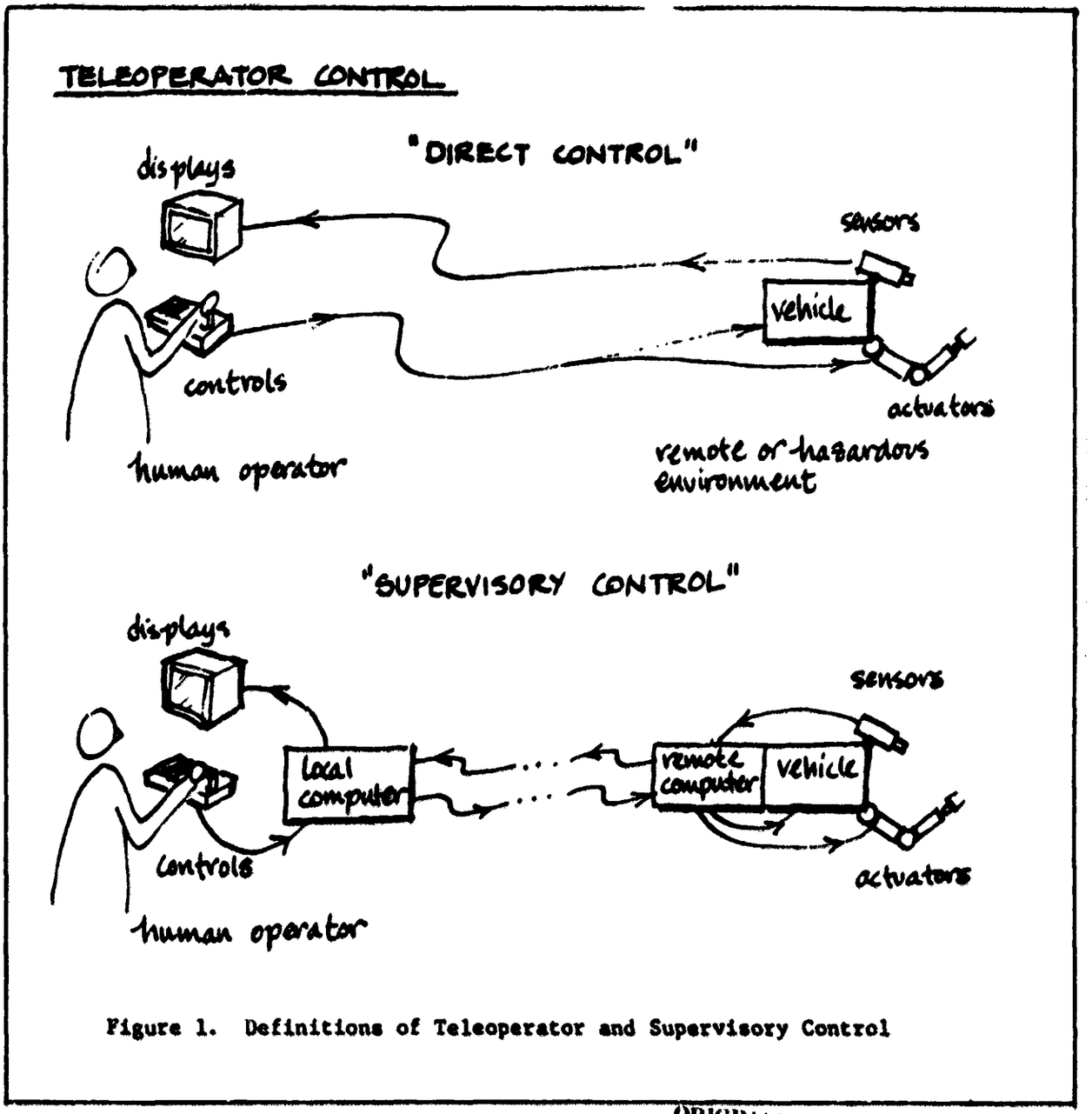

Figure 1. Definitions of Teleoperator and Supervisory Control

ORIGINAL PAGE IS
OF POOR QUALITY

Definitions

TELEOPERATOR

A vehicle having sensors and actuators for mobility and/or manipulation controlled by a human operator, and thus enabling him to extend himself to physically remote or hazardous environments.

SUPERVISORY CONTROL

A heirarchical control scheme whereby a device having sensors, actuators and a computer, and capable of autonomous decision making and control over short periods and restricted conditions is remotely monitored and intermittently operated directly or reprogrammed by a person.

the upper figure the human directly controls, over either a wire or sonic communication link, the separate propulsive actuators of the vehicle, the actuators for the separate degrees of freedom of the manipulator, and the pan and tilt actuators of the video camera. The video picture is sent back directly to the operator. The "hand control" can be a master-slave positioning replica or a rate joystick.

In the lower figure a computer is added to the teleoperator, and for short periods and limited circumstances this teleoperator may function autonomously.

At the bottom are generic definitions of teleoperator and supervisory control. The upper drawing portrays the former without the latter. The lower drawing is the combination.

In supervisory control the teleoperator's (remote) computer communicates at high bit-rate with the teleoperator's sensors and actuators. But because of bandwidth constraints on the signal transmission link, or because of teleoperator sensing limitations, communication may be restricted to low-bit-rate with the human operator's (local) computer. For this reason, and also because of the intermittent nature of human monitoring and reprogramming of commands on a keyboard (and possibly joystick or other controls), the human supervisor's communication with the teleoperator tends to be at a slow rate, i.e., intermittent symbol strings or movement sequences on a master-controller with relatively many bits per instruction package. His communication with the local computer to refresh TV images or to edit or "dry run" his commands on a model before committing them to action may be constrained only by his own speed limitations.

The physical separation of local and remote computer is not necessary in aircraft, industrial plants or other systems where the operator is physically nearby, and where supervisory control is used for reasons other than physical remoteness and limited communication channel capacity between human operator and the object of control. In such situations supervisory control may be advantageous, nevertheless, to achieve faster or more accurate control, or to control simultaneously in more degrees-of-freedom than the operator can achieve by direct servo-control, or to relieve him of tedium. The latter reasons for supervisory control can apply to undersea vehicles when the human operator is not physically distant (as with manned submersibles) or to undersea teleoperators when a reliable high-bandwidth communication channel (wire or optical tether) is available.

2. Why Teleoperators Underseas? The Limits of Divers and Manned Submersibles.
The principal reasons for interest in using teleoperators for underseas tasks are dollar costs and safety.

Operations, including exploration, inspection, construction, maintenance, salvage and rescue, are having to be performed at increasing depths. At such depths - below, say 300m. (depending upon the paticular task) the time required for divers - mostly compression/decompression time - becomes excessive; factors having to do with depth per se, including life support equipment,become increasingly costly; personal safety is more and more difficult

ORIGINAL PAGE IS
OF POOR QUALITY

to maintain. These assertions are borne out by rather alarming mortality figures for commercial divers in the North Sea.

Water turbidity and other depth-related factors may require greater bottom-time, thus compounding the decompression-time factor. Under such conditions, a fixed-capability teleoperator, which sometimes is seen as too clumsy by comparison to a human diver at shallower depths, becomes much more attractive economically.

Happily, there is progress in the development of teleoperators, and they are becoming less clumsy. Inspection and manipulation tasks which simply could not be accomplished a few years ago are now achievable, due to steady progress in the design of video systems, mechanical valves and actuators, etc. For the immediate future, however, the primary technological factor which is changing the prospects for undersea teleoperation is the computer.

Circa 1970 divers seemed to have the edge on manned work-vehicles with manipulators in terms of maneuverability, manipulation, tactile sensing, and covertness. Because of smaller unmanned vehicles and eventually through unmanned untethered vehicles, however, the diver (especially the tethered diver) is losing his edge. Manipulation, sensing and cognition remain the primary advantages for the diver, but the computer is changing these also.

The comparison between teleoperators and manned submersibles is more clear-cut. The fact is that television cameras can now "see" with less light than the human eye, and new sonic imaging systems can see through densely turbid waters where neither human vision nor video can function. Spatial resolution or video can be made to approximate that of the eye by focusing. Present advantages of manned submersibles or teleoperators as work vehicles (neglecting for the moment personnel rescue) are: steropsis for close-up objects, and the ability of a human observer with a wide angle of view to keep track of the relative location of different objects. As the communication channel improves, to the point where the manipulator itself is the limiting factor, a man in a submersible can control manipulators or video pan-tilt controls just as well as a man on the surface. The major difference remaining between manned submersible and teleoperator are then cost and safety, as with the diver. The pressure vessel and life-support equipment make the manned submersible much more costly than the same vehicle without the pressure vessel and life-support equipment but with remote control instead. The factors of quality and reliability of communication and remote control then become the key factors.

3. Why Supervisory Control of Teleoperators Underseas? Some Assertions about the Problem.

a. Demands are increasingly stringent in terms of depth, sensory resolution, speed and accuracy of power of response for accomplishment of undersea tasks. Some of these tasks are always the same and are amenable to fixed automation, but many are different each time they occur and therefore cannot be done by fixed automation.

b. In terms of depth and skill human divers are reaching their limits, or when they go beyond these limits they do so at significant risk to life and cost in support equipment and personnel.

c. Teleoperators, i.e.,submersibles having video and other sensors, actuators for mobility and manipulation, and remotely controlled by human operators, offer much promise for extending man's flexible, adaptable, perceiving and control capabilities into remote and hazardous environments.

d. Present teleoperators are quite limited in sensory capability (e.g.,in turbid water), in manipulation capability (in speed and dexterity as compared to human hands), and in dealing with distortion in man-machine communication (misorientation of teleoperator to human body, time delays and noise).

e. Computers are rapidly getting smaller in size and power requirement and cheaper in cost for a given computing capability.

f. While accomplishment of one-of-a-kind undersea tasks by intelligent and completely autonomous robots may have appeal, we simply do not have available at this time such devices or the understanding to build such devices.

g. Undersea systems, like aerospace systems, demand conservative design because unreliability poses severe costs.

h. The most immediate and reliable approach would appear to be to add modest computer aiding and "artificial intelligence" to teleoperators, retaining human sensing, motor, memory and decision capability, at least for higher level planning, decision-making, and control.

i. Over a longer period of years, as computer control and artificial intelligence become more sophisticated, certain human functions in teleoperation may be replaced, but greater need and demand will be placed upon other human functions, and in these respects the need for improved man-computer interaction will increase, not diminish.

4. Relative Roles of Man and Computer, and Man-Computor Communication.

In analyzing the relationship between human operator and computor in teleoperation, it is useful to consider how human behavioral components, through two basic forms of communication are used in four human supervisory roles. Figure 2 summarizes the situation by arrows indicating causality between descriptors.

Commanding the computor is done by either typing strings of symbols or pushing dedicated buttons or switches (symbolic commands) or moving a joystick or replica controller, where there is a geometric isomorphism between control movement and its meaning (analogic commands). Observing can also be of symbolic displays (alphanumerics) or analogic displays (pictures or geometric diagrams). Imagining(internal mental visualization) may also be symbolic or analogic.

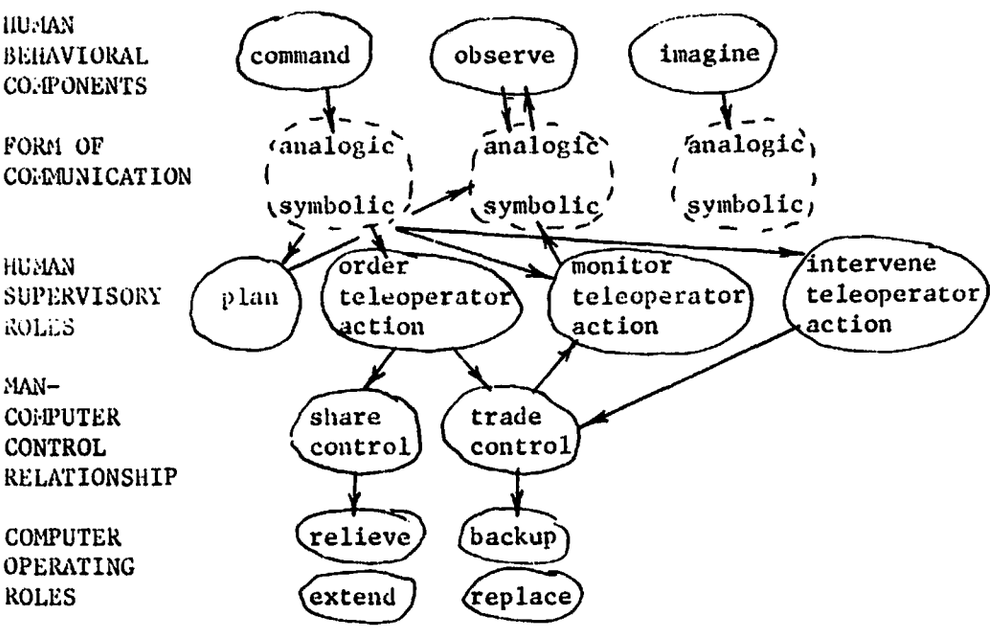

Figure 2. Relative Roles of Man and Computer

ORIGINAL PAGE IS
OF POOR QUALITY

Supervisory commands may be for purposes of planning information, such as referencing computer memory or testing a potential future action on a model; they may be for ordering teleoperator action; they may be for making computer adjustments while monitoring teleoperator action; or they may be for intervening in teleoperator action to assume direct manual control. Observation of displays is indicated in both the planning and the monitoring role of the operator.

As shown in the fourth row, the teleoperator may be ordered to act in two different ways. One is where the man shares control with the computer, i.e. the two work on the same task at the same time. The other is where the man trades control on all or some of the tasks, i.e. for those tasks he gives over complete control to the computer. Intervention means that the computer trades control back to the man. When control has been traded to the computer, part of the act of monitoring is to observe (analogic and symbolic) displays of its performance, as shown by the upward arrows.

The computer's alternative operating roles when sharing control with the human operator are relieve, i.e. do things which make his work easier, and extend, i.e. pushing his performance beyond where it would normally be. When control is traded to it the computer may backup the operator by being ready to take over in case he fails, or it may replace him altogether.

While this taxonomy of relationships at the present has no corresponding quantitative theory, it has been useful to the authors in thinking about what is desirable for man-computer control of teleoperators. In particular it has helped us think through the various forms of computer aiding which might be programmed into an experimental system. And it has clarified for us the potential of using a combination of general purpose typewriter and dedicated on special-purpose keyboard commands (symbolic)and force-reflecting master-slave and rate commands (analogic).

5. SUPERMAN: A System for Supervisory Manipulation

A brief description of a thesis by T.L. Brooks in progress at the Man-Machine Systems Lab at MIT is given on the following pages as an example of a supervisory manipulator system. This system is called SUPERMAN. Figure 3 shows the general relationships between the multiple inputs (keyboard, dedicated symbolic keys, and analog inputs), the computer states (STANDBY, DEFINE, EDIT, EXECUTE, AND TAKEOVER) and the control modes (RATE, MIXED MASTER/SLAVE AND RATE, MASTER/SLAVE, and COMPUTER control).

STANDBY State - When the computer is in this state, control resides with the main program and the operator. By pressing the proper button on the control console, the user can enter a particular manual control mode or another computer state (see Figure 4).

Manual Control Mode - A manual control mode is the method through which the user analogically interacts with the arms. A control mode is independent of the state. For example, the control mode might be MASTER/SLAVE while the state is EDIT. There are three kinds of modes:

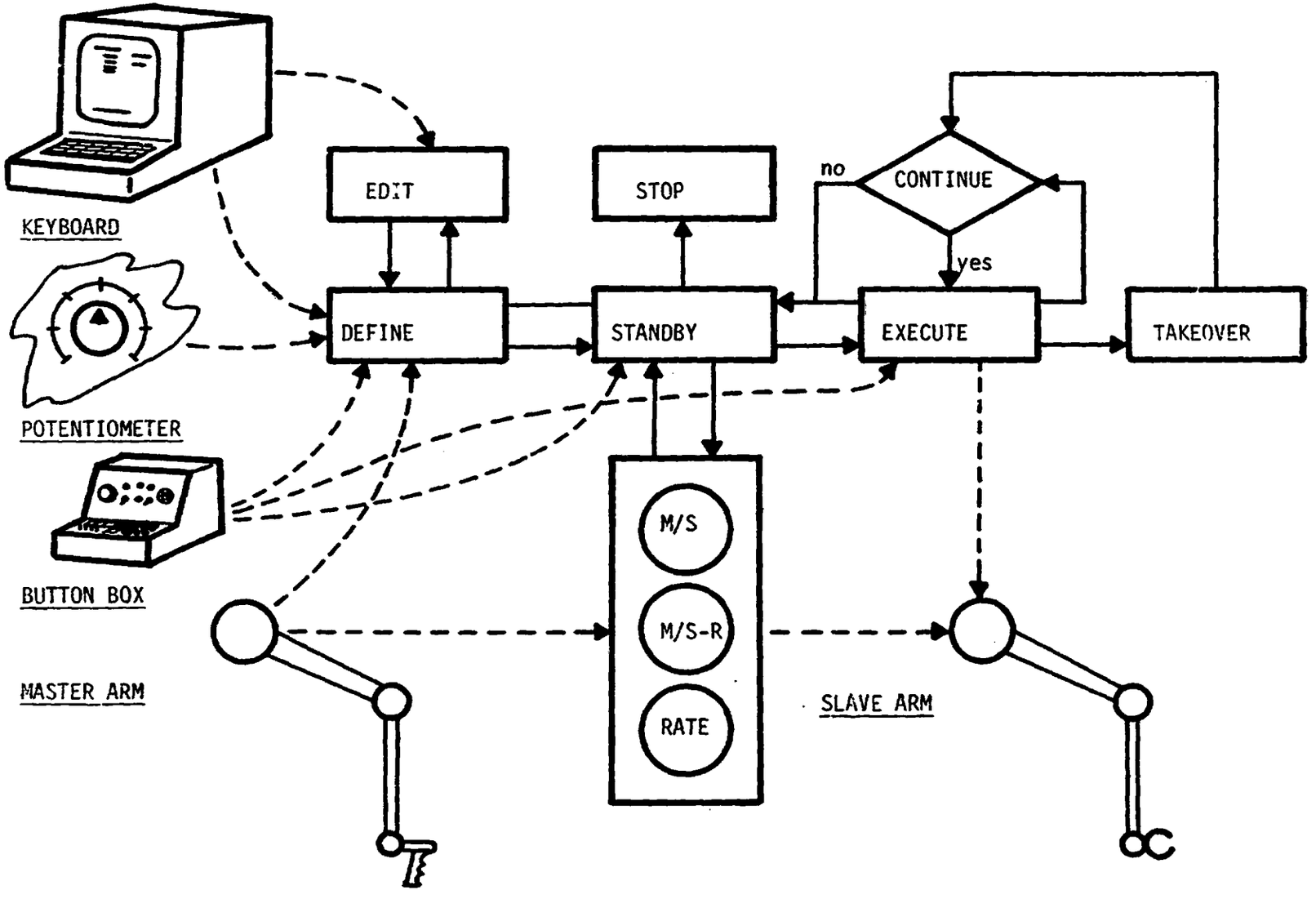

Figure 3. Block Diagram of SUPERMAN System

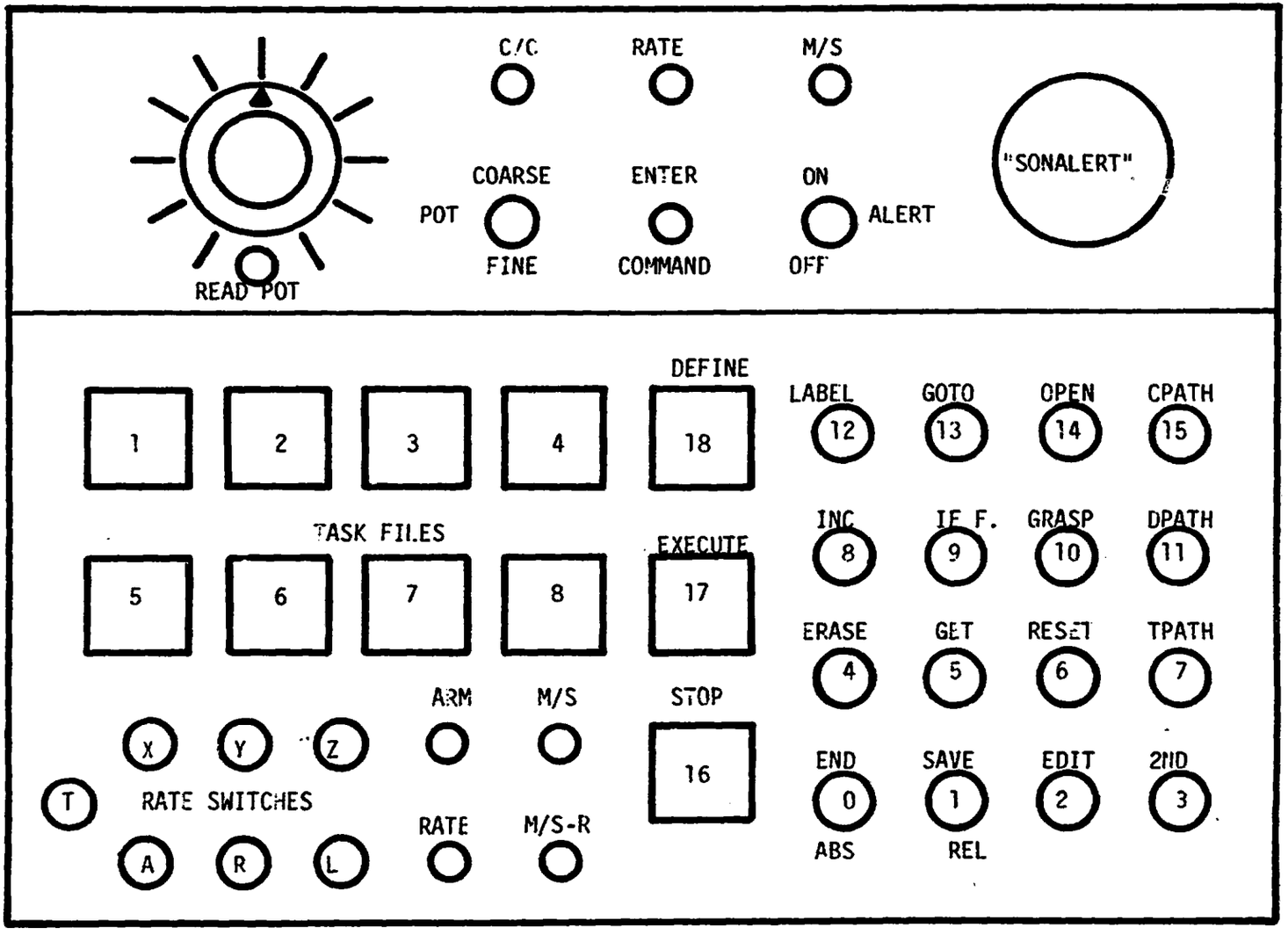

Figure 4. Special Control Console for SUPERMAN System

ORIGINAL PAGE IS
OF POOR QUALITY

a) RATE - The individual degrees of freedom are controlled through rate commands by switches on the control console and a potentiometer for rate adjustment. Both rate and resolved-motion rate are available.

b) MIXED MASTER/SLAVE AND RATE - The master acts as a spring-loaded joystick in the X, Y and Z axes, giving rate commands to the X, Y and Z axes of the slave proportional to displacement of the master. (The rate of the slave arm is then reflected in the force feedback level which the operator feels in the master.) Both rate and resolved motion rate control are available. The remaining degrees of freedom, the left and right elevation, the azimuth and the end-effector are controlled in a master/slave mode.

c) MASTER/SLAVE - The slave arm is driven to duplicate in position the action of the master. Any force felt by the slave is reflected to the master giving the operator force feedback (i.e. proportional to position disparity between master and slave).

DEFINE - DEFINE is the primary state through which the operator enters a string of commands to be executed. Commands are entered by pressing specially dedicated buttons for each function. All of the buttons used in the DEFINE state have dual functions (see Figure 4 - dual function buttons are 0-15).

EXECUTE State - As the title implies, the string of commands is executed through this state. During the execution of the command register, if the operator desires to take control, there are two methods available. The operator can take immediate control: (1) by pulling on the appropriate control stick (i.e. the MASTER in the case of MASTER/SLAVE or MIXED MASTER/SLAVE AND RATE modes or the rate switches in the RATE mode), or (2) by pressing the STOP button (all action ceases after the STOP button has been pressed until the operator signals for continuation or return to STANDBY). The operator can execute a string of commands which have been saved as a task file by pressing one of the lighted TASK FILE buttons. The operator also has the option of executing the current command register by pressing the EXECUTE button. This allows the operator to define a string of commands and immediately execute them to determine if any modifications are necessary. After the operator is sure the command string performs the desired function correctly, that function can then be saved as a task file or a named file.

TAKEOVER State - TAKEOVER is a transition state between control modes, i.e. from computer control to the control mode in effect before the EXECUTE command. Special problems result during this state due to the mismatch between the master and the slave at the time of the takeover. The diamond in Figure 3 signifies that after the mismatch has been dissolved, the operator has the option of moving into the STANDBY state or continuing the EXECUTION state.

The detailed meanings of the DEFINE buttons 0-15 are given below:

BUTTON Number	Command
0	END Final command used to signal completion of DEFINE state.
1	SAVE Used to save the command register on the disk as either a task file or a named file. A task file can be recalled only by one of eight buttons in the STANDBY state, whereas a named file is saved under a user-designated title and can only be recalled by the same name through the GET button (6) in the DEFINE state.
2	EDIT The EDIT command allows the user to modify the command register. The following options are available through the keyboard after entering the EDIT state; a) CHANGE A LINE b) INSERT A LINE c) DUPLICATE A LINE d) DELETE A LINE e) LIST COMMAND REGISTER f) RETURN TO DEFINE
3	2ND Used to enter the second function of dual command keys. The first function of each key is printed in black letters above the button. The second function is written below the button in gold letters. To enter a second function command, press the 2ND key and then the desired second command.
4	ERASE LAST LINE [ERASE] Used to erase the last entry in the command register.
5	GET Used to retrieve a named command file from the disk. GET asks for the name of the command file to be recalled and then locates the file, reads it into the command register (and returns to DEFINE state).
6	RESET Used to initialize the necessary internal variables and the command register to zero.

7 THROUGH PATH [TPATH]

Records the present position of the arm for use in EXECUTE as a through point. (A through point is a position which the operator desires the arm to move through without stopping, i.e. non-zero velocity point.)

8 INCREMENT (DOF) (XXXX)

Makes an incremental motion in the desired degree of freedom by a selected value. The user enters the INCREMENT command, then the degree of freedom (DOF), adjusts the desired increment (XXXX) through the potentiometer and presses the READ POT VALUE button directly beneath the potentiometer.

9 IF (DOF) FORCE.GT.
EXECUTE NEXT COMMAND

If the force level in the desired degree of freedom (DOF) is greater than the level set by the operator (XXXX) the following command is executed. If the force level is less than the level set by the operator, the command immediately following the IF FORCE.GT. statement is skipped during execution. The user enters the IF FORCE.GT. command, then the desired degree of freedom, adjusts the force level through the potentiometer.

10 GRASP WITH FORCE (XXXX) [GRASP]

The user enters the GRASP command and adjusts the force level through the potentiometer.

11 DISCRETE PATH [DPATH]

Records the present position of the arm for use in EXECUTE as a stopping point. During execution, the slave arm is moved from its current position to the recorded position with zero final velocity.

12 LABEL (XXXX)

Labels a position in the command register which can be returned to through a GOTO command. The user presses the LABEL button and then the number (XXXX) of the desired label.

13 GOTO (XXXX)

GOTO is a conditional command which moves to label (XXXX), unless the operator signals during execution to change the branch to (YYYY) by pressing a different button. To enter the command the operator presses the GOTO button and then the number (XXXX) of the label to which GOTO should branch.

14	OPEN Open jaws.	
15	CONTINUOUS PATH Records the position of the master manipulator every 0.1 second for use in EXECUTE. A continuous path is achieved by interpolating between the recorded positions.	[CPATH]
2ND - 0	ABSOLUTE Informs the execution compiler that the command register is to be executed exactly as recorded (see RELATIVE). The user enters the absolute command by pressing the 2ND button (#4) and then the ABSOLUTE button (#0).	
2ND - 1	RELATIVE Informs the execution compiler that the positions in the command register are to keep the same relative displacement with respect to each other, but are to be transformed so that the first position following the RELATIVE command corresponds to the position of the slave at the time of execution. A RELATIVE command can be cancelled by an ABSOLUTE command, with the result that only the positions between the RELATIVE and ABSOLUTE commands are transformed. The user presses the 2ND button (#4) and then the RELATIVE button (#1) to enter the command in the register.	
2ND - 2 through 2ND - 15	not assigned.	

As an example program consider a string of commands to take a nut off of a bolt and put it in a box. This program can be broken down into two major sections, one removes the nut and the other places it in the box. Since the user would prefer one nut removal program to be used for all nuts regardless of the orientation of the nut, a RELATIVE command should obviously be the first command in the register (the RELATIVE command and all of the following commands are briefly described under DEFINE). The entire command register for the nut removal program would be as follows. The following general formats will be followed throughout this example:

[BUTTON PUSH]
(POT READINGS)
"KEYBOARD COMMANDS"
COMPUTER REPLIES.

1	[RELATIVE]	
2	[LABEL] [1]	
3	[DPATH]	Place the slave on a nut and record that position by pressing the DPATH button.
4	[GRASP](200)	
5	[DPATH]	Turn the end effector 180° and record the position.
6	[INCREMENT] [Y](300)	Increment the slave by 300 counts in the direction that would pull the nut off.
7.	[IF FORCE.GT.][Y] (100)	If the force is greater than 100 in the Y direction, the nut is still on the bolt, therefore execute the next command.
8	[GOTO] [2]	
9	[GOTO] [3]	If the force had been less than 100 in the Y direction, the nut is free and this command would be executed.
10	[LABEL] [2]	
11	[INCREMENT] [Y] (-300)	Return the arm to position before incrementing in #6.
12	[OPEN]	Release the nut.
13	[GOTO] [1]	Return to LABEL 1 and continue turning the nut.
14	[LABEL] [3]	End of the first part of task - nut is off.
	[SAVE] "NUT-OFF"	Save command register as the named file "NUT-OFF" (typed in at the keyboard).

The second part of the task requires the manipulator to place the nut in a box. The entire command register for the program to put the nut in the box would be as follows:

1.	[ABSOLUTE]	The box would always be in the same place.
2	[TPATH]	Move the slave to a position just over and above the outside edge of the box and record this position by pressing the TPATH button.
3	[DPATH]	Move the slave to a position over the center of the box and record the position.
4	[OPEN]	
5	[TPATH]	Enter same position as in #2 by duplicating line 2.

[SAVE] "NUT-IN-BOX"

At this point the operator could call either program and execute it. The NUT-OFF program would simply take the nut off and return control to the operator as soon as the nut was free. But the present status of each file (i.e., a named file) requires that the operator type in each name to obtain the file to execute it. If the operator performs the following commands the file will be saved as a task file which is immediately executed at the touch of a button:

[GET] "NUT-OFF"

[GET] "NUT-IN-BOX"

The computer will reply by stringing the two files together as one file. Then enter:

[SAVE] "TASK-FILE"

and press the button which will retrieve the file (e.g., button #1). To remove a nut and put it in the box the operator simply presses the same button, the execution compiler transforms the first half of the register relative to the position of the slave at the instant the button is pressed and then executes the program. After the nut is removed and placed in the box the slave returns to the operator's position and the computer relinquishes control.

SESSION G: DISPLAYS

Chairman: H. Jex

358
PAGE INTENTIONALLY BLANK

D25

DISPLAY AIDS FOR REMOTE CONTROL OF UNTETHERED UNDERSEA VEHICLES*

W. L. Verplank

Man-Machine Systems Laboratory
Department of Mechanical Engineering
Massachusetss Institute of Technology
Cambridge, Massachusetts 02139

N79-15613

Abstract

A "predictor" display superimposed on slow-scan video or sonar data is proposed as a method to allow better remote manual control of an untethered submersible. Simulation experiments show good control under circumstances which otherwise make control practically impossible.

1. Introduction

Untethered, unmanned submersibles have been limited to automatic control on simple pre-programmed or target-seeking trajectories. More precise navigation and obstacle avoidance will require increasingly sophisicated automatic control and/or direct control from the surface. Direct human control through a sonic communication channel will be difficult because of the low bandwidth and the signal travel time. Probably the most productive approach will be a combination of elementary automatic control such as is possible with some present-day tethered submersibles (e.g., altitude or depth and heading control) plus display aids which make control easier for the operator. This paper proposes a display aid which is particularly applicable to the problems of time-delay and slow frame-rate.

2. The Problem

For remote control, there are two sources of difficulty with sonar communications: time-delay and slow-frame-rate. Round trip time-delay is the time for a command to travel to the vehicle and the first indication of response to travel back. At a minimum this will be two times the distance divided by the speed of propagation, 2T. For example, T = 1 second at about 5,000 feet.

Pictorial information from television camera or obstacle avoidance sonar will be further delayed because of limited channel capacity. Assuming a low resolution picture of 80 K bits and a channel capacity of 10K bits/sec., there would be at most, one picture every 8 seconds (S = 8 seconds).

The effects of trying to navigate with just this pictorial information are illustrated in Figure 1.

---

* This work was supported in part by ONR Contract N00014-77-C-0256. The untethered vehicle control problem was suggested in discussions with the Harbor Branch Foundation and the M.I.T. Office of Sea Grant.

360 PAGE INTENTIONALLY BLANK

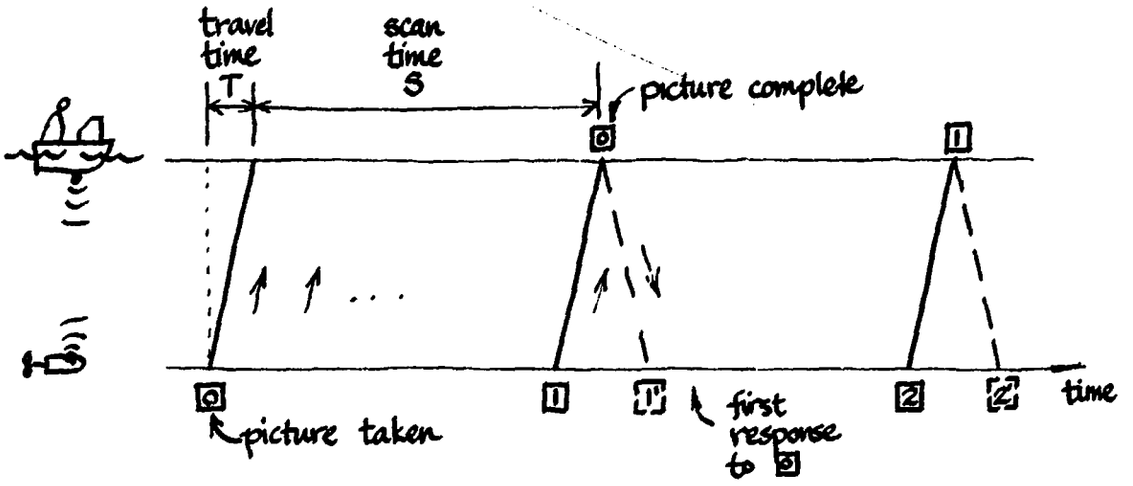

Figure 1a. Effect of delays from transport time (T) and scan time (S).

The picture from 2 is received T + S seconds after it is taken; the first operator response is received by the vehicle at least T seconds later, for a total delay of 2T + S seconds. While the operator is looking at the still picture from 2 the commands he is sending are actually moving the vehicle from 1' to 2', as illustrated in Figure 1b.

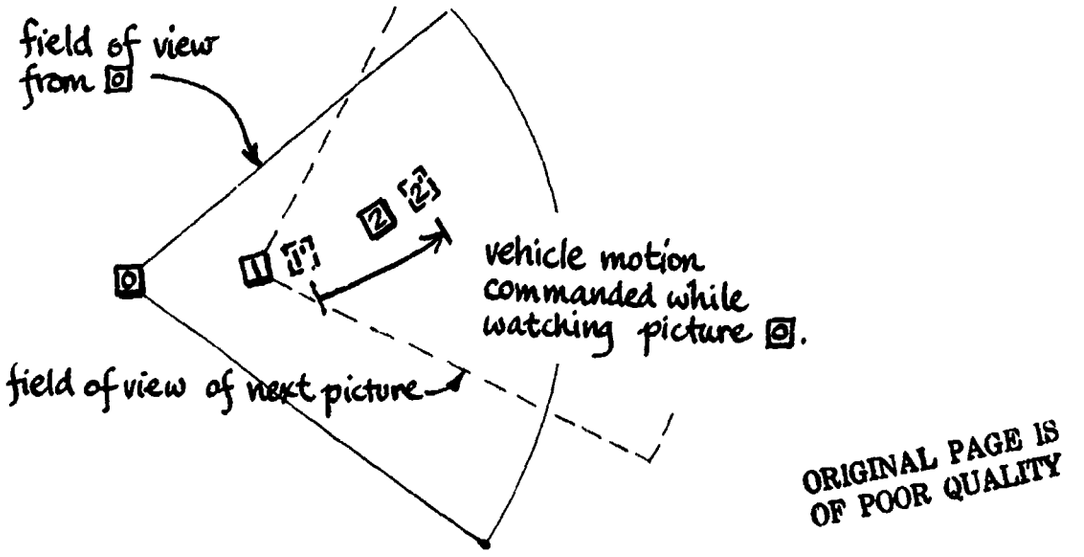

ORIGINAL PAGE IS OF POOR QUALITY

Figure 1b. Positions of vehicle at times in Figure 1a.

ORIGINAL PAGE IS
OF POOR QUALITY

3. Predictor Display

Predictor displays were first used for submarine control (Kelley, 1968). NASA considered predictor displays for remote control of unmanned lunar roving vehicles (Arnold, 1963) but sent men instead.

The predictor display proposed here presents a symbol superimposed on the slow-frame-rate and time-delayed picture from the vehicle's television camera. The symbol responds instantansously and continuously to the operator's commands predicting "future" positions of the vehicle. For example, refering to Figure 1b, when 2 is complete the predictor symbol would show the position 1'. Before the next picture from 1 arrives, the symbol will be moved, in response to the operator's commands, to position 2'.

The position of the vehicle is computed from a local model of the vehicle response and the operator's commands u(t), as shown in Figure 2.

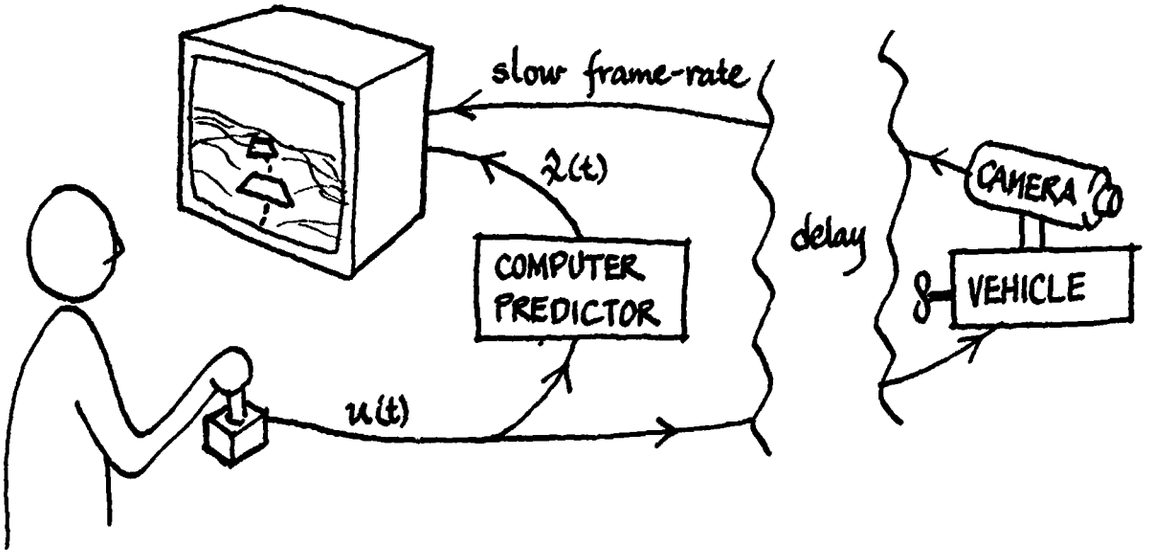

Figure 2. Predictor display superimposed on pictorial data

Pictorial or Map Displays

The predictor symbol may prove useful both on pictorial displays (superimposed on television or obstacle-avoidance sonar) and on map-like position displays. Map displays would avoid one difficulty of pictorial displays, which is loosing the predictor symbol when it moves out of the field of view of the camera (for example, moving sideways or backward).

Auxiliary Position Data

If position data is available from transponders or locator beacons, it could be used to update the vehicle model. With just the pictorial data, the open-loop prediction would have to span an interval of (at least) 2T + S to (at most) 2T + 2S seconds. With auxiliary feedback the open-loop estimate will only need to span the delay of that auxiliary data (at minimum 2T). The signals and corresponding delays are shown in Figure 3. (u(·), command vector; x(·), vehicle location data).

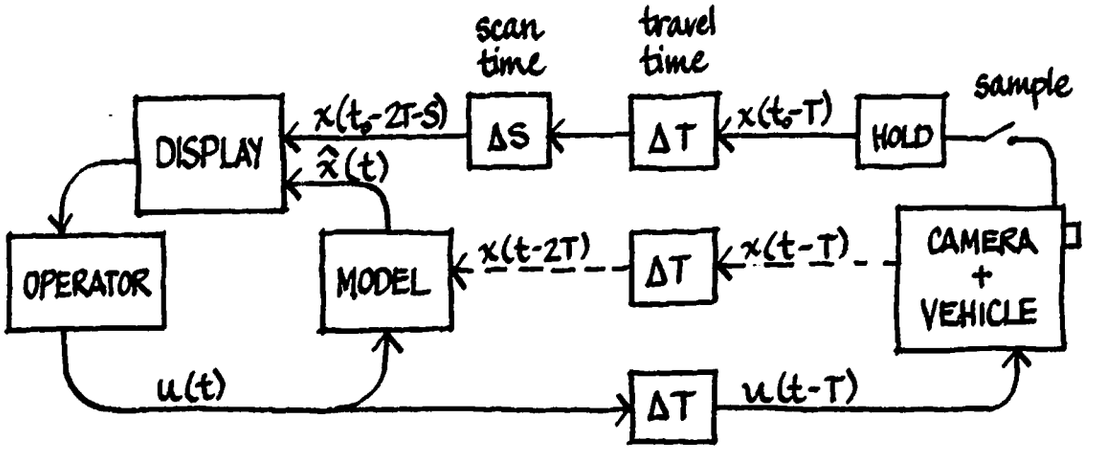

Figure 3. Delays associated with predictor calculation

Adaptive Estimation

Another feature that could be built into the local model of the vehicle is some estimate of the disturbances (such as current). The current model as well as the vehicle model could be updated on the basis of the mismatch between predicted and measured vehicle position.

4. A Demonstration Experiment

In order to explore the effects of the predictor display, an interactive simulation was written on an Interdata 70 computer and Imlac graphic display. A random terrain was generated and displayed in perspective, updated every 8 seconds, to simulate the pictorial information. A moving predictor symbol was generated respresenting the vehicle as a square in perspective. Two straight ridges were added to the random terrain to serve as a test course. (Figure 4).

ORIGINAL PAGE IS
OF POOR QUALITY

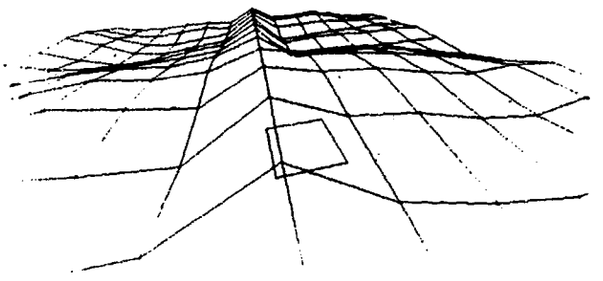

Figure 4. Computer-generated terrain with predictor symbol

The simulated vehicle was controlled by the operator with a spring-centered 2-degree-of-freedom joystick. The dynamic response of the vehicle was simple integration with forward speed proportional to forward-back position of the stick and turn-rate proportional to left-right position of the stick. The vehicle was always the same height above the terrain (simulating automatic altitude hold). No disturbances such as currents were simulated. Also, it was found important to have a good detent and dead-zone on the stick to avoid inadvertent commands.

A stationary "table" was drawn to indicate where the next picture was to come from while the "real-time" predictor continued to move in response to the operator's commands (Figure 5). Dotted lines were added to this table to indicate the field of view. This reduced the considerable confusion about how the picture was expected to change and served as a guide for keeping the vihicle within its own field of view, which is the best strategy for using this kind of predictor on the pictorial display.

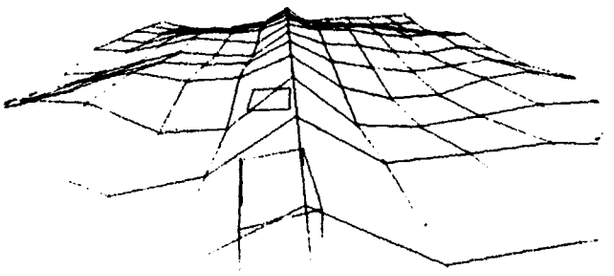

Figure 5. Predictor plus "table" showing from where next picture will come

Results

A typical path, without the predictor, is shown in Figure 6. The dotted lines represent ±1 terrain-unit from the ridge. The circles represent the vehicle's position every 2 seconds. V's represent the field of view of each picture sent. Quite often there is no movement between successive dots (2 secs.) or successive pictures (8 seconds.)

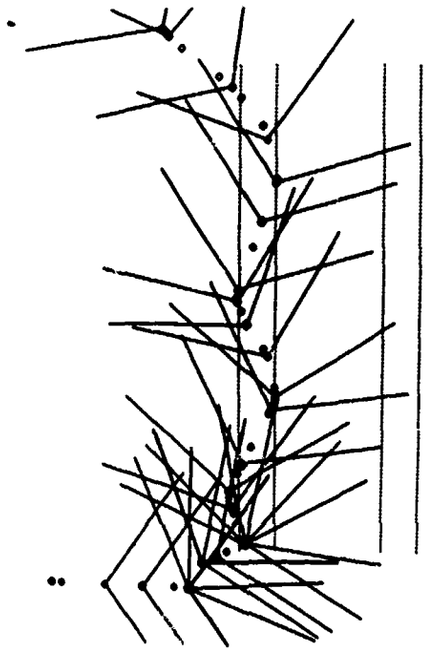

Figure 6. Typical path with no predictor

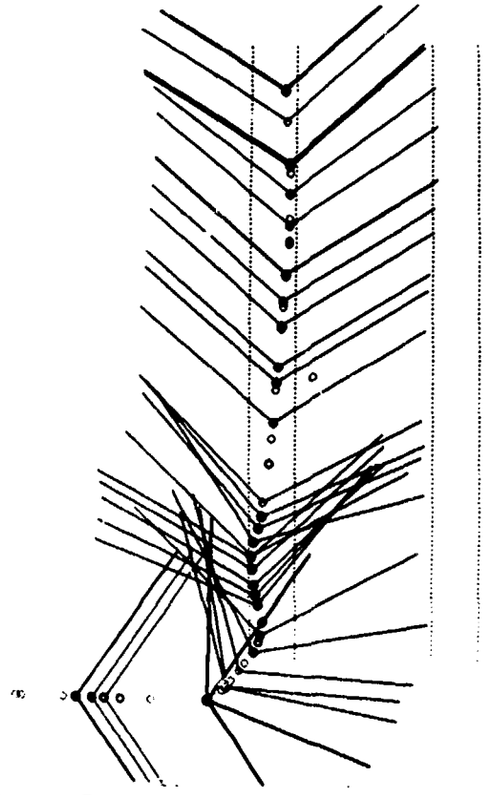

Figure 7. Success at slow speed with no predictor

Only with extremely slow speed was it possible to keep track of the ridge. Approximately five minutes and 40 pictures were required to traverse just one of the ridges (half the course) This is shown in Figure 7.

With the predictor symbol, practically continuous motion was possible. A typical path is shown in Figure 8. The course was completed in 3 minutes and 23 pictures.

ORIGINAL PAGE IS
OF POOR QUALITY

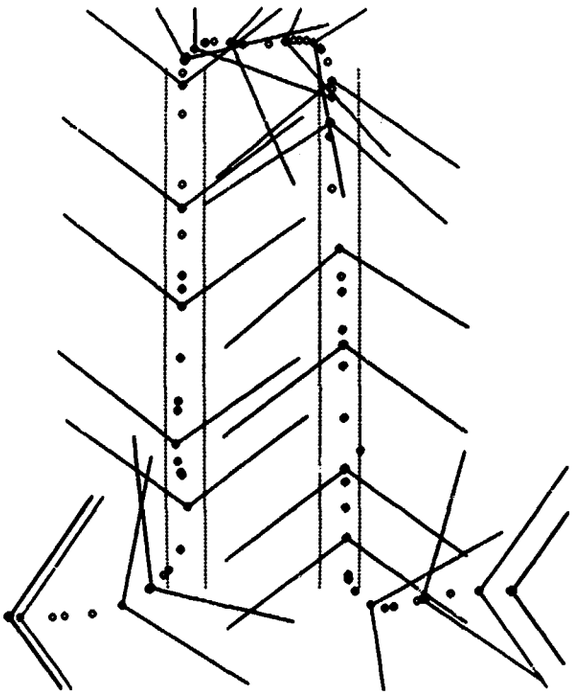

Figure 8. Path with predictor display

Request Mode

One unexpected finding from these experiments was that rather than sending the picture periodically every eight seconds, sending the picture only upon the operator's request reduces the total number of pictures necessary and encourages a "move and wait" strategy which avoids confusion. The difference is illustrated in Figure 9.

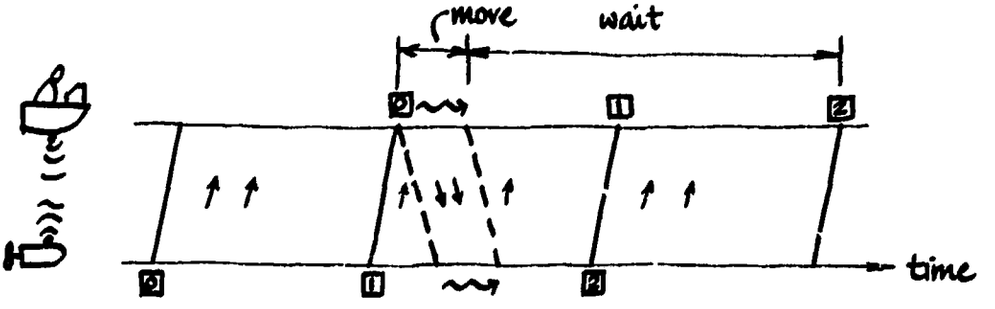

Figure 9a. New picture every 8 seconds: "periodic mode"

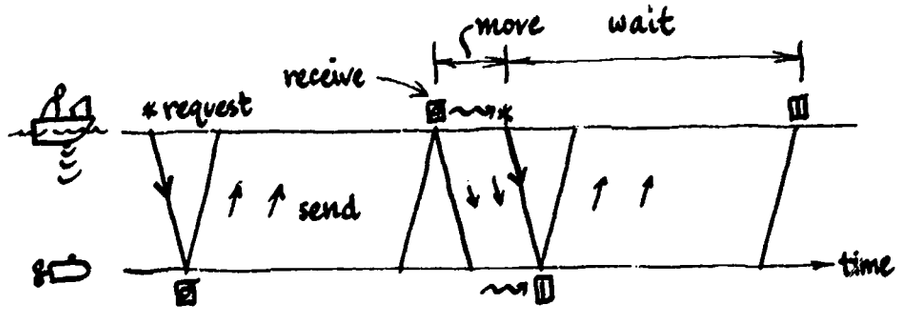

Figure 9b. New picture upon request: "request mode"

In the periodic mode (Figure 9a) a short move starting with the receipt of picture 2 will not be reflected in the next picture, 1 , as the operator might expect; instead he has to wait for 2 . In request mode (Figure 9b), the wait for pictorial confirmation is minimized.

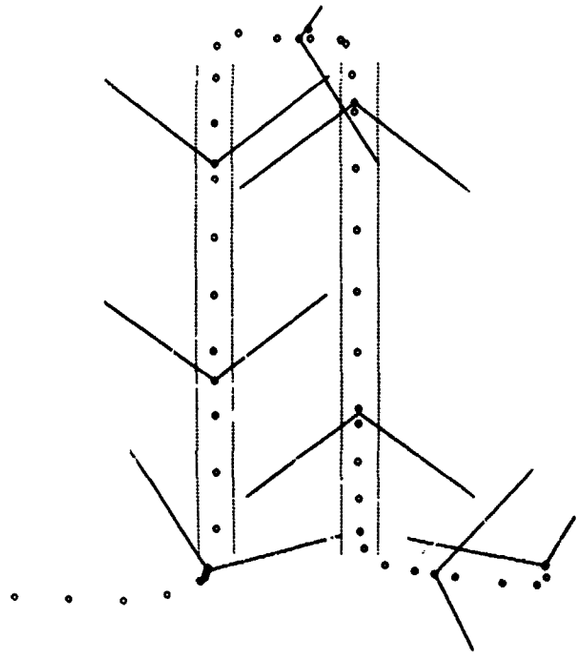

Figure 10. Typical path in the request mode

A typical path in request mode (using the predictor) is shown in Figure 10. Compared to periodic mode, the time is about the same but the number of pictures used in one-half to one-third; velocities are higher but there is a wait for 10 seconds as each picture is taken and sent.

On an actual vehicle, probably both modes should be available with the request mode used when move-and-wait strategy is appropriate (for precise positioning based on pictorial feed-back, and when environmental disturbances are small). Periodic mode is probably more appropriate for less precise navigation and continuous motion when the predictor symbol can be relied upon.

Another trade-off that should probably be built into the pictorial feed-back is variable frame-rate/resolution. In a more dynamic and uncertain environment (i.e., larger bandwidth disturbances or target motion) sampling rate will want to be higher at the expense of resolution.

6. Conclusions and Recommendations

For the conditions studied (T = 1 sec., S = 8 sec.) manual control is not feasible without display aids such as the predictor symbol. The request mode is preferred as it seems to avoid confusion and reduce the number of pictures necessary.

The present results are at best preliminary. We studied only very simple vehicle dynamics and only one set of delay conditions. Further study with laboratory simulation can investigate:

1) more realistic vehicle dynamics,

2) environmental uncertainties such as drift,

3) a broader range of delay conditions and

4) various degrees of partial automation.

Also, the predictor displays (both pictorial and map) could be used on existing tethered vehicles to simulate untethered operation and evaluate the potential for untethered operation.

References

Kelley, C. R., Manual and Automatic Control, Wiley, New York, 1968.

Arnold, J. E., and Braisted, P. W., Design and Evaluation of a Predictor for Remote Control Systems Operating with Signal Transmission Delays, NASA TN D2229, 1963.

N79-15614

A SAFETY MARGIN AND FLIGHT REFERENCE SYSTEM AND DISPLAY FOR POWERED-LIFT AIRCRAFT*

by Robert K. Heffley
Systems Technology, Inc.

and Gordon H. Hardy
NASA Ames Research Center

SUMMARY

A study was conducted to explore the feasibility of a safety margin and flight reference system for those powered-lift aircraft which require a back-side piloting technique. The main objective was to display multiple safety margin criteria as a single variable which could be tracked both manually and automatically and which could be monitored in order to derive safety margin status. The study involved a pilot-in-the-loop analysis of several system concepts and a simulator experiment to evaluate those concepts showing promise. A system was ultimately configured which yielded reasonable compromises in controllability, status information content, and the ability to regulate safety margins at some expense of the allowable low speed flight path envelope. It was necessary, however, to utilize an integrated display of two variables — one to be tracked in a compensatory manner and one to be monitored. The variables themselves consisted of linear combinations of the computed critical safety margin and pitch attitude, and the proportions of the combinations were definable in terms of the aforementioned compromises.

SYMBOLS

k	Weighting coefficient for pitch attitude
N_H	Engine rpm
V	Airspeed
V_{Lin}	Minimum airspeed at approach thrust
V_{min_m}	Minimum airspeed at maximum thrust
α	Angle of attack
α_{max}	Maximum allowable angle of attack
γ	Aerodynamic flight path angle
θ	Pitch attitude

* This study was performed under Contract NAS2-9418.

PAGE INTENTIONALLY BLANK

INTRODUCTION

The pilot's control technique for a powered-lift aircraft in the approach flight phase is inherently different from that for a conventional aircraft. The pilot (or autopilot) of the powered-lift aircraft cannot simply use 1.3 times the power-off stalling speed (for the approach configuration) as the target airspeed or "flight reference" and be guaranteed adequate safety margins. Since a powered-lift aircraft derives a significant part of its lift from a thrust vector which is inclined nearly perpendicular to the flight path, the minimum speed is determined to a large extent by the thrust or power setting. This is in dramatic contrast to the characteristics of a conventional aircraft as shown in Fig. 1. Note that the approach speed for a powered-lift aircraft may be in the neighborhood of the idle thrust stalling speed (Point A in Fig. 1).

In addition to the problem of selecting a suitable speed (or other parameter) to use as a flight reference which will ensure adequate safety margins, the pilot may have to cope with some other unusual flight characteristics. For example, most powered-lift aircraft approach at speeds on the "backside" of the thrust required curve. Consequently, a "backside" or "STOL" control technique is usually used, i.e., the pilot uses pitch attitude to regulate airspeed and modulates thrust to control flight path. A typical flight characteristic resulting from this mode of control and from the thrust vector being inclined nearly perpendicular to the flight path is shown in Fig. 2. That is, if the pilot is using airspeed as a flight reference (i.e., maintaining a constant airspeed), it can be seen that to steepen the descent path angle the pilot must increase pitch attitude! This is contradictory to all normal practice and can make airspeed a very confusing flight reference.

Because of these problems, the pilots of airplanes such as the NASA Augmentor Wing Jet STOL Research Aircraft (AWJSRA) must use a combination of airspeed, angle of attack, and pitch attitude as a flight reference. Only through extensive experience are these pilots able consistently to maintain adequate safety margins. While this use of a complex flight reference has been acceptable in the research environment, it would not be acceptable operationally.

OBJECTIVE

The objective of the program, therefore, was to find a single display to be used for maintaining a safe flight condition in powered-lift aircraft. Several features needed to be considered, however, which significantly complicated the design of such a system. These are shown in Fig. 3.

The present study was primarily a feasibility study and was limited to an analysis and simulation phase. The results to be presented were obtained in the context of (i) an existing powered-lift STOL airplane (NASA AWJSRA),

ORIGINAL PAGE IS
OF POOR QUALITY

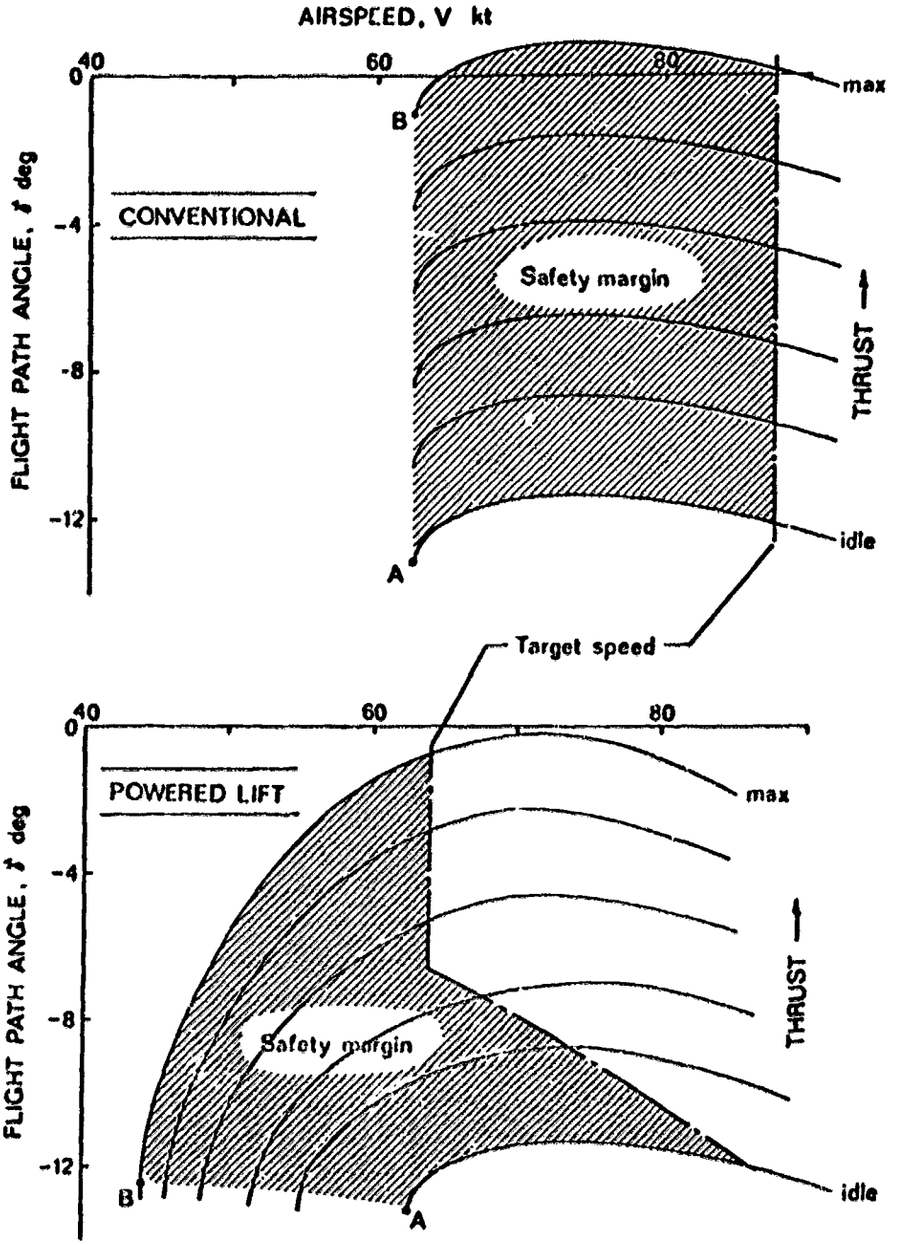

Figure 1. Comparison of γ - V Plots Between a Conventional and a Powered-Lift Aircraft.

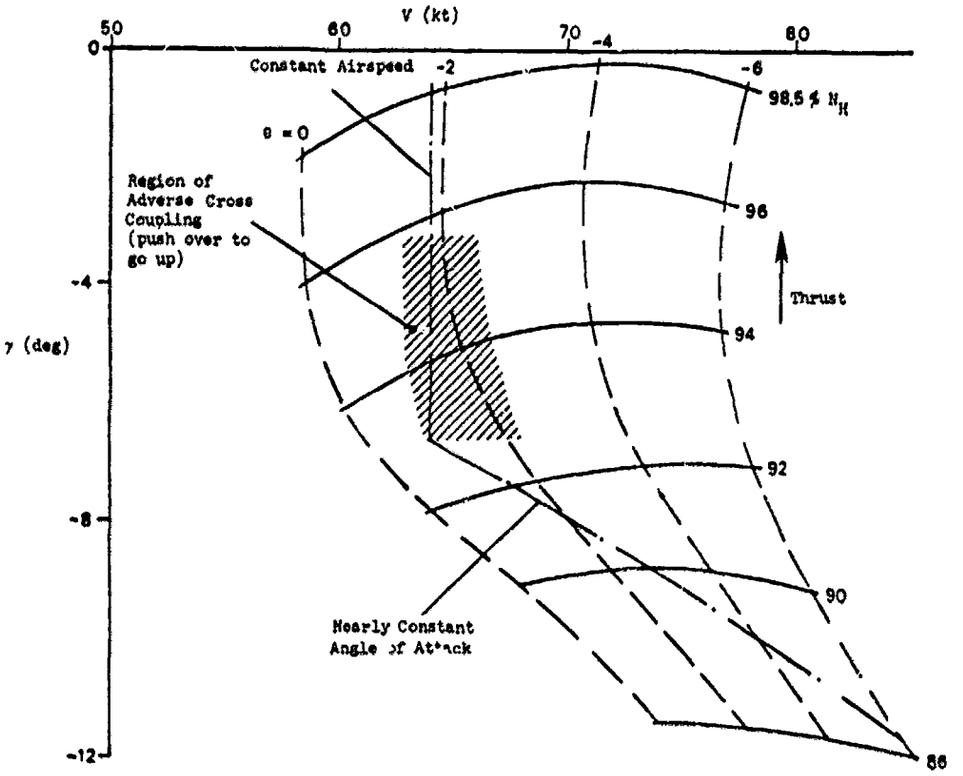

Figure 2. γ - V Curve Showing Region of Adverse Cross Coupling Along Trajectory of Desired Airspeed.

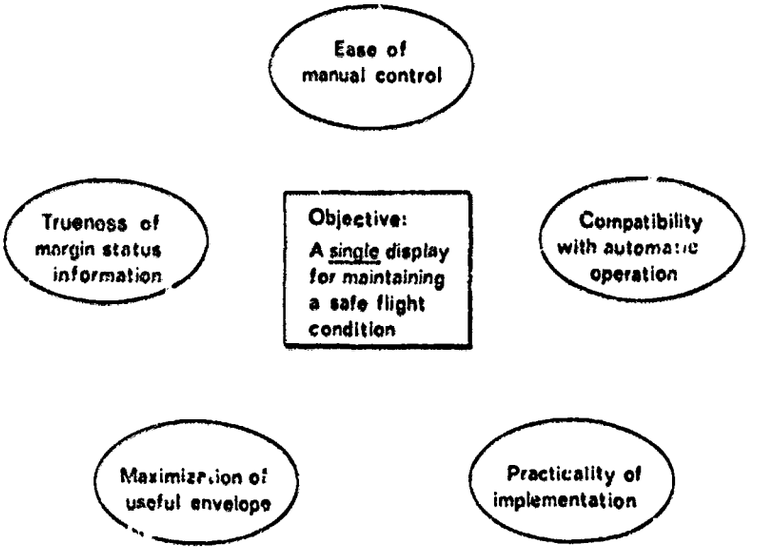

Figure 3. Tradeoffs Involved in the System Design.

C-5

(ii) existing avionics hardware (STOLAND guidance, control, and navigation system, Ref. 1), and (iii) severe atmospheric disturbances encountered during the landing approach flight phase.

TECHNICAL APPROACH

An extensive study of airworthiness requirements which is described in Refs. 2 and 3, defined the required safety margin criteria for powered-lift aircraft in terms of the instantaneous angle of attack and airspeed. The suggested criteria from Ref. 2 are listed in Table 1. Figure 4 shows these criteria superimposed on the AWJSRA flight envelope. The present study assumed these safety margin criteria for the purpose of defining the available flight envelope. Note that only two criteria dominate, i.e., airspeed must be greater than the minimum speed at maximum thrust plus 20 knots and the angle of attack must be such that a 20 knot vertical gust will not result in exceeding the maximum allowable angle of attack. The resulting flight envelope is bounded in Fig. 4 by the lines labeled "minimum safe airspeed."

Table 1. Safety Margin Criteria.

(All Engines Operating)

$V > 1.15\, V_{min}$ (approach thrust)	
$V > V_{min} + 10$ knots (approach thrust)	
$V > 1.3\, V_{min_m}$ (maximum thrust)	
$V > V_{min_m} + 20$ knots (maximum thrust)	Most Critical Criteria
$\alpha < \alpha_{max} - \sin^{-1} \frac{20 \text{ knots}}{V}$ (vertical gust margin)	Most Critical Criteria

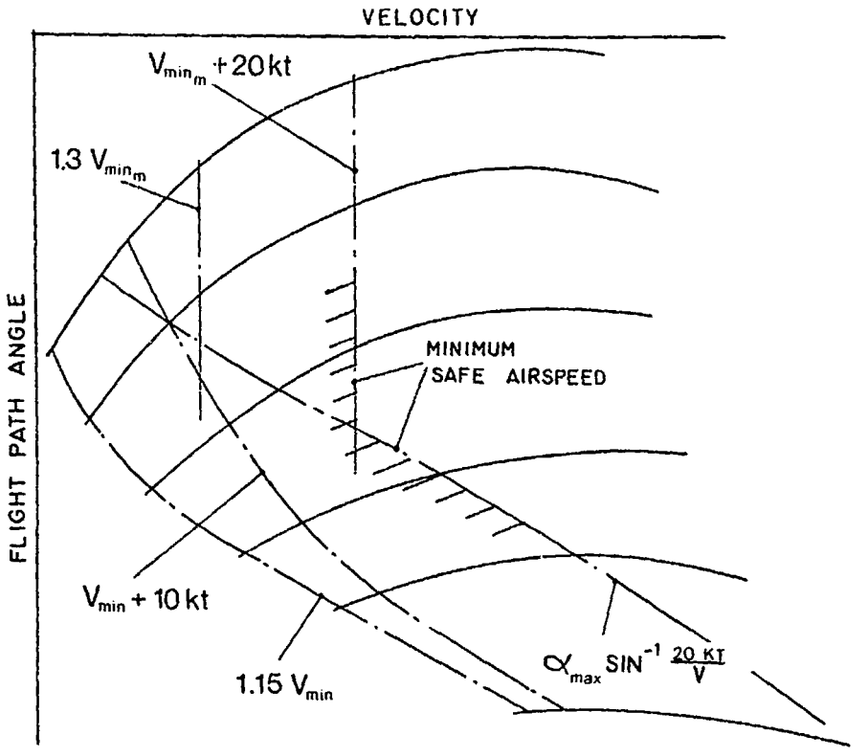

Figure 4. Relationship of Various Safety Margin Criteria.
(Corresponding to Table 1 for the AWJSRA)

A large number of possible flight reference and safety margin mechanizations that were consistent with this flight envelope were examined and are described in detail in Ref. 4. The analysis utilized multiloop control system analysis methods and considered: (1) ease of control, (2) display of safety margin status, (3) pilot and automatic system performance in maintaining safety margins, and (4) system mechanization as they relate to sensor and computational requirements. The purpose of the analysis was to sort through the large number of possibilities to find a few which would be worthwhile examining during the simulation phase.

RESULTS

From the large number of implementation concepts considered, one was found to meet design objectives satisfactorily. Although it consisted of a single display, two variables were involved. One variable was actively tracked and thus served as a flight reference. The other variable was simply

ORIGINAL PAGE IS
OF POOR QUALITY

monitored in order to obtain high quality status information. This implementation can be summarized as:

$$[\text{Tracked Variable}] = [\text{Actual Margin}] + k \cdot [\text{Pitch Attitude}]$$

$$[\text{Monitored Variable}] = [\text{Actual Margin}]$$

where the actual margin is taken as the most critical of applicable airspeed and angle of attack safety margin criteria from Table 1.

It is significant that the tracked variable was composed of a simple linear combination of actual margin and pitch attitude. This implementation permitted a direct tradeoff between ideal status information and easy controllability depending upon the weighting factor, k. A single value of k was found to provide satisfactory compromises in the various tradeoffs shown previously in Fig. 3*.

The manner in which the two variables were displayed was important to the success of the system. The main hardware element of the display was the SUNDSTRAND Electronic Attitude Director Indicator (EADI) shown in Fig. 5. Safety margin information was presented along the vertical scale on the far left-hand side.

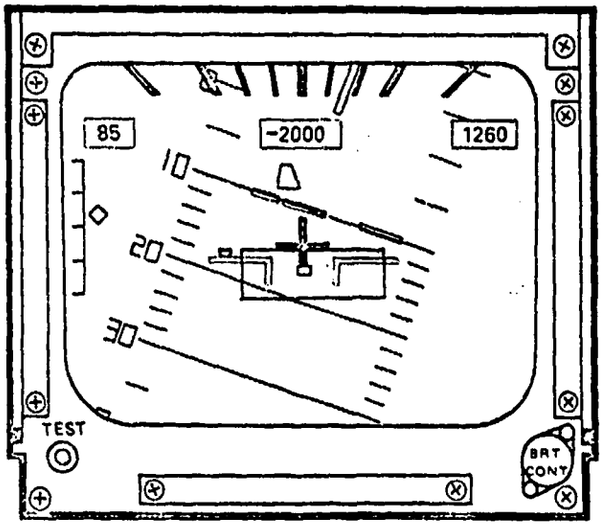

Figure 5. Overall EADI Presentation.

* This value amounted to 10% safety margin change per degree pitch attitude change where the nominal operating point was at 100% allowable safety margin.

Details of the safety margin system presentation are described in Fig. 6. Note that the tracked variable is displayed directly on the moving pointer, but that the monitored variable is displayed as the distance between the moving pointer and a moving scale "floor." This configuration provided good relative emphasis on the two variables and did not confuse their respective roles in the pilot's mind.

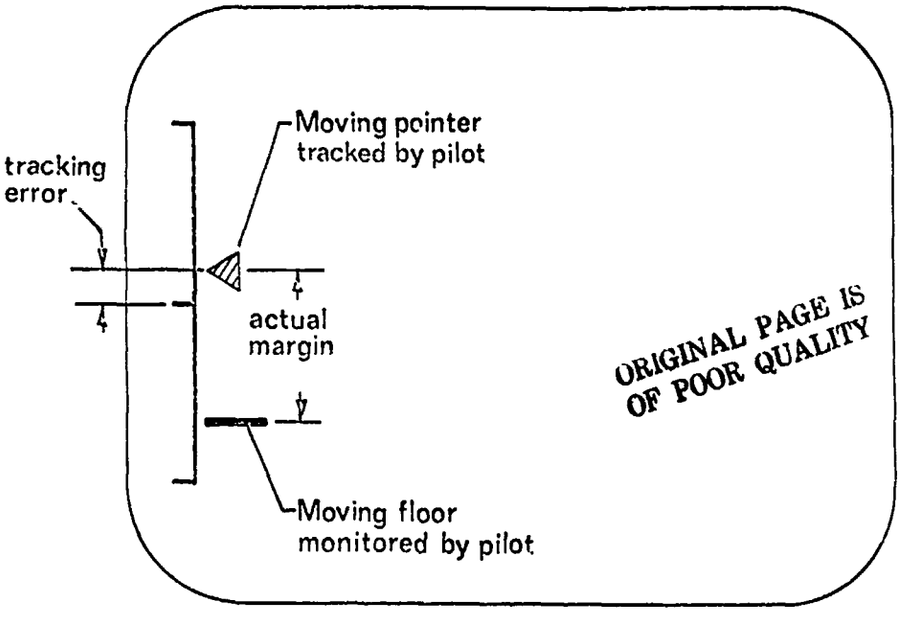

ORIGINAL PAGE IS OF POOR QUALITY

Figure 6. Details of Safety Margin System Display on EADI.

CONCLUSIONS

The study reported in this paper was successful in evolving a useful safety margin system and display for a powered-lift aircraft. The flight reference implementation found most effective involved a blend of the safety margin and a linear function of pitch attitude. This concept provided (i) an easily controlled variable, (ii) correct sensitivity to gusts, (iii) a guide to correct control action for obtaining good safety margin performance, (iv) acceptable performance in the presence of large atmospheric disturbances, and (v) the concept was relatively easily implemented. The main compromise resulting from the use of this concept was a reduction in available flight envelope in order to enhance certain controllability features. (The nominal operating point was approximately 5 knots faster than the minimum approach speed permitted by applicable safety margin criteria.) The envelope compromise was, however, controllable in a rational and predictable way by the flight reference weighting coefficient. Finally, the results of the study have provided the necessary groundwork for a flight investigation.

ORIGINAL PAGE IS
OF POOR QUALITY

REFERENCES

1. Grgurich, John; and Bradbury, Peter: STOLAND Final Report. NASA CR-137972, 1976.

2. Scott, Barry C.,; Martin, Paul W.; Hynes, Charles S.; and Bryder, Ralph B.: Progress Toward Development of Civil Airworthiness Criteria for Powered-Lift Aircraft. FAA-RD-76-100, 1976.

3. Heffley, Robert K.; Stapleford, Robert L.; and Rumold, Robert C.: Airworthiness Criteria Development for Powered-Lift Aircraft. A Program Summary. NASA CR-2791 or FAA-RD-76-195, 1977.

4. Heffley, Robert K.; and Jewell, Wayne F.: Study of a Safety Margin System for Powered-Lift STOL Aircraft. NASA CR-152139, 1978.

D27

N79-15615

A HEAD-UP DISPLAY FOR MID-AIR DRONE RECOVERY

W. L. Augustine, E. L. Heft

Air Force Flight Dynamics Laboratory
Wright-Patterson AFB, Ohio 45433

T. G. Bowen

11th Tactical Drone Squadron
Davis-Monthan AFB, Arizona 85707

and

R. L. Newman

Crew Systems Consultants
Yellow Springs, Ohio 45387

SUMMARY

During mid-air retrieval of parachute packages, the absence of a natural horizon creates serious difficulties for the pilot of the recovery helicopter. A head-up display (HUD) was tested in an attempt to solve this problem. Both a roll-stabilized HUD and a no-roll (pitch only) HUD were tested.

The results show that fewer missed passes occured with the roll-stabilized HUD when the horizon was obscured. The pilots also reported that the workload was greatly reduced. Roll-stabilization was required to prevent vertigo when flying in the absence of a natural horizon. Any HUD intended for mid-air retrieval should display pitch, roll, sideslip, airspeed, and vertical velocity.

INTRODUCTION

One of the most successful ways to recover drones is the mid-air retrieval system (MARS). During these recoveries, a parachute system is deployed from a descending drone prior to retrieval. A typical parachute system consists of an engagement parachute connected by a load line to the drone and a main parachute canopy supporting the drone. The main canopy is designed to release when the load line from the drone to the engagement parachute is under tension. The load line is routed up the main canopy risers to a break-tie at its apex, then up to the engagement parachute.

To recover the drone or other object, the pilot flies the helicopter to approach the engagement parachute from the side opposite the load line.

PAGE 380 INTENTIONALLY BLANK

This location is shown by an aiming panel on the main canopy. The helicopter has three hooks rigged below it which catch load carrying members in the engagement parachute. These hooks are connected to an energy absorbing winch aboard the helicopter. As the load line absorbs the tension after engagement, the apex tie releases, followed by main canopy separation, and the drone is carried by the load line supported from the helicopter. Figure 1 shows the helicopter and parachute system just prior to engagement.

Safe and consistent MARS operations depend on the pilot's ability to match the helicopter's vertical velocity with the parachute's while closing with the top of the engagement parachute. At the same time, the helicopter must approach from a specific direction to ensure that the load line will not be pulled through the main canopy.

The pilot's primary visual cue is the alignment of the helicopter, the top of the engagement parachute, and the horizon. If the horizon is obscured by smoke, haze, or clouds, or if false horizons are present, the pilot has extreme difficulty in judging his position relative to the target. Under these circumstances, attempted recovery can be dangerous and fruitless.

Variations in the size of the parachute canopies can produce illusions of being too high or too low relative to the engagement parachute. The pilot must allow the canopy top to pass beneath the fuselage as the helicopter closes with the engagement parachute. The apparent change in position from level to approximately twelve feet below the helicopter can make engagement difficult to judge. These visual problems are compounded by the need for precise heading and roll control since any degree of uncoordinated flight is magnified in the pole position. Airspeed must be maintained within a small band (45 to 60 knots) for proper operation of the energy absorbing winch.

The head-up display has been used to assist pilots during visual tracking tasks. The HUD is an outgrowth of the reflecting gunsight and presents flight instrument data in the pilot's field of view as he looks at external visual cues. To date, HUDs have been applied to two main areas: weapons delivery(1) and landing approach(2,3). A survey of HUD technology is also available(4).

HUDs serve to combine real world visual cues with derived data. These data sources are complementary. It would be difficult to reproduce the real world cues artificially. At the same time, the derived data presents information that the pilot cannot perceive directly, or only with great difficulty. One must be careful, however, to ensure that both data fields are compatible. As Singleton points out(5), there is a basic incompatibility between the redundant, analogue data of the real world and the symbolic, often digital data of artificial displays. The problem is further complicated by the need for careful attention to retain proper balance, so that the proper display (real world or artificial data) dominates. During visual tracking, the real world must dominate with the flight instrument data providing supplementary information. The roles reverse during instrument flight. However, the HUD must not be such a compelling sight that the pilot fixates on it to the exclusion of the real world. This has definite implications on pilot learning and has been reported elsewhere(2). These comments were verified by conversa-

tions with HUD-qualified pilots prior to the development of the test plan for this study, as well as during preliminary HUD flights.

EQUIPMENT DESCRIPTION

The particular HUD evaluated in this study is a modified electro-mechanical unit manufactured by Sundstrand Data Control. The system consists of two pilot display units, a control module, and a computer. The HUD was developed from a commercial transport display known as the Visual Approach Monitor (VAM). The VAM presents pitch and longitudinal flight patch information to the pilot. No roll or heading information is supplied. The VAM was designed to minimize the problems of judging final approach path angles during visual approaches. It is presently in operational use with Pacific Western Airlines in their arctic support flights(3). It has also been evaluated in several military and civilian airplanes.

Roll information is not considered essential since the VAM was designed for use on final approach in visual conditions only. Later VAMs incorporate an airspeed index showing deviation from a reference speed. A color-coded index shows deviation with a red S for slow, a yellow F for fast, and a green O for correct airspeed. This peripheral cue is similiar to the angle-of-attack indexes on some military airplanes.

The Light Line is a further development of the basic VAM display. Developed under support from the AFFDL, the Light Line presents both pitch and roll information as well as a flight path angle display appearing as a beam of light emanating from the airplane to the projected impact point. This display was evaluated as an approach aid in USAF T-38 airplanes at the Instrument Flight Center(6).

The HUD used in this study is a further development of the VAM/Light Line displays. At the start of the program, it was not clear if roll-stabilization would be required. Therefore a roll/no-roll option was provided through a roll cut-out switch. Airspeed data was provided with a VAM-type airspeed index, and a "ball bank" indicator showed sideslip information. Figure 2 shows the symbology of the test MARS HUD.

SCOPE OF EXPERIMENT

The overall purpose of this program was to determine whether a HUD will assist the pilot of a MARS helicopter with recoveries in low visibility conditions and will also enhance training and standardization. The experimental objective was to determine whether a no-roll presentation is acceptable for MARS operations. If not, is a roll-stabilized horizon bar acceptable? Specific questions to be answered were: (1) What changes in MARS performance (precision and smoothness of control, airspeed control, and maintenance of the sight picture) are attributed to the HUD? (2) What is the pilot workload change induced by the HUD? (3) What are pilot preferences for, and potential

operational problems associated with roll-stabilized and non-roll-stabilized HUD formats? and (4) What changes in HUD format, data, or procedures will help improve MARS performance?

The evaluation was originally planned to be conducted in two phases, both to be flown from Davis-Monthan AFB, Arizona, in visual flight conditions. Phase I was to be flown using 80 lb weights with modified personnel parachutes (TWs) as targets. Actual engagement was not planned. A counterbalanced experiment was designed using the two HUD presentations (roll-stabilized - RH, and no-roll - NR) and a no HUD control (NH). The experiment was arranged to yield useful data with as few as four subjects and six sorties, although the planned numbers were six subject pilots and ten sorties.

Phase II was to follow and consist of two MARS recoveries of 1800 lb dummy vehicles (DVs) with tandem parachutes (main and engagement parachute system described above). This phase was intended to validate the results of Phase I which used single parachutes as targets with no recoveries. During Phase I, the advantages of the HUD were so obvious that Phase I was curtailed at the minimum allowed in the experimental design. Phase II was expanded to include a thirty day operational evaluation at an operating location (OL). During this evaluation, eighteen operational drones were recovered using the HUD.

PHASE I: INITIAL TESTING

Each subject pilot flew on one or two sorties. A sortie consisted of approximately thirty minutes of familiarization with the HUD, followed by up to twelve simulated MARS passes to TWs. All three HUD configurations were used on a given sortie: RH, NR, and NH. The order was varied to minimize the effect of learning. Each subject pilot completed a pre-experiment questionnaire, rating cards after each series of passes, a post-flight questionnaire, and a post-experiment questionnaire. The safety pilot completed a rating card after each pass.

A total of six sorties were flown using four subject pilots. All four subjects were well qualified in CH-3 MARS operations. CH-3 flying experience ranged from 800 to 1800 hours with a total flying experience range of 2500 to 2950 hours. All pilots were CH-3 instructor pilots. The safety pilots were also CH-3 instructor pilots. One of the subjects also served as a safety pilot after he completed his flights as a subject. None of the pilots had flown any HUD-equipped aircraft prior to this evaluation.

Pre-experiment Questionnaire

In addition to establishing the subjects' qualifications, the questionnaire asked for their assessment of the MARS mission. Counting the safety pilot and the copilot on one Phase II DV recovery, six questionnaires were completed. The consensus was that the most significant visual problem was determining the position relative to the engagement parachute in the absence

of a natural horizon. The pilots also commented on the difficulty of transitioning from keeping the parachute on the horizon to passing over the canopy just prior to engagement. Two pilots felt that roll information would be very important in a MARS HUD, but not essential. Three felt that it would be desirable, and one pilot had a neutral opinion.

Subjective Workload

There was no major change in overall subjective workload as reported by the pilots. However, sideslip was perceived as easier to control with either HUD than with no HUD. Roll was reported to be easier with the RH configuration than with the NR HUD. Table I shows the data.

Need for Additional Data

The pilots all felt a need to come "inside" for more data than was shown on the HUD. All reported a need for airspeed until they adapted to the airspeed indexes. All required vertical velocity data. Most required sideslip information with NH, but either HUD provided this data to the pilots' satisfaction. Roll and pitch data were required in the absence of a HUD by some pilots; the RH configuration eliminated the need to come inside for either. One pilot felt a need for torque or RPM.

The need for additional data is summarized in Table II. The HUD was felt to be useful only during final approaches since the horizon bar was displaced beyond the limits of the combiner glass during the turns to final approach.

No focus or visual conflict was reported. Two pilots reported difficulty with the airspeed cue. Comments were also made about the HUD blocking the view of the parachute as it passed beneath the helicopter.

Performance

Under the excellent visibility conditions present at Davis-Monthan AFB, there was no difference in the miss rates (reported by the safety pilot or by the pole operator) between the RH and the NH configurations. Both had miss rates of 22% (4 misses in 18 passes). The absence of roll data causes the miss rate to increase to 28% (4 misses in 14 passes). This is not statistically significant.

Concern Over High or Low Passes

The pilots were generally less concerned over high or low passes with the HUD than without. One pilot commented that while he was less concerned in general, the loss of sight of the parachute on short final (blocked by the HUD hardware) did bother him. (Note: this subject pilot also flew as a safety pilot and as a subject pilot during Phase II and felt that it was not a problem after adaptation.) Either HUD configuration caused the "hits" to be concentrated at the pole tips.

Other Comments

Additional comments were made. Significant comments (paraphrased) are: (1) Airspeed too far from center (3 subjects), (2) Display should be moved closer to pilot (3 subjects), (3) HUD would help training by providing a common sight picture to instructor and student (3 subjects), (4) Practice time was too limited (3 subjects) and the learning curve was slow for airspeed control (1 subject), and (5) The horizon line should be made more intense than the aiming V (1 subject).

PHASE II: OPERATIONAL EVALUATION

Following the decision to conduct an operational evaluation at the OL, the two pilots chosen to fly the evaluation each flew a training sorties consisting of practice MARS approaches to two TWs, followed by a sorties with an actual recovery of an 1800 lb DV. The two pilots were already experienced with the HUD, having flown as safety pilots in Phase I (one also flew as the first subject).

The HUD was removed from the helicopter used for Phase I and for the four sorties described above. It was then taken to the OL and installed in another CH-3. Eighteen operational recoveries were made at the OL during the month of April 1975. Only the RH display was used for recoveries during this phase, although the NR mode was briefly evaluated during other flying in the haze conditions prevalent at the OL.

Both DV recoveries at Davis-Monthan AFB were made on the first pass. Of the eighteen HUD-assisted engagements at the OL, sixteen were made on the first pass*, one on the second, and one on the third pass. One mission had a no-HUD recovery (4th pass) because of excessive display vibration. The miss rate using the HUD was 14% (per pass).

Benefit of HUD

The second operational sortie typifies the benefit of the HUD. On this sortie, the load line break-ties had separated from the main canopy resulting in the engagement parachute lying over and remaining at the same altitude as the main canopy. With the horizon obscured by haze, rain, and clouds, the HUD allowed a successful recovery on the first pass. The pilots felt that in the absence of a HUD, there would have been multiple missed passes and very likely a lost drone.

The pilots felt that pilot workload was much lower with the HUD.

Visual Illusions

Both pilots commented on an illusion during passes with the HUD in marginal weather. They had the illusion of being correctly lined up with the engagement parachute, but the HUD showed them to be high. Confidence in the

---

* Counting one tear-out as a successful pass

HUD from their experience in Arizona allowed them to use the HUD to correct their flight paths and make consistent catches.

Need for Roll-Stabilization

The HUD proved to be highly satisfactory under adverse weather conditions with roll-stabilization; but without roll a serious problem was encountered. Both pilots felt that manuevering in haze induced vertigo. They considered that roll-stabilization was an essential requirement for use in reduced visibility.

DISCUSSION

Operational Effectiveness

There were 77 MARS passes during the evaluation. Of these, fifty passes were made to 80 lb TWs and success/failure was estimated by the safety pilot or pole operator. The remaining 27 passes were made to DVs or to actual drones with success being defined as an engagement (or a tear-out). Of the 77 total passes, twenty-five were made during drone recoveries in haze at the OL. The remaining passes (50 TWs and 2 DVs) were made in good weather in Arizona.

We must further separate the data into learning and steady-state performance. To do this, we shall classify all no-HUD passes as steady-state since all subjects were considered to be highly qualified by their organizations. All Phase I passes with either HUD should be considered as learning passes. The actual recoveries made using the roll-stabilized HUD, both DVs and operational drones, can be classed as steady-state performance. Thus we have 32 learning passes and 45 steady-state performance passes.

The performance comparison between the two HUD versions can only be based on the learning data. Because of the small sample size, the difference in miss rates is not significant.

To compare the performance of the RH and the no-HUD baseline, we must use steady-state performance and, as a result, equate the difficulty of making passes to TWs and to tandem parachutes, although the motion of the tandem parachute system makes actual recoveries harder. Likewise, we must equate the difficulty of operating in Arizona in good visibility to the difficulty of operating at the OL in haze and smoke. Since the NH passes were mostly made to TWs at Davis-Monthan AFB, these assumptions are heavily weighted against the HUD.

Nevertheless, the miss rates were much lower with the HUD (3 misses in 23 passes or 13%) than without the HUD (32% missed). Again the limited data precludes any statistical test ($\chi^2=2.29$, df=1, $0.2>p>0.1$). However, in view of the heavily biassed test conditions, this difference in miss rates should be considered valid.

Mission Success Rate

To convert from miss rate (i. e., fraction of passes missed) to mission success rate (i. e., fraction of drones recovered), we use the familiar parallel redundancy formula:

$$\text{MISSION SUCCESS RATE} = 1 - (\text{MISS RATE})^n$$

where n is the number of passes possible before the drone is too low for a safe pass. With a typical value of n = 3, we can compute the mission success rates. For the roll HUD, the learning curve performance is 98.9% and the steady-state performance in 99.8% of all drones recovered. The steady-state baseline (no HUD) performance is 96.8%.

Again, the assumptions favor the no HUD case. If we look at the one sortie where the HUD malfunctioned (3 misses out of four passes), the corresponding mission success rate for no HUD in haze would be 58%. This figure is consistent with mission recovery rates of less than fifty percent which have been reported in no-horizon conditions.

Flight Safety

The primary hazard during MARS operations is collision with the parachute. During Phase I, it was noticed that the successful passes with the HUD were concentrated at the pole tips. This effect is probably the result of the aiming V helping the pilot to make a smooth transition to allow the parachute to pass beneath the helicopter into the engagement window. While this effect was only noticed with passes to TWs, it will undoubtedly reduce the number of nose or belly slaps during training and certainly minimize the risk of a catastrophic collision. It is not clear whether the aiming V should be adjustable to accommodiate different size parachutes. The pilot opinions were divided and no tests were conducted.

While no particular problems with the no-roll HUD were noted during flights in good weather, the pilots at the OL did report a strong tendency toward vertigo when flying the no-roll HUD in restricted visibility. This represents an unacceptable hazard.

One sortie was cancelled because of invalid pitch data on one HUD. This can be a serious hazard in instrument weather conditions or if the horizon is not visible. Serious consideration should be given to incorporating an instrument comparator to warn against invalid data. Failing this, crew procedures must be developed to ensure that discrepancies are noted. However, it will be difficult for the non-flying pilot to crosscheck his HUD with his panel instruments.

Displayed Data Requirements

The basic MARS HUD was intended to display pitch, sideslip, and airspeed with an optional roll display. The pitch display was the primary display needed for MARS. Since sideslip and airspeed were critical for successful engagements, they were also included. Part of the experimental design was to

evaluate the need for roll. The HUD also included an aiming V to assist the pilot during the transition just prior to engagement. During the evaluation, pilot comments suggested that vertical velocity data be added.

Pitch. Lack of adequate pitch cues from the horizon was the original reason for the HUD. We can, therefore, presume that pitch is a requirement for a MARS HUD. However, with a pitch malfunction, the airspeed, sideslip, and vertical velocity data would still be useful. Pitch failure, then, need only extinguish the pitch and roll displays (and the aiming V).

Roll. Roll can be considered a requirement primarily as a vertigo avoiding measure. Roll failure must extinguish the pitch and roll displays.

Airspeed. No test without airspeed was conducted. We conclude from pilot comments that it is required. Airspeed failure need only extinguish the speed indexes.

While the use of the three symbol airspeed display is adequate for determining both the actual airspeed and trends, some learning over and above the normal HUD familiarization seems to be needed.

Sideslip. Likewise, no specific evaluation of a no-sideslip HUD was done. Based on pilot comments, we conclude that it is a requirement. The original ball bank display was too hard to read for small sideslip angles. As a result, the opaque ball was changed to a triangular shaped sideslip index. The display, as modified, is adequate for the MARS mission. Bad sideslip data need only extinguish the ball bank display.

Vertical Velocity. The original display had no vertical velocity data. However, the majority of the pilot comments indicated a need for such data. The reason for this can be found in the Air Force handbook on instrument flying(7). This approach divides the flight instruments into control and performance instruments. The pilot makes his control inputs be reference to the control instruments (such as ADI or power/thrust) and monitors the aircraft's response by reference to the performance instruments (airspeed, heading, or vertical velocity).

The MARS pilots, having made a pitch or power correction to fly up or down relative to the parachute, felt the absence of a vertical performance instrument to monitor their corrections. This explains the need for vertical velocity data. Apparently, they felt able to do without a power control instrument. Perhaps, kinesthetic feedback from the collective position was sufficient. One pilot did comment on the absence of torque or RPM data.

During the recovery after engagement, the pilot must, at maximum torque, trade altitude for airspeed. During this transition, the vertical velocity data is also needed. A torque display is not needed since the pilot can sense maximum torque from the RPM droop. As a result of these observations, the production MARS HUD incorporates a vertical velocity display. Preliminary pilot comments to this addition were favorable.

Aiming V. The aiming V was commented on favorably by the subject pilots. However, no concensus could be reached on the need for different Vs for different sized parachute canopies.

Modified Display. As a result of the testing and pilot comments, the symbology was changed for the production MARS HUD hardware. The revised format it shown in Figure 3.

CONCLUSIONS

The HUD system (with roll) will enhance MARS performance during periods of reduced visibility. It will also enhance safety during training by causing the passes above the target parachute to be higher — reducing the chances of the helicopter's striking the parachute. Roll stabilization is a safety-of-flight requirement to avoid vertigo in no-horizon weather conditions. Roll-stabilization appeared to improve performance over the no-roll case; however insuffient data was available for a statistically valid test.

Pilot workload is much lower when using the HUD. Training to use the HUD should require practice passes to 2-4 training weights, assuming a MARS-qualified pilot. The ability to make full use of the airspeed cue on the HUD may require additional time. The airspeed learning curve seems to be quite variable from pilot to pilot.

The MARS HUD should display pitch, roll, sideslip, airspeed, and vertical velocity data. A reliable self-test circuit is highly desirable. The horizon line should be more distinct than the aiming V.

While the HUD should enhance crew training and standardization as well as mission performance, operational flight procedures should be reviewed shortly after fleet use begins.

REFERENCES

1. A-7D Navigation/Weapon Delivery System, Vought Report 2-14000/412-10, 1974

2. Naish, J. M., Properties and Design of the Head-Up Display (HUD), McDonnell-Douglas Report MDC-J1409, 1968; revised 1970

3 Mackie, R., Jet Transport Operations in the Arctic, presented at the Aircraft Operations in the Canadian Arctic Meeting of the Canadian Aeronautics and Space Institute, Edmonton, 1973

4 Augustine, W. L., Head-Up Display Area Survey, AFFDL-TM-72-11-FGR, 1972

5 Singleton, W. T., Display Design: Principles and Procedures, ERGONOMICS, 12, 1969, 519-531

6. Tapia, M. and Intano, G., Light Line Visual Landing Head-Up Display Evaluation, USAF IFC-TR-76-1, 1976

7. Instrument Flying, USAF Manual AFM-51-37, 1971

8. Partial (MARS) Flight Manual, USAF CH-3E Helicopters, USAF Technical Order 1H-3(C)C(I)-1, 1974

HUD	Controlled Parameter	Number of Responses 1 Very Easy	2 Easy	3 Medium	4 Hard	5 Very Hard	Mean Value
No HUD	Airspeed		1	2	1	1	3.4
	Vertical Velocity		1	2	1	1	3.4
	Pitch		2	3			2.6
	Sideslip		2	2	1		2.8
	Roll		3	2			2.4
	Overall		1	2	1	1	3.4
Roll HUD	Airspeed		1	3	1	1	3.33
	Vertical Velocity			4	1	1	3.5
	Pitch		3	2	1		2.67
	Sideslip	1	4	1			2.0
	Roll		5	1			2.17
	Overall		1	3	1	1	3.33
No-Roll HUD	Airspeed		2	1	3		3.17
	Vertical Velocity		2	1	3		3.17
	Pitch		3	2			2.4
	Sideslip	1	4	1			2.0
	Roll		4		1	1	2.83
	Overall		1	3	2		3.17

TABLE I

SUBJECTIVE DIFFICULTY OF MAKING PASSES

Configuration	Number of Questionnaires	Number of Times Parameter Cited by Pilot						
		Airspeed	Pitch	Roll	Sideslip	Altitude	Vertical Velocity	RPM or Torque
No HUD	6	6	2	3	4	1	6	1
Roll HUD	6	3				1	3	1
No-Roll HUD	5	3		2		1	2	1

TABLE II

NEED FOR ADDITIONAL DATA

NOT SUPPLIED BY HUD

ORIGINAL PAGE IS
OF POOR QUALITY

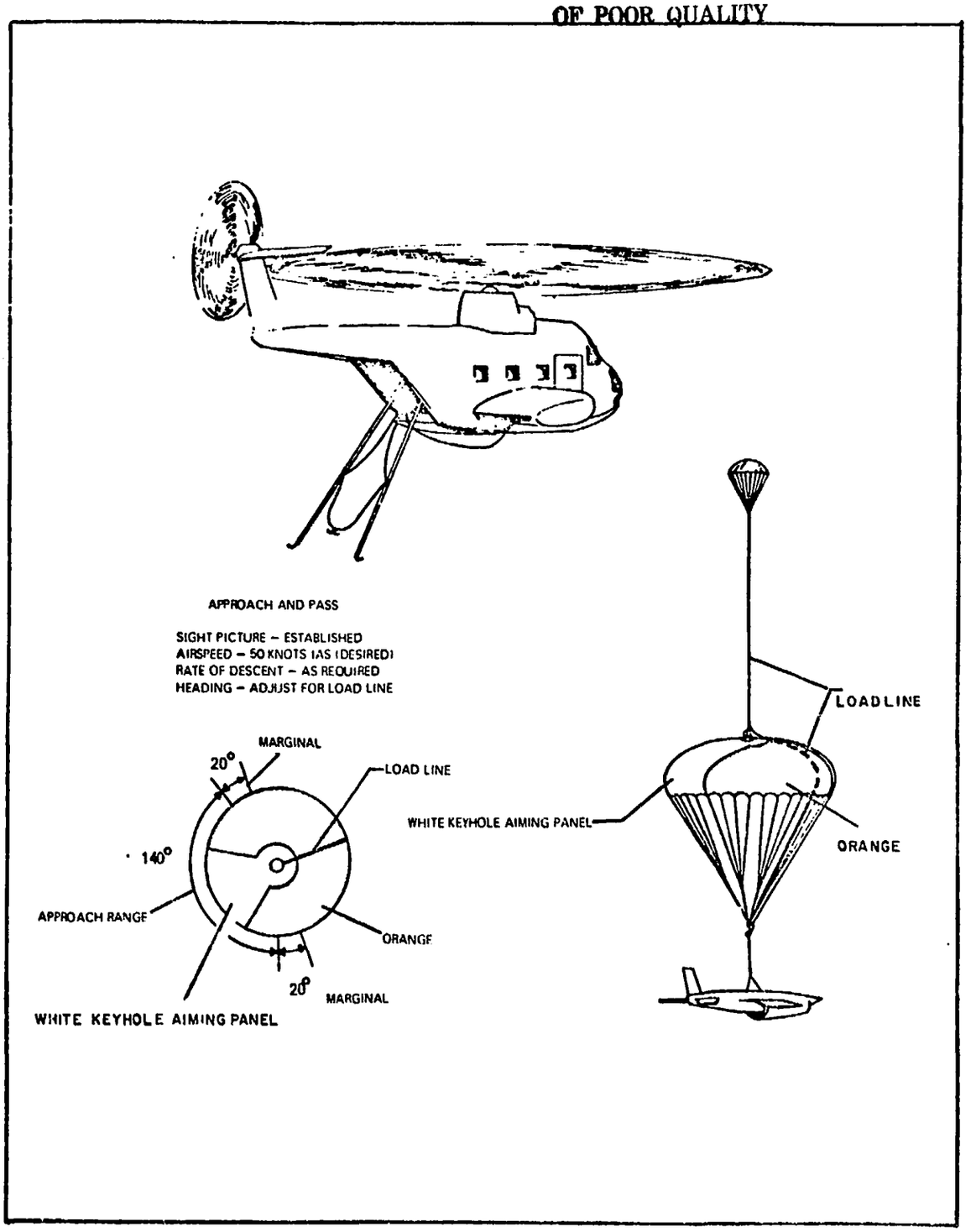

Figure 1

Helicopter Approach and Pass

(From Reference 8)

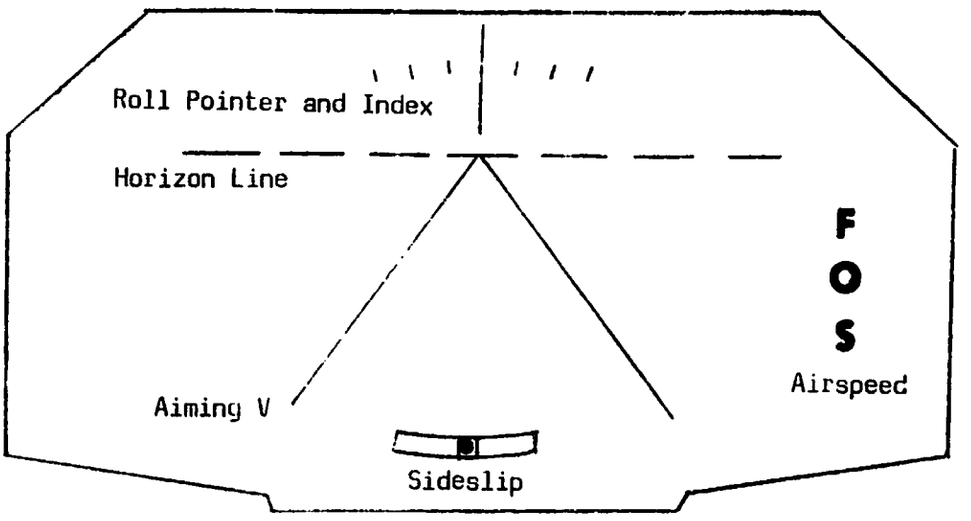

Figure 2

MARS HUD Display Format

(As Tested)

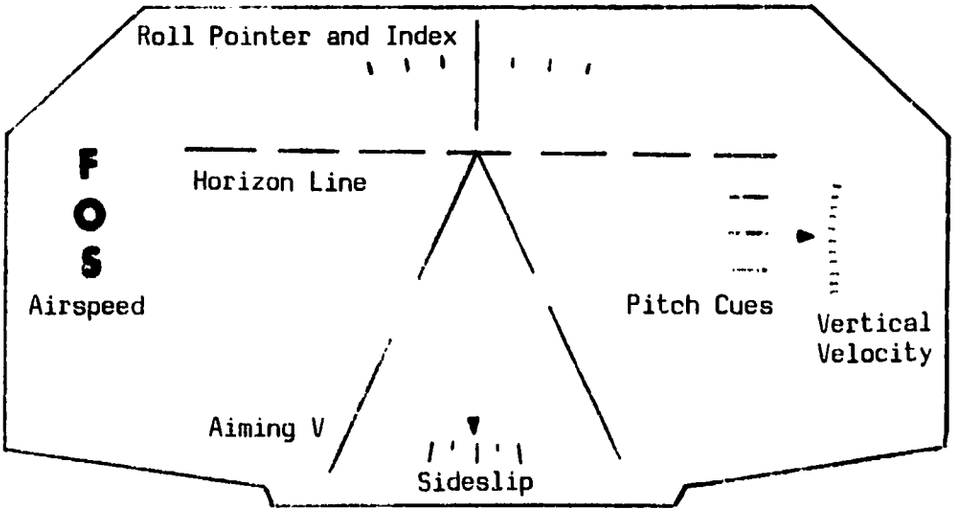

Figure 3

Revised Display Format

28

N79-15616

EVALUATION OF DISPLAY AND CONTROL CONCEPTS FOR A TERMINAL CONFIGURED VEHICLE IN FINAL APPROACH IN A WINDSHEAR ENVIRONMENT*

William H. Levison
Bolt Beranek and Newman Inc.
Cambridge, Mass. 02138

Presented at the fourteenth Annual conference on Manual Control, University of Southern California, April 25-27, 1978.

ABSTRACT

The effects of display and control parameters on approach performance of a simulated Terminal Configured Vehicle (TCV) were explored experimentally in a manned simulation study and analytically using a state-of-the-art pilot/vehicle model. A revised treatment of nonrandom inputs was incorporated in the model. Response behavior was observed for two display configurations (a pictorial EADI presentation and a flight-director configuration requiring use of a panel-mounted airspeed indicator), two control configurations (attitude and velocity control wheel steering), and two shear environments, each of which contained a head-to-tail shear and a vertical component.

In general, performance trends predicted by the model were confirmed experimentally. Experimental and analytical results both indicated superiority of the EADI display with respect to regulation of height and airspeed errors. Velocity steering allowed tighter regulation of height errors, but control parameters had little influence on airspeed regulation. Model analysis indicated that display-related differences could be ascribed to differences in the quality of speed-related information provided by the two displays.

*This research was supported by the National Aeronautics and Space administration under contract No. NAS1-13842.

INTRODUCTION

Windshear constitutes one of the major threats to flight safety in approach and landing operations. This threat is enhanced not only by the potential severity of the shear (defined as a wind whose velocity changes with altitude), but also by the tendency of the shear profile to change rapidly over time. This lack of predictability has led to the need for control and display aids to help pilots better cope with the presence of windshears.

This paper summarizes the second phase of a program to analyze display-control configurations for the Terminal Configured Vehicle (TCV). This work was performed for NASA Langley Research Center and was intended to augment a simulation study conducted there.

The first phase of this study explored the effects of certain control and display configurations on approach performance in a zero-mean, random turbulence environment. The LRC simulation was augmented by an analytic study performed at Bolt Beranek and Newman Inc. using the "optimal-control" pilot/vehicle model to explore both performance and workload differences among control/display configurations of interest. The reader is assumed to be familiar with the features of this model, which has been well documented in the literature. Frequent reference is made below to the report by Levison and Baron [1] which documents the results of the first study phase and which demonstrates application of the pilot model to analysis of TCV approach performance.

Approach performance of a TCV in windshear environments was studied in the second study phase, with control and display configuration (along with windshear profile) the major variables of interest. The existing pilot/vehicle model was modified to allow a revised treatment of nonrandom inputs; because the longitudinal and vertical components of the shear have greatest impact on path and airspeed regulation, only longitudinal-axis performance was explored in the analytic study. The results of the windshear study are documented in [2].

PROBLEM DEFINITION

Description of the Flight Task

The flight task of interest was the standard straight-in (3 degree) approach of a simulated TCV. The simulated atmospheric environment contained low-level zero-mean gusts plus a wind shear consisting of a rotating horizontal component and a brief interlude of either an updraft or a downdraft.

Speed and flight path were controlled manually. Flight-path control was aided by one of the following control augmentation schemes: "Attitude Control Wheel Steering (ACWS) or "Velocity Control Wheel Steering" (VCWS). Basically, these modes provide attitude-rate stabilization and allow the pilot, in effect, to command either attitude (ACWS) or path angle (VCWS). A more detailed description of control wheel steering is given in Levison and Baron [1]. In order to use the existing man-machine model, the track-hold feature of the CWS was approximated by continuous linear feedback law as shown in Figure 1.

Displays

Flight control information was provided primarily by an electronic attitude/director indicator (EADI). Two display configurations were considered: (1) "advanced" display, which presented information in an integrated (pictorial) format, and (2) the flight director display, which provided director information based on path, path angle, and attitude errors.

The advanced display provided the following flight-control information (as diagrammed in Figure 2): (a) an aircraft symbol to serve as x-axis airframe reference, (b) an artificial horizon and pitch attitude scale, (c) a roll attitude scale and pointer, (d) a pair of so-called "gamma wedges" to indicate path angle, (e) a dashed line to indicate a point 3 degrees below the horizon, (f) a perspective runway symbol, (g) an extended runway center line to aid in lineup regulation, (h) a symbol to indicate track angle, (i) a glideslope indicator, (j) a localizer indicator, and (k) a so-called "potential gamma" symbol to provide information pertaining to speed management.

Except for the potential gamma symbol, this display was indentical to the advanced display described in [1], to which the reader is referred for additional details on the structure and use of this display. A weighted sum of airspeed error and rate of change of vehicle velocity was used to drive the potential gamma symbol, relative to the gamma wedge, in the vertical dimension.

The "flight director display" consisted of a raw status display plus director information. The EADI provided attitude information, glideslope and localizer errors in symbolic format, and director information. Airspeed and rate-of-climb were displayed by conventional panel meters. Perspective runway, gamma wedges, and potential gamma were omitted from the EADI in this display configuration.

Director information was provided with a pair of crossbars

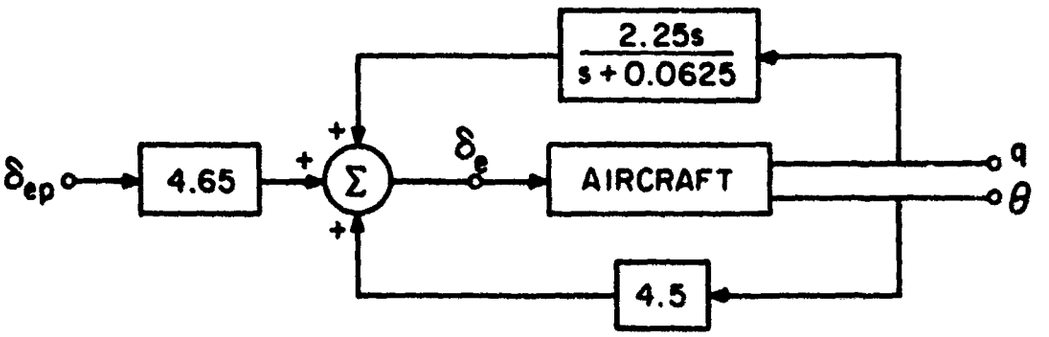

(a) ATTITUDE CWS

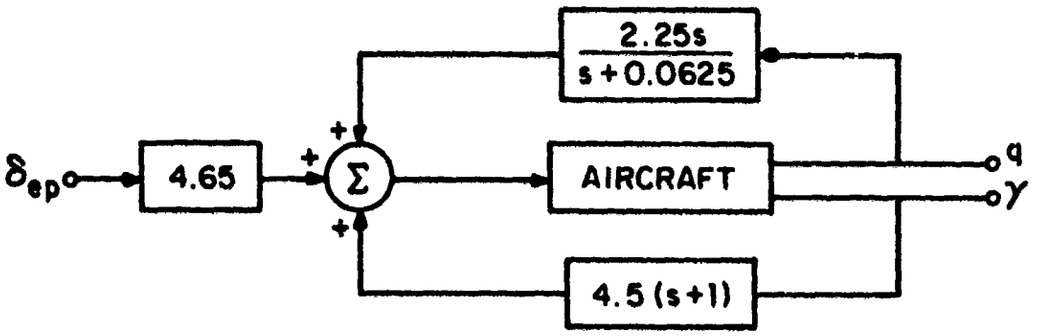

(b) VELOCITY CWS

Figure 1. Linear Approximation to Control Wheel Steering

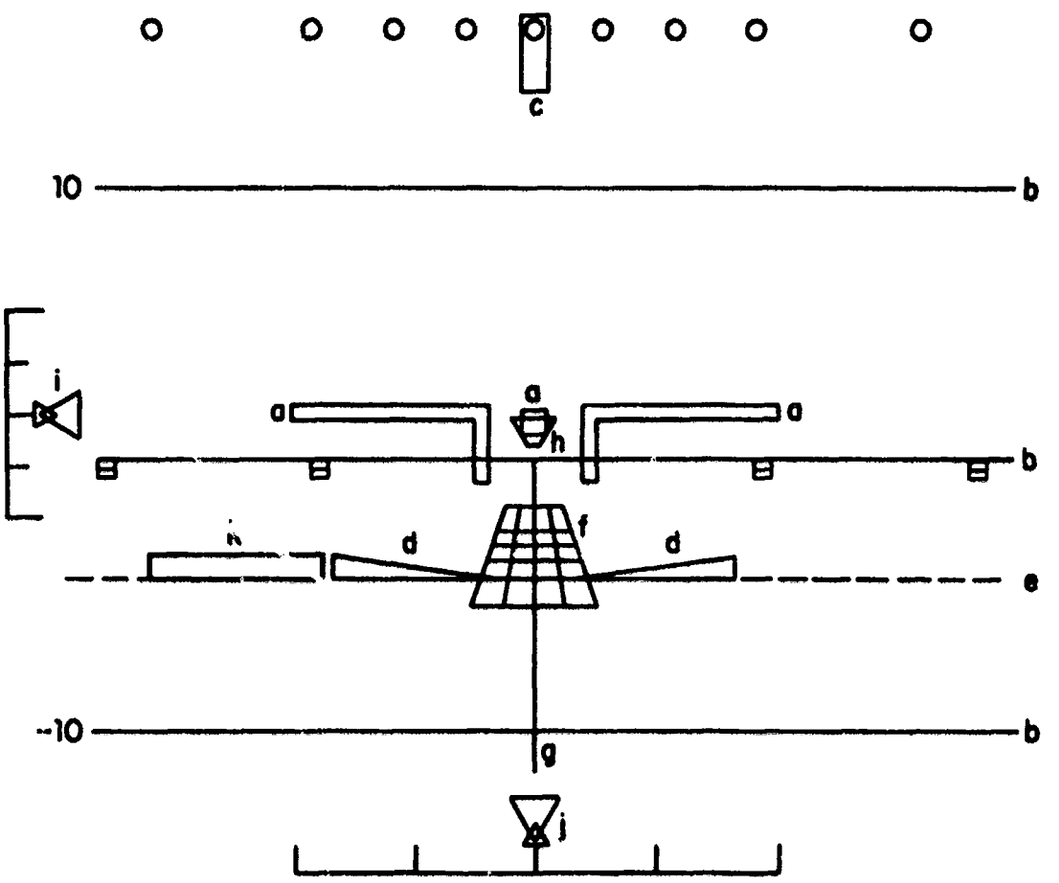

Figure 2. Sketch of the EADI Display
(Display elements defined in the text)

that deviated from the x-axis reference symbol in a "fly-to" mode. The director indicator was driven by a weighted sum of height, path angle, and pitch-rate errors as described in [2].

Wind Environment

Wind shears as well as zero-mean random gusts were simulated in the NASA-LRC experiments. In order to simplify problem formulation and reduce computational requirements, the effects of these simulated gusts were approximated in the bulk of the model analysis by including wide-band disturbances added in parallel with the control deflections. Preliminary model analysis was conducted to select disturbance levels that would give nearly the same predicted path and airspeed errors as would be obtained from a more faithful representation of the simulated gust inputs [2].

Each of the simulated windshears used in the experimental and analytical study contained a rotating horizontal component plus a brief vertical component. Figure 3 shows the relationship between wind speed and range for points along the nominal 3 degree glide path for two of these shears.* (Note that the horizontal and vertical wind components have been scaled differently in this figure.)

METHODS

Model Analysis

The model employed in this study was basically the so-called "optimal-control model" described extensively in the literature, modified to treat non-zero-mean (i.e., deterministic) inputs. As the treatment of the deterministic input (i.e., the windshear) was different from that used in previous studies (3-5), a brief discussion of this treatment is given below. A more detailed exposition of this aspect of the pilot model is given in the appendix to [2].

Modeling the pilot's response to a deterministic input involves two basic considerations: (1) the degree to which the

*Since windspeed is an explicit function of altitude, rather than range, deviation of the aircraft from the desired glide path would modify somewhat the range dependency shown in Figure 3.

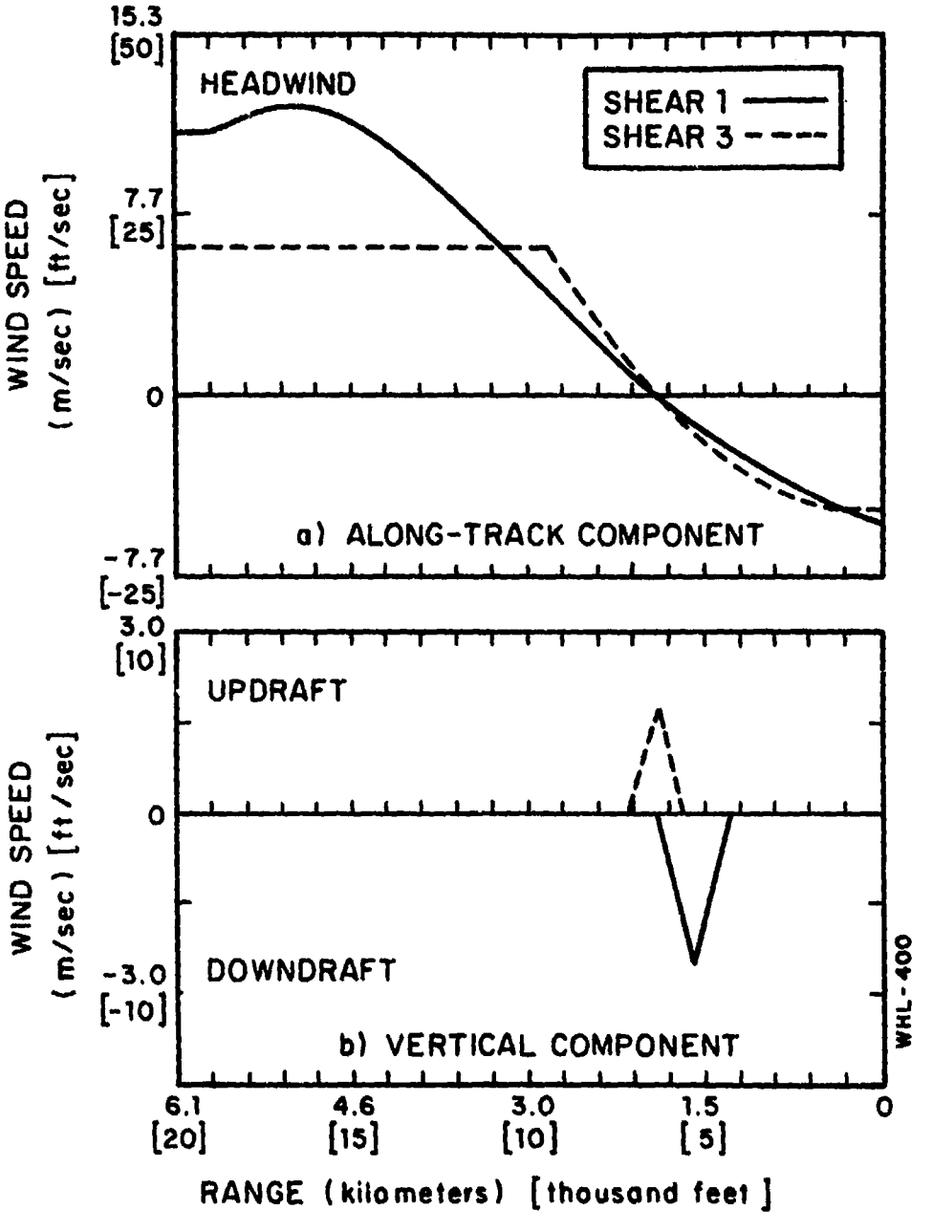

Figure 3. Windshear Profile

pilot understands the nature of the input (i.e., his "internal model"), and (2) the way in which the pilot detects and responds to the input. A simple representation of the pilot's knowledge of the windshear was adopted for the study; basically, we assumed no specific knowledge of the shear, only the knowledge that a non-zero-mean wind might exist. We assumed that the pilot would not try to anticipate changes in the wind, but would, at best, attempt to estimate the current wind vector. This level of pilot knowledge was modeled by simply implementing a stepwise-constant representation of the wind. Since the wind varied relatively slowly with time, an integration time step of 1 second was sufficiently fine to allow an adequate representation of the continuously-varying wind speed.

The pilot/vehicle model was modified to reflect the following assumptions concerning pilot behavior in a non-zero-mean input environment:

a. The pilot continuously anticipates the behavior of the display variables he is utilizing, given his current estimates of system states and his internal model of system parameters.

b. The pilot performs a short-term average on the difference between expected and actual behavior of each display variable.

c. If average prediction error is sufficiently large with respect to the variability of this error, the pilot becomes additionally uncertain about his estimates of system state variables, and he attempts to upgrade these estimates.

Implementing this set of assumptions led to the following additional pilot-related model parameters: (1) the short-term averaging time, (2) the magnitude of the prediction error considered large enough to warrant special action, and (3) specific state variables to which the pilot attributes his uncertainty. In addition, an algorithm had to be formulated for relating prediction errors to increased uncertainty.

Model predictions were obtained with the assumptions that (1) prediction errors were averaged over about two seconds, (2) an average deviation of two standard deviations from the expected value warranted special consideration by the pilot, and (3) uncertainty could be associated with any of the principal state variables, including the state variables representing the horizontal and vertical shear components.

To obtain a model solution it was necessary to describe the task environment in a suitable mathematical format and to assign values to model parameters related to pilot limitations. System dynamics were modeled as described in [1], with the modification indicated in Figure 1 of this paper to account for control wheel steering augmentation.

The pilot was assumed to adopt a control strategy that minimizes a weighted sum of mean-squared response variables. In this study, the "cost function" included height error, sinkrate error, airspeed error, angle-of-attack error, control deflection, and rate-of-change of control deflection. Because the results of the previous study suggested that pilots tended to regulate height error in terms of an angular, rather than a linear, criterion, weightings associated with height and sinkrate errors were varied inversely with range. Weightings for other variables were kept fixed throughout the "flight" as documented in [2].

When tracking with the advanced display, the pilot was assumed to perceive height error, sinkrate error, pitch and pitch rate, flight path angle and path angle rate, and potential gamma. Because movement of the perspective runway with respect to the nominal glideslope was proportional to error in angular terms, the thresholds for height and sinkrate errors (in terms of feet and ft/sec) varied linearly with range. The height error threshold was based on an "indifference threshold" of 1.4 meters at the 30 meter decision height as determined from previous analysis. Other threshold values were based on considerations of visual resolution as described in Levison and Baron. The noise/signal ratio of -17 dB associated with use of the advanced display reflects a moderate-to-high level of workload with no interference among display elements (i.e., we assume integration of the displayed information).

When tracking with the director display, the pilot was assumed to rely primarily on the director symbol and the airspeed indicator for continuous flight-control information, with a negligible amount of time spent scanning the status information for monitoring purposes only. The threshold of 1.0 m/sec. on airspeed was based on the assumption that the pilot was indifferent to airspeed errors smaller than the calibration increments of the airspeed indicator (2 kts); threshold values for perception of director displacement and rate were based on visual resolution limitations. The noise/signal level of -14 dB reflects the same overall level of attention to the task as before, with the requirement to share attention between the director and airspeed indicators. For simplicity, equal sharing of attention between the two displays was assumed, and loss of visual inputs associated with eye movements was neglected.

Experimental Procedures

The experimental task was to track a 3° ILS beam to touchdown. Each experimental trial began at a simulated range of 6700 m from the runway threshold at an altitude of approximately 366 m. The aircraft was initially trimmed on the desired glide path for a 3° path angle in its approach configuration: 120-knot airspeed laps, gear down. Rudder was automatically controlled.

Zero-mean random gusts and wind shears were both simulated during each experimental trial. Three shear environments were explored, including those designated as "Shear 1" and "Shear 3", profiles of which are given in Figure 3.

Gust disturbances having an rms variation of 0.3m/sec were simulated for all three translational axes. Gust spectral characteristics were varied with altitude according to the wind models suggested by Chalk et al. [6].

Data were obtained from three NASA test pilots. Practice trials were provided using shears other than those specified for data collection. Each pilot "flew" two sessions of 18 approaches each for data collection; each session consisted of two replications of 3 control/display configurations and 3 shear environments presented in a balanced order. Thus, four replications per experimental condition per pilot were obtained.

Ensemble statistics were computed for selected response variables for each experimental condition. First, within-subject replications were analyzed to provide trajectories of mean response and of the standard deviation of the response. These measures were processed further to provide across-subject averages of the mean and standard-deviation response trajectories. Mathematical definitions of these statistical variables are given in Levison and Baron.

For purposes of data presentation, statistical analysis was performed for height and airspeed errors, sampled at 305 meter intervals beginning at a range of 4572 m from the ILS origin.

SUMMARY OF RESULTS

Considerations of space preclude an extensive presentation of either theoretical or experimental results. A sampling of results is presented to demonstrate three applications of the pilot/vehicle model in the context of this study: (1) prediction, (2) diagnosis, and (3) extrapolation. Additional results are documented in [2].

Prediction

The following four figures compare display and control trends for predicted and experimental mean response trajectories for the "Shear 1" environment.* Because the experiment was not full factorial, display differences are shown for the Attitude CWS configuration only, and control differences are compared for the advanced display configuration.

Effects of display on mean height error and mean airspeed error are shown, respectively, in Figures 4 and 5. In general, the trends predicted by the model are confirmed, but the differences observed experimentally are smaller than predicted. Model and experimental correlation is generally better for height than for speed response.

As predicted, experimental height error is generally more negative for the director than for the advanced display. The data also confirm the prediction that the director display leads to a larger swing in error over the course of the approach. There was also a tendency (not predicted) for the pilots to fly above the nominal glide path.

Figure 5 shows that the test pilots flew the director display with less negative (or more positive) airspeed errors than achieved for the advanced display--a trend the reverse of which was predicted by the model. Given the reported tendency of pilots to fly approach speeds greater than nominal when windshears are anticipated [7], we suspect that the test subjects attempted to compensate for the lack of good airspeed information from the director configuration by intentionally carrying excess airspeed. Experimental results confirm the prediction of greater swings in error with the director display, although the magnitudes of the display-related differences are less than predicted.

Figures 6 and 7 confirm the major trends predicted for control effects; namely, tighter regulation of height error was observed for velocity CWS, whereas control configuration had little effect on regulation of speed error.

Results for the Shear 3 environment, documented in [2], showed similar types of correlation between predicted and measured mean error trajectories.

---

*Model results shown in these figures are true predictions in the sense that they were obtained before the experimental data were analyzed. Pilot-related model parameters were not adjusted to provide a best match to the data.

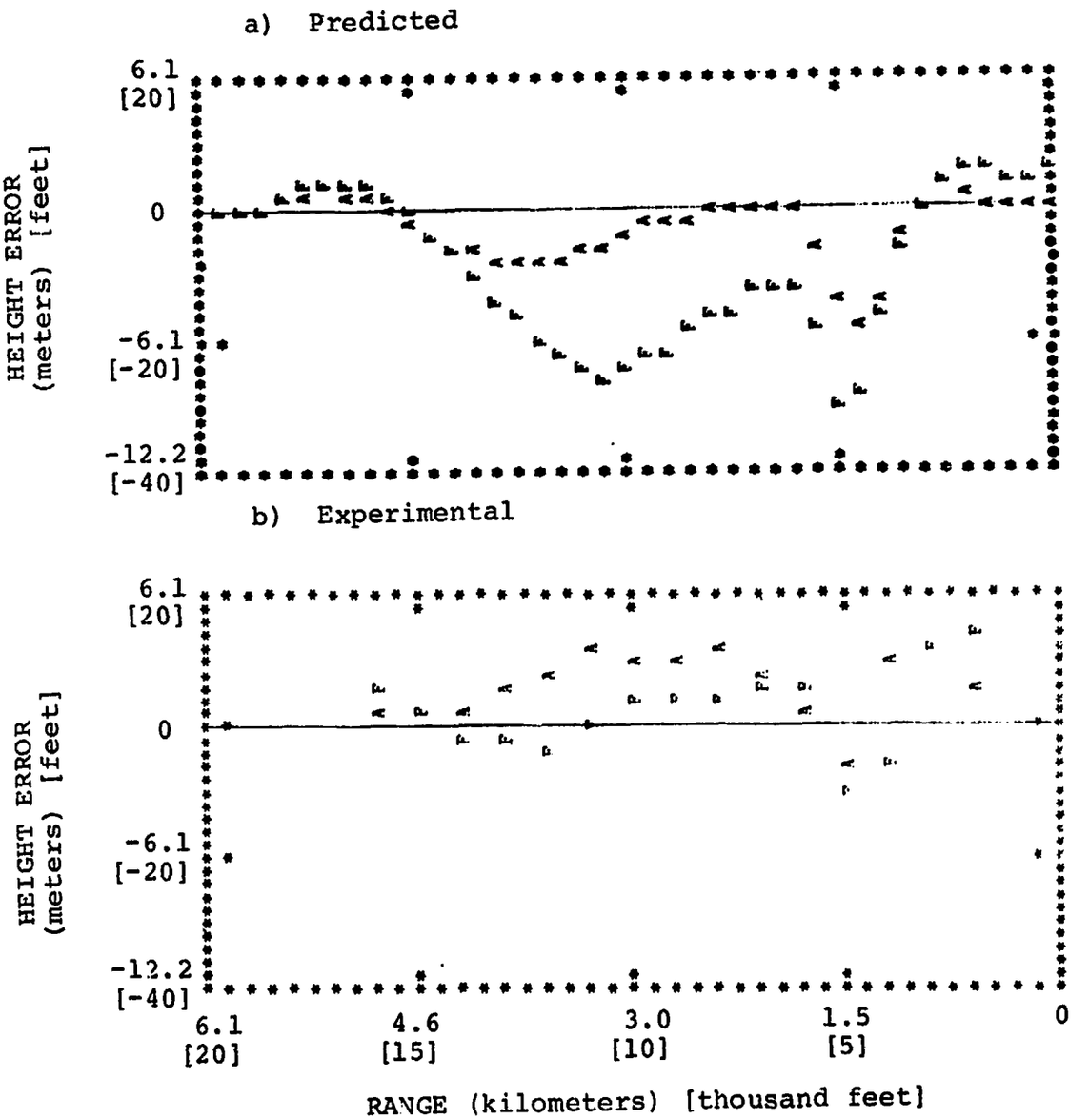

Figure 4. Effect of Display on Mean Height Error, Shear 1 Attitude CWS.
A = advanced display, F = flight director

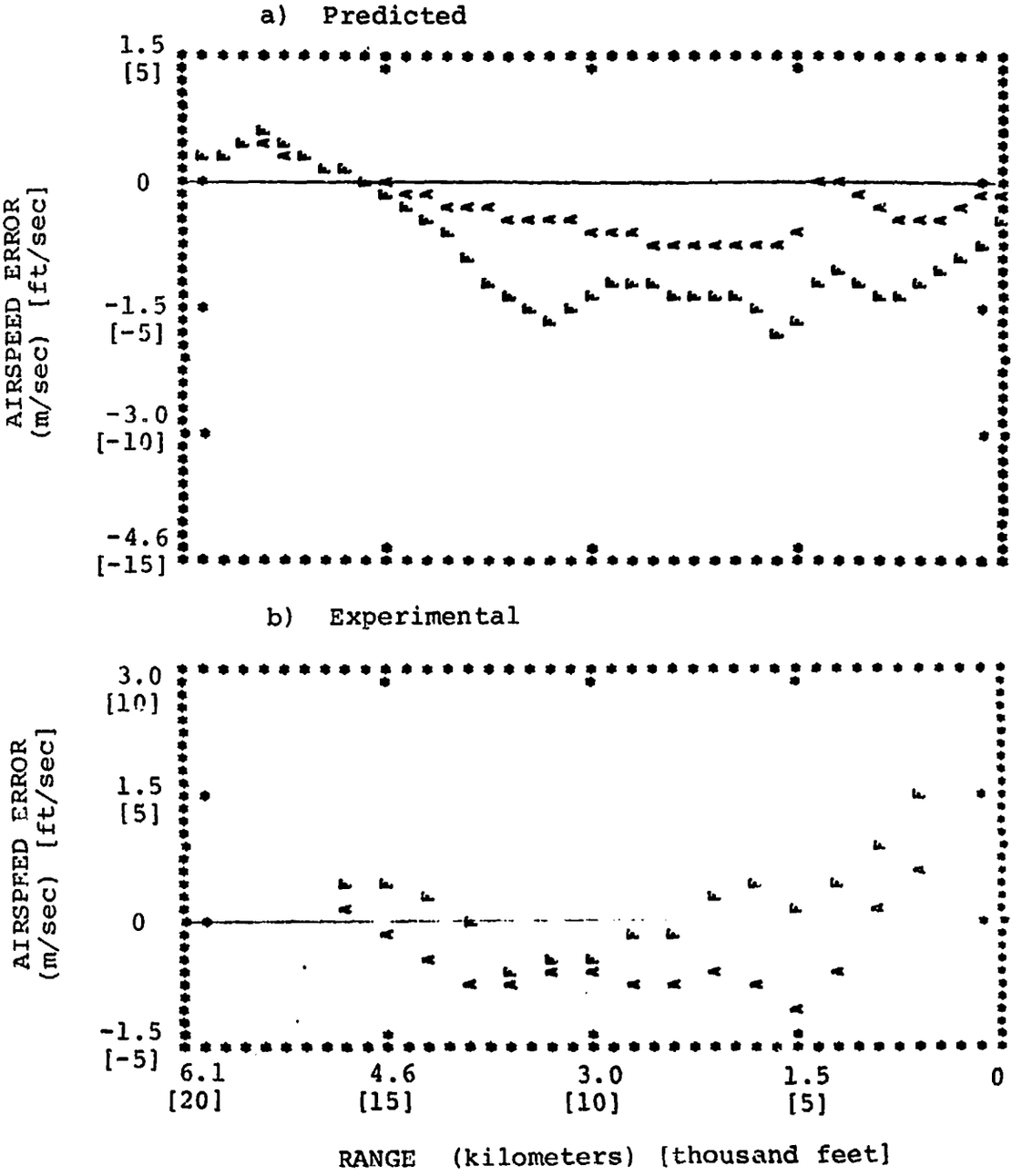

Figure 5. Effect of Display on Mean Airspeed Error, Shear 1

Attitude CWS.
A = advanced display, F = flight director

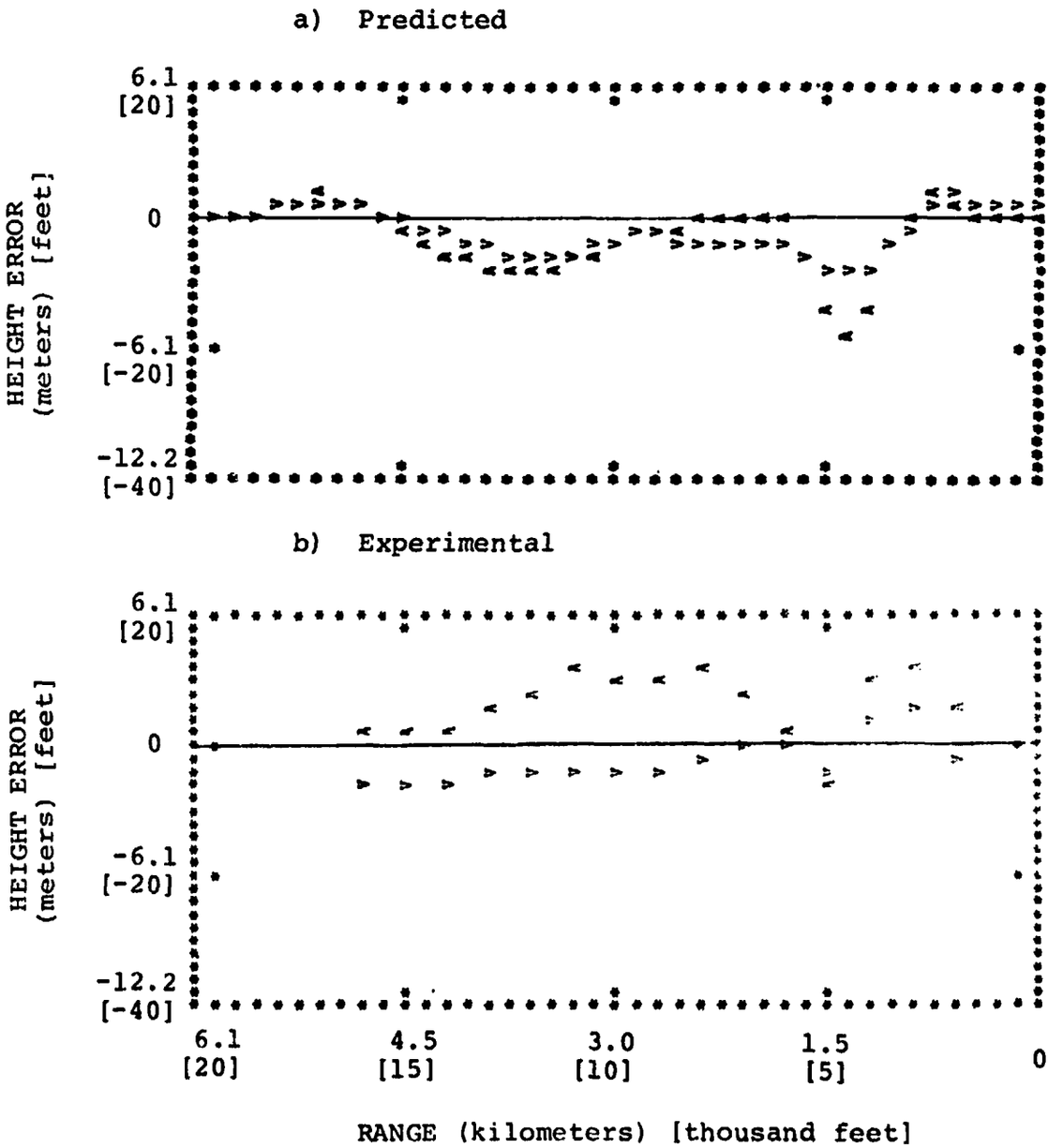

Figure 6. Effect of CWS on Mean Height Error, Shear 1

Advanced Display.
A = attitude CWS, V = velocity CWS.

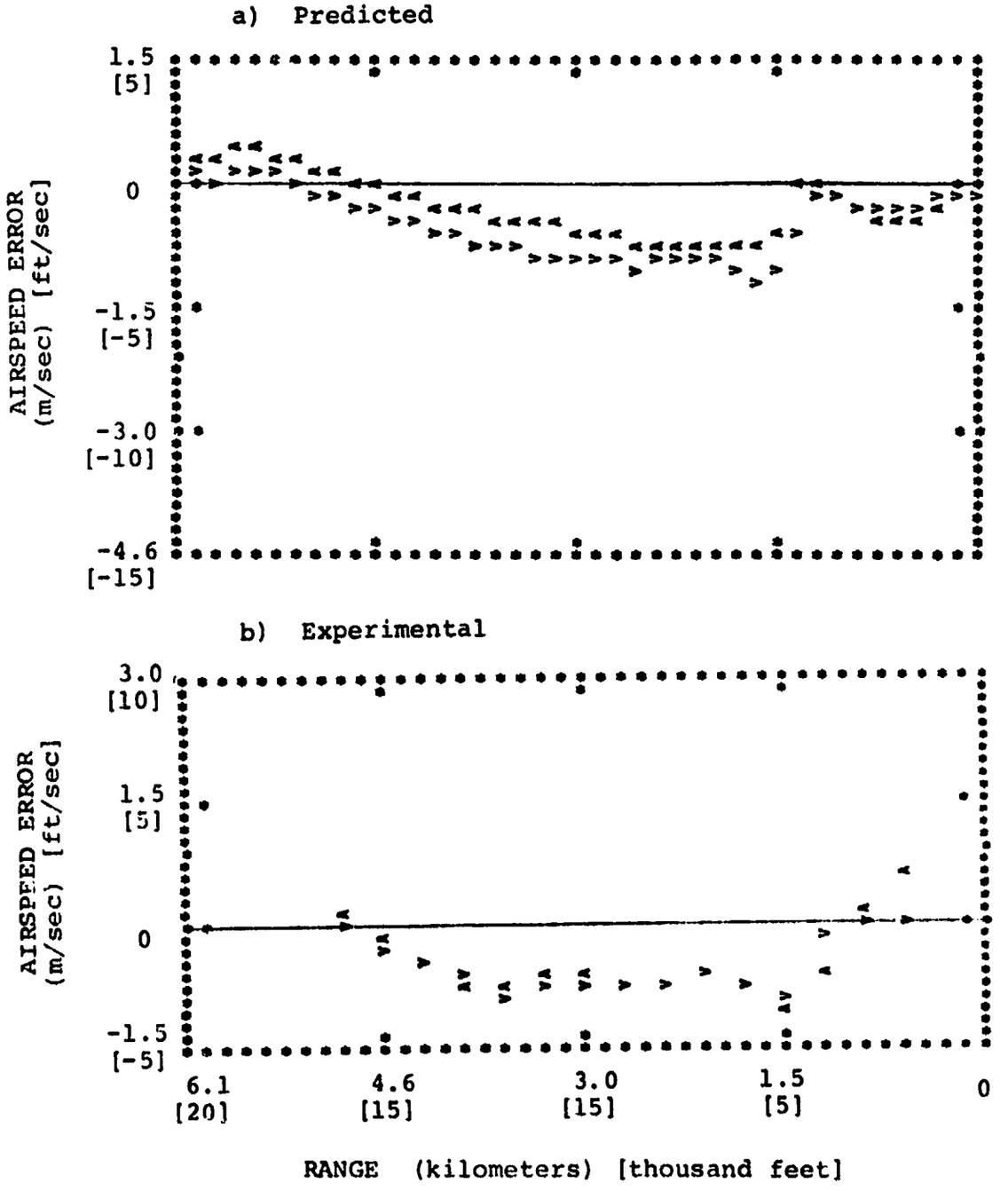

Figure 7. Effect of CWS on Mean Airspeed Error, Shear 1

Advanced display.
A = attitude CWS V = velocity CWS

Diagnosis

In order to ascertain the cause of the performance differences observed for the two display configurations, the director display configuration was reanalyzed with the threshold of 0.024 m/sec (as opposed to 1.0 m/sec assumed previously). This reduced threshhold was equivalent to that which would be associated with the potential gamma indicator of the advanced display if potential gamma were driven solely by airspeed error. Director laws and scaling were unchanged, and, as before, the pilot was assumed to share attention equally between the director and speed indicators.

Figure 8 shows that predicted performance with the director display, given improved airspeed resolution, is comparable to that achievable with the advanced display for the Shear 1 environment. Thus, reducing the perceptual threshold on airspeed should substantially improve performance with the flight director.*

Extrapolation

A reliable pilot/vehicle model provides a convenient tool for answering various "what if" questions that may not be readily explored experimentally. In this study we used the model to explore the consequences of providing the pilot with better knowledge of the wind environment. Specifically, the "advanced" display was considered with additional, direct, displays of horizontal and vertical wind assumed. Thresholds relating to perception of wind velocities were neglected, and an integrated display was assumed (i.e., noise/signal ratios remained at -17 dB for all display quantities). The intent here was not to simulate a physically realizable display, but to determine the performance potential associated with improved estimation of the wind environment.

Figure 9 shows that predicted performance with the two displays is nearly identical over most of the approach. Thus, it would appear that little overall improvement in performance can be expected from a display which provides the pilot with improved estimates of the instantaneous wind environment.

This latest result is contingent on the assumption that the pilot does not attempt to estimate the altitude- (hence, time-) varying nature of the shear but attempts only to estimate the current wind vector. It is possible that performance could be improved if the pilot were to attempt to extrapolate the wind--

*As of the writing of this paper, this prediction has not been tested experimentally.

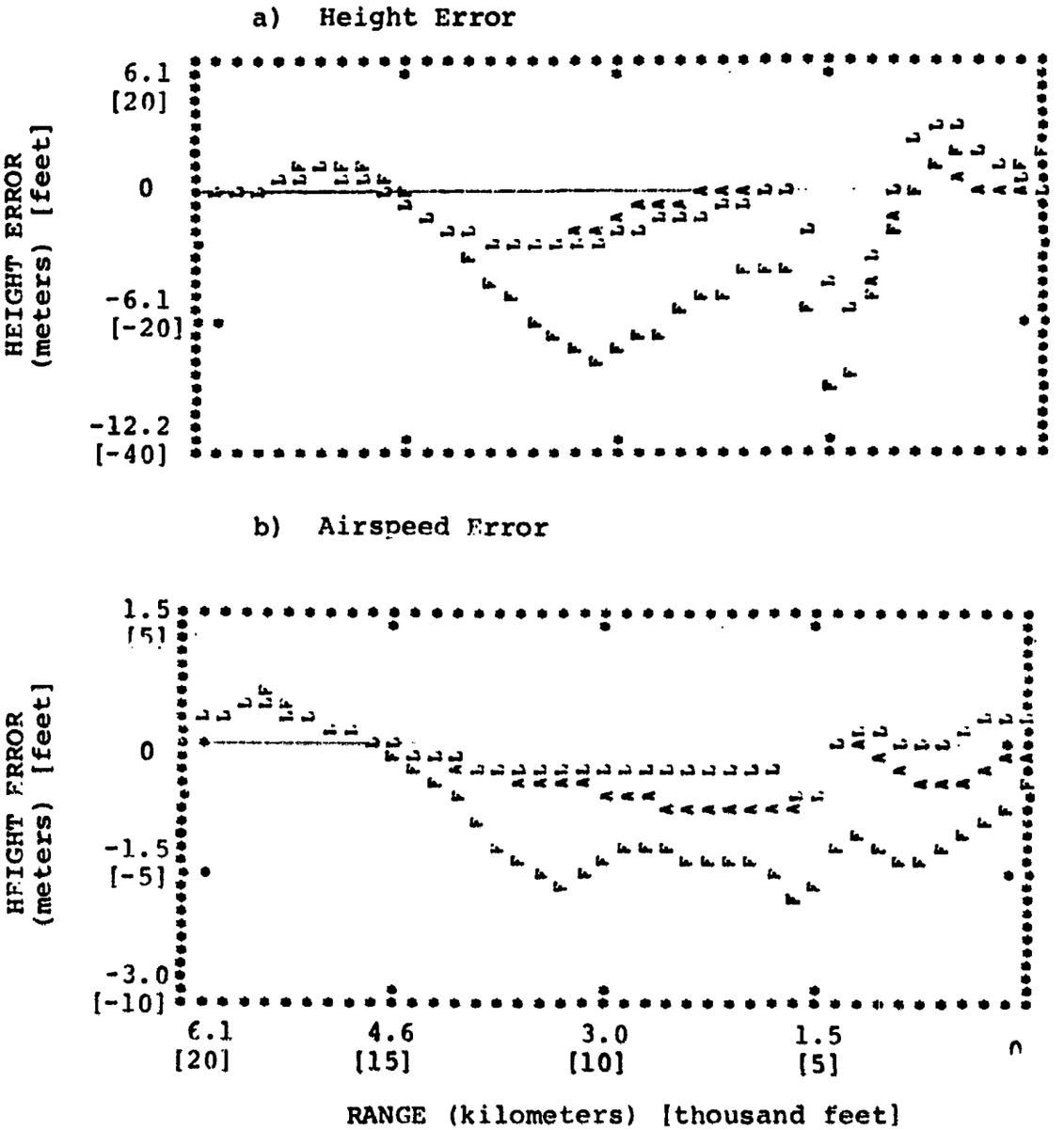

Figure 8. Effect of Reduced Threshold for Perception of Airspeed Error

Shear 1, attitude CWS
A = advanced display, F = flight director,
L = director with lowered perceptual threshold.

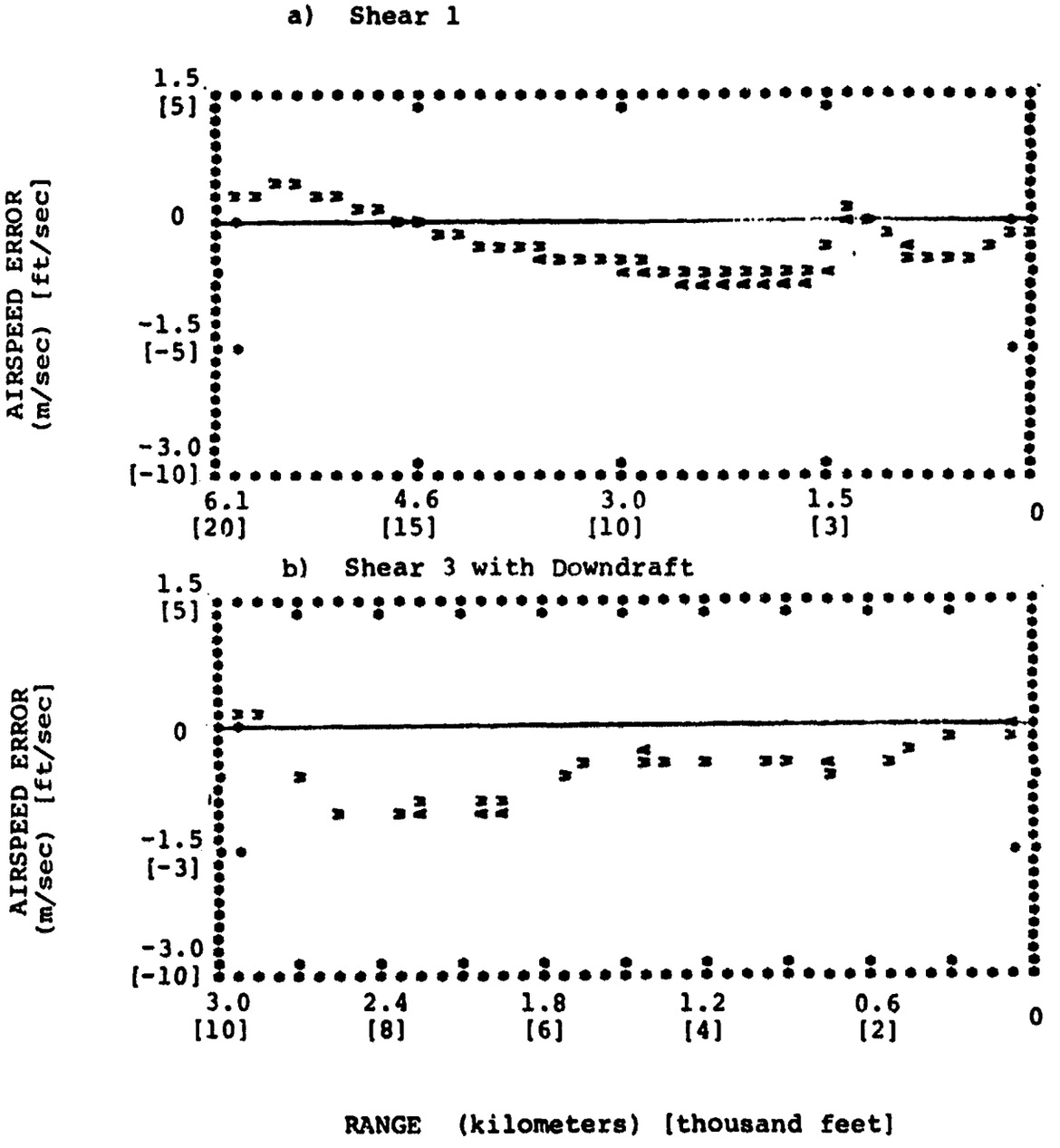

Figure 9. Effect of Explicit Display of Wind on Predicted Mean Height Error

Attitude CWS
A = advanced display, W = additional wind display

especially if the display were augmented to provide such predictive information. The potential for predictive capabilities of both pilot and display is a relevant area for future study.

DISCUSSION

In general, performance trends predicted by the model were confirmed experimentally. Experimental and analytical results both indicated superiority of the "advanced" display with respect to regulation of height and airspeed errors. Velocity steering allowed tighter regulation of height errors, but control parameters had little influence on airspeed regulation. Model analysis indicated that display-related differences could be ascribed to differences in the quality of speed-related information provided by the two displays.

Predictions were most accurate with regard to display-and control-related differences in the total swing of the mean error over the course of the approach, and least accurate with regard to response variability and absolute levels of mean error. Experimental run-to-run variability was from 2 to 3 times as great as predicted for both height and speed errors, [2], and mean errors tended to be less negative (or more positive) than predicted. The relatively large experimental variability may have been, in part, a result of keeping the data base small to prevent the pilot's learning of the shear profile. In addition, there appeared to be a tendency for the pilots to fly high and/or fast on some trials and not on others, a factor that could contribute to predictive inaccuracies.

With regard to future application of the pilot/vehicle model to the study of approach performance in windshears, one might profitably address questions relating both the pilot's conception of the behavior of the wind as well as to the wind information explicitly displayed. For example, one can assume that the pilot knows that the wind will change with altitude (and thus with time) in a smooth manner, and one can explore the consequences of displaying (a) the same variables displayed in this study, (b) additional variables relating to the current wind state, and (c) additional variables relating to the rate-of-change of wind. Furthermore, one can explore the interaction of these factors with the type and severity of shear. Additional factors that can be explored are the relation between performance and workload for candidate controls and displays, as well as the utility of motion cues in detection of windshears.

In conclusion, the model employed in this study has been validated with regard to its ability to predict important performance trends related to controls and displays in windshear environ-

ments. Because of the operational necessity of understanding performance in windshears, we suggest that the pilot/vehicle model be applied further to aid in the design of simulation experiments and to explore a variety of factors that cannot be readily studied in the laboratory. While we cannot guarantee accurate predictions of absolute performance levels at this stage of model development, the model should provide reliable indications of the nature of performance and workload improvements that can be achieved with candidate controls and displays in a variety of windshear environments.

REFERENCES

1. Levison, W. H. and S. Baron, "Analytic and Experimental Evaluation of Display and Control COncepts for a Terminal Configured Vehicle", Report No. 3270, Bolt Beranek and Newman Inc., Cambridge, Mass., July 1976.

2. Levison, W. H.; "Analysis and In-Simulator Evaluation of Display and Control Concepts for a Terminal Configured Vehicle in Final Approach in a Windshear Environment", Report No. 3632, Bolt Beranek and Newman Inc., Cambridge, Mass., August 1977. To be published as NASA CR-3034, 1978.

3. Baron, S. and W. H. Levison, "Analysis and Modelling Human Performance in AAA Tracking", Report No. 2557, Bolt Beranek and Newman Inc., Cambridge, Mass., March 1974.

4. Kleinman, D. L. and W. R. Killingsworth, "A Predicative Pilot Model for STOL Aircraft Landing", NASA CR-2374, March 1974.

5. Kleinman, D. L. and T. Perkins, "Modeling the Human in a Time-Varying Anti-Aircraft Tracking Loop", Trans. of the First NWC Symposium on the Application of Control Theory to Modern Weapons Systems, China Lake, California, June 1973. Also IEEE Trans. on Auto. Control, Vol AC-19, No. 4, pp. 297-306, August 1974.

6. Chalk, C. R., T. P. Neal, T. M. Harris, F. E. Pritchard and R. J. Woodcock, "Background Information and User Guide for MIL-F-8785B(ASG), "Military Specification - Flying Qualities of Piloted Airplanes." AFFDL-TR-69-72, U.S. Air Force, August 1969. (Available from DDC as AD 860 856.)

7. Foxworth, T. G. and H. F. Marthinsen, "Another Look at Landing and Stopping Criteria", AIAA Paper No. 74-956, AIAA 6th Aircraft Design Flight Test and Operations Meeging, Los Angeles, California, August 13-14, 1974.

SESSION H: EYE/HEAD TRACKING AND SCANNING

Chairman: K. Ziedman

416

D29

N79-15617

TWO DIMENSIONAL EYE TRACKING: SAMPLING RATE OF FORCING FUNCTION

John P. Hornseth, Donald L. Monk, James L. Porterfield
Crew Station Integration Branch
Human Engineering Division
6570 Aerospace Medical Research Laboratory
Wright-Patterson AFB, Ohio 45433

Robert L. McMurry
Systems Research Laboratory
2800 Indian Ripple Road
Dayton, Ohio 45440

INTRODUCTION

This study was conducted to determine the minimum update rate of a forcing function display required for the operator to approximate the tracking performance obtained on a continuous display. Previous studies (see review by Frost, 1972, p. 287) using time on target as a measure of performance, obtained a breakdown in performance around 15 samples per second. In this study, frequency analysis was used to determine whether there was an associated change in the transfer function characteristics of the operator. It was expected that as the forcing function display update rate was reduced, from 120 to 15 samples per second, the operator's response to the high frequency components of the forcing function would show a decrease in gain, an increase in phase lag, and a decrease in coherence.

APPARATUS

The forcing function, in each dimension, consisted of the sum of nine sine waves and simulated a Gaussian noise passed through a second order filter with a roll-off frequency at 1 Hz. The forcing function was generated at rates of 120, 60, 30, or 15 samples per second and presented on the screen at these update rates. An optical projection system consisting of a low power laser and a pair of galvo-mirrors rear projected the forcing function onto a cloth screen in the form of a spot of red light randomly moving in two dimensions about a center spot marked on the screen. The maximum excursion of the forcing function was $\pm 5°$ visual angle in azimuth and elevation, as viewed by the subject (S). The $\pm 5°$ visual angle positions were also marked on the screen and, along with the center spot, served as

PAGE INTENTIONALLY BLANK

calibration points for both the forcing function and S's eye movement response. The subject tracked the forcing function from a position on the opposite side of the screen from the optical projections system and equidistant from the screen.

The subject's eye line-of-sight was computed using the AMRL Honeywell Remote Oculometer. For a complete description of the Oculometer, see Merchant, et. al., 1974. Calibration of the Oculometer prior to each tracking run was accomplished by using a second optical projection system positioned adjacent to the forcing function optical projection system. The movement of the laser spot generated by this second system corresponded to the subject's eye line-of-sight. The Oculometer-driven laser spot was turned off during the tracking run.

Five channels of a seven channel 1/2-inch Ampex 300 instrumentation tape recorder were used to record: (1) time code, (2) horizontal forcing function, (3) vertical forcing function, (4) horizontal eye movements, and (5) vertical eye movements.

PROCEDURE

Four students, two male, two female, from the University of Dayton served as subjects for this study. Each subject tracked the forcing function twice at each sampling rate (eight tracking runs per subject) in a partially balanced design. The data for each subject was collected in two test sessions of four tracking runs each. After seating the subject, the operation of the Oculometer was checked and calibrated. The subject was instructed to sit in a natural, comfortable position. The only constraint placed upon the subject was the instruction to refrain from making large head movement. The subject was instructed to follow (pursue) the moving spot of light with his eyes as the spot moved on the screen. The subjects were screened for uncorrected 20/20 vision. Between runs subjects were given a short rest.

RESULTS

Frequency analyses of the data from the four subjects were accomplished using an IBM 370 Computer and the BMD X92 program. For each run the power spectral density of the forcing function, the power spectral density of the eye response output, the cross power spectral density, the cross correlation, the coherence, and the transfer functions in gain and phase were computed. The data for the two runs for a given sampling rate condition were averaged, for each subject, at each of the nine sine wave component frequencies of the forcing function.

The average transfer function gain, averaged across subjects, for each of the four sampling rates, are presented in Figure 1 (Horizontal) and Figure 3 (Vertical). No differences attributable to sampling rate are present.

The average transfer function phase, averaged across subjects, for each of the four sampling rates, are presented in Figure 2 (Horizontal) and Figure 4 (Vertical). An increase in transport delay of approximately 30 msec was observed at the 15 samples per second update rate for both the horizontal and vertical tracking data.

The coherence data averaged around .98 with a slight drop off at the high frequencies and showed no differences attributable to the sampling rate of the forcing function.

DISCUSSION

The lowest update rate used in this study (15 samples per second) was not low enough to have an appreciable effect upon the transfer function characteristics of the operator. Further research is planned using lower update rates. Expected changes at the high frequency sine waves components of the forcing function not observed in this study may be observed at lower update rates. A time on target analysis of the data is planned to determine whether the results of this study correspond with the results previously reported.

REFERENCES

1. Frost, G., Man-Machine Dynamics. In Vancott, H.P. and Kinkade, P.G. (Eds), Human Engineering Guide to Equipment Design, (Revised Edition), McGraw-Hill, 1972.

2. Merchant, John, Morrissette, Richard, and Porterfield, James L., "Remote Measurement of Eye Direction Allowing Subject Motion Over One Cubic Foot of Space," IEEE Transactions in Biomedical Engineering, Vol BME-21, No. 4, July 1974.

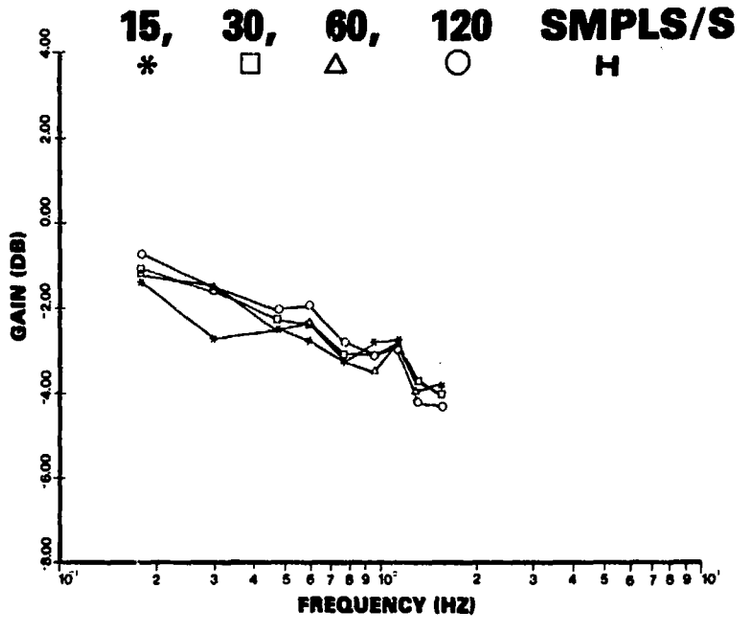

Figure 1. Horizontal Gain as a Function of Update Rates

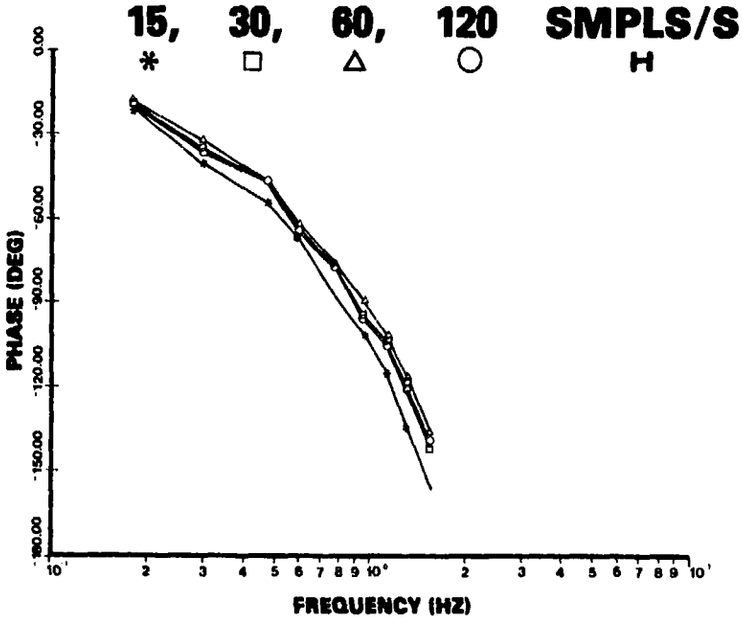

Figure 2. Horizontal Phase as a Function of Update Rates

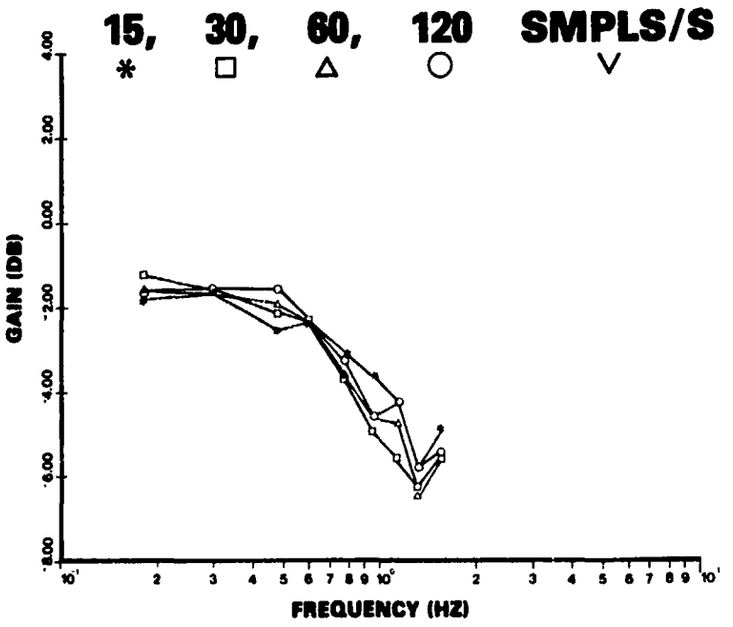

Figure 3. Vertical Gain as a Function of Update Rates

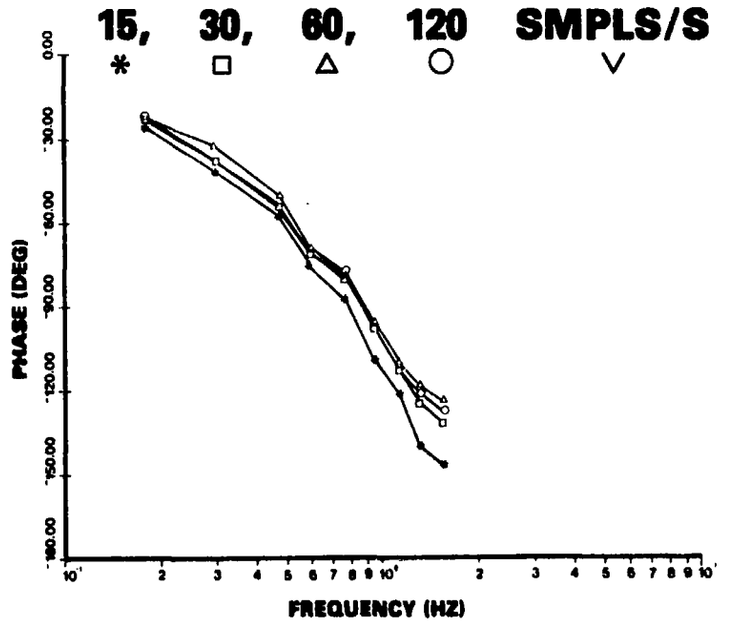

Figure 4. Vertical Phase as a Function of Update Rates

N79-15618

HEAD TRACKING AT LARGE ANGLES FROM THE STRAIGHT AHEAD POSITION

Donald L. Monk, James L. Porterfield, John P. Hornseth
Crew Station Integration Branch
Human Engineering Division
6570 Aerospace Medical Research Laboratory
Wright-Patterson AFB, Ohio 45433

Robert L. McMurry
Systems Research Laboratory
2800 Indian Ripple Road
Dayton, Ohio 45440

INTRODUCTION

The basic purpose of this experiment was to compare head tracking performance at various angles from the straight ahead position. In our previous laboratory studies (e.g. Shirachi and Black, 1975; Hornseth, Stanley, and Carson, 1976; and Shirachi, Monk, and Black, 1976) head tracking was performed within a ± 15° or less cone about the straight ahead or boresight position. Honeywell has conducted studies in which the subjects aimed their heads as far off boresight as 40° (Hughes, et al, 1970). Their subjects slewed their heads in the direction indicated by an arrow, on the head position display they were using, until a target came into the field of view of the helmet mounted display. At this point their task became that of laying a reticle over the target to achieve lock on. The length of time the subjects were actually tracking was only a few seconds. Flight test studies conducted at Tyndall AFB and China Lake (Dietz et al, 1971 and Grossman, 1974) investigated head tracking performance which included large off-boresight angles. The target motion in these two studies was highly predictable.

One of the big advantages of a helmet sight in a high performance aircraft is its off-boresight capability in aiming a fire control system. However, tracking data using a target that is moving rapidly and randomly for an extended period of time is missing. This study is intended to provide data in this area that will be of value to engineers in designing head control systems.

424
PAGE INTENTIONALLY BLANK

METHOD

Apparatus:

A PDP 11/34 minicomputer with floating point hardware was used to generate the forcing function, digitize and record 4 analog data channels (azimuth and elevation of both the target and head motion), and perform some data analyses. A Honeywell helmet mounted sight (HMS) was used to sense the subject's head angles as he tracked the target. This helmet system weighed 1.65 kg. A Hughes, side mounted, helmet display was used to present the moving target and head position reticle to the subject's right eye. This helmet mounted display weighed .54 kg. An IMLAC PDS-4 computer graphics display generated the target and reticle symbology using the forcing function and the head position signals to position the target symbol relative to the reticle. An Ampex FR-1300 instrumentation tape recorder was used to record the subjects' responses, the forcing function, and a time code. An IBM 370/155 was used for data analysis and plotting.

The forcing function was updated at a 90 Hz rate. The HMS provided head azimuth and elevation angles at a 30 Hz rate. The IMLAC was "free running" at approximately a 1000 Hz refresh rate.

Forcing Function:

The forcing functions were generated from a sum of sine waves with the amplitudes scaled to simulate white noise passed through a second order filter with a break frequency of 0.7 Hz. More information on the forcing function can be found in Appendix A. The phase relationships between the sine waves were randomly varied from subject to subject but remained constant across a given subject's conditions. Pilot study data indicated that there was negligible learning across 6 runs with the same forcing function.

Procedure:

Each subject performed the head tracking under 6 head position conditions. The following mean azimuth and elevation angular positions were used:

0°, 0° (center-center); 0°, +30° (center-up); 0°, -30° (center-down); -45°, 0° (left-center); -45°, +30° (left-up); and -45°, -30° (left-down). Because of symmetry of the left-right neck muscles and pilot study data, only the left hemisphere of head motion was investigated. Performance at angles further off-center were not selected for examination because pilot study data suggested that the limits of head and neck motion may be exceeded at larger angles for some subjects. Other supporting data give the average limit of male neck movement for up flexion at 61° with S.D. of 27° down

flexion at 60° with S.D. of 12°, and left or right rotation at 79° with S.D. of 14° (Van Cott and Kinkade, 1972). The maximum excursion of the target from each of the 6 head positions was ±10°. This small excursion was used to increase the probability the target would remain on the subjects' display at all times and not require the subject to search for it. Also, the small target excursions constrained the subjects to track at various mean angular positions within the head motion envelope to provide an adequate representation of head tracking at the specified off-center positions.

Each tracking run was 100 seconds long. The first 9 seconds of tracking were not scored to allow the subject to overcome the initial "start up" error induced by the target suddenly jumping to a random starting position and beginning to move. The following 91 seconds of tracking data were recorded and scored. At the end of each run a rest period of 1 minute was given. After each group of 3 runs, the rest period was extended to 5 minutes. The first 6 runs were practice runs, allowing for the subjects to adjust to head tracking at each angular position. All practice runs were presented to each subject in the same order. The data runs were presented in a randomized order to reduce any possible ordering effects. All subjects' scores asymptoted to an acceptable level of performance during the practice runs.

Subjects:

Fourteen male subjects were used with ages ranging from 16-40. Eye dominance was tested for each subject with about half reporting right eye dominance. The subjects'instructions are given in Appendix B.

RESULTS & DISCUSSION

A subject's performance scores were computed from his radial error data. Radial error is the visual angle from a subject's line of sight to the target at each instant in time. The Duncan's New Multiple Range Test (NMRT) was used to test for statistical differences in performance at the 6 head angle positions. Table 1 shows the 3 homogenous subsets of head positions found using the 50% circular error probability (CEP) metric (a 50% CEP refers to that radius, about the target, within which the subject tracked 50% of the time). The best performances (lowest CEP), denoted by the A subset, was found when the head faced center-center, left-center, and left-down. The next best performance, the B subset, was obtained when the head faced center-center, left-up, left-down, and center-up. The worst performance, subset C, was found when the head faced center-down, center-up, and left-up. It should be noted that the differences between the best position (-45°, 00°) and the worst position (00°, -30°) is small, .15° or 6%. While this difference is statistically significant, it is left up to the designers/engineers to determine if the difference is of practical significance.

Establishment of on target gate rings were done as an analysis procedure after data collection. However, during the experimental runs, the subjects were not required to keep the target within a gate ring, nor were they shown any rings. In analyzing the data, a subject was considered on target if his radial error was less than a specified tolerance. Six on target tolerance rings were used in analyzing the data collected in this experiment. They ranged from 1° to 6°, in 1° increments. Gate times were computed for each tolerance ring. Gate time was defined to be the amount of time a subject kept the target inside the ring. As soon as the target was outside the ring, that gate time ended. If the target was again inside the ring, another gate time was started. To reduce "noise" effects in this gate time measure, an arbitrary dead time zone of .1 seconds was used. This meant that not only must the target be within the ring to start a gate, it must also be within for .1 second. Likewise, it must be outside of the ring for .1 second to end the gate. The mean gate times for each ring, averaged over all positions, are shown in figure 1. Using the Duncan's test, the gate time metric did not prove to be a sensitive measure for distinquishing among the angular positions (Tables 2-7). For all of the tolerance rings, except the 4° ring, performance at the 6 head positions did not differ significantly from each other. The 4° ring indicated that the longest gate times were obtained at all positions except left-up and center-down. The next subset included all positions except left-center.

The time on target (TOT) scores, for each tolerance ring, were computed by multiplying the mean gate times by the number of times the target stayed within the ring. The mean TOTs for each ring, averaged across all positions, is shown in figure 2. The Duncan's test was applied to each of the 6 rings to determine homogenous subsets. As shown in Table 8 for the 1° tolerance band, there are no significant differences among any of the 6 angular positions. As the task becomes easier, by increasing the tolerance ring to 2°, the Duncan's test indicates that 3 homogenous subsets exist. As with the CEP metric, the TOT with a 2° ring has the best scores at the center-center, left-center, and left-down (Table 9). Next best scores are center-center, left-up and down, and center-up. The worst scores are center-center, left-up, and center-up and down. Increasing the ring size to 3°, there are still 3 homogenous subsets (Table 10). The best and second best scores remain the same, while the worst score is found to be the center-down position. With the rings at 4° and 5°, only 2 homogenous subsets are found (Tables 11 and 12). The best scores are the same positions as those in the 2° and 3° rings. The second best positions are also the same as in the 2° and 3° ring plus the center-down position is included in this subset. The 6° tolerance ring, the easiest task, also has 3 homogenous subsets (Table 13). The best positions were found to include all positions except center-down, while the next best included all positions except left-center. For this condition, both significantly different subsets have almost merged into a single subset.

A two way analysis of variance was used to test for significances in RMS error scores. No significant difference was found between azimuth versus elevation RMS errors (Table 14). Significance at the p = .001 level was found between the 6 angular positions. The head position by azimuth-elevation dimension interaction was also found to be significant at p = .001 level.

A Duncan's test was performed to compare RMS error scores between the 6 angular positions for both azimuth and elevation. Two homogenous subsets were found with the azimuth scores (Table 15). The best performance was the center-center and all left positions. With the elevation RMS error scores, 3 homogenous subsets were found, but with a different grouping than the other metrics have found (Table 16). The best performance was at left-center, left-down, and center-down. This was the only time that the center-down position was in the best performance grouping when multiple groups were found. The next subset contained the left-down, center, center-up, and center-down conditions. The worst position was the left-up position.

CONCLUSIONS

The 3 primary metrics, CEP, TOT, and gate times, all emphasize a different aspect of tracking performance, but they are not independent of each other. Thus, it is not surprising that the Duncan's test should generally designate the same position subsets. In almost all the tests, the best position was the left-center, followed by the center-center and left-down positions. Again, it should be emphasized that all of the differences found were small but statistically significant. However, they may or may not be practically significant. The helmet mounted sight and helmet mounted display used for this experiment were early prototypes. The later models of each unit are lighter and have a much improved center of gravity. Both of these factors may eliminate even the statistical significant differences among the positions within the envelope $\pm 45°$ azimuth and $\pm 30°$ elevation.

APPENDIX A

The sum of sine wave input was chosen such that it simulated white noise passed through the second order system $\left(\frac{A}{S+A}\right)^2$. Eleven sine frequencies, for azimuth were selected on the basis of being equal spaced between 0.10 Hz and 2.00 Hz on a $\log_{10}$ scale. For elevation, the 11 sine frequencies were also spaced equally on a $\log_{10}$ scale with the frequencies being midway between the azimuth frequencies. Their frequencies ranged from 0.12 Hz to 2.32 Hz. An additional requirement placed upon frequency selection was that the resultant input must complete a full cycle at the run's end. Thus, all frequencies must be a harmonic of the fundamental frequency. For this experiment, the fundamental frequency, $f_o = \frac{1}{91.02 \text{ seconds}} = .01099$ Hz.

APPENDIX B

Subject Instructions: "Your task in this experiment will be to head track a rapidly moving target. In the head mounted display, located in front of your right eye, you will notice a reticle at the center of the display. This reticle will always remain at the center of the display as you move your head. Please move your head around a little so that you can see which of the two objects is actually the reticle. The object that moves around on the display, as you move your head, is the target. During the test runs, the target will move around in a rapid, random pattern. Your task will be to move your head so as to keep the center of the reticle as near the center of the target as you can. The test runs will last 90 seconds. After each test run, you will be given a 1 minute rest period before the next run. Please remain seated during these short rest periods. Each test run will require you to track the target with your head aimed in a different direction. You will first be given some practice in tracking at each of the 6 head positions used in the experiment. Then you will be given the experimental runs. After each group of 3 runs you will be allowed to get up out of the chair to stretch and walk around. If at any time you have any questions about what you are to do, be sure to ask for additional instructions or clarifications. Do you have any questions at this time?"

REFERENCES

Dietz, F. and Wise, J., "Evaluation of the Helmet Mounted Sight" (Title Unclassified, Confidential Report) ADC/ADWC, Project 69-19, December 1971.

Grossman, J., "Flight Evaluation of Pilot Sighting Accuracy Using a Helmet-Mounted Sight, "NWC TP5638, Naval Weapons Center, China Lake, California, April 1974.

Hornseth, J., Stanley, G., and Carson, P., "Head Tracking: A Fatigue Study," NASA TMX-73 170, Twelfth Annual Conference on Manual Control, Ames Research Center, Moffett Field, California, May 1976.

Hughes, J., Henke, A., and Schultz, R., "Helmet Mounted Sight/Display Applications," AFFDL-TR-69-118. Air Force Flight Dynamics Laboratory, Wright-Patterson AFB, OH, April 1970.

Shirachi, D., and Black, J., "Head-Eye Tracking in Two-Dimensional Pursuit Tasks," NASA TMX-62-464, Ames Research Center, Moffett Field, California, May 1975.

Shirachi, D., Monk, D., and Black, J., "Effects of Headgear and Visual Angle on Head Rotation Spectral Characteristics," NASA TMX-73-170, Ames Research Center, Moffett Field, California, May 1976.

ORIGINAL PAGE IS
OF POOR QUALITY

Van Cott, H., Kinkade, G., Editors; Human Engineering Guide to Equipment Design", Superintendent of Documents, U. S. Government Printing Office, Washington, D.C., 20402, 1972.

FIGURES AND TABLES

FIGURE 1

MEAN GATE TIMES FOR EACH GATE TOLERANCE RING, AVERAGED ACROSS ALL HEAD POSITIONS

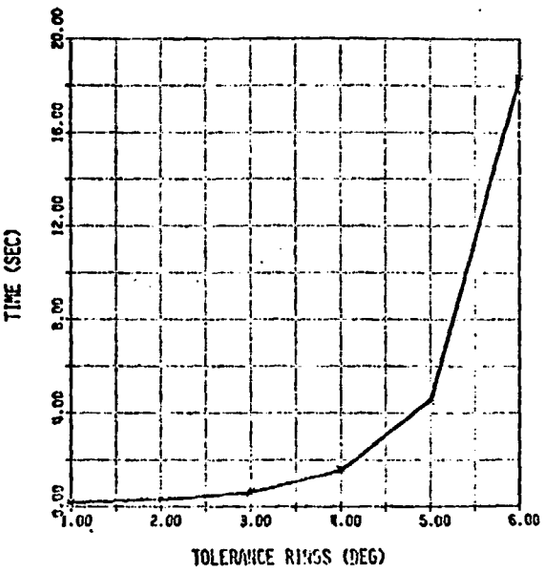

FIGURE 2

MEAN TIME ON TARGET FOR EACH TOLERANCE RING, AVERAGED ACROSS ALL HEAD POSITIONS

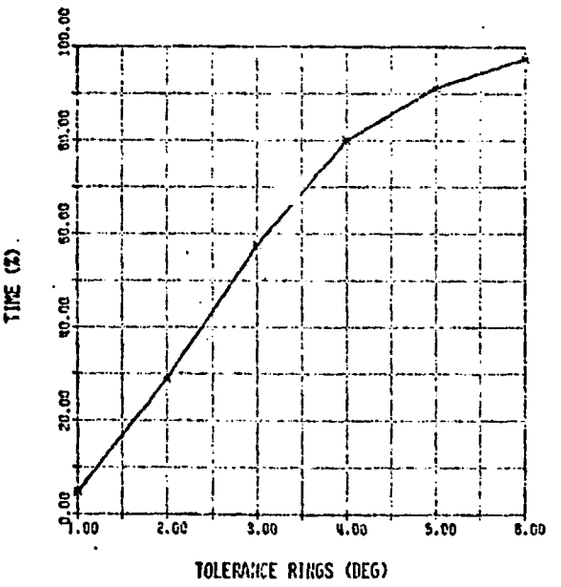

TABLE 1

DUNCAN'S NMRT FOR THE MEAN CEP SCORES AT THE 6 HEAD POSITIONS

CEP (DEGREES)		
EL (DEG)	AZ (DEG)	
	-45	0
+30	2.60 BC*	2.61 BC
0	2.51 A	2.55 AB
-30	2.57 AB	2.66 C

TABLE 2

DUNCAN'S NMRT RESULTS FOR THE 1° GATE TIME SCORES AT THE 6 HEAD ANGLE POSITIONS

1° GATE TIMES (SEC)		
EL (DEG)	AZ (DEG)	
	-45	0
+30	0.15 A	0.16 A
0	0.16 A	0.15 A
-30	0.16 A	0.15 A

TABLE 3

DUNCAN'S NMRT RESULTS FOR THE 2° GATE TIME SCORES AT THE 6 HEAD ANGLE POSITIONS

2° GATE TIMES (SEC)		
EL (DEG)	AZ (DEG)	
	-45	0
+30	0.28 A	0.28 A
0	0.29 A	0.28 A
-30	0.29 A	0.28 A

TABLE 4

DUNCAN'S NMRT RESULTS FOR THE 3° GATE TIME SCORES AT THE 6 HEAD ANGLE POSITIONS

3° GATE TIMES (SEC)		
EL (DEG)	AZ (DEG)	
	-45	0
+30	0.60 A	0.59 A
0	0.64 A	0.62 A
-30	0.62 A	0.58 A

* For all Duncan's NMRT tables in this report, letters represent homogenous subsets. The mean performance scores contained in a subset do not differ significantly from other means contained in that subset. The means not contained in the same subset are significantly different at the p = .05 level. A given mean can belong to more than one subset.

ORIGINAL PAGE IS
OF POOR QUALITY

TABLE 5
DUNCAN'S NMRT RESULTS FOR THE
4° GATE TIME SCORES AT THE
6 HEAD ANGLE POSITIONS

4° GATE TIMES (SEC)		
EL (DEG)	AZ (DEG)	
	-45	0
+30	1.44 B	1.52 AB
0	1.85 A	1.57 AB
-30	1.59 AB	1.33 B

TABLE 6
DUNCAN'S NMRT RESULTS FOR THE
5° GATE TIME SCORES AT THE
6 HEAD ANGLE POSITIONS

5° GATE TIMES (SEC)		
EL (DEG)	AZ (DEG)	
	-45	0
+30	4.54 A	4.62 A
0	5.12 A	4.59 A
-30	4.42 A	4.13 A

TABLE 7
DUNCAN'S NMRT RESULTS FOR THE
6° GATE TIME SCORES AT THE
6 HEAD ANGLE POSITIONS

6° GATE TIMES (SEC)		
EL (DEG)	AZ (DEG)	
	-45	0
+30	17.2 A	19.2 A
0	20.0 A	20.3 A
-30	19.5 A	13.6 A

TABLE 8
DUNCAN'S NMRT RESULTS FOR THE
1° TIME ON TARGET SCORES AT
THE 6 HEAD ANGLE POSITIONS

1° TOT (%)		
EL (DEG)	AZ (DEG)	
	-45	0
+30	4.52 A	4.56 A
0	5.15 A	4.73 A
-30	5.22 A	4.66 A

TABLE 9
DUNCAN'S NMRT RESULTS FOR THE 2° TIME ON TARGET SCORES AT THE 6 HEAD ANGLE POSITIONS

2° TOT (%)		
EL (DEG)	AZ (DEG)	
	-45	0
+30	28.2 BC	28.4 BC
0	30.7 A	29.3 ABC
-30	29.6 AB	27.4 C

TABLE 10
DUNCAN'S NMRT RESULTS FOR THE 3° TIME ON TARGET SCORES AT THE 6 HEAD ANGLE POSITIONS

3° TOT (%)		
EL (DEG)	AZ (DEG)	
	-45	0
+30	57.4 B	56.8 B
0	60.3 A	58.7 AB
-30	58.3 AB	55.7 C

TABLE 11
DUNCAN'S NMRT RESULTS FOR THE 4° TIME ON TARGET SCORES AT THE 6 HEAD ANGLE POSITIONS

4° TOT (%)		
EL (DEG)	AZ (DEG)	
	-45	0
+30	79.2 B	78.8 B
0	82.0 A	80.5 AB
-30	79.9 AB	78.3 B

TABLE 12
DUNCAN'S NMRT RESULTS FOR THE 5° TIME ON TARGET SCORES AT THE 6 HEAD ANGLE POSITIONS

5° TOT (%)		
EL (DEG)	AZ (DEG)	
	-45	0
+30	91.6 B	91.7 B
0	93.6 A	92.5 AB
-30	92.2 AB	91.0 B

ORIGINAL PAGE IS
OF POOR QUALITY

TABLE 13

DUNCAN'S NMRT RESULTS FOR THE 6° TIME ON TARGET SCORES AT THE 6 HEAD ANGLE POSITIONS

6° TOT (%)		
EL (DEG)	AZ (DEG)	
	-45	0
+30	97.2 AB	97.4 AB
0	98.2 A	97.7 AB
-30	97.7 AB	96.9 B

TABLE 14

ANALYSIS OF VARIANCE TABLE OF RMS ERROR

Source of Variation	DF	Sum of Squares	Mean Square	F	P
A (AZ-EL Dimension)	1	.17	.17	4.53	>.05
B (Angular Positions)	5	.46	.09	5.01	<.001
C (Subject)	13	7.16	.55	65.82	
A X B	5	.27	.05	6.42	<.001
A X C	13	.50	.04	4.56	
B X C	65	1.19	.02	2.19	
A X B X C	65	.54	.01		
Total	167	10.30			

TABLE 15

DUNCAN'S NMRT RESULTS FOR THE AZIMUTH RMS ERROR SCORES AT THE 6 HEAD ANGLE POSITIONS

AZ RMS E (DEG)		
EL (DEG)	AZ (DEG)	
	-45	0
+30	2.23 AB	2.25 B
0	2.15 A	2.15 A
-30	2.23 AB	2.31 B

TABLE 16

DUNCAN'S NMRT RESULTS FOR THE ELEVATION RMS ERROR SCORES AT THE 6 HEAD ANGLE POSITIONS

EL RMS E (DEG)		
EL (DEG)	AZ (DEG)	
	-45	0
+30	2.29 C	2.20 B
0	2.05 A	2.16 B
-30	2.11 AB	2.13 AB

ORIGINAL PAGE IS
OF POOR QUALITY

N79-15619

D31

LIGHTWEIGHT HELMET-MOUNTED EYE MOVEMENT MEASUREMENT SYSTEM

John A. Barnes

US Army Human Engineering Laboratory
Aberdeen Proving Ground, Maryland

We first realized the need for a simple, easy to use, lightweight device to determine the aircrewman's fixation points and paths of eye movement between fixation points when we performed our initial eye movement measurement work. We used a Mackworth EMC-2 device, figure 1, to determine a helicopter pilot's visual work load during actual flight.

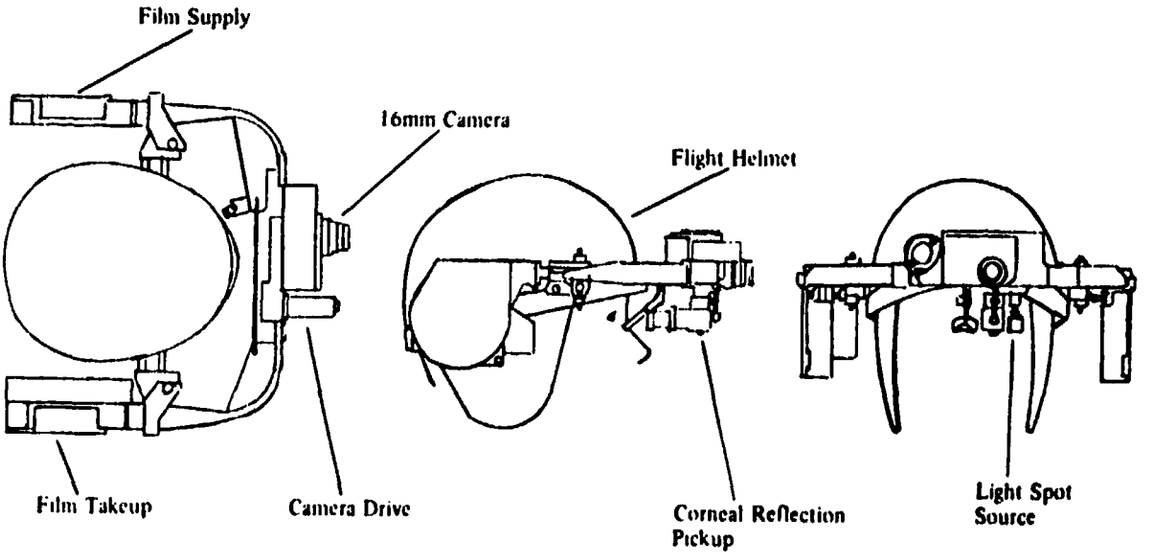

Figure 1. EMC-2 Eye-Movement Camera

The development of the present system has been a "spare-time" project since 1971. The components have been procured whenever funds were available or a particular project required their use. The interface components were constructed by our shop personnel during slack periods in their work schedules. There are no custom designed components in the present system; every item is, or is made up from commercially available components.

The helmet we used is the type that preceded the present US Army aviators' helmet. It has been modified slightly; a small amount of material has been removed from immediately above the brow to accommodate the camera case, the visor has been removed and the suspension system has been replaced with a removable, subject-fitted, molded plastic foam inner helmet similar to the one used in the USAF HGU-2 flight helmet. The fitted helmet

stabilizes the optical head and helps to keep the system in calibration during use. The helmet-mounted eye movement measuring system, figure 2, weighs 1,530 grams; the weight of the present aviators' helmet in standard form with the visor is 1,545 grams.

Front view of the system.

System in the stowed position.

Figure 2. Lightweight Helmet-Mounted Eye Movement Measurement System

The optical head is a standard NAC Eye-Mark. This optical head was mounted on a magnesium yoke which in turn was attached to a slide cam mounted on the flight helmet. The slide cam allows one to adjust the eye-to-optics system distance quite easily and to secure it so that the system will remain in calibration. The design of the yoke and slide cam is such that the subject can, in an emergency, move the optical head forward and upward to the stowed and locked position atop the helmet. This feature was necessary for flight safety.

The television camera that is used in the system is a solid state General Electric TN-2000 with a charged induced device (CID) imager used as the vidicon. This particular device has 45,000 cells which form the video picture. The charged coupled device (CCD) solid state imagers are also available but the CID imagers have an advantage in that they do not "bloom" as badly when they are struck by a bright light. Fairchild now offers a CCD imager which contains 185,440 cells and produces a more detailed video picture; this was not available when our system was assembled. The CID imager is mounted on the NAC optical head in place of the standard fiber optics. The camera electronic package which measures 7½ x 2 x 4 inches and weighs less than two pounds is placed in the pocket of a vest worn by the subject. The imager and electronic package are connected by a very thin ribbon cable which is 42 inches long.

The output of the system can be sent to the video monitor and recorder by direct wire or by the use of video transmitter. It can be transmitted over a range of 3,000 feet. The video transmitter measures 7½ x 3 x 3¼ inches and weighs 1½ pounds; it can be placed in another pocket of the subject's vest.

ORIGINAL PAGE IS
OF POOR QUALITY

All components of this system operate on 12 volts or less. The power can be supplied from a belt-type battery pack or can be taken from the vehicle electrical system; the total power requirement for the subject mounted equipment is less than three amperes.

A coupling lens is required to match the optical output from the NAC optical head to the CID imager. The design of the lens used determines the distance between the optical head and the CID imager.

For applications where the helmet is not necessary, the system's video components can be used with the standard EYE-MARK face mask mount. For our own laboratory use we have replaced the snap fasteners of the face mask mount with VELCRO for easier and faster adjustments.

This system is not without its difficulties; the video presentation is not as precise as a film rendition of the same scene but the instant feedback is worth the degradation of the presentation. For most purposes little or no information is lost by using the video recordings. When the system is used to investigate visual behavior where the fixation points will be at distances greater than 100 meters, there is an inherent problem in the EYE-MARK. The light marker that indicates the subject's fixation point is a fixed size, .5 mm, and as the scene lens presents an increased scene area this fixed mark increases in size relative to the rest of the presentation. We have had limited success in decreasing the size of the light marker by reducing the size of its aperture. This also decreases the marker's brightness and it will no longer be visible on the scene presentation. The minimum aperture size that we have been able to use is .11 inches (normal is .16), this reduces the light marker size by about one-third. One further problem that might bother some is that the video presentation is a mirror image of the real world, the fiber optics systems contains a mirror which is not used with this video system. We rectify this by placing a front surface mirror at some comfortable angle in front of the monitor and view the video picture from a position above and behind the monitor.

The Fiscal Year 1977 cost to the Government for the system components was:

NAC EYE-MARK Optical Head	$ 3,420.00
GE TN-2000 CID Video Camera	2,925.00
Sony AV-3400 Video Recorder	888.75
Sony CVM-115 Monitor/Receiver	252.00
VM-2200 Video Transmitter 15 mw	1,584.00
Coupling Lens	400.00

The "off-of-the-shelf" cost of the complete system was $9,469.75. This cost does not reflect the cost of interfacing these components into a system; this will vary with the user's support resources but should not exceed $500.00.

We have field tested the system to check its performance with the performance specifications given by NAC for the optical head. The subject's

head was fixed in position so that all recorded movement was pure eye movement and the recorded errors were from eye movement only. The targets were set at a distance of 100 meters from the subject and extended in an arc of 11^{o} either side of the center target. The NAC specifications indicated a maximum error of 2^{o} of arc at 10^{o} either side of the center position; this is 3.5 meters error at 100 meters range. We measured 3.6 meters at 10^{o} on a smoothed curve of the 42 data points recorded. We have found in our work that a 3^{o} eye movement will be tolerated before the head is moved, thus with this system for 3^{o} of eye movement we have an error of 1 meter at 100 meters range, 10 cm at 10 meters range and 1 cm at 1 meter range.

The listing of trade name products in this article is not to be taken as an indorsement of these products. They were the products that were available at the time of procurement which met our requirement that all elements of the system operated on 12 volts DC. They were the least costly items that met that requirement and that were compatible with, or could easily be made compatible with, the other elements of the system.

SESSION I: MOTION SIMULATION AND EFFECTS

Chairman: R. Stapleford

D32

N79-15620

THE EFFECTS OF CLOSED LOOP TRACKING ON A SUBJECTIVE TILT THRESHOLD IN THE ROLL AXIS

By Marvin Roark* and Andrew Junker**

*Systems Research Laboratories, Inc.
Dayton, Ohio 45440

**Aerospace Medical Research Laboratory
Wright-Patterson Air Force Base, Ohio 45433

SUMMARY

The indifference thresholds for the perception of tilt in the roll axis were experimentally determined in a moving base simulator under three tracking task difficulties. The threshold level determined in this experiment is approximately 5 to 7 degrees (.1g).

INTRODUCTION

In ground based simulators, unlike aircraft, false tilt cues may occur when they are rolled. The amount of tilt which can be detected by the pilot in the simulator, defined as the indifference threshold, appears to be a function of the task being performed. To eliminate the false tilt cues that occur when the indifference threshold is exceeded, washout schemes are used to limit the motions of the simulator. This is often accomplished by limiting the amount of roll of the simulator while still allowing the acceleration and other helpful cues to be felt by the pilot. In the past the washouts used were based on what felt good to the pilot in the simulator. Very little data is available relative to what this threshold is, see reference 1, and what factors, if any, alter the level of indifference. Data in the past has dealt with determining the absolute threshold. One set of data, see reference 2, does show that the "absolute" threshold increases when workload is increased. This prompted an investigation to determine the effect of workload on the indifference threshold level for use in washouts and in motion related parameters of pilot modeling.

An experiment was performed to determine the indifference threshold and the interactive effect of the tracking task on the threshold value. This experiment and associated results are presented in this paper.

METHOD

The basic idea behind the experiment was to have a subject track a closed loop disturbance nulling task and then superimpose a random appearing ramp (tilt input) to the motion loop of the simulator. Figure 1 is a block diagram

442

INTENTIONALLY BLANK

of the motion and visual systems used in the experiment showing the location of the disturbance input and the tilt input to the motion plant in the system. The only input was the disturbance input so the display was the negative of the simulated plant position. When the subject could detect the tilt input, he was to indicate the direction of the tilt via a hand-held indicator containing a left and a right thumb actuated pushbutton. The subject was instructed to hold the pushbutton down until he no longer felt that he was tilted. The time histories of the chair position, the tilt input and the hand-held indicator signals were recorded and later analyzed.

The experiment was run on the Roll Axis Tracking Simulator (RATS) at the Aerospace Medical Research Laboratory at Wright-Patterson Air Force Base. The RATS is capable of simulating the roll dynamics of a high performance aircraft, in this case, an F-16. The plant dynamics are described by equation 1 with limits of 180°/sec and 400°/sec^2. The cab contains a CRT mounted at the axis of rotation which is through the head of the subject. The subject viewed the display shown in figure 2 which was 26 inches away. The subject used a force stick mounted on the right side of the cab to control the tracking task. To prevent the subject from experiencing any external cues, a shroud inclosed the cab, white noise was injected in the helmet and the room lights were extinguished. In addition, a harness was used to keep the subject in his seat while the cab was in motion.

Three sum of sine inputs, simulating white noise passed through a low-pass filter with a double pole at 2 radians, were used with RMS values of .933, 1.40, and .467 pounds which resulted in 14, 21, and 7 degrees/second root mean squared (RMS) variance in the visual error. A group of ten subjects were exposed to the inputs in the order mentioned above. They ran 4 runs a day for 3 days, with each run lasting 165 seconds. The subjects had been trained from a previous experiment, therefore, minimum training was required. Data from the last two days was used for subsequent analysis. An example of a data run can be seen in figure 3. The top trace is a time history of the negative visual error (simulated plant position) seen by the subject. The negative of the visual error is shown so that it can easily be compared to the actual motion plant seen in trace 3. This was the tracking task he was trying to null out by keeping the wings on the display level with the dashed reference line. The second trace shows the offset signal that was added to the cab position. The resulting cab position during the tracking task is shown in trace 3. A run consisted of from zero to four of the offset signals to maximize randomness between runs. The offset signal itself occurred at a rate of 1°/sec with limits of ±20 degrees. The 1°/sec value was chosen because it is below the roll velocity threshold of 2°/sec, see reference 1. The last graph is the output of the hand-held indicator the subject used to indicate when the tilt was felt.

In addition to the tracking data taken, a set of baseline data for each subject was recorded. This data provides a baseline indifference threshold, comparable to the absolute threshold data taken in previous experiments. The subject was asked to sit quietly in the cab while the cab was tilted, using the same tilt input described earlier. The subject was to indicate the direction of tilt as he did before. The tracking task was not present and the

display remained fixed on the screen.

RESULTS

The results are shown in figures 4 through 7 and summarized in figure 8. For each group, the offset angle, at the point when the indicator button was pressed was recorded and placed in groups of half degree increments. The number of points recorded in each half degree group was then plotted in histogram form with the mean and standard deviation shown for each group. The mean values for the indifference threshold increases with the difficulty of the task. Fewer data points were needed for the baseline data due to the smaller amount of variance across subjects.

The summary shows a baseline level of 3.48° (.06g) which jumps to 6.46° (.113g) with the least difficult task and 7.56° (.132g) with the most difficult. These results are discussed in the following section.

DISCUSSION

From the baseline data, the indifference threshold level is 3.48° (.06g). This value can be compared to data taken from other experiments where the absolute threshold was determined but, the results from this experiment are 3 to 30 times higher, see reference 1. This is due to the conditions under which the experiment was run. These conditions added extra loading to the subjects tilt detection, similar to the kind of loading he would receive when running in a simulator. Under these "real world" conditions, the simulator environment, a useful measurement of the indifference threshold is made and can be directly applied to washout designs and used in pilot modeling.

Figures 5 through 7 show the results when tracking tasks of varying difficulties are added to the baseline conditions. The results of all four conditions, summarized in figure 8, contained the type of trend as expected, see reference 2. The summary shows a sharp jump from the baseline to the least difficult of the three tracking tasks and then increasing threshold levels with the difficulty of the task. The various difficulties were obtained by increasing the tasks RMS value which had the effect of changing the signal to noise ratio of the system. This change accounts for part of the increase in the threshold levels as well as the increase in the variance of the data. The relatively large jump from the baseline is due to the initial loading of the subject by the tracking task.

CONCLUSIONS

In this paper, an experiment to investigate the effects of the tracking task workload on the indifference threshold is described. Based on the results and the discussion, the following conclusions can be drawn.

1) The indifference threshold increases with task loading.

2) The tilt indifference threshold while performing a tracking task is approximately .1g.

REFERENCES

1. Zacharias, G.: Motion Cue Models for Pilot-Vehicle Analysis. Technical Memorandum, Bolt Beranek and Newman Inc., Cambridge, Mass., under Contract No. F33615-77-C-0506, September 1977.

2. Hosman, R.J.A.W., van der Vaant, J.C.: Thresholds of Motion Perception Measured in a Flight Simulator. Proc. of the Twelfth Annual Conference on Manual Control, Ames Research Center, Moffett Field, California, May 1976.

3. Peters, R.A.: Dynamics of the Vestibular System and Their Relation to Motion Perception, Spatial Disorientation and Illusions, NASA CR-1303, 1969.

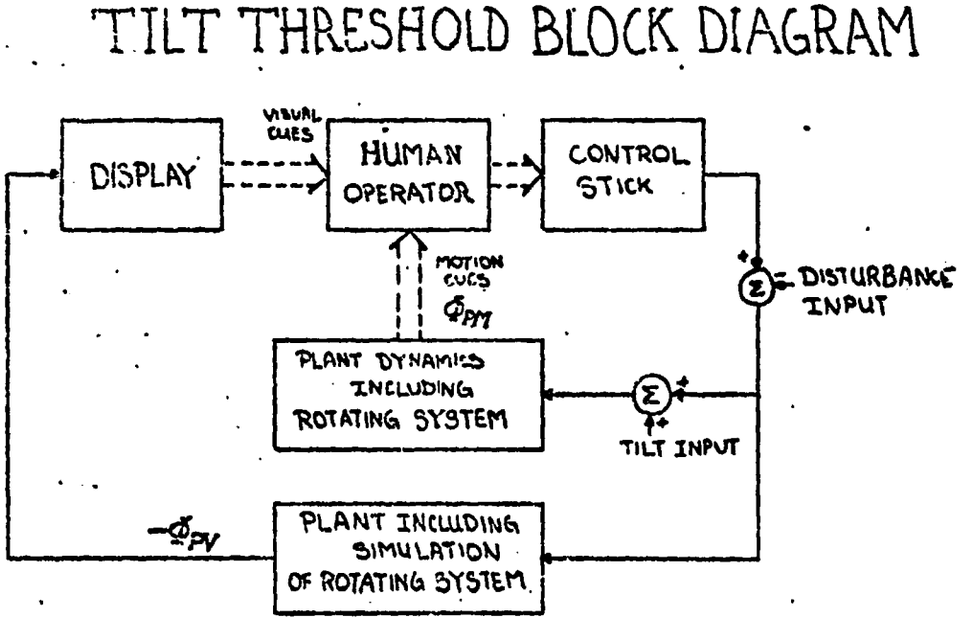

Fig. 1. Experimental Block Diagram

ORIGINAL PAGE IS
OF POOR QUALITY

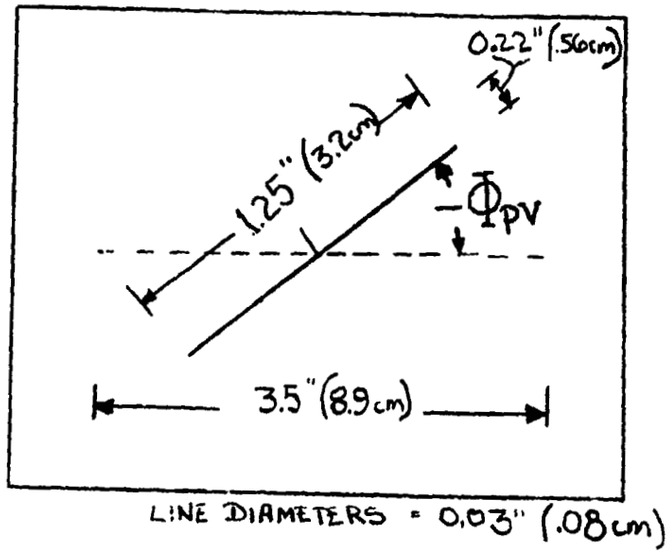

Fig. 2. Visual Display

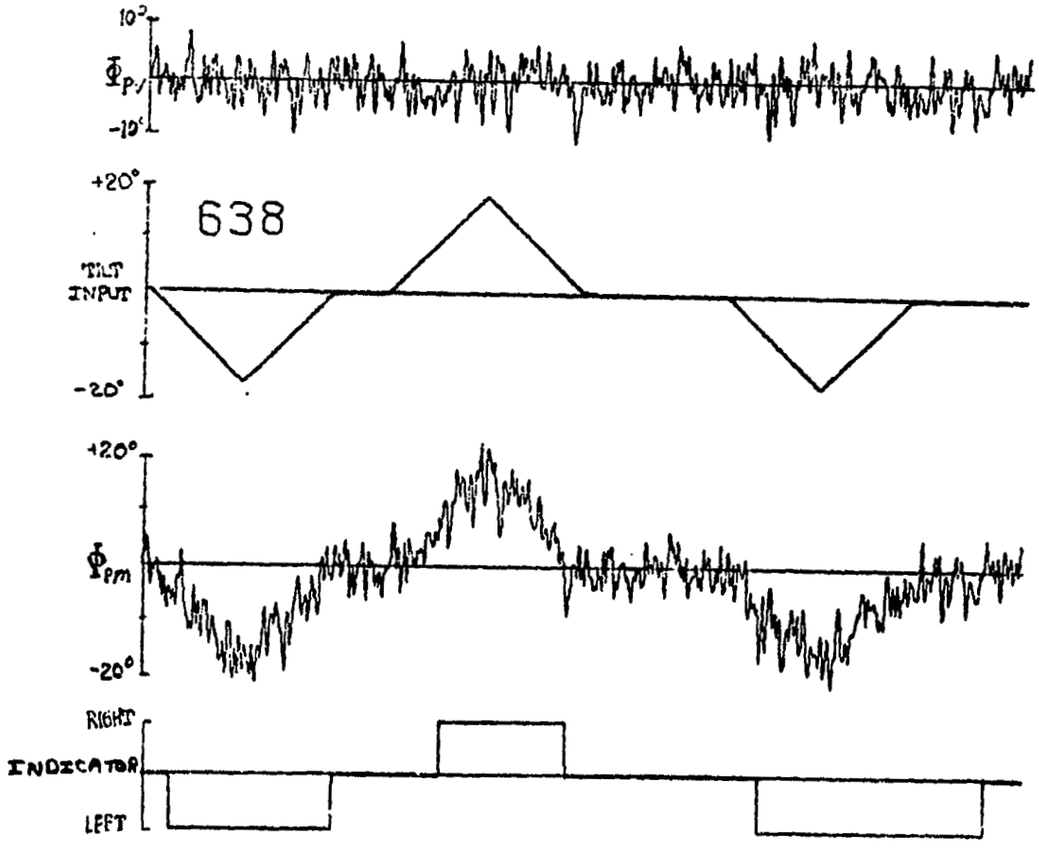

Fig. 3. Sample Data

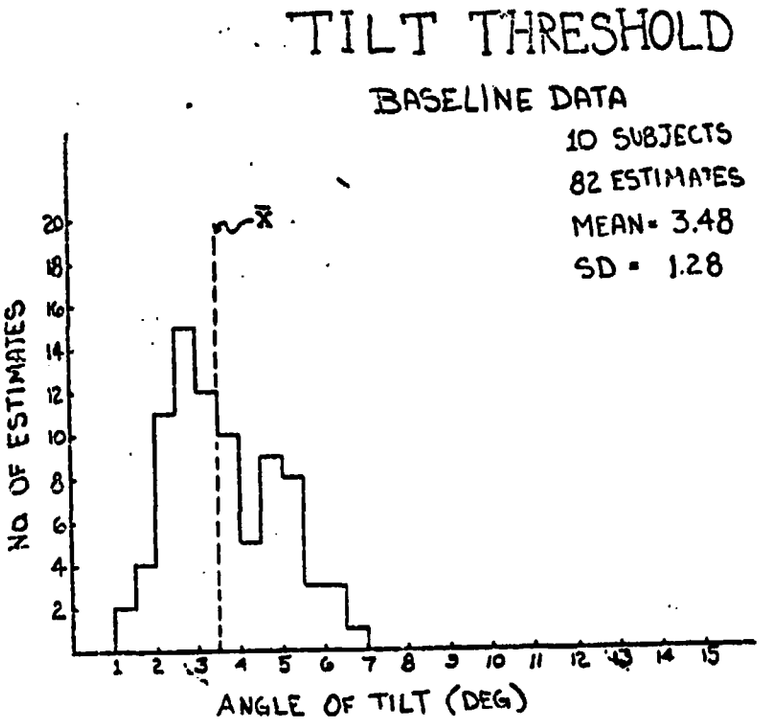

Fig. 4. Results of the Baseline Data

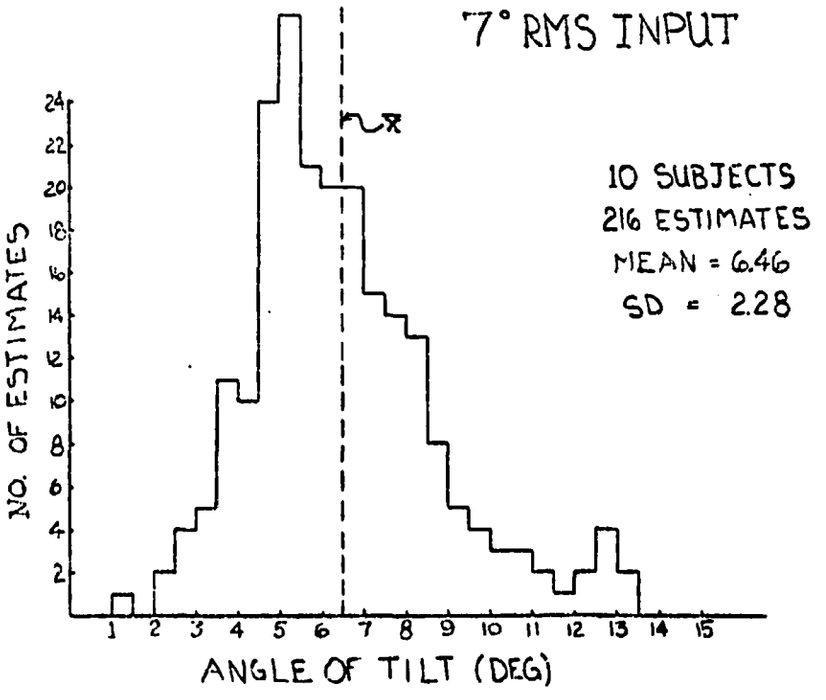

Fig. 5. Results of the 7° RMS Tracking Task

ORIGINAL PAGE IS
OF POOR QUALITY

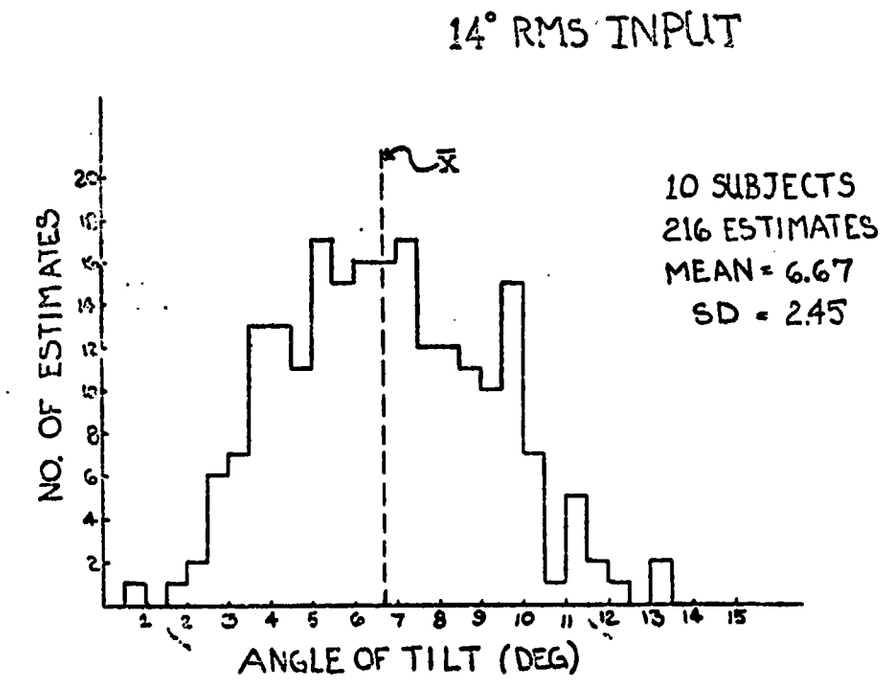

Fig. 6. Results of the 14° RMS Tracking Task

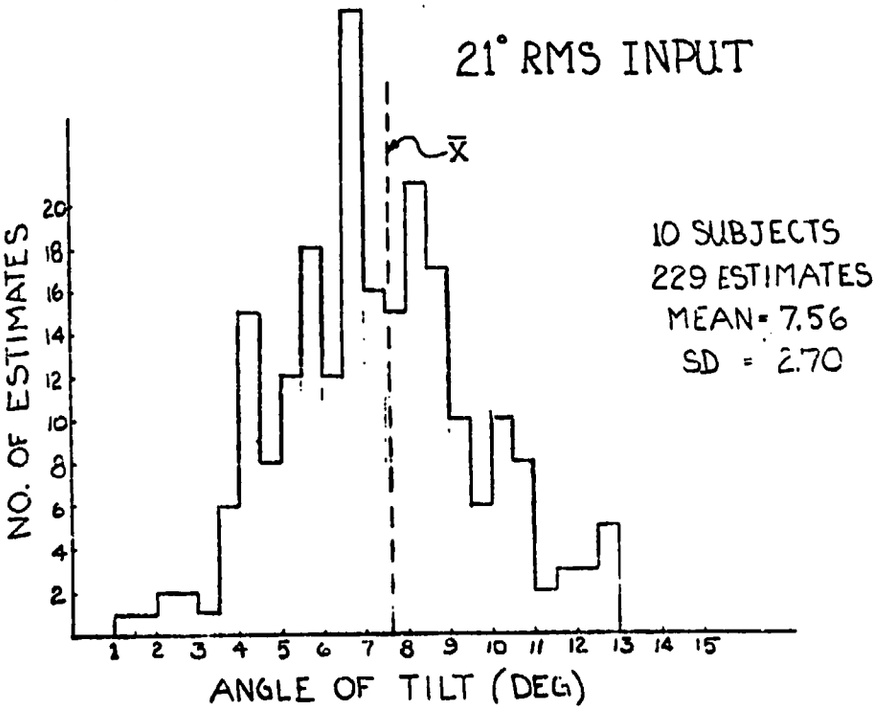

Fig. 7. Results of the 21° RMS Tracking Task

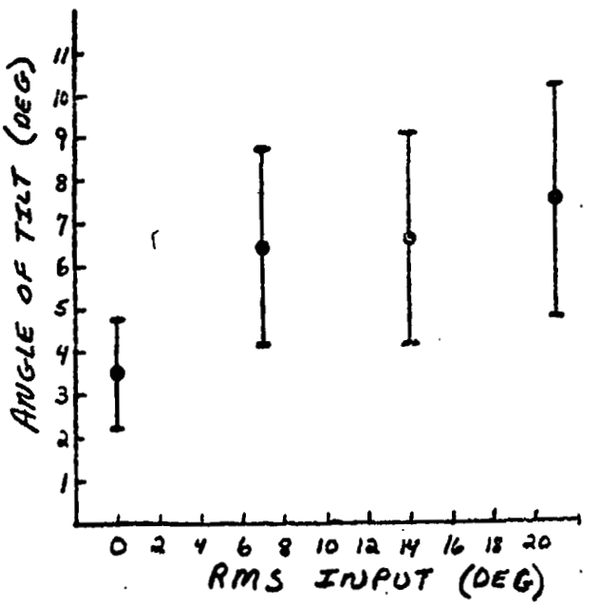

Fig. 8. Data Summary

D33

N79-15621

USE OF THE TILT CUE IN A SIMULATED HEADING TRACKING TASK*

William H. Levison
Bolt Beranek and Newman Inc.
Cambridge, Mass. 02138

and

Andrew M. Junker
Aerospace Medical Research Laboratory
Wright-Patterson AFB, Ohio

Presented at the Fourteenth Annual conference on Manual Control, University of Southern California, Los Angeles, California, May 25-27, 1978.

ABSTRACT

An experimental and analytical study was undertaken jointly by the Aerospace Medical Research Laboratory and Bolt Beranek and Newman Inc. to explore the effects of the tilt cue on pilot/vehicle performance in a simulated heading tracking task. The task was performed with subjects using visual-only cues and combined visual and roll-axis motion cues. Half of the experimental trials were conducted with the simulator rotating about the horizontal axis; to suppress the tilt cue, the remaining trials were conducted with the simulator cab tilted 90° so that roll-axis motions were about earth vertical.

The presence of the tilt cue allowed a substantial and statistically significant reduction in performance scores. When the tilt cue was suppressed, the availability of motion cues did not result in significant performance improvement. These effects were accounted for by the optimal-control pilot/vehicle model, wherein the presence or absence of various motion cues was represented by appropriate definition of the perceptual quantities assumed to be used by the human operator.

* This research was supported in part by AFOSR under Contract No. F44620-74-C-0060.

INTRODUCTION

One of the problems associated with ground-based motion simulation is the introduction of unwanted or "false" cues that are not present in three dimensional flight. The particular set of such false cues present in a given simulation depends both on the nature of the flight task and the degrees of freedom of the moving-base simulator.

This paper reviews the results of a recent experimental and analytical study to explore the pilot's ability to use the "tilt cue" (i.e., the deviation of the effective "gravity vector" from the usual head-to-seat orientation). Such a cue is "false", for example, if it is present in the simulation of a constant rate coordinated turn. This study was performed as part of a multi-year collaborative effort between Bolt Beranek and Newman and the Aerospace Medical Research Center to develop a model of the pilot's use of roll-axis motion cues. Results obtained in the preceding phases of this program have been reported in References [1-5]; documentation of the study reviewed below is in preparation.*

DESCRIPTION OF EXPERIMENTS

Preliminary model analysis was conducted using the optimal-control pilot/vehicle model to search for an experimental task for which performance would be sensitive to the presence or absence of the tilt cue. This analysis revealed that simple roll-axis tasks of the type explored previously would not be sufficiently sensitive. When the addition of another integration to the system dynamics was found to provide the desired predicted sensitivity, the heading tracking task diagrammed in Figure 1 was adopted for this study. In all experimental trails the subject was provided with a visual display of heading error as sketched in Figure 2.

Motion about the roll axis was provided by the Dynamic Environmental Simulator (DES). When the roll axis of the simulator was in the normal horizontal orientation, a roll displacement provided the subject with a tilt cue. The tilt cue was suppressed by rotating the DES 90 degrees so that the pilot was in the supine position. In this position gravity acted normally to the plane of rotation and could not provide the pilot with information related to the tracking task. Motion was provided only in the roll axis; yaw motion was absent.

Vehicle dynamics were of a higher order than those explored in the preceding study. The DES itself provided approximate dynamics of a single pole

* Levison, W. H. and A. M. Junker, "Modeling the Pilot's Use of a Roll-Axis Tilt Cue", BBN Report No. 3802, Bolt Beranek and Newman Inc., Cambridge, Mass. (in preparation).

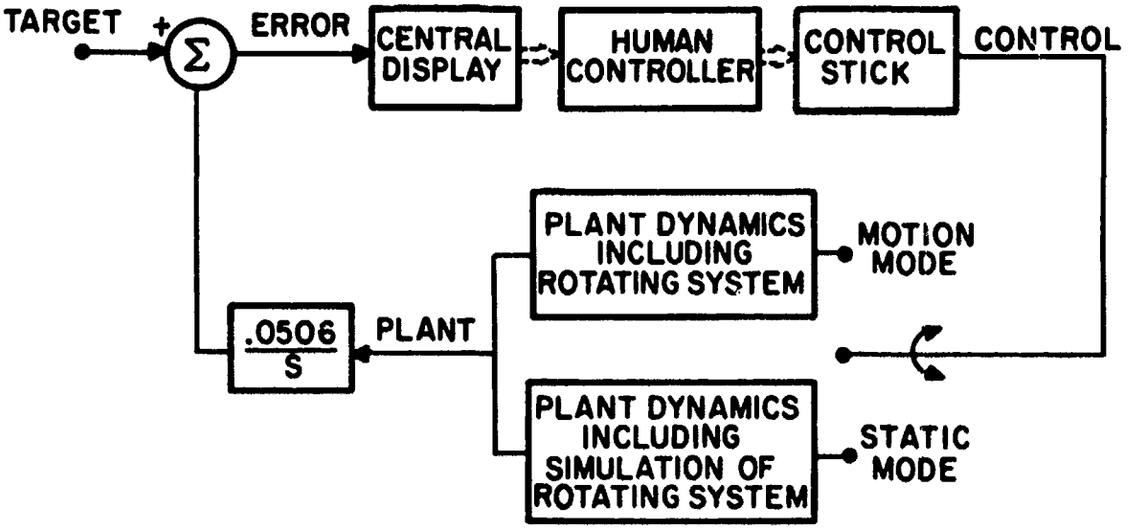

Figure 1. Block Diagram of the Tracking Task

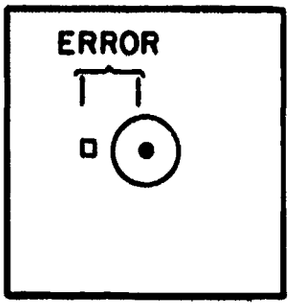

Figure 2. Sketch of the Central Visual Display

at 2 rad/sec and a complex pole pair having a natural frequency at about 10 rad/sec. "Target" motion was provided by a sum of sinusoids designed to approximate a second-order noise process.

Subjects were instructed to minimize a weighted sum of mean squared heading error and mean squared roll acceleration and were trained to near asymptotic performance on each of the four experimental conditions.

SUMMARY OF RESULTS

The comparison between predicted and measured rms performance scores presented in Figure 3 shows that the model predicted the major trend of the experiment: namely, that motion cues would benefit performance to a greater extent when the tilt cue was present (i.e., horizontal roll axis). This comparison is perhaps better illustrated in Figure 4 in which static-motion differences in rms scores are shown for all performance measures. For the most part, predicted differences were within one standard deviation of the difference scores obtained experimentally. For roll axis horizontal, the model predicted a smaller decrease in the error score and a greater decrease in the acceleration score than revealed by the data. Predicted static/motion performance differences were generally less than observed experimentally for roll about the vertical; however, observed differences were largely not statistically significant.

Model predictions shown in Figures 3 and 4 were obtained with pilot-related parameters selected as indicated in Table 1. On the basis of results obtained in a study of simulator washout effects [3], a "residual noise" of 15 degrees was associated with perception of plant roll angle from the tilt cue. Because of the relatively large roll rates and accelerations required to perform the tracking task, perceptual thresholds and residual noise terms for other motion-related cues were considered negligible.

The informational analysis adopted in previous studies was used to account for the presence or absence of motion cues. For roll about the horizontal axis, moving-base simulation was assumed to provide the pilot with information related directly to vehicle roll angle, roll rate, roll acceleration, and roll acceleration rate. We further assumed that attention would be shared between visual cues as a group and motion cues as a group and that the pilot would allocate attention between these two sets of cues in a way that would minimize the objective performance cost. A similar treatment was adopted for roll about the vertical axis, only in this case the pilot was assumed to obtain no cue related directly to plant position, and zero attention was ascribed to this variable. The model for static tracking was

* The reader is directed to References 1-5 for a review of the optimal-control model and its treatment of motion cues.

ORIGINAL PAGE IS
OF POOR QUALITY

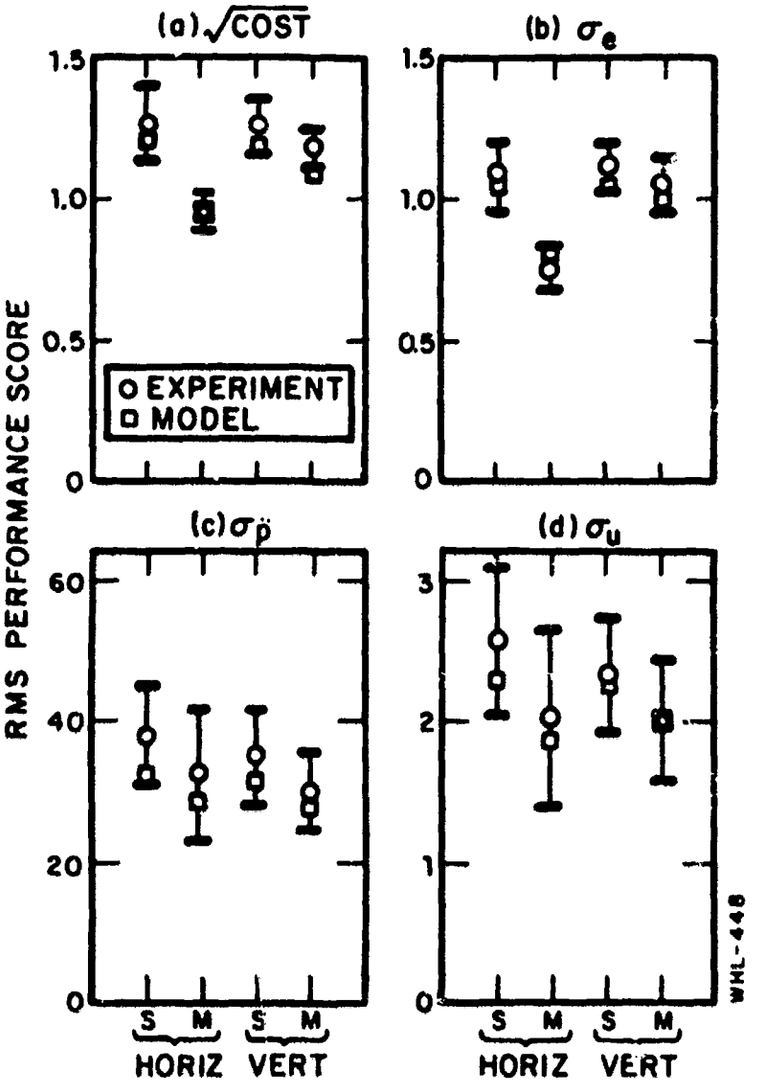

Figure 3. Comparison Between Model and Experimental Performance Scores, Nominal Parameter Values

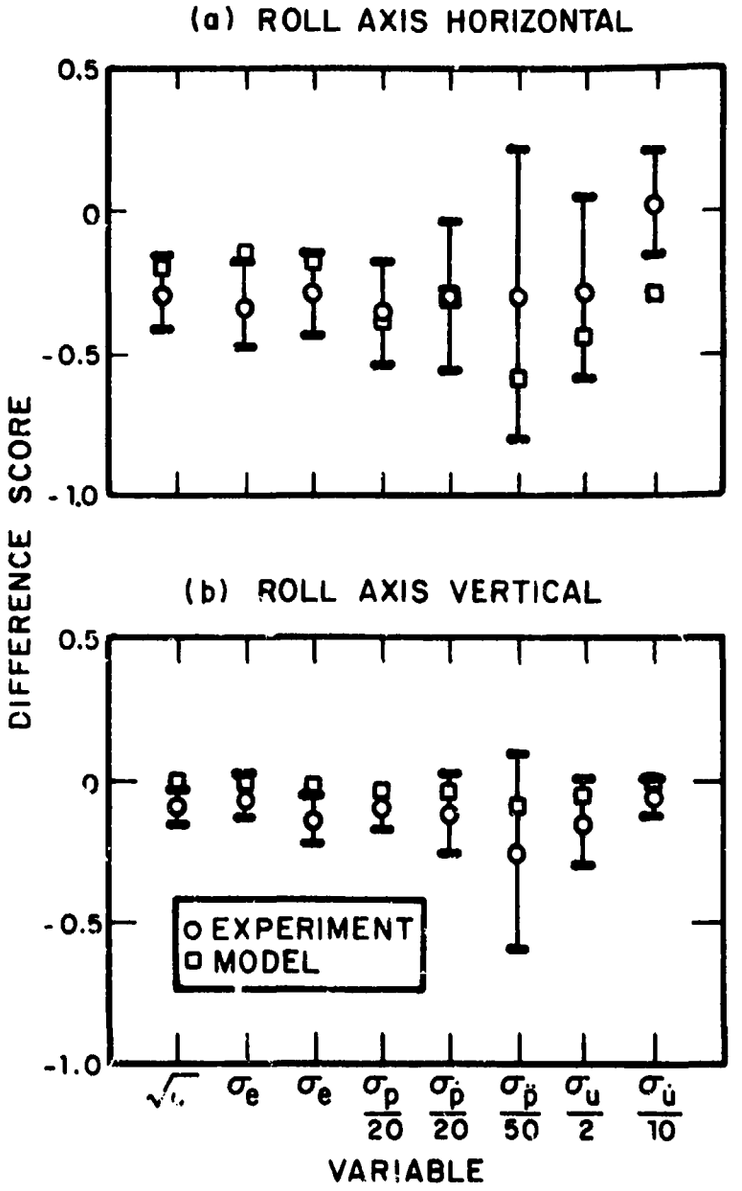

Figure 4. Differences Between Motion and Static Performance Scores

identical for the pilot in the upright and supine positions. Relative attentions of 0.5 and 0.2 to motion variables were predicted, respectively, for the cases of tilt cue present and tilt cue absent.

Table 1

Nominal Values for Pilot-Related Model Parameters

Motor time constant	0.1 seconds
Time delay	0.2 seconds
Driving motor noise/ signal ratio	(negligible)
Pseudo motor noise/ signal ratio	-35 dB relative to control variance
Observation noise/signal ratio for "full attention"	-20 dB relative to signal variance
Perceptual threshold, indicator displacement	0.05 degrees visual arc
Perceptual threshold, indicator velocity	0.05 degrees/second visual arc

Figure 5 shows that the model correctly predicted many of the detailed changes in pilot response behavior induced by the moving-base simulation. For roll about the horizontal, the model showed a substantial increase in low-frequency phase shift, a small decrease in amplitude ratio, and a decrease in input-correlated control power at low frequencies. For vertical-axis roll, the model correctly predicted a small increase in low-frequency phase and, in general, no appreciable changes in other frequency-response measures.

The model also predicted the following effects that were not observed experimentally: decreased input-correlated and remnant-related control power at high frequencies for horizontal-axis roll, and increased low-frequency remnant power for roll about the vertical. Errors in predicting the effects of motion simulation on low-frequency remnant power arose primarily from the tendency of the model to predict considerably less remnant in the static case than was observed experimentally.

The subjects used in these experiments were instructed only to minimize total "cost"; they were not instructed as to the desired control strategy. One might, therefore, expect the subjects to have adopted strategies different from that predicted by the model, provided such non-optimal behavior had neglible effect on total cost.

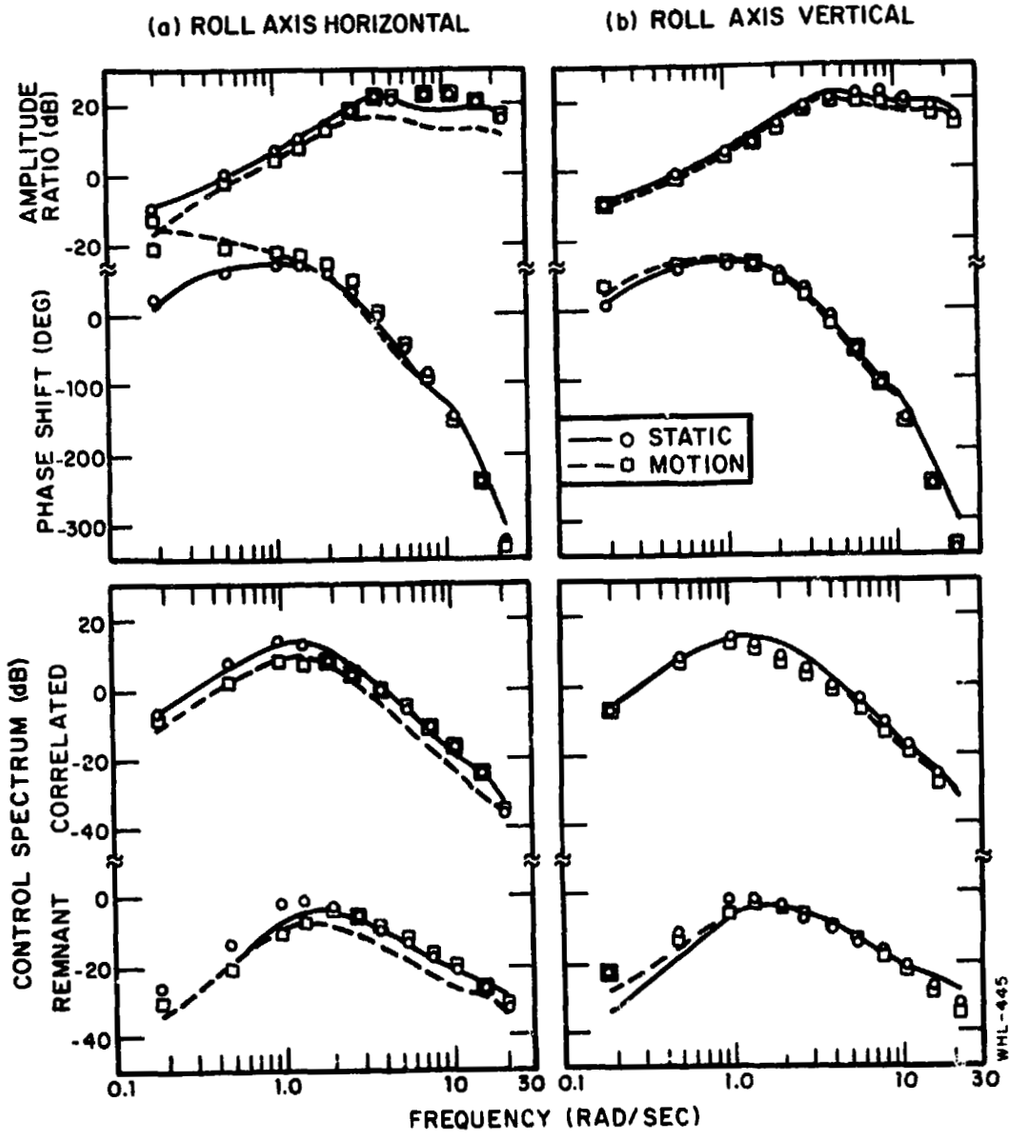

Figure 5. Comparison Between Model and Experimental Frequency-Response, Nominal Parameter Values

Selected pilot-related parameters were varied to determine the extent to which matching errors could be attributed to performance insensitivity. Specifically, time delay and cost weightings were modified in such a way that total cost was virtually unchanged (an increase of less than 3%.) Figure 6a shows that the ability of the model to match pilot response behavior at high frequencies was substantially improved by this procedure. To this extent, differences between predicted and observed measurements can be attributed to "pilot preference" of the type that does not noticeably affect performance.

Errors in modeling low-frequency aspects of response behavior could not be attributable to pilot preference, however. Low-frequency remnant power for static tracking was matched only by an increase in observation noise - specifically, noise associated with perception of heading error. The match to low-frequency phase shift for the motion case was improved by assuming less than optimal attention to motion cues. The resulting improvement in model-matching capability is demonstrated in Figure 6b.

DISCUSSION OF RESULTS

The results of this study indicate that a simple informational analysis is sufficient to account for much of the influence of the tilt cue in tasks involving roll-axis motion. Specifically, one assumes that the pilot directly perceives the bank angle of the (moving) vehicle if the tilt cue is present; otherwise, this element is omitted from the pilot's "display vector". The remaining motion-related cues of roll rate, roll acceleration, and roll acceleration rate are assumed available in both situations.

One should not interpret the results of this study as indicating that the tilt cue will generally be of significance in a task involving roll-axis motions. On the contrary, the degree to which the tilt cue provides usable information to the pilot depends on the details of the tracking task. (In fact, considerable pre-experimental model analysis was required to design an experimental task in which performance would be significantly influenced by the presence or absence of the tilt cue.)

The "residual noise" of 15 degrees associated with perception of the tilt cue is not to be interpreted as a detection threshold, but rather as a measure of uncertainty associated with this perceptual variable in the context of a continuous tracking task. Since a "residual noise" is roughly equivalent to a "threshold" of one-third the value in terms of the optimal-control pilot model [6], the residual noise of 15 degrees is consistent with an indifference threshold of about 5 degrees recently obtained in an experiment requiring simultaneous detection of tilt and continuous roll-axis control [7].

To some extent, insensitivity of performance to pilot response strategy appears to have allowed the subjects to "trade" acceleration score for error score when performing the tracking task with roll motion about the

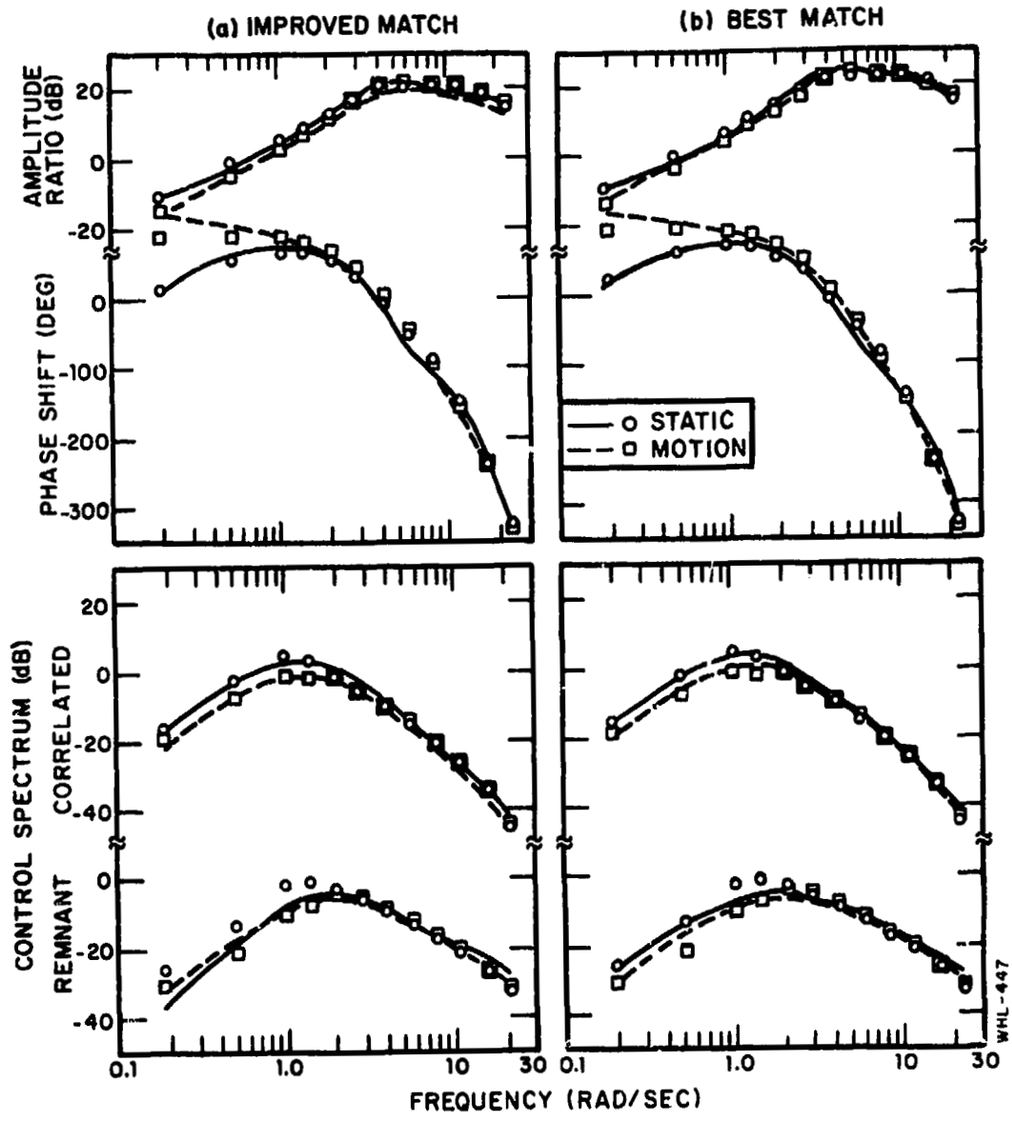

Figure 6. Comparison Between MOdel and Experimental Frequency Response, Parameter Values Adjusted for Better Match

ORIGINAL PAGE IS
OF POOR QUALITY

horizontal axis. However, performance insensitivity does not explain the relatively large noise/signal ratio (equivalently, low attention) associated with perception of heading error in the fixed-base tracking task. Increasing this parameter from the nominal -20 dB to -5 dB to provide the best match to the experimental results increased the predicted total cost by about 20% - an increase too large to ascribe to pilot indifference.

A more consistent explanation of these results is that the high noise level may have reflected increased uncertainties about vehicle response characteristics caused by the relatively high order of the plant dynamics (two pure integrations plus additional lags to represent the dynamics of the rotating simulator). When motion cues were present, the controllers may have obtained sufficient additional information about the state of the controlled plant to minimize this uncertainty; hence, the ability to match moving-base response behavior with nominal noise levels. Improved modeling of pilot response behavior in situations involving high-order dynamics is a possible area for future research.

REFERENCES

1. Levison, W. H., S. Baron and A. M. Junker, "Modeling The Effects of Environmental Factors on Human Control and Information Processing," AMRL-TR-76-74, Wright-Patterson Air Force Base, Ohio, August 1976.

2. Levison, W. H. and A. M. Junker, "A Model for the Pilot's Use of Motion Cues in Roll-Axis Tracking Tasks," AMRL-TR-77-40, Wright-Patterson Air Force Base, Ohio, June 1977.

3. Levison, W. H., "A Model for the Pilot's Use of Roll-Axis Motion Cues in Steady-State Tracking Tasks", Bolt Beranek and Newman Inc. Report No. 3808, May 1978.

4. Levison, W. H., "Use of Motion Cues in Steady-State Tracking", NASA TM X-73, 170, Twelfth Annual Conference on Manual Control, Urbana, Illinois, May 1976.

5. Levison, W. H. and A. M. Junker, "Use of Motion Cues in Two Roll-Axis Tracking Tasks", Procedings of the Thirteenth Annual Conference on Manual Control, M.I.T., Cambridge, Mass., June 15-17, 1977.

6. Kleinman, D. L. and S. Baron, "Analytic Evaluation of Display Requirements for Approach to Landing", NASA CR-1952, November 1971.

7. M. Roark and A. Junker, "The Effects of Closed Loop Tracking on a Subjective Tilt Threshold in the Roll Axis", Procedings of Fourteenth Annual NASA-University Conference on Manual Control, University of Southern California, April 25-27, 1978.

U34

N79-15622

ROLL TRACKING EFFECTS OF G-VECTOR TILT AND VARIOUS TYPES OF MOTION WASHOUT

Henry R. Jex and Raymond E. Magdaleno
Systems Technology, Inc.
Hawthorne, California

and

Andrew M. Junker
6570th Aerospace Medical Research Lab, EM Branch
Wright-Patterson AFB, Ohio

SUMMARY

The aim of this research was to discover the basic effects on pilot roll tracking behavior, performance, and impressions for several types of motion-reducing logic ("washouts") used in moving-base simulators. It was a joint program between the 6750 Aerospace Medical Research Laboratory (AMRL-EM Branch) and Systems Technology, Inc.

The experiments were performed on the AMRL Dynamic Environment Simulator (DES), in the roll degree of freedom only. The g-vector was oriented both normally (pilot erect, tilt cue present) and 90 deg nose-up (pilot supine, no tilt cue). Washout filters included: second order, first order, attenuated first order, attenuated, and static (fixed base).

In a dogfight scenario, the task was to follow the target's roll angle while suppressing gust disturbances. The two independent inputs (interleaved sum-of-sines) enabled identification of both the visual and motion response parameters of the pilot by the STI Model Fitting Program (MFP'77). A 12-parameter multiloop model structure fitted includes separate visual and roll motion sensing channels, with a common neuromuscular actuator block.

Excellent describing function and performance data as well as subjective impressions were obtained on four non-pilot subjects, each well trained in the "real-world" case (full motion; 90 deg nose-up). All subjects adopted the same behavioral strategies in following the target while suppressing the gusts, and the MFP-fitted math model response was generally within one "data symbol width."

The results include the following:

- Comparisons of full roll motion (both with and without the spurious gravity tilt cue) with the static case. These motion cues help suppress disturbances with little net effect on the visual performance. Tilt cues were clearly used by the pilots but gave only small improvement in tracking errors.

- The optimum washout (in terms of performance close to "real world," similar behavioral parameters, significant motion attenuation (60 percent), and acceptable motion "fidelity") was the combined attenuation and first-order washout.

- Various trends in parameters across the motion conditions were apparent, and are discussed with respect to a comprehensive model for predicting pilot adaptation to various roll motion cues.

The detailed data base (spectra, remnant, describing functions, model fits) are compiled in a separate document available to interested researchers through AMRL-EM.

INTRODUCTION

Objectives and Background

A joint experimental/analytical effort by the Aerospace Medical Research Laboratory (AMRL/EM) and Systems Technology, Inc. (STI) was conducted to define a pilot's use of motion cues in moving-base simulators free to rotate only in the roll degree of freedom. This situation provides the pilot an intrinsically spurious roll attitude or "tilt" cue. This effect can be reduced by "washing out" the cab motion so the cab always tends to return to an upright orientation, although this distorts the true angular motions. The optimization of the washout dynamics to achieve the best compromise between realistic roll rate cues and suppression of the spurious tilt cue is an important facet of the immediate future work to be done in the AMRL/EM laboratory.

The basic objective was to determine what form and degree of washout dynamics achieves the highest simulation realism, while engendering true-to-life behavior of the pilot, and producing the correct performance effects due to environmental stressors. Longer range objectives include the possible correlation of these experiments with other ground-based simulations and later with in-flight experiments.

To accomplish the above objectives this investigation had to consider two basic problems in moving-base simulation: the use of motion cues by the pilot in the actual ("real world") case and the effects of spurious motion cues in modifying that usage in the simulator. A brief examination of the piloting task involved in the first problem is useful before proceeding to the second.

Consider a situation of primary interest to the Air Force — air-to-air combat — and focus upon the pilot's response to the dynamic (non-steady) components of motion. Assume that, initially, the pilot has his wings lined up with those of a target aircraft that he perceives against a murky or night-time background (no horizon visible). In this "impoverished display" situation he can visually perceive only the difference (error) between the target's wings and his own. Further, the pilot has two tasks to perform, often simultaneously:

a. Regulate (suppress) disturbances, e.g., due to gusts or swirls from the target's wingtip vortices. In this task the pilot's role is to reduce motions, and if he suppresses the gusts with small error, the physical motions become small.

b. Track (follow) the target roll motions (e.g., by keeping one's wings parallel with the target). In this task the pilot's role is to produce motions, and if he tracks with small error, the physical motions become larger (approaching the target motions).

In the general case, where both inputs are present, the pilot is faced with a continual conflict between reducing disturbance motion and producing correct following motions. The figure-of-merit (at least in air combat and landing tasks) is primarily low roll error (and, perhaps, limited roll acceleration or its rough equivalent — aileron control deflection). Because multiple sensory feedbacks are involved, with more than one input, the problem is a multiloop one, and this greatly complicates the control system analysis as well as the attempt to infer the pilot's behavioral "structure" and parameters, as will be demonstrated, herein.

Most of the earlier research in measuring the use of visual and motion cues, such as that of Stapleford, et al (Ref. 1) and Shirley (Ref. 2), tended to have either the target input or disturbance, as dominant, such that the possible cue conflicts were minimized. Stapleford, et al were able to infer the separate visual and motion pathway dynamics by using mathematically independent target and disturbance inputs comprising sums-of-sinusoids interleaved in frequency, then interpolating between frequencies to solve the simultaneous vector equations required to untangle the loops (this process will be shown later herein). However, these pioneering results were not fitted in any form suitable for efficient use. Thus, the secondary objectives of this program were to improve the reduction and analysis of multisensory manual control data, and to structure and parameterize the results. Here, where the target following and disturbance motions were comparable, in bandwidth and amplitude, new techniques were required.

Such a situation seem natural for an optimal control model of the human operator, and Levison, working with AMRL experimenters has put forth a first-cut at just such a model in Refs. 3 and 4. The forcing functions were either target inputs or disturbances, and effects similar to Stapleford's and Shirley's were obtained. Whether or not their (implicitly) assumed feedback structure is valid is hard to say without more data on the all important dual-input case treated here.

In another approach Zacharias (Ref. 5) has tackled the problem of sensory conflict of visual and vestibular sensors in conjunction with regulation of purely visual, purely motion or conflicting cue situations, and has speculated on a cue-conflict resolving model for the human operator, in the yaw-only degree of freedom. Testing the validity of such cue-conflict-resolution approaches as these requires a very solid data base to exercise one's model against, and this is still largely lacking. In light of the above needs, a

ORIGINAL PAGE IS
OF POOR QUALITY

third objective was to establish a very solid and comprehensive data base, using inputs, controlled elements, and washouts that were analytically tractable and fairly linear, so that future validation of cue-utilization models would be facilitated.

Scope

To meet these objectives, the AMRL Dynamic Environmental Simulator (DES) was employed, which permits pilot rolling motions with his rolling axis horizontal (normal spurious tilt cues present) as well as vertical (tilt cues absent). Details are given later. The scenario selected was that of air-combat with a set of fairly sluggish aircraft roll dynamics, so that motion cues would be useful. As will be described, the target and disturbances were carefully designed to provide strong motion-usage conflicts as well as easy analytical modeling. Several motion cases, ranging from full motion, various washouts to fixed base were included. Based on prior work, a plausible structure for the pilot's use of visual and motion inputs was proposed, and a newly developed technique was used to fit these model parameters quite precisely to the frequency-domain data.

We show how some of the past results are explained on the basis of differences in the apparent "opened-loop" transfer functions for target vs. disturbance inputs, despite identical pilot behavior with respect to either by itself.

To obtain reliable measurements, worth fitting by the relatively high-order models selected, extremely consistent pilot behavior is necessary. This was obtained by a combination of the sluggish controlled element (which had a fairly well-defined optimum strategy) and very well-trained subjects.

The results show clear answers to the questions raised earlier, when analyzed with respect to various performance and behavioral (dynamic) parameters, and some interesting trends are evident in the pilot parameters vs. motion measures, even for fairly small motions. Nevertheless, this report does not attempt to interpret these covariations in terms of an overall model of operator adaptation to pure and distorted motion feedbacks.

EXPERIMENTAL DESIGN

Approach

As noted in the introduction, there were two facets of roll motion-cue usage to be investigated: "real-world" motion vs. no-motion and distortions of real-world motion by various washout filters. In the actual flight case, where gradual bank angles result in translation of the aircraft, there is no way to tell vertical by seat-of-the-pants or other vestibular sensors. A set of realistic rolling cues were provided by tipping the roll-axes of the simulator 90 deg nose upward so that the spurious tilt cues were absent. This full-motion at 90 deg inclined roll axis (F-90) case was given the most

ORIGINAL PAGE IS
OF POOR QUALITY

practice and became the "real-world" reference for all other motion cases. By comparing it with the static case, the basic effects of motion were revealed. To check effects of the conflicts between target following vs. disturbance regulation, both forcing functions were given alone and together (dual input) for the F90 case. If the dual case gave similar data as either input alone, then the dual input could be used throughout, with consequent savings in runs and data analysis.

The washouts in roll-only simulators are used for two main purposes, a) to reduce the tilt cues (largely a low frequency effect) and b) to reduce any or all motions (accelerations, rates, displacements) to fit into a limited capability simulator, always with a horizontal orientation of the roll-axis. Consequently the effects of simulated roll only motions were covered by the full motion at 0 deg roll axis inclination and various washouts — all selected to give substantial reduction in roll displacement.

To keep the number of runs within bounds, it was decided to keep constant the plant and the spectrums of forcing functions; and to try only one variation of each washout filter scheme.

Control Task

Block Diagram — a scenario with high face validity relevant to Air Force problems is air-to-air gunnery. In a modern high thrust/weight fighter, combat maneuvers take place at all flight path angles, hence the horizon is relatively unimportant. The main criterion for accurate tail chase is to match the roll angle of the target aircraft. The pilot is attempting to follow an evasive target while at the same time he may be buffeted by gusts, a component of which could be wing tip vortices of the target. To simplify the simulation and subsequent modeling and interpretation, a compensatory display (error only) was used and the subjects were instructed to minimize the bank angle error.

Fig. 1-a illustrates the basic elements involved: the Human Operator, Controlled Element, and Washout dynamics. The multiloop nature is evident in that the Motion Path senses physical (inertial) bank angle while the Visual Path senses the error between target and task bank angle. (The four-character "names" on the signals in Fig. 1 represent the Fourier coefficients and are used to label some power spectra and describing functions later in this report).

Controlled Element

The controlled element (Eq. 1 on Fig 1-b) represents an approximation to the roll dynamics of a fighter. The Roll Subsidence mode, having a time constant of $1/1.6 = 0.63$ sec, is typical of a loaded fighter (i.e., with external stores). This value was selected as it would require a significant amount of lead generation by the pilot, because the Crossover-Law for human operator equalization (e.g., Ref. 5) predicts that in such cases the ideal pilot lead

a. Block Diagram Showing Definitions of Elements and Signals

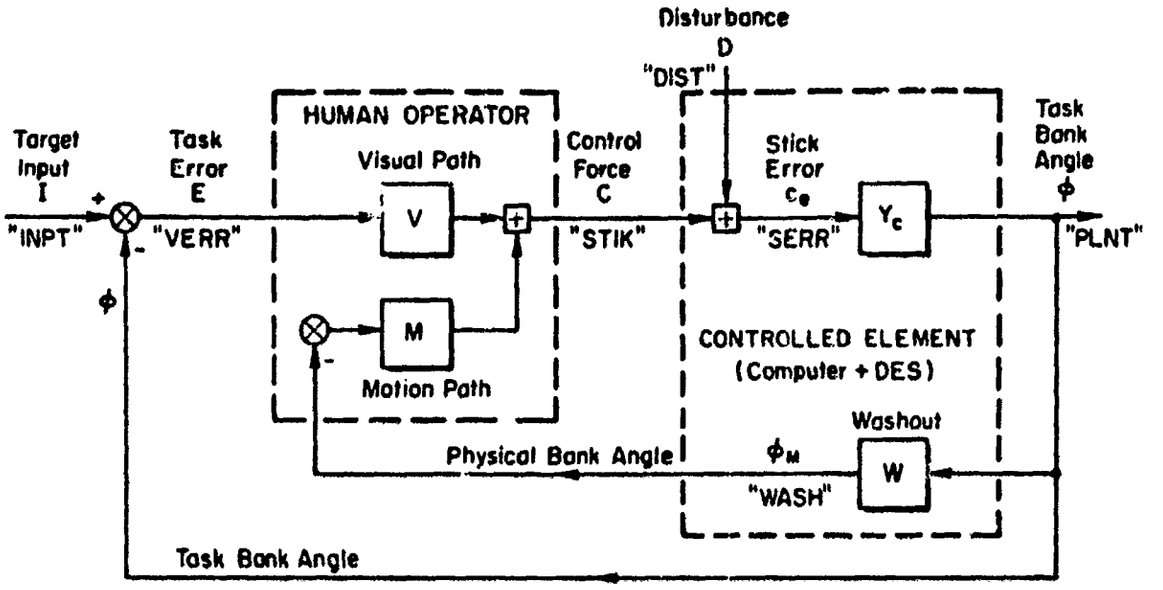

b. Controlled Element Transfer Function

$$Y_c(s) \equiv \frac{\Psi}{c_e} \triangleq 17 \; \frac{\overbrace{(-s/25 + 1)}^{\text{DES Lags}}}{\underbrace{s}_{\substack{\text{Spiral} \\ \text{Mode}}} \; \underbrace{\left(\frac{s}{1.6} + 1\right)}_{\substack{\text{Roll} \\ \text{Subsi-} \\ \text{dence}}} \; \underbrace{\left(\frac{s}{5} + 1\right)}_{\substack{\text{"Servo"} \\ \text{Lag}}} \; \underbrace{\left[\frac{s^2}{11^2} + \frac{2(.3)s}{11} + 1\right]}_{\substack{\text{"Structural"} \\ \text{Mode}}}} \quad \left(\frac{\text{deg/sec}}{\text{lb}}\right) \qquad (1)$$

ORIGINAL PAGE IS
OF POOR QUALITY

Figure 1. Roll Tracking Task Block Diagram and Transfer Function

C-6

would be about $T_L \doteq T_R \doteq 0.5$-$0.7$ sec. The "Structural Mode" and "DES lags" represent the unavoidable and measured response characteristics of the DES motion simulator, while the "Servo" Lag represents actuation lags of a (poor) aircraft control system. It was raised to 0.2 sec to prevent excessive acceleration or rate commands to the DES which would cause its drives to operate in a partly saturated (hence nonlinear) manner.

Analysis of this controlled element showed that it requires a fairly tightly constrained pilot equalization, with some lead to offset the roll-subsidence lag, but not too much or else the structural mode and lag elements would destabilize the system. Thus, there was a clearly optimum control strategy for the subjects to learn, which was important because they were not experienced pilots.

Forcing Functions

Quasi-random target and disturbance inputs were constructed from eight sinusoids each (Table 1). The frequencies were selected so as to have an integer number of cycles in the run length as shown. To assure statistically independent inputs, target and disturbance frequencies were interleaved, yet each was approximately evenly spaced on a log-frequency plot. After these choices were made the amplitudes were "shaped" to simulate a random noise process that would result from white noise being filtered by the shaping filter forms given in Table 1. Finally, these "shaped amplitudes" were scaled so as to give the listed rms and peak amplitude values.

The target's shaping filter was selected to simulate a low pass spectrum typical of an evasive target. The disturbance's shaping filter was selected so that under static conditions (and, as further shaped by the controlled-element) the spectral content and rms values would be nearly equal to that of the target, as seen on the error display. Thus the pilot could not use input frequency properties to separate target motions from disturbance motions.

Multiloop Pilot Model and Identification Procedure

Analysis. — The measurement problems involved in the multiloop system of Fig. 1-a can be illustrated by examining the task error components resulting from target and disturbance inputs, shown in Fig. 2.

First consider the static case, where the Motion Path is inoperative: $M(j\omega) = 0$. Then the task error vector (frequency response function) becomes that given by Eq. 2 in Fig. 2 (for convenience, we have dropped the arguments $s = j\omega$ in each of the inputs and transfer functions; $E(j\omega) = E$, etc.).

Equation 2 has been written in the form of a conventional single loop system, wherein the [ ] term is the closed-loop error-to-input describing function, so the product $V \cdot Y_c$ is recognized as the open-loop describing

TABLE 1. FORCING FUNCTIONS FOR DUAL INPUT RUNS

TARGET (rms = 7.1 deg)*			DISTURBANCE (rms = .74 lb = 3.4 N)*		
Cycles / Run Length†	ω (rad/sec)	A_{dB} 0 = 1. deg	Cycles / Run Length	ω (rad/sec)	A_{dB} 0 = 1. lb
5	0.19	13.6	9	0.35	−20.6
13	0.50	11.6	17	0.65	−16.5
23	0.88	8.7	30	1.15	−13.6
37	1.42	5.6	49	1.88	−11.4
63	2.42	1.0	83	3.18	− 9.7
107	4.10	− 5.8	141	5.41	− 9.2
182	6.98	−14.4	241	9.24	−10.0
309	11.85	−24.4	410	15.72	−11.7
SHAPING FILTER FORM					
$\frac{1}{(s+0.5)(s+1.7)(s+5.0)}$			$\frac{s}{(s+0.5)(s+5.)}$		

* For single input runs the values were increased by $\sqrt{2}$:1
† Run length = 163.84 sec

function, G_{OL} for purely visual feedbacks. Recall that increasing the magnitude of G_{OL} reduces tracking errors, etc.

Similarly, in hypothetical situations where the operator would close his eyes and operate solely on motion cues (V = 0), the task errors would be given by Eq. 3 in Fig. 2. The input is unaffected, while the disturbances are suppressed.

When both visual and motion paths are active the multiloop relationships become more complex, but can still be written so as to reveal the effective opened-loop dynamics (similar to Eqs. 2 and 3), as shown in Eq. 4. Now, however, the "opened-loop" describing function for target errors (G_T, of Eq. 4a) contains the closed-motion loop $1/(1 + MWY_c)$, while G_D for the disturbance errors contain the sum of motion and visual effects $(V + MW)Y_c$.

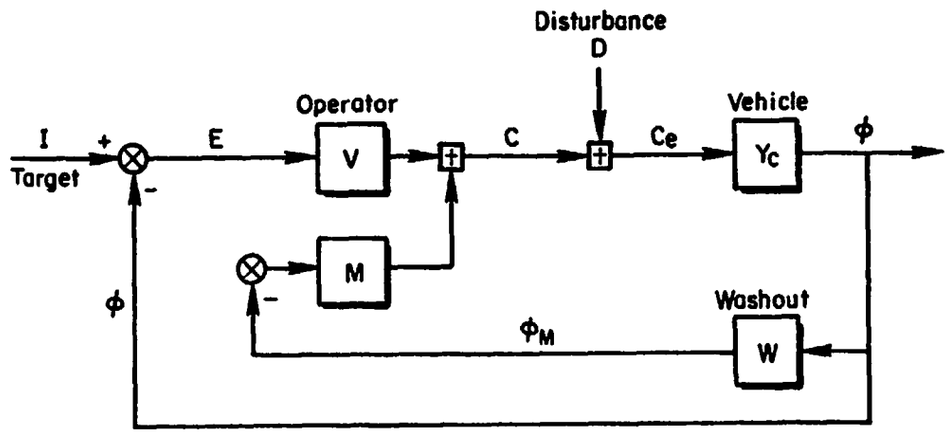

Note: All blocks and signals are vector functions of frequency: $E = E(j\omega)$ etc.

For Visual only: (Static; $M \equiv 0$)

$$E = (I - DY_c)\left[\overbrace{\frac{1}{1 + VY_c}}^{(E/I)_{CL}}\right] \qquad (2)$$

Open-loop DF: "G_{OL}" for Visual Loop alone

For Motion Only: (Eyes closed; $V \equiv 0$)

$$E = I - DY_c\left[\frac{1}{1 + \underbrace{MWY_c}_{G_{OL}}}\right] \qquad (3)$$

Open-loop DF: G_{OL} for Motion Loop alone

For Visual-Plus-Motion:

$$E = I\left[\frac{1}{1 + G_I}\right] + (-DY_c)\left[\frac{1}{1 + G_D}\right] \qquad (4a)$$

where "Opened-loop" DF's

$$G_I = \frac{VY_c}{1 + MWY_c} \qquad (4b)$$

$$G_D = (V + MW)Y_c \qquad (4c)$$

Figure 2. Closed-loop Error Relationships to Target and Disturbance Inputs for Various Single and Multiloop Structures

In the single loop cases of Eqs. 2 and 3 a high-gain (V or M) reduces errors, but in the multiloop case there is a conflict:

- A high-gain motion feedback (large M) reduces the disturbance errors via Eqs. 4a and 4c, but increases the target errors via 4a and 4b.

- A high-gain visual loop (large V) reduces both error components.

- The optimum strategy (to minimize E) is a complicated function of the spectra of I and $D \cdot Y_c$, as well as of Y_c and W.

These are the analytical expressions for the qualitative motion/visual cue conflict mentioned in the introduction. Further, notice that analytically opening the loop for either target or disturbance inputs will give different apparent "opened-loop" describing functions (Eqs. 4b vs. 4c) even with identical V and M operations in both equations. This has led in the past to some misinterpretation of results for mostly-target or mostly disturbance inputs.

Finally, it can be seen that, knowing the vehicle and washout dynamics (Y_c and W) and with simultaneous independent inputs I and D, the independent estimates of the visual and motion operations (V and M) are theoretically possible if the signals are not confounded with noise. The temptation to measure V and M from static and motion-only runs, respectively, is precluded by the adaptive nature of the human operator. In general, the pilot will adopt different parameter values for his gains, leads and lags in the above special cases compared to the combined case, as will be shown later.

Model Structure and Parameters. — The criteria for selecting the model structure were that it be:

1. The simplest form capable of capturing all of the significant frequency-domain characteristics of the measured data, both with and without motion.

2. Have components structurally related to previously well known visual-motor elements, such as neuromuscular (NM) and, central-nervous system (CNS) components, as well as motion sensing elements from afferent vestibular and proprioceptive signals.

3. Compatible with prior manual-control models, e.g., those in Ref. 5.

Figure 3 details the assumed pilot model structure and forms for the Visual and Motion paths of Fig. 2. The rate and displacement elements in the "VISUAL PROCESSES" group are used to generate a lead time constant ($T_L = K_R/K_D$) which pilots typically adopt to cancel the roll-subsidence mode in the controlled element (Ref. 3). The "integral" term is sometimes needed to represent the pilot's trimming actions and other low frequency behavior. (e.g., the so called "α-effects" in the Extended Crossover Model of Ref. 5)

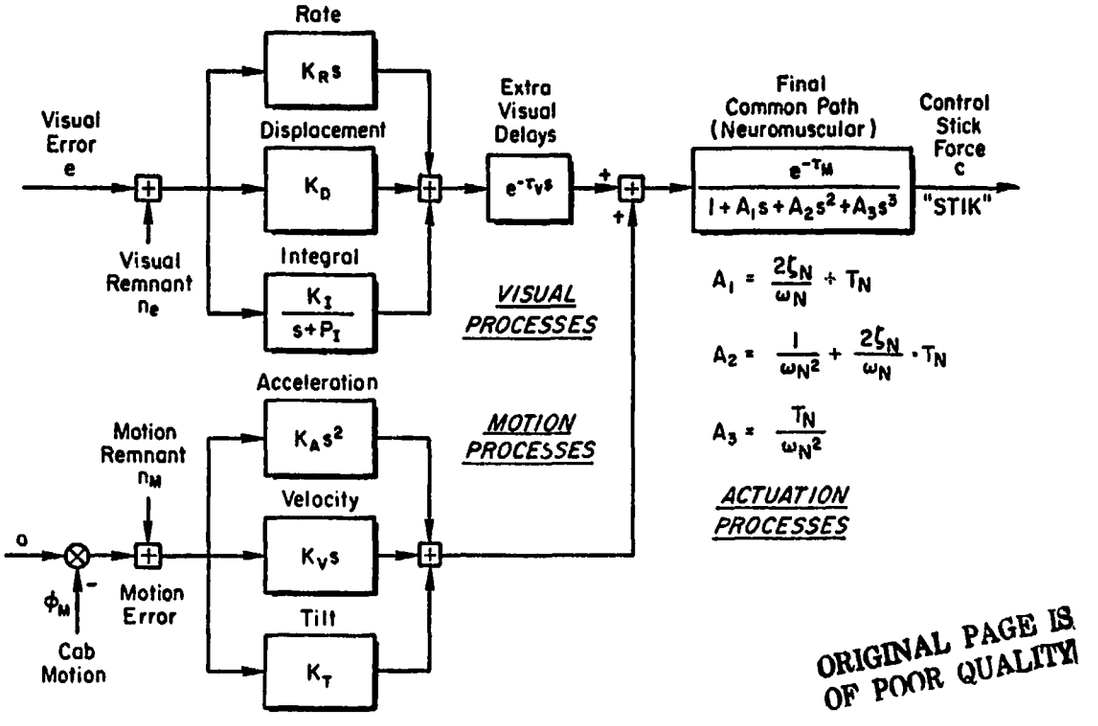

ORIGINAL PAGE IS OF POOR QUALITY

Figure 3. Assumed Pilot Model for Roll-Only Tracking

The extra visual time delays account for retinal and central (e.g., rate) processing as well as computational and display lags.

The tilt, velocity and acceleration terms in the "MOTION PROCESSES" are the simplest possible descriptors of the pilot's use of physical bank angle. These are not intended to represent motion sensors directly although the velocity term is very similar to the output of the semicircular canals over the forcing function frequency region. The tilt angle cue K_T is actually due to the lateral specific force due to the tilted g-vector.

The "ACTUATION PROCESSES" include a time delay and a third order neuromuscular system, the latter readily simplified to a second or even a first order approximation, as noted in the figure (e.g., for a second-order system set $T_N = 0$, whence $A_3 = 0$, $A_2 = 1/\omega_N^2$ and $A_1 = 2\zeta_N/\omega_N$). The delay terms τ_V and τ_M were actually modeled as first-order Pade polynomials, and by breaking up the net delays into two small portions the Pade roots (at $2/\tau$) are at sufficiently high frequency to give an excellent fit up to over 10 rad/sec.

Identification. — The two "opened-loop" expressions in Eq. 4a can be used to identify the two unknown paths (Visual and Motion) only if the Target and Disturbance inputs are independent. For signals constructed as a sum of sine waves this means that there can be no common frequencies. However this precludes the direct solution for the unknowns (V and M) since the "opened loop" expressions cannot be evaluated at the same frequencies. This dilemma was dealt with in Refs. 1 and 2 by linearly interpolating the measurements at the interleaved frequencies. This can lead to difficulties and inaccuracies in the vicinity of lightly damped modes, where the transfer functions are not smooth. A different technique is used where specific model forms are assumed for the Visual and Motion paths and the equations of motion are written for all elements and loops, so that in effect the "interpolations" are made with appropriately shaped math models. The unknown parameters are then adjusted by the STI Model Fitting Program (MFP; described below) so as to fit simultaneously the closed loop error and stick describing function responses to the Target and Disturbance inputs.

The STI Model Fitting Program was developed to fit high order multiloop models to frequency domain data (e.g., from Fast Fourier transforms and is described in Ref. 7. It evaluates selected transfer functions from fixed-form adjustable-parameter equations-of-motion written in a special way such that each adjustable parameter appears only once in the "matrix-of-equations." Thus, the influence of each parameter on any system response to any input is available. The program minimizes the vector difference between model and data transfer function responses using a variety of steepest descent techniques to minimize a cost function. This cost function is evaluated by squaring and amplitude weighting the difference in the real and imaginary parts of the data and model responses. In the present case, five frequencies of the task error-to-disturbance, four of the stick-to-disturbance and five of a linear sum of error- and stick-to-target were fit. The amplitude-weighting was the inverse of the data magnitude, thus each frequency was uniformly represented except that the highest frequency of the stick-to-disturbance was weighted 10 dB less.

Since the target and disturbance are sums of sinusoids, the effective "opened-loop" expressions in Eq. 4 were estimated using ratios of Fourier coefficients:

$$\hat{G}_I\,(j\omega)\Big|_I = \frac{\varphi}{E} = \left(\frac{PLNT}{VERR}\right) \text{ at Target frequencies, } \omega_I \qquad (5)$$

$$\hat{G}_D\,(j\omega)\Big|_D = \frac{-C}{C_e} = \left(\frac{-STIK}{SERR}\right) \text{ at Disturbance frequencies, } \omega_D \qquad (6)$$

where the four character names PLNT, VERR, STIK and SERR are defined in Fig. 1 and will be used to identify various responses in the remainder of this report.

To check the accuracy of this procedure an analog "autopilot" operation on both task error and measured motion was mechanized on the DES setup and the recorded signals were processed thru MFP. Table 3 summarizes the results of

TABLE 3. ORIGINAL AND RECOVERED PARAMETERS FOR DUAL AUTOPILOT

$$\text{Visual Path:} \quad V = \frac{K_R s + K_D}{T_V s + 1} e^{-\tau_V s}$$

$$\text{Motion Path:} \quad IM = \frac{K_V s + K_T}{T_M s + 1}$$

CASE	"VISUAL LOOP"				"MOTION LOOP"		
	K_D	K_R	T_V	τ_V	K_T	K_V	T_M
Original	.133	.067	.100	.018	.040	.100	.100
Recovered by MFP	.134	.062	.098	.023	.040	.104	.092

this check, using the forms indicated. The time delay shown is an approximation to the net phase effects of various hybrid computation delays and high-frequency anti-aliasing filter lags. Some errors could be due to the fact that the "dialed-in" computer settings did not accurately represent the effective parameters. Generally the recovered parameters in Table 3 are quite close to the nominal, such that a transfer function plotted from the recovered parameters would be indistinguishable from one plotted for the original parameters.

Washout Dynamics

In addition to the static (no motion) case ("ST"), and full-motion cases with roll axis at 0 deg inclination "F0", and nose up 90 degrees, "F90"; four different washout schemes were tested:

- Purely Attenuated, "A" wherein the plant motions at all frequencies were multiplied by 1/2 in commanding the DES.
- First-Order, "W1"; where the low frequency motions are attenuated by a first-order high pass filter of the form:

$$\left.\frac{\varphi_M}{\varphi}\right|_{W1} = \frac{K_{hi}\, s}{s + 1/T} \qquad (7)$$

where

K_{hi} = high frequency gain (near 1.0)

T = time constant ("break frequency" = 1/T)

With this washout a step bank angle command returns experimentally to zero with a time constant of T sec.

- First-Order, Attenuated, "W1,A"; a combination of the two foregoing washouts, with different gains and break frequencies.

- Second-Order "W2"; the low frequency terms are washed out by second order high pass filter of the form

$$\left.\frac{\varphi_M}{\varphi}\right|_{W2} = \frac{K_{hi}\, s^2}{s^2 + 2\zeta\omega s + \omega^2} \qquad (8)$$

where

ω = the break frequency, and
ζ = the damping ratio (typically .7)

With such a second-order washout an initial step bank angle returns with minimal overshoot with an effective delay (to half amplitude) of $(2\zeta/\omega)$ seconds. A constant roll rate input still ends up at zero bank angle.

The various washout parameters were originally selected to produce a reduction in rms roll amplitude to about 50 percent of the full motion case, based on a more-or-less arbitrary a priori assumption of a typical, invariant, second-order closed-loop pilot-simulator response to roll commands, characterized by a bandwidth of 3.6 rad/sec and a closed-loop damping ratio of $\zeta_{CL} \doteq 0.6$. It was realized that in practice the pilot might change his response characteristics for different washouts, but this procedure was used to select the different parameters on a more rational basis than (say) fixed break frequencies of all the washouts.

In the simulation, inadvertent problems with mechanization of the filters and DES response properties slightly modified the intended wash-out dynamics. The actual response properties of the washout plus DES combination were fitted by the appropriate forms of Eqs. 7 and 8 and the effective washout-filter parameters were extracted. These are summarized in Table 4. Most of the effective parameters were close to the intended ones, except for the W2 high frequency gain which was 1.2 instead of the 1.0 desired. In Table 4 the cases are arranged in order of decreasing magnitude of rms physical roll angle, and this order will be used throughout the presentations to follow.

Measurements

A comprehensive set of measurements were made in an attempt to quantify all aspects of the pilot's performance, behavior, and effort.

TABLE 4. MOTION CONDITIONS AND WASHOUT DYNAMICS

Case:	F_{90}	F_0	W2	W1	W1, A	A	ST
Washout Type:	"Full Motion" at 90°	"Full Motion" at 0°	"Second Order"	"First Order"	"First Order, Attenuated"	"Attenuated"	"Static"
High Frequency Gain	1.0	1.0	1.2	1.0	0.7	0.53	0
Break	—	—	$\omega = .85$ r/s $\zeta = .7$	1.0 r/s	.40 r/s	—	—

1. Performance Measures: Overall statistics (mean, variance, rms) of all signals, with emphasis herein on: tracking error stick force and physical roll-angle and rates.

2. Pilot Behavior Measures: Describing functions are the primary indicators of pilot behavior. The fitted parameters are useful for encoding efficiently the data, but the actual plots are often most informative. We use the "opened-loop" describing function, as they are the most useful and tie in with past experience on single loop systems.

3. Subjective Evaluations: Each subject was given a questionnaire about his tracking strategy, effects of motion cues and, differences due to washouts. Because these were not experienced pilots, no comparison to actual flight could be made; instead, subjects were asked to compare the motion cues with those of the F90 "real world" case.

APPARATUS AND PROCEDURES

Apparatus

The experiment was performed on the Dynamic Environmental Simulator (DES) at the Aerospace Medical Research Laboratory at Wright-Patterson Air Force Base. The DES is a man-rated centrifuge with independent roll and pitch cab control. For this experiment only the roll tracking motion was used, with the roll-rate limited to 90 deg/sec and the roll acceleration limited to 90 deg/sec^2. There are no limits on roll angle in the DES.

Within the cab, the subject seat was mounted such that the roll axis of rotation was roughly through the subject's head. Mounted on the seat was a right-side-mounted force stick for vehicle control. The elbow was braced, so that when the roll axis was 90 deg nose up, the hand was still comfortably over the stick. The cab contained a computer generated display, Fig. 4,

which was centered in azimuth a distance of approximately 17 inches from the subject's eyes. Subject's sitting height were such that the display was within 0 to 10 degrees of eye level. The "inside-out" display of target tracking error consisted of a 3.5 inch long rotating "target wing" whose center was superimposed upon a stationary horizontal dashed line nine inches in length. A .25 inch perpendicular "fin" at the center of the rotating line provided upright orientation.

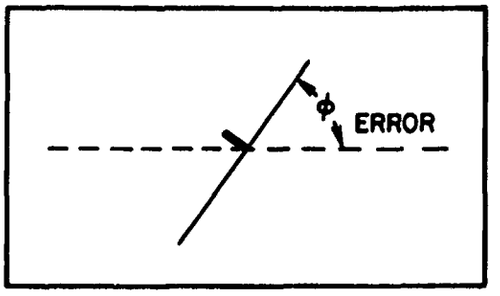

Figure 4. Sketch of the Roll Tracking Display

The DES is configured such that the pitch gimbal is outside of the roll gimbal. Thus it is possible to pitch the simulator nose up 90 degrees without affecting the roll axis tracking system. The cab pitched up 90 degrees was used for the "real-world" condition, as noted earlier.

Experimental Procedure

Four healthy college students between 18 and 25 years of age were used for the experiment. None were experienced pilots, so extensive training was necessary. Training was first accomplished for the static and two Full-Motion conditions. Tracking under each condition was considered one run. Each run lasted 165 sec and the three conditions or runs were presented in a random order each day. At the end of each run, subjects were presented their mean-squared-error score for that run. Training continued for approximately three weeks, three to six runs per day, at which time error scores began to reach asymptotic levels. Once performance leveled off, four more runs per subject per condition were performed and time history data was recorded for subsequent analysis.

For the second part of the study in which we investigated washout filter effects, we used the experimental design philosophy stated earlier — that washout filter effects should be compared to the "real-world" motion cues as encountered in the full motion no-tilt-cue case (F90). Therefore at the start of the evaluation of each washout filter, we let each subject first track in the F90 condition for one day. Following this we had each subject track normally (roll axis at 0 deg) with a given washout filter for three days, four runs per day. The last four runs for each subject with the washout filter were saved for data analysis. The procedure was followed for each washout filter investigated. As in the first part of the study, subjects were told their scores for motivational purposes.

Data Collection

A hybrid computer system was used for: display generation, forcing function creation, on-line error score computation, and time history data collection. From the time history data, root-mean-squared values and Fast Fourier Transforms (FFT) of each time signal were computed. From the FFT's power spectral densities and opened-loop describing functions (e.g., Eqs. 7 and 8) were computed. The frequency response data reduction, based upon the sum of sine waves generation, was similar to that employed in a preceding study (Ref. 3).

Comparisons among individual data showed good consistency, once sufficient training had occurred. Therefore, for each motion condition, the last four runs of every subject were averaged (16 runs total) by AMRL to give mean ± standard deviation values for model fitting by STI. It is these averaged data that are analyzed in the following section on Results.

RESULTS

Limited space precludes the presentation, here, of all the reduced and averaged data. Instead we present typical time histories for one subject, averaged spectra and describing functions for a typical motion case, and then, after demonstrating that the fitted transfer functions truly represent the data, we present the "opened-loop" curves for various cases, and analyze the resulting performance and behavioral measures to answer the questions in the Introduction.

Typical Time History

A pair of time-histories of the various inputs and outputs for corresponding segments of static and full-motion runs, is given in Fig. 5. For these plots, identical target and disturbance inputs (top and bottom traces) were used in each run, to reveal the differences more clearly. The following features of the time histories should be noted:

- The disturbance input, which is summed downstream of the stick (and shown to the same scale) is effectively integrated by the vehicle dynamics to yield roll motions comparable in amplitude and frequency to the target input.
- In the static case the roll angle does not follow the target very well, because of these simultaneous, large disturbance inputs.
- Comparison of the E and C traces for the static case (where only the visually displayed error can be used) shows that the pilot is using both error displacement and rate in his compensating control actions.

ORIGINAL PAGE IS
OF POOR QUALITY

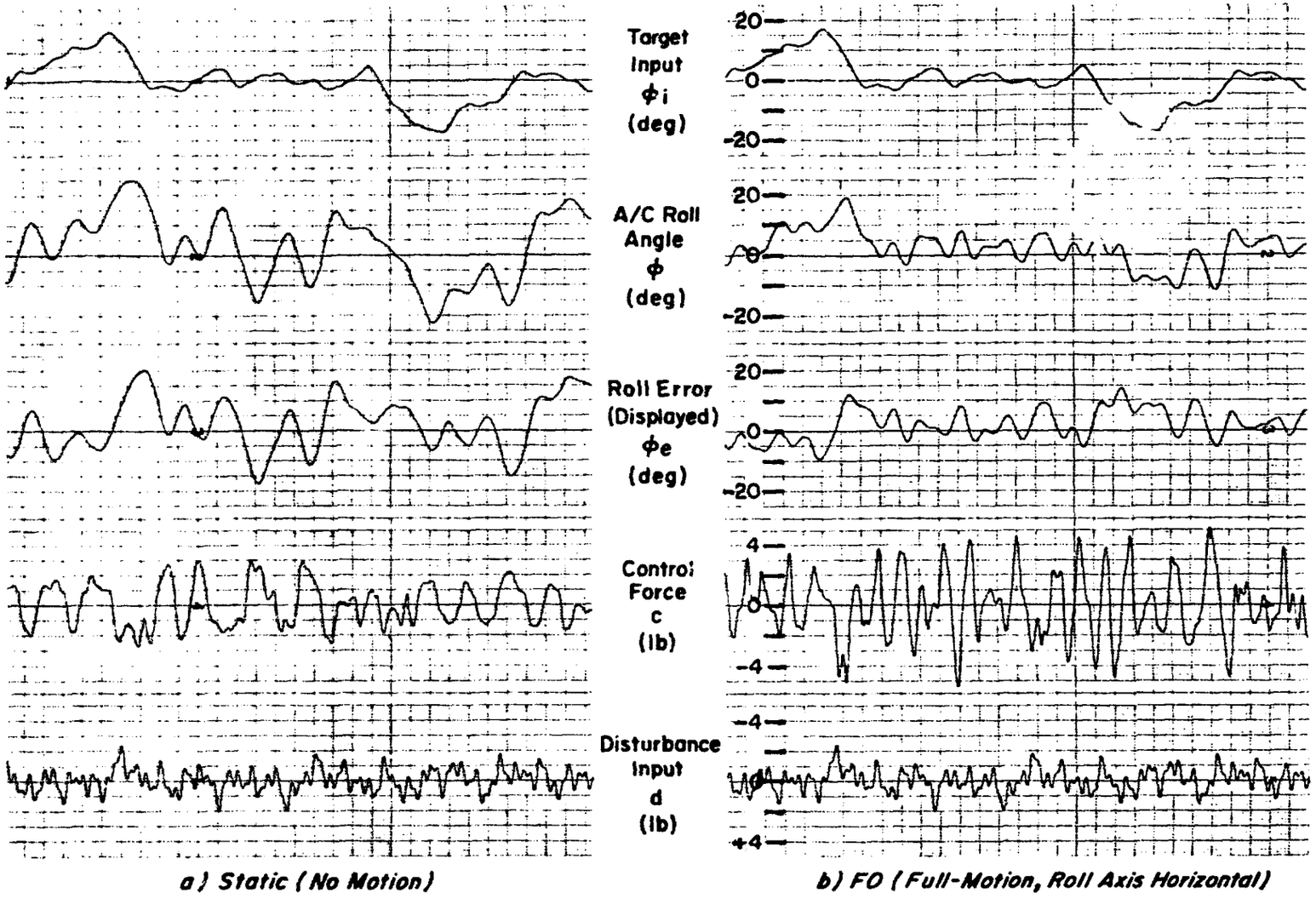

Figure 5. Typical Time Histories with No- and Full-Motion

- Comparing the motion case to the static case, the control response is obviously a more aggressive and higher bandwidth (due to motion cues), while the tracking error is reduced.

- (Not shown) There is a remarkable consistency in the φ, E and C traces for repeated portions of the same inputs, showing a highly input-coherent and consistent operator response, as will be shown by the reduced data, later.

Frequency-Domain Data

Examination of the individual error scores and closed-loop describing functions showed that each of the subjects adopted similar behavior and so the results could be validly averaged, without loss of significant details in the average. Thus, approximately four runs each of four subjects were averaged for the data shown (a few runs were dropped due to data problems). The data shown here for the Full Motion Case with roll axis at 0 degrees (F0) is genuinely typical of all the cases investigated and was not selected as the best-examples available.

Spectra. — Figure 6 shows power spectra for the control stick, displayed error, and aircraft bank angle. The remnant shown (plotted at forcing function frequencies by the X symbols) is actually an average over neighboring (non-overlapping) estimates. The small standard deviations shown for all signal components indicate that all subjects had essentially the same, low variability, behavior. The signal-to-noise ratio is quite good at all but the very highest frequencies and implies a high coherency between the two inputs and responses. This permits the major part of the responses to be described by linearized describing functions. Notice that the spectrum of Φ_{plant} (+) is large at low target frequencies (to follow the target) while its spectrum at low disturbance frequencies (◇) is lower, as desired.

Closed-Loop Describing Functions. — Figure 7 illustrates typical closed-loop describing function data (to which the model was fitted by the MFP procedure described earlier) for the control stick and task error responses to target and disturbance inputs. The frequencies used in the model fits are indicated by the arrows labeled "Fitted Freqs". Not all data points were used for computational economy. A preliminary analysis indicated that the selected frequency response points were the most sensitive indicators of pilot behavior.

Generally, the closed-loop data exhibit very low variability and the model fits capture every nuance of all the responses, using one set of model parameters and the various closed-loop relationships (e.g., in Fig. 2). The wiggles in the describing functions due to various low-damped modes, would greatly complicate simple interpolations between target frequencies to obtain vectors at disturbance frequencies, as done by earlier investigators (Refs. 1,5).

Model Fits. — Table 5 summarizes the model parameters fit to the data for all dual-input cases. Only nine of the twelve parameters in Fig. 3 were

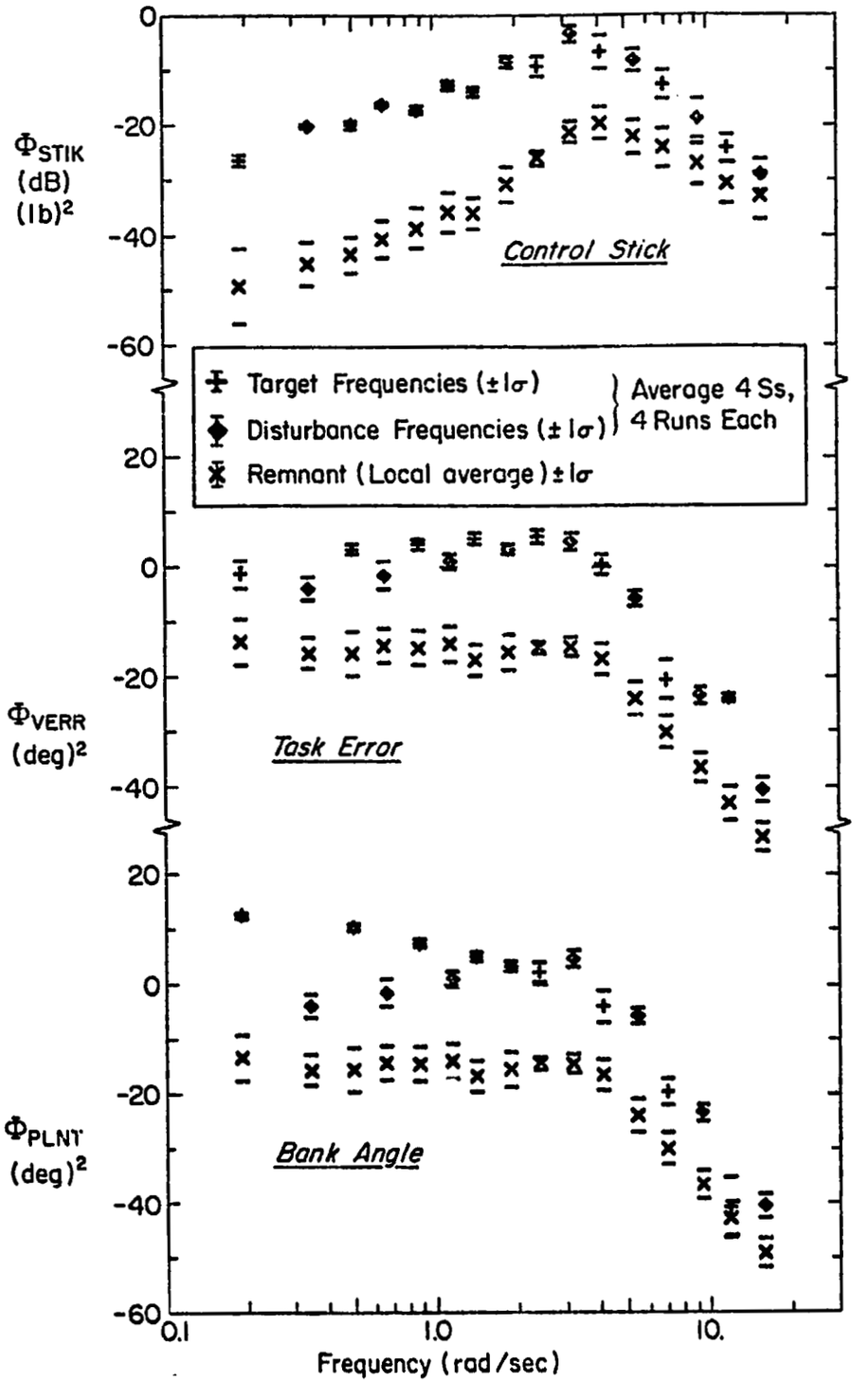

Figure 6. Typical Power Spectra for Full Motion, Erect (Case FO)

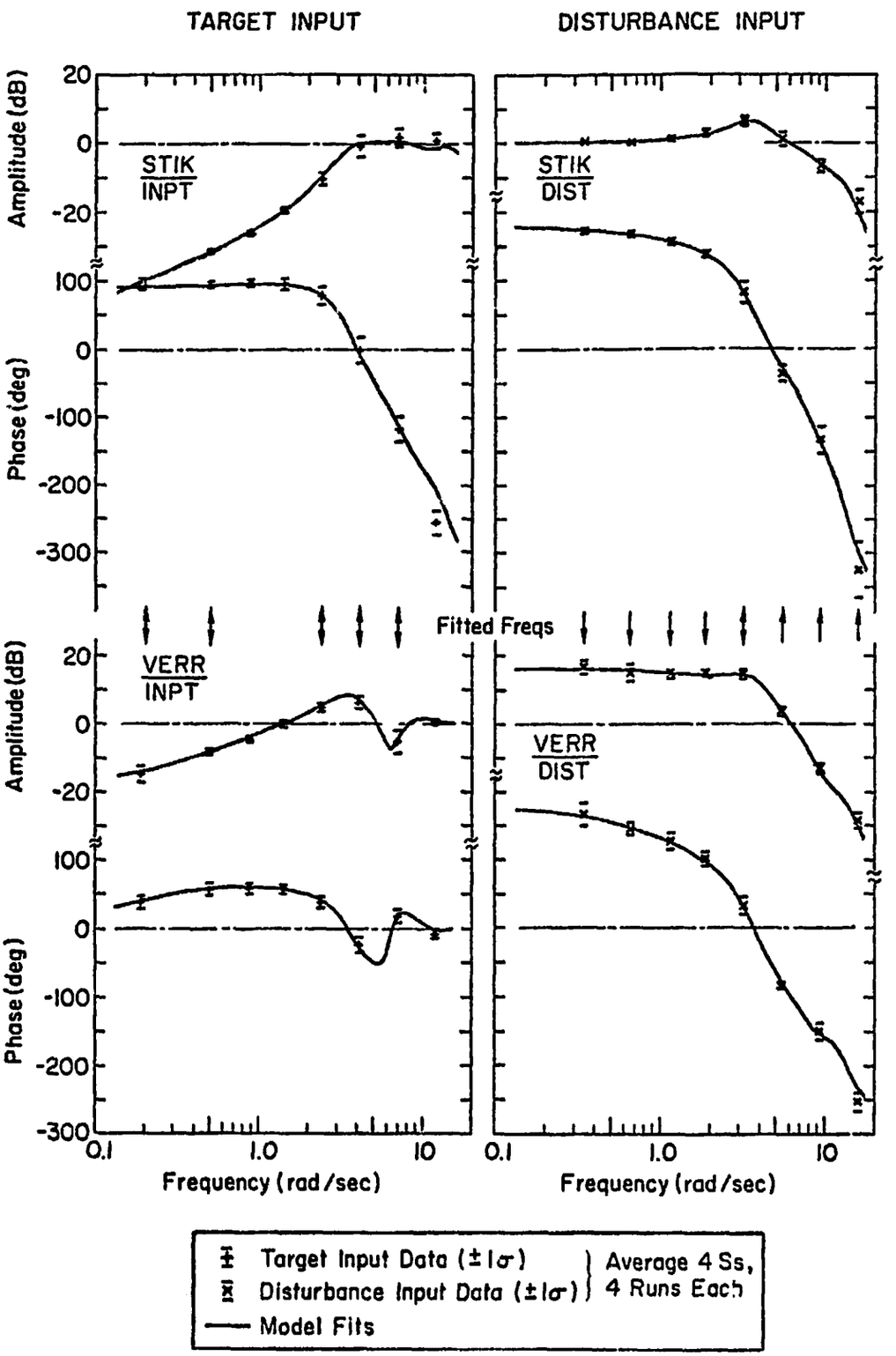

ORIGINAL PAGE IS
OF POOR QUALITY

Figure 7. Typical Closed Loop Describing Function Data and Model Fits for Full Motion, Erect (Dual Input, Case FO)

TABLE 5. SUMMARY OF MODEL PARAMETERS FIT TO DATA

CASE Motion Condition	MODEL PARAMETERS												REMARKS
	Visual					Motion			Neuromuscular				
	K_D	K_R	τ_V	$\frac{K_R}{K_D}$	$\frac{K_R}{K_D} - \tau_V$	K_T	K_V	K_A	τ_M	ζ_N	ω_N	$\tau_M + A_1$	
	$\frac{lb}{deg}$	$\frac{lb}{deg/s}$	sec	sec	sec	$\frac{lb}{deg}$	$\frac{lb}{deg/s}$	$\frac{lb}{deg/s^2}$	sec	--	$\frac{rad}{sec}$	sec	
F90 Real World	0.149	0.068	0.16	0.46	0.30	-.0001	0.076	0.020	0.15	0.26	9.3	0.20	Theor. $K_T \approx 0$
FO Full Motion	0.136	0.074	0.15	0.54	0.39	0.022	0.070	0.022	0.15	0.29	10.4	0.20	$\tau_M + A_1$ = Effective Delay
W2 2nd Washout	0.134	0.090	0.12	0.67	0.55	0.023	0.048	0.019	0.11	0.39	7.6	0.22	
W1 1st Washout	0.130	0.079	0.12	0.61	0.49	0.034	0.060	0.022	0.11	0.38	7.6	0.21	
W1, A 1st Wash + Atten.	0.119	0.070	0.08	0.59	0.51	0.040	0.081	0.031	0.17	0.28	9.0	0.23	
A Atten. Motion	0.122	0.053	0.06	0.43	0.37	0.056	0.131	0.028	0.15	0.13	8.2	0.19	K_T, $K_V \approx$ twice Values for FO
ST Static	0.072	0.064	—	0.89	—	—	—	—	0.18	0.18	7.0	0.23	

(K_1, P_1, A_3 set to 0)

needed, as preliminary fits showed that a second order fit was sufficient for the neuromuscular mode ($T_N = 0$) and there appeared to be no error integrating action ($K_I = P_I = 0$). Lack of K_I and P_I (the so called α-effect in the Extended Crossover Model) may have been due to presence of the tilt cue in the motion cases with roll axis at 0 deg, but its absence at F90 and Static conditions is unusual.

The additional columns in Table 5 detail the effective lead time constant in the visual path ($T_L = K_R/K_D$) and the effective time delay in the neuromuscular path ($\tau_e \doteq \tau_M + A_1$). Note that the visual displacement gain, K_D, nearly doubles when going from Static to any Motion condition, and the tilt sensitivity, K_T, is negligible for the F90 case, as it should be, since no tilt cue is available.

Opened-Loop Describing Functions. — A number of other trends and covariations among parameters are evident; however, these effects can best be illustrated by using the "opened-loop" responses calculated using the measured closed-loop data along with the loop structure of Fig. 2 or the parameters in Table 5 with the model of Figs. 2 and 3. Figure 8 shows the resulting "opened loop" data and computed model curve for the Full Motion, F0 Case. As with the closed loop responses the model curve fits the actual "opened-loop" data very well — it truly represents the data. These data and fits for this example are typical; i.e., the other cases show effects similar in kind, differing only in degree. Thus, comparisons among cases can be made using the curve fits, as we will do in the remainder of this paper.

These multiple "opened-loop" describing functions have all of the appearance and significance of single open-loop transfer functions, and similar descriptive parameters apply. Some of these have been noted on Fig. 8, as defined below:

ω_u = "unstable frequency" (180 deg phase crossover). This sets the maximum bandwidth of the loop, and is the frequency at which oscillations set in if the gain were further increased by K_M dB.

ω_c = "crossover frequency" (0 dB gain crossover). This sets the effective bandwidth of the loop, and determines the resulting stability margins.

K_M = "gain margin" — allowable gain increase for incipient loop instability.

φ_M = "phase margin" — allowable phase lag for incipient loop instability.

In Fig. 8, it is apparent that the disturbance loop (dominated by the motion pathway) has a higher bandwidth and lower phase margin than the target loop (dominated by the visual pathway). This implies lower tracking errors, as will be shown later.

ORIGINAL PAGE IS
OF POOR QUALITY

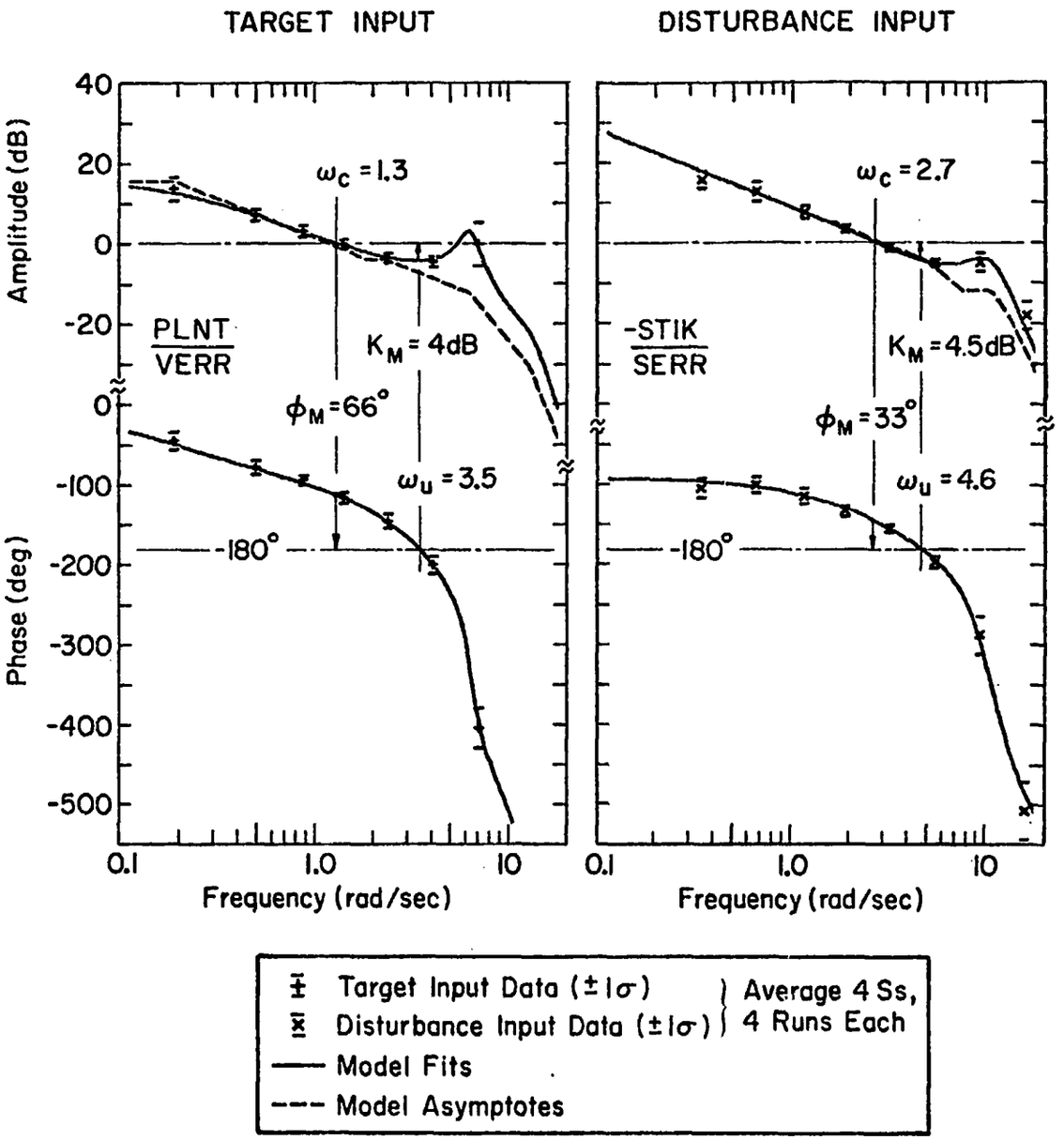

Figure 8. Typical Effective "Opened Loop" Data and Model Curve for Full Motion, Erect (Dual Input, Case F0)

The kinks in the dashed "asymptotes" in Fig. 8 show the poles (break downwards) and zeroes (break upward) of the model. The need for the relatively high order pilot-vehicle model used here is clearly shown by the spread between the asymptote breaks and the model fits as well as the different asymptotes in each "opened-loop."

Effects of Full Motion vs. Static Conditions

Figure 9 compares various performance measures for Full Motion and Static cases. Variances are used because they can be partitioned into summable vector components due to: Target, Disturbance and Remnant. Concentrating on task error, Fig. 9b, for the STATIC Case, the error components from Disturbance (D) and Target (T) inputs are essentially the same, reflecting the dual input spectrum design objective mentioned earlier. For the Full Motion at 90 deg (F90) case the target errors (T) are the same as for a Static cab, while the disturbance errors (D) are much smaller. Going from Full Motion, at 90 deg to the 0 deg (F0) case shows that the target following errors (T) are reduced slightly while the disturbance errors are unchanged.

These basic trends in the tracking performance are explained by the changes in the opened-loop describing functions (DF) shown in Fig. 10. For the Target Input DFs the Supine and Static cases having no tilt cues show essentially the same DF (which results in the same target following errors) whereas the Erect case (with the maximum tilt cue) has a smaller target error. For the Disturbance Input DF both motion cases (F0, F90) have the same DF, which explains why their "D" components were the same in Figs. 9a,b,c,d. Furthermore, the "Rate Cue Effect" (lower loop lags leading to higher crossover frequencies with motion) leads to the motion/static performance effects denoted by the arrows. Thus Figs. 9 and 10 show that the subjects used motion cues to improve performance in two main ways.

- The lower lags (and higher ω_u) permitted by the vestibular sensory-motor loop enables, in effect, a "roll-rate damper loop" to be closed by the pilot, thereby allowing a tighter disturbance regulation loop to be used by him (a loop gain increase of about 2.7/1.7 = 1.6). Consequently, the disturbance variance is reduced significantly.

- The tilt-cue was used at low frequencies to provide a sense of zero reference and, thereby, to avoid drifts and overshoots, the effects showing up as a low frequency phase reduction on the target "opened-loop."

Components of the Multiloop Describing Function Under Motion

Further insight may be gained into the complexity of the multiloop interactions and motion effects via Fig. 11, in which the fitted model has been used, via the loop structure and equations of Fig. 2, to examine: each

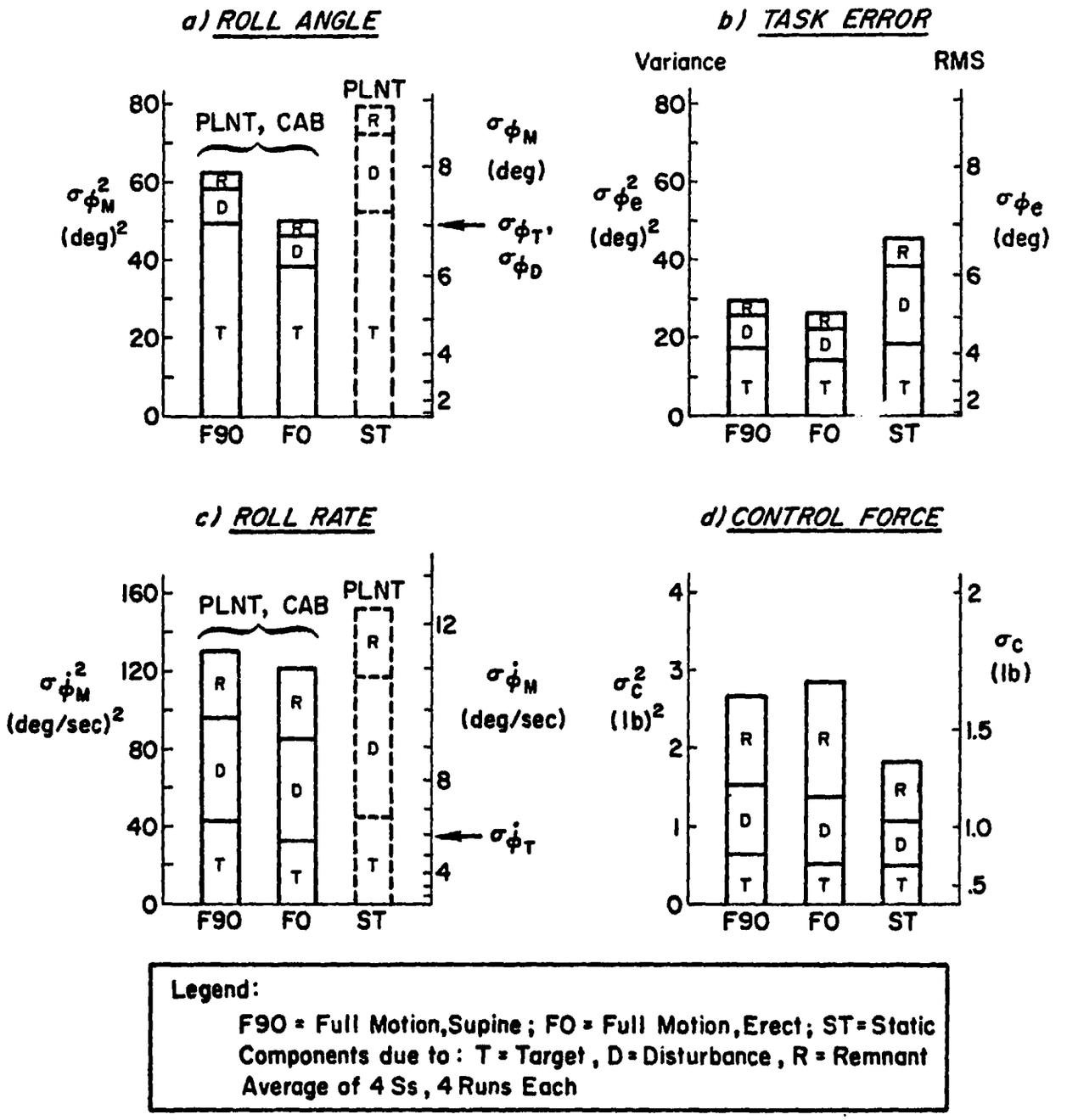

Figure 9. Effects of Full Motion (Supine, Erect) and Static Cases on Performance

ORIGINAL PAGE IS
OF POOR QUALITY

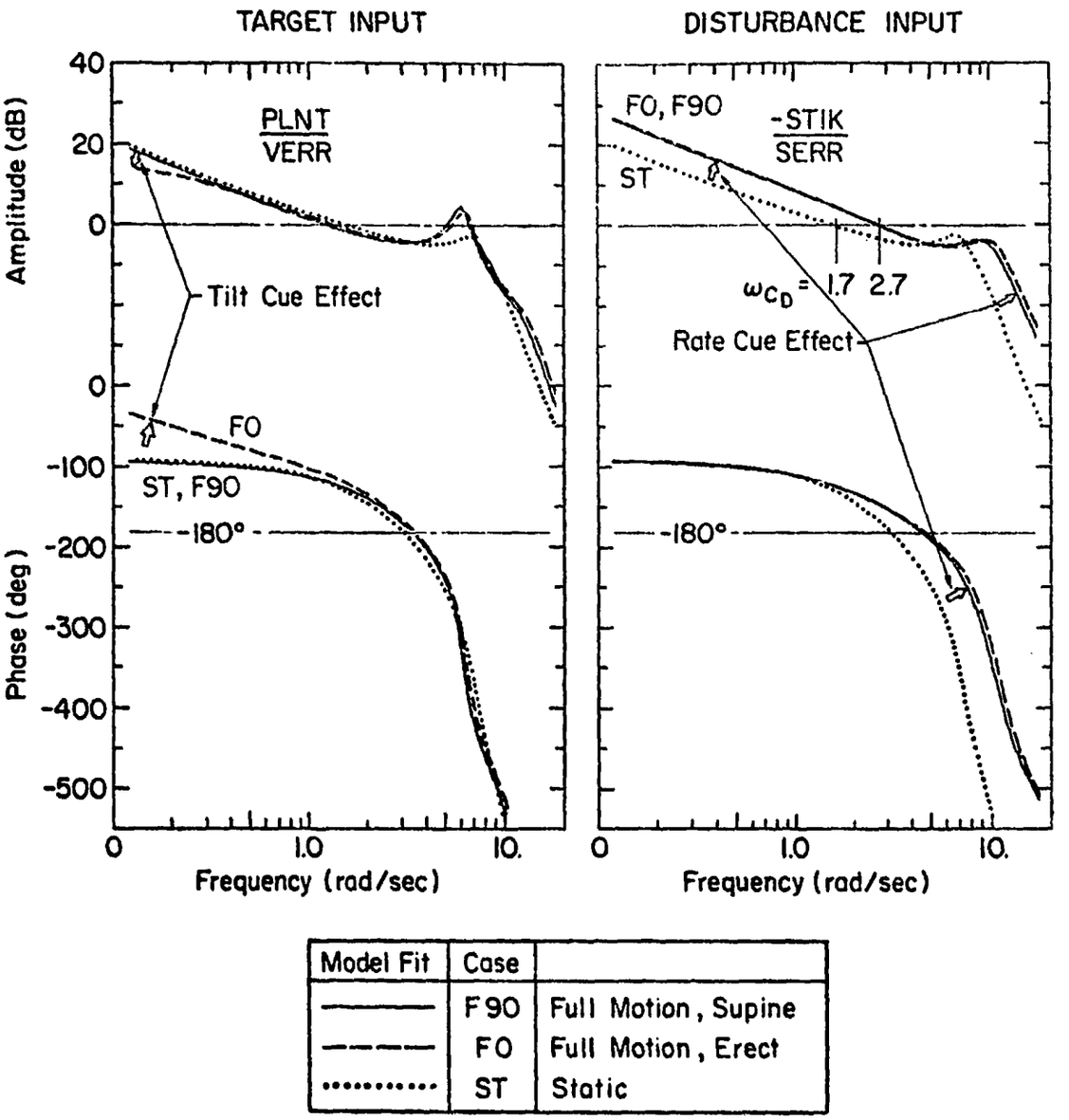

Figure 10. Effect of Motion Cues on "Opened Loop" Describing Functions (Dual Input Cases)

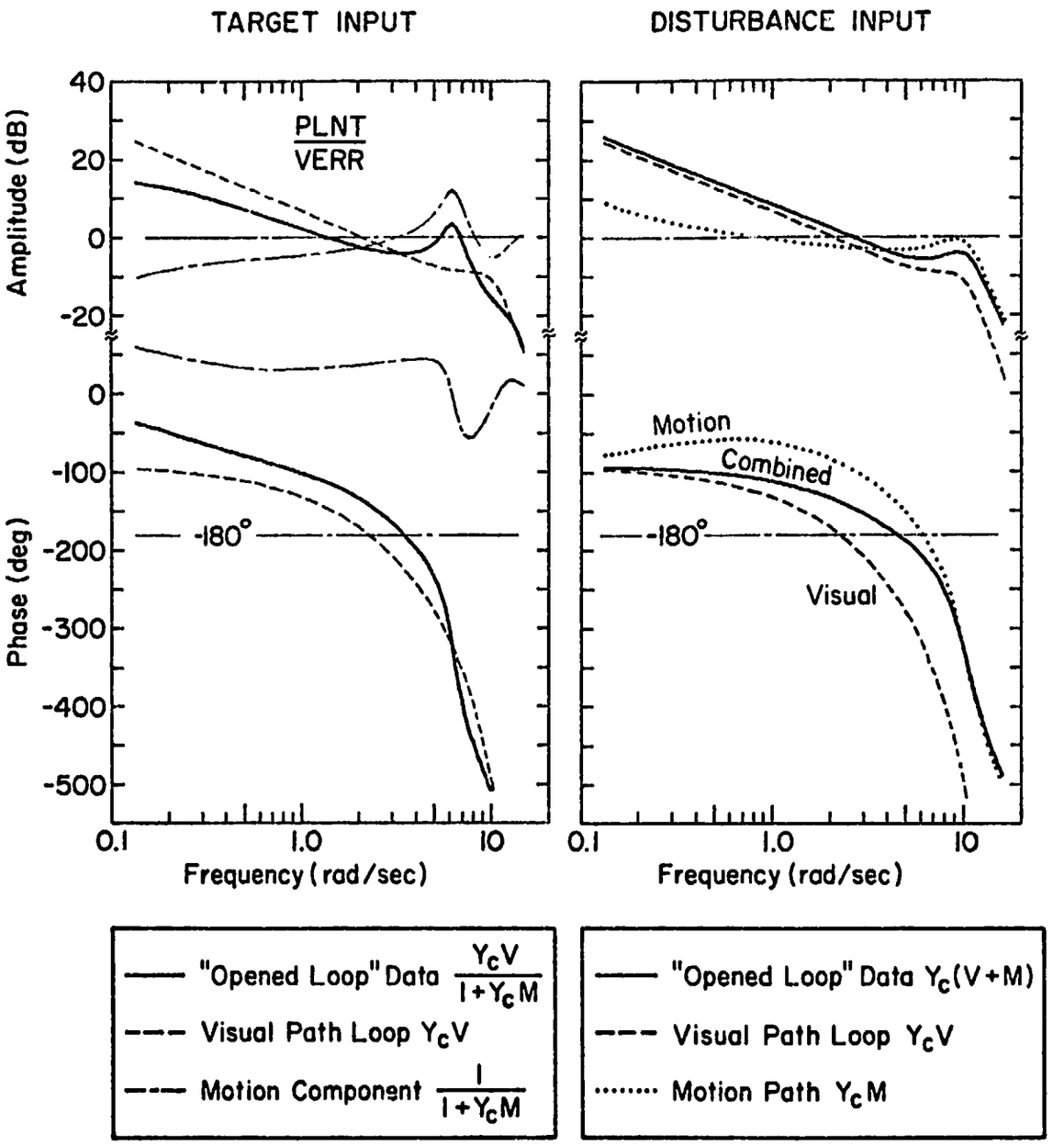

Figure 11. Behavioral Components of "Opened Loop" Data
(Dual Input, Full Motion Erect Case F0)

sensory loop individually (visual = dashed, motion = dotted) with the other simply turned off, and then the combined "opened-loop" (solid line) as discussed earlier in Section II-C. Remember that the "opened-loop" DF is a complex vector function of V and M, as noted in the legend.

Without going into details, the key points revealed by Fig. 11 are as follows:

- The Disturbance Input loop (on right) is a simple vector sum of VY_c and MY_c. The flat amplitude of the motion loop (dotted) shows that MY_c acts like a roll-rate feedback loop with an effective time delay, τ_e, appreciably less than the visual loop (for MY_c; $\tau_e \doteq .20$ sec, for VY_c; $\tau_e \doteq .20 + .15 = .35$s). Over the important crossover frequency region of 0.5-5.0 r/s, their vector sum (solid) has an apparent τ_e even <u>less</u> than MY_c alone! This is consistent with and "explains" the results of Stapleford (Ref. 1) and Shirley (Ref. 2).

- At low frequencies the Disturbance regulation (solid) is dominated by (closest to) the visual loop at low frequencies and motion loop at high frequencies.

- The Target following loop (on the left) is a more complex function of VY_c and MY_c as seen in the equations in the box. (The motion component $(1 + Y_cM)^{-1}$ is shown dash-dotted to distinguish it from Y_cM alone. Here, the solid curve is the vector <u>product</u> of the two components). In both amplitude and phase, the Target following loop dynamics are dominated by the visual loop (dashed) at all frequencies.

- A comparison (not shown here) of the purely visual static case <u>per se</u> (dotted curve of previous Fig. 10) and the isolated VY_c (dashed curve of Fig. 11) shows that they are <u>not</u> the same. When <u>motion is present</u>, the visual loop can be (and is) operated at higher gains, albeit with a slightly larger lead equalization (T_L) and consequently larger τ_e. (Per Table 5, $T_L \doteq 0.89$ sec and $\tau_e \doteq 0.23$ sec for the ST case; while $T_L = 0.54$ sec and $\tau_e = 0.20 + 0.15 = 0.35$ sec for the FC Case).

This analysis of Fig. 11, and others like it, clearly shows that one cannot simply add a motion feedback loop to the static case dynamics to get the combined result. Instead the operator optimizes his combined loop properties for the case at hand.

Effects of Single vs. Dual Forcing Functions

For some Full Motion cases (F90, F0), data were taken for Target input alone; and for Case F90, Disturbance input alone, to compare with the dual input case. When either input was used alone, it was increased by the square-root-of-two to keep the rms input the same as in the dual input case.

In general one might expect that if the disturbance alone were present, the pilot would adopt a different optimum behavior, because all he would have to do is to suppress both the felt and seen motions. Conversely, for the target alone, the pilot might more agressively track the error, because the unseen disturbances were absent.

The results, shown in the opened-loop describing functions in Fig. 12, did not follow these expectations! For simplicity, the curve in Fig. 12 is that fitted to the corresponding dual input case, for which it passed precisely thru every data point on both sets of DF (e.g., see Fig. 8). The single-input data are shown relative to this dual-input curve in Fig. 12, remembering that each of the data plots represents a different set of runs. Somewhat to our surprise, the single input data are not significantly different from the dual input case, for the points generally lie within one symbol width of the curve and almost all lie well within ± 1 standard deviation of the dual-input curve.

How can this be, in the light of the theoretical expectations discussed above, considering that all pilots were given plenty of practice on every case, and noting that all behaved similarly (evidenced by the low scatter)?

Some hypotheses are:

- The "optimum" behavior was, perhaps fortuitously, nearly identical for the single and dual input cases. The combination of lightly damped modes in the controlled element near the neuromuscular modes plus stick lags has been identified as the so-called "Pilot Induced Oscillation Syndrome" of Ref. 8. These restrict the degree of equalization which can be used by the pilot to improve performance. Consequently, he may be operating near this constrained limit in all cases.

- The pilots were so overtrained in the dual case that they did not adapt "optimum" behavior in the single input cases despite plenty of practice with it. If so, this raises questions with respect to the assumption that pilots adopt an "optimum" behavior.

- There was some error in the experiment, such that dual inputs were really present. We checked this and verified that only the specified single input spectra and rms signals were present.

Here is an ideal, simple test case against which to validate the optimal adaptation models (e.g., Ref. 4). The inputs are analytically tractable, the good model fits show that the data are representable by linear, modest-order state equations, and the data are precise, have high signal-to-noise, and are internally self consistent. Such a validation remains as a future task.

Meanwhile, this result tentatively implies that the dual-input results should apply to the single input situations, if the inputs and controlled elements are similar to those used herein.

ORIGINAL PAGE IS
OF POOR QUALITY

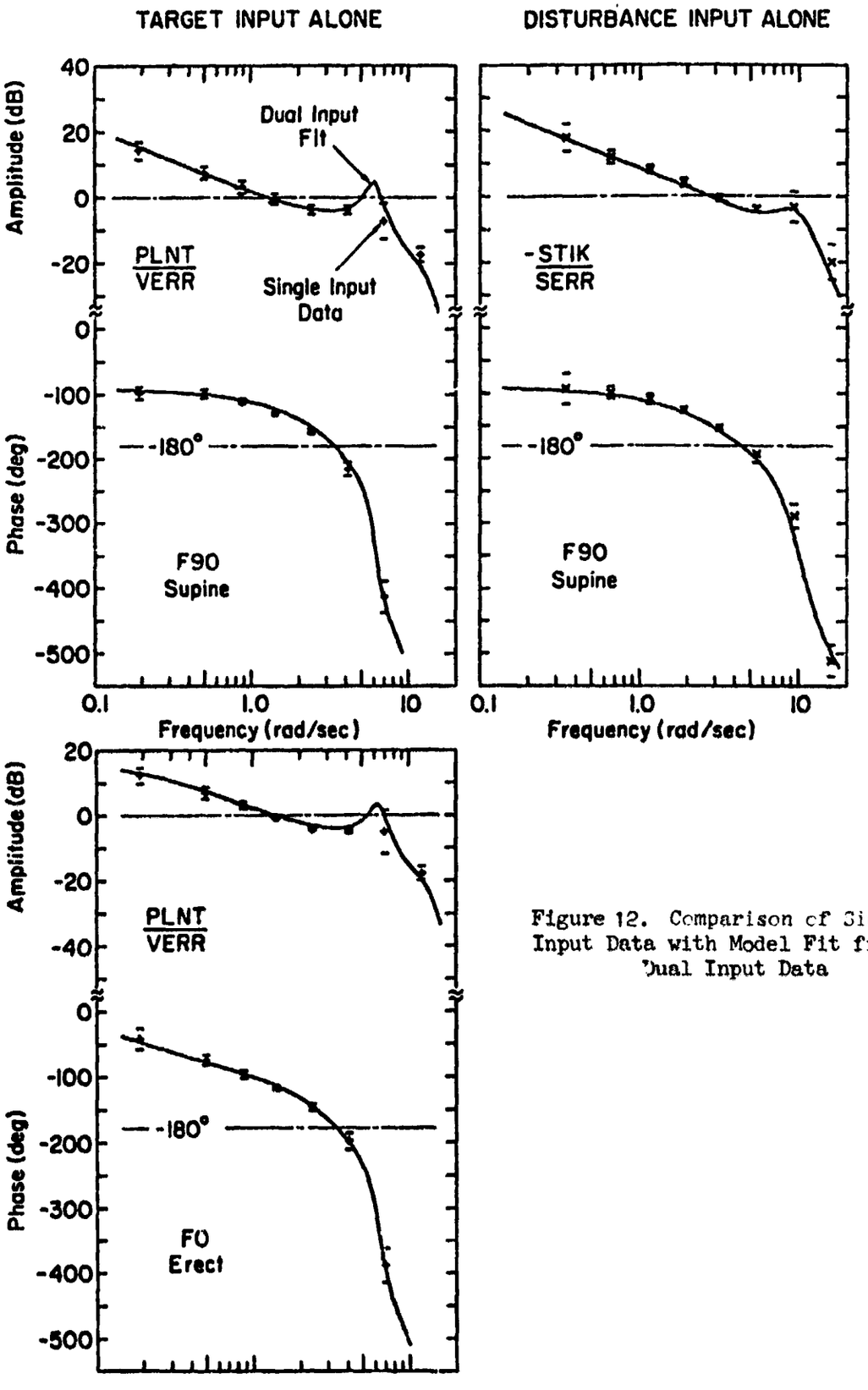

Figure 12. Comparison of Single Input Data with Model Fit from Dual Input Data

Effects of Motion Shaping (Washouts)

Having presented the results on our first question — that of basic motion effects vs. no motion, we turn now to the second question: What are the effects of various motion "shaping" (attenuations and/or washouts)? For this purpose, the data will be restricted to the dual-input cases, all with roll axis horizontal, i.e., FO, W2, W1, W1A, ATT, in the order of decreasing recovered roll angle.

Figure 13 shows various performance measures for these cases. Consider first the variance of recovered (measured physical) roll angle, $\sigma^2_{\Phi M}$, shown at the upper left, each case broken down in terms of the components due to target, disturbance and remnant. Noted on the margin are the variances for the target (or disturbance) alone, and their sum. Ideally, the recovered variance would consist of only the target component (equal to $\sigma^2_{\Phi T}$, attenuated by the motion shaping washout) and no disturbance or remnant portions. It may be recalled from Fig. 9 that in the (real-world) "F-90" case this ideal is approached, in that the target component nearly equals the commands, while the disturbance and remnant portions were small fractions of that.

With these standards in mind, let us consider the effects of various washouts. As described in Section II on Experimental Design, the overall scheme was to select different forms of motion washout, each selected (albeit crudely) to give the same attenuation of roll angle to about 50 percent of the basic, FO, case (i.e., the target roll variance of 1/4 of the basic level). As seen in Fig. 13a, this was achieved closely only for the pure attenuation case ($\sigma_{\Phi M} \doteq 3.6$ deg vs. $\sigma_{\Phi T} \doteq 7.0$ deg). The ATT computed roll motions (shown dashed) were nearly equal to the FO case, as were the other task performance measures in Fig. 13 (e.g., tracking error and control force) implying a close matching of the visual and motion-loop behavior in the basic and ATT cases, despite the lower magnitude of motion cues in the latter. (More on this later).

The Second Order Washout (W2) (which greatly attenuates the lowest frequencies) distorted the perceived motion cues (per the subjective questionnaire) and failed to reduce the motions as intended. Analysis of these results showed that this was due to the following reasons:

a. The washout was a compromise design* such that the high-frequency asymptote magnified the roll angles (and rates) above the break frequency of .85 r/s by a factor of about 1.2, causing the roll rate variance (Fig. 13-c), and high frequency portions of the roll angle variance, to be increased by $(1.2)^2 = 1.4$ relative to the intended case.

* The DES is a velocity system and as such would drift whenever a cascade washout was used. Consequently, a feedback scheme was devised that approximated the desired cascade washout but a perfect match at both high and low frequencies was not possible.

ORIGINAL PAGE IS
OF POOR QUALITY

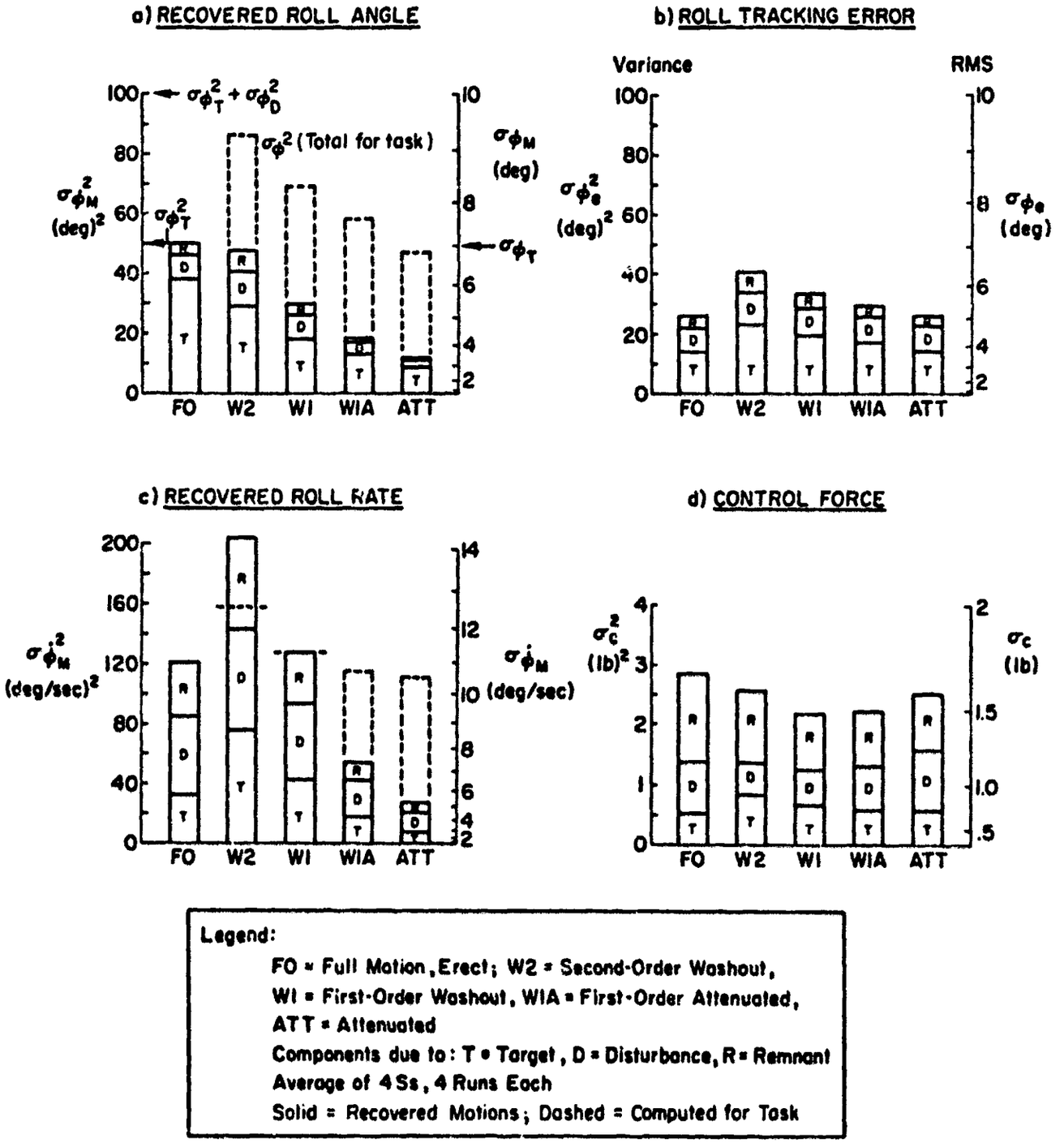

Figure 13. Effects of Motion Shaping on Performance

b. The distortion of the felt motions relative to the visual motions caused the pilots to perform even worse than in the static case.

The other washouts were intermediate in recovered motion and plant motion between the Full and Attenuated cases.

Attenuation reduces both the recovered roll angles and roll rates in the same proportion, but washout reduces mainly the low frequency components and, thereby, reduces the roll rates less than the roll angles. This can be seen by comparing Figs. 13a vs. 13c for the W2 and W1 cases, especially.

Except for the anomalous W2 case, discussed above, the performance measures of tracking error and control force were not significantly different among any of the first order or attenuated wash out cases (See Figs. 13b and 13d. Even the proportions of each variance due to: target inputs, disturbances, and remnant were about the same as for the full motion case (FO).

Further insight into the pilot's tracking behavior under these washouts is given by the opened-loop describing functions in Fig. 14. It is immediately apparent that the disturbance-loop describing functions are nearly identical, implying the following:

- Despite attenuated, reduced-low-frequency motions, and phase distortions, the pilot compensated to give the same opened-loop DF.

- In the ATT case, the rms roll angle was reduced from 7 deg to 3.6 deg, the pilot had double his tilt and roll rate gains, (K_T, K_V) as verified by the fitted coefficients in Table 5, and summarized below:

Case:	σ_Φ	K_T	K_V	K_A
FO	7°	.022	.070	.022
ATT	3.6°	.056	.131	.028
Ratio: (ATT/FO)	.51	2.55	1.87	1.27

Despite the fact that the rms tilt angle in the ATT case represents a lateral-specific-force cue of less than $3.6/57.3 = .063\ g_y$, the roll rates were apparently sufficiently high to be readily sensed and used to compensate for the reduced motion cue over the FO case.

On the left of Fig. 14 is the target-loop DF, where the following effects of washout are clearly apparent:

- the FO and ATT cases are nearly identical for the same reasons given above for the invariant disturbance loop DF.

ORIGINAL PAGE IS
OF POOR QUALITY

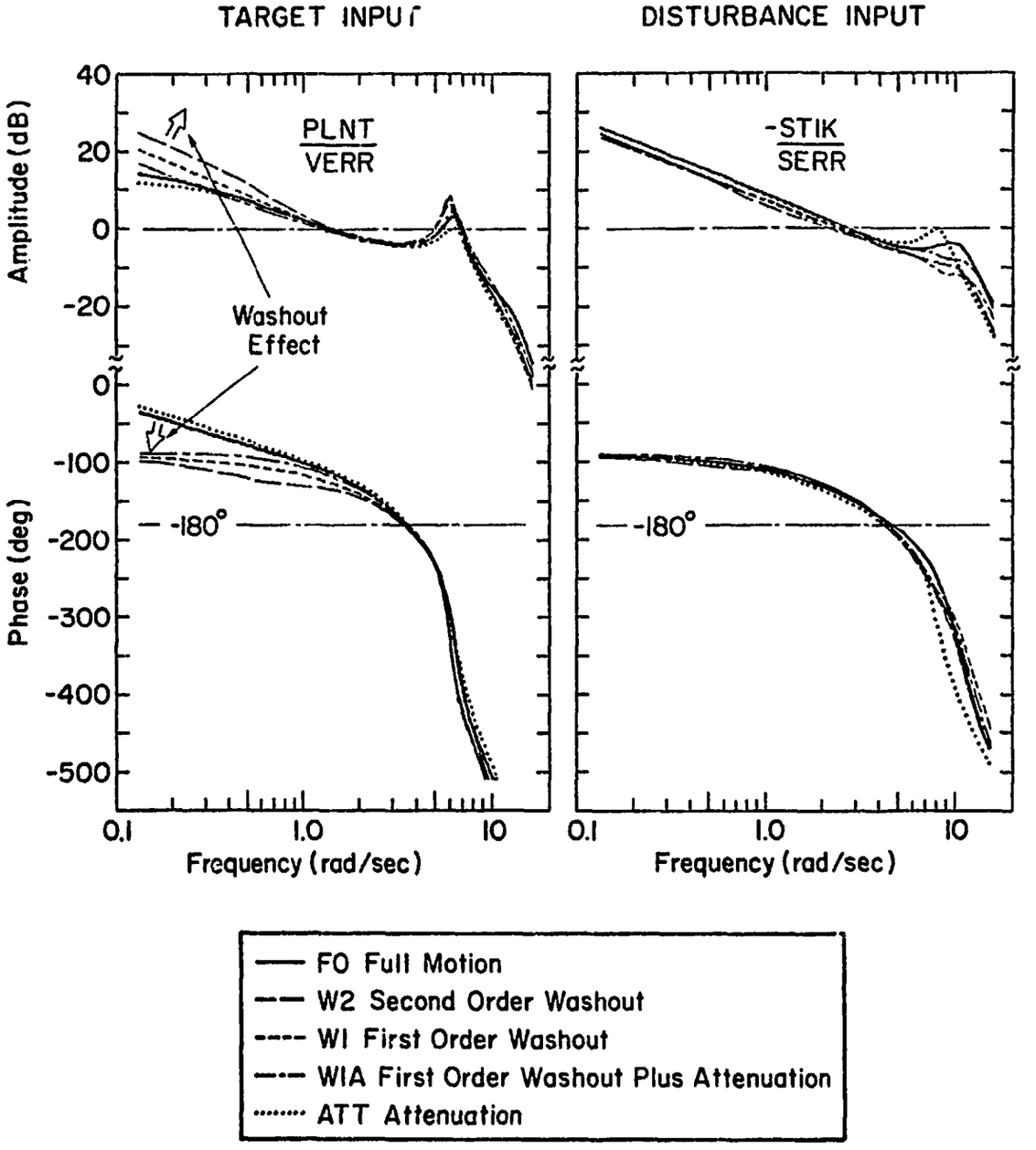

Figure 14. Effects of Motion Shaping for "Opened Loop" Describing Function (Dual Input Cases, Roll Axis Horizontal)

- the other washouts induce (at low frequencies) higher amplitude ratio and more phase lag as the washout degree is increased from ATT, to W2. An analysis indicates that these trends reflect fairly complex interactions similar to that of Fig. 11 (Left side). Note that inserting a low frequency washout to the motion path (M in Fig. 11) causes the resulting curve to start (at low frequencies) on the dashed curve and transition to the solid curve with increasing frequency. These amplitude and phase trends explain the "Washout Effect" in Fig. 14.

Optimum Washout

One of the objectives of this experiment was to find the optimum washout for AMRL's roll-only simulators. The desirable criteria are relative to the "real-world" case: a) significant reduction in roll amplitude and rates, and b) similar pilot behavior and performance.

Inspection of the foregoing results reveals that the clear choice is the first-order attenuated washout (W1A). Figure 15 justifies this selection based on the following comparisons with the F90 ("real-world" baseline) case:

- Large reduction is recovered roll-angle and rate — as shown in Fig. 15a — with similar plant roll angles and rates.

- Very similar tracking error performance and control activity, as shown in Fig. 15b and 15c. Even the distributions of each variance from target, disturbance, and remnant inputs is closely matched.

- The opened-loop describing functions, shown in Fig. 15d, are practically identical. This is because the effect of tilt cue usage previously described in connection with Fig. 10, is almost exactly cancelled by the washout-break effect noted in Fig. 14.

- (Not shown) The subjective comments were more favorable for this washout than any other except pure attenuation.

Thus, we recommend first-order attenuated washout for use on all AMRL roll-only type simulators. The degree to which this form can be extended has not been determined, but the data suggest the following as likely to be both useful and satisfactory to pilots:

- Attenuation factor of 0.5 to 0.7

- Break frequency of 0.3+ to 0.5 rad/sec (Washout time-constant of 2-3 sec).

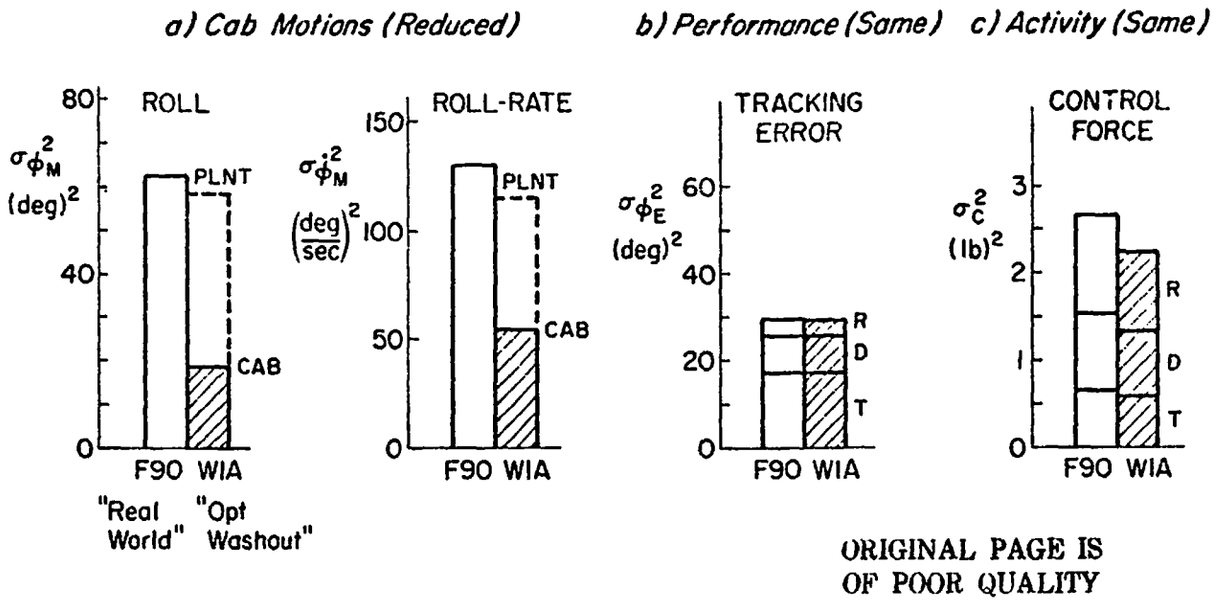

ORIGINAL PAGE IS
OF POOR QUALITY

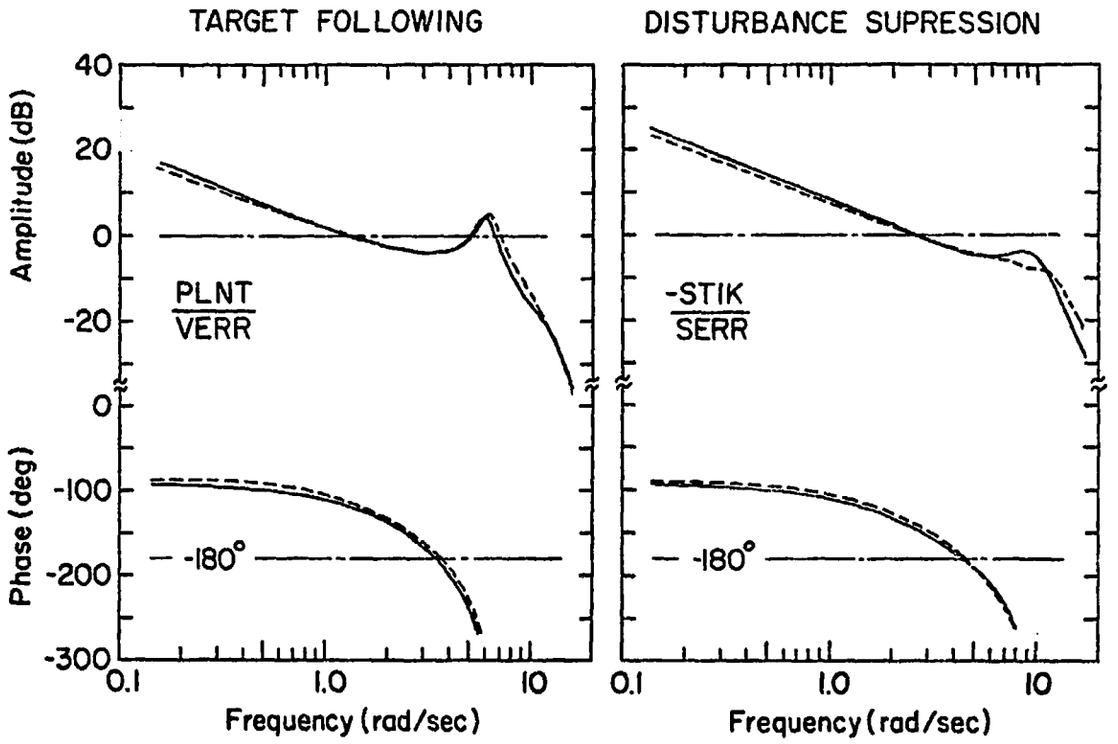

Motion Fit	Case	
———	F90	"Real World", Full Motion, Supine
– – – –	WIA	Optimum Washout (first order washout plus attenuation) 1/T = 0.4 rad/sec, Attenuation = 0.7

Figure 15. Comparison of Optimum Washout with "Real World" Case

CONCLUSIONS

This research has covered several very well trained subject's responses to a variety of motion cases in a roll-only motion simulator, with simultaneous target and disturbance inputs. The results presented here support the following conclusions:

1. Across all seven conditions the four subjects were very consistent in their tracking behavior and scores, providing an exceptionally, reliable, and definitive data base worthy of detailed analysis, even beyond that performed herein (e.g., on remnant effects).

2. The multiloop model structure presented in Fig. 1, which has both visual, motion and (a common) neuromuscular dynamic elements, proved capable of accurately fitting the closed- and "opened"-loop describing functions at all measurable signal points within the loop. In combination with the interleaved sum-of-sinusoids target and disturbance inputs the new STI Multiloop Fitting Program (MFP) provided efficient fits of 10 parameters in a multiloop situation which had heretofore been very difficult to fit because of the complex interactions involved between the visual and motion feedback paths.

3. Untangling the closed-multiple loop describing function data in the "opened-loop" manner shown here provides a ready comparison with traditional single open-loop data. Similar effects (e.g., the Crossover-law adaptive behavior) are shown for the dual input case, with the disturbance loop having the higher bandwidth (limited mainly by the controlled element and vestibular rate-sensing dynamics).

4. After lots of analysis and digesting of complex trends in the various cases, the key to understanding it all seems to be the following:

   - Given reasonable rate motion cues at frequencies above about 0.5-1.0 rad/sec, the pilot's motion feedback system acts like an adaptive roll-rate damper with a bandwidth of nearly 3 rad/sec. This tends to suppress disturbances but opposes target following motions, while stabilizing both loops.

   - The pilot then uses sufficient extra visual compensatory (error correcting) gain to follow target commands as well under motion as in the static case, and with less remnant and disturbance components.

5. The affects of motion are consistent with the prior work of Stapleford (Ref. 1), Shirley (Ref. 2) and Levison et al (Ref. 4), while extending this work to the new case of equally strong target and disturbance inputs each having comparable apparent spectra at the display.

6. The describing functions and fitted tilt-cue parameter clearly showed that the spurious tilt cues from rolling with roll-axis horizontal are used, even though the rms lateral specific force was in some cases much less than 0.1 g_y. A very simple model for the use of this cue is given. Nevertheless, use of this cue resulted in only small improvements in tracking performance in this random-input tracking task.

7. The four types of motion washout investigated (second-order, first-order, first-order-attenuated, and purely-attenuated) showed distinct effects compared to the "real-world" reference case of full motion about a vertical roll axis; the second-order case was the least desirable because of large differences in performance, behavior, (describing functions) and subjective ratings. The other cases provided roughly similar performance measures with some small differences in relative remnant, describing functions, and ratings.

8. The pilots clearly adapted differently to the various washouts, thus complicating the job of predicting the net effects for a given washout.

9. The optimum washout for roll-only-simulators (from the standpoint of performance, behavior and ratings similar to the "real-world" reference case) was clearly the first-order, attenuated washout. Recommended parameters (for this type of task) would be: attenuation factor 0.5-0.7, and washout time-constant of 2-3 seconds (break at 0.3-0.5 rad/sec).

The data base for this paper is being prepared for permanent filing and general access at the U.S. Defense Documentation Center (DDC); and may be requested through the third author, at AMRL.

It would be interesting and fruitful to analyze and model the remnant portion of these data, using the closed-loop spectral data available (e.g., as in Fig. 6). Because the inputs were carefully selected and shaped to be representable by filtered white noise, various optimal-control-theories could be tested against this very consistent, accurate, and definitive data base. Finally, using these model and parameters (which precisely fit almost every data point,) various analytical manipulations of the data can be performed to gain further insight about pilot adaptation to motion cues and washouts.

REFERENCES

1. Stapleford, Robert L., Richard A. Peters, and Fred R. Alex, Experiments and a Model for Pilot Dynamics with Visual and Motion Inputs, NASA CR-1325, May 1969.

2. Shirley, R. S., "Motion Cues in Man-Vehicle Control," M.I.T., Cambridge, MA, Sc.D. Thesis, Jan. 1968.

3. Levison, W. H., S. Baron, and A. M. Junker, Modeling the Effects of Environmental Factors on Human Control and Information Processing, AMRL-TR-76-74, Aerospace Medical Research Laboratory, Wright-Patterson AFB, Ohio, Aug. 1976.

4. Levison, W. H. and A. M. Junker, A Model for the Pilot's Use of Motion Cues in Roll-Axis Tracking Tasks, Bolt Beranek and Newman, Inc., Cambridge, MA, Report No. 3528, Apr. 1977.

5. McRuer, Duane T., and E. S. Krendel, Mathematical Models of Human Pilot Behavior, AGARDograph No. 188, Jan. 1974.

6. Zacharias, G. L., and L. R. Young, Manual Control of Yaw Motion with Combined Visual and Vestibular Cues, presented at 13th Annual Conf. on Manual Control, M.I.T., Cambridge, MA, 15-17 June 1977.

7. Magdaleno, Raymond E., and R. Wade Allen, Modeling Biodynamic Effects of Vibration, AFOSR 75-1236 TR, July 1975.

8. Ashkenas, I. L., H. R. Jex, and D. T. McRuer, Pilot-Induced Oscillations: Their Cause and Analysis, Northrop Corp., Norair Div., Rept. NOR 64-143, June 1964 (AD 481994).

N79-15623

A METHOD OF MOTION SIMULATOR DESIGN BASED ON MODELING CHARACTERISTICS OF THE HUMAN OPERATOR

D. W. Repperger A. M. Junker

Aerospace Medical Research Laboratory
Wright-Patterson Air Force Base, Ohio 45433

Introduction

A problem of interest in the design of simulators is the development of a design criteria such that the simulators can be adjusted until they emulate real world situations. In this paper such a design criteria is obtained to compare two simulators and evaluate their equivalence or credibility. In the subsequent analysis the comparison of two simulators can be considered as the same problem as the comparison of a real world situation and a simulation's representation of this real world situation.

The design criteria developed here involves modeling of the human operator and defining simple parameters to describe his behavior in the simulator and in the real world situation. In the process of obtaining human operator parameters to define characteristics to evaluate simulators, measures are also obtained on these human operator characteristics which can be used to describe the human as an information processor and controller. Such modeling is motivated by the work of Fitts [1], Senders [2], Verplank [3], and others. First a study is conducted on the simulator design problem in such a manner that this modeling approach can be used to develop a criteria for the comparison of two simulators.

Symbols

ST(t)	Stick response of the human operator.
$\hat{x}(t)$	The Kalman filter's best estimate of ST(t),
$\nu(t)$	The residuals, innovations, or modeling error.
S	An approximation to signal power generated by the human.
N	An approximation to noise power generated by the human.

Symbols

$e(t)$, $E(s)$	The closed loop error signal and its Laplace transform.
ϕ	The discrete state transition matrix.
1σ	One standard deviation of a parameter estimate.
K_o	The Kalman Gain matrix.
A,B,H	The system gain matrices.
$x_1(t), x_2(t)$	State variables which describe ST(t) and $\frac{d}{dt}$ ST(t).
P,R,Q	Unknown covariance matrices.
$\hat{C}_k$	Sample covariance function (from the data).
$\hat{\rho}_k$	Sample, normalized autocorrelation function.
BW	An approximation to bandwidth of the human operator.

THE SIMULATOR DESIGN PROBLEM

In the comparison of two simulators or in the comparison of a simulator with a real world situation, an assumption is made as follows:

Assumption (1):
Simulator A = Simulator B if the human operator in Simulator A has the same "model characteristics" as the human operator in Simulator B.

The key term, "model characteristics" will be more explicitly defined via the modeling procedure. An alternative problem that can be solved via this procedure is the validation of a simulator in comparison to a real world situation. In this case the definition of simulator credibility is best described by assumption (2)

Assumption (2):
Simulator A = the real world if the human operator in Simulator A has the same "model characteristics" as the human operator in the real world situation.

In practice, the usefulness of assumption (2) has application if it is possible to take data in the real world situation as well as in the simulator. If the simulator can be adjusted so that the human operator parameters in the real world situation are close to the human operator parameters in the simulator, then the simulator has replicated the real world situation. This agrees intuitively with the definition of a replication of an experiment. A replication of an experiment is simply two empirical runs of data in which some variable shows consistency in both of the two empirical runs. In this case the variables that are to show consistency are the human operator model parameters. If these parameters show consistency between the real world situation and the simulator, then the simulator has replicated the real world situation. If the human operator appears the same in both the simulator and in the real world situation, and he rates the two to be the same subjectively, then the simulator has reproduced the desired environment from the point of view of the human.

The data base used to study the measures of simulator credibility involves a washout experiment as discussed in [4]. This experiment provides a unique opportunity to study how well the simulator replicates the real world situation.

THE G-VECTOR TILT WASHOUT EXPERIMENT

The G-Vector tilt washout experiment conducted at the Aerospace Medical Research Laboratory provides a data base to investigate the simulator credibility question. The data base used here involved a large centrifuge which has the capability of positioning the roll axis normal to the earth's gravity (called 0°) or parallel with the earth's gravity vector in which the subject is on his back or supine (called 90°). Six experimental conditions were considered in this study.

0° Conditions (Upright Position)	90° Condition (Subject on his back)
0° Motion	90° Motion
0° Washout - Attenuation only	
0° Washout - 1st. order washout	
0° Washout - 1st. order + attenuation	
0° Washout - 2nd. order	

As the subject makes a command stick response, the simulator rolls to simulate an aircraft in a banking maneuver. It is obvious that in the 0° (upright) motion case the human has both tilt cue information as well as angular acceleration cue information. In the 90° (subject on his back) motion case, the human does not have the tilt cue information. The four washout conditions were conducted at 0° (upright position) and a washout circuit was installed between the stick response and the plant's roll characteristics (Fig. (1a-b)). The effect of the washout circuit is to distort the motion cues to the human.

The manner in which this data base is equivalent to the simulator credibility problem is that the "real world" is defined as the 90° motion case.

The question is then asked, which washout scheme at 0^{o} is closest to the real world 90^{o} motion case? The 0^{o} washout conditions contain reduced tilt cue information and also contain some distorted motion cues from the washout circuits. The modeling procedure which enables the determination of an equivalence definition between two simulators is presented next.

THE MODELING APPROACH

Figure (2) illustrates how the modeling approach was conducted here. After the data was collected from the various experimental conditions a post experimental analysis was conducted with a model developed in such a manner that the human operator can be modeled as an information processor and controller. With reference to figure (2), the input to the model is the time series e(t) (the displayed error signal). The purpose of this modeling approach is to choose model parameters such that the model's output $\hat{x}(t)$ is an accurate representation of the measured stick response of the human. The measure of modeling accuracy is expressed in the residuals or output modeling error $v(t)$ which satisfies:

$$v(t) = ST(t) - \hat{x}(t) \tag{1}$$

If the model is appropriately fitted to the data, then $v(t)$ should be a random white process which satisfies:

$$\text{mean } [\ v(t)\ ] = E[v(t)] = 0 \tag{2}$$

$$\text{var } [v(t)] = E[v(t)v^{T}(\tau)] = R\ \delta(t-\tau) \tag{3}$$

It will be necessary in the subsequent analysis to test $v(t)$ for whiteness and determine R of equation (3). If $v(t)$ is a random white process, then the expected value of the model is equal to the expected value of the human's output. This is one method to validate such a model. A simple model structure is discussed next to describe the human's characteristics of interest.

A SIMPLE MODEL TO DESCRIBE HUMAN OPERATOR CHARACTERISTICS

It is desired to develop a model to characterize the human operator parameters of interest for this study. From previous studies [5,6], other simple representations of the human which have application in specific situations have been developed. In this paper a modeling approach will be used that will give rise to simple methods to characterize human operator parameters across several experimental conditions (or simulator designs). These modeling characteristics turn out to be analogous to an information theory representation of the human. Using the definition of channel capacity:

$$\text{channel capacity} = \text{Bandwidth} * \log_{10}\left(\frac{S+N}{N}\right) \tag{4}$$

The Bandwidth term is analogous to speed and the term $\log_{10}(\frac{S+N}{N})$ is analogous to accuracy. If the human operator has characteristics similar to an information channel, one would expect a product of the form of equation (4) to be invariant over several experimental conditions. It is then necessary to determine only two characteristics of the human operator in this representation of responses. To determine bandwidth, use is made of the human describing function plots. In the determination of the accuracy measure, a Kalman filter must be used.

From figure (3), it is desired to have a method by which an approximate measure of human operator signal/noise ratio can be determined. In this modeling procedure, the Kalman filter is initially specified to have input-output characteristics similar to those obtained from the describing function with the addition of some phase lag to account for the time delay of the human. The unknown Kalman gain coefficients (which represent the uncertainty terms or covariance matrices) are updated [7] in such a manner that the residuals $\nu(t)$ are white. The signal to noise ratio can then be approximated by:

$$\frac{S+N}{N} \approx \frac{\sum_{i=1}^{N} [ST(t_i)]^2}{\sum_{i=1}^{N} [\nu(t_i)]^2} \qquad (5)$$

It is noted that the variance of the residuals $\nu(t)$ are a measure of human uncertainty with respect to the error signal. This is true because the Kalman filter output $\hat{x}(t)$ is that portion of the stick response correlated with the error signal. The residuals $\nu(t)$ are that portion of the stick output not correlated with the error signal. This definition of human uncertainty differs from the classical definition of remnant [8,9] which is defined as that portion of human response not correlated with the input forcing function. This definition of human uncertainty is concerned with that part of the human response which is totally non-productive in reducing the error signal. This is easily seen to be true by noting that $\nu(t)$ when passed through the plant and around the loop still is uncorrelated with the error signal. Hence it cannot constructively be used to reduce the error signal because of its orthogonality to it. This measure of human uncertainty is a true measure of human output not useful in the tracking task. Next, a description of the measures of bandwidth and accuracy obtained from this modeling procedure are presented.

CALCULATION OF BANDWIDTH

In the computation of a measure of the bandwidth of the human operator, several difficulities exist in attempting to treat the human as an information channel [10]. This is due to difficulities in determining the true describing function from measured data variables and the effects of correlation between the human's remnant response and portions of the measured error signal. In this paper several approximations will be made. Figure (4) illustrates the

describing function of the human for the 0° motion case. Across the six experimental conditions considered here, the shape of the human operator describing function remained essentially the same; the major change between experimental conditions was only due to the d.c. gain values where the describing function was at a maximum. The ensuing analysis was conducted on the spectrum generated by the target frequencies. The reason it is necessary to work with the target frequencies is that if the target forcing function were zero, the describing function of the human operator obtained from only the human operator response (or for small values of disturbance input) is just equal to -1/plant. This result is well known [10,11].

From the target spectrums all experimental conditions are rated in order of their maximum gain value (table I). From table I it is seen that 0° static has the lowest gain value. The largest frequency the human will pass for this value of gain is now determined for each experimental condition.

This definition of the human operator bandwidth is the highest frequency at which the human will respond with gain of 0.5 db. In other words across all experimental conditions, the range of frequencies (from 0.0 radians and upward) is obtained that the human will pass with gain greater than 0.5db. In this manner a normalization is conducted on one experimental condition versus the remaining experimental conditions. This is a logical definition of human bandwidth and is one of many possible methods to approximate the bandwidth of a control system [12]. Measures of human uncertainty in tracking are determined next.

Table I - Bandwidth Computation - Subject - Eric

Experimental Condition	Maximum Gain in db	Bandwidth $\triangleq$ Higest Frequency where gain $\geq$ 0.5 db	1σ
0° Motion	6.5db	10.8 Rad/Sec	2.0
Washout Attenuation only	4.8db	9.8 Rad/Sec	0.3
90° Motion	4.5db	9.5 Rad/Sec	0.7
Washout 1st Order + Attenuation	3.5db	9.2 Rad/Sec	1.1
Washout 1st Order	2.9db	8.3 Rad/Sec	0.8
Washout 2nd Order	3.3db	8.2 Rad/Sec	1.1
0° Static	0.5db	7.3 Rad/Sec	1.0

MEASUREMENT OF ACCURACY OR SUBJECT UNCERTAINTY

With reference to figure (5) it is desired to update the model parameters in such a way that the innovations sequence $\nu(t)$ is a white, random process. The method of updating the parameters is based on an algorithm [7] which is actually a maximum liklihood procedure. In this manner a unique value of the optimal gain can be determined which maximizes the probability density function of the structure of the assumed model based on all the available data points. The optimal gain is the principal part of the discrete Kalman filter model which is described by:

$$\hat{x}_{i+1/i} = \phi \hat{x}_{i/i} + \int_0^{\Delta t} e^{A\tau} d\tau B \, \mathrm{col}[e(t), \dot{e}(t)] \quad (6)$$

$$\hat{x}_{i/i} = \hat{x}_{i/i-1} + K_o [z_i - H \hat{x}_{i/i-1}] \quad (7)$$

where $\hat{x}_{i/i}$ is the minimum variance estimate of the human's stick response. The matrix ϕ is the discrete transition matrix associated with the human's transfer function determined as follows:

$$\text{Let} \qquad \frac{ST[s]}{E[s]} = \frac{d(s+a)}{(s+b)(s+c)} \quad (8)$$

i.e. a fit of one zero and two poles is conducted on the human's transfer function to the describing function data (Bode plot). The coefficients a,b,c, and d are adjusted to try to match the phase data as well as the magnitude data. Implicitly the human's time delay has been included in the representation (8) through the adjustment of the parameters b and c. Future work will be done to study more exact fits. The matrix ϕ is then determined via $\phi = e^{A\Delta t}$ where $\Delta t = .04$ seconds (the sampling rate) and the matrix A is determined via:

$$\begin{bmatrix} \dot{x}_1 \\ \dot{x}_2 \end{bmatrix} = A \begin{bmatrix} x_1 \\ x_2 \end{bmatrix} + B \begin{bmatrix} e(t) \\ \dot{e}(t) \end{bmatrix} \quad (9)$$

where

$$x_1(t) = ST(t)$$

$$x_2(t) = \frac{d}{dt} ST(t)$$

and equation (9) is the time domain representation of equation (8). The matrix H in equation (7) is specified by $H = [1,0]$. The Kalman gain K_o satisfies:

$$K_o = P H^T (HPH^T + R)^{-1}$$

$$P = \phi [P - PH^T (HPH^T + R)^{-1} HP] \phi^T + Q$$

where the covariance matrices Q and R describe the human's uncertainty in the tracking task. The manner of obtaining the Q and R matrices is based on the algorithm in [7]. Initial matrix values denoted as Q_o and P_o are chosen. In order to establish the updating rule, it is necessary to define the sample covariance function.

Let:
$$\hat{C}_k = \frac{1}{N} \sum_{i=k}^{N} \nu_i \nu_{i-k}^T$$

is a sample covariance function. The matrices R and Q are now updated [7] via:

$$R_k = \hat{C}_o - H(P_k H^T)$$

where
$$P_k H^T = K_o \hat{C}_o + A^* \begin{bmatrix} \hat{C}_1 \\ \hat{C}_2 \end{bmatrix}$$

where
$$A^* = (\bar{A}^T \bar{A})^{-1} \bar{A}^T$$

and
$$\bar{A} = \begin{bmatrix} H\phi \\ H\phi(I-K_o H)\phi \end{bmatrix}$$

and finally Q is determined via:

$$Q_k = P - \phi K R_k K^T \phi^T - \phi(I-KH)P(I-KH)^T \phi^T$$

This algorithm has been shown to converge [7] and is equivalent to maximizing the log-likelihood function of the model structure conditioned on the data.

The final validation of this modeling effort is the need to test the residuals for whiteness. To accomplish this goal the normalized auto correlation function $\hat{\rho}_k$ is computed as follows:

$$\hat{\rho}_k = \frac{\hat{C}_k}{\hat{C}_o}$$

The test of whiteness of the residuals is a 95% whiteness test on $\hat{\rho}_k$. The 95% confidence limits for $\hat{\rho}_k$ are $1.96/\sqrt{N}$ where N is the number of samples. The band $\pm 1.96/\sqrt{N}$ is constructed about zero. If less than 5% of the sample points lie outside the band, the sequence is white. If more than 5% of the sample points lie outside the band, then a significant correlation exists in the residuals and the sequence is not white. Figure (6) illustrates the sample auto-correlation function obtained here from the data after the residuals have been whitened via this algorithm.

RESULTS FROM THIS ANALYSIS

Figure (7) represents the type of diagram obtainable from this type of

analysis procedure. The vertical axis is a plot of the measure of bandwidth as shown in Table I. The horizontal axis indicates numerical values of the accuracy measure or S/N ratio obtained here. Also plotted is the curve of constant capacity based on this analysis procedure. The numerical values resulting from this investigation of the data are given in Table II:

Table II - Speed - Accuracy Results

Exp Condition	Mean BW	1σ of BW	N=Mean $\log_{10}$S/N	1σ $\log_{10}$S/N	Mean Capacity BW*$\log_{10}$(1+S/N)
0° motion	10.8	2.0	3.265	.191	34.346
Washout Attenuation only	9.8	0.3	3.278	.088	31.719
90° motion	9.5	0.7	3.358	.089	31.5025
Washout 1st order + Attenuation	9.2	1.1	3.378	.064	30.79
Washout 1st Order	8.3	0.8	3.373	.043	27.813
Washout 2nd Order	8.2	1.1	3.412	.082	27.634

Also plotted in figure (7) is the invariant rule:

$$BW * \log_{10}(1+S/N) = \text{Constant} = 30.6 \qquad (11)$$

The constant 30.6 is the mean of the values of capacities obtained in the right most column in Table II. From figure (7) it is noted that most of the experimental conditions fall near this line.

Figure (7), by itself, is the diagram which can be used to assess the fidelity of a simulator in comparison to the real world data. If 90° motion is considered the real world situation, the washout scheme closest (distance wise) to this situation is 1st. order + attenuation. The other washout schemes are sucessively further away in this diagram and therefore, further from reality. The reason why it is said that the two experimental conditions best replicate each other is that the human exhibits almost the same bandwidth (or speed characteristics in tracking) and almost the same uncertainty characteristics (as measured by the S/N ratio).

Another interpretation of figure (7) is to consider the inverse problem associated with modeling; i.e. given the model parameters, can an analog simulation be built which will recreate the original empirical data. If the human in the loop were replaced by a quantitative description (e.g.

bandwidth and S/N ratio), the analog simulations of the 90^{o} motion case and washout 1st order + attenuation would most closely replicate one another. This is true because the only difference between the two simulations would be the parameters which describe the human operator. If these parameters are close to one another in some sense, then these simulations would best match. This is the motivation for using figure (7) to study simulator fidelity.

One additional comment needs to be made about why the washout scheme of 1st. order + attenuation best matched the 90^{o} motion case. The 0^{o} washout condition provided tilt cue information but the 1st. order + attenuation washout filter phase lag had the effect of distorting these tilt cues sufficiently to replicate the 90^{o} motion case. For the case of attenuation only, the tilt cue had an effect closer to 0^{o} motion (as expected). Also, as the washout scheme added more phase lag (2nd order case), the deviation from reality became more pronounced and the human operator dropped his bandwidth accordingly.

Future Research

The primary approximation used here was in the evaluation of human operator bandwidth. This approximation also effected the S/N ratio because the A matrix in the Kalman filter depends on this approximation. Future research will consider more accurate methods of evaluating bandwidth and including human time delay. In addition, a comparison will be made in the information rate obtained here to results from discrete tasks (approximately 3.0 bits/sec [13]) and to other information measures obtained from vision [14], reading [15], and control systems in general [16]. Another approximation utilized here was that the S/N ratio of the human was assumed to be constant over the entire frequency spectrum. In [3] the analysis procedure was able to study the capacity measure across the entire frequency spectrum. The procedure considered here can be extended in this respect. Also, since the analysis conducted here only involved one subject, future work will consider this analysis across different subjects, and use will be made of these measures of human invariance and subjective uncertainty in various task situations.

SUMMARY AND CONCLUSIONS

A study of design rules for the evaluation of a simulator's fidelity to the real world situation was conducted. The measures of model parameters obtained here give rise to information-theoretic models of the human operator. It appears that an invariant rule may exist on the human's ability to do information processing over a variety of different experimental conditions.

REFERENCES

1. Fitts, P.M.,"The Information Capacity of The Human Motor System in Controlling the Amplitude of Movement", Journal of Experimental Psychology, 1954, 47, pp. 381-391.

2. Senders, J.W. and J.J.M. Posner,"A Queueing Model of Monitoring and Supervisory Behavior", in Monitoring Behavior and Supervisory Control, by T.B. Sheridan and G. Johannsen, Plenum Press, 1976.

3. Verplank, W.L.,"The Facilitating Effects of Uncertainty in Long-Term Manual Control", Proceedings of the 1977 International Conference on Cybernetics and Society, September, 1977, Washington, D.C.

4. Jex, H.R. and A.M. Junker, "Roll Tracking Effects of G-Vector Tilt and Various Types of Motion Washout", The Fourteenth Annual NASA - University Conference on Manual Control, April 25-27, 1978, Los Angeles, California.

5. Repperger, D.W. and A.M. Junker, "Using Model Order Tests to Determine Sensory Inputs in a Motion Study", The Thirteenth Annual Conference on Manual Control, MIT, Cambridge, MA., 1977

6. Repperger, D.W. and A.M. Junker, "Performance Evaluation of Tracking Based on a Low Pass Filter Model", Eleventh Annual Conference on Manual Control, NASA TM X-62,464, pp. 599-624.

7. Mehra, R.K.,"On The Identification of Variances and Adaptive Kalman Filtering", IEEE Transactions on Automatic Control, Vol. AC-15, No. 2, April, 1970, pp. 175-184.

8. Jex, H.R.,R.W. Allen, and R.E. Magdaleno, "Display Format Effects on Precision Tracking Performance, Describing Functions, and Remnant", AMRL-TR-71-63, August, 1971.

9. Levison, W.H., S. Baron, and D.L. Kleinman,"A Model for Human Controller Remnant", IEEE Transactions on Man-Machine Systems, Vol. MMS-10, No. 4, pp. 101-108, December, 1969.

10. Wingrove, R.C., "Comparison of Methods for Identification of Pilot Describing Functions From Closed Loop Operating Records", NASA TN D-6235, 1971.

11. McRuer, D.,D. Graham, E. Krendel, and W. Reisener, "Human Pilot Dynamics in Compensatory Systems - Theory, Models, and Experiments with Controlled Element and Forcing Function Variations", AFFDL-TR-65-15, July, 1965.

12. Lynch, W.A., and J. G. Truxal, "Introductory System Analysis", McGraw-Hill, 1961.

REFERENCES

13. Miller, G.A.,"The Magical Number Seven, Plus or Minus Two: Some Limits on Our Capacity for Processing Information", The Psychological Review, vol. 63, No. 2, March, 1956, pp 81-97.

14. Kelly, D.H.,"Information Capacity of a Signal Retinal Channel", IRE Transactions on Information Theory, April, 1962, pp 221-226.

15. Pierce, J.R. and J.E. Karlin, "Reading Rates and The Information Rate of a Human Channel", The Bell System Technical Journal, March, 1957, pp 497-516.

16. Rink, R.E., "Optimal Utilization of Fixed-Capacity Channels in Feedback Control", Automatica , Vol. 9, pp 251-255, 1973.

ORIGINAL PAGE IS
OF POOR QUALITY

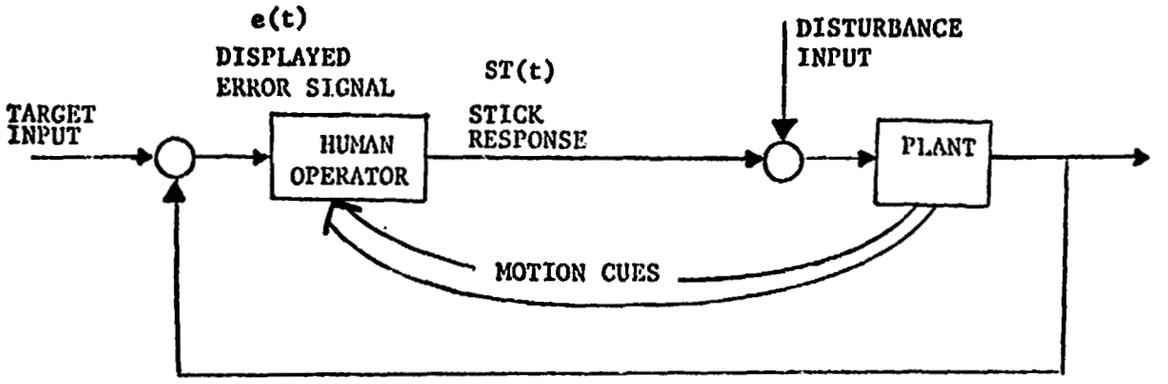

FIGURE (1a) -90° Motion Tracking

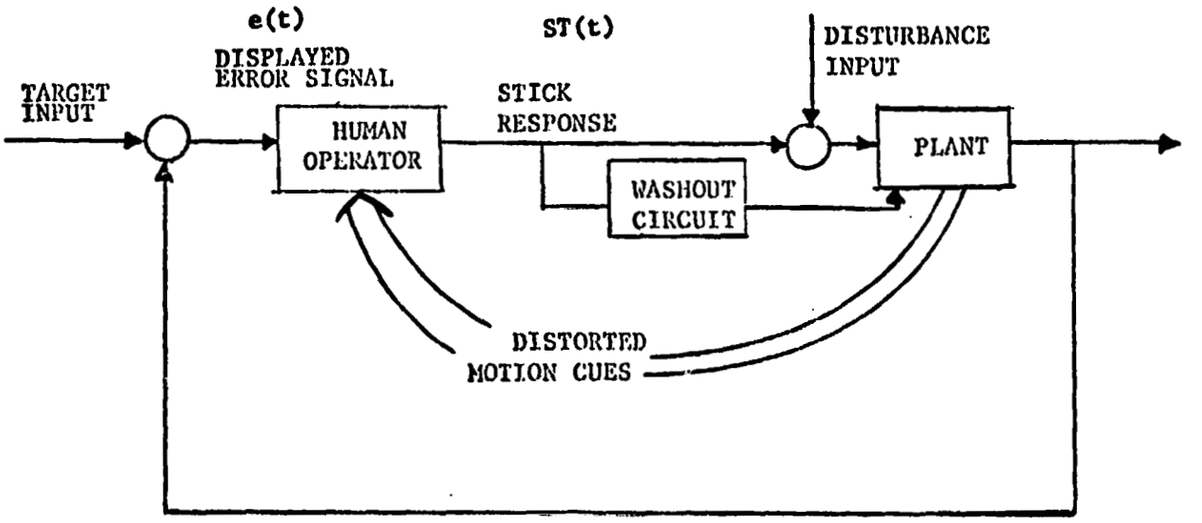

FIGURE (1b) -0° Washout Circuit

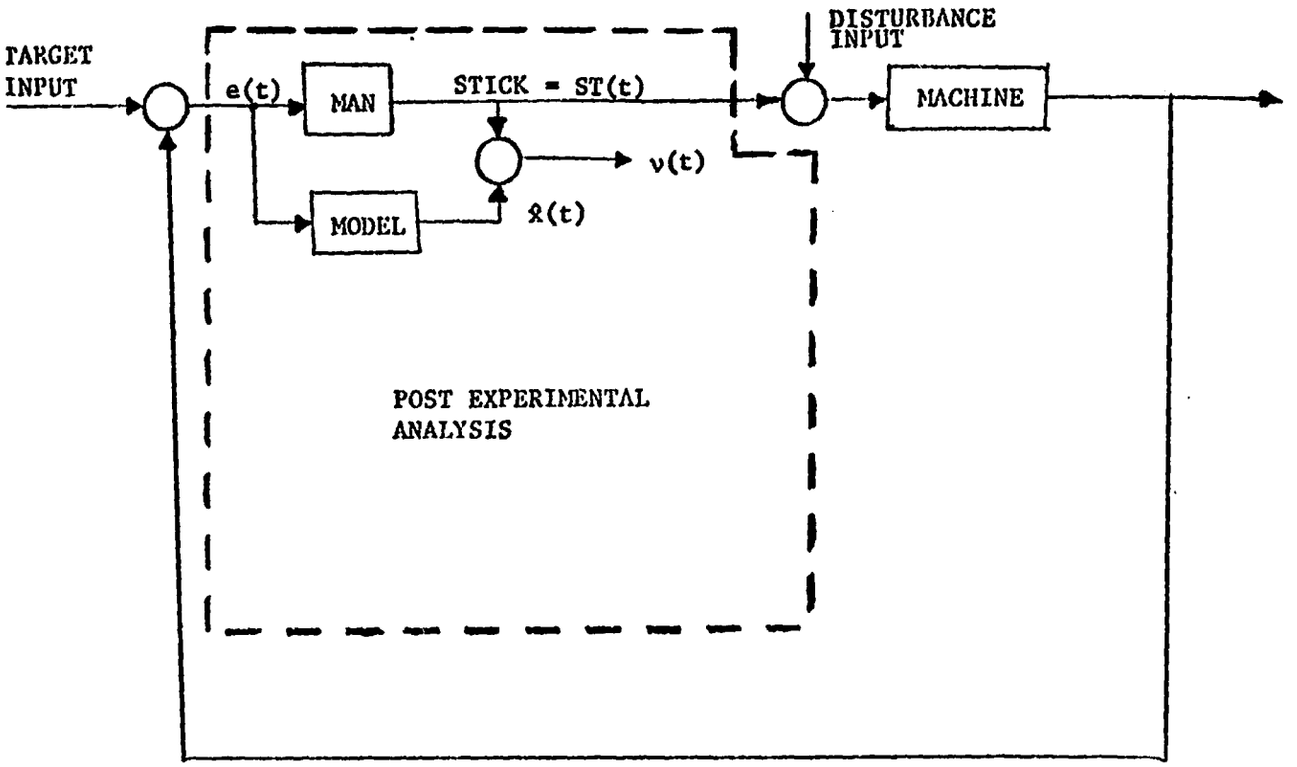

FIGURE (2)

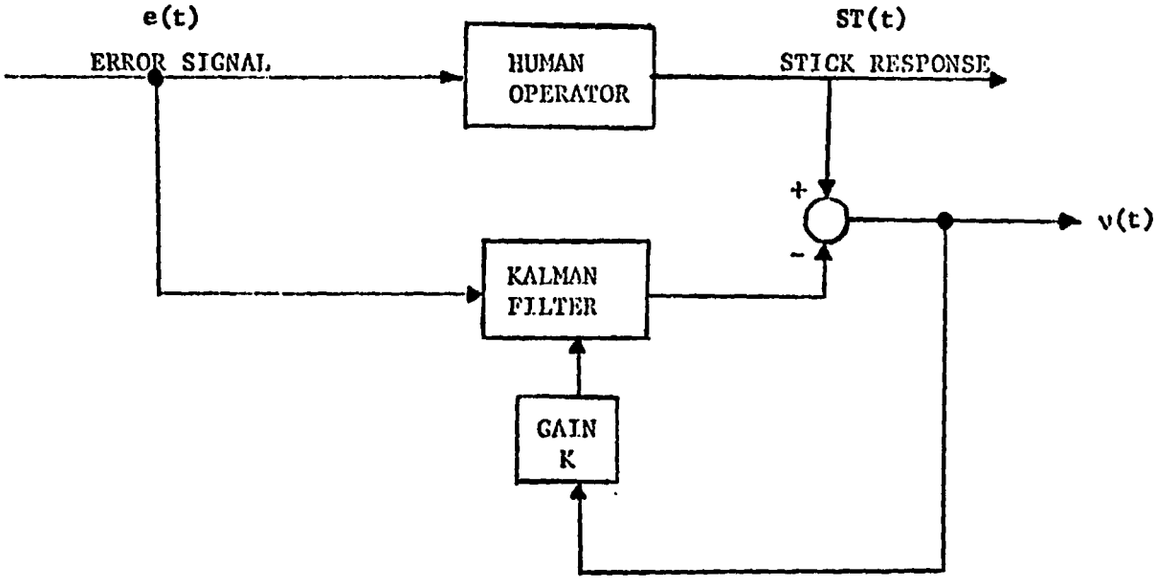

FIGURE (3)

ORIGINAL PAGE IS
OF POOR QUALITY

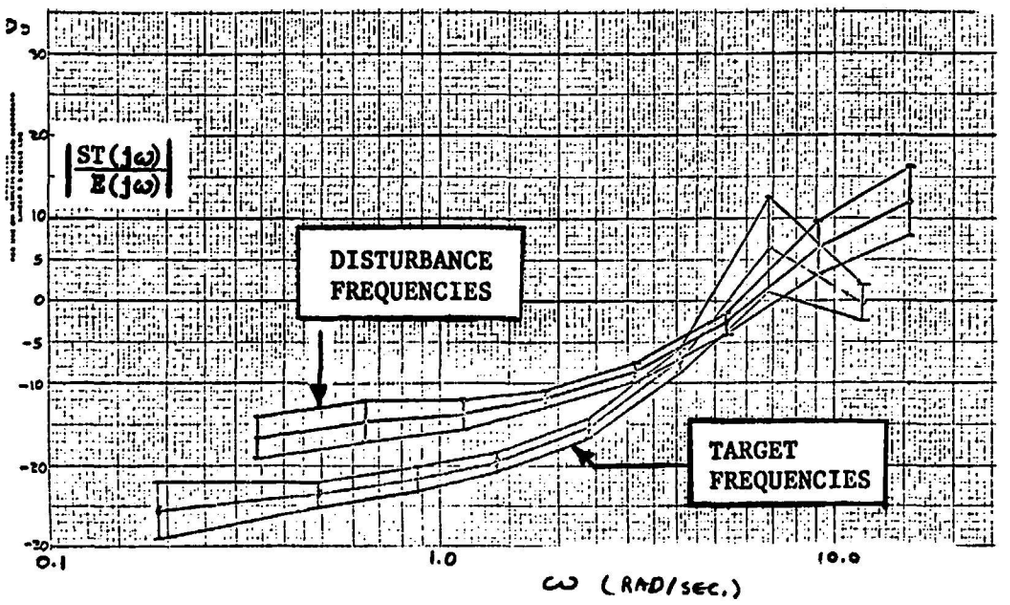

FIGURE (4) - The Human Operator Describing Function
0° Motion Case

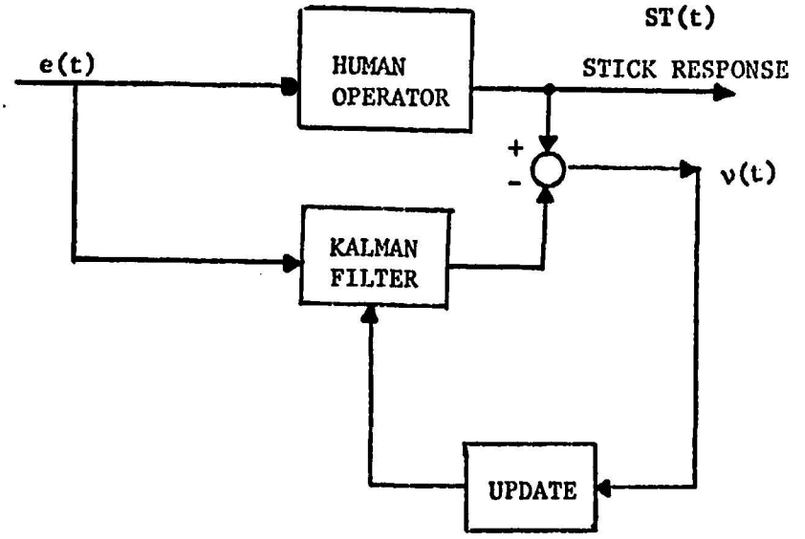

FIGURE (5) - Calculation of Subject Uncertainty

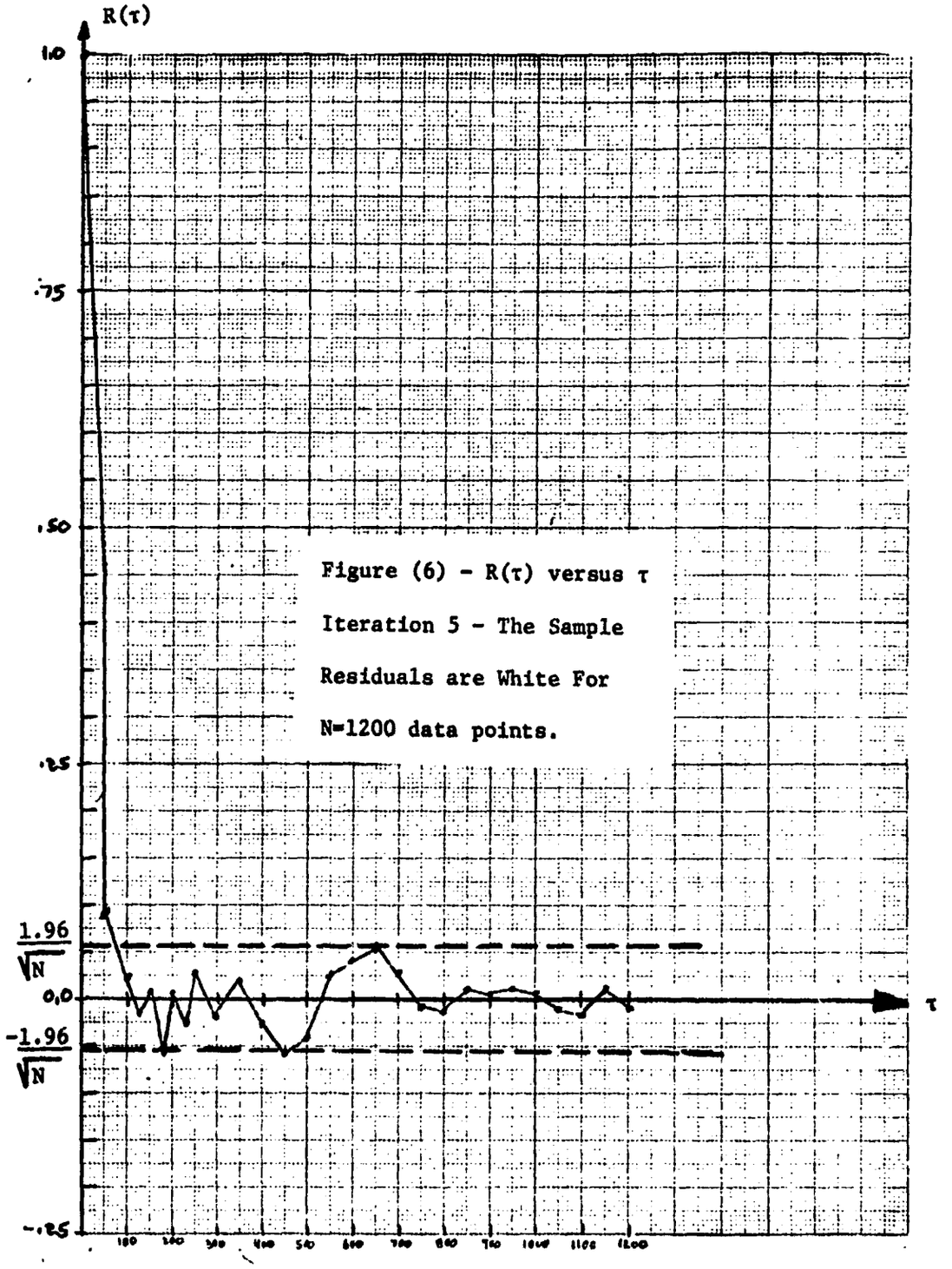

Figure (6) - $R(\tau)$ versus τ

Iteration 5 - The Sample Residuals are White For N=1200 data points.

ORIGINAL PAGE IS
OF POOR QUALITY

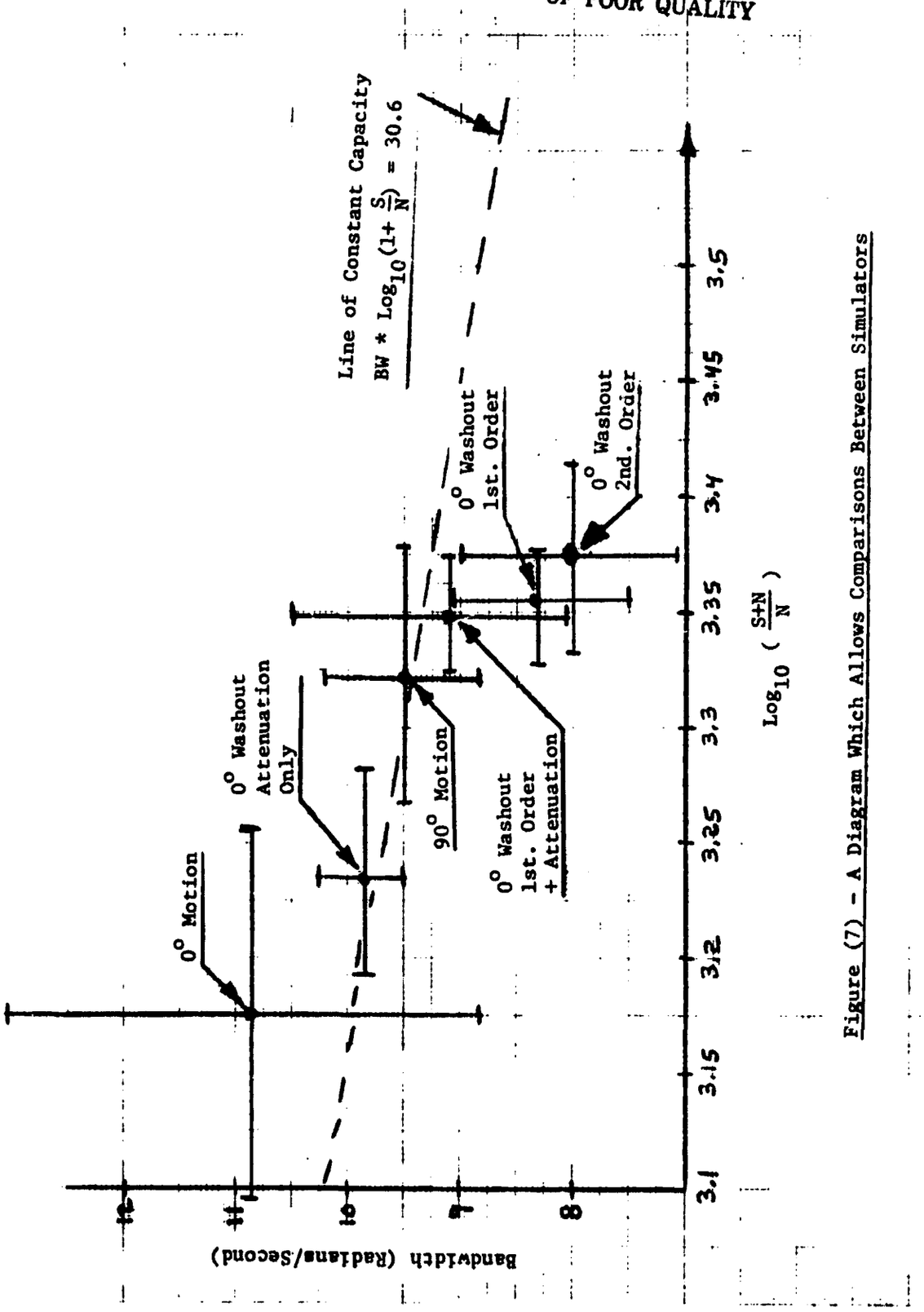

Figure (7) - A Diagram Which Allows Comparisons Between Simulators

D36

N79-15624

INVESTIGATION OF NONLINEAR MOTION SIMULATOR WASHOUT SCHEMES

By Susan A. Riedel and L. G. Hofmann

Systems Technology, Inc.

Hawthorne, California

INTRODUCTION

Research interest in washout filters for motion simulator drives arises out of a desire to maximize the fidelity of motion cues presented to simulator pilots. Washout filters must satisfy two important, usually conflicting, requirements:

1. The filter (along with the limiters) must prevent the simulator from reaching the mechanical limits imposed on displacement, velocity and acceleration in each axis.

2. The filter must reproduce actual motion cues without perceptible distortion. That is, motions contributed because of the washout must be imperceptible to the pilot.

The first requirement basically dictates integrated consideration of known motion base limits, existing limiter circuitry and the proposed washout design. The result should be a design which is not at crossed purposes with the limiters. The second requirement, however, demands knowledge of the physiology of motion perception. Research in engineering, physiology and psychology has lead to models of certain mechanisms for motion perception, and has greatly sharpened our knowledge of human motion perception capability. These capabilities (or lack thereof) can then be exploited by the washout designer in fulfilling the second requirement.

The first section of this paper presents an overview of some of the promising washout schemes which have recently been devised. The four schemes presented fall into two basic configurations; crossfeed and crossproduct. Various nonlinear modifications further differentiate the four schemes.

The second section of this paper discusses one nonlinear scheme in detail. This washout scheme takes advantage of subliminal motions to speed up simulator cab centering. It exploits so-called perceptual indifference thresholds to center the simulator cab at a faster rate whenever the input to the simulator is below the perceptual indifference level. The effect is to reduce the angular and translational simulator motion by comparison with that for the linear washout case.

520

The final section of this paper presents the conclusions and implications for further research in the area of nonlinear washout filters.

An Overview of Nonlinear Washout Techniques

All nonlinear washout schemes presented here are modifications to one of the two basic linear designs shown in figure 1. For simplicity, a single set of coupled axes for each design is depicted. The crossproduct scheme, attributed to Schmidt and Conrad (reference 5), is currently implemented on the Large Amplitude Multimode Aerospace Research Simulator (LAMARS) (reference 7). The crossfeed scheme (reference 6) attributed to Bray is implemented on the Flight Simulator for Advanced Aircraft (FSAA) (reference 8).

An interesting aspect of the crossproduct scheme is that the recovered specific force always equals the input specific force in the absence of any additional filtering of translational acceleration. In the figure, this implies $\dot{V}_{po} = \dot{V}_{poF}$. This result is due to the configuration of the residual tilt and coordinating crossfeed paths. Notice that because of the different arrangements for the coordinating crossfeed and residual tilt paths in the crossfeed scheme, $\dot{V}_{po}$ and $\dot{V}_{poF}$ are not necessarily equal.

Table 1 compares four nonlinear washout schemes which are in various stages of development. Because of the nonlinear nature of these schemes it is not possible to predict the outcome of a given experiment based on the results of previous experiments. Thus, conclusions drawn from test results for these nonlinear schemes are, at best, tentative.

Figure 2 presents a roll axis example of the adaptive gain (Parrish, references 2 and 3) scheme. The gain K_p is computed on-line based upon a cost function. This cost function is a function of roll rate, roll angle and initial K_p. It includes several constants which can be varied to "tune" the filter. The cost function is integrated and limits are imposed to obtain the filter gain. This gain varies with time. When the filter is tuned for a particular application, Parrish and Martin found it helpful for reducing the so-called "false cue" observed in pulse-type maneuvers.

Figure 3 illustrates a sway-axis example of the varying break frequency (Jewell, reference 1) scheme. In this case a cost function is used to compute the time-varying break frequency of the second-order translational washout. The cost function is a function of the translational acceleration, velocity and position as well as break frequency itself. Constants are available to tune the filter. The cost function is then integrated and a limit is imposed to obtain the break frequency. Jewell has demonstrated in a computer simulation that a two-fold reduction in translational motion can be achieved for a quasi-random input.

Figure 4 presents a portion of the surge axis as it appears in a signal compression scheme which incorporates parabolic limiting. While both the Parrish and the Jewell schemes addressed the problem of increased simulation fidelity and decreased motion base requirements, this scheme proposes a solution for the problem of the hardware motion base limits. The essence of this

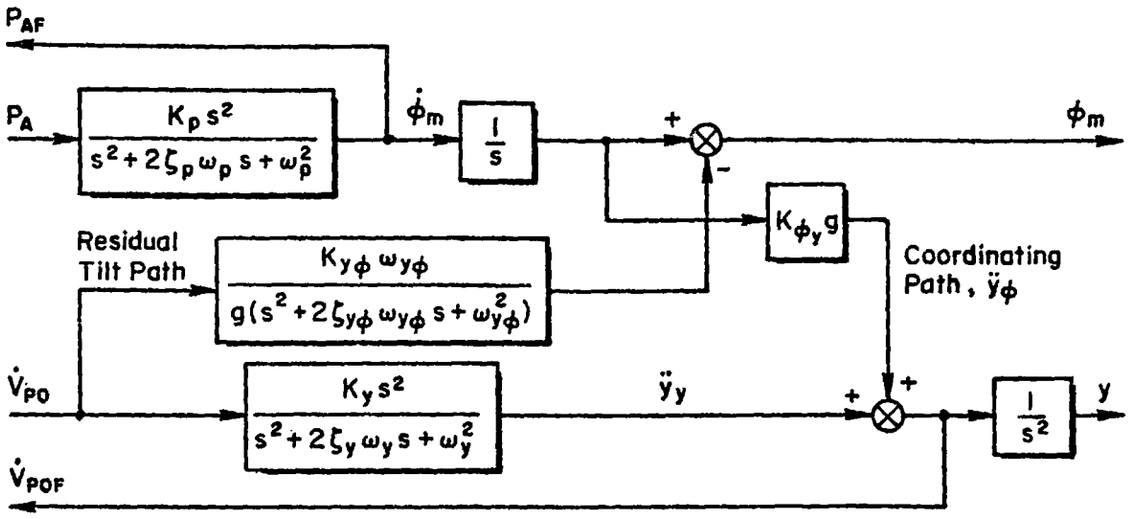

Crossfeed Scheme - Bray - FSAA

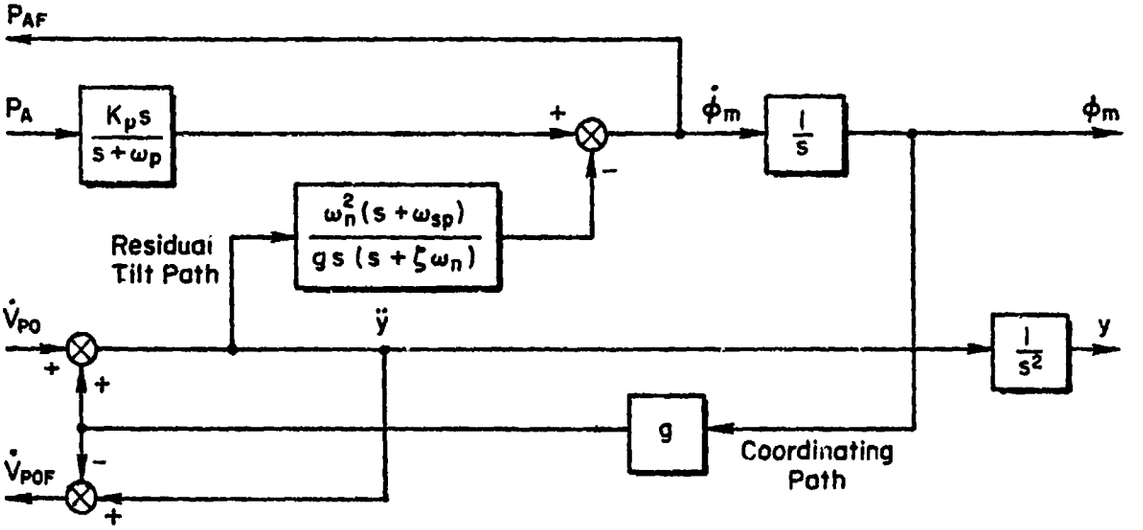

Crossproduct Scheme - Schmidt and Conrad - LAMARS

Figure 1. Basic Single-Axis Linear Washout Circuit Framework

ORIGINAL PAGE IS
OF POOR QUALITY

TABLE 1. COMPARISON OF FOUR NONLINEAR WASHOUT SCHEMES

	Adaptive Gain	Variable Break Frequency	Parabolic Limiting	Subliminal
Description	Varies washout gain K using a cost function	Varies washout break frequency ω_ϕ using a Parrish-type cost function	Incorporated in electrical drive to command maximum deceleration to stop simulator at limits	Increases washout rate when input is subthreshold to force cab back to zero position faster
Purpose	Eliminate "false cue"	Reduce motion base displacement requirements	Back-up system for hardware and software units	Reduce motion base displacement requirements
Principal Investigators	NASA-Langley Parrish Martin	STI Jewell Jex	NASA-Ames Bray Sinacori	STI Hofmann Riedel
Level of Investigation	Implemented on Langley Visual Motion Simulator	Computer model roll-sway axes	Implemented on FSAA	Computer model roll-sway axes
Underlying Linear Basis	Crossproduct	Crossproduct	Crossfeed	Crossproduct
Inputs for Which Scheme Is Most Effective	Pulse-type inputs	All inputs	Large inputs which could cause limiting	Small, subthreshold inputs
Level of Success	May eliminate "false cues"	Twofold reduction in lateral displacement requirement	Avoids hitting hardware limits	Twofold reduction in lateral displacement requirement
Side Effects	Increased nonlinearity with increased motion	Increase in lateral specific force miscoordination		Increase in lateral specific force miscoordination
References	2, 3	1	6	4

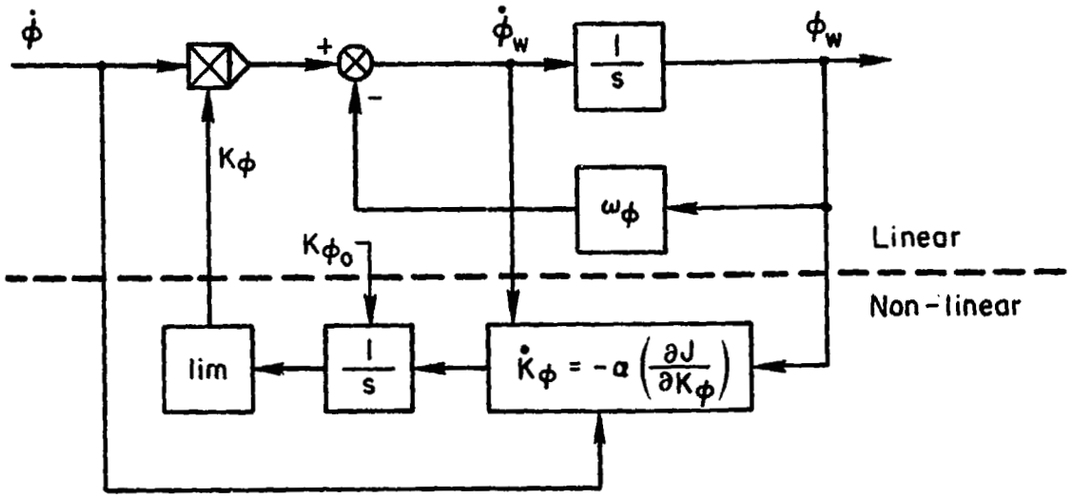

$$\dot{\phi}_\omega = K_\phi \dot{\phi} - \omega_\phi \phi_\omega$$

$$\dot{K}_\phi = -\alpha(\partial J/\partial K_\phi)$$

$$J = 1/2\left[(\dot{\phi}-\dot{\phi}_\omega)^2 + b_\phi \phi_\omega^2 + b_{K\phi}(K_\phi - K_{\phi_0})^2\right]$$

Figure 2. Adaptive Gain Scheme

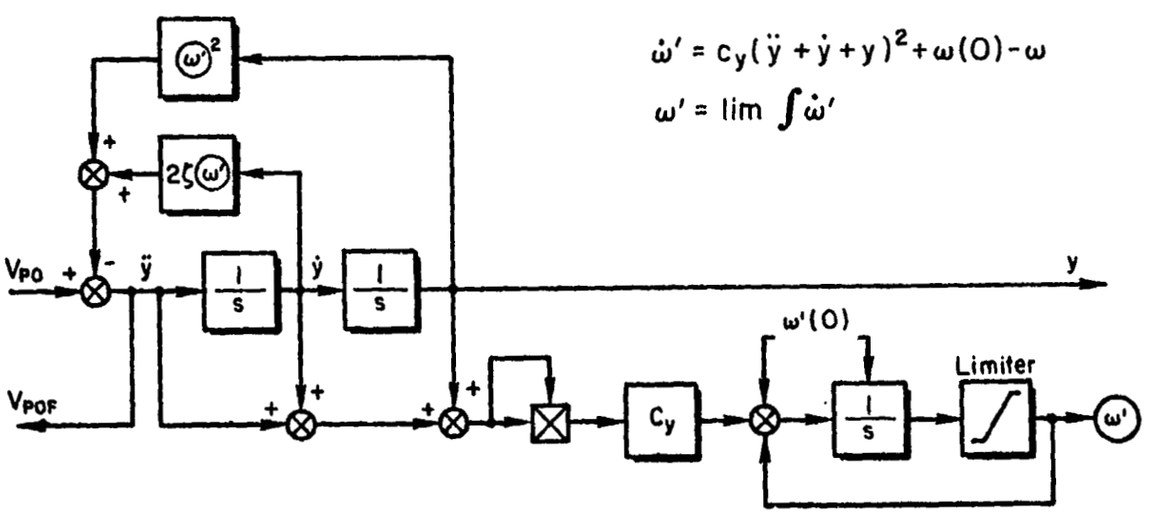

$$\dot{\omega}' = c_y(\dddot{y} + \ddot{y} + \dot{y} + y)^2 + \omega(0) - \omega$$

$$\omega' = \lim \int \dot{\omega}'$$

Figure 3. Varying Break Frequency Scheme

ORIGINAL PAGE IS
OF POOR QUALITY

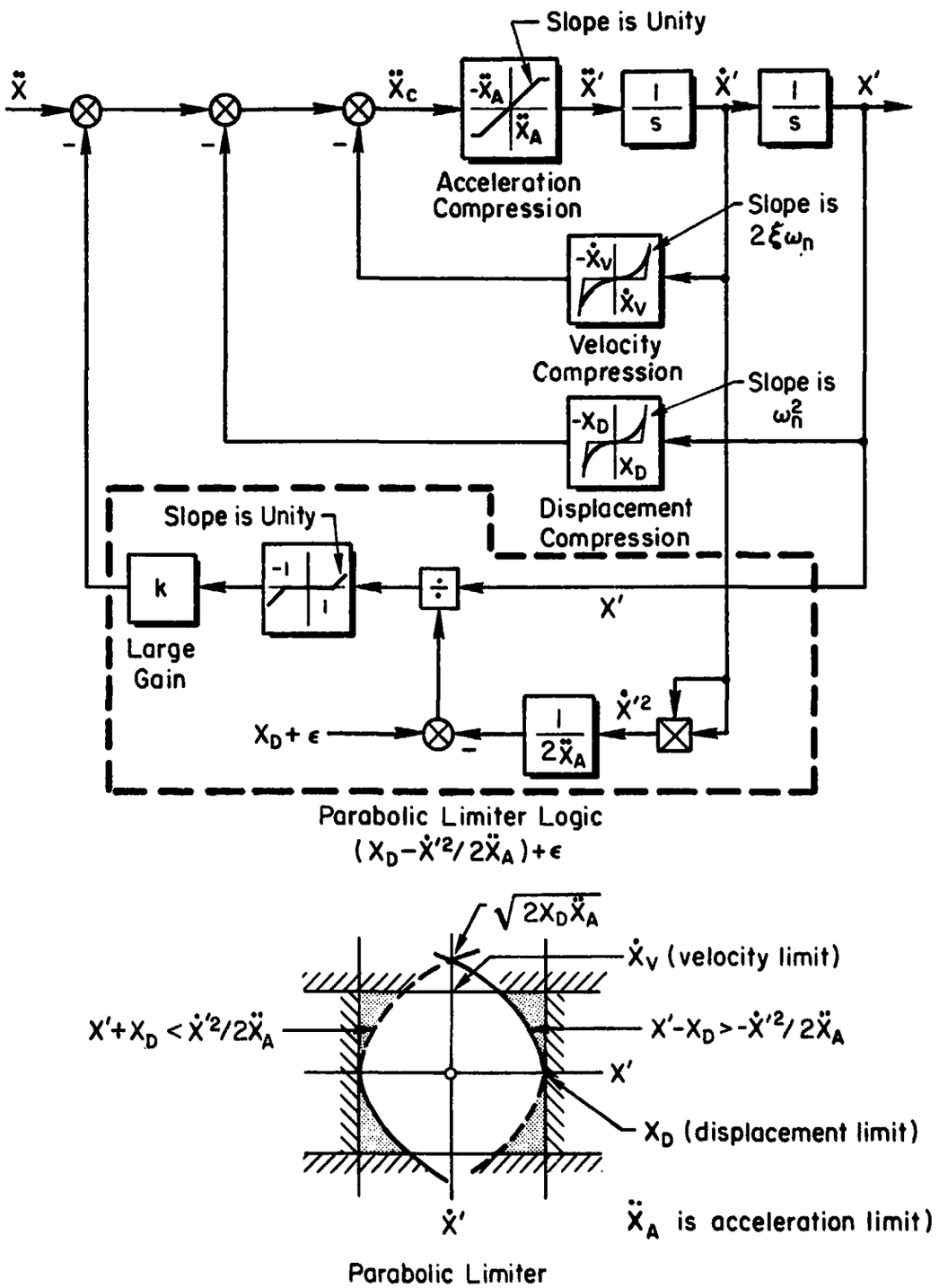

Figure 4. Parabolic Limiting Scheme Incorporating Signal Compression

scheme is a continuous calculation to assure that the cab can be brought to zero velocity before displacement limits are reached. The commanded motion is reproduced to the extent that a margin between the calculated stopping point and the displacement limits exists. In this way, maximum use may be made of the available motion capability.

The fourth washout, the subliminal scheme, is the subject of the next section of this paper.

THE SUBLIMINAL WASHOUT SCHEME

Figure 5 presents an application of the subliminal washout scheme to a first-order roll axis washout. This concept came about as the result of an attempt to utilize so-called "indifference" thresholds which pilots exhibit under normal workload. These thresholds may be operative for both angular velocity and specific force perception under normal workload. The hypothesis is that pilots do not perceive angular velocities and specific forces which are below the respective indifference thresholds. The washout design objective is to exploit this particular phenomenon to obtain reduced simulator motion requirements or increased motion fidelity.

The overall design goal is to drive the cab back to its zero position more rapidly than would the underlying linear washout whenever the motion stimulus is below the indifference threshold level. This is accomplished with the use of the two nonlinear functions in boxes A and B in figure 5. The input to the function in Block A is the scaled angular velocity. This function produces a weighting factor which serves as a variable feedback gain in the washout circuit. If the input magnitude is larger than the indifference threshold p_T, the weighting factor is zero. If the input is zero, the weighting factor is 1.0. Otherwise, the weighting factor is some fraction of 1.0 which is a sinusoid-like function of the input for the form of the weighting function used here.

The input to Block B, a soft saturation nonlinear function, is cab roll angle, φ. If φ is large, the value of the function output is the value of the indifference threshold level, $\pm p_T$. If φ is small the value of the function output is proportional to φ.

The outputs from Blocks A and B are then multiplied to arrive at an incremental washout rate command signal. The particular choice of functions in Blocks A and B assures that this signal's magnitude never exceeds the indifference threshold level. The smoothness of the functions in Blocks A and B tends to prevent discontinuous commanded changes in the washout rate. The value of this incremental washout rate command signal will be non-zero whenever the cab roll angle is non-zero and the input angular velocity is below the indifference threshold level. The signal is then subtracted from

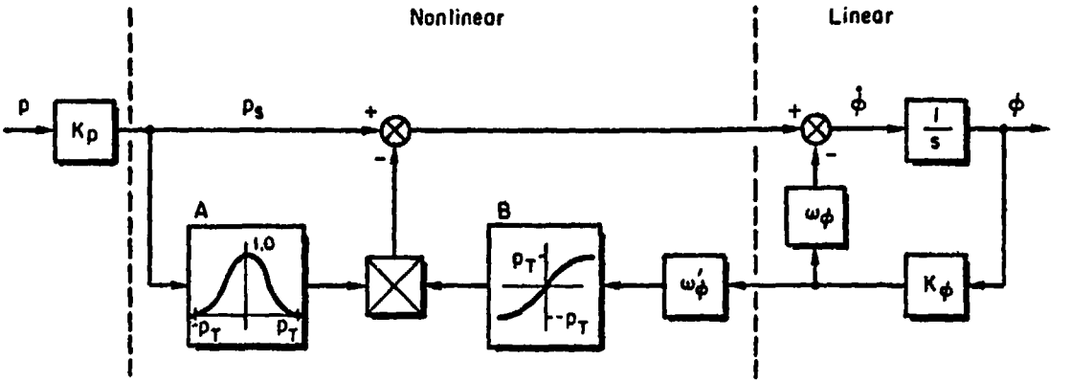

p = Input Angular Velocity

p_s = Scaled Angular Velocity

p_T = Indifference Threshold Level

$\dot{\phi}$ = Commanded Cab Roll Rate

ϕ = Commanded Cab Roll Angle

Figure 5. Nonlinear Washout Scheme (First-order Washout)

the scaled input angular velocity. The result is a smaller away-from-center angular velocity input to the integrator than would result for the underlying linear scheme. Thus, the cab is driven back to its zero position more quickly than it would be for the linear scheme, during intervals of sub-threshold inputs in angular velocity.

Preliminary tests of this subliminal washout concept for the roll axis showed it to be ineffective. There was some reduction in simulator motion requirements, but not really enough to warrant further investigation.

Figure 6 shows an application of this same washout concept to the lateral specific force channel of a crossproduct washout configuration for roll-sway axes.

It was pointed out in the discussion of the crossproduct scheme that the input specific force, V_{po}, and the recovered specific force, V_{poF}, are always equal for the crossproduct washout configuration. In this case the subliminal washout introduces intentional miscoordination of specific force. The indifference phenomenon allows this deliberate introduction of specific force miscoordination, and as long as this miscoordination does not exceed the specific force indifference threshold level, the pilot under normal workload will not detect the miscoordination.

ORIGINAL PAGE IS
OF POOR QUALITY

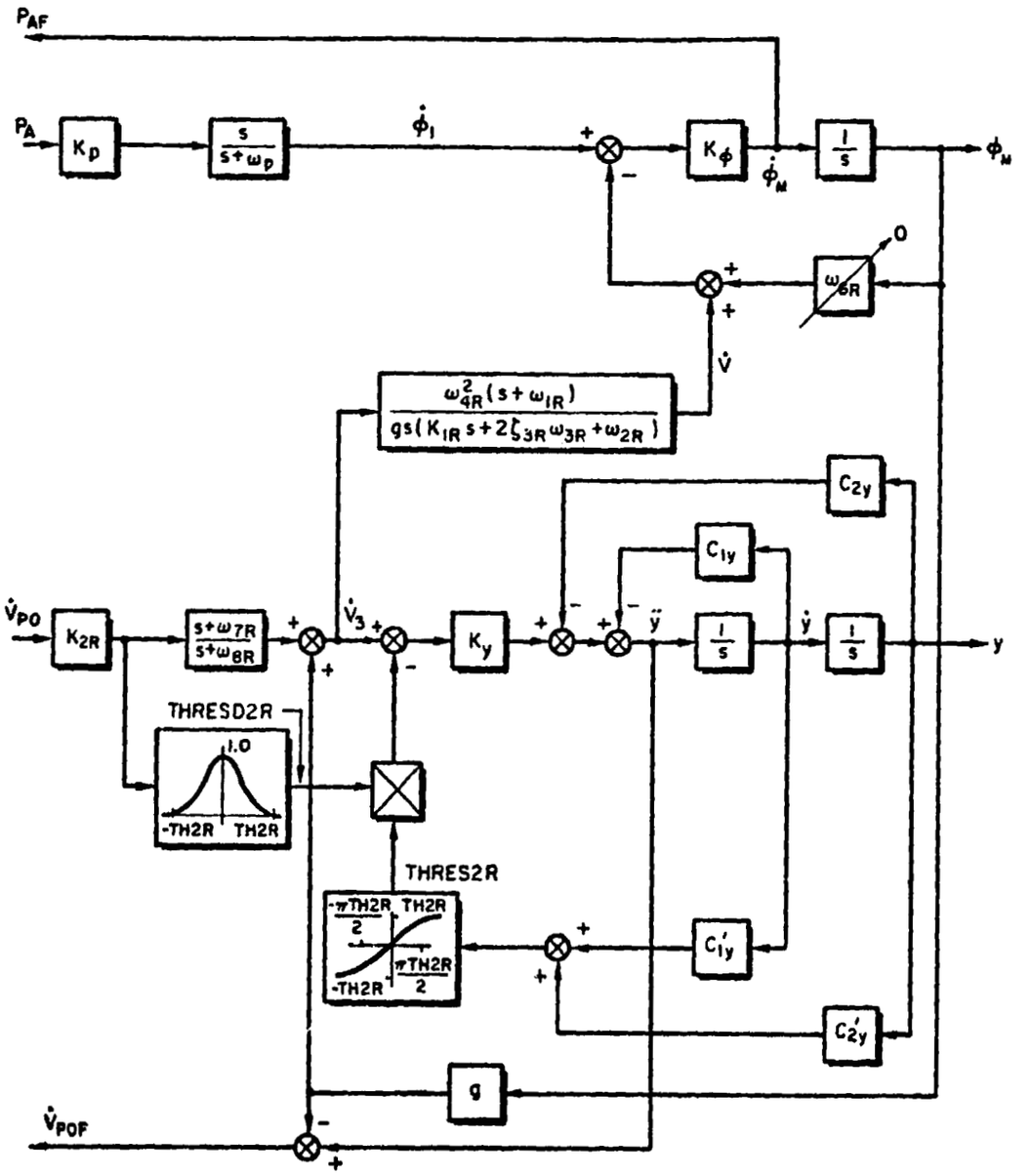

Figure 6. LAMARS Drive Logic Washout with Nonlinear Feedback Added to Specific Force Path Only

Computer simulation results for the washout in figure 6 are presented in figure 7. The input to the simulation corresponds to a roll-in to a constant 4 g turn. The inputs are roll rate, P_A, and lateral specific force, $\dot{V}_{po}$. There is no reduction in acceleration, $\ddot{y}$, slight reduction in velocity, $\dot{y}$, and significant reduction in lateral translation, y. These results show clearly that the subliminal washout substantially reduces simulator displacement motion requirements. Lateral translation reduction is 70 percent, i.e., from a maximum linear displacement of 4.05 m (13.5 ft) to a maximum displacement of 1.2 m (4 ft).

In order to accomplish this substantial reduction in lateral translational requirements, however, a substantial change in recovered specific force is generated because of miscoordination. This is due to the increased washout rate for the subliminal washout scheme. Since the increase in washout rate is constrained to at or below an indifference threshold level of 0.1 g, the change in recovered specific force is also constrained to that level. Thus, under normal workload the pilot should not be able to detect this level of miscoordination.

The computer simulation of the subliminal washout has been exercised for a variety of inputs. Significant reductions in motion base requirements have been observed. On the basis of these results the following conclusions can be drawn:

1. The subliminal washout concepts, as implemented in the translational axes of the crossproduct scheme, are effective in reducing the velocity and displacement requirements of the motion base.

2. The subliminal washout scheme is most effective for sub-indifference threshold specific force inputs. The washout reduces to the underlying linear scheme when inputs exceed this threshold.

3. The use of the subliminal threshold scheme results in an increase in recovered specific force which is spurious. This spurious motion is due to additional miscoordination. The nonlinear implementation insures that this miscoordination component is never greater than the assumed indifference threshold level. Thus under normal workload, the pilot should be unable to detect this false cue.

Much work remains to be performed in the investigation of this subliminal washout scheme. The initial results of the computer simulation have shed light on the scheme's major uses, and encourage further research and eventual simulator implementation.

ORIGINAL PAGE IS
OF POOR QUALITY

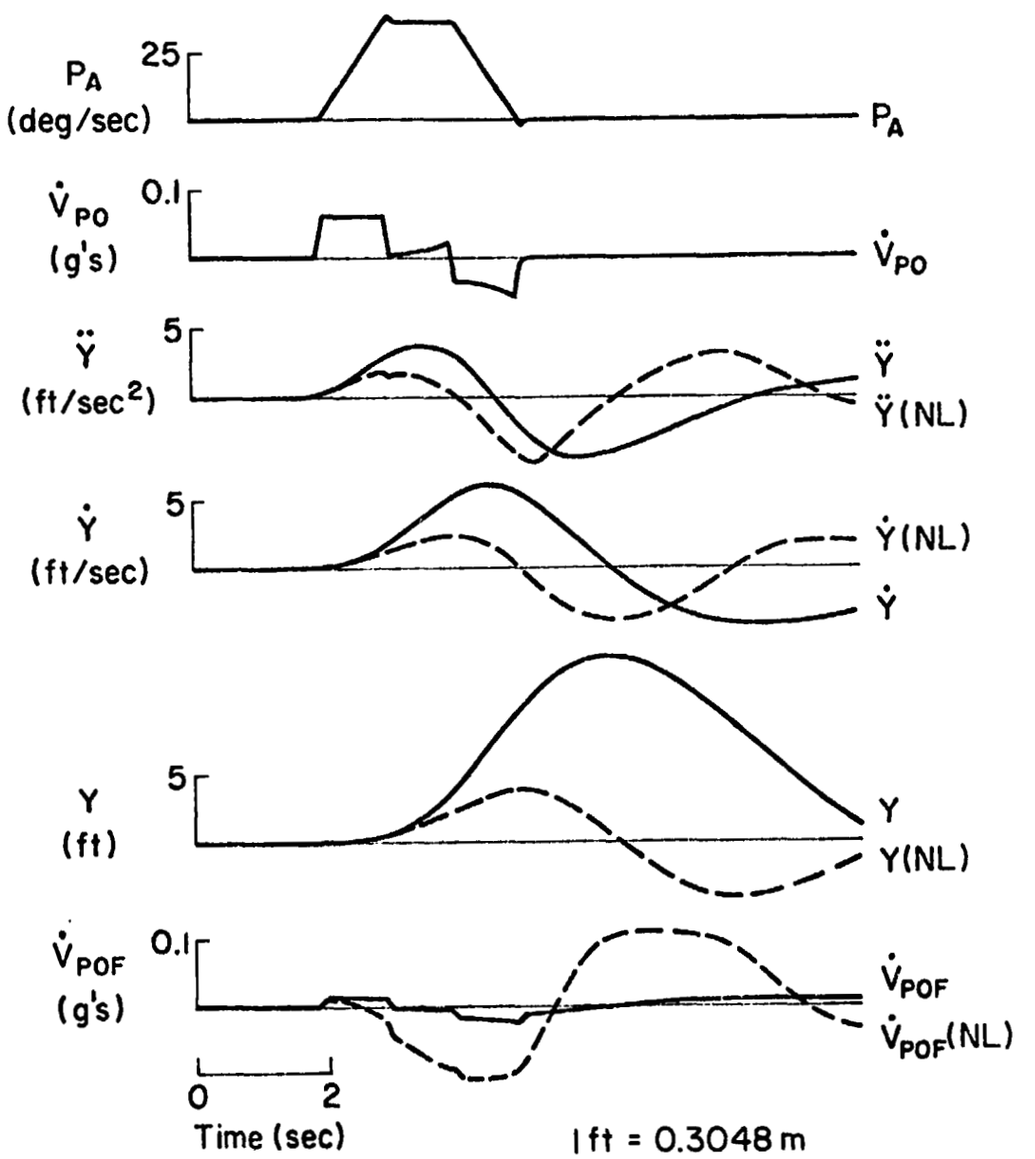

Figure 7. Comparison of Linear and Nonlinear Outputs

CONCLUSIONS

A sample of some new concepts in nonlinear washout filters has been presented here. Since each scheme addresses a different aspect of the washout problem, it may be desirable to combine several nonlinear concepts in a single, grand scheme. In this way, several problems in a particular simulation could be handled by a single washout circuit. Further research along these lines might lead to a well-defined method for designing a washout circuit to suit particular simulation needs, taking into account the peculiarities of the motion base as well as a description of the flying task to be simulated.

The research reported herein was sponsored by the Air Force Flight Dynamics Laboratory under Contract F33615-77-C-2065. (W. Klotzback, AFFDL/FGD and J. Bankovskis, AFFDL/FGD)

REFERENCES

1. Jewell, Wayne F., and Henry R. Jex, "A Second Order Washout Filter With a Time-Varying Break Frequency," STI WP-1094-9, Feb. 1978.

2. Parrish, R. V., and D. J. Martin, Jr., Comparison of a Linear and a Nonlinear Washout for Motion Simulators Utilizing Objective and Subjective Data from CTOL Transport Landing Approaches, NASA TN D-8157, 1976.

3. Parrish, R. V., J. E. Dieudonne, R. L. Bowles, and D. J. Martin, "Coordinated Adaptive Washout for Motion Simulators," AIAA Paper No. 73-930, Sept. 1973.

4. Riedel, Susan A., and L. G. Hofmann, "Preliminary Investigation of a New Nonlinear Washout Scheme," STI WP-1110-1, Dec. 1977.

5. Schmidt, S. F., and B. Conrad, Motion Drive Signals for Piloted Flight Simulation, NASA CR-1601, 1970.

6. Sinacori, J. B., "A Brief Survey of Motion Simulators' Drive Logic with Emphasis on the Roll Axis," STI WP-1094-2, May 1977.

7. Sinacori, J. B., "A Practical Approach to Motion Simulation," AIAA Paper No. 73-931, Sept. 1973.

8. Sinacori, J. B., Robert L. Stapleford, Wayne F. Jewell and John M. Lehman, Researchers Guide to the NASA Ames Flight Simulator for Advanced Aircraft (FSAA), STI-TR-1074-1, May 1977.

SESSION J: PERCEPTION AND ATTENTION ALLOCATION

Chairman: W. Rouse

D37

N79-15625

A THEORETICAL AND EXPERIMENTAL ANALYSIS OF THE OUTSIDE WORLD PERCEPTION PROCESS

by P.H. Wewerinke
National Aerospace Laboratory NLR
the Netherlands

SUMMARY

The outside scene is often an important source of information for manual control tasks. Important examples of these are car driving and aircraft control. This paper deals with modelling this visual scene perception process on the basis of linear perspective geometry and the relative motion cues.

Model predictions utilizing psychophysical threshold data from base-line experiments and literature of a variety of visual approach tasks are compared with experimental data. Both the performance and workload results illustrate that the model provides a meaningful description of the outside world perception process, with a useful predictive capability.

INTRODUCTION

Many manual control tasks depend on the visual perception of the outside scene. In the context of aircraft control, the most important example is the visual approach scene. So, in order to investigate a great many flight situations in the approach and landing, it is mandatory to take into account this visual scene perception process which has often a major impact on mission performance.

Based on a concise inventory of the most important characteristics (cues) of the visual scene the visual scene perception process is described (modelled) on the basis of the linear perspective geometry and the relative motion cues. This involves mathematical relationships between these visual cues and the aircraft state variables. After linearization this model can be integrated in the existing framework describing piloted aircraft behavior (the optimal control model). This is the subject of the next chapter.

The visual scene perception model involves assumptions concerning perceptual thresholds of the various cues, noise levels associated with observing these cues and interference among them. Values for these parameters are derived from baseline experimental data supplemented by the psychophysical literature. Based on these values a theoretical analysis is performed dealing with a variety of visual approach conditions.

534

Furthermore,the results of an experimental program are compared with the model predictions. In addition, model predictions of pilot workload are compared with subjective ratings.

VISUAL SCENE PERCEPTION MODEL

One of the earliest studies of visual scene perception directly related to flight control problems has been performed by Gibson (Refs. 1 and 2). According to Gibson, the most important visual cues which can be derived from the visual field are related to

- the linear perspective geometry
- relative motion or motion parallax
- the apparent size of objects whose real size is known
- a far object covered by a near one
- the distribution of flight and shade over an object
- aerial perspective and the loss of detail with distance.

Of these, the linear perspective geometry provides a variety of cues. This is illustrated by the schematic version of the visual scene in figure 1a which can be thought of to consist of lines and points (textural elements). This involves not only the linear and angular position of the observer with respect to the outside world but also (dynamically) the relative motion. The point of the visual field toward which the observer is moving appears to be stationary ("focus of expansion"). All other textural points move with respect to the observer which can be indicated by velocity vectors ("streamers"). This is shown in figure 1b for the case of rectilinear motion. Various other references mention visual cues which can be conceived as examples of the afore-mentioned basic elements. Most of them are related to the landing approach scene (Refs. 3-5).

From the foregoing it can be derived that a reasonable approach is to model the visual scene perception process on the basis of the linear perspective geometry and the relative motion cues. Following reference 6 this involves a description of the cues which can be derived from the visual scene and their functional relationships with linear and angular positions and velocities of the observer. When, in addition, the relationships between the moving observer and the visual scene can be linearized about a nominal condition, the perception process can be described in standard estimation theoretical terms and included in the optimal control model structure in the following manner.

Let the observer (aircraft[*]) moving with respect to the outside world be described by the system state x(t). This involves the common linear and

[*] Although the following applies to a variety of man-machine situations, this analysis is directed at the aircraft control problem.

angular positions of the aircraft as well as additional parameters to describe relevant characteristics of the moving visual scene (with respect to the aircraft). After linearization about a nominal path the result will be a set of linear, (in general) time-varying equations given by

$$\dot{x}(t) = A(t)\, x(t) + \mathfrak{E}(t)\, w(t) \qquad (1)$$

where A(t) describes the process of the aircraft moving with respect to the outside world, and w(t) represents system disturbances (e.g. turbulence). Furthermore, the visual cues will be described by the display vector y(t). The relationships between these displayed variables and the system state is given by

$$y(t) = C(t)\, x(t) \qquad (2)$$

The perception of these variables is accompanied with an equivalent time delay, perceptual thresholds and observation noises. Also the interference between the various visual cues, a.o. arizing from the necessity to scan the visual field and to divide the attention among the various cues, has to be considered (Refs. 7 and 8). Now, these observations of the visual scene are dealt with in the same fashion as observations from other sources (e.g. displays, motion cues, etc.). The system state is estimated optimally (by means of a Kalman-Bucy filter) on the basis of the known (learned) dynamics involved and the observations. This state estimation process can be considered as an internal representation of the task environment.

Relationships between visual scene characteristics and the system state

A schematic version of the visual scene (Fig. 1) can be assumed to comprise textural elements and known objects. Both provide linear perspective geometrical cues (basically, the inclination of lines) and impressions of relative position and velocity.

The inclination Ω, of a line element of the visual scene is given by

$$\Omega = \tan^{-1} Y/H \qquad (3)$$

where Y is the distance betwe n the observer and the pertinent line element perpendicular to the looking direction and H is the vertical position of the observer. Assuming small perturbations (y, h and ω) around the trim condition (Y_o, H_o and Ω_o) results after some manipulation (to a first order) in the linear expression

$$\omega = C_h\, h + C_y\, y \qquad (4a)$$

where

$$C_h = -\sin 2\,\Omega_o / 2H_o \qquad (4b)$$

Differentiating eq (4a) yields the expression for the inclination rate

$$\dot{\omega} = C_h \dot{h} + C_y \dot{y} \tag{4c}$$

The small perturbations of the relative position and velocity of an element of the visual scene is simply given by

$$\alpha_h = h/R \; ; \; \alpha_y = y/R$$

and

$$\dot{\alpha}_h = \dot{h}/R \; ; \; \dot{\alpha}_y = \dot{y}/R \tag{5}$$

where α is the visual angle and R is the distance between the object and the observer.

Furthermore, when the attitude of the observer (aircraft) is taken into account (with attitude angles φ, Θ and ϕ) eqs. (4) and (5) become

$$\begin{aligned} \omega &= C_h h + C_y y + \varphi \\ \alpha_h &= h/R + \Theta \\ \alpha_y &= y/R + \phi \end{aligned} \tag{6}$$

and the corresponding time-derivatives $\dot{\omega} = \ldots$, etc.

Next, these expressions are utilized to describe the cues which can be derived from the visual approach scene.

Visual approach scene

A schematic version of the visual approach scene is shown in figure 2. The cues which are assumed to be derived from this scene are indicated.
The most important cue for lateral guidance is derived from the inclination of the runway sides and/or centerline. The lateral deviation y, is zero if the inclination of both runway sides is the same ($\omega_r = \omega_l$) and the inclination of the centerline is zero ($\omega_c = 0$).
Vertical guidance has to be based on the (average) inclination of the runway sides when no runway end and no horizon is visible. In that case, the observer has to know the nominal inclination (Ω_o), which is range-varying. The following model analysis and experimental results will show that a better indication of the vertical position is obtained when the length of the runway α_h (or, almost equivalently, the depression of runway threshold with respect to the horizon) is visible. Also in that case, the observer has to know the nominal depression which is, however, constant during a standard approach (e.g., 3 deg).
Glide slope information requires also the estimation of the distance to touchdown. This can be based on the apparent size of ground objects, of which the most important is often the runway width.
Aircraft attitudes provide "inner-loop" information and can be derived from the relative position and inclination of (e.g.) the horizon and any aircraft reference. The pitch angle Θ, which has to be estimated with respect to its (non-zero) nominal value and the bank angle φ are indicated in figure 2.

MODEL ANALYSIS

The linear visual scene perception model (VSPM) can be implemented in the optimal control model (Refs. 6 and 7). Based on the foregoing discussion, a variety of visual approach conditions are selected to analyze theoretically. In addition, an experimental program has been conducted to provide a critical test for the hypotheses (assumptions) underlying the model results. In order to obtain detailed information concerning the information processing involved in the manual approach task, no range-varying effects are considered in the following analysis. In other words, it is assumed that the aircraft is "frozen" at a fixed point of the approach path corresponding with a nominal altitude of 200 ft for a 3° approach ("hovering"). The consequence is a stationary process involved allowing frequency domain measures such as human describing functions and observation noise spectra. Especially the latter will provide a sensitive check on the exactness of the values used for the model parameters under investigation. The primary model parameters are the perceptual thresholds of the various visual cues (display elements) involved because these represent the most uncertain model parameters. The results of several previous experimental studies suggest reasonable accurate values for the remaining model parameters.
Therefore, base-line experiments have been conducted and relevant psychophysical literature have been searched resulting in reasonable reliable estimates for the perceptual thresholds involved. Finally, the last section contains the model analysis proper and the resulting model predictions.

Visual scene configurations

Referring to the foregoing discussion the configurations given in figure 3 were selected for the following model analysis and formal experiment.

Vertical control on the basis of the inclination of the runway sides can be compared with the condition that the depression of the runway threshold below the runway end (α) or below the horizon is visible (configurations 1 and 2). Furthermore, the effect of an aircraft reference providing explicitly pitch information is of interest (configuration 3).

Lateral control utilizing the inclination of the centerline is represented by configuration 4. In case the runway sides are available, the inclination of both sides has to be estimated and compared with each other (configuration 5). A simple model analysis shows that this process is associated with the same observation noise as in the case of a center line. Only the perceptual thresholds involved are different (next section). This will be tested against the experimental results. Again the effect of explicit roll information provided by the aircraft reference is considered by including configuration 6. Configuration 7 concerns roll tracking based on the aircraft reference. This (presumably) easy task is included to evoke some variation in workload in order to yield additional experimental evidence for the workload model of reference 8 and to test the perceptual threshold assumptions involved.

Configurations 8 and 9 are selected to investigate the interference between vertical and lateral control. It is assumed that the pilot has to divide his attention between the various display variables (visual scene cues) involved. This interference is assumed not only within a control task (e.g. attention has to be divided between pitch angle and altitude) but also between vertical and lateral control when performing both tasks simultaneously. This represents a crucial hypothesis which will be tested in the following as the visual scene is widely assumed to represent integrated information and it is a non-trivial question whether the visual scene can be "broken down" into separate elements. Finally, configuration 10 is included to investigate the effect of additional texture. This has, in principle, its implications for the information contents of the visual scene which turned out to be of no interest but also for the psychological aspects (perspective illusion and realism).

Perceptual thresholds

It was anticipated that perceptual threshold phenomena could be important for the foregoing visual scene cues. Thresholds can be accounted for in the optimal control model by modifying the observation noise covariance associated with a particular visual cue.

Although the psychophysical literature reports a wealth of emperical threshold data, these data are known to be affected by numerous experimental conditions which easily explains the typical scatter in "comparable" data. Therefore, a baseline experiment has been conducted to determine the position thresholds of the display elements involved in the visual scene configurations shown in figure 3. These thresholds are primarily due to the lack of explicit visual references concerning zero or nominal, visual scene conditions.

This involves that learning (experience) and temporal cues (memory functioning) are important in measuring and interpreting thresholds.

Experimental details are given in reference 9. The resulting measurements are "translated" to values suitable for (as required by) the describing function representation for the assumed dead-zone non-linearity. The results are summarized in table 1.

As discussed in reference 9 thresholds associated with the perception of motion in the visual field can be related to resolution properties. This implies that the motion detection thresholds can be inferred from the foregoing discrimination data. The result is also contained in table 1.

Apart from these (nominal) threshold estimates, in table 1 it is also indicated how reliable these estimates are assumed to be. A sensitivity analysis in the following will serve to relate this incertainty in threshold values to a confidence interval associated with the system performance predictions of the model.

Model predictions

A block diagram of the control task(s) is given in figure 4. System disturbance enters the system parallel to the control input. The resulting

output is displayed to the human operator as the pitch and roll angle (for the pertinent configurations) representing K-dynamics. The integral of these outputs are the altitude (or approach angle) and lateral deviation (or center line inclination), respectively (K/s-dynamics). The disturbances are white noise processed by two first order filters with poles at one rad/sec and two rad/sec. The disturbance levels are for the vertical task given by a resulting pitch variance of 0.068 deg^2 and for the lateral task given by a resulting roll variance of 10.5 deg^2 (corresponding with the values used for the experimental program). Details concerning sensitivities and gains involved are contained in reference 9.

Model parameters can be divided in parameters which are constant for all configurations and parameters which are considered as the remaining model variables. Also the experimental results of the next chapter will be related to these (dependent) variables. The key variables are the perceptual thresholds. The nominal values of table 1 are assumed for the model predictions. Furthermore, the effect of the upper- and lower threshold values on the system outputs is also determined and discussed in the following chapter. The overall level of attention (P_o) is also, to same extent, variable, although this value has been shown in previous studies to be relatively constant. A nominal value of -20 dB is assumed and the effect of $\pm$ 2 dB on the system outputs is considered.
The constant model parameters are: a neuro-motor time constant of 0.1 sec, a perceptual time delay of 0.2 sec and a motor noise ratio of -30 dB.

Now, assuming that the human operator divides his attention among the visual cues (position and velocity of all display elements) optimally, i.e., minimizing the given cost functional* (Ref. 8), system performance can be predicted for the various configurations. The results are given in table 2.

Vertical control is superior for the condition that the runway depression angle and the pitch angle can be observed (conf. 3). The contribution of the pitch information amounts to a 20 % reduction of the approach angle variance (σ_α^2 of conf. 2). When the viewing condition is such that no horizon or runway end is visible and control has to be based on the runway sides (ω_l and/or ω_r) and runway threshold variation ($\dot{a}$) the vertical approach performance is degraded substantially. This clearly demonstrates the contribution of the various visual cues involved. Furthermore, in the case of both vertical and lateral control, the vertical approach performance is predicted to deteriorate with 30 % to 50 % (due to the assumed interference between both tasks). The last column of table 1 contains the (optimal) fractions of attention dedicated to the various cues.

The best lateral approach performance is obtained when the runway centerline inclination (ω_c) cue is available (conf. 4). Lateral control utilizing the runway sides is substantially degraded (conf. 5) due to the larger perceptual threshold of this cue. The bank angle provides useful

* According to the instructions given to the subjects in the experiment the system output is assumed to be minimized. In addition the control rate is weighed yielding the neuro-motor time constant of 0.1 sec.

inner loop information (conf. 6). When performing the vertical and lateral task simultaneously, the model predicts a deterioration in lateral performance (confs. 8 and 9) of about 100 %. The model predicts that the effect of the texture (conf. 10) on system performance is negligible.

The effect of the model parameter variations (thresholds and overall attention) on the system scores and additional theoretical results will be discussed in the next chapter where the model predictions will be compared with the experimental results.

EXPERIMENTS

The first objective of the experimental program was to test the foregoing model results with respect to both the fundamental hypotheses involved (optimality in control and attention allocation, interference between cues) and the assumed numerical values of the key model parameters. Secondly, in case significant discrepancy occurs between model and experimental results the appropriate adjustments can (hopefully) be made in the model assumptions underlying the model results.

Experimental procedures

The same 10 configurations as discussed previously are investigated in the experimental program. These configurations were four times presented to the (four) subjects (general aviation pilots) in a random order. Each run lasted 200 sec. Between the runs the subjects were asked to give their impression of the exerted workload (Reference 9 contains the rating scales used and additional experimental details). The subjects were instructed to minimize the mean-squared system output. They were trained on the ten configurations in a random order till a relatively stable performance level was reached. All together, about 250 training trials were performed.

An analog computer was used to simulate the vehicle dynamics and to generate the visual scene characteristics. This visual scene was presented to the subjects on a TV monitor located 2.5 m in front of their point of regard, They manipulated a two-axis isometric hand control. The system parameters were recorded on FM magnetic tape for off-line mean-squared scores and frequency domain computations*.

Comparison of experimental results and model scores

In this section the experimental results in terms of mean-squared performance scores are compared with the model predictions. Based on the results of table 2 firstly the approach angle (α)- and centerline inclination (ω_c) scores are considered (the model predicts attitude- and control scores which are relatively insensitive over the configurations).

* Unfortunately, these frequency domain data were not available in time to include in this paper. These results will be included in reference 9.

Apart from the nominal model predictions (of table 2) the effect of the uncertainty in underlying assumptions (i.e., numerical values of the thresholds and overall attention) on system performance is determined. For the upper- and lower threshold values given in table 1 and, in addition, + 2 dB and -2 dB variation in overall attention the corresponding performance scores are determined. It is hypothesized that the experimental scores lie within the resulting performance interval.

In figures 5 and 6 both the experimental means and standard deviations (of 16 runs) and the model predictions are given. For all single-axis tasks the experimental scores lie well within the predicted interval. This indicates not only that the model is "right" but also that the assumed numerical values for the thresholds and overall attention are close to the "real" values.

For the dual-axis tasks the experimental results do clearly not match the model predictions. The experimental data of configuration 9 and 10 have been pooled because both the model predictions and the experimental results for both configurations indicate that the only effect of the texture information is the enhancement of the perspective illusion. This was also apparent during the learning phase. An adjustment of the model parameter values (which has to be appropriate for the single-axis tasks as well) does not result in a good agreement with the experimental scores. Therefore, it is tentatively concluded that the assumed hypothesis of interference between the two tasks has to be rejected. Instead, the following hypothesis is considered: the visual scene stimulates the human operator to perform the dual-axis task just as well as the single-axis task (thus, vertical control is not degraded when the lateral control task is added, and vice versa). So, it is assumed that there is no performance interference. This will be further discussed in the following.

Comparing also the attitude scores (Θ and φ) and the control scores (δ_e and δ_a) of the model predictions in table 1 and the measured scores given in table 3 it is apparent that both the measured attitude scores and the measured control scores are much lower than predicted. This indicates that the subjects (being pilots) performed the - to some extent realistic appearing - "approach" tasks in a much smoother fashion than the model predicts on the basis of an assumed neuromotor time constant of 0.1 sec. This is confirmed by pilot commentary indicating that the pilots were reluctant to make rapid control movements and "chase the needles".
Based on this observation the neuromotor time constant was adjusted to a value of 0.25 sec. This value which was kept constant in the following analysis is apparently more representative for outer-loop control behavior. In addition, figure 5 suggests that for the vertical control tasks a better agreement between measured and model results will be obtained when the lower threshold values given in table 2 will be assumed ($0.2\ ^{o}$/sec and 0.4^{o}). This is the only minor adjustment of the model variables.

The resulting model scores are compared with the measured mean-squared values in table 3. In general, the agreement between the measurements and the refined model scores is quite good. Now (with a neuromotor lag of 0.25 sec) the control scores match, on the average, very well. The same can be

said of the system outputs α and, to less extent, ω_c.
A comparison of the pitch attitude scores shows that the pilots were somewhat more conservative in making pitch corrections than the model predicts (apart from configuration 1). These lower pitch scores (and the corresponding somewhat lower control scores) could easily be duplicated by the model, however, by an appropriate weighting of the pitch angle. The mean-squared roll angles match again, rather well*.

The system output scores are summarized in figure 7. For the dual-axis configurations, both the scores corresponding with the assumption that there no performance interference between the two axes and the "full interference" scores are indicated. The results strongly support the hypothesis that there is no interference between the vertical- and lateral axis thanks to the visual scene.

In summary, it can be concluded that for the relatively realistic, outer-loop control tasks under investigation a neuromotor time constant of (say) 0.25 sec is appropriate. Furthermore, only one minor adjustment of the nominal model variables was required to yield, on the average, a good agreement between model results and measurements: a position threshold for α and θ of 0.4° and a velocity threshold for $\dot{\alpha}$ and $\dot{\theta}$ of 0.2°/sec (the same value as found in reference 10). Finally, the experimental results provided convincing support for the hypothesis that the visual scene perception process can be described on the basis of the, mutually interfering, various (separate) visual cues considered. There is no performance degradation (interference) when both the vertical and lateral control task are performed simultaneously.

Workload model results and subjective ratings

Using the foregoing model results human operator workload can be computed. The workload model (a.o. discussed in reference 8) involves not only the level of attention, P_o, dedicated to the task in accordance with the model of reference 11, but also the aspect of arousal ("uncertainty").

The model predictions are compared in figure 8 with subjective ratings on the workload scale given in references 8 and 9. Apart from configuration 1 the linear correlation between subjective ratings and workload model predictions is quite good ($r = 0.88$). This result provides additional support for the workload model.

The model predicts a much lower workload level for configuration 1 than reflected by the subjective ratings. The explanation for this is that for this configuration the subjects were not sure what the right (nominal) vertical position was. Not only they learned slowly on this configuration (somewhat discouraged by their varying learning-performance) but also they clearly did not like the uncertainty involved in performing the task which can also be related to training. So, the model, not including this learning aspect, predicts that the workload corresponding with this configuration will

* For the roll-only task (conf.7) an overall level of attention, P_o, of -18 dB had to be assumed in order to match the measured scores.

substantially reduce when the subjects are more trained on (familiar with) this task.

CONCLUSIONS

The visual scene provides a variety of perspective geometrical and relative motion cues. The experimental results have supported that these characteristics can be considered as separate cues among which the human operator has to divide his attention. The commonly accepted idea that pictorial information is better integrated (less interfering) than separate display elements is in the present study specifically demonstrated in that there is no performance interference between the vertical and lateral task. Both the workload model results and the subjective ratings indicate that the workload is increased indeed when performing both tasks.

In the case of guidance control tasks (e.g., the visual approach task) pilots are reluctant to make rapid control movements. This is represented in the optimal control model by a weighting on control rate corresponding with a neuromotor time constant of about 0.25 sec. This outer-loop control behavior is distinguished from attitude (inner-loop) control tasks which can be modelled with a neuromotor time constant of 0.1 sec (Ref. 7).

Furthermore, the assumptions concerning the key parameters of this investigation, i.e. the perceptual thresholds, could (indirectly) be checked against the experimental data. Apart from one minor adjustment the a priori assumed threshold values yielded a good agreement between model scores and measurements. The sensitivity analysis visualized in figures 5 and 6 indicates that this result allows a reasonable accurate verification of the underlying model parameters (thresholds and level of attention).

Finally, the workload model predictions have been confirmed convincingly by subjective ratings. Apart from configuration 1 (the performance of which task must have been dominated by a psychologigal effect not included in the model) the linear correlation between model predictions and subjective ratings was 0.9.

REFERENCES

1. Gibson, J.J. The perception of the visual world. The Riverside Press. Cambridge, Mass. 1950.

2. Gibson, J.J. et al., Parallax and perspective during aircraft landings. Amer.Journ. Psych. 68 (1955).

3. Havron, M.D., Information available from natural cues during final approach and landing. Human Sciences Research Inc., HSR-RR-62/3-Mk-X, March 1962.

4. Bronw, J.L., Visual elements in flight simulation. Rochester University TR 73-2, December 1973.

5. Naish, J.M., Control information in visual flight. Seventh annual conference on manual control, NASA SP-281, June 1971.

6. Baron, S. and Berliner, J., Manmod 1975: Human internal models and scene-perception models. US Army Missile Command, TR RD-CR-76-3, September 1975.

7. Baron, S. and Levison, W.H., Display analysis with the optimal control model of the human operator. Human Factors, 1977, 19(5).

8. Wewerinke, P.H., Performance and workload analysis of in-flight helicopter missions. Paper presented at the 13th Annual conference on manual control, MIT, June 1977. (also NLR MP 77013 U).

9. Wewerinke, P.H., Visual scene perception process involved in the manual approach. NLR TR 78 (forthcoming).

10. Levison, W.H., The effects of display gain and signal bandwidth on human controller remnant. AMRL-TR-70-93, March 1971.

11. Levison, W.H., A model for mental workload in tasks requiring continuous information processing. Nato symposium on mental workload, Mati, Greece, September 1977.

Table 1 Thresholds

PAR	DISPLAY	THRESHOLD	CONFIDENCE INTERVAL
	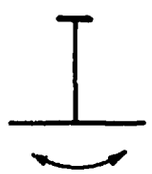	1° $1^{\circ}/s$	- $0.5 - 2^{\circ}/s$
ω_c $\dot{\omega}_c$		5° $3^{\circ}/s$	$4 - 6^{\circ}$ $2 - 4^{\circ}/s$
		2° $2^{\circ}/s$	- $1 - 3^{\circ}/s$
θ $\dot{\theta}$	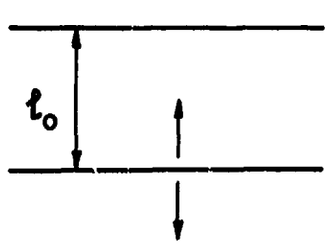	0.5° $0.3^{\circ}/s$	$0.4 - 0.6^{\circ}$ -
α $\dot{\alpha}$		0.5° $0.3^{\circ}/s$	$0.4 - 0.6^{\circ}$ $0.2 - 0.4^{\circ}/s$
φ $\dot{\varphi}$	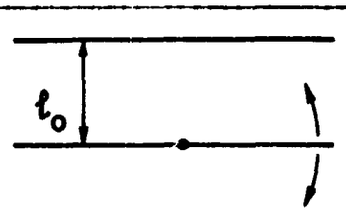	0.7° $1^{\circ}/s$	- -

Table 2 Model predictions

a) VERTICAL CONTROL

Configuration	$\sigma_{\alpha}^2(\text{deg}^2)$	$\sigma_{\theta}^2(\text{deg}^2)$	$\sigma_{\delta_e}^2(\text{N}^2)$	attention allocation f_i
1	0.211	0.242	57.6	$f_{\omega_1} = 0.55$ $f_{\dot{\alpha}} = 0.45$
2	0.121	0.239	57.3	$f_{\alpha} = 0.6$ $f_{\dot{\alpha}} = 0.4$
3	0.103	0.247	58.8	$f_{\dot{\alpha}} = 0.6$ $f_{\theta} = 0.4$
8	0.156	0.319	70.2	$f_{\alpha} = 0.42$ $f_{\dot{\alpha}} = 0.13$
9	0.157	0.331	72.4	$f_{\alpha} = 0.06$ $f_{\dot{\alpha}} = 0.27$ $f_{\theta} = 0.23$

b) LATERAL CONTROL

Configuration	$\sigma_{\omega_c}^2(\text{deg}^2)$	$\sigma_{\varphi}^2(\text{deg}^2)$	$\sigma_{\delta_a}^2(\text{N}^2)$	attention allocation f_i
4	1.86	9.68	13.1	$f_{\omega_c} = 0.37$ $f_{\dot{\omega}_c} = 0.63$
5	4.22	14.7	15.7	$f_{\omega_c} = 0.42$ $f_{\dot{\omega}_c} = 0.58$
6	2.96	9.35	12.9	$f_{\omega_c} = 0.35$ $f_{\varphi} = 0.65$
8	8.01	24.8	20.9	$f_{\omega_c} = 0.27$ $f_{\dot{\omega}_c} = 0.18$
9	6.71	19.6	18.2	$f_{\omega_c} = 0.22$ $f_{\varphi} = 0.22$

Table 3 Comparison of measured scores and model results

VERTICAL CONFIGURATION		$MS_{\alpha}(deg^2)$	$MS_{\theta}(deg^2)$	$MS_{\delta_e}(M^2)$
1	model	0.189	0.095	26.7
	measured	0.193	0.098	26.4
2	model	0.082	0.096	26.9
	measured	0.077	0.054	23.0
3	model	0.072	0.091	26.4
	measured	0.081	0.047	21.2
8	model	0.085	0.110	28.4
	measured	0.083	0.061	24.6
9, 10	model	0.072	0.095	26.9
	measured	0.065	0.040	20.1

LATERAL CONFIGURATION		$MS_{\omega_c}(deg^2)$	$MS_{\varphi}(deg^2)$	$MS_{\delta_a}(N^2)$
4	model	2.78	5.82	9.76
	measured	3.62	7.82	10.9
5	model	5.42	8.40	10.6
	measured	4.72	7.90	10.9
6	model	3.40	5.46	9.62
	measured	3.99	5.40	9.43
7	model	-	2.89	4.54
	measured	-	2.99	4.99
8	model	6.37	10.0	11.2
	measured	6.20	12.1	14.0
9, 10	model	4.14	6.66	10.8
	measured	4.52	6.90	10.8

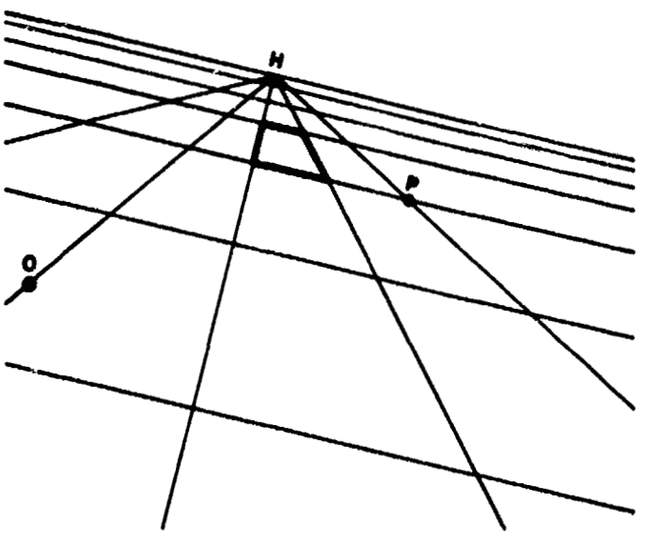

1a OUTSIDE VIEW

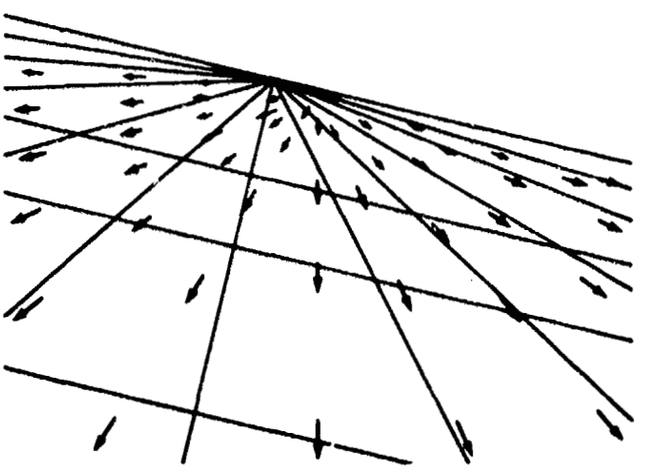

1b RELATIVE MOTION OF THE VISUAL FIELD

Fig. 1: Visual scene

ORIGINAL PAGE IS
OF POOR QUALITY

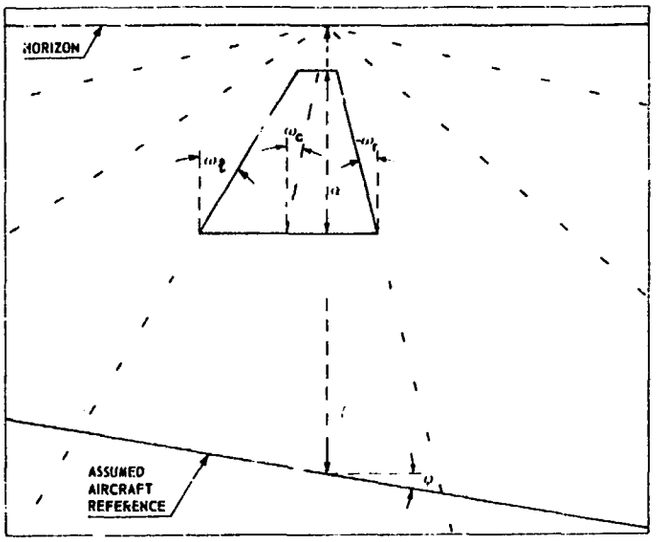

Fig. 2: Cues derived from the visual scene

VIEWING CONDITION	CONTROL		
	VERTICAL	LATERAL	BOTH
	1		
		4	
	2	5	8
	3	6	9
			10

N.B. CONFIGURATION 7 CONCERNS ROLL TRACKING BASED ON ROLL BAR ONLY

Fig. 3: Viewing conditions and selected configurations

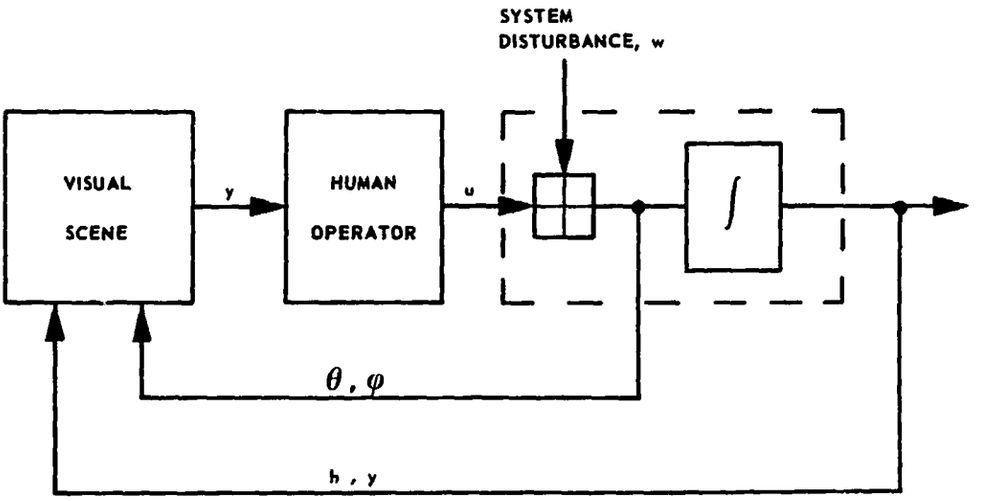

Fig. 4: Control task

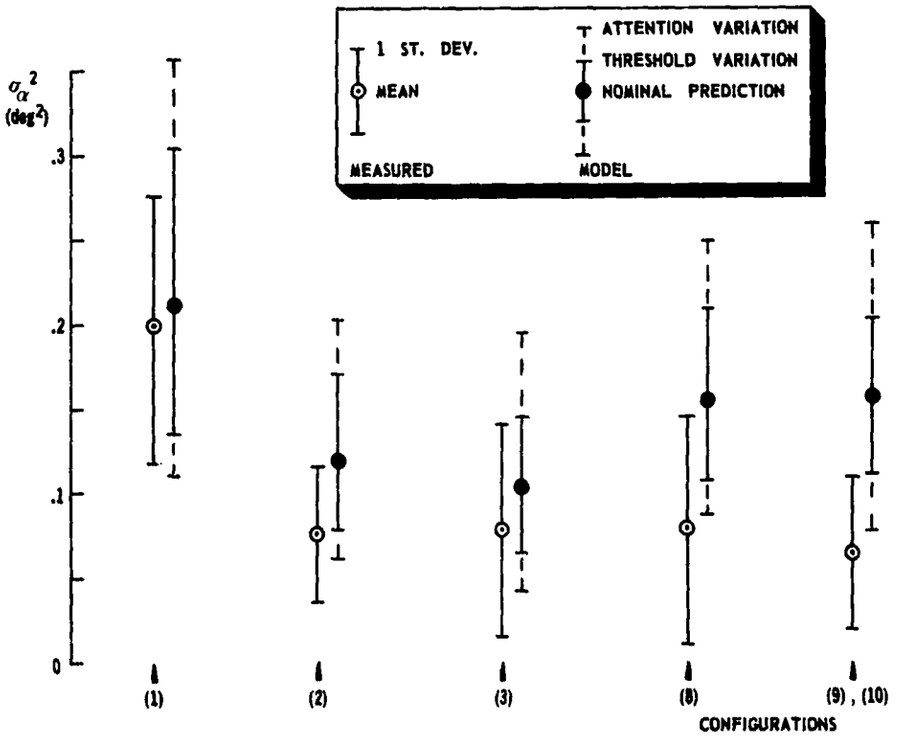

Fig. 5: Comparison of experimental scores and model predictions -- vertical control

ORIGINAL PAGE IS
OF POOR QUALITY

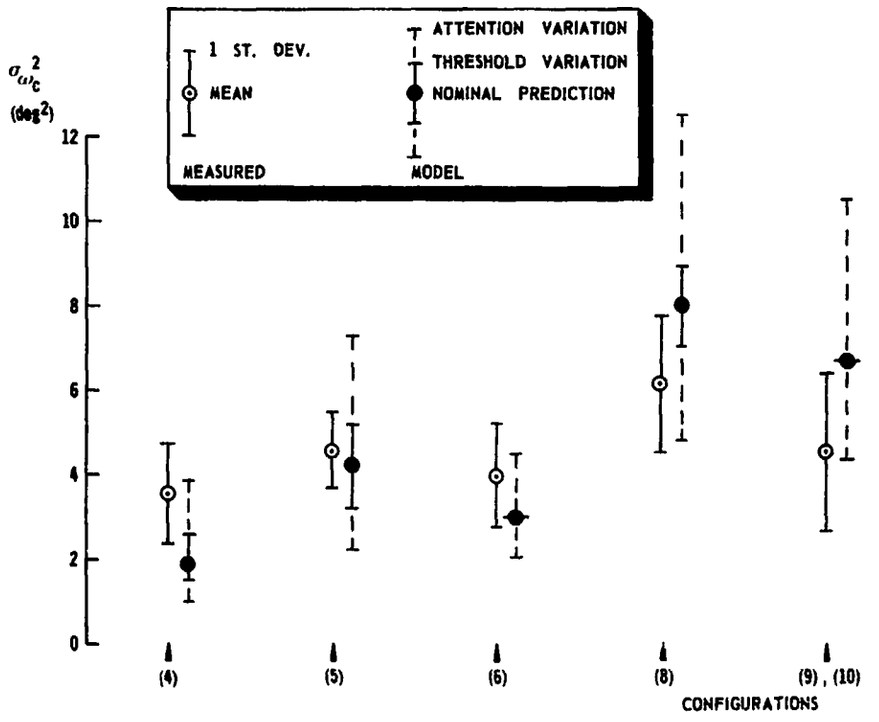

Fig. 6: Comparison of experimental scores and model predictions - lateral control

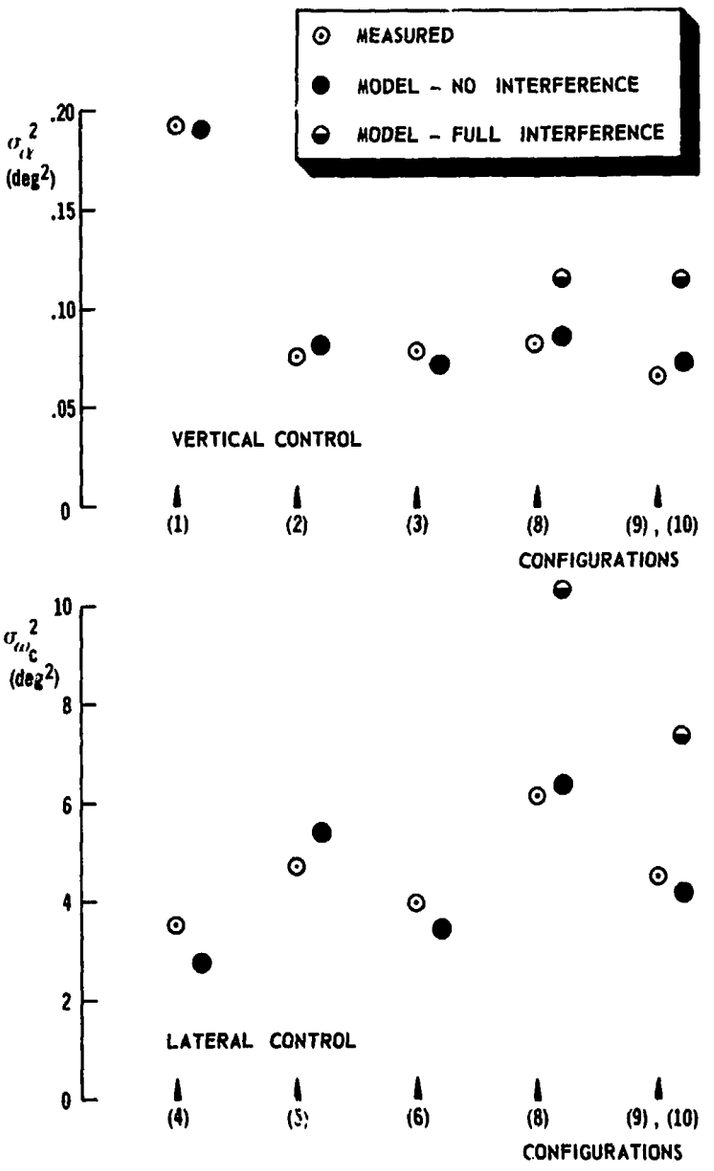

Fig. 7: Refined model scores and experimental results

ORIGINAL PAGE IS
OF POOR QUALITY

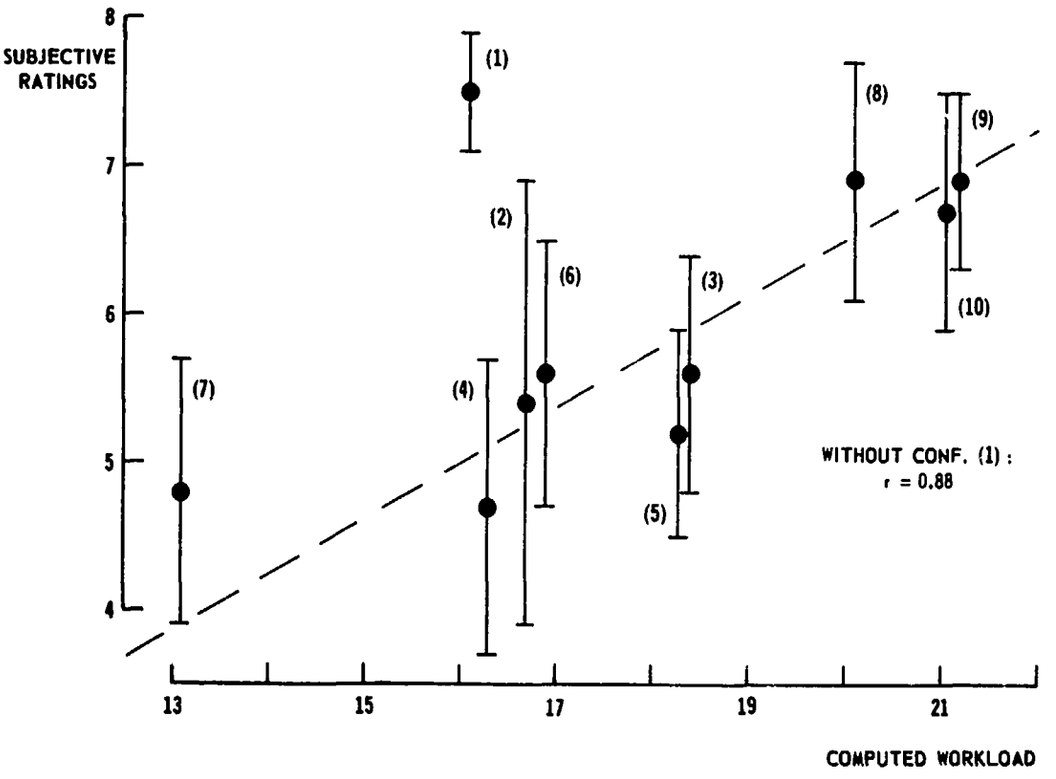

Fig. 8: Subjective workload ratings and computed workload

ORIGINAL PAGE IS
OF POOR QUALITY

D38

N79-15626

LINEAR MODELLING OF ATTENTIONAL RESOURCE ALLOCATION[1]

by Byron Pierce[2] and Christopher D. Wickens

University of Illinois Department of Psychology

SUMMARY

Eight subjects time-shared performance of two compensatory tracking tasks under conditions when both were of constant difficulty, and when the control order of one task (designated primary) was varied over time within a trial. On line performance feedback was presented on half of the trials. The data are interpreted in terms of a linear model of the operator's attention allocation system, and suggest that this allocation is strongly suboptimal. Furthermore the limitations in reallocating attentional resources between tasks, in response to difficulty fluctuations were not reduced by augmented performance feedback. Some characteristics of the allocation system are described, and reasons for its limitations suggested.

INTRODUCTION

A common requirement imposed upon the human operator engaged in time-sharing performance under time-varying environmental conditions results when changes occur in the difficulty of one of two concurrently performed tasks, as its performance constraints are held constant. Such changes thereby force a reallocation of attentional resources toward the task whose difficulty is increasing. Thus for example in precision flight, an increase in lateral air turbulence will require re-allocation of resources away from tasks of lesser demand (communications, pitch control) toward control along the lateral axis.

The entire process of task demand evaluation and resource allocation can be conceptualized as a two stage process. The operator must first evaluate the error, or discrepancy between desired and actual performance on the task or tasks required (error evaluation). If such an error is perceived to exist, the attention allocation system then must respond by shifting resources in a manner to restore the desired level of performance and nullify the original error (resource allocation). This closed feedback loop describing the resource allocation system is analogous in some respects to a compensatory tracking task, in which position error is evaluated and a manual control response is executed to nullify the error. Because of this similarity, modelling techniques borrowed from manual control will be utilized in

[1]This research was supported by a grant from Air Force Office of Scientific Research Life Sciences directorate. AFOSR77-3380. Dr. Alfred Fregly was the contract monitor.

[2]Now at Williams Air Force Base.

556
PAGE INTENTIONALLY BLANK

the current investigation to describe and evaluate the human's attention allocation system.

Delp and Crossman (Reference 1) have provided an analytical framework for describing the linear relation between time-varying task parameters and single task performance in terms of a higher level "meta transfer function." The objective of the present research is to apply similar procedures to analyze the meta transfer function of the resource allocation system to task demand (difficulty) changes in the dual task environment. In the paradigm employed, subjects perform two concurrent tracking tasks. One task is designated as primary--a high priority task whose performance is to be maintained at or above some criterion for the duration of a trial. During the trial, the difficulty of the primary task is varied in a semi-periodic fashion. It is assumed that, to the extent that he is capable, the subject follows the priority instructions, and primary task performance remains constant in the face of varying primary task difficulty. To achieve this optimal allocation behavior, the subject is therefore required to withdraw processing resources from performance of the secondary task, and its performance should then vary, more or less phase-locked to the difficulty variations of the primary task.

An hypothetical example of this "optimum allocation response" to a ramp increase in primary task difficulty is depicted by the solid lines of Figure 1. The time-varying performance on both tasks is portrayed, along with the inferred allocation of processing resources between the tasks. Note the differential sensitivity of primary vs. secondary task performance to the increase in primary task difficulty, and the corresponding optimum allocation of resources. Naturally, other varieties of allocation responses may be observed as well. The dashed lines in Figure 1 depict that of a non-optimum allocator in which resources are not at all redistributed, and primary task performance varies with its difficulty. Naturally a hybrid response between that of the optimal and nonoptimal allocator is possible, in which there is some reallocation of resources, but in insufficient degree to meet the new primary task demands.

The model that will be employed to describe the allocation system is portrayed in Figure 2. Here the allocation system is assumed to be a linear dynamic system in the sense that it receives inputs (task demands and subjectively assessed performance) and generates outputs in response (mobilized processing resources). While these outputs cannot be directly observed, they may be inferred from an appropriately filtered on-line performance measure. Thus in dual task performance, depicted in Figure 2, the dynamic relation between the four inputs to the allocation system (difficulty and performance demands on both tasks) and the two outputs (task performance on each task) can be evaluated to determine the extent to which these are described by a linear transfer function or orderly mathematical relation. Such a procedure is analogous to the analysis of dual axis tracking (Reference 2).

When analyzing dual task performance, one may examine for each task, the sensitivity of its allocated resources (inferred from performance) to changes in its own difficulty (D_1P_1 and D_2P_2 in Figure 2) and to changes in the difficulty or performance of the concurrent task (D_1P_2 and D_2P_1). In the

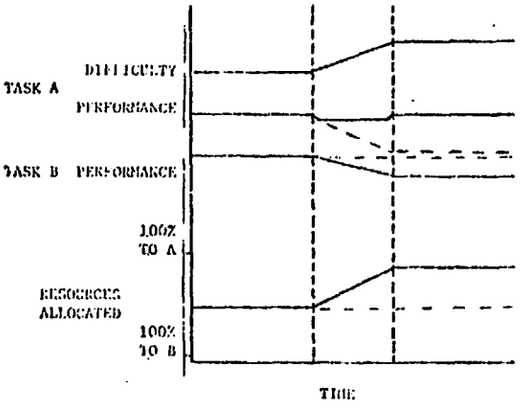

Figure 1. Hypothetical response depicting optimal allocation adjustment (solid lines) and nonoptimal allocation (dashed lines)

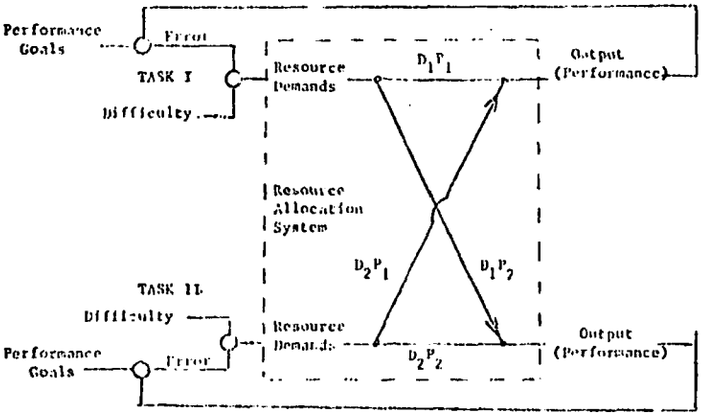

Figure 2. Schematic representation of dual task performance

current study Fourier analysis will be employed to determine the relations between time-varying inputs (tracking task difficulty) and time-varying outputs (filtered performance). To the extent that the resource allocation system is sensitive at all to these variations, the linear coherence measure, correlating variations over time between the input and output signals, should be non-zero. More specifically the cross-channel (D_1P_2 and D_2P_1) and like-channel (D_1P_1 and D_2P_2) coherence measure will be examined as a means of determining the optimality of the allocation system. For a highly optimal system, the like channel coherence (D_1P_1) should be a low (near 0), with the crosschannel coherence (D_1P_2) high (near 1.0). For the non-optimal allocator the values should be reversed, and for the hybrid case both coherence values should be relatively high.

If suboptimal allocation is observed in the present results, then an important question that can be asked relates to the source of the limitation in the allocation system. In terms of the two-phase description of the allocation process as shown in Figure 2, one may ask whether the limitation results from the operator's inability to perceive discrepancies between desired and actual performance (failure of error evaluation), or from the inability to reallocate resources in response to an accurately evaluated error. In an analogous manner it is possible to ask whether inadequate performance in a compensatory tracking task results from poor perceptual evaluation of the displayed error, or from an inability to execute an appropriate control response.

To investigate the source of potential limitations, a separate set of experimental conditions were included in which the conventional instantaneous tracking error display was supplemented by augmented performance feedback that displays the discrepancy between the desired level of primary task performance, and the running average of that performance (e.g., Reference 3). To the extent that limitations in the allocation system result from inadequate error evaluation, rather than limits of allocation, then the explicit display of the discrepancies in performance should produce a corresponding approach toward optimality of allocation (i.e., an increase in the cross-channel, and decrease in the like-channel coherence).

METHOD

ORIGINAL PAGE IS
OF POOR QUALITY

Tasks. Subjects performed two compensatory tracking tasks, displayed one above the other with a slight horizontal offset. The left display was controlled by left-right manipulation of a spring loaded controller held in the left hand. The right display was similarly controlled with the right hand. The total visual angle subtended by both displays was 4^{o} (horizontal) x 1^{o} (vertical). Disturbance inputs consisted of band-limited white noise with an upper cutoff frequency of .32 Hz. Separate uncorrelated disturbances were employed on each task and were added to the output of the control dynamics. Control dynamics were of the form:

$$Y_c = K\left(\frac{1-\alpha}{s} + \frac{\alpha}{s^2}\right)$$

On trials of constant difficulty, the value of the difficulty parameter alpha was set at .50. On variable difficulty trials, the value of alpha on one task, designated primary, was driven by the function: $\alpha = .50 + \sin(.1884\ t) + \sin(.0628\ t)$, $(0 < \alpha < 1)$. This produced a system that varied continuously between second order unstable dynamics, first order stable dynamics, and intermediate levels in a series of spikes and ramps (see Figures 3 and 4). Secondary task difficulty was always held constant with alpha = .50.

Supplementary performance feedback of the primary task, used in variable difficulty trials, appeared as a bar graph varying in height to reflect changes in performance (Reference 3). The performance bar represented in-

ORIGINAL PAGE IS
OF POOR QUALITY

tegrated primary task error, averaged over a sliding 5-second window. The desired performance level, indicated by a short horizontal line positioned about half the distance from the zero point (no bar graph showing) to the top of the display, reflected the subject's average performance assessed for trials of constant difficulty. By tracking so that the bar graph remained at or above the desired performance line, the subject attained desired standards of primary task performance.

Root mean squared error (RMSE) was computed on line for each task and recorded at the end of each trial. Control stick and cursor error positions were sampled and recorded on tape every 120 msec. Experimental control was governed by a Raytheon 704 computer.

Design and Procedure. Eight right-handed male students at the University of Illinois participated in the experiment and were paid for participation. A within-subjects design was employed so that all subjects performed all experimental conditions. Following one day's session of practice on the dual axis tracking tasks, four experimental sessions were conducted. Within each session, subjects performed 24 two minute dual task trials. These consisted of 8 trials of constant difficulty, of which the final 4 were used for data analysis (Phase I), followed by 12 trials of variable difficulty, of which the final 8 were used for data analysis (Phase 2). Finally the subjects received four more trials of constant difficulty (Phase 3). During constant difficulty trials subjects were instructed that the two tasks were of equal priority, while in Phase 2, the task of variable difficulty was designated as primary--its performance to be held constant. On alternating Phase 2 trials, either the left hand task or the right hand task was primary (and was therefore variable). Similarly on alternating pairs of Phase 2 trials, supplemental feedback was either present or absent.

RESULTS

RMS Error. Two 1-way repeated measure analyses of variance were performed on the RMS tracking errors, one for primary and one for secondary task performance. The four levels of each ANOVA consisted of Phase 1, Phase 2 feedback, Phase 2 no-feedback, and Phase 3. The effect of condition on the performance measures in both ANOVAs was highly reliable (Primary Task, $F_{3,21} = 107.98$, $p < .001$; Secondary Task, $F_{3,21} = 54.93$, $p < .001$). The mean values of primary and secondary task error for the four conditions are shown in Table 1. It is apparent that large differences in both tasks

Table 1: RMS Error (Proportion of Scale

	Phase 1	Phase 2 Feedback	Phase 2 No Feedback	Phase 3
Primary Task	.1164	.1808	.1869	.1166
Secondary Task	.1206	.2058	.1806	.1147

were evident between the variable (Phase 2) and constant difficulty (Phases 1 and 3) trials, a difference substantiated by the experimental contrast of Phase 1 with Phase 3 no-feedback (Primary Task, $F_{1,7} = 153.0$, $p < .001$; Secondary Task, $F_{1,7} = 31.8$, $p < .001$). The effect of feedback, however, examined in the contrast between the two Phase 2 conditions, was only reliable for the Secondary Task ($F_{1,7} = 59.03$, $p < .001$).

Coherence Analysis. The response of performance to the time-varying changes in task difficulty is illustrated in Figures 3 (feedback) and 4 (no-feedback). The error measures were smoothed by averaging tracking RMS error within a sliding 2.4 second window. These smoothed performance records were then ensembled over trials and subjects to produce the data portrayed in Figures 3 and 4. It is evident in these figures that to some extent performance on both tasks "tracked" the time-varying difficulty parameter, an observation that was born out by the analysis of linear coherence.

The linear coherence analysis employed a Fast Fourier Transform algorithm (Reference 4) to transform time variations of primary task alpha and within trial error measures to power spectra in the frequency domain. From these transformed measures, linear coherence values (Reference 5) were computed correlating variations over time between Primary Task difficulty (alpha level) and the performance measures (within trial error averages) on both tasks.

Obtained linear coherence values, assessed at the six lowest frequency values that best account for variations of the task one alpha signal, are displayed in Figure 5. It is evident in Figure 5 that linear coherence is reasonably high in both conditions for both measures. However, primary task difficulty fluctuations seem to induce greater variation in primary task than in secondary task performance. Similarly feedback demonstrated little effect on primary task coherence but a small but consistent effect on the coherence with the secondary task.

DISCUSSION

The most striking aspect of the data relates to the marked deterioration in performance on both tasks that results when the difficulty of one is made variable. This was manifest in a 60-70% increase in RMS error, despite the fact that the average value of the difficulty parameter alpha (= .50) in the variable difficulty tasks was equivalent to its value in the constant condition.

A reasonable explanation for this difference can attribute the performance decrement to the higher level cognitive process required to deal with varying task demands, in an effort to meet performance requirements. In short, the operation of the attention allocation system itself requires processing resources in order to function in continuously reevaluating and responding to resource demand changes.

ORIGINAL PAGE IS
OF POOR QUALITY

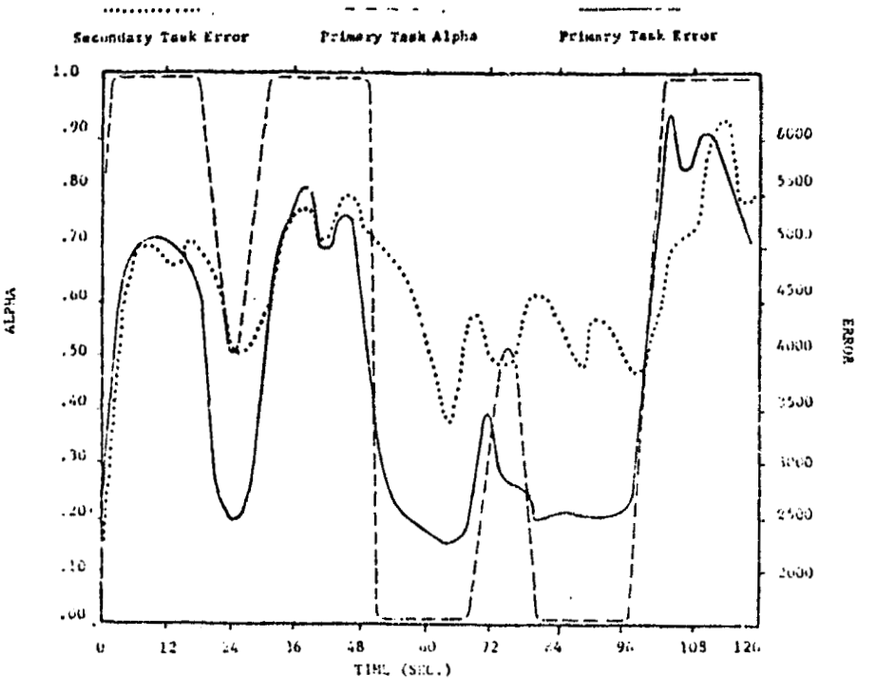

Figure 3. Average time history of within trial dual task error

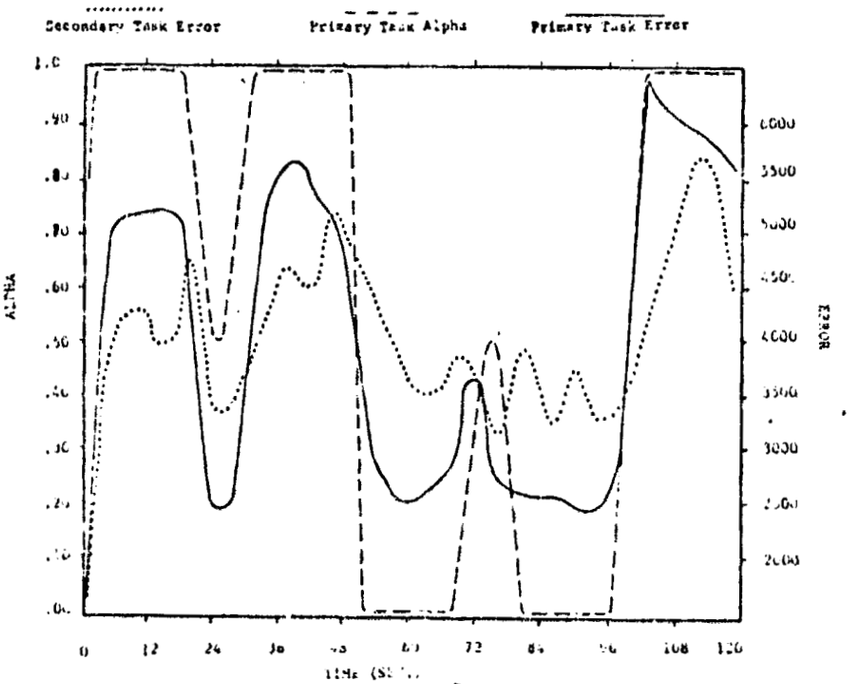

Figure 4. Average time history of within trial dual task error and primary task alpha--no-feedback condition

ORIGINAL PAGE IS
OF POOR QUALITY

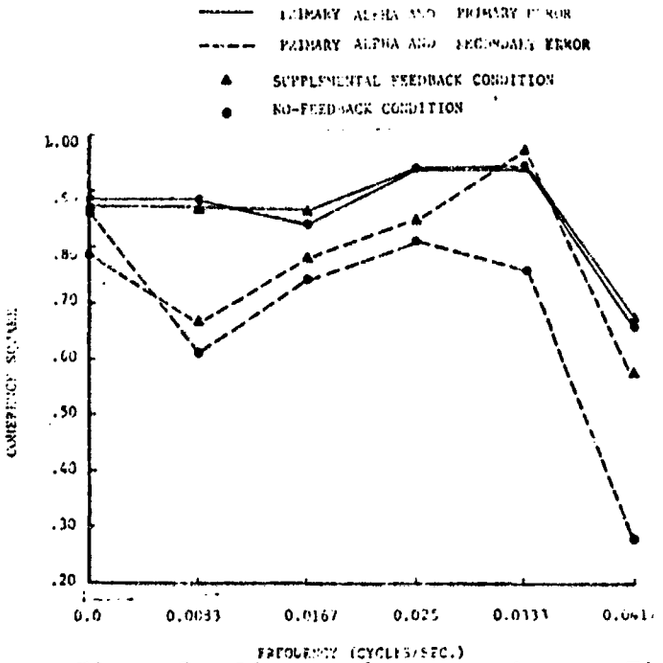

Figure 5. Linear coherence values between alpha and tracking error measures

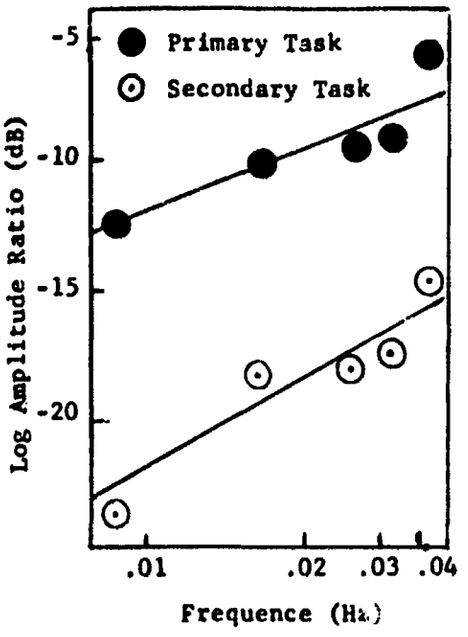

Figure 6. Gain plot of transfer function. Ratio of tracking error (range 0-1.0) to alpha.

Properties of the Allocation System. The proposition that the system may be modelled approximately as a linear dynamic system received some support in the current results, both from the relatively high linear coherence values obtained at the frequencies corresponding to difficulty variation, and on the basis of visual examination of Figures 3 and 4. In addition to the general responsiveness of performance on both tasks to the difficulty fluctuations described above, two additional characteristics of these figures that are not revealed by the coherence analysis are particularly relevant.

1. The transfer function of the alpha-performance data was computed, and the amplitude ratio data are plotted in the gain portion of the Bode plot shown in Figure 6. While the linear correlation of this slope is not high, and the number of points (6) is too few to allow any strong conclusions, the implication of these data is that the response of the allocation system, as inferred from subjects' performance is to lead the difficulty variation as a KS system. That is, performance is sensitive to the rate of change or first derivative of difficulty, rather than to the absolute level of difficulty itself. This behavior is graphically illustrated in the response of primary task performance to the spike increase in alpha at time t = 72 in Figures 3 and 4. This result is in contrast to that observed by Delp and Crossman (Reference 1), who modelled the performance response to difficulty changes (their "meta"-transfer function) as a first order, K/S, or integral system.

The source of this difference is not immediately apparent; it may be attributable to either the repeated nature of the difficulty function employed in the current study that allowed the subjects some degree of anticipation, to the discrete steplike changes of that function, or to the dual task environment used here.

2. Both figures indicate the presence of relatively high frequency oscillations in secondary task performance that do not correspond to variations in alpha. While these oscillations might at first be described as "noise," it should be noted that they correspond very closely, point-for-point in time between the separate and independent replications depicted in Figures 3 and 4. A close correspondance of this nature would not be predicted from random variability in the two replications. Instead, these oscillations bear a resemblance to the frequency response that a second order physical system with spring loading might show to a step or impulse input, approximating the nature of the difficulty changes presently employed. While the precise nature or source of these oscillations cannot be established, their presence nevertheless provides supportive evidence for the linearity, and invariant properties of the allocation mechanism, and encourages further investigation.

Optimality of the Allocation System. The coherence analysis performed indicated clearly that subjects did not behave as the optimum allocator of Figure 1. In marked contrast to the instructions delivered to the subjects, primary task performance was highly sensitive to primary task difficulty. It is therefore important to ask why, in the present results, subjects appeared unable to follow the imposed priority instructions. Wickens and Kessel (Reference 6) showed that when the difficulty of a task (instability tracking) is increased between sessions in a dual task environment, it is possible for subjects to hold that task performance constant--at the expense of secondary task performance. Why then, when difficulty was manipulated within a session in the current experiment, was the severe limitation observed?

It appears unlikely that subjects simply ignored the instructions, as resources clearly were withdrawn from the secondary task to deal with the difficulty increase and were returned when demands were lowered, thus producing the high secondary task coherence measure. Instead it appeared that either the resources withdrawn were not delivered to the primary task, or alternatively that the changes in difficulty were sufficiently abrupt that smooth resource modulation could not occur (i.e., resource adjustment did not have sufficient time to operate). This second hypothesis is supported by visual inspection of Figure 3. Note following the difficulty step increases at times t = 24-28 and t = 96 seconds that in both instances primary task error begins gradually to reduce as secondary task error undergoes a corresponding increase, as if at this point the subject begins a gradual and appropriate reallocation of processing resources away from the secondary task toward the primary, in accordance with instructions. In fact a rough estimate of the lag between difficulty increases and secondary task error increases places this lag at approximately 2-3 seconds, a value that corresponds reasonably well to the 2.8 second lag observed by Delp and Crossman.

The implication of this observation is that the appropriate resource mobilization might be within the capabilities of the operator to a greater extent, had the difficulty transitions been of the more gradual nature employed by Delp and Crossman.

Feedback. The contrast in performance measures between the augmented feedback and no-feedback conditions indicated further that the operator's limits were manifest in the second stage of the closed loop allocation system--the reallocation of resources--rather than in the first stage--the error evaluation process. When this evaluation process was presumably aided by explicit presentation of the discrepancy between desired and obtained performance, no reliable improvement in allocation behavior was observed, either in the form of a reduction of primary task error, or a reduction in its linear coherence function with alpha. In fact, the only effect of feedback that was observed was a reliable increase in secondary task error, and a corresponding increase in the secondary task coherence measure, as this task apparently became more responsive to the changes in primary task difficulty.

While augmented feedback did not prove to be useful in the current investigation, the conclusion drawn must of necessity be limited. It is quite likely that the difficulty changes were sufficiently dramatic that their presence, and the resulting performance changes, were easily observable by the subjects. Changes of a more subtle nature might have produced a sub-threshold deterioration in performance that could only be detected with the aid of the augmented feedback.

CONCLUSION

The major limitations of human performance in the variable difficulty paradigm, demonstrated in the present results, suggest that this area warrants further exploration. Research is needed to determine the effect on allocation ability of such variables as training, the nature of the difficulty time functions, and the qualitative similarity between the time-shared tasks. Through this research a better appreciation can be gained not only of the mechanism by which attentional resources are allocated, but of the fundamental nature of those resources themselves.

REFERENCES

ORIGINAL PAGE IS
OF POOR QUALITY

1. Delp, P. and Crossman, E. Transfer Characteristics of Human Adaptive Response to Time-varying Plant Dynamics. Proceedings 8th Annual Conference on Manual Control. Wright Patterson Air Force Base. AFFDL-TR-72-92. June 1972.

2. Damos, D. and Wickens, C. A Quasi-linear Control Theory Analysis of Time-sharing Skills. Proceedings 13th Annual Conference on Manual

Control. U.S. Government Printing Office, 1977.

3. Wickens, C. and Gopher, D. Control Theory Measures of Tracking as Indices of Attention Allocation Strategies. Human Factors, 1977, 19, 349-366.

4. Shirley, R. Application of a Modified Fast Fourier Transform to Calculate Operator Describing Functions. Proceedings 5th Annual Conference on Manual Control, NASA, SP-215, 1969.

5. Sheridan, T. and Ferrell, L. Man-machine Systems. Cambridge, Mass.: MIT Press, 1974

6. Wickens, C. and Kessel, C. The Effect of Participatory Mode and Task Work-load on the Detection of Dynamic System Failures. Proceedings 13th Annual Conference on Manual Control. U.S. Government Printing Office, 1977.

D39

N79-15627

A MODEL FOR DYNAMIC ALLOCATION OF HUMAN ATTENTION AMONG MULTIPLE TASKS +

Thomas B. Sheridan and M. Kamil Tulga
Man-Machine Systems Laboratory
Department of Mechanical Engineering
Massachusetts Institute of Technology
Cambridge, Massachusetts 02139

Abstract

This paper consists of two parts. The first part describes the problem of multi-task attention allocation with special reference to aircraft piloting, the experimental paradigm we use to characterize this situation and the experimental results obtained in the first phase of our research. A qualitative description of an approach to mathematical modeling, and some results obtained with it are also presented to indicate what aspects of the model are most promising. The second part of the paper consists of two appendices which (1) discuss the model in relation to graph theory and optimization and (2) specify the optimization algorithm of the model.

1. Introduction

We think that an increasingly crucial aspect of piloting an aircraft is "multi-task allocation of attention". The pilot must monitor many more systems than before, most of which are growing in complexity. In earlier days flying the aircraft "by the seat of the pants" was difficult, but piloting was, more or less, a constant task. It was obvious that the pilot could keep track of what was being controlled at what time and how well that was working because he was doing it; he was in the loop and could see or feel it directly.

As systems become automatic the pilot himself tends to lose track of what signals are coming into what subsystem and what response that subsystem is making. Most of the time when everything is normal the automatic systems do just fine. Indeed if we demanded that the pilot actually perform all functions which are now automated it is clear he couldn't do a fraction of such tasks. Yet we expect him to monitor all such functions, and at the first overt alram or even subtle evidence of failure we expect him to be able to render a quick accurate diagnosis of the problem and set it straight.

We call the pilot a "flight manager" or "supervisory controller" and we see him in the image of a corporation manager with legions of dutiful automatic servants doing his will and bringing him information as he desires it. The problem is that the corporate manager has time to ponder and investigate and weigh evidence and consider his decisions. He operates

+ research supported by NASA Grant NSG 2118.

568

PAGE INTENTIONALLY BLANK

on a human time scale: if the corporation manager sees his "production vehicle" about to go bankrupt he has at least a few minutes to decide what's wrong and what to do about it. The flight manager doesn't.

The general research questions implied are:

a) What are the expected behaviors and what are the limits of a person's capability to allocate his attention among many simultaneous tasks of varying importance and varying urgency, as a function of the number of tasks, the general pace at which they occur and other salient parameters?

b) If there is a normative or optimal way a person should perform such a task, can it be specified as a quantitative model, and how close does a trained person come to behaving optimally?

c) What are the implications for improving the design of the man-machine systems in which the pilot must perform such multi-task allocation decisions?

2. Experimental Paradigm

To characterize such a multi-task decision-making situation we have developed a very general experimental paradigm and an associated model. The experimental paradigm requires the subject (or decision-maker DM) to select one at a time from among a number of blocks ("tasks") of different heights and widths displayed simultaneously on a CRT (Figure 1). His selection, made by holding a cursor even with the block "attended to" is in order to maximize his reward, where the earning rate is proportional to the displayed "importance" (indicated by the height of each block) and the "productivity rate" (the rate at which the block decreases in width when "attended to"). Blocks appear at random distances from a "deadline" and move at constant velocity toward that deadline, disappearing when they first touch it. Various task parameters have to do with the frequency at which new blocks appear, the speed with which they move toward the deadline, the variability in importance, the variability in how far from the deadline they first appear, and so on. The toal is to "remove" as much block area as possible.

In one experiment blocks continually appear with exponential distribution in time. In a second experiment all blocks appear at the start of the run; no new ones appear thereafter.

An important feature of the experiment is that blocks do not queue up for service, i.e., if a block reaches the deadline the opportunity to earn its reward is lost. We cannot say for sure, however, whether blocks queue in the operator's mind for attention in correspondence to the fact that at any one instant of time there may be some blocks which are far from the deadline and others which are close. The close ones, of course, may be of little importance, so often it is better to attend to more important tasks which are farther from the deadline in order to ensure that all of the really important ones do get attended to before the deadline.

ORIGINAL PAGE IS
OF POOR QUALITY

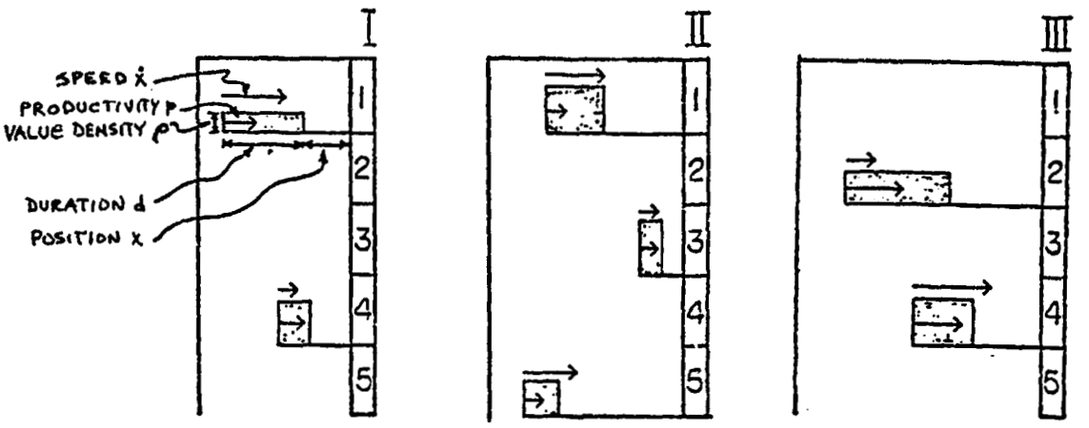

Figure 1. Experimental Computer Display of Moving Blocks Representing Tasks

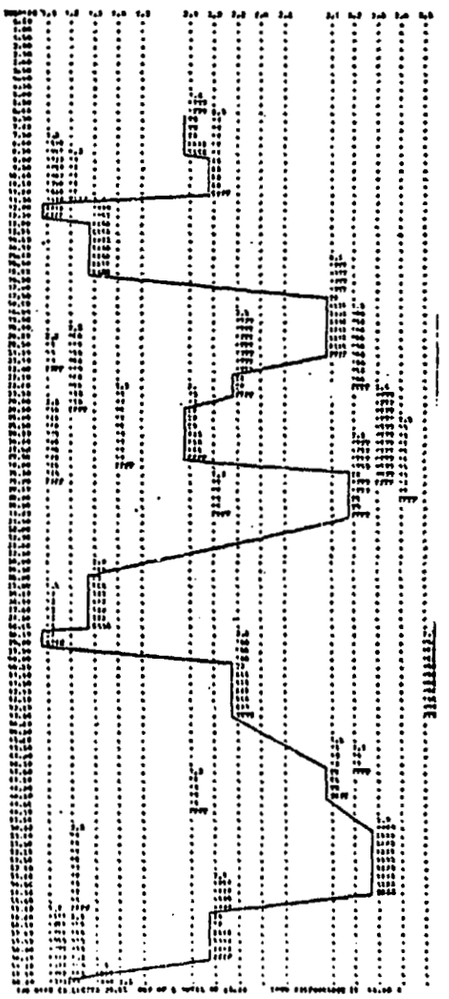

Figure 2. Record of D.M.'s Action Trajectory in Real Time

Figure 2 illustrates a means we have used to obtain a time-plot of which block the subject selects in which queue (column headings). Printed symbols in each column tell the service time the block requires, the time the block will be available, and the value to be obtained.

Having informally experimented with this situation with a variety of parameter combinations we are now in a position to claim that the experiment does seem to simulate various attentional demands which are placed on the pilot. These vary considerably in duration. Some tasks are urgent, but of modest importance; some are urgent and of great importance; some are not urgent and of modest importance; some are not urgent but of great importance to be done before the deadline.

3. Experimental Results

As the first phase of the second author's doctoral thesis, experiments with human subjects have been run with various experimental parameter combinations. Because the number of such possible combinations is so large we have investigated the effects of changing one parameter at a time, relative to a "baseline condition". Table 1 indicates that for all runs the subject worked with 3 queues of blocks (tasks) and runs lasted 400 seconds. The baseline parameters are given above. Seven changes in parameters are indicated below, made one run at a time, all other parameters matching the baseline condition in each case. For each the values gained by each of three subjects, the range of their data, the average, and the total possible are given.

In Table 1 it is seen that a considerably higher speed of blocks moving toward the deadline (2) reduces the score, but not much, compared to the baseline (1). Greater variation in block speed (3) makes little difference. A reduction of interarrival time (4) of blocks means more blocks become available - more opporunity is there for earning a score - but a smaller fraction of these are completed. As the height of blocks (task value densities) become more variable (5) the net earnings are little affected, though the presence of a few very lucrative blocks doubles the total possible score. Giving partial credit (6) for productivity (allocation) on a task when it hits the deadline increases the earnings little more than one percent, which is surprising. Lowering productivity (7) has the most significant effect, as seems intuitively reasonable - but the reduction in score is not quite in proportion to the forced reduction in rate of doing tasks.

4. A Mathematical Modeling Approach

To accompany the experimental task, we have developed a mathematical model which can be run on the computer immediately after any human data run. (The relationship of the model to graph theory in general and the full specification of the model algorithm given in Appendices 1 and 2 respectively).

ORIGINAL PAGE IS
OF POOR QUALITY

COMMON CONDITIONS

3 queues, 400 sec duration

BASELINE CONDITION

Task Interrival time, exponential distribution, mean = 20 sec/queue

all tasks appear 5 units away from the deadline

all tasks 2.5 units in duration

all tasks speed toward deadline at 0.1 units/sec.

productivity on all tasks 0.5 units per sec.

value density rectangular distributor 0 - 1 utiles/sec

No partial credit was given in the baseline case.

	CONDITION	% AVAILABLE VALUE GAINED BY SUBJECTS				AVG.	TOTAL POSSIBLE VALUE (UTILES)
		DY	KT	SJ	RANGE		
1	Baseline, B	.913	.931	.942	.029	.929	98.7
2	More speed (2.5 B)	.917	.880	.878	.061	.891	98.7
3	Variable speed (rect, .05-2.5)	.934	.907	.912	.027	.918	98.7
4	Less interarrival time (0.75B)	.803	.809	.795	.014	.802	122.2
5	More varied value density (rect dist 0-2)	.946	.940	.902	.044	.929	197.6
6	Baseline, but with partial credit	.943	.949	.926	.023	.940	98.7
7	Less productivity (0.5B)	.642	.660	.650	.018	.650	98.7

Table 1

Some Experimental Results

The model is essentially a dynamic program which calculates an optimal "attention allocation trajectory" for all the blocks present, and then takes the first step of that trajectory. As soon as each new block appears, the dynamic programming calculation is repeated. The model is constrained by three parameters to make it human-like. The parameters may be adjusted according to various criteria until the model best fits experimental data. One parameter is a time delay τ, simply adjusted to match human motor reaction time plus decision time.

A second parameter is a linear discounting of importance of later blocks in various alternative trajectories which the dynamic programming algorithm compares to determine which trajectory costs least. This discount rate we call β. Zero β means that, in present evaluation of alternative trajectories for future action, what the model earns in the more distant future weights just as heavily as what it earns in the very next step. Large β means the model discounts the future completely and only considers alternative next steps.

A third parameter, γ, is a linear discount rate on distance of blocks (tasks) from the deadline, determined anew at each successive model iteration. Zero γ means that, in deciding what to do next, blocks far from the deadline are just as heavily weighted as those close to it (multiplied by the blocks' individual importance). Large γ means the model only attends to what is close to the deadline. It is a "putting out bonfires" strategy.

It may seem at first reading that β and γ mean the same thing, but this is not true, and in fact it was our experiments which led us to see this distinction: this aspect of the model grew out of the research. The point is that time into the future, with respect to alternative sequences of (planned) action, is quite different from opportunity time available. In other words, the task which is far from the deadline can be done first, and the one which is close to the deadline done later. The only absolute constraint, of course, is that no task can be "done" after it crosses the deadline.

5. Results from the Model

We now have experimented with the model itself on various multi-task situations. In those situations cited above where all blocks appear at the outset we have verified, as expected, that zero β and zero γ are best. All information is known from the start, and an optimal trajectory as determined by dynamic programming is optimal in an absolute sense.

Curiously, this is not true of the experiment where blocks appear continually. Let us recall that the dynamic programming algorithm computes an optimal trajectory based on what blocks are in view at the time, then commits itself to the first step of that optimal trajectory. Thus, if there is discounting in "planning time", optimal may be to do a relatively unimportant but about-to-disappear task, since there is just time

then to complete an important task which is the only one available. But, while doing the unimportant task, suppose a new important task appears with the same opportunity time as the other important one. A choice must be made between the two important tasks, since only one task can be attended to at a time; one important task must be lost. Had the model expected the new important task was coming it would have attended first to the available important task, ignoring the unimportant close-to-deadline one, and then had time available for the new important one. Instances of this effect are revealed in simulation runs described below.

Our model runs thus far had been made with varying τ values (reaction times) and either varying β or varying γ. τ values have been matched to average reaction times of experimental subjects on a one-run-at-a-time basis.

We have let the computer compare human DM results with computer results separately on the basis of five different criteria: 1) percent value gained for the given run out of the total possible value obtainable; 2) percentage of all completed tasks independent of duration or importance; 3) percentage of time both model and human subject acted on the same tasks at the same time; 4) squared differences between cumulative value gained by model and human, summed over the entire run; 5) squared differences between incremental value gained by model and human for brief time interval, summed over the entire run.

Figures 3 through 7 show examples of five model runs. Figure 3 is for subject KT for the baseline experimental conditions. Figure 4 is for the same subject for a speed 2.5 times as great as the baseline. Figures 5, 6, and 7 are for three different subjects for a productivity half that of the baseline. On each page are ten plots, each plot representing a series of model runs at different values of β (left column, see abscissa below for value of β) with $\gamma = 0$, or model runs at different values of γ (right column) with $\beta = 0$. Points symbolized by X are model runs. The horizontal lines represent human data for the given experimental condition. Circles are comparisons between human and model. Each row is for measures according to a different criterion, as indicated. Thus all points on any vertical slice represent the same model run. Ordinate values of the performance criteria are shown at the right.

Thus, considering the plots in order from top criterion to bottom, the top one is to be maximized (or matched to the line for best fit to human). The X plot of the second one is to be maximized (or matched to the line for best fit to human); the circles on this plot represent % of tasks which are common to model and human, and are to be maximized. The third plot is to be maximized, the fourth and fifth are to be minimized.

For the first criterion (% value gained) it is evident that the model closely approximates the human, at lower values of β or γ doint slightly better (as one would expect for little or no discount) while at higher values doing slightly worse (where the model is not allowed to "plan ahead", i.e., β is large, or is not allowed to consider blocks

ORIGINAL PAGE IS
OF POOR QUALITY

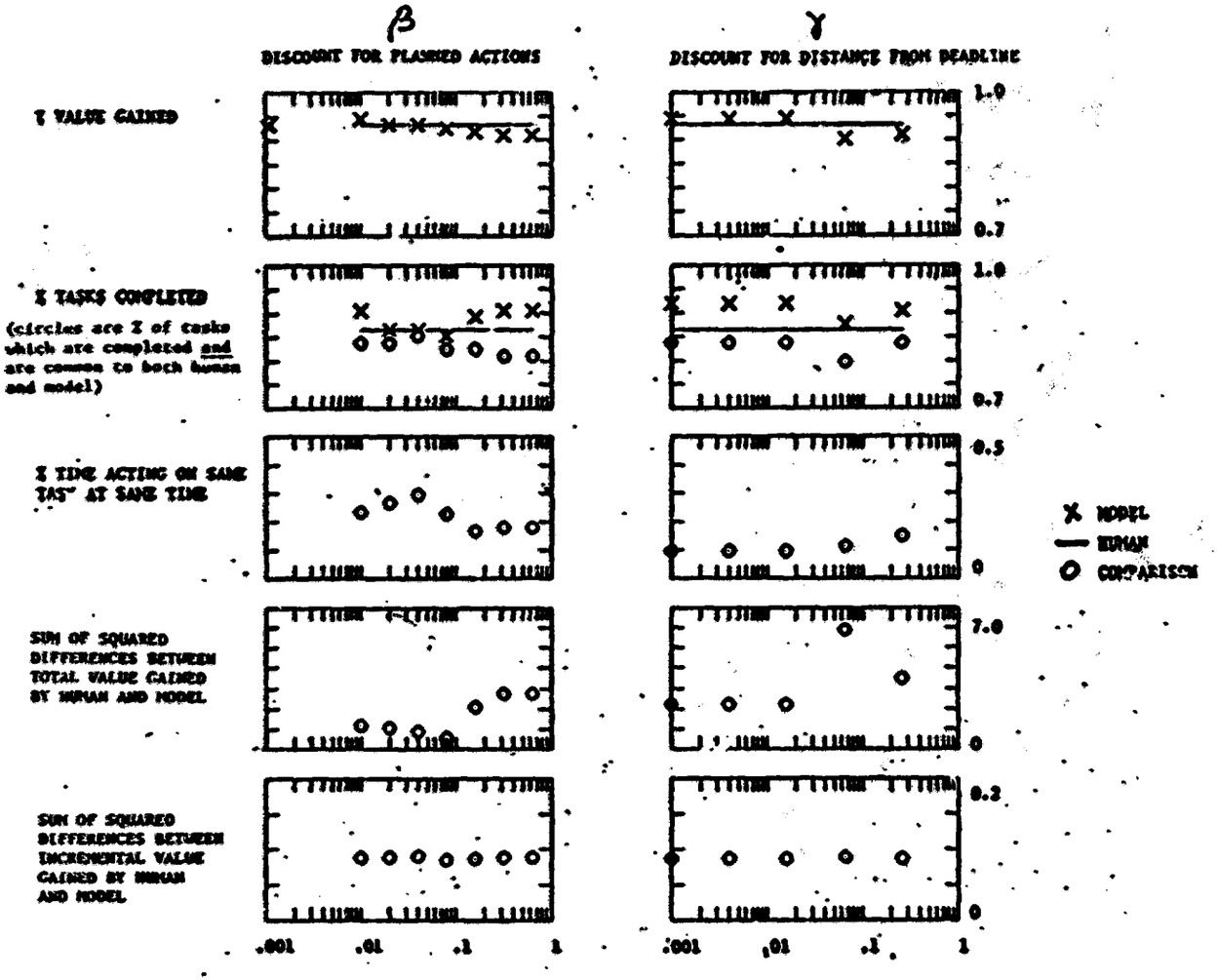

Figure 3. Condition 1. BASELINE:
interarrival 20 sec/queue
speed 0.1 units/sec
productivity 0.5 units/sec
Subject: KT

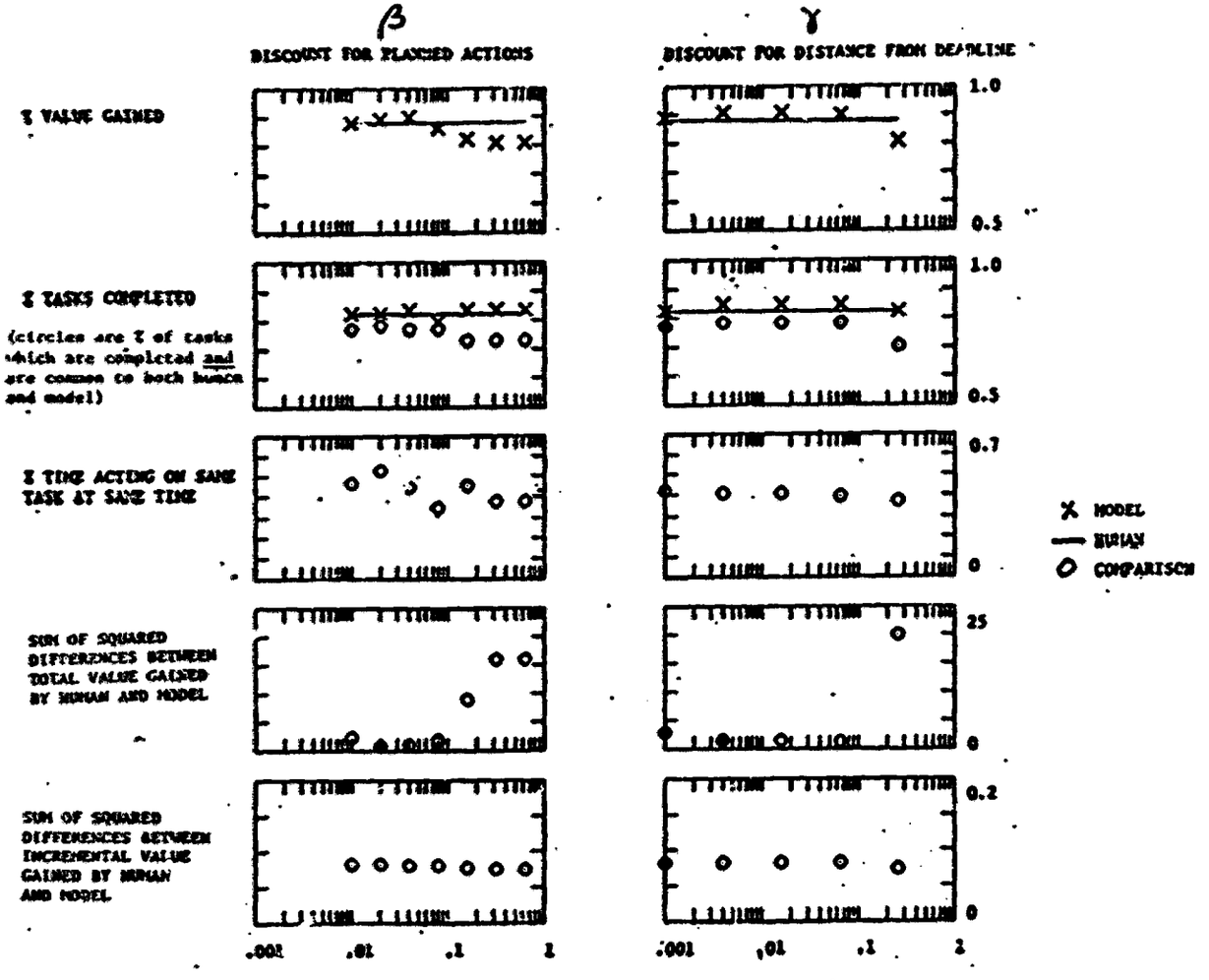

Figure 4. Condition 2
interarrival 20 sec/queue
speed 0.25 units/sec
productivity 0.5 units/sec
Subject: KT

ORIGINAL PAGE IS
OF POOR QUALITY

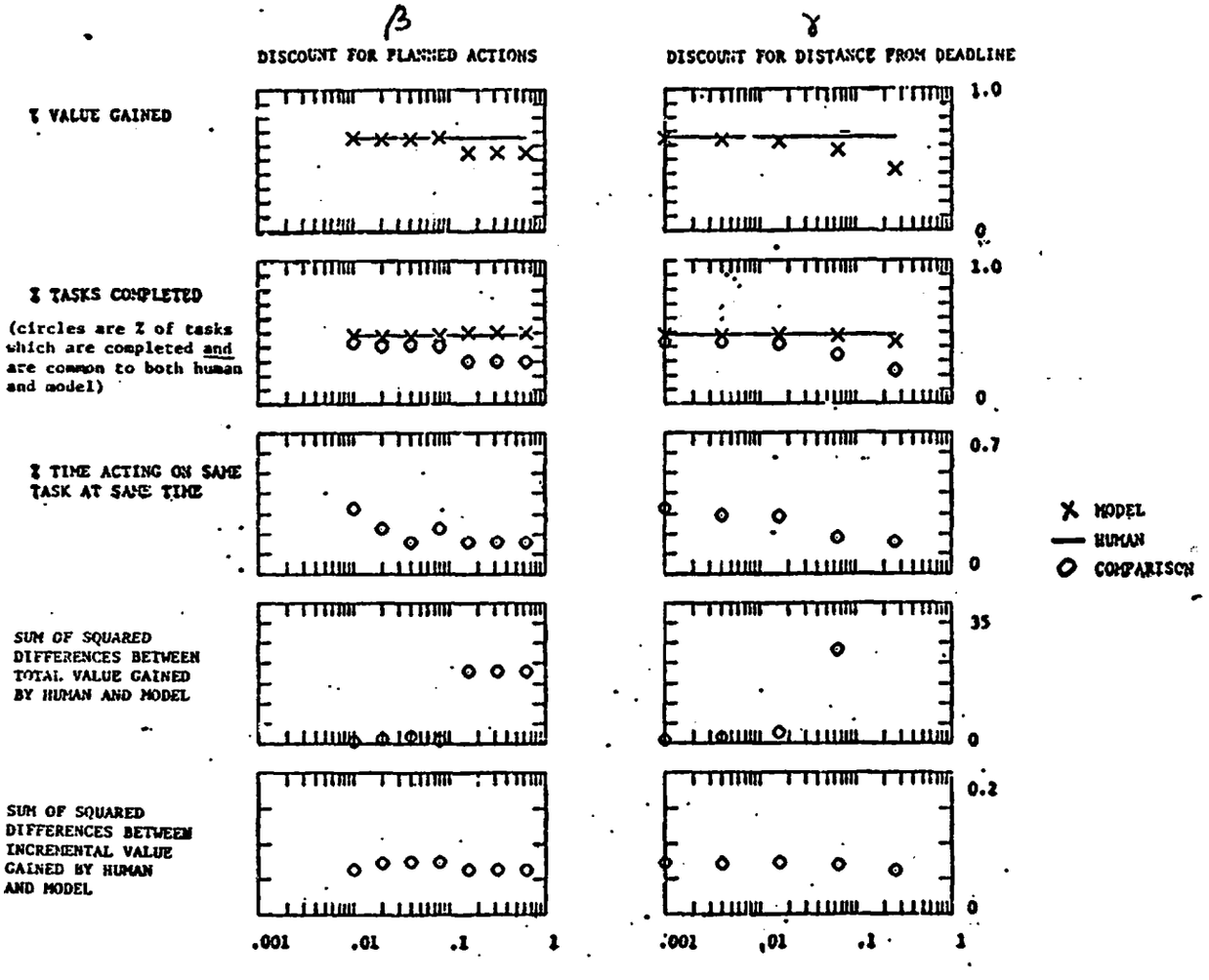

Figure 5. Condition 7
interarrival 20 sec/queue
speed 0.1 units/sec
productivity 0.25 units/sec
Subject: KT

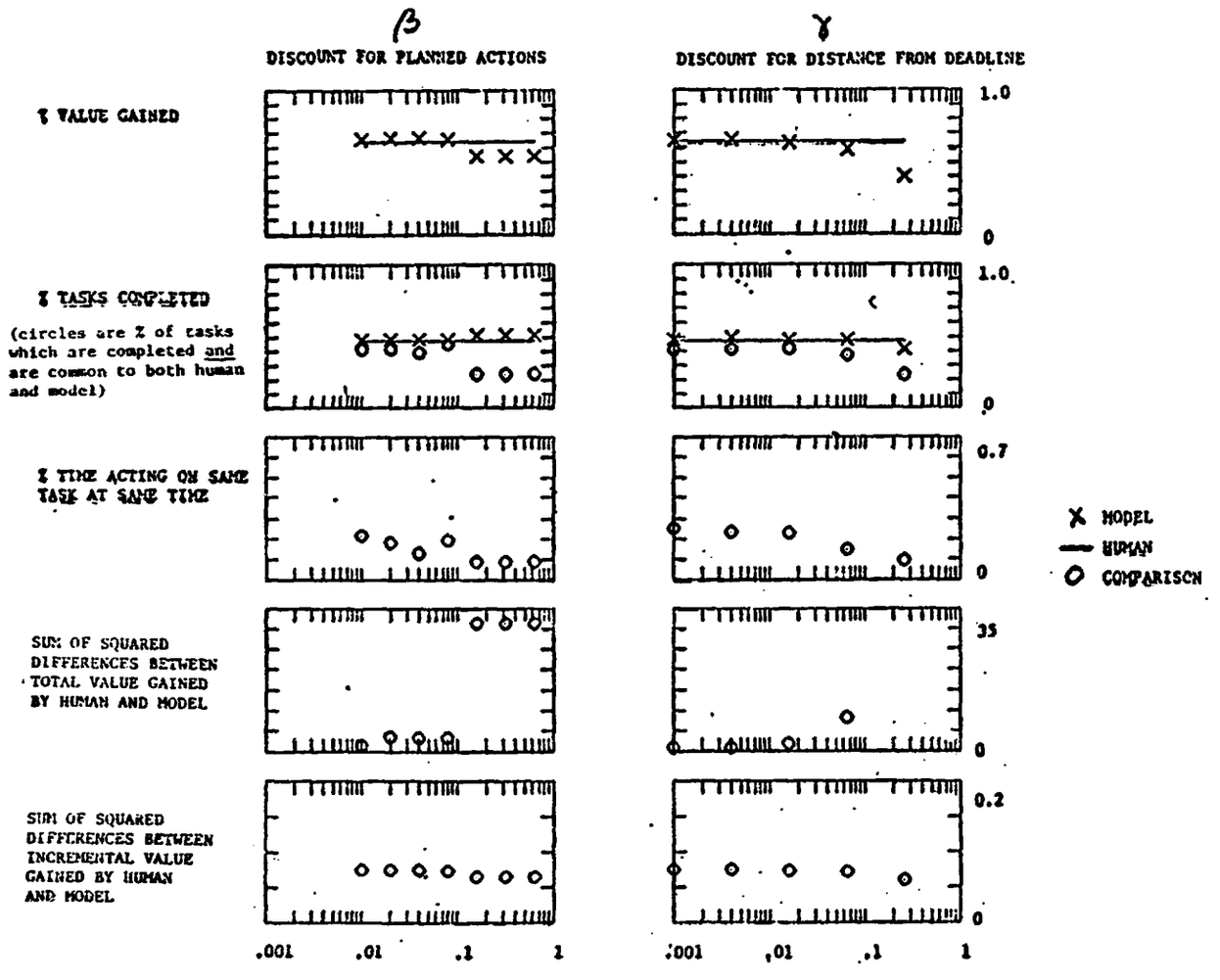

Figure 6. Condition 7.
interarrival 20 sec/queue
speed 0.1 units/sec
productivity 0.25 units/sec
Subject; DY

ORIGINAL PAGE IS
OF POOR QUALITY

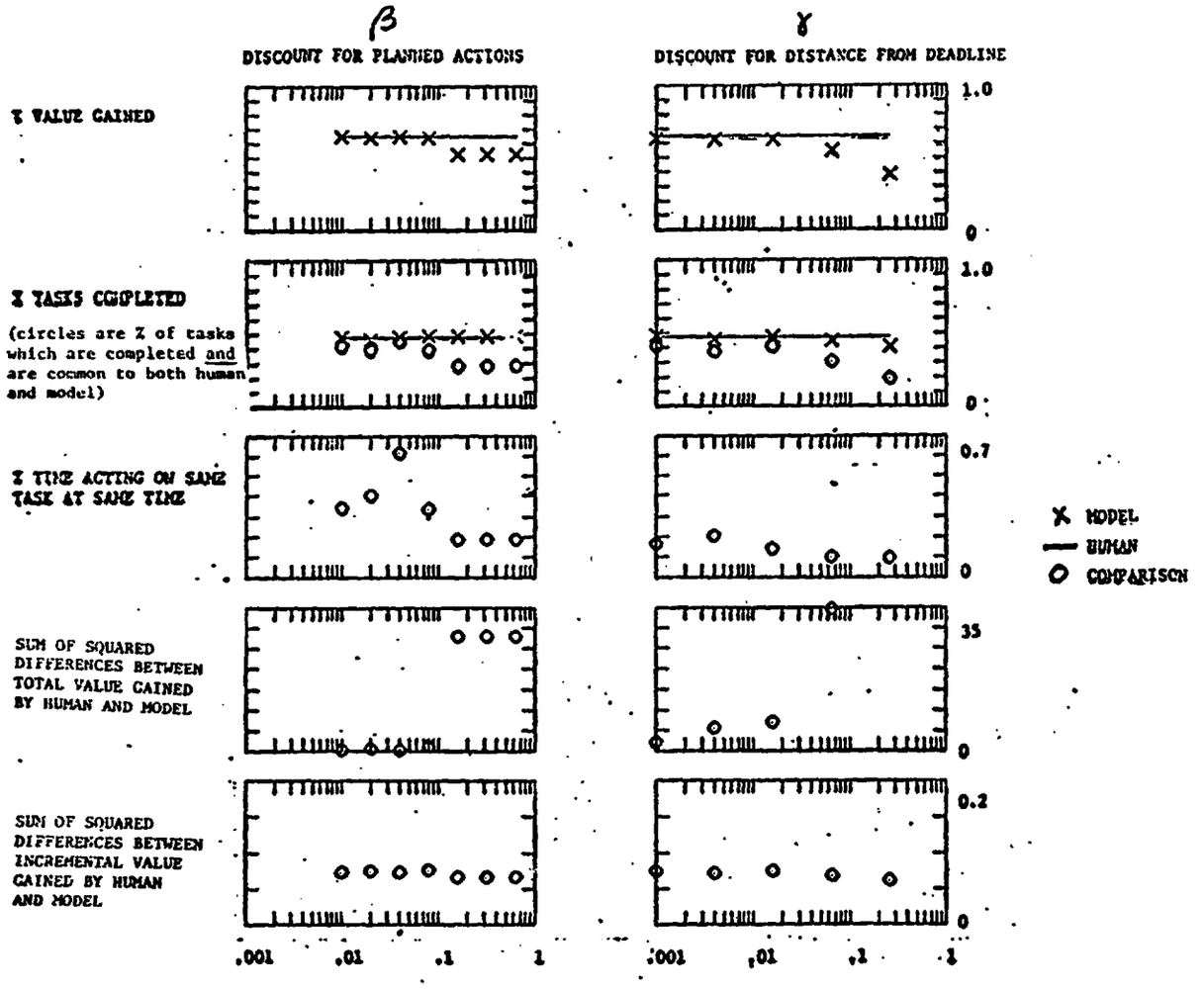

Figure 7. Condition 7.
interarrival 20 sec/queue
speed 0.1 units/sec
productivity 0.25 units/sec
Subject: SJ

far from the deadline, i.e., γ is large). Interestingly, however, for data on the first two pages zero β is not quite as good as a slightly larger β. The theoretical reason for this was discussed above, i.e., with a slight discounting of the future the model is more apt to do the most important block first, and be more open to new blocks which have high payoff.

In everyday terms, this suggests that a person with lots to do, little time to do it, and new tasks continually popping up with relatively short deadlines, should not plan too far ahead. Mostly he should do the most important thing first, ignoring the closest-to-deadline factor. As he has time to see what's coming farther into the future and doesn't expect many new opportunities to be popping up, he should plan ahead.

With respect to the second criterion (% tasks completed) it is interesting that the model and human match precisely in a mid range of β which is also the best match of model to human for tasks which are common to both model and human. This suggests (1) that a β in this range is a good candidate for a model, (2) that the higher task completion capability of the model in other β ranges, without concommitant increase in total value gained, meant it was wasting time on unimportant tasks. The γ fits for this criterion are not so good or so consistent, and we begin to see that γ seems not to be a very meaingful parameter.

As for the next parameter, % of time acting on the same task at the same time, it appears that the β curve peaks at approximately the same value for several of the subjects, but again the γ curve is not very interesting.

The curves for the final two criteria seem to have little to offer, except that the fourth curve consistently takes a jump (gets worse) for β values at 0.1 or larger.

Further experiments will seek to refine the model, the fitting criteria, and possibly add an estimator of future tasks to the optimization algorithm.

Appendix 1. The Model in Relation to Graph Theory*

The paradigm described in the paper will result in a graph $G_T(t) = G(N;A)$ with N nodes and A arcs, where each node represents a task and arcs represent the transfer properties between these tasks. Note that rewards associated with different nodes can be different and delay-(time-) dependent. Also the processing (or service) and availability times of the nodes and the transfer times between them can be different. Therefore in a reward-time (r-t) coordinate framework we have graph $G_T(t)$ as shown in Figure A1.

Note that in Figure A1 τ values represent transfer times between nodes, which incidentally can be direction-dependent, such that precedence constraints can be imposed. t^R, t^D and t^P are "ready-time", "deadline time" and "processing time", respectively. Note that when the rewards associated with the tasks are constant until they hit the deadline, the r-t curve associated with a node will be as shown in Figure-A2a. For the case in which the DM can get partial credit, however, the rewards, rather than being Fixed-Loss, will be as shown in Figure-A2b.

In the Figure A2 t^S is the slack time, i.e. the latest time; if, during which the task is completed all the reward associated with the task can be gained. Note that "time available" is deadline-time minus ready-time:

$$t^A = t^D - t^R.$$

One interesting observation that can be made from Figure-A1 is that in $G_T(t)$ graphs there may not be enough time to get the rewards of all nodes N. In fact, we can infer from the same figure that the best schedule that can be chosen in the particular graph $G_T(t)$ is $\Pi = (2,1,4)$ which does not include node (task) 3.

At this point we digress and consider this sequencing problem in relation to other common combinatorial problems like Job-Shop Scheduling, Traveling Salesperson, etc. (Golden and Magnanti, 1977).

We can differentiate the sequencing problems listed in Table-A1 according to the following criteria:

1) Will multiple journeys between the nodes be counted multiple?
2) Can we add extra nodes?
3) Can the rewards associated with the nodes be delay-dependent?
4) Can the transfer delays between different pairs of nodes be different?
5) Is it imperative to return to the base node?
6) Is it necessary to satisfy the above requirement before a certain delay, T_R?
7) Can the graph G, desribing the problem change dynamically in time?

*See list of symbols at end of Appendix 2.

ORIGINAL PAGE IS
OF POOR QUALITY

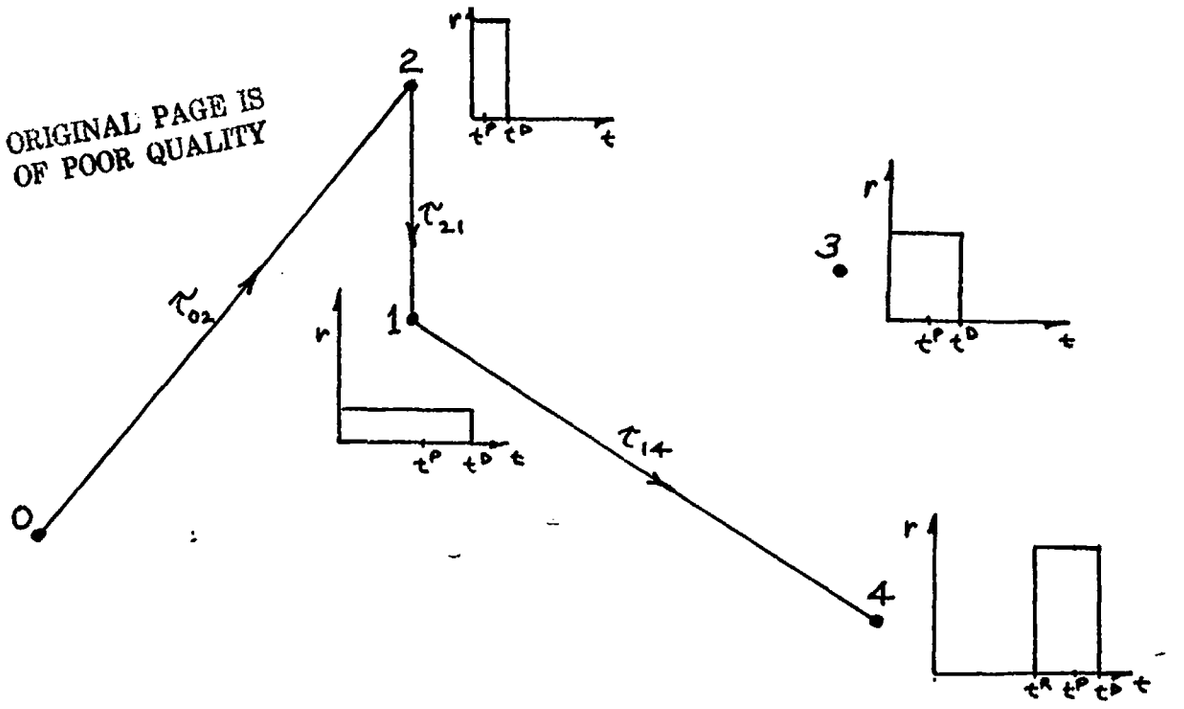

FIGURE A1. A Schedule π = (2,1,4) for Multi-Task Attention Allocation on Graph $G_T(t) = G (N ; A)$.

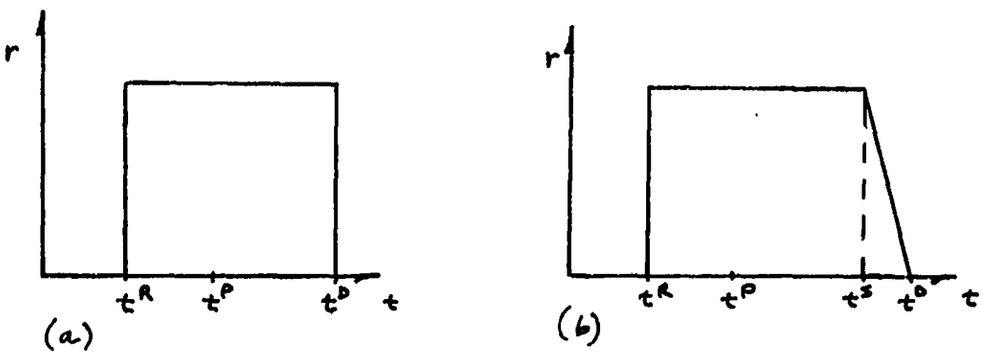

FIGURE A2 Reward-Time Curves for a Task (a) when no Partial Credit is Given, and (b) when Partial Credit is Given.

Using these criteria we have listed some common combinatorial optimization problems with two new ones:

a) Minimum Spanning Trees, MST (Kruskal, 1956)

b) Steiner Tree Problem, STP (Nijenhuis & Wilf, 1975)

c) Job-Shop Scheduling, JSS (Elmaghraby, 1968 and Sahni, 1976)

d) Hamilton Cycle, HC; alias the Traveling Salesperson Problem (Held & Karp, 1962)

e) Open Tulga-Path, OPT; alias Multi-Task Attention Allocation,

f) Closed Tulga-Path, CTP

Note that in Table-A1 the indicator '0' means that the particular criterion need not be satisfied for the problem at hand, while indicator '1' is for the opposite case, with 'N/A' indicating that the criterion is not applicable for the problem. Figure-A3 is a schematic representation of some of the problems. OTP describes Multi-Task Attention Allocation.

Problems vs. Criteria:	MST	STP	JSS	HC	OTP	CTP
1	0	0	1	1	1	1
2	0	1	N/A	N/A	N/A	N/A
3	0	0	1	0	1	1
4	1	1	0	1	1	1
5	0	0	0	1	0	1
6	0	0	0	0	0	1
7	0	0	0	0	1	1

Table-A1. Properties of Various Sequencing Problems.

Before returning to the Multi-Task Supervisory Control, the reader can observe from Figure-A3 that, if the requirement was to serve all the nodes (tasks) with minimum number of controllers (or processors or vehicles or people, etc.) another controller might have been assigned to node-3 in Figure-A3(iii), and the OTP problem will become an advanced version of the 'Bin-Packing Problem'. (Johnson, 1974) The reader may note here the case of computer aiding (2nd. controller) of the human operator (1st. controller). (Rouse, 1977) Similarly in Figure-A3(iv) an extra vehicle can serve node-3 and come back to the base node before T_R; however, unless the return time T_R is sufficiently large, node-4 cannot be served whatever the number of vehicles, but as T_R increases 3, then 2 vehicles will be enough to serve all the nodes: the CTP then becomes an advanced 'Vehicle-Routing Problem". (Golden, 1976)

We can see from Figure-A3 that Multi-Task Attention Allocation Paradigm is representable by the OTP Combinatorial Problem when we consider that node 0 (base node) is where the DM currently is, and 4 tasks

ORIGINAL PAGE IS
OF POOR QUALITY

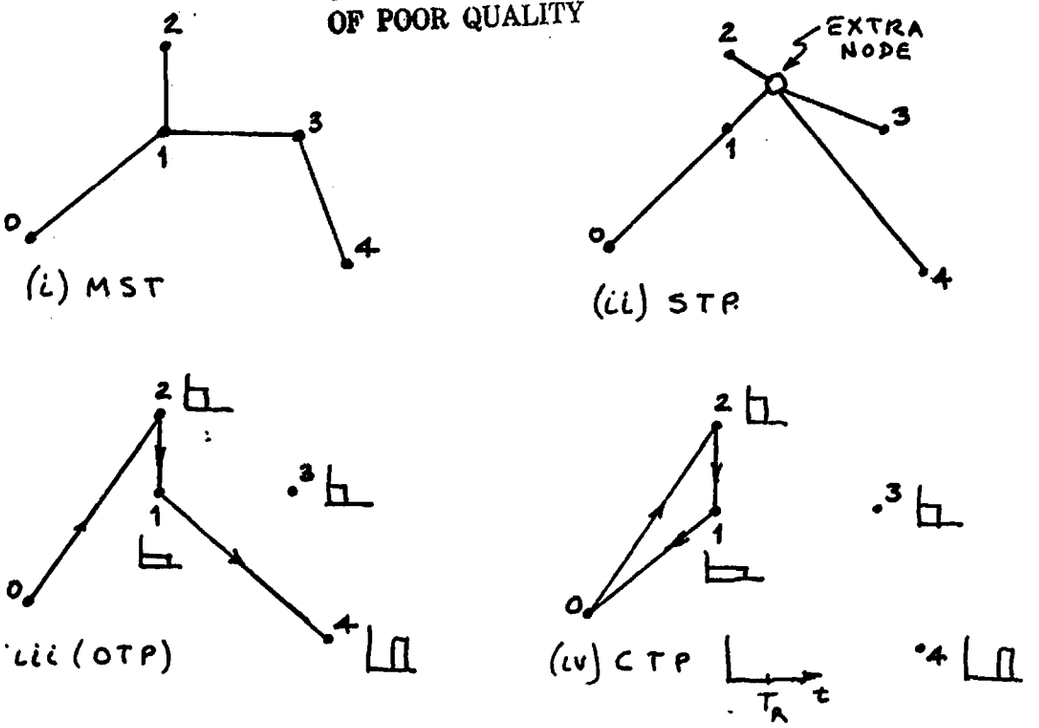

FIGURE A3 Graphical Representation of Some Sequencing Problems

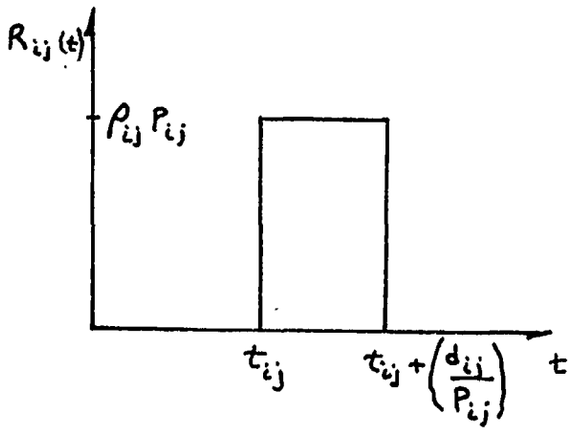

FIGURE A4. The Return, for a Task, as a Function of Time for the Partial Credit Mode

are (or will be) available with different properties. The DM will then act on the first task of the optimal schedule, $\Pi^\circ = (2,1,4)$, i.e. task 2.

Note however, that new tasks may appear on this graph $G_T(t)$ probabilistically according to the interarrival rates and with the task parameters explained in the paradigm section, and the thing to be maximized is the reward gained at the end of the experiment, so that tasks that are going to appear cannot be ignored. That is to say: since graph $G_T(t)$ is time-dependent, then the optimal schedules $\Pi^\circ(t)$ on them are time-dependent too.

Appendix 2. Optimization Algorithm of the Model

In choosing his control, i.e., which task to at upon, we can model the DM as an optimal controller who maximizes his expected returns over a planning horizon. (Koopmans, 1964). In particular, the DM will act to maximize his expected total returns over a finite planning horizon, T, with a discount function $B(\beta, t)$:

$$\max_{\Pi} \quad r(\Pi) = E\left[\int_0^T R_\Pi(t)\,dt \right]$$

where $$R_\Pi(t) = \sum_{(i,j)\in\Pi} R_{ij}(t) \cdot B(\beta, t)$$

in which the summation is over all the tasks (i,j), which collectively make up the ordered task set, schedule Π, that the DM expects to act upon over his planning horizon. $R_{ij}(t)$ is the return he gets for acting on (or completing) the task (i,j) during (or at) time t.

For the case in which the DM gets credit continuously while acting on a task, the $R_{ij}(t)$ will be as shown in Figure-A4.

In Figure-A4, t_{ij}, P_{ij}, d_{ij}, p_{ij} represent the time at which the DM plans to start acting on the task, the value density of the task, the duration of the task, and the productivity of the DM for the task (i,j), respectively.

If however, the DM is going to get (full) credit only after successfully completing a task, then the $R_{ij}(t)$ will be as shown in Figure-A5.

The DM, in effect, will choose at each decision point a schedule $\Pi^\circ = (\Pi_1^\circ, \Pi_2^\circ, \ldots)$ that he intends to act upon to maximize his expected returns, and then he will actually act upon the first task Π_1°, in this ordered set of tasks.

It is probable and acceptable that he might have to give up on acting on some tasks when their 'available times' are small - due to their high speed and/or due to their proximity to the deadline - or when they have comparatively low value densities, especially in compe-

ORIGINAL PAGE IS
OF POOR QUALITY

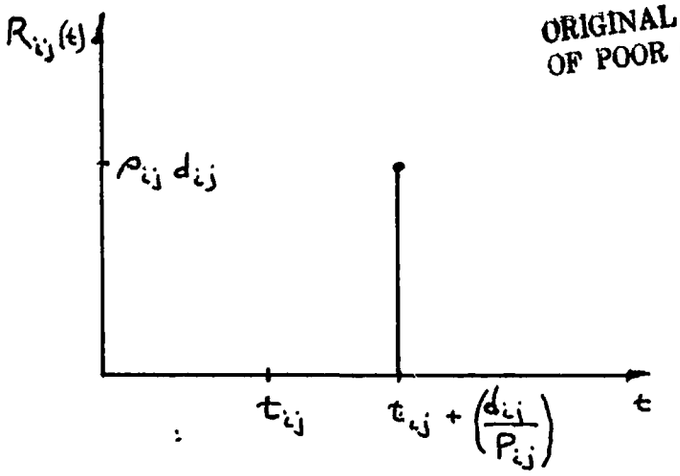

FIGURE A5. The Return, for a Task, as a Function of Time for the No-Partial Credit Mode.

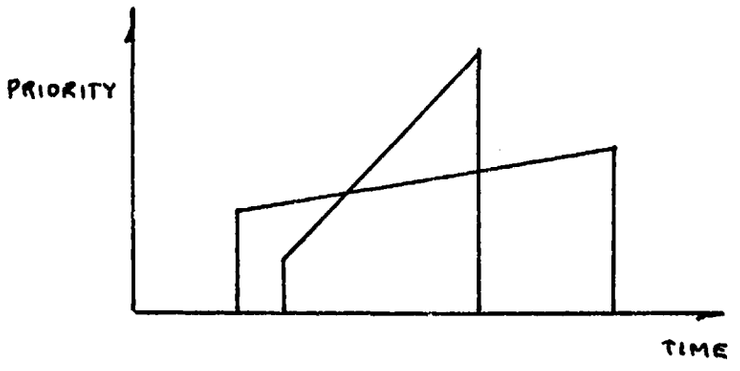

FIGURE A6. Increasing Priorities of Different Tasks as They Wait to be Served.

tition with other simultaneously available tasks which are preferred in these respects. Another important parameter, of course, is the transfer time $\tau_{ii'}$, between the queues. He has to consider the fact that he will end up getting no credit for a period of time when he transfers his control from the i.th queue to the i'.th one.

The algorithm for finding the optimal schedule of tasks Π°, to act upon is:

Algorithm T_PATH

Input (usage, T_R, $\tilde{X}_{ijk}$, $\tau_{ii'}$, B, G)

The input parameter 'usage' indicates whether an OTP or a CTP is desired, and if it is a CTP, T_R is used as the required return time to the base node. τ is the transfer-delay time matrix between the queues of tasks and B, and G are discount functions on future returns and on tasks away from the deadline-tasks with larger slack-times -, respectively.

Note that the system state tensor $\tilde{X}_{ijk}$ specifies the various task parameters for each given instant of time like:

1) whether the task is available (display) or not, L_{ij} (=1 or 0)
2) the return associated with the task as a function of time, $R_{ij}(t)$
3) the processing/service time of the task $t^{P}_{ij}(t)$
4) the 'available time' of the task, $t^{A}_{ij}(t)$

Output optimal schedule Π°, and discounted present value $r(\Pi^{\circ})$ and completion time $c(\Pi^{\circ})$ associated with it.

Step-1 [Initialize]

```
for i = 1 to I do
for j = 1 to J_i do
while L_ij = 1 do /* is the task available ? */
transform (i,j) to ℓ and
generate the tuple (r(ℓ), c(ℓ))

r(ℓ) = R_ℓ(t = 0)
c(ℓ) = τ_0ℓ + t^P_ℓ(t = 0)
end
end
```

Note that $R_{\ell}(t) = \int_{\tau=t}^{\infty} R_{ij}(\tau), B(\beta, \tau) \cdot d\tau$

Furthermore, the tasks currently available are summed to give N, which is also the maximum number of stages, M, the optimal schedule can have.

Step-2 [Generate schedules that are m stages deep]

ORIGINAL PAGE IS
OF POOR QUALITY

for m = 2 to M do

generate all m-member-subsets = S

and for each task $\ell \varepsilon S$
generate the $(r(\Pi)\ ,\ c(\Pi))$ tuple(s)
-where $\Pi = \{\Pi'\ ,\ \ell\}$, i.e. schedule Π is schedule Π' with task ℓ at stage m.
-for each $\Pi' = \text{order}\{S-\ell\}$, i.e. for each $\Pi' \overline{\equiv} \{S-\ell\}$,
-where the '$\overline{\equiv}$' operator tests whether each member of one set is also contained in the other. (Weinberg, 1971)

$$r(\Pi) = r(\Pi') + R_{\ell}(t = c(\Pi'))$$

$$c(\Pi) = c(\Pi') + \tau_{\ell'\ell} + t^{P}_{\ell}(t = c(\Pi'))$$

where ℓ', is the last task - task at stage (m-1) in schedule Π'.

Eliminate schedules according to the rules:

1) Eliminate the tuples which are infeasible, that is credit cannot be obtained from the last task ℓ in schedule Π before it reaches the deadline; or if usage is CTP, before $(T_R - \tau_{\ell o})$, where $\tau_{\ell o}$ is the transfer time between the queue of task ℓ and the base node 0.

2) Eliminate schedule Π^1, if there is a schedule Π^2, such that:

$$\Pi^1 \overline{\equiv} \Pi^2$$

and $\ell^1 = \ell^2$ or queue of ℓ^1 = queue of ℓ^2

-ℓs are the last tasks -at stage m- in the respective schedules-

and $r(\Pi^1) \leq r(\Pi^2)$

and $c(\Pi^1) \geq c(\Pi^2)$

3) Eliminate the schedules that are less than (m-1) stages deep.

end

Step-3 [Return to the base node if usage is CTP]

if usage = Closed Tulga-Path then
for all schedules Π do

$$r(\Pi) = r(\Pi) + R_{o}(t = c(\Pi))$$

$$c(\Pi) = c(\Pi) + \tau_{\ell o}$$

with ℓ being the last task of schedule Π.

end

Step-4 [Optimal]

The optimal schedule Π° is the one with the property:

$$r(\Pi^\circ) > r(\Pi) \quad \text{for all } \Pi \neq \Pi^\circ.$$

and if

$$r(\Pi^\circ) = r(\Pi) \quad \text{then } c(\Pi^\circ) < c(\Pi)$$

Note that when the rewards of nodes are delay-independent then this algorithm reduces to the dynamic programming formulation of the Traveling Salesperson Problem. (Held & Karp, 1962). On the other hand, when transfer delays between all tasks are equal and when rewards of all tasks are Fixed-Loss, i.e. constant up to a certain delay (time) and then zero, then the solution will reduce to Job-Shop Scheduling with Deadlines. (Elmaghraby, 1968 and Sahni, 1976).

Several things should be clarified at this point. First, if the model is permitted to get partial credit, as in Figure-A4, then the tasks which will hit the deadline before they can be complted will also be included in the optimization, although with their returns $R_{ij}(t)$ appropriately adjusted to reflect the gain that can be obtained from them before they disappear.

Another point that should be emphasized is that, since all the dynamics of the tasks are known a-priori by the algorithm (and also by the human), there is no need to repeat the optimization unless there is a new task arrival; when no new information is presented, the optimal plan, i.e., the currently optimal schedule will be followed in real time as the tasks in this linked list are completed. It has also been proven theoretically (McNaughton, 1959) that there is nothing to be gained by shifting attention from one task to another and back again, even in the case of no time penalties for doing so. On the other hand, if after a new task arrival the first task in the new optimal schedule is not the task that is currently being attended, then the model will pre-emptively leave the current task to serve the first task in the new optimal schedule. However, the task that was pre-emtively abandoned might still be in the new schedule, and conditions permitting may eventually be re-attended.

The effect of $G(\gamma, t^s)$ will be to adjust the return $R_{ij}(t)$ for acting on task (i,j), by changing the effective value density of the task (i,j) as:

$$R_{ij}(t) = R_{ij}(t) \cdot G(\gamma, t^s_{i,j})$$

where t^s_{ij} is the slack-time of the task, i.e., $t^s = \max\left\{0, \left[(x/\dot{x}) - (d/p)\right]\right\}$, with $x, \dot{x}, d, p$ representing the current position, speed, current duration and the productivity associated with the particular task, respectively.

Note that the idea of weighing tasks according to their initial priorities plus incremental priority increases as they wait in a queue (Carbonell, 1966 and Jackson, 1965), as shown in Figure-A6, corresponds to the $G(\gamma, t^s)$ function, where the initial priority is determined by the initial proximity of the task to the deadline, and this priority increases as the task approaches the deadline.

It is interesting to note also that, as the speeds of the tasks approach zero, i.e., the deadlines are at infinite future time - and if the transfer times between all the tasks are equal, then the DM is modeled to choose the new task to act upon, according to:

$$\max_{(i,j)} \rho_{ij} p_{ij}$$

This, of course is the familiar result from the Queueing Theory (Smith, 1956) when we consider the productivity of the DM, p_{ij}, as the service rate μ_{ij} and the value density of the task (i,j) ρ_{ij} as the negative cost per unit time delay c_{ij}:

$$\min_{(i,j)} c_{ij}\mu_{ij} \text{ where } c_{ij} < 0$$

List of Symbols

G	graph
t	time
τ	transfer time
τ	dummy time
r	reward available at a node (task)
R	reward gained for a given plan
Π	a schedule: $r(\Pi)$ total discounted return of a schedule; $c(\Pi)$ completion time of a schedule
Π°	that schedule which is optimal
T_R	deadline time for return to base node
T	planning horizon
B	discount function on future returns
β	discount parameter (rate in this case) on future returns
G	urgency discount function
γ	urgency discount parameter (rate in this case)
I	total number of queues
J_i	total number of tasks in queue i.
ℓ	combination of i & j for any task
ℓ	maximum number of stages that optimal schedule can have
m	stage index
d	duration
s	speed
ρ	value density
p	productivity
x	position

t^P processing time

t^R ready time

t^D deadline time

t^A available time

t^S slack time

References

Elmaghraby, S.E., "The One Machine Sequencing Problem with Delay Costs", J. Ind. Eng., Vol. 19, No. 2, p. 105-108, February 1968.

Golden, B.L. and Magnanti, T.L., "Deterministic Network Optimization: A Bibliography",Networks, Vol. 7, No. 2, p. 149-183, Summer 1977.

Golden, B.L., Ph.D. Dissertation, Sloan School of Management, M.I.T., 1976.

Held, M. and Karp, R.H., "A Dynamic Programming Approach to Sequencing Problems", J. SIAM, Vol. 10, No. 1, p. 196-210, March 1962.

Johnson, D.J., Ph.D. Dissertation, Mathematics Department, M.I.T., 1974.

Koopmans, T.C., "On Flexibility of Future Preference", in Human Judgements and Optimality", (eds. M.G. Shelly II and G.I. Bryan), John Wiley 1964.

Kruskal, J.P., Jr., "On the Shortest Spanning Subtree of a Graph and the Traveling Salesman Problem", Proc. Amer. Math. Soc., Vol. 7, No. 1, p. 48-50, February 1956.

McNaughton, R., "Scheduling with Deadlines and Loss Functions", Management Sci., Vol. 6, No. 1, p. 1-12, October 1959.

Nijenhuis & Wilf, Combinatorial Algorithms, Academic Press, 1975.

Rouse, W.B., "Human-Computer Interaction in Multitask Situations", IEEE Trans. Syst. Man and Cybern., Vol. SMC-7, No. 5, p. 384-392, May 1977.

Sahni, S.K., "Algorithms for Scheduling Independent Tasks", J.ACM, Vol. 23, No. 1, p: 116-127, Jan. 1976.

Smith, N.E., "Various Optimizers for Single-Stage Production", Naval Res. Logist. Quart., Vol. 3, No. 1, p:59-66, Mar. 1956.

Weinberg, P., "Betriebswirtschaftliche Iogik", Bertelmans Universitaetsverlag* Duesseldorf, 1971.

D40

N79-15628

PERCEPTUAL FACTORS INVOLVED IN PERFORMANCE OF AIR TRAFFIC CONTROLLERS USING A MICROWAVE LANDING SYSTEM

Gary Gershzohn*
San Jose State University Foundation
San Jose, Calif.

SUMMARY

This study investigated performance of air traffic controllers using a Microwave Landing System (MLS). Eight professional radar air traffic controllers acted as subjects and performed their normal duties within the constraints of the experimental design and simulation. The task involved the control of two simulated aircraft targets per trial, in a 37.0-km (20-n. mi.) radius terminal area, by means of conventional radar vectoring and/or speed control. The goal was to insure that the two targets crossed the Missed Approach Point (MAP) at the runway threshold exactly 60 sec apart. The effects on controller performance of the MLS configuration under wind and no-wind conditions were examined.

The data for mean separation time between targets at the MAP and the range about that mean were analyzed by appropriate analyses of variance. Significant effects were found for mean separation times as a result of the configuration of the MLS and for interaction between the configuration and wind conditions. The analysis of variance for range indicated significantly poorer performance under the wind condition. These findings are believed to be a result of certain perceptual factors involved in radar air traffic control (ATC) using the MLS with separation of targets in time.

INTRODUCTION

This study was designed to investigate some of the perceptual factors which affect performance of air traffic controllers using an MLS to control the landing of aircraft. The MLS is a new type of landing guidance aid and is still in an experimental phase. When fully operational its primary purpose will be to facilitate the safe an expeditious flow of a new generation of aircraft into airports with an efficiency that cannot be duplicated today. The implementation of the MLS will require an alteration of the physical structure of airways and the ATC system.

A radar scope was simulated on a cathode-ray tube (CRT) and displayed

---

*This author's research was supported by NASA Grants NGL 05-046-002 and NSG-2269 to San Jose State University.

a terminal area with the MLS. The controllers were presented with several air traffic situations and were required to separate targets. The experimental goal was to identify some of the perceptual factors involved in and the performance of controllers using the MLS.

Although the MLS is one of the most recent developments in ATC, and as such has not been the subject of lengthy investigation, research in aeronautics has placed considerable emphasis on developments in human factors aspects of ATC. The literature contains numerous reports on topics such as mental processes of controllers (1), workload (11), and the role of automation (10). The general picture of the evolution of ATC responsibilities and required performance has also been outlined (8, 9). By and large, data on basic human perceptual processes specifically involved in ATC has received only scant attention. Therefore, this study, in part, examined pertinent psychological literature on visual motion perception in order to analyze performance of controllers using the MLS.

METHOD

The geometric arrangment of the MLS as viewed on the radar scope is significantly different from conventional Instrument Landing Systems. Whereas current Instrument Landing Systems employ a single, straight course to the runway, the complex MLS in this experiment was composed of five courses, both straight and curved. In order to evaluate the effects of this particular configuration on controller perception and performance, a specific task was developed.

Subjects

Eight professional air traffic controllers served as paid participants. All had extensive experience in radar ATC either with the military or FAA at high traffic density locations.

Apparatus

A 25.4- by 25.4-cm (10- by 10-in.) CRT display was generated by an Evans & Sutherland Line Drawing System interfaced with a Digital Equipment Corporation PDP 11/40 computer. Figure 1 illustrates the simulation that represented the ATC scope with the MLS. The scale of 2.9 km/cm (4 n. mi./in.) was close to standard usage.

Aircraft targets were represented by triangles measuring .45 cm (.18 in.) on each side. Each symbol was labeled by a single alphanumeric tag for use by the controller in identifying and tracking targets. The targets appeared to move in a manner not unlike those on conventional radar ATC scopes. Simulated aircraft had several basic movement capabilities: (a) entry along an MLS route at the periphery and complete tracking to the MAP, (b) automatic landing and exit from the display at the MAP, (c) heading change at a rate of 3^{o}/sec, and (d) acceleration at a rate of 3.7 km/hr

(2 knots)/sec (equivalent to .0003 cm/sec^2 on the CRT). Altitude information was not required for this experiment.

The computer generated movement of targets was controlled by the subject. His verbal commands were transmitted by a standard microphone. Receiving and acknowledging these ATC instructions was the experimenter in the role of pilot of the simulated aircraft. Communication between the controller and experimenter reflected standard ATC operations and phraseology. Upon receipt of the controller's commands, the experimenter input the information to the PDP 11/40 computer via a high speed interface device which then altered the flight dynamics of the simulated aircraft accordingly.

Procedure

The task required that the controller control two targets per trial in order to achieve the desired goal of 60-sec separation between targets at the MAP. At the beginning of each trial one target appeared at the start of the VIKING route at the 37.0-km (20-n. mi.) hash mark at an airspeed of 464 km/hr (250 knots). It was followed approximately 60 sec later by a second target at the same airspeed which entered either along the VIKING route or one of the other four MLS routes. Since the second target traversed one of the five routes in following the first target, there were five different perceptual relationships between the two targets. These will be called path combinations of target movement. For example, a target entering on the VIKING route followed by a target on the GEMINI route would be called the VIKING-GEMINI (V-G) path combination.

The controller was instructed to adjust the movement of one or both targets by use of speed and/or directional control in order to insure that the two targets crossed the MAP exactly 60 sec apart. Each target automatically reduced its airspeed to 167 km/hr (90 knots) by the time it reached the 9.3-km (5-n. mi.) fix; this was in keeping with normal aircraft operating limitations. The airspeed of 167 km/hr (90 knots) was then maintained to the MAP. As the controller perceived the continuing relationship between the targets, he had to make a decision to issue or not to issue ATC instructions to change the relative movement or position of one or both in order to reach the goal of 60-sec separation. The airspeed and heading of either target could be changed only during the time that target was between the 37.0-km (20-n. mi.) fix and 9.3-km (5-n. mi.) fix; the controller had received instructions that no control was to be applied to a target after it had passed the 9.3-km (5-n. mi.) fix. When the second target reached the MAP the trial was at an end. The actual separation in seconds was recorded by the computer and used as the raw data for that trial. In order to measure performance in several situations, trials were conducted under wind (360^0 at 46 km/hr (25 knots)) and no-wind conditions.

An introductory session familiarized the controller with the general nature of the experimental purposes and MLS. Written instructions were supplied. Three practice trials with no-wind and three with wind before the respective experimental trials were used for the purpose of acquainting the controller with the appearance of the MLS and movement dynamics of targets. At the conclusion of each practice trial, the controller was told exactly how much separation in time existed between the two targets as they successively

crossed the MAP. This gave the controller an indication of the spatial and temporal relationships between targets under his control. This feedback, however, was not given during experimental trials.

Experimental Design

Two dependent variables were studied: (a) the mean separation time between targets at the MAP, and (b) the average range about that mean. A 5 X 2 X 2 factorial design for repeated measures was used to analyze the data. The five path combinations served as five levels of one independent variable. Two wind conditions constituted conditions of a second independent variable and the order of presentation of wind conditions was the third independent variable. The wind treatment condition was presented first to one half of the controllers and the reverse order was administered to the other half. There were 15 experimental trials under the no-wind condition and another 15 under wind. The same path combination was administered to each controller three times.

RESULTS AND DISCUSSION

The mean of the three separation times for each controller was calculated and constituted the data on which the analysis of variance was performed. For the purpose of noting the variability of controller performance, a second analysis of variance was performed on the range of the separation times per subject. Results of the analysis of variance for means are shown in Table 1 and for range in Table 2. A summary of the means and average ranges for each condition is presented in Table 3 and Table 4, respectively.

The effect of the order of presentation of wind conditions was not statistically significant. Therefore, for the purpose of analysis of other results, these data were combined.

The analysis of variance for means showed a significant difference between path combinations ($F = 3.84$; $df = 1, 10$; $p < .05$). This indicated that controller performance in attaining 60-sec separation between targets was affected by the different path combinations. The analysis of variance for range did not indicate any significant effects ($F = .98$; $df = 4, 24$; $p > .05$) due to different path combinations (fig. 2).

The mean separation times between targets under the no-wind condition (60.6 sec) and under the wind condition (57.0 sec) were close to the 60-sec target value, yet the magnitude of the average range of times about these means was quite large (fig. 2 and 3). Under the no-wind condition, the average range was 19.6 sec, and under wind, 43.2 sec. The analysis of variance for range showed a statistically significant difference in controller performance as a function of wind condition ($F = 12.42$; $df = 1, 6$; $p < .05$). The analysis of variance for means revealed no significant results ($F = .48$; $df = 1, 6$; $p > .05$). While the overall mean separation time between targets under the no-wind and wind condition were not significantly different, the average ranges about these means were. Both the no-wind and wind mean times indicated a high degree of accuracy on the average in attaining the 60-sec

target value. But the 19.6 and 43.2 sec ranges showed the accuracy reflected in the mean times to be a result of the high separation times between targets cancelling out the low separation times, especially under the wind condition.

These results will be discussed from three points of view: (a) the perceptual factors involved in performance of controllers using the MLS, (b) controller performance using time as a relevant separation criterion rather than distance, and (c) the implications of the findings for future development of the ATC system with the MLS.

The controller's perception of the ATC situation constitutes an important factor in understanding the results. Three primary perceptual factors are considered to be of importance in the controller's task in this experiment: (a) spatial separation of targets, (b) figure-ground (map overlay) effects, and (c) the perception of wind-generated accelerated motion. The latter point appeared to be most significant in evaluating the data and requires special consideration.

The mean separation time under the no-wind condition was closer to the 60-sec target value than under the wind condition. This was due primarily to the controller's difficulty in taking into account the differential effects of wind on ground speed as the target changed heading. The difficulty in perceiving the onset of of accelerated motion had several consequences for controller performance. First, the reduction of the ground speed of a target, either in the automatic speed reduction phase of the approach or as a result of the wind, altered the separation between it and the other target. Should the velocity change have gone undetected, the result would have been a new amount of separation between targets of which the controller was completely unaware. Obviously, a continuous series of such changes by one or both targets would lead to inaccurate and erratic performance such as was evident under the wind condition. Second, the perception of acceleration of one or both targets required an evaluation by the controller of the actions necessary to maintain or change the relationship between the targets. This necessitated the ability to make an accurate prediction of the future progress of the target undergoing acceleration. It has been shown by Gottsdanker (4-6) and Gibson (3) that future target position during constant velocity motion can be predicted with considerable accuracy. However, predicting target position during accelerated motion was found to be generally inaccurate and appeared to be based on the last perceived velocity rather than on acceleration (2, 7). The apparent inability of the controller to successfully predict the accelerated motion of targets, and hence future positions in time, was associated with high variability in performance. Third, the changes in ground speed of a target traversing that part of the MLS course that curved toward the airport were difficult to assess. The controllers reported that the point in time when the ground speed began to slow was not immediately apparent nor was it possible to accurately predict the future motion of targets: The large magnitude of the change in ground speed in those MLS courses with long curved segments made accurate perceptions difficult and inaccurate performance most evident in the results. The accelerations that occurred within the curving courses were most significant under the wind condition and posed a situation which the controllers were unable to gauge precisely.

On the basis of discussions with the controllers after the experiment, it would appear that the controllers' attempt to separate the two targets by

60 sec at the MAP was not accomplished merely by estimating time. Rather, they used a time-distance conversion (distance = airspeed x time). This was not surprising since controllers perform their normal ATC duties using mileage not time as the separation criterion, and consequently they were faced with a novel and difficult task.

Two factors involving time and distance conversions were involved. The first concerned a principle that specific separation in time between two targets will remain constant if the ground speeds of the two targets remain unchanged. Secondly, separation in time will remain constant when ground speeds change if, and only if, the place and rate of change of ground speed of one target is identical to that of the other. The realization of these phenomena led to another point. Since time separation was held constant between the targets during the automatic speed reduction (under conditions heretofore described), the establishment of 60-sec separation between targets prior to the commencement of the speed reduction (which entailed accelerated motion) was seen as desirable. Once the automatic speed reduction began, the controller had no means of adjusting the airspeed of a target. This required action to be taken earlier in order to have control capability of a useful and realistic magnitude and to set up a relationship between the two targets when they proceeded at a constant velocity. Since the judgment of constant velocities is more accurate than accelerated velocities, the controller was able to judge the separation in time more precisely when targets moved at constant rates.

The results of the present experiment indicate that the control of aircraft using an MLS with curved courses and temporal separation may be subject to a number of limiting factors. The different path combinations had an effect on both the mean separation between targets and the variability of the controller's performance under the wind condition. Under the no-wind condition, there was little difference in performance by path combination. The controllers' comments indicated that they attributed this to their careful and precise attention to the position of the targets with reference to hash marks and the calculation of time-distance equations. The wind condition posed more serious difficulty since the use of hash marks and the time-distance equation did not provide information which could be used to compensate for the perceptual factors associated with the wind.

In consideration of the perceptual factors involved in controller performance, it seems unlikely that the addition of any appreciable workload (in the form of more targets) would permit positive and accurate control. One of the most important influences on performance is workload. It may be measured by the number of targets a controller has to deal with at one time. By current standards in the current ATC system, with complicating intersecting and converging routes, a light workload might be five targets; a heavy workload might reach as high as 15 targets. In this experiment, which employed only two targets at one time, the workload was minimal yet the variability in performance with wind was high. This was true in spite of the fact that the controller had enough time to calculate time-distance relationships for the two targets. With more than two targets, it is not likely that the controller would be able to maintain the mental strategies of control found in this experiment. Furthermore, an increase in workload that would reflect a busy terminal area would make accurate and successful separation between aircraft, with time as the separation criterion, a most unlikely occurrence.

Yet, innovations in ATC systems, cockpit displays, and possible alterations of the MLS configuration may alleviate some of the problems that faced controllers in this simulation. Such improvements may allow conventional radar ATC using the MLS with a real world workload.

REFERENCES

1. Bisseret, A.: Analysis of Mental Processes Involved in Air Traffic Control. Ergonomics, vol. 14, 1971, pp. 565-570.

2. Filion, R. D. L.: On the Visual Detection of Accelerated Motion. Unpublished doctoral dissertation, Princeton Univ., 1964.

3. Gibson, J. J.: Research on the Visual Perception of Motion and Change. In Second Symposium on Physiological Psychology. Office of Naval Research: 1958.

4. Gottsdanker, R.: The Accuracy of Prediction Motion. J. Exp. Psych., vol. 43, 1952, pp. 26-36.

5. Gottsdanker, R.: A Further Study of Prediction Motion. Amer. J. Psych., vol. 68, 1955, pp. 432-437.

6. Gottsdanker, R.: The Ability of Human Operators to Detect Acceleration of Target Motion. Psych. Bull., vol. 53, 1956, pp. 477-487.

7. Gottsdanker, R; Frick, J.; and Lockard, R.: Identifying the Acceleration of Visual Targets. Brit. J. Psych., vol. 52, 1961, pp. 31-42.

8. Litchford, G.: Aeronautics and Air Traffic Control. NASA CR-1833, 1971.

9. Roberts, L.: Future Trends in Air Traffic Control Technology. Paper presented at the 19th Conference of the International Air Transport Association (Dublin, Ireland), 1972.

10. Secretariat of the 19th Conference of the International Air Transport Association: An Assessment of the Expected Aircraft Movement Demand on Typical Air Routes and for Representative Terminal Areas, and the Consequent Impact on Air Traffic Handling Capabilities. Paper presented at the 19th Conference of the International Air Transport Association (Dublin, Ireland), 1972.

11. Sperandio, J.: Variations of Operator's Strategies and Regulating Effects on Workload. Ergonomics, vol. 14, 1971, pp. 571-577.

TABLE 1

Analysis of Variance for Mean Separation Time Between Aircraft Targets at the MAP

Source	df	MS	Error Term	F
Order of presentation of wind condition (A)	1	18.15	D	.03
Path combination (B)	4	589.68	B X D	3.83[a]
Wind condition (C)	1	258.13	C X D	.48
Subjects (D)	6	655.18		
A X B	4	46.23	B X D	.31
A X C	1	200.66	C X D	.37
B X C	4	532.82	B X C X D	6.48[b]
B X D	24	163.66		
C X D	6	542.16		
A X B X C	4	63.02	B X C X D	.77
B X C X D	24	82.19		

[a] $p < .05$

[b] $p < .01$

ORIGINAL PAGE IS
OF POOR QUALITY

TABLE 2

Analysis of Variance of Range About Mean Separation Times between Aircraft Targets at the MAP

Source	df	MS	Error Term	F
Order of presentation of wind condition (A)	1	68.45	D	.07
Path combination (B)	4	556.32	B X D	.98
Wind condition (C)	1	11,092.05	C X D	12.42[a]
Subjects (D)	6	929.25		
A X B	4	451.45	B X D	.80
A X C	1	344.45	C X D	.39
B X C	4	551.98	B X C X D	1.03
B X D	24	565.02		
C X D	6	892.91		
A X B X C	4	178.89	B X C X D	.33
B X C X D	24	536.10		

[a] $p < .05$

TABLE 3

Summary of Mean Separation Times (in seconds) between Aircraft Targets at the MAP by Path Combination and Wind Condition

Path combination	Wind condition		
	no-wind	wind	across no-wind/wind
V-V	62.6	71.5	67.1
V-G	58.1	56.2	57.1
V-A	59.1	41.4	50.2
V-P	65.4	52.4	58.9
V-M	57.7	63.4	60.6
Across all path combinations	60.6	57.0	58.8

ORIGINAL PAGE IS
OF POOR QUALITY

TABLE 4

Summary of Average Ranges (in seconds) about Mean Separation Times between Aircraft Targets at the MAP by Path Combination and Wind Condition

Path combination	Wind condition		
	no-wind	wind	across no-wind/wind
V-V	19.1	24.8	21.9
V-G	20.9	54.5	37.7
V-A	20.1	42.9	31.5
V-P	24.0	45.1	34.6
V-M	14.1	48.8	31.4
Across all path combinations	19.6	43.2	31.4

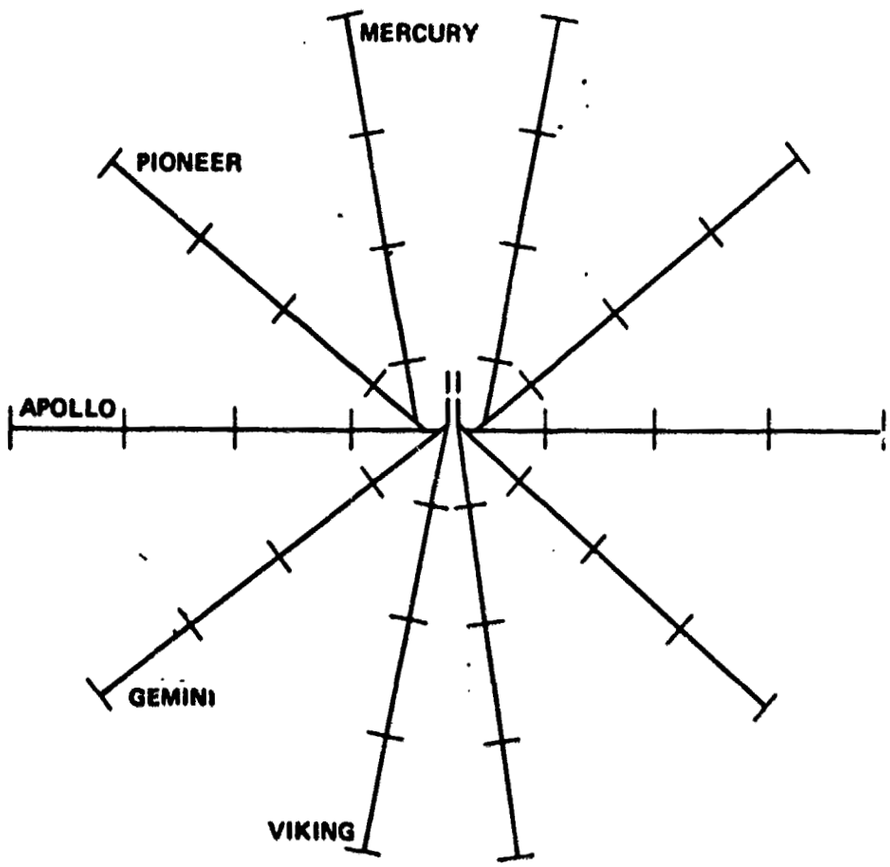

Figure 1.- MLS route configuration as seen on controller's display.

ORIGINAL PAGE IS
OF POOR QUALITY

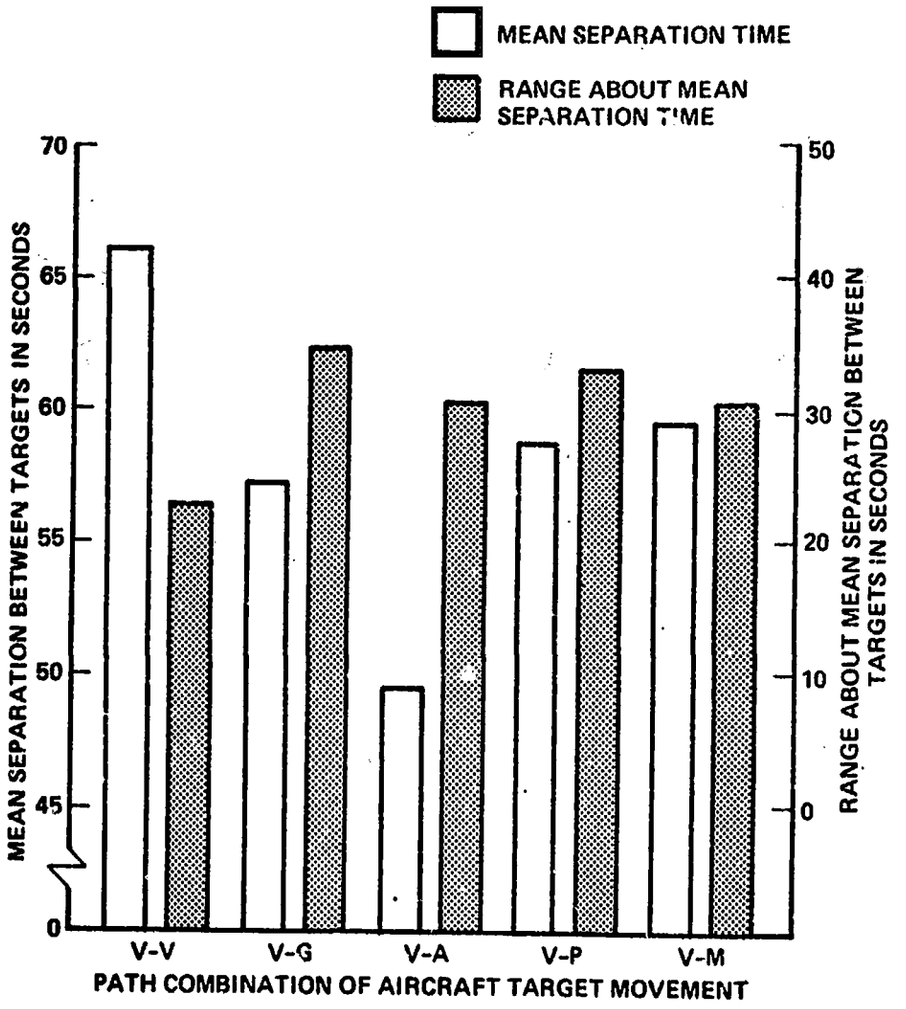

Figure 2.- Mean separation time and range about mean separation time between aircraft targets at the MAP by path combination.

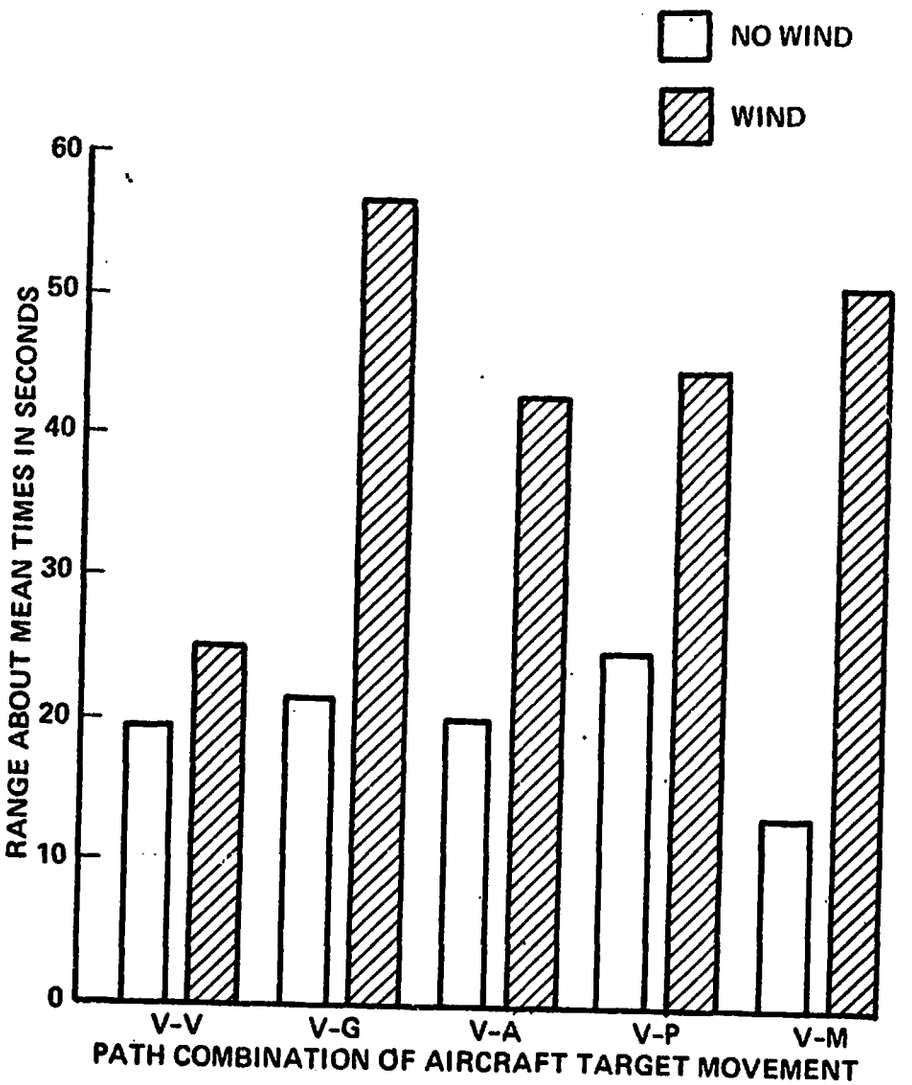

Figure 3.- Average range about mean separation time between aircraft targets at the MAP by path combination and wind condition.

SESSION K: DECISION-MAKING BEHAVIOR AND MODELING

Chairman: R. Curry

N79-15629

THE EFFECTS OF ALCOHOL ON DRIVER PERFORMANCE IN A DECISION MAKING SITUATION*

By R. Wade Allen, Stephen H. Schwartz,
Anthony C. Stein and Jeffrey R. Hogge

Systems Technology, Inc.
Hawthorne, California

ABSTRACT

This paper reviews the results of driving simulator and in-vehicle field test experiments of alcohol effects on driver risk taking. The objective was to investigate changes in risk taking under alcoholic intoxication and relate these changes to effects on traffic safety.

The experiments involved complex 15 minute driving scenarios requiring decision making and steering and speed control throughout a series of typical driving situations. Monetary rewards and penalties were employed to simulate the real-world motivations inherent in driving. A full placebo experimental design was employed, and measures related to traffic safety, driver/vehicle performance and driver behavior were obtained.

Alcohol impairment was found to increase the rate of accidents and speeding tickets. Behavioral measures showed these traffic safety effects to be due to impaired psychomotor performance and perceptual distortions. Subjective estimates of risk failed to show any change in the drivers' willingness to take risks when intoxicated.

INTRODUCTION

Alcohol has been shown to be overrepresented in accident statistics (Refs. 1 and 2). Recent surveys have subdivided accident causation into a variety of factors including vehicle, environmental and driver factors (Ref. 3). Driver behavior can be further subdivided roughly into perception, psychomotor skill and higher cognitive factors including decision making. Alcohol effects on driver psychomotor skill in steering control have been previously studied in some detail (Ref. 4), and the objective of the work reported here was to investigate the alcohol impairment in driver decision-making situations.

*This work was supported by the Office of Driving and Pedestrian Research, National Highway Traffic Safety Administration, Department of Transportation. The views expressed in this paper are those of the authors and do not necessarily represent those of the National Highway Traffic Safety Administration.

608 PAGE INTENTIONALLY BLANK

An important aspect of this research was to determine whether driver risk taking changes with Blood Alcohol Concentration (BAC) and, further, to partition the changes in risk taking into changes in driver perception, psychomotor factors and the acceptance of risk. These three factors combine to determine performance in a decision-making task and, singly or in combination, give rise to performance that we objectively observe as risk taking. Take, for example, the situation where a driver has run a red light. This could be due to the driver's having misperceived his speed or the time interval of the amber light; it could also be due to the fact that he took too long in making a decision and thus his reaction time for accelerating or braking to a safe stop was delayed; or the driver may merely have elected to accept the risk of running a red light because he was motivated to minimize the delays caused by stopping.

In previous research on driver risk taking, no consistent approach has been used to differentiate between the various factors contributing to decision task performance. Several studies have measured driver risk taking, which has been found to increase with BAC (blood alcohol concentration) (Refs. 5-7). More recently, however, it was found in a gap acceptance task using significant rewards and penalties that intoxicated subjects did not consciously accept greater risks (Ref. 8). Impaired psychomotor skill did result in degraded performance, however.

The inconsistency in past research has been in the definition and simulation of driver risk taking, the analysis of all behavior components in risk taking, and the use of tangible risks. Based on a review of the literature, the following elements were felt to be essential to adequately determine the effects of alcohol on driver decision making: 1) division of driver behavior into perceptual, psychomotor and cognitive components; 2) use of rewards and penalties to simulate real-world risks (e.g., accidents, tickets, lost time); 3) use of tasks which simulate the temporal pressure of normal driving. The experimental methods for accomplishing these goals are discussed below.

EXPERIMENTAL METHODS

Approach

This research was accomplished in two separate experiments, the first a simulator study and the second involving field validation trials. The two experiments were designed to be as similar as possible in order to allow direct comparison of results. The specific setup for each was as follows.

Simulation. The simulation was configured to present a plausible driving scenario, requiring both steering and speed control in driving decision-making situations. The functional details of the simulation have been described previously (Ref. 9). Basically, the simulator consisted of an actual car cab and controls with a two lane roadway drawn on a 0.25 x 0.32 m

(10" x 12")* CRT mounted on the cab cowl 0.76 m (30 in.) in front of the driver as illustrated in Fig. 1. Equations of motion for the car steering and speed control were solved on an analog computer, which generated car heading angle, lateral position, and forward speed in response to steering wheel, accelerator and brake commands. The car motion variables drove special purpose electronic circuits which generated a dashed line two lane roadway [3.65 m (12 ft) lane width] with 0.76 m (2.5 ft) shoulders. The roadway was presented in correct perspective, but reduced scale (roughly two-thirds) in order to fit on the CRT and yet subtend a 22 degree perceptual field of view.

Driving events were controlled by a paper tape programmer at a rate proportional to forward speed. From a cross section of the many typical driving decision-making situations three events were selected that could be easily implemented in a laboratory simulation. The functional details of each event and related measurements are described further on.

Field Validation. This study was conducted in an instrumented vehicle described elsewhere (Ref. 10). Special equipment was added to allow the car to interact with the test course. A photo detector mounted on the vehicle sensed reflective strips on the test course and triggered a programmer which controlled event sequences in the field course driving scenario. Instrumentation was also added to allow experimenter feedback in scenario conditions and subject progress. Details of the field setup are illustrated in Fig. 2.

Driving Tasks and Measurements

The driving scenario was designed to allow implementation both in the simulator and on the field course. A variety of events were considered, and events that could be conveniently mechanized were selected for each experiment as indicated in Table 1 (Ref. 11). A signal light situation was selected as a classical single stage decision event. Vehicle control in a curve was selected to investigate the large number of single vehicle loss of control accidents that occur with alcohol involvement (Ref. 12). The remaining situations selected from Table 1 involve divided attention, a driver behavior factor which has been shown to be sensitive to alcohol impairment (Ref. 13). Details of the driving tasks and overall scenario were as follows.

Signal Light. A model signal light was mounted directly above the horizon of the roadway display in the simulator (Fig. 1a), and an actual signal light was set up on the test course in the field validation study (Fig. 2a). Signal timing was controlled as a function of car speed and distance from the intersection in order to control the time-to-go to the intersection. Several timing conditions were used ranging from a sure stop to a sure go. Details of the signal timing and task kinematics have been presented elsewhere (Ref. 11).

*Customary units were used for the measurements and calculations of this study.

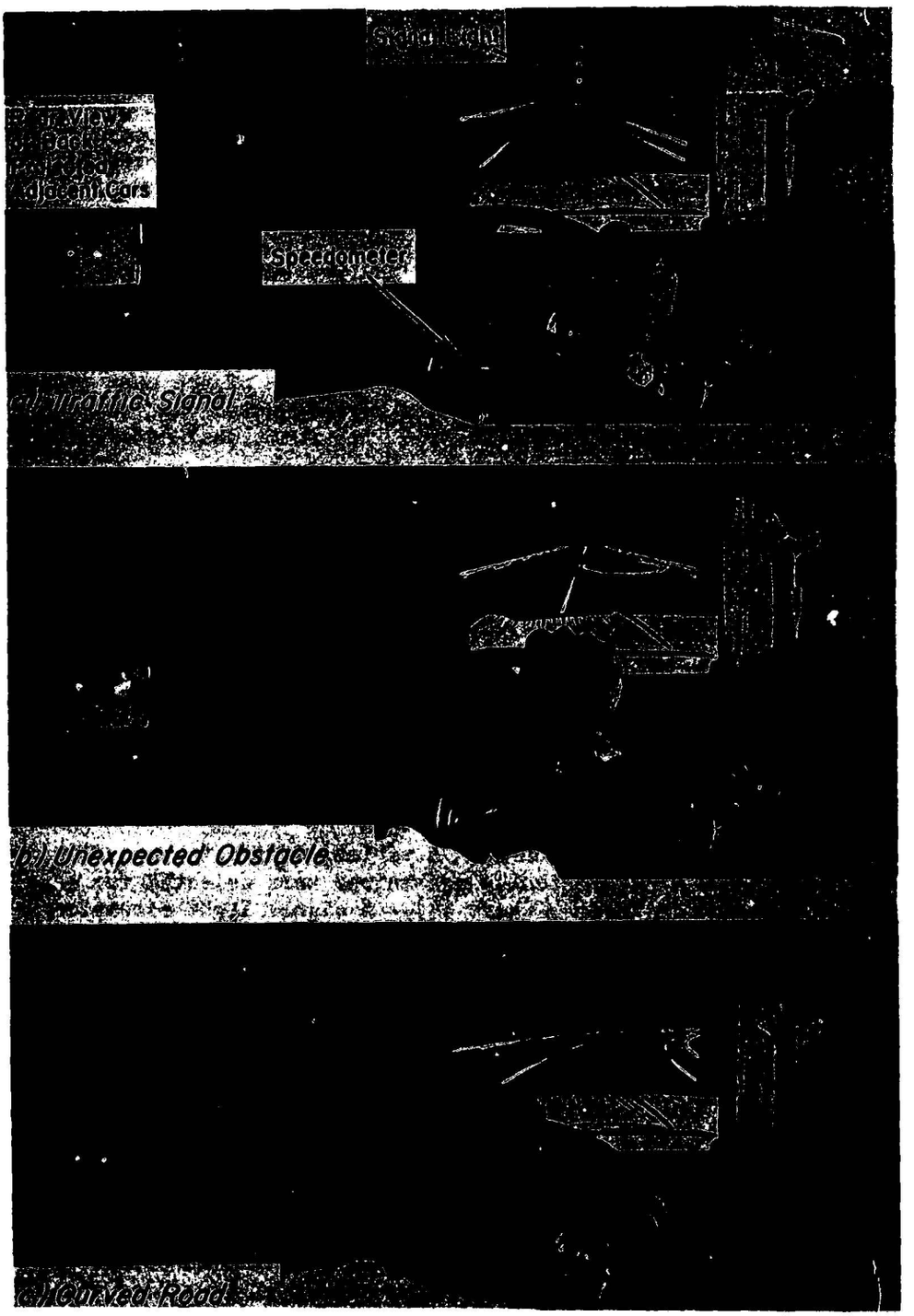

Figure 1. Simulation Setup

ORIGINAL PAGE IS
OF POOR QUALITY

ORIGINAL PAGE IS
OF POOR QUALITY

a) Course Layout Showing Car Approoching Signal Light

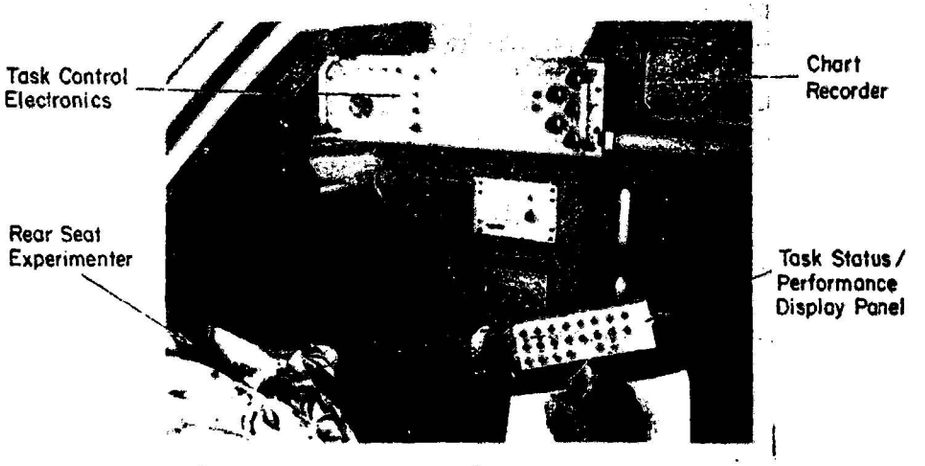

b) Back Seat Experimenter's Station

c) Front Seat Experimenter's Station

Figure 2. Equipment Setup for the Field Validation Study

TABLE 1. DRIVING DECISION-MAKING SITUATIONS

DECISION CLASS	BASIC TYPE	SPECIFIC SITUATIONS	SELECTED TASKS	
			SIMULATION	IN-VEHICLE
Single Stage	Traffic Control	• Signal light	X	X
		• Course navigation		X
	Unexpected Threats	• Car, pedestrian, object unexpectedly enters roadway	X	
		• Object in/on roadway		
Sequential	Maneuvers	• Speed and steering control in a curve	X	X
		• Lane changing and merging		
		• Road entry and merging		
		• Over[illegible]ng and passing		

The perceptual requirements of this task were to estimate car speed and distance to the intersection which the driver then uses to determine the probability of making the light. Driver perception is based on motion of the dashed lines and the intersection, auditory feedback of car speed, and position of the intersection when the light changes from green to amber. The driver does not separately estimate speed and distance, but makes a "Gestalt" estimate of the chance of entering the intersection before the light turns red. The amber light interval was held constant at 3 seconds which is typical of urban signal timing.

Driver signal timing perception was measured by having the subjects verbally report their chance of failing to make a given signal situation immediately after passing through the intersection. Failure was defined as entering the intersection after the light had turned red. This amounts to measurement of a subjective probability in decision theory context, and care was taken to insure that these estimates were unbiased by task performance (Ref. 11). Psychomotor performance was measured in terms of brake reaction times in the situations where the driver stopped.

Curve. The curved portion of the simulation and field test driving scenarios (Figs. 1c and 2a, respectively) required specific steering and speed control in order to avoid loss of control. Tire forces were limited in the simulator equations of motion such that peak curvatures could not be negotiated at speeds greater than about 45 km/h (28 mph) although the

scenario legal speed limit was set at 72 km/h (45 mph). Also 40 km/h (24 mph) speed advisory signs were displayed to the simulator drivers in advance of the curves.

In the field test a special circuit was set to activate an alarm at greater than 0.5 g lateral acceleration in order to simulate a loss of control accident. The car was capable of 0.7-0.8 g turns but actual loss of control had to be avoided for safety reasons. The field course speed limit was 40 km/h (25 mph) and the curve radii were such as to require significantly lower speeds in order to avoid exceeding the imposed g limit.

The critical perceptual task in the curve situation was speed judgment. Speed was represented by visual field motion and auditory feedback, as in the signal event, plus quantitative readout on the speedometer. Use of the speedometer is more appropriate here than for the signal event because of the quantitative nature of the curve limit speed and a lower time pressure on perception and psychomotor action. Perception in this task was again measured by driver-reported subjective probability of crashing which was solicited directly after curve exit. Speed at peak curvature was obtained as an objective measure of risk, i.e., the higher the speed, the greater the risk. Comparison of subjective risk estimates with speed then gives a measure of driver risk perception in the curve situation.

Divided Attention. In the simulator the divided attention situation involved obstacle avoidance. This task consisted of a circular object at the right side of the displayed roadway which sometimes remained stationary at the side of the road or, more frequently, moved laterally into the subject's (right) lane (Fig. 1b), requiring either stopping or steering avoidance. The subject also had to contend with adjacent cars in the left lane which were simulated by a projected slide viewed in the side view mirror (Ref. 9). Changing lanes in the presence of an adjacent car led to a crash as simulated by a buzzer and display jitter. Crashes also resulted from striking the obstacle or running off the road shoulder.

The obstacle avoidance task was a conflict situation. The subject was encouraged by a time reward to continue going if possible, but was penalized for crashing as described further on. This task primarily provided a measure of the driver's visual monitoring and steering control. Comments were solicited from subjects on monitoring behavior in the event of an adjacent crash.

Mechanization of the obstacle avoidance task was deemed too difficult for the field study so a simple route guidance task was substituted. A dashboard mounted indicator was used to direct the subject either left, right or straight after he had passed the signal light intersection. The course layout and timing were such that the route decision was made under a reasonable amount of time pressure.

Driving Scenario and Reward/Penalty Structure

Each run in the simulator and field tests consisted of an approximately 15 minute drive which included a pseudo-random sequence of the above tasks. Program starting points were varied and counterbalanced between subjects in order to avoid learning the event sequences. Circuits for detecting red light and speeding violations were activated at approximately 30 percent of the events to simulate occasional police surveillance.

Audio alarms were activated when violations were detected, and when the lateral g limit for loss of control was exceeded in the field test. A crash buzzer was activated in the simulator when subjects exceeded the road shoulder limits, or ran into obstacles or adjacent cars. Accidents in the field test were further defined by striking the tires and cones used to define the edge of the course (Fig. 2a). Thus subjects were given complete feedback on traffic safety related variables (accidents and tickets) as they would in the real world. In addition the number of accidents and tickets were used as traffic safety measures on the overall driving scenario and were also accounted for in the reward/penalty structure as described below.

Subjects were instructed to behave as they normally would in a driving situation with a reasonable motivation for timely progress while avoiding traffic violations and accidents. In addition, the monetary reward/penalty structure given in Table 2 was used to simulate real-world driving motivations and risks (Ref. 14), and provide a quantitative value structure for expected value modeling of decision-making behavior (Ref. 15). The overall

TABLE 2. REWARD/PENALTY STRUCTURE FOR SIMULATING REAL-WORLD MOTIVATIONS IN DRIVERS

COMPONENT	LAB SIMULATION	FIELD VALIDATION
Run completion bonus	$10	$10
Time saved reward	$2/min	$2/min
Low ticket penalty group	$1/ticket	$1/ticket
High ticket penalty group	$2/ticket	$4/ticket
Accident penalty	$2/crash	$2/crash
Route error penalty	—	$0.50/error

scaling of the structure was made large enough to be meaningful and comparable to the subjects' hourly wages. The run completion bonus was included to insure subjects completing each run, and the time saved reward was set to encourage the subjects to make timely progress on the drives and not become excessively cautious. Penalties were assessed for tickets, accidents and route errors (traffic safety factors). Ticket penalties are one factor that can be manipulated in the real-world (i.e., traffic court fines) and a between group comparison was included for two levels of this variable. Results of the simulator study showed no significant differences between the $1 and $2 penalty groups so the high ticket penalty was increased to $4 for the field experiment. Results on the ticket penalty variation are fully discussed in Ref. 14.

Design, Treatments and Procedures

Subjects were selected from the male licensed driving population through a newspaper ad and screened to insure heavy drinking tendencies (defined as the capability for reaching a peak BAC of 0.15). Based on age and scores on a hostility test (Ref. 16) and betting test (Ref. 17), subjects were matched and divided into the two penalty groups. During training sessions subjects were given several one-half hour exposures to the simulated driving scenarios and reward/penalty structure in order to minimize learning effects during the formal data sessions.

The experimental design shown in Fig. 3 was completed by 12 subjects in the simulator experiment and at a later date by a different group of 14 subjects in the field tests. Session order was counterbalanced between subjects. Performance was measured in four separate runs during sessions of nominally eight hours in length. During alcohol days runs were administered at sober, ascending, peak and descending levels of Blood Alcohol Concentration (BAC) in the simulator tests. The ascending BAC runs were subsequently dropped in the field tests based on minimal differences in simulator performance levels on the ascending and descending portions of the BAC curve. During placebo days runs were administered at roughly the same times as on the alcohol days. Thus subjects served as their own controls for alcohol effects, and penalty structure was between group effect.

Actual times and blood alcohol levels are illustrated in Fig. 4. BAC was measured with a gas chromatograph breath analyzer. Placebo drinks were made by floating a small amount of liquor on top of mixer. Subjects were allowed to select their own mixed drinks in order to maximize subject morale; however, combinations which would not allow credible placebos were tactfully avoided. Alcohol was administered proportional to body weight in three drinks.

The facility layout and personnel assignments were designed to maintain subject motivation and experimental efficiency. Recreational areas were set up adjacent to the simulator and included a bar, breath test area, lounge and dining area, and a restroom. This provided a relaxing atmosphere for the

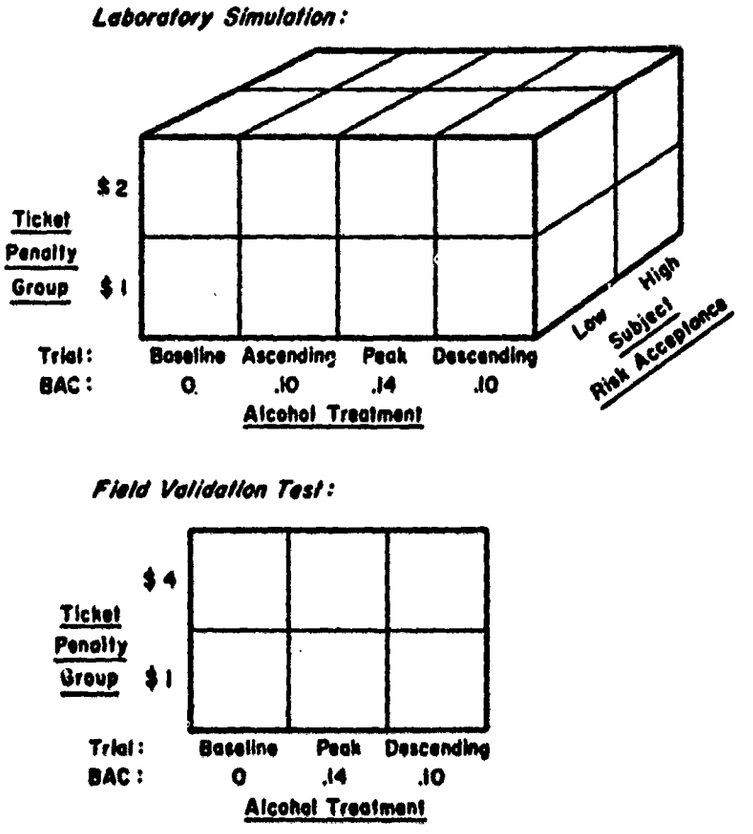

Figure 3. Experimental Design

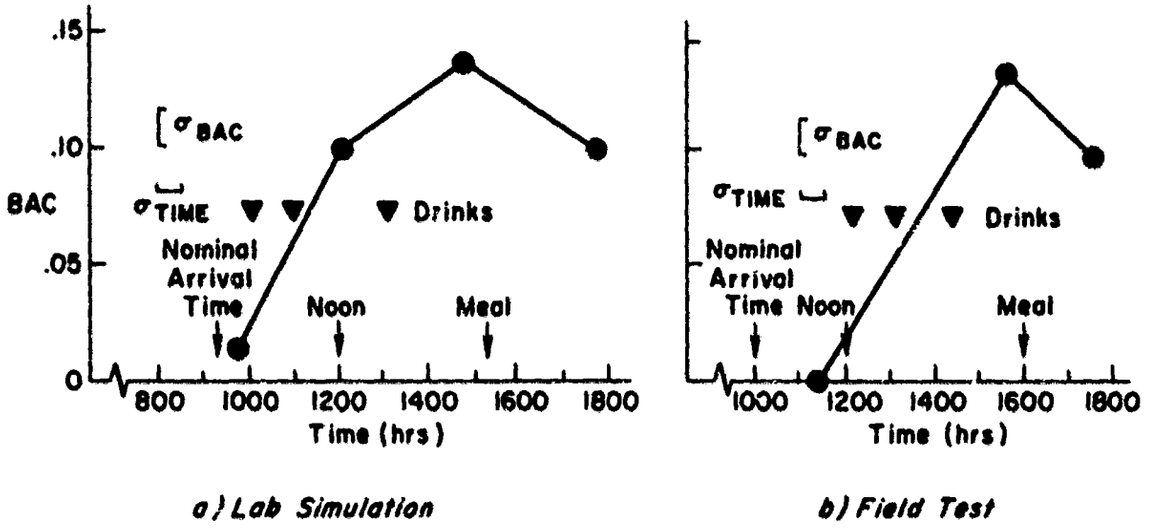

Figure 4. Alcohol Treatment Procedure Summary

ORIGINAL PAGE IS
OF POOR QUALITY

subjects between experimental trials and isolated them from laboratory activity other than when they were being tested.

RESULTS AND DISCUSSION

Overall Performance

Performance measures accumulated over the whole driving scenario are plotted in Fig. 5, which show excellent agreement between the simulation and field test experiments. The total payoff per run gives an overall combined performance measure of the reward/penalty structure components. Average payoff was appreciably affected by BAC as illustrated in Fig. 5a. Sober subjects were making an average $12.50 per run, which dropped to $5 at the peak BAC condition. Analysis of variance procedures (ANOV) proved these results to be reliable ($P < 0.01$), but showed no significant difference between the two ticket penalty groups. The payoff levels were quite substantial, as the average sober subject made roughly $30-50 during his placebo session, and subject comments indicated these payoff levels motivated performance.

Component measures of the reward/penalty structure are also given in Fig. 5. Average driving time to complete the driving scenario (Fig. 5b) was remarkably insensitive to BAC, while speeding tickets and accidents were appreciably elevated with BAC (Figs. 5c and 5d). Since driving completion time was constant, the increased incidence of speeding tickets with BAC implies increased speed variability. Subjects were well aware of the speed limit and speeding penalty, and feedback of speed was available both visually and aurally. Thus, increased speed variability suggests decrements in perception and/or speedometer monitoring.

Considering a speed versus accuracy paradigm, it is apparent here that these subjects maintained average speed levels (and thus average rate of event occurrence) under alcohol impairment at the expense of accuracy (increased tickets and accidents). Thus risk taking increased with BAC, but the question remains as to whether the drivers were aware of the increased risk and thus were willingly accepting greater risk.

The simulator driving scenario provided for three types of accident exposure, and these accident results are plotted in Fig. 6. Crashes on the curve resulted from excessive speed and/or poor steering control and were the most prevalent accident. The adjacent car crashes arose from the driver not monitoring his rearview mirror when he decided to steer around the obstacle (subject reported). This result is consistent with previously reported monitoring failures in driving situations (Ref. 4). Observations during the experiment indicated that obstacle crashes occurred either because the driver took too long to decide to stop and then hit the obstacle, or tried to steer around and clipped it from the side.

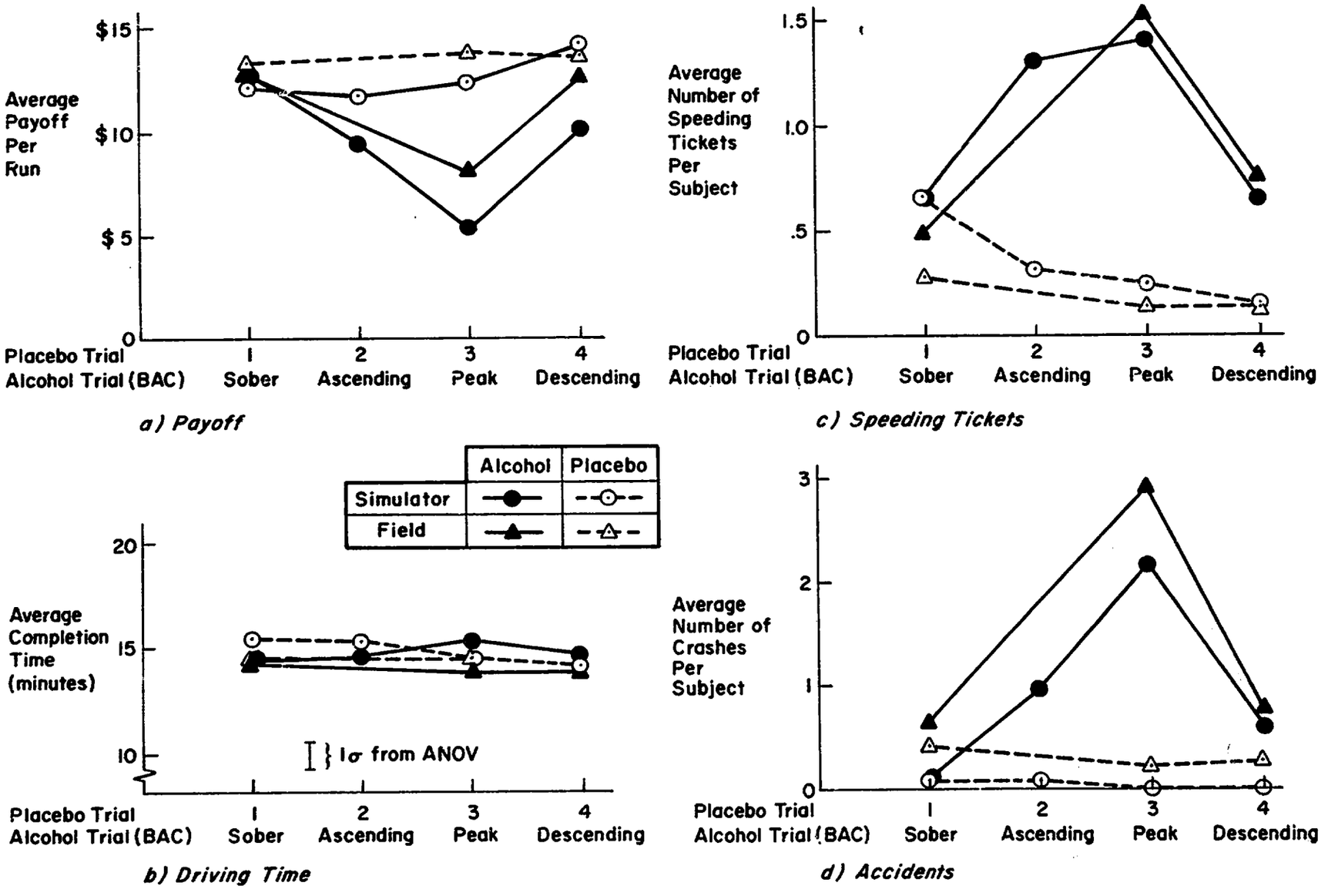

Figure 5. Overall Driving Scenario Performance Measures

ORIGINAL PAGE IS
OF POOR QUALITY

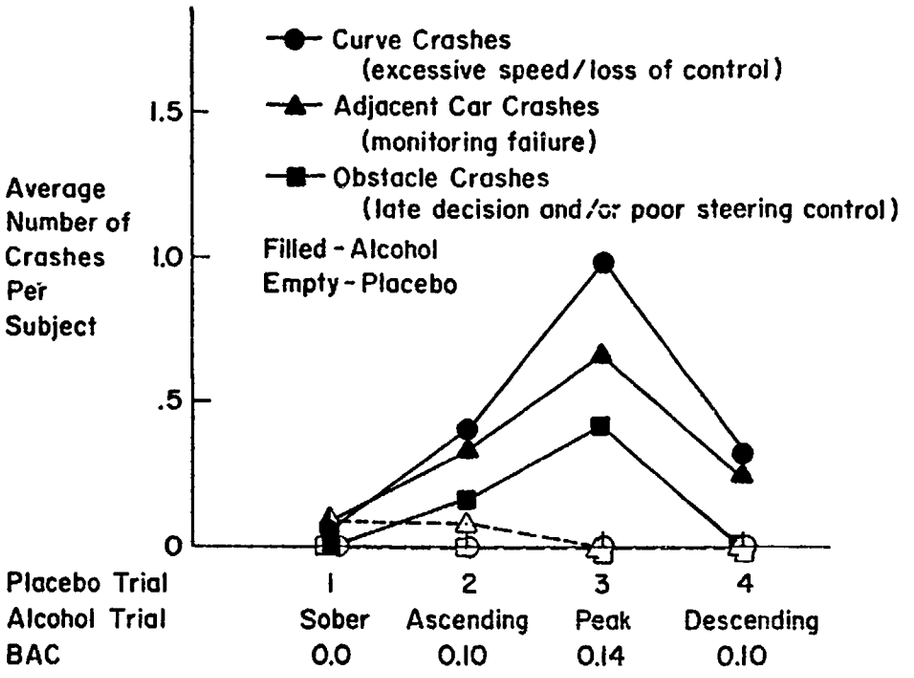

Figure 6. Simulator Curve, Adjacent Car and Obstacle Crash Results

The relative increase in experimental accident rate with BAC is compared with real-world data (Ref. 18) as shown in Fig. 7. Although there is some difference between the two experiments reported here (primarily due to different placebo accident rates), the data are still consistent with epidemiological statistics. The knee of the experimental data occurs in the region of 0.10 BAC and the data bracket the real-world rates. This data thus lend credibility to alcohol sensitivity of our simulated driving scenarios.

Signal Light Behavior

The probability of going on a given signal timing condition and the driver's estimate of failure (i.e., running the red light) are plotted in Fig. 8. There were 5 signal timings randomly distributed throughout the scenario, and the amber light timing was set to change the light when the driver was 3.4 seconds from the intersection (traveling at constant speed) in the simulator and 4.2 seconds in the field test for the data illustrated. The amber light interval was only 3 seconds long so the subjects would invariably run the red light under these conditions if they decided to go. There was some probability of going under this condition, however, which increased under alcohol.

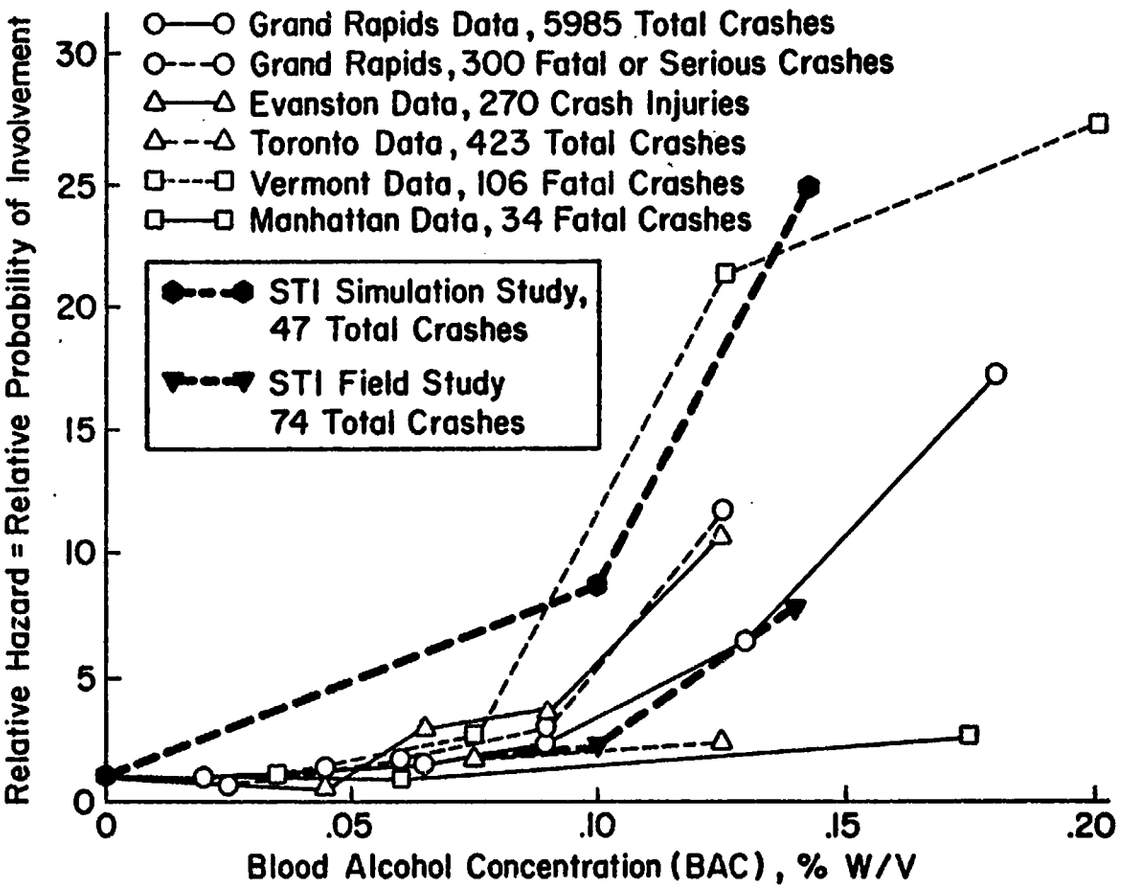

Figure 7. Comparison of Experimental Accidents With Real World Data (after Hurst, Ref. 18)

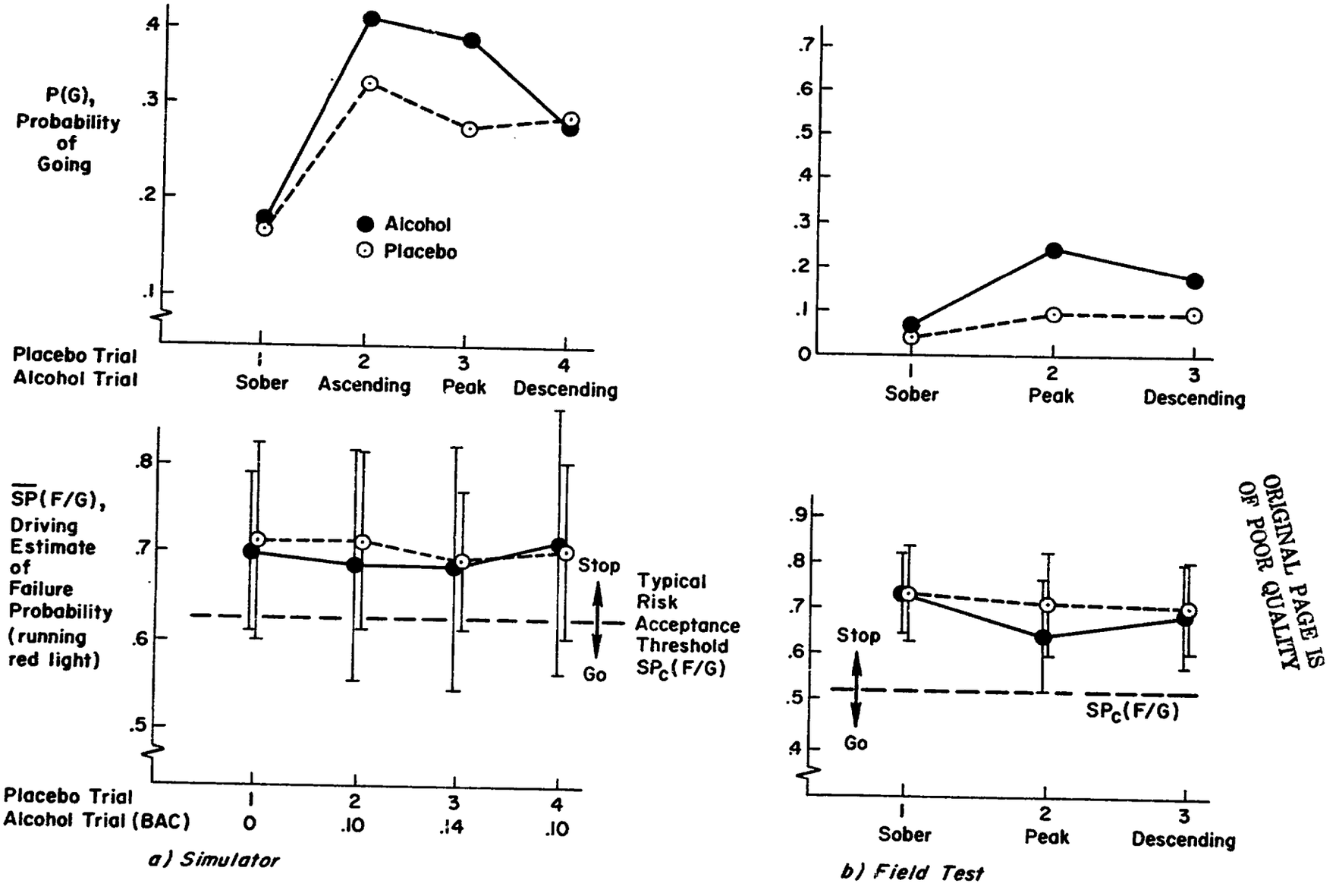

Figure 8. Signal Light Behavior Probability of Going and Driver Estimates of Failure (Running the Red Light) Given a Go

ORIGINAL PAGE IS OF POOR QUALITY

The drivers' subjective estimates of failure given that they decided to go, SP(F/G), are consistent with the probability of going. In the simulation experiment variability in the estimates increased with BAC. If we hypothesize a risk acceptance threshold for going, we see that the increased variability leads to an increased probability of going. In the field test a combination of increased variability and lower mean estimate of risk led to increased probability of going.

The subjects' failure probability estimates were obtained as soon as possible after passing through the intersection on randomly selected events where the subject did not receive a ticket (the police circuit was activated only 30 percent of the time). In order to check for performance biasing (probability estimates influenced by events after the decision point), a separate set of runs were conducted in the simulation where the whole roadway display and signal light were blanked at the end of the amber light interval. The estimates were no different under these circumstances than when the task was carried to completion. These results indicate that the failure estimates were a reflection of the drivers' perception or "Gestalt" of the time distance relationship existing at the appearance of the amber light and the decision point. These points and a complete decision theory analysis of the signal light behavior is given elsewhere (Ref. 15).

Brake response time on the signal light task was used as a measure of signal task psychomotor behavior. The results in Fig. 9 show no effect of alcohol on either the mean or variability in response time.

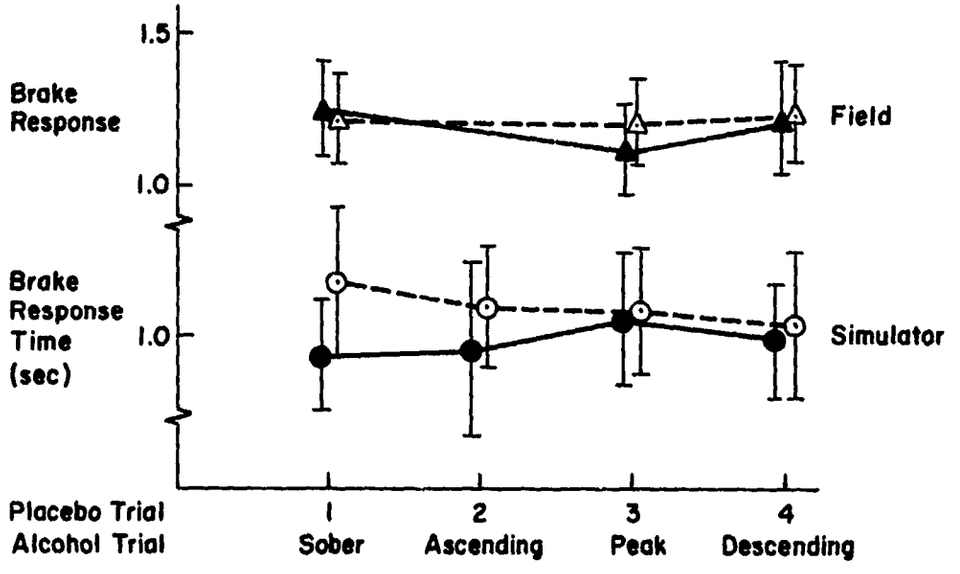

Figure 9. Alcohol Effects on Brake Response Time in the Signal Light Task

Curve Behavior

Drivers had to carefully control speed on the curves to avoid loss of control. As illustrated in Fig. 10, drivers did maintain safe speeds on the average with no significant effect due to BAC level. However, speed variability between curves (computed across several repeat curves/run/subject) did significantly increase under peak BAC. ANOV procedures showed this effect to be significant at the 0.05 level. By taking into account the speed mean and standard deviation values and assuming a normal distribution, we can compute the probability of exceeding the critical curve speed, which should equal the probability of crashing. In Fig. 11 computed and measured crashed probabilities for the simulator data are compared. The computed probabilities show an increase in the region of peak BAC, but are generally lower than the data by 30 percent. In the field test the mean and variability does not explain the increase in accident rate (field accidents were primarily due to g limit exceedences in the curves). However, experimenters noted that g exceedence often occurred with steering corrections. Steering actions by the driver can exceed the g limit at speeds below the critical speed. In the linear region of tire force characteristics, lateral acceleration for a neutral steer car can be expressed approximately as a function of the car's speed (U_o), wheelbase ($a + b$), and front wheel steer angle, δ_w:

$$a_y = \frac{U_o^2}{a + b} \delta_w < a_{y_{max}}$$

The driver could enter a curve and establish safe steady-state conditions (i.e., constant U_o and δ_w), then provide steering corrections which command lateral accelerations beyond the acceleration limit according to the above. As noted, the higher the speed (U_o), the less additional steering angle can be tolerated before the tires reach their acceleration limit. Errors in this mode might result from the driver not establishing a large enough steering angle at the beginning of the curve, then having to make a correction in midcourse which is beyond the acceleration limits of the tires.

Subjective estimates of risk or 'crash' probability were obtained in both studies at the end of selected curves. No effect of alcohol was noted on these estimates. Thus in spite of the increased accident rate under alcohol which was primarily due to loss of control on curves, drivers did not exhibit any perception of the elevated risk.

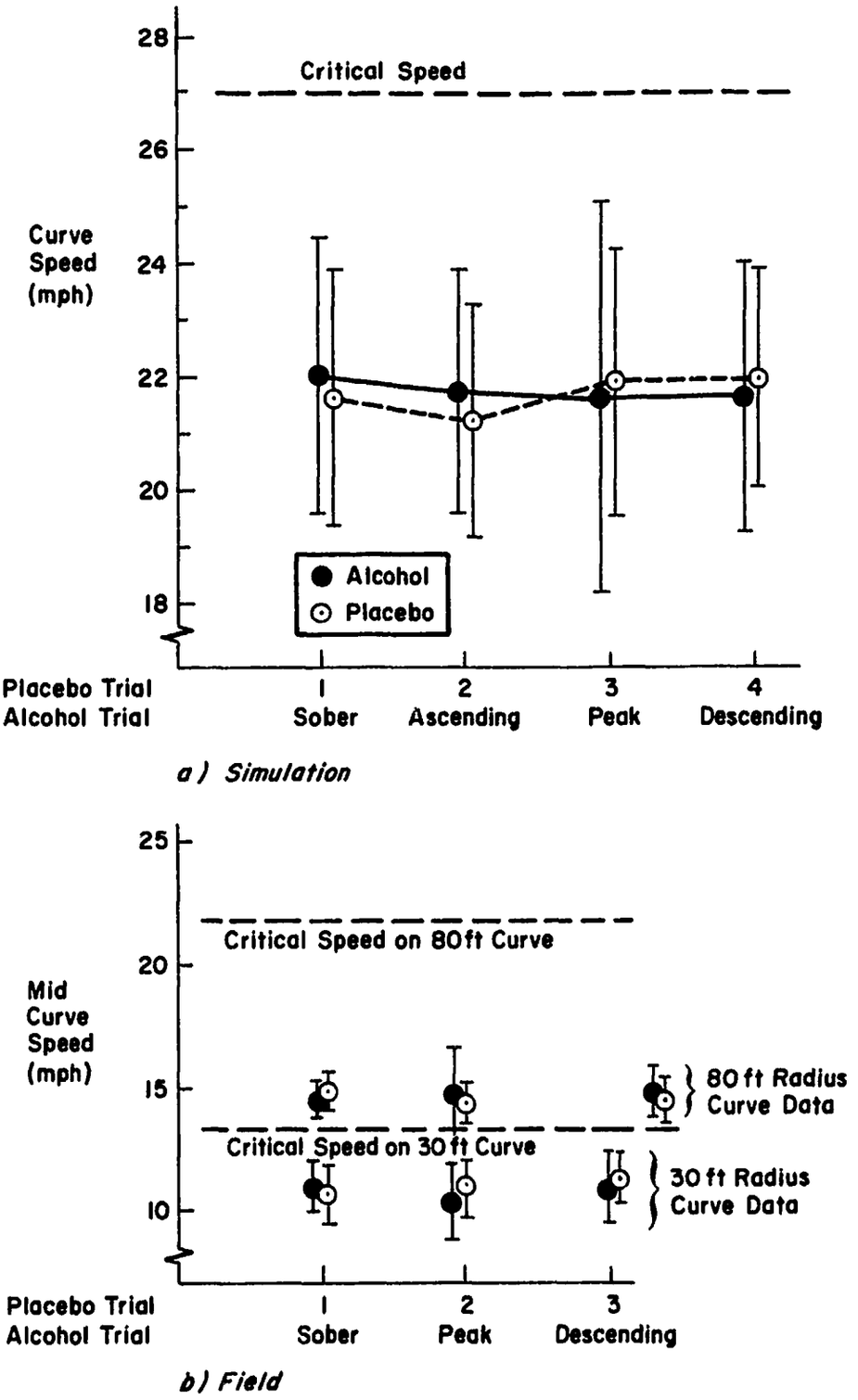

Figure 10. Mean and Variability of Speed on Curves in the Simulator and Field Driving Scenarios

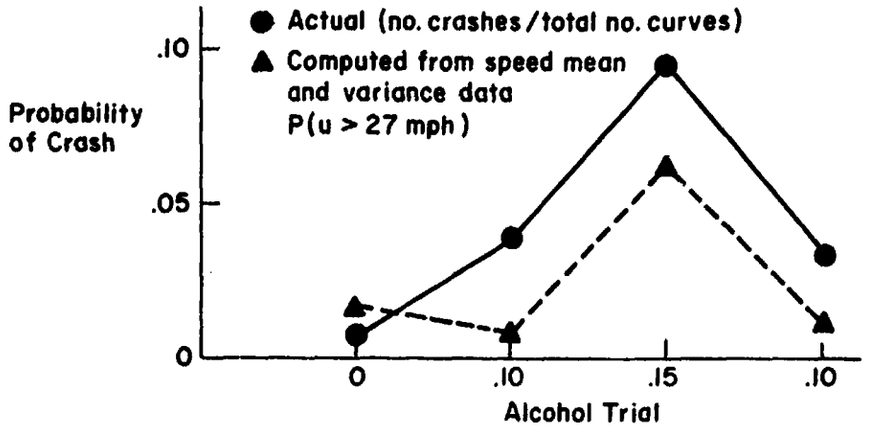

Figure 11. Comparison of Actual and Computed Curve Crash Probabilities for the Simulator Driving Scenario

SUMMARY AND CONCLUDING REMARKS

Overall performance on the driving scenario, as measured by accumulated payoff according to a reward/penalty structure, was appreciably degraded by BAC (blood alcohol concentration). Penalties due to accidents and speeding tickets increased with BAC and were primarily responsible for the decline in payoff.

Increased speed variability under alcohol was responsible for the increase in speeding tickets and curve accidents. On the average drivers did not perceive the increased hazard of the curve task with alcohol impairment as indicated by subjective estimates of risk; however, speed variability did increase, probably due to impaired perception of speed. Similarly, going behavior on the signal task increased under alcohol due to an increase in the variability of risk perception.

The above changes in speed variability and signal risk perception with increased BAC imply perceptual impairment unknown to the drivers. Alcohol increased perceptual variability which increased the driver's risk exposure. However, the mean level of subjective risk estimates was unchanged with alcohol in this experiment, which indicates the subjects were not aware of their increased risk exposure. The incidence of tickets and accidents under alcohol, although increased, was still a low probability event (roughly 1.5 and 1 incident per subject per run, respectively, at the peak BAC level). Although degraded psychomotor skill and perception combined to increase the changes of violations and accidents under alcohol, the subjects were not aware of these changes in risk.

REFERENCES

1. 1968 Alcohol and Highway Safety Report. Committee on Public Works, U.S. Congress, 90th, 2nd Session, Aug. 1968. (Available from Government Printing Office, Washington, D.C.)

2. Filkins, Lyle D.; Clark, Cheryl D.; Rosenblatt, Charles A.; et al.: Alcohol Abuse and Traffic Safety: A Study of Fatalities, DWI Offenders, Alcoholics, and Court-Related Treatment Approaches. Univ. of Michigan, Highway Safety Research Institute, 26 June 1970.

3. Study to Determine the Relationship between Vehicle Defects and Failures, and Vehicle Crashes, Volume I. DOT/HS-800 850, Univ. of Indiana, Inst. for Research in Public Safety, May 1973.

4. Allen, R. W.; Jex, H. R.; McRuer, D. T.; and DiMarco, R. J.: Alcohol Effects on Driving Behavior and Performance in a Car Simulator. IEEE Trans. on Systems, Man and Cybernetics, Vol. SMC-5, No. 5, Sept. 1975, pp. 498-505.

5. Cohen, John; Dearnaley, E. J.; and Hansel, C. E. M.: The Risk Taken in Driving Under the Influence of Alcohol. British Medical Journal, 21 June 1958, pp. 1438-1442.

6. Lewis, Everett M. Jr.; and Sarlanis, Kiriako: The Effects of Alcohol on Decision Making with Respect to Traffic Signals. ICRL-RR-68-4, Dept. of Health, Education and Welfare, 1969.

7. Ellingstad, V. S.; McFarling, L. H.; and Struckman, L. L.: Alcohol, Marijuana and Risk Taking. DOT-HS-801 028, Univ. of South Dakota, Human Factors Lab., Apr. 1973.

8. Snapper, Kurt; and Edwards, Ward: Effects of Alcohol on Psychomotor Skill and Decision-Making in a Driving Task. Paper presented at the SAE International Automotive Engineering Congress, Detroit, Mich., Jan. 1973.

9. Allen, R. W.; Hogge, J. R.; and Schwartz, S. H.: An Interactive Driving Simulation for Driver Control and Decision-Making Research. Proc. Eleventh Annual Conference on Manual Control. NASA TM X-62,464, May 1975, pp. 396-407.

10. Klein, Richard H.; Allen, R. Wade; and Peters, Richard A.: Driver Performance Measurement and Analysis System (DPMAS) Description and Operational Manual. TM-1039-1, Systems Technology, Inc., Jan. 1976.

11. Allen, R. W.; Schwartz, S. H.; and Jex, H. R.: Driver Decision-Making Research in a Laboratory Simulation. Paper presented at the NATO Symposium on Monitoring Behavior and Supervisory Control, Berchtesgaden, Federal Republic of Germany, Mar. 8-12, 1976.

12. Perchonok, K.: Accident Cause Analysis. DOT HS-800 716, National Highway Traffic Safety Administration, July 1972.

13. Moskowitz, H.: Alcohol Influences upon Sensory Motor Function, Visual Perception, and Attention. Alcohol, Drugs, and Driving, Perrine, M. W., Ed., DOT HS-801 096, National Highway Traffic Safety Admin., Mar. 1974, Chapter 3, pp. 49-69.

14. Stein, A. C.; Schwartz, S. H.; and Allen, R. W.: Use of Reward-Penalty Structures in Car-Driving Research. Proc. Fourteenth Annual Conference on Manual Control. USC, May 1978.

15. Allen, R. Wade; Schwartz, Stephen H.; and Jex, Henry R.: Driver Decision-Making Research in a Laboratory Simulation. Proc. Eleventh Annual Conference on Manual Control. NASA TM X-62,464, May 1975, p. 170.

16. Pelz, Donald C.: Hostility Questionnaire. Univ. of Michigan, Inst. for Social Research, Survey Research Center.

17. Hurst, P. M.; and Siegel, S.: Prediction of Decisions from a Higher Ordered Metric Scale of Utility. J. Exper. Psychology, Vol. 2, 1956, pp. 138-143.

18. Hurst, P. M.: Epidemiological Aspects of Alcohol in Driver Crashes and Citations. Alcohol, Drugs, and Driving, Perrine, M. W., Ed., DOT HS-801 096, National Highway Traffic Safety Admin., Mar. 1974, Chapter 6, pp. 131-171.

19. McRuer, D. T.: Simplified Automobile Steering Dynamics for Driver Control. Paper presented at the SAE Aerospace Control and Guidance Systems Committee Meeting No. 35, Palo Alto, CA, Mar. 19-21, 1975.

D42

N79-15630

A DECISION MODEL APPLIED TO ALCOHOL EFFECTS ON DRIVER SIGNAL LIGHT BEHAVIOR

Stephen H. Schwartz and R. Wade Allen

Systems Technology, Inc.
Hawthorne, California

ABSTRACT

A decision model including perceptual noise or inconsistency is developed from expected value theory to explain driver stop and go decisions at signaled intersections. The model is applied to behavior in a car simulation and instrumented vehicle. Objective and subjective changes in driver decision making were measured with changes in blood alcohol concentration (BAC). Treatment levels averaged 0.00, 0.10 and 0.14 BAC for a total of 26 male subjects. Data were taken for drivers approaching signal lights at three timing configurations. The correlation between model predictions and behavior was highly significant. In contrast to previous research, analysis indicates that increased BAC results in increased perceptual inconsistency, which is the primary cause of increased risk taking at low probability of success signal lights.

INTRODUCTION

One of the motivations for developing the driver decision model described here was to measure and analyze the behavior of alcohol-impaired drivers. We desired to separate risk taking into components of risk perception and acceptance. If a driver takes increased risks, is it because he perceived the risk and decided to accept it or because he does not perceive the increased risk? Expected value theory provides a simple construct for making this distinction and has been applied in the past to describe impaired driver behavior, (References 1, 2, and 5).

Here we apply a Subjective Expected Value (SEV) model to explain driver stopping and going behavior at signaled intersections. Perceptual noise is included to reflect one type of driver inconsistency in the decision-making process (Reference 3). The model is applied to data collected as part of an automobile simulator study involving a typical drive-home scenario. Although measures were taken throughout the scenario on several tasks, we concentrate here on signal light behavior. We briefly present the decision model, the experimental results, and our analysis and interpretation in view of previous studies.

DECISION-MAKING MODEL

The model was derived to guide experimental design and measurement. The expected value approach is not new; however, the inclusion of perceptual noise as applied to signal light behavior is original. The basic scenario is a signal light at an intersection which has changed from green to amber and will change to red in 3 seconds. Based on his perception of speed and distance the driver must then decide whether to stop or go. The kinematics for this task have been described previously, Reference 4. Here we briefly derive an appropriate decision model subject to several assunptions.

We begin by simplifying what is actually a complex decicion task, Reference 11, in a simple two-alternative situation. Conceptually we are assuming this decision process takes place in parallel with the driver's continuous speed control behavior as illustrated in Figure 1. Perceptions of vehicle

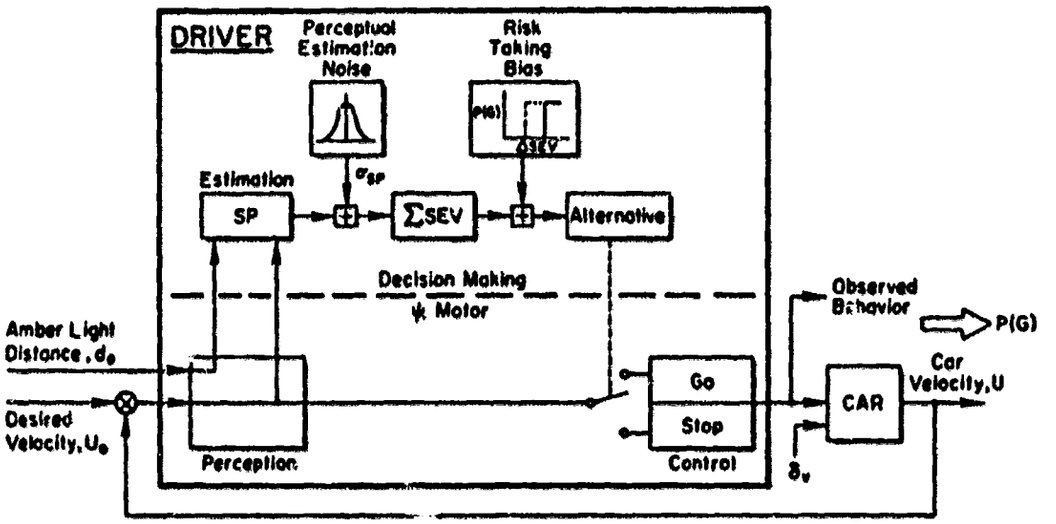

Figure 1. Signal Light Risk Acceptance Model

velocity and distance to the signal at the time the light changes to amber are used to form a subjective estimate of the probabilities of success and failure for the various alternatives. As indicated in the figure and discussed further below, these subjective probabilities are stochastic in nature. They are weighted with appropriate utilities or values and the driver selects the alternative with the highest expected value. We define Subjective Expected Values (SEVs) for the two alternatives, go or stop, respectively:

$$SEV(Stop) = SP(Pass/Stop)V(Pass/Stop) + SP(Fail/Stop)V(Fail/Stop) \quad (1)$$

$$SEV(Go) = SP(Pass/Go)V(Pass/Go) + SP(Fail/Go)V(Fail/Go) \quad (2)$$

ORIGINAL PAGE IS OF POOR QUALITY

where SP(·) and V(·) are conditional subjective probabilities and values, respectively. From these equations and the several other simplifying assumptions, we can express the probability that a driver will attempt to go through the signal light. Further simplifying notation so that F = Fail and G = Go, the probability of Going is:

$$P(G) = \iint_{\text{Region}} f[SP(F/G),\ SP(F/S)]\ dSP(F/G)\ dSP(F/S) \qquad (3)$$

where the region is defined by:

$$P(G) = P[SEV(G) \geq SEV(S)] \qquad (4)$$

With the assumptions listed in Table 1, it can be shown (see Reference 6 for derivation) that the P(G) is the Gaussian integral:

$$P(G) = \frac{1}{\sigma_{SP(F/G)}\sqrt{2\pi}} \int_{o}^{SP_c(F/G)} \exp\left\{\frac{-[SP(F/G) - \overline{SP}(F/G)]^2}{2\sigma^2_{SP(F/G)}}\right\} dSP(F/G) \qquad (5)$$

TABLE 1. SOME MODEL ASSUMPTIONS

1. Operator selects decision alternative with largest subjective expected value. Values reflect utilities and are constant.
2. Subjective probabilities are mutually exclusive and exhaustive.
3. Subjective probabilities are Gaussian random variables in the region of interest.
4. Increased SP(F/G) decreases P(G), i.e., the values discourage go-failures.
5. The verbal estimates of SP(F/G) linearly reflect subjective perception.
6. The threshold value of SP(F/G), below which the operator selects the go alternative is $SP_c(F/G)$:
   - $\triangleq \overline{SP}(F/G)$ where P(G) = 0.5
   - is a constant as compared with being a random variable
7. SP(F/S) = 0.

A typical example of these concepts is illustrated in Figure 2. Repeated observations for a given situation, e.g., signals with the same time to the intersection, result in a distribution of subjective estimates illustrated by the top probability density curve. Assuming a cutoff subjective probability, $SP_c(F/G)$, as illustrated, the area under the density curve and to the left of the criterion is P(G). This is illustrated in the bottom of Figure 2, where the relationship of P(G) as a function of the average subjective estimate, $\overline{SP}(F/G)$, is illustrated. The slope of this relationship is determined by the variability of the subjective estimates, σ_{SP}. Note that the effect of increasing the variance of the subjective estimates is to increase P(G) for the case illustrated. Also shown is the consequence of a change in the driver's risk acceptance, $SP_c(F/G)$.

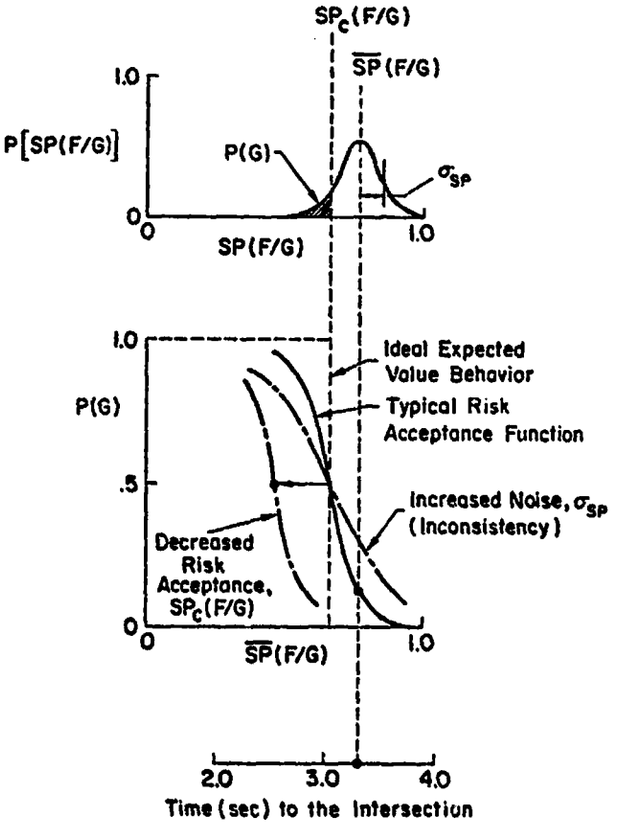

Figure 2. Typical Relationship Between Probability of Going, P(G), Subjective Probabilities of Fail Given a Go, SP(F/G), and Signal Timing

A useful empirical relationship is also apparent in Figure 2. Evaluation of Eq. 5 for the condition $SP_c(F/G) = \overline{SP}(F/G)$ results in $P(G) = 0.5$. Thus, the subjective cutoff $SP_c(F/G)$ can be determined empirically from objective behavior probabilities by selecting the value of $\overline{SP}(F/G)$ at $P(G) = 0.5$.

THE EXPERIMENTS

The signal light task was simulated in both a fixed-base simulator and instrumented vehicle on a closed course as described in the companion paper (see Reference 14). The signal light timing was controlled similarly in both simulation and field studies. When the vehicle approached the intersection, the signal light initially turned green. At a random-appearing time later, the signal turned amber. This time was controlled by a circuit which compensated for car speed such that the time interval to the intersection was the same for a given intersection type, regardless of the approach speed, if the driver maintained that speed. The amber light interval was fixed at 3 seconds, following which the light turned red. Thus, the probability for successfully making a light was controlled without placing an artificial speed restriction on the subject. Five signal timings were automaticlly commanded. One was set to require a sure stop (early yellow) and another a sure go (long green). The remaining three timings ranged from a probable stop to a probable go. The times to the intersection from the amber light typically ranged from 2.0 to 3.5 seconds. (The kinematics of stopping or going for these timings are discussed more fully in Reference 4.)

The subjects were instructed to behave as they normally would in a driving situation with a reasonable motivation for timely progress and a desire to avoid tickets and accidents. Also, a monetary incentive structure was provided as a tangible and quantifiable motivation for performance (see Reference 14).

Subjects were trained until objective performance and subjective estimates were consistent in the view of the experimenter. Subjective estimate training began with a short tutorial written exam used as a basis for discussion of the concepts of probabilities. Following this, each subject received two to three hours of practice driving in half-hour sessions spread over two days. Feedback on performance and subjective estimates was given throughout these training trials.

Subjects completed trials on each of two days. During an alcohol day, the trials corresponded to an across-subject average blood alcohol concentration (BAC) of 0.00 (baseline), 0.10 (ascending — when measured), 0.14 (peak), and 0.10 (descending). During the placebo day, the trials were given at approximately the same time of the day as for the above trials. The day order was counterbalanced among subjects.

Objective and subjective measures were taken, and the number of stop and go decisions was recorded. The number of failures and successes for each decision was detected automatically and recorded irrespective of whether or

not the driver received a ticket. Corresponding subjective estimates were recorded during the run. Subjects were asked to give their estimate of failure on a scale of 0 to 100 percent immediately following randomly selected intersections. Nominally, six of each type of intersection were selected. Intersections for which the driver received a ticket were ignored. (A tacit assumption in using subjective estimates received after the execution of the signal task is that the subjective probabilities were unbiased by performance outcomes as perceived by the subject. To test this assumption, a parallel simulation experiment used selected intersections where the visual scene was blanked out immediately following the driver's commitment to a decision and prior to going through the intersection. Thus the driver received no feedback on his performance for these selected intersections. These results were similar to the "after the fact" estimates.)

RESULTS

The data were examined for each intersection independently over the eight trial conditions (four trials per session for placebo and alcohol sessions). Both objective and subjective data were analyzed to differentiate between changes in risk acceptance vs. risk perception.

In Figure 3 the objective probabilities of going, P(G), and failing given a go, P(F/G), for both the simulation and field test are compared to determine driver risk-taking behavior. The probabilities were computed by dividing the total number of outcomes by the total number of opportunities (e.g., P(F/G) = Number of go failures/Number of go's). For example, Intersection 2 in the simulation resulted in the subjects always going, P(G) = 1, and the timing was such as to preclude go failures, P(F/G) = 0. The timing was also adequate on Intersection 3 to allow safe go's; however, in this case the drivers did not always go, i.e., P(G) $\doteq$ 0.75. This behavior was not sensitive to alcohol, and the subjects appear to have been behaving conservatively on Intersection 3. Subjects did not go very frequently on Intersection 4 and had a high failure rate when they did. There is an indication of increased go behavior under alcohol for Intersection 4. This is also apparent for all the intersections in the field test.

Part of the reason for this increased going behavior on some intersection timing in spite of increased failures is illustrated in Figure 4. Here we note that the variability of the subjective risk perception, σ_{SP}, increases although the average perception of risk, $\overline{SP}(F/G)$, remains relatively constant. Considering a typical switching criterion, as shown in Figure 4, we see that the increased variability of risk perception with increased alcohol leads to a greater percentage of subjective estimates below this criterion. The justification for this interpretation was validated via statistical analysis of parameters for the proposed model.

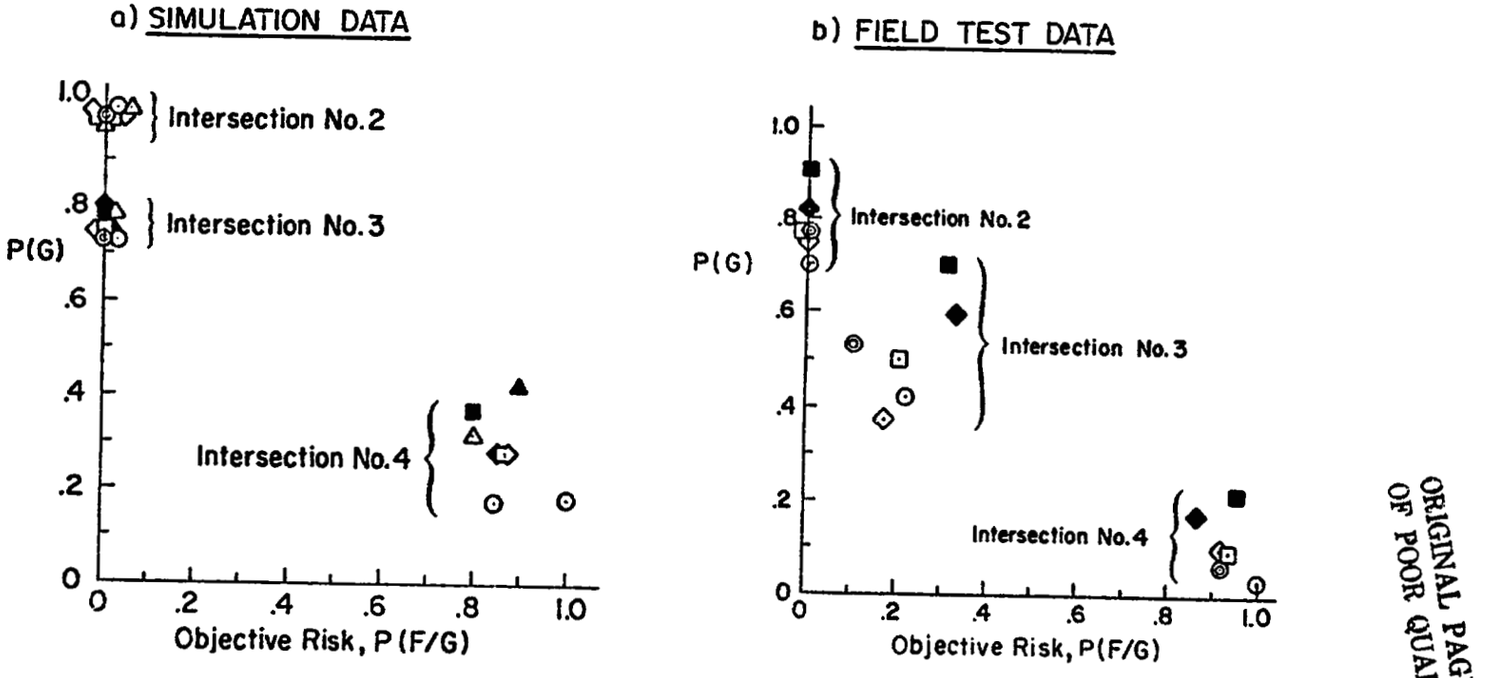

Figure 3. Alcohol Effects on Signal Light Risk-Taking Behavior

ORIGINAL PAGE IS
OF POOR QUALITY

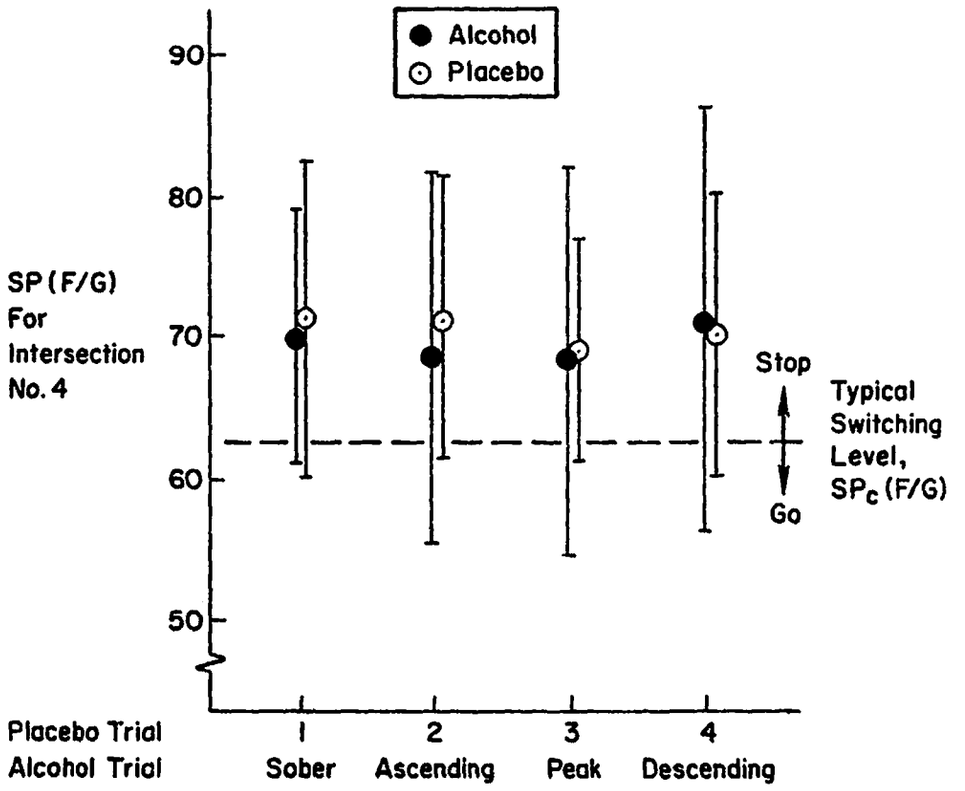

Figure 4. Changes in Subjective Estimates of the Probability of Failure Given a Go Attempt, SP(F/G) with BAC Condition

MODEL EVALUATION

The decision-making model discussed above was used to analyze driver risk acceptance behavior. This was accomplished in three steps. First, driver risk acceptance thresholds, $SP_c(F/G)$, were computed for each experimental treatment. Then the threshold data were analyzed to investigate changes under intoxication. Finally, the various risk perception data were combined according to Eq. 5 and resulting computed or estimated values of the probability of going, $\hat{P}(G)$, were compared with actual P(G) data to establish model validity.

Risk acceptance thresholds were computed for each subject and each run by curve fitting a risk acceptance function (Figure 5) to P(G) and $\overline{SP}(F/G)$ data for the three intersection timing conditions. A trigonometric function was used to describe the risk acceptance function:

$$P(G) = \frac{1}{2}\left[1 + \sin\left(\overline{SP}(F/G) - SP_c(F/G)\right)\right] \qquad (6)$$

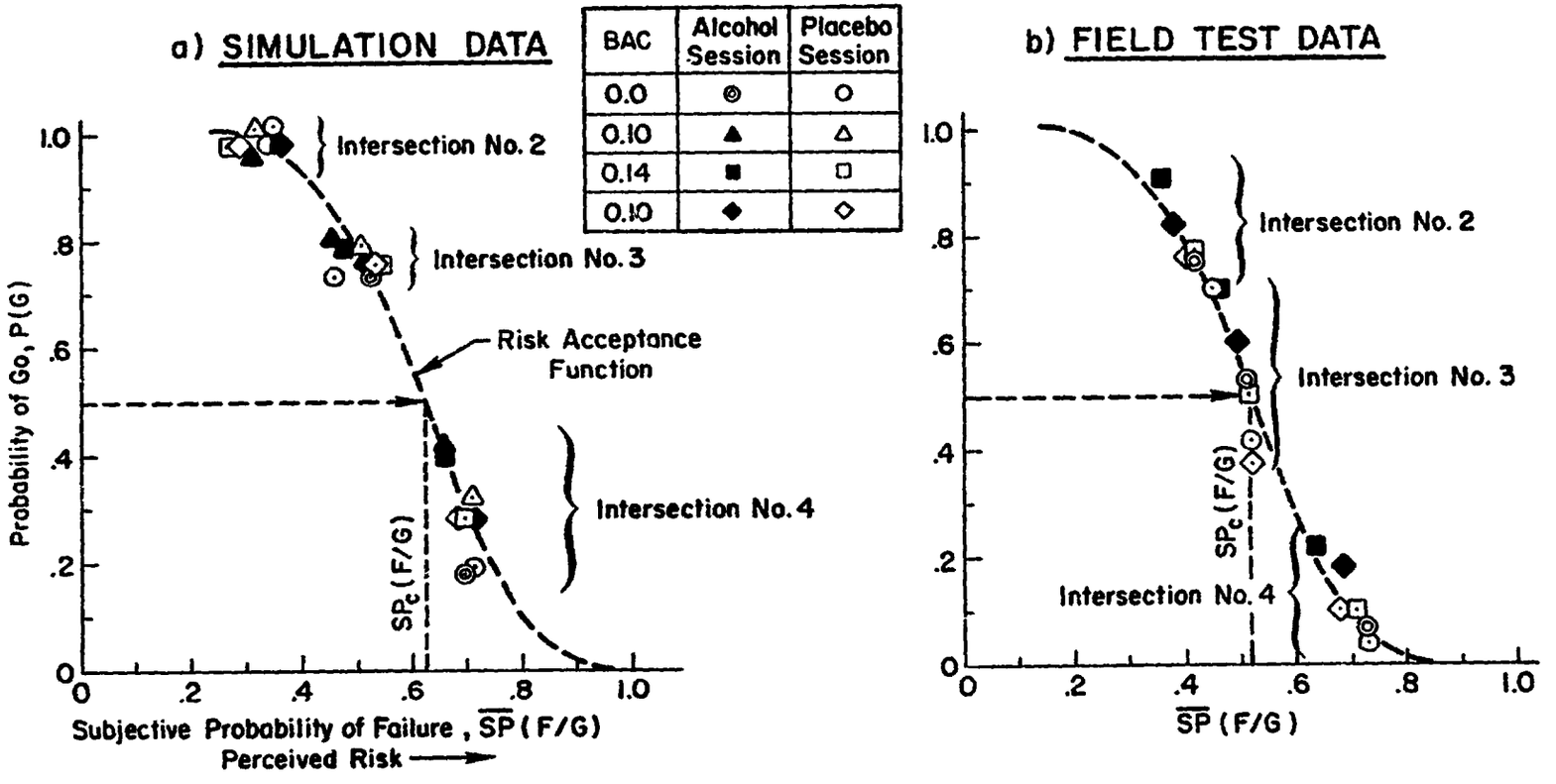

Figure 5. Alcohol Effects on Signal Light Decision Making Behavior

By rearranging this formula we obtain a relationship which can be used for a linear regression fit:

$$a\overline{SP}_i(F/G) - aSP_c(F/G) = \sin^{-1}[2P_i(G) - 1] \qquad (7)$$

The data input for this regression fit is the mean subjective probability of failure and probability of going for each intersection. The derived values are then a and the risk acceptance threshold $SP_c(F/G)$. The parameter a describes the slope at the midpoint of the risk acceptance and is inversely proportional to the risk perception variability σ_{SP}.

The $SP_c(F/G)$ were computed and analyzed with no indication of alcohol effects on driver risk acceptance. The SP_c and $\overline{SP}(F/G)$ data were then used to compute probability of go estimates, $\hat{P}(G)$, according to Eq. 5. These compare favorably as shown in Figure 6. Analysis of covariance procedures were employed to compare the actual and estimated values of P(G). The F ratios indicated that P(G) was highly correlated with the computed estimate $\hat{P}(G)$, Reference 6.

These results suggest that the alcohol effects on the drivers' subjective risk perception, both $\overline{SP}(F/G)$ and σ_{SP}, are responsible for drivers increased going behavior while intoxicated. They also validate the usefulness of the model in analyzing that behavior.

There are other possible interpretations of these results. An intuitive one is that the variations in subjective estimates are due to variations in the time of the decision and not to variations in perception for a given time and distance relation. However, a preliminary analysis of the time histories for several of the subjects indicated that the response times did not change significantly under alcohol, Reference 7. In addition, there are other models which could be applied to the observed signal light behavior. A potentially fruitful approach is the signal detection model as developed by Green and Swets, Reference 8, expanded for application to man/vehicle problems by Curry, et al., Reference 9, and applied to the lane change maneuver by Cohen and Ferrell, Reference 10. Other types of criteria suggested in this work, such as likelihood ratio threshold and Newman-Pearson strategy, may be applicable. However, it is apparent from Figure 6 that the additional refining assumptions used in these models may not be necessary for interpreting the major effects of alcohol on decision behavior.

PREVIOUS RESEARCH

While increasing frequency of driving decision errors with increased BAC has been found by other researchers, the interpretation of which behavior component is primarily responsible for this increase has been inconsistent. Comparison between studies is confounded because of differences in tasks, reward and penalty conditions, alcohol treatment methods, and analytical approaches. However, the results can be interpreted and compared as follows.

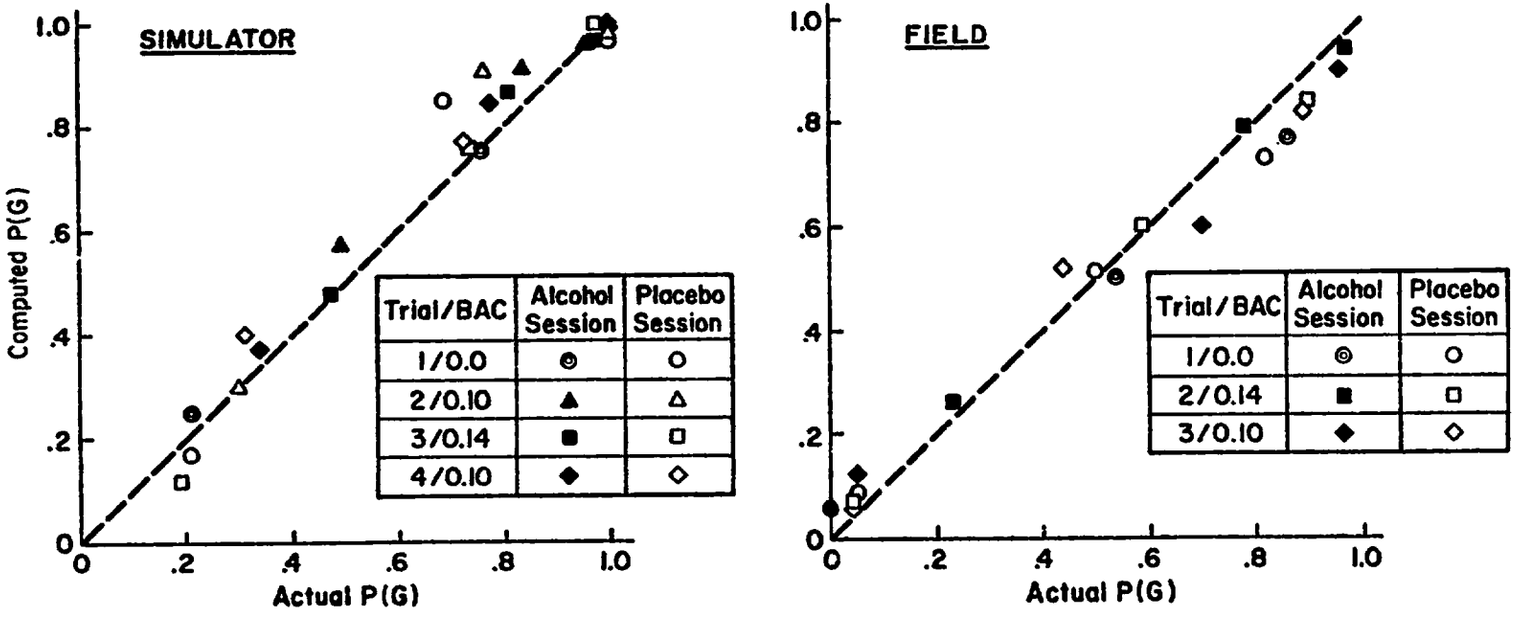

Figure 6. Comparison of Measured Versus Computed Probability of Going. $\hat{P}(G)$ Estimates Computed Using Measured Values of $SP(F/G)$, σ_{SP}, and $SP_c(F/G)$

In agreement with our results, four of the five other studies commented on here found increased risk taking with increased alcohol intake. Cohen, Dearnaley, and Hansel, Reference 1, in evaluating bus drivers' willingness to drive through a cone-delineated gap found the number of attempts increased with alcohol intake. Lewis and Sarlanis, Reference 11, using a simulated traffic signal, found the number of go responses significantly increased under alcohol. Light and Keiper, Reference 12, also found an increased number of attempted passes in a simulated overtaking and passing task. Finally, Ellingstad, McFarling, and Struckman, Reference 13, in evaluating performance on laboratory analogs of automotive passing tasks with multiple discriminant analysis, found the discriminant "riskiness/indecisiveness" increased with alcohol. This discriminant included a positive loading on passing attempts. The only exception to this trend was presented by Snapper and Edwards, Reference 2, who found no significant change with BAC in the number of attempted lane changes through a given gap size on their closed course.

The interpretation of these data as resulting from changes in psychomotor skill, perceptual ability, or cognitive risk acceptance varies between authors. Re-analysis is difficult because only two of these studies took sufficient measures to delineate changes in decision strategies. Cohen, et al., Reference 1, asked the bus drivers to indicate levels of confidence expressed as the number of times out of five the driver thought he could succeed in driving through the different size gaps. The estimates did not change significantly on the average for the narrowest accepted gap; however, the accepted gap size decreased with increased alcohol intake. Therefore, he assumed "If the difficulty of the task remained unchanged, they became more optimistic and attached a higher subjective probability to the task." The variances in the estimates were not reported. Cohen concluded that the primary effects of alcohol were to decrease psychomotor skill and deteriorate "judgment," where we interpret judgment to include mean perception. Snapper and Edwards, on the other hand, asked their subjects for subjective probabilities and found no significant change in the mean for a given gap size. As they found no change in the mean subjective estimates and no increased risk taking, but with increased failures in execution, they concluded that the primary effect of increasing BAC was degraded psychomotor skill. Again, no data on the effects of BAC on the consistency or variability of the subjective probabilities were presented.

By comparison, our findings agree with most of these results but not with the authors' interpretations. As in most of these studies, we found increased risk taking and no change in risk acceptance, i.e., no change in the mean subjective estimate for a given intersection. However, our data suggest that increased risk taking is primarily due to increased variance or inconsistency in perceptual estimates. This interpretation could also explain the results found by the first four authors mentioned above if data on mean and variances of subjective estimates were available. The disparity between this conclusion and Snapper and Edwards' conclusion may be due to at least two factors. Their lane change task placed more emphasis on psychomotor execution than does the current signal light task; hence their results may have been more sensitive to this type of degradation. In fact, we found considerable degradation in the consistency of psychomotor performance in the other tasks in our driving scenario (Reference 7). In addition, a fundamental difference between our

simulated driving tasks and those of both of the previous studies using subjective estimates is addition of temporal pressure. Our subjects were required to form their estimates in "real time" as opposed to the "stop action" type of judgments and driving scenarios used in previous studies.

Thus, the behavior skills required for the decision-making tasks of the other researchers are somewhat different from those studied here. Allowing for these differences, the other studies may have had the same cause for the increased risk taking as measured here, namely, distorted perception, but they did not present sufficient data to determine it.

In summary of previous decision-making studies, those aspects of our results which are directly comparable with previous research largely agree with those findings. Risk taking generally increased with increasing BAC. Interpretation of previous work beyond this point is difficult because of insufficient measures. However, that work does not disagree with the current conclusion that there is no change in risk acceptance. Our interpretation of these results, that perceptual distortion is a primary cause of alcohol-induced increased risk taking observed for simple tasks, is new.

CONCLUSIONS

An expected value model accounted for the effects of perceptual noise on decisions for drivers in a simulated signal light task. With this model, analysis of the significant changes in behavior for increasing BAC indicated no changes in risk acceptance; that is, subjects did not change their subjective criterion level. The primary cause of the increased risk taking found for intersections timed with a low probability of success was increased inconsistency or variance in their subjective perceptual estimates.

These results have ramifications both for researchers in this field and those attempting to apply the results. In future human decision-making work, measures of inconsistency in perception should be given as much attention as measures of central tendency. Also suggested by these results is that one method of reducing drinking driver errors may be to improve the driver's perceptual environment to decrease his inconsistency. We could expect these results to generalize the effects of alcohol on other such real-time decision tasks as aircraft and spacecraft control. In addition, the analytical framework used here may be useful in evaluating the effects of other drugs and stressors on human decision behavior.

ACKNOWLEDGMENT

This work was supported by the Department of Transportation, National Highway Traffic Safety Administration, under Contract No. DOT-HS-4-00999. The views expressed in this paper are those of the authors and do not necessarily represent those of the National Highway Traffic Safety Administration.

REFERENCES

1. Cohen, J.; Dearnaley, E. J.; and Hansel, C. E. M. The Risk Taken in Driving Under the Influence on Alcohol. Brit. Med. J., 21 June 1958, pp. 1438-1442.

2. Snapper, K.; and Edwards, W. Effects of Alcohol on Psychomotor Skill and Decision-Making in a Driving Task. Univ. of Michigan, Department of Psychology, NIAAA Grant No. MN22063-01, 1973.

3. Hurst, P. M. Consistency in Driver Risk Taking. Behavioral Res. in Driving Safety, combined issues, vol. 2, nos. 1-2, Spring-Fall 1971, pp. 73-82.

4. Allen, R. W.; Schwartz, S. H.; and Jex, H. R. Driver Decision-Making Research in a Laboratory Simulation. NATO Symposium on Monitoring Behavior and Supervisory Control, Berchtesgaden, 8-12 Mar. 1976.

5. Rapoport, A.; and Wallsten, T. S. Individual Decision Behavior. Ann. Review of Psych., vol. 23, 1972, pp. 131-176.

6. Allen, R. W.; Schwartz, S. H.; Hogge, J. R.; and Stein, A. C. The Effects of Alcohol on the Driver's Decision-Making Behavior. Systems Technology, Inc., TR-1053-1, Feb. 1978.

7. Allen, R. W.; Schwartz, S. H.; Stein, A. C.; and Hogge, J. R. The Effects of Alcohol on Driver Performance in a Decision-Making Situation. Presented at the 14th Annual Conference on Manual Control; published in this volume.

8. Green, D. M.; and Swets, J. A. Signal Detection Theory and Psychophysics. New York: Wiley, 1966.

9. Curry, R. E.; Gai, E. G.; and Nagel, D. C. Decision Behavior with Changing Signal Strength. In Proc. 10th Annual Conf. on Manual Control, Wright-Patterson AFB, OH, 9-11 Apr. 1974.

10. Cohen, H. S.; and Ferrell, W. R. Human Operator Decision-Making in Manual Control. IEEE Trans., vol. MMS-10, no. 2, June 1969, pp. 41-47.

11. Lewis, E. M., Jr.; and Sarlanis, K. The Effects of Alcohol on Decision Making with Respect to Traffic Signals. Dept. of Health, Education, and Welfare, Rept. No. ICRL-RR-68-4, 1969.

12. Light, W. O.; and Keiper, C. G. Effects of Moderate Blood Alcohol Levels on Automobile Passing Behavior. Dept. of Health, Education, and Welfare Report No. ICRL-RR-69-4, 1971.

13. Ellingstad, V. S.; McFarling, L. H.; and Struckman, L. L. Alcohol, Marijuana and Risk Taking. Dept. of Transportation, Rept. DOT HS-801 028, Apr. 1973.

14. Stein, A. C.; Schwartz, S. H.; and Allen, R. W. Use of Reward-Penalty Structures in Human Experimentation, published elsewhere this volume.

D43

N79-15631

COMBINED MONITORING, DECISION AND CONTROL MODEL FOR THE HUMAN OPERATOR IN A COMMAND AND CONTROL TASK

by

Ramal Muralidharan, Sheldon Baron
Bolt Beranek and Newman Inc., Cambridge, MA

SUMMARY

This paper reports on the ongoing efforts to model the human operator in the context of the task during the enroute/return phases in the ground based control of multiple flights of remotely piloted vehicles (RPV). This is a part of our research aimed at investigating human performance models and at modeling command and control systems.*

The approach employed here uses models that have their analytical bases in control theory and in statistical estimation and decision theory. In particular, it draws heavily on the models and the concepts of the optimal control model (OCM) of the human operator. We are in the process of extending the OCM into a combined monitoring, decision, and control model (DEMON) of the human operator by infusing Decision theoretic notions that make it suitable for application to problems in which human control actions are infrequent and in which monitoring and decision-making are the operator's main activities. Some results obtained with a specialized version of DEMON for the RPV control problem are included.

1. INTRODUCTION

1.1 Modeling Goals

We are involved in a program of research aimed at investigating human performance models and approaches to modeling command and control systems (see reference 1). A part of our research effort concerns the study of the feasibility of modeling the human operators in command and control systems via control and decision theoretic models. This paper describes the salient aspects of this part of our ongoing research effort.

1.2 Modeling Approach

The approach employed here uses models that have their analytical bases in control theory and in statistical estimation and decision theory. In particular, it draws heavily on the models and concepts of the OCM (references 2-6). The modeling approach is normative, in that one determines what the human operator ought to do, given the system objectives and the operator's

* The research reported in this paper was supported by the Air Force Office of Scientific Research under contract F44620-76-C-0029.

646

PAGE INTENTIONALLY BLANK

limitations, and this serves as a prediction of what well-trained, motivated operators will do.

In the basic OCM concern is more with the operator's continuous interact. ' ı with the system, as demanded by closed loop analysis, than with his response to discrete events. The development of the basic OCM and its model structure has been dictated by the principal areas of its previous application, viz., vehicle control. We shall extend the OCM by incorporating structures and notions that make it suitable for application to problems in which human control actions are infrequent and in which monitoring and decision-making are the operator's main activities.* The expected end product is a combined monitoring, decision, and control model for the human operator in a command and control task.

1.3 Task definition

In this paper we shall discuss our modeling effort as it relates to the task facing the human operator during the enroute/return phases in the ground based control of multiple flights of remotely piloted vehicles (RPV).

The enroute/return phases together with a terminal control phase constitute an "RPV mission". An RPV-mission consists of coordinated flights of several RPV-triads. Each triad has a strike vehicle (S), an electronics countermeasures vehicle (E) and a low- reconnaisance vehicle (L). Each RPV is automatically controlled along a pre-programmed flight plan assumed optimal with respect to terrain and defenses. The RPVs deviate from their flight plan due to navigation system errors, position reporting errors, communication jamming by the enemy, equipment malfunctions etc. These deviations are kept in check by external monitoring and control from the ground station. This supervision is provided by human enroute controllers, who are equipped with CRT displays for monitoring flight path and vehicle status and with keyboards and light pens for introducing changes in RPV flight parameters. The ultimate objective of the enroute controllers is to ensure that the S and E RPVs fly on schedule over the target 15 seconds apart followed by the L RPV two minutes later to assess damage. This time-phasing at the target is accomplished by time-phased handoffs at designated hand-off coordinates on the flight plan. The S RPV's are handed off to the terminal controller (pilot) equipped with a televised view from the nose of the RPV and with standard aircraft controls and displays in order to direct each vehicle to a specific designated target, release its payload, and hand it back to one of the enroute controllers.

Terminal phase control is achieved only if the S RPV is within a 1500' corridor around its flight plan. It is the responsibility of the enroute operator to command "patches" to alter the flight plan as necessary to achieve terminal phase control. These patches are acceptable ("GO") only if they satisfy constraints such as turning radius, available fuel, command link status etc.

---

* This type of extension is feasible because of the basic information processing structure of the OCM. Indeed, there have already been applications of OCM to account for visual scanning(references 7,8) and decision making(references 9,10).

In summary, the enroute operator's task is to monitor the trajectories and ETAs of N vehicles, to decide if the lateral deviation or ETA error of any of these exceeds some threshold, and to correct the paths of those that deviate excessively by issuing acceptable patches.

2. THE CLOSED LOOP MODEL

A block diagram modeling the flow of information and the control and decisions encountered by the human operator (enroute operator) is shown in Figure 1.

ORIGINAL PAGE IS
OF POOR QUALITY

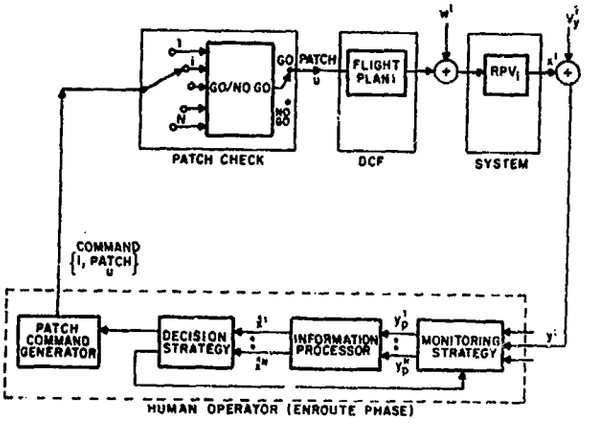

Figure 1. Block Diagram for RPV Monitoring/Control Decision Problem

DCF: The DCF (Drone control facility) contains the stored flight plans that drive the N subsystems RPV_i, i=1,2,...,N. They are usually "optimal" with respect to current terrain and other information. We will assume they can be computed using state-variable equations.

System: The N RPVs undergoing monitoring/control constitute the system. A simple non-linear representation of their dynamic behavior will be assumed for this analysis. Linearization will be carried out if necessary for implementation of the model. The true status x^i of the i-th RPV may be different from the stored flight plans due to "disturbances" w^i. The reported status y^i will be different from the true status x^i due to reporting error v_y^i. The observed status y_p^i will depend on the reported status y^i and on the "monitoring strategy" (to be discussed later on).The disturbances w^i and reporting error v_y^i will be modeled by suitable random processes. The y^i are the displayed variables corresponding to RPV_i.

Monitoring Strategy: Since the human must decide which RPV or which display to look at, he needs to develop a monitoring strategy. This is important because his estimates of the true status of each RPV (and hence his patch decision strategy) will depend upon his monitoring strategy. To account for the interaction of the patch decision strategy with the monitoring strategy we formulate and solve a combined monitoring and patching decision problem (Appendix B has the details).

Monitoring strategies may be distinguished by whether they predict temporal (time histories of) monitoring behaviour or average monitoring behaviour over some chosen time horizon. Most of the earlier work in the literature, including that with the OCM, falls in the latter category. The monitoring strategy we derive will predict temporal behaviour which can be simulated . Some of the monitoring strategies derived in the literature which we expect to investigate in the DEMON setup are:

(i) A simple strategy involving cyclical processing of the various RPVs(reference 11).

(ii) A strategy generalizing the Queueing Theory Sampling Model (reference 12), which would minimize the total cost of not looking at a particular RPV at a given time. This strategy is mainly useful for maintaining lateral deviations within allowable limits. The costs for errors and for the different RPVs would be functions of the time-to-go and, possibly, RPV type.

(iii) A strategy of sampling when the probability that the signal exceeds some prescribed limit is greater than a subjective probability threshold(references 13,14).

(iv) A strategy aimed at minimizing total estimation error(reference 7). This strategy would be consistent with monitoring for the purpose of minimizing lateral deviation errors.

Information Processor: This block models the processing that goes on in the human operator to produce the current estimate of the true RPV status from past observed status. This block is the well known control- theoretic model consisting of a Kalman filter-predictor which produces the maximum-likelihood, least-squares estimate $\hat{x} = (\hat{x}^1, \hat{x}^2, \ldots, \hat{x}^N)$ of the true status x of all the RPVs. It also produces the variance of the error in that estimate.(Note that an estimate of the state of each RPV is maintained synchronously at all times. Observation of a particular RPV improves the accuracy of the estimate of the status of that RPV while uncertainty about the status of the remaining, unobserved vehicles increases.) Given the assumptions generally made for this kind of analysis, the information processor can thus generate the conditional density of x based on the past observations y.

Decision Strategy: This block models the process of deciding which, if any, RPV to patch. We consider the decision process to be discrete (it takes 5 sec to get a new display). The cost of making a patch would reflect the lost opportunity to monitor and/or patch other RPVs as well as breaking radio-silence; the gain (negative cost) is the presumed reduction in error for the "patched" vehicle. The decision strategy attempts to minimize the (expected) cost. This block translates the best estimate $\hat{x}$ into a decision to (i) command a patch to one of the RPVs and/or (ii) modify the future monitoring strategy.

Patch Command Generator: This block generates the commanded patch. We shall investigate a strategy based on minimizing a weighted sum of the time to return to the desired path and the total mean-square tracking error. The allowable paths would be constrained by the RPV turning radius limits. Random execution errors would be added to the commanded patch to represent human errors.

Patch Check: This consists of a GO/NO GO check on the patch using conditions on turning radius, command link status, etc.

3. MATHEMATICAL DETAILS OF THE MODEL

3.1 System

The system under study consists of the N-RPV subsystems and may be described by the state equations:*

$$\dot{x} = Ax + dBu + Ew + Fz \qquad , x(t_0) = x_0 \tag{1}$$

where the state vector x includes the states x^i of the N-RPV subsystems. Here d is a vector of decision variables (to be explained below) and z is a non-random input vector which will be used to model non-zero means of the random inputs w as well as any predetermined command inputs. In the present RPV context z will be used to generate the flight plan for the RPVs. The vector u denotes the patch control input to the RPVs. In partitioned form equation (1) appears as follows:

$$\begin{bmatrix} \dot{x}^1 \\ \dot{x}^2 \\ \vdots \\ \dot{x}^N \end{bmatrix} = \begin{bmatrix} A^{11} & A^{12} & \cdots & A^{1N} \\ A^{21} & A^{22} & \cdots & A^{2N} \\ \vdots & & \ddots & \\ A^{N1} & A^{N2} & \cdots & A^{NN} \end{bmatrix} \begin{bmatrix} x^1 \\ x^2 \\ \vdots \\ x^N \end{bmatrix} + \begin{bmatrix} d_1 I & & & \\ & d_2 I & & \\ & & \ddots & \\ & & & d_N I \end{bmatrix} \begin{bmatrix} B^1 \\ B^2 \\ \vdots \\ B^N \end{bmatrix} u + \begin{bmatrix} E^{11} & E^{12} & \cdots & E^{1N} \\ E^{21} & E^{22} & \cdots & E^{2N} \\ \vdots & & \ddots & \\ E^{N1} & E^{N2} & \cdots & E^{NN} \end{bmatrix} \begin{bmatrix} w^1 \\ w^2 \\ \vdots \\ w^N \end{bmatrix} + \begin{bmatrix} F^{11} & F^{12} & \cdots & F^{1N} \\ F^{21} & F^{22} & \cdots & F^{2N} \\ \vdots & & \ddots & \\ F^{N1} & F^{N2} & \cdots & F^{NN} \end{bmatrix} \begin{bmatrix} z^1 \\ z^2 \\ \vdots \\ z^N \end{bmatrix} \tag{2}$$

For the system under study, the following observations hold:

A1: Only one of the N-RPV subsystems may be controlled by the patch-control u at any given time. A decision to control the i-th RPV subsystem then implies the following conditions on the decision variables:

$$d_i = 1 \quad , d_j = 0 \quad , j \neq i \tag{3}$$

A2: The N-RPV subsystems are decoupled (except for the interdependence of the decision variables via (3)), that is,

---

* For the purpose of discussion, a linear model is assumed. In actual implementation, we may use a simple non-linear model in which case (1) would represent a linear perturbation equation for the system about some nominal trajctory.

$$A^{ij} = 0,\ E^{ij} = 0\ ,\ F^{ij} = 0,\ i \neq j \tag{4}$$

The N-RPV subsystems may thus be described by

$$\dot{x}^i = A^{ii}\, x^i + d_i B^i u + E^{ii} w^i + F^{ii} z^i,\ x^i(t_0) = x_0^i \tag{5a}$$

$$d_i = 0 \text{ or } 1 \tag{5b}$$

$$\sum d_i = 1 \text{ or } 0 \tag{5c}$$

3.2 Flight Plan (DCF)

When there is no disturbance w^i and no (patch) control u then the N-RPV subsystems follow the flight plan $\bar{x}^i$

$$\dot{\bar{x}}^i = A^{ii}\, \bar{x}^i + F^{ii} z^i,\ \bar{x}^i(t_0) = \bar{x}_0^i \tag{6}$$

Flight plans made up of straight lines are easily generated using a piecewise constant time function for z^i and $\bar{x}_0^i$ as the launch point.

3.3 Patching

Any disturbance w^i causes the i-th RPV to deviate from its flight plan. Denoting these deviations by $e^i = x^i - \bar{x}^i$ it follows from (5) and (6) that

$$\dot{e}^i = A^{ii}\, e^i + d_i B^i u + E^{ii} w^i\ ,\ e^i(t_0) = x_0^i - \bar{x}_0^i \tag{7a}$$

$$d_i = 0 \text{ or } 1 \tag{7b}$$

$$\sum d_i = 1 \text{ or } 0 \tag{7c}$$

It is the purpose of the (patch) control u to correct any such deviation. Since w^i is an unknown random disturbance and d^i is nonzero for at most a single RPV subsystem, it is not possible to maintain $e^i=0$ for all i. The operator thus faces the patching problem which consists of the following three sub-problems:

(i) Monitoring decision - which RPV to monitor?
(ii) Patching decision - whether to patch the monitored RPV?
(iii) Patch computation - what patch command to issue?

3.3.1 Monitoring Decision

As mentioned before, the monitoring decision is intimately connected with the patching decision because it restricts the available patching options. For example, in the present RPV context only a monitored RPV can be patched. The combined monitoring and patching decision problem is analyzed in appendix B.

3.3.2 Patching Decision

A patching decision consists of deciding if the monitored RPV subsystem is to be patched. At most one of the RPVs may be patched at a given time. One idea of patching is to reduce deviations from the flight plan to below some threshold values. Some facts to note are:

(i) Cross-track error of less than 250' is desired for type-S RPVs

(ii) Terminal-phase control not possible if cross track error exceeds 1500'

We assume a normative model, in which the operator attempts to optimize some (subjective) measure of performance via a patching decision. This performance measure would depend on his understanding of the mission objectives. Some of the objectives of the RPV mission are: Don't lose an RPV, maintain ETA, maintain lateral position, maintain radio silence. We consider two alternative cost functions to help in arriving at a patching decision:

Piecewise constant cost function

$C(e^i) = \bar{C}^i$ if $e^i \in e_T^i$, a threshold set

$C(e^i) = C^i$ if $e^i \notin e_T^i$

Quadratic Cost function

$C(e^i) = e^{i'} K e^i$

The choice of e_T^i and K will be made based on facts of the type (i) and (ii) noted above. The costs C^i, $\bar{C}^i$, $C(e^i)$ will be chosen to be functions of mission time to reflect the importance of ETA. As mission time gets closer to ETA for RPV-i, C^i will be made larger and/or e_T^i will be shrunk to reflect "urgency". The optimal patch decision will be chosen to minimize the expected cost using subjective probabilities computed with the help of the information processor. The details are in Appendix B.

3.3.3 Patch Control Computation and Generation

Once a decision is made to patch a particular RPV-subsystem, it is necessary to compute and execute the patch control. The purpose of a patch control is to guide the aircraft from its initial location and heading to intercept and fly along the planned flight path. Various criteria may be considered to compute the optimal patch control, for example, a strategy that minimizes the time to return to the planned flight path (see appendix A and also reference 15).

4. IMPLEMENTATION OF THE MODEL

DEMON, the combined monitoring, decision, and control model of the human operator is being implemented in FORTRAN. The program has a modular structure to facilitate ease of adding further modules to include alternative monitoring, control, and decision strategies that may appear promising at a future date.

To accomodate the random aspects of the problem, the program will basically have a Monte-Carlo simulation character. The specialized version of DEMON for

the RPV problem will produce as outputs the "true" time-histories of the RPV flights, the sequence of monitoring and patching decisions made, and the resulting performance.

The important aspects of the simulation program implementing Demon are

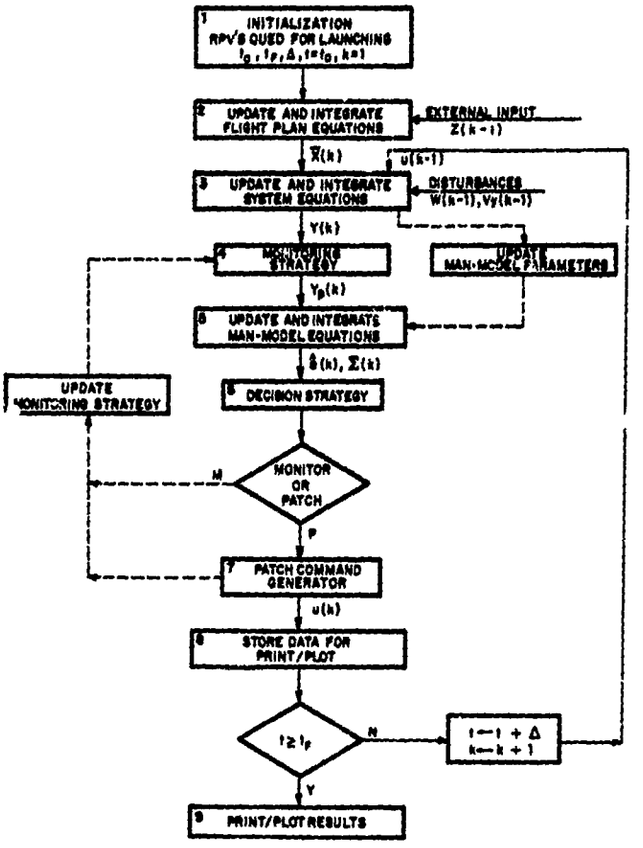

ORIGINAL PAGE IS
OF POOR QUALITY

Figure 2. Flow Diagram for the simulation program implementing DEMON

shown in the flow diagram in Figure 2. There are, as indicated, nine major modules in the program. Modules 4, 6 and 7 are of special interest because they do not arise in the usual manual control models. The theory behind these modules is developed in Appendices A and B. As indicated in Appendix A, the patch command generator could involve a non-linear control law.

5. EXAMPLE

In order to test some of the modeling concepts and to debug the DEMON program we consider a simple example which captures the essence of the RPV mission while discarding the nitty gritty details. The lateral motion of the RPVs about their flight plan is represented by random walk processes over the assumed mission duration of 600 frames (the display frame update rate is every 5

ORIGINAL PAGE IS
OF POOR QUALITY

seconds). Each RPV is observed via a single lateral deviation display and controlled via a constant velocity comand. The permissible patch back to the flight plan is constrained by the maximum allowable speed which represents the turning radius constraint. The patch control strategy is to use maximum allowable speed adjusted by a "safety factor" which depends on the "NO GO" patches issued previously by the operator for that RPV.

Some preliminary results have been obtained using DEMON on the above simplified RPV mission. The flavour of the results we obtained is indicated in Figure 3 which shows the combined effect of ETA dependent (shrinking) threshold and different RPV priority on the simulated simple RPV mission. As mission time increases RPV monitoring frequency increases . But there comes a time when monitoring resources are not adequate to satisfy the increasing needs of each of

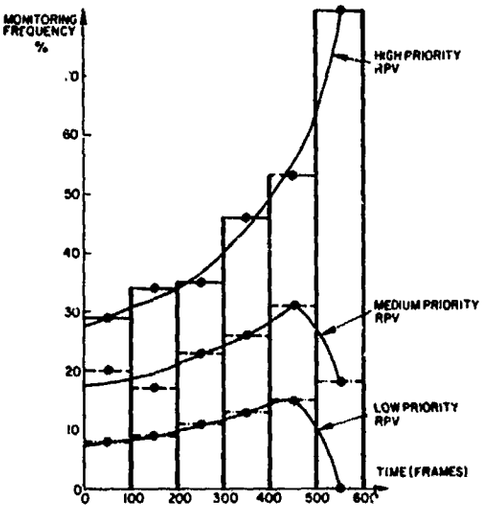

Figure 3. Effect of Shrinking Threshold and RPV Priority

the RPVs and then the highest priority RPV demands most of the attention it can get while the lowest priority RPV gets no attention from the operator.

6. CONCLUSION

We have developed DEMON, a combined monitoring, decision and control model for the human operator in the context of the enroute phase of an RPV mission. Since the monitoring strategy derived from DEMON is temporal it has obvious application to developing instrument scanning strategy for flight control and management. We have structured the model to have wider applicability (than the problems addressed by the basic OCM or the RPV control problem) and expect it to be useful to model human operators whose control actions may be infrequent but whose monitoring and decison making may be the primary activities. We anticipate testing and refining the DEMON model furthur using an existing data base for the RPV control problem(reference 16).

7. APPENDIX A: PATCH CONTROL STRATEGY

7.1 System Dynamics and Patch Computation

In Section 3, the N-RPV system dynamics were considered in general terms. Here, we shall use a simple model for the RPV-subsystem dynamics and derive a specific patch control strategy. Considering only the projected motion in the horizontal plane we shall re-write the normalized equations of motion derived in

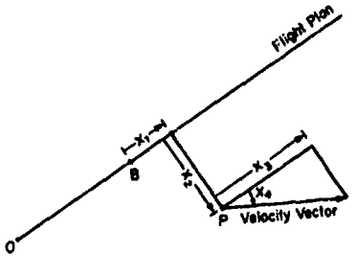

Figure 4. Choice of Co-ordinates for System Equation

reference 15, using the state variables(see Figure 4) x_1 = ground-speed error, x_2 = cross-track error, x_3 = velocity component along track, x_4 = heading relative to track:

$$\dot{x}_1 = \cos x_4 - 1 \ , \ x_1(0) \text{ given}, \ x_1(T) \text{ free}$$

$$\dot{x}_2 = \sin x_4 \ , \ x_2(0) \text{ given}, \ x_2(T) = 0$$

$$\dot{x}_3 = u \ \sin x_4 \ , \ x_3(0) \text{ given}, \ x_3(T) = 1$$

$$\dot{x}_4 = -u \ , \ x_4(0) \text{ given}, \ x_4(T) = 0$$

T free

$$x_3^2 + x_4^2 = 1$$

Once a decision is made to patch a particular RPV-subsystem, it is necessary to compute and execute the patch control. The purpose of a patch control is to guide the aircraft from its initial location and heading to intercept and fly along the planned flight path. Various criteria may be considered to compute the optimal patch control. Many criteria may be written in the form,

$$J = 1/2K_1x_1^2(T) + 1/2K_2 \int_0^T x_2^2 \, dt + K_3 \int_0^T dt$$

which is a weighted sum of the square of the ground speed error, integral square of the cross-track deviation, and time to return to the planned flight path.We shall only solve the special problem of minimum time to return to the flight path by choosing the weights to be $K_1=0=K_2$ and $K_3=1$.

ORIGINAL PAGE IS
OF POOR QUALITY

7.2 Minimum Time Patch Strategy

Using the necesssary conditions for minimum time it is easy to see that the optimal control is Bang-Bang except for possible singular arcs. It can furthur be shown that the singular control is identically zero.

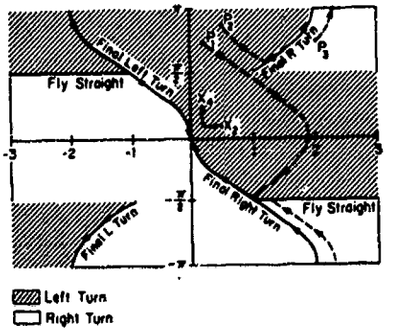

Figure 5. Minimum Time Patch Control Strategy

The computed minimum-time patching strategy is indicated in Figure 5. For example, all points in state space that can be brought to the planned flight path using a single left turn u=1 are characterized by the equation $x_2(0) = \cos x_4(0) - 1$.

The minimum time required for the patch will be checked against the scheduled hand-off times for the given RPV to determine if the computed patch should be executed. Velocity patches to correct for ETA errors with due regard to fuel constraints may be included by a simple extension of the above problem (for example, append to the minimum time patch a velocity patch to minimize ETA errors).

The operator does not observe the states x directly, and will base his control actions instead on the best estimates of these states available to him based on all his observations. This disjoining of estimation and control is justified by the "separation principle" (see reference 17).

8. APPENDIX B: PATCH DECISION STRATEGY

8.1 Introduction

In this appendix we shall formulate and solve the combined monitoring and patching decison problem encountered by the enroute operator in the RPV mission. As stated in section 3, the information processor produces the current estimate $\hat{x}$ of the true status x of all the RPVs at any time. It also produces the variance of the error in that estimate. The information available for making monitoring and patching decisions may be summarized in terms of the posterior distribution of x^i conditioned on all observations based on past monitoring and patching decisions and control. Under the usual assumptions, this posterior distribution for x^i is $N(\hat{x}^i, X^{ii})$.

Let x_T^i denote a threshold set associated with the i-th RPV, that is, $x^i \in x_T^i$ is a desirable condition. Let H^i denote the hypothesis that $x^i \notin x_T^i$ and P^i be the probability that H^i is true. P^i is easily calculated using the available information on the posterior distribution of x^i:

$$P^i = 1 - \int_{x_T^i} N(\hat{x}^i , X^{ii})\, dx^i$$

Monitoring the i-th RPV results in a tighter distribution for x^i around its mean $\hat{x}^i$ because it reduces the uncertainty X^{ii} associated with $\hat{x}^i$. Patching the i-th RPV requires monitoring as well. The effects of patching are: first, to correct the error e^i which might have 'wandered off' from zero due to disturbances, by assuring that $\hat{x}^i \in x_T^i$; and second, to provide a tighter distribution of x^i around its mean $\hat{x}^i$.

To formulate and solve the combined monitoring and patching decision problem, we shall assume that C_i is the cost if H^i is true. Recall that H^i has a (subjective) probability P^i of being true. Just as H_i, P^i, C_i were defined in relation to the set x_T^i, let $\bar{H}_i$, $\bar{P}^i$, $\bar{C}_i$ be defined in relation to the set $\bar{x}_T^i$, the complement of x_T^i. We shall use minimum expected cost EC(d*) as the criterion for selecting the best monitoring and patching decision d*.

Let d_{ij} denote a decision to monitor RPV-i and patch RPV-j in the combined monitoring and patching decision problem. Since a patch can be done only on a monitored RPV, there are only 2N+1 available decisions. They are:

(i) Do nothing decision d_{00}, that is, monitor no RPV and patch no RPV.*

(ii) N pure monitoring (no patching) decisions d_{j0}, j=1,2,..,N.
(iii) N patching (and monitoring) decisions d_{jj}, j=1,2,...,N.

Let P_{ijk} denote the probability that the hypothesis H^i is true when the decision is d_{jk}. Because the RPV subsystems are non-interactive, it follows that the probabilities associated with RPV-i when some other RPV is monitored and/or patched is same as that associated with RPV-i when no RPV is monitored. That is,

$$P_{i00} = P_{ijk} \quad \text{any } j \neq i,\ i=1,2,\ldots,N;\ k=j \text{ or } 0$$

Thus, there are only 3N distinct probabilities to be computed
(i) N probabilities P_{i00} associated with do-nothing decision d_{00}
(ii) N probabilities P_{ii0} associated with pure monitoring decision d_{i0}
(iii) N probabilities P_{iii} associated with patching decision d_{ii}

Let $(PP)_i$ denote the probability that the patch decision d_{ii} "takes", that is, results in $x^i \quad x_T^i$, and let T_{ij} denote the cost of implementing decision d_{ij}. The costs T_{ij} will be chosen to be functions of mission time to reflect the importance of ETA. As mission time gets closer to ETA for RPV-i, T_{ij} will be made larger and/or x_T^i will be shrunk to reflect "urgency".

---

* This could correspond to performing some other task such as communication.

The combined monitoring and patching decision problem is described in terms of a decision-tree diagram in Figure 5.* The actual cost of a particular

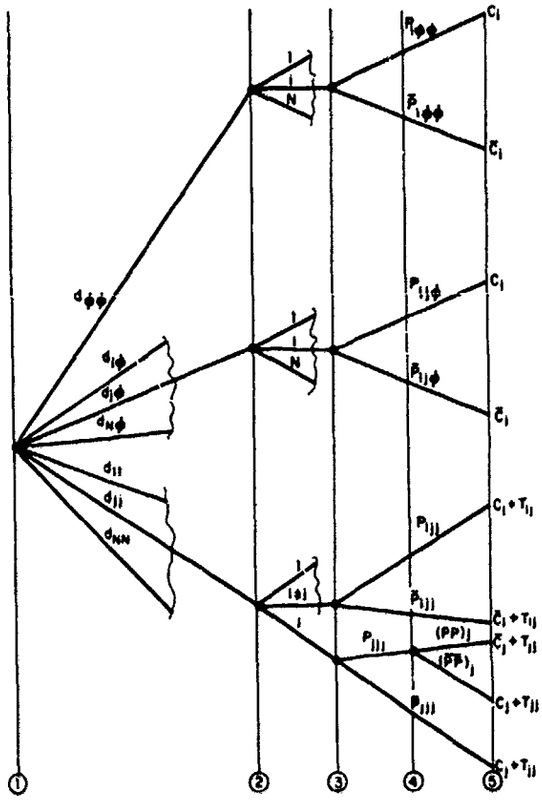

ORIGINAL PAGE IS
OF POOR QUALITY

Figure 6. Decision Tree Diagram for Combined Monitoring and Patching

decision depends on the path chosen to traverse the tree from level 1 to level 5. The exact path from level 1 to level 5 for the N-RPVs are determined both by the decision maker (the human operator) and by Nature (the random elements in the problem) . Since a decision has to be made at level 1 before Nature has

* For reasons similar to the one we stated for combining the monitoring and patching decision problem, one might argue that the decision problem over the rest of the mission duration must be considered by the operator at any decision instant during the mission. We shall not do this because: first, the analysis for this case is no different from the one we present here - only the expressions are messier; and second, the actual computations of the decisions would become infeasible .

taken its course at the monitoring level 3 and at the patching level 4 , the decision maker can only evaluate his 2N+1 alternative decisions in terms of their expected costs. This he can do as follows: The expected cost of the do-nothing decision d_{00} is

$$EC(d_{00}) = \sum_1^N (C_i P_{i00} + \bar{C}_i \bar{P}_{i00})$$

Expected cost of pure monitoring decision d_{j0} is

$$EC(d_{j0}) = EC(d_{00}) - (C_j P_{j00} + \bar{C}_j \bar{P}_{j00}) + C_j P_{jj0} + \bar{C}_j \bar{P}_{jj0}) + T_{j0}$$

Expected cost of a patching decision d_{jj} is,

$$EC(d_{j0}) = EC(d_{00}) - (C_j P_{j00} + \bar{C}_j \bar{P}_{j00}) + (C_j P_{jjj} + \bar{C}_j \bar{P}_{jjj}) - (PP\ P \qquad T_{jj})$$

The optimal decision d^* is the one which results in maximum opportunity gain, that is,*

$$d^* = \arg\min\ (\ EC(d_{00}, EC(d_{m0}), EC(d_{kk})\ )$$

where

$$m = \arg\max_j\ ((C_j P_{j00} + \bar{C}_j \bar{P}_{j00}) - (C_j P_{jj0} + \bar{C}_j \bar{P}_{jj0}) - T_{j0}\ )$$

$$k = \arg\max_j\ ((C_j P_{j00} + \bar{C}_j \bar{P}_{j00}) + (C_j P_{jjj} + \bar{C}_j \bar{P}_{jjj}) - (PP_j P_{jjj}(C_j - \bar{C}_j) - T_{jj})\ )$$

Consider a specialization of the above decision problem where the probabilities P_{ijk} are assumed to be independent of the decisions d_{jk} (that is, $P_{ijk} = P_i$) , the costs $\bar{C}_i$ and T_{ij} are all zero, and the patch success probabilities $(PP)_i = 1$ for each subsystem RPV. Then the optimal decision is

$$d^* = d_{jj}$$

where

$$j = \arg\max_i\ (P_i\ C_i)$$

This is the result obtained by Carbonell(reference 12).

An implicit assumption made in the computation of expected cost in the combined monitoring and patching decision problem is that the costs are constant over the entire sets $\bar{x}_I^j$ and x_I^j. This assumption is easily dropped when non-constant cost functions are desired, e.g.,

$$C(e^i) = e^{i'}\ M\ e^i$$

In such a case, $P_{ijk}C_j$ in the above analysis will be replaced by an appropriate integral which would yield $P_{ijk}C_i$ as a function of $\hat{x}^i$ and X^{ii} and appears amenable for computations.

---

* The notation arg. min. implies $d^* = d_{00}$ or d_{m0} or d_{kk} depending on which of the three values $EC(d_{00})$, $EC(d_{m0})$, $EC(d_{kk})$ is the smallest. Here d_{m0} is the best monitoring decision and d_{kk} is the best patching decision.

We close this appendix, with an example of a piecewise-constant cost function that appears meaningful for the N-RPV system under study. Recall from appendix A that the first two components of x^i are:

x_1^i = ground speed error (along track)

x_2^i = cross-track error

One choice for the piecewise-constant cost function is:

$$C(e^i) = 1 \text{ if } |x_2^i| > x_{2T}^i = 250$$
$$= 0 \text{ if } |x_2^i| \leq 250$$

REFERENCES

1. Miller, D., Feehrer, C., Muralidharan, R., Pew, R. and Baron, S., "Development of Human Performance models for Man-Machine System Simulation", BBN Report No. 3739, December 1977.

2. Baron, S., "A Model for Human Control and Monitoring Based on Modern Control Theory," **Journal of Cybernetics and Information Sciences**, Vol. 4, No. 1, Spring 1976.

3. Baron, S. and W. Levison, "An Optimal Control Methodology for Analyzing the Effects of Display Parameters on Performance and Workload in Manual Flight Control, "**IEEE Trans. on Systems Man and Cybernetics**, Vol. SMC-5, No. 4, July 1975.

4. Baron, S., D. L. Kleinman, et al., "Application of Optimal Control Theory to the Prediction of Human Performance in a Complex Task," Wright Patterson Air Force Base, Ohio, AFFDL-TR-69-81, March 1970

5. Kleinman, D. L. and S. Baron, "A Control Theoretic Model for Piloted Approach to Landing," **Automatica**, Vol. 9, 1973, pp. 339-347

6. Kleinman, D. L., S. Baron and W. H. Levison, "An Optimal-Control Model of Human Response, Part 1: Theory and Validation," **Automatica**, Vol. 6, 1970, pp. 357-369

7. Baron, S. and D. L. Kleinman, "The Human as an Optimal Controller and Information Processor," **IEEE Trans. on Man Machine Systems**, MMS-10, No. 1, March 1969

8. Kleinman, D. and R. Curry, "Some New Control Theoretic Models for Human Operator Display Monitoring", **IEEE Trans. on Systems , Man and Cybernetics**", Vol. SMC-7, No.11, November 1977, pp. 778-784

9. Levison, W. and R. Tanner, "A Control Theoretic Model for Human Decision-Making", NASA CR-1953, December 1971

10. Gai, E. and R. Curry,"A Model of the Human Observer in Failure Detection Tasks", **IEEE Trans. System , Man and Cybernetics**, Vol. SMC-6, No. 2, February 1976

11. Senders, J., "The Human Observer as a Monitor and Controller of Multidegree of Freedom Systems", **IEEE Trans. Hum. Factors Electron.**, Vol. HFE-5, No. 1, September 1964

12. Carbonell, J. R.,"A Queueing Model of Many-Instrument Visual Sampling," **IEEE Transactions on Human Factors in Electronics**, Vol. HFE-7, No. 4, December 1966, pp. 157-164

13. Senders, J.,J. Elkind, M. Grignetti and R. Smallwood, "An Investigation of the Visual Sampling Behaviour of Human Observers", NASA CR-434, April 1966

14. Gai, E. and R. Curry, "Failure Detection by Pilots During Automatic Landing: Models and Experiments", **J. Aircraft**, February 1977

15. Erzberger, H. and H. Q. Lee, "Optimum Horizontal Guidance Techniques for Aircraft," **J. Aircraft**, Vol. 8, No. 2, February 1971, pp. 95-101

16. Mills, R.,R. Bachert and N. Aume, "Supplementary Report of the RPV System Simulation Study II : Evaluation of RPV Position Report Smoothing and Automatic Heading Correction", AMRL-TR 75-87, September 1975.

17. Bryson, A. E. and Y. C. Ho, "**Applied Optimal Control**", Hemisphere, newyork, 1969

D44

N79-15632

A MODEL OF HUMAN EVENT DETECTION IN MULTIPLE PROCESS MONITORING SITUATIONS*

Joel S. Greenstein and William B. Rouse

Department of Mechanical and Industrial Engineering
Coordinated Science Laboratory
University of Illinois
Urbana, Illinois 61801

SUMMARY

It is proposed that human decision making in many multi-task situations might be modeled in terms of the manner in which the human detects events related to his tasks and the manner in which he allocates his attention among his tasks once he feels events have occurred. A model of human event detection performance in such a situation is presented. An assumption of the model is that, in attempting to detect events, the human generates the probabilities that events have occurred. Discriminant analysis is used to model the human's generation of these probabilities. An experimental study of human event detection performance in a multiple process monitoring situation is described and the application of the event detection model to this situation is addressed. The experimental study employed a situation in which subjects simultaneously monitored several dynamic processes for the occurrence of events and made yes/no decisions on the presence of events in each process. Input to the event detection model of the information displayed to the experimental subjects allows comparison of the model's performance with the performance of the subjects.

INTRODUCTION

In many systems, the human operator spends much of his time monitoring subsystems for events which call for action on his part. Aircraft, power stations, and process control plants are examples of such systems. As the complexity of these systems increases, the operator becomes responsible for more subsystems of greater variety. There is consequently a greater probability that the operator will encounter situations in which there are more tasks than he can acceptably perform.

One means of maintaining the operator's workload at a satisfactory level is the introduction of automation capable of performing some of the operator's tasks. Models of the operator's task performance would be of use

*This research was supported by the National Aeronautics and Space Administration under NASA-Ames Grant NSG-2119.

in predicting the performance gains to be expected from the introduction of such aids. Further, in systems in which the responsibilities for some tasks are shared by the operator and an automated decision maker, these models might also be used within the system to coordinate the actions of the two decision makers.

Senders [1] and Smallwood [2] have modeled human decision making in multiple process monitoring tasks. Senders postulated that the human monitor samples his displays in a manner which allows reconstruction of the displayed signals. An information theory approach is employed to determine how often and for what duration the human must sample each display. Smallwood proposed that the human operator forms an internal model of the processes he is monitoring and of the environment relevant to his task as a result of his past perceptions of them. A situation is considered in which the operator seeks to detect excursions of instruments beyond threshold values. The operator is modeled as directing his attention to the instrument whose current probability of exceeding threshold (based on the operator's internal model) is greatest. It might be noted, in passing, that the internal model concept discussed by Smallwood is perhaps as appropriate to the design of automated decision makers as it is to modeling the human decision maker. If the automated decision maker is to interact appropriately with the human, it would seem that its internal model of the relevant environment should include a model of the human.

Carbonell [3,4] and Senders and Posner [5] have proposed queueing theory approaches to the modeling of human decision making in multiple process monitoring tasks. Carbonell uses a priority queueing discipline. He assumes that the human operator attempts to minimize the risk involved in not observing other instruments when he chooses to monitor a particular instrument. Senders and Posner employ a first come first served service discipline. They suggest two models which might be used to estimate the inter-observation intervals for an instrument (i.e., the time between arrivals of the instrument to the queue of instruments awaiting observation by the human monitor). The first model involves the degree of the observer's uncertainty about the value of the variable displayed on the instrument. The second model involves the probability that the displayed variable will exceed an acceptable limit.

The models cited above emphasize the monitoring of displays, rather than the decisions or actions that result from the human operator's perception of the displayed values. The operator's motivation for monitoring the displays is the possibility that an event which requires his action will occur. The multi-task decision making problem addressed in this paper concerns the event detection and action selection decisions the operator makes on the basis of the information he gains through monitoring.

Human decision making in such multi-task situations, then, might be modeled in terms of the manner in which the human detects events related to his tasks and the manner in which he allocates his attention among his tasks once he feels events have occurred. Gai and Curry [6] have developed a model of the human monitor in a failure detection task. The model has two stages, the first being a Kalman filter which estimates the states and observations

of the monitored process and the second a decision mechanism which operates on the Kalman filter residuals using sequential analysis concepts. The model can be used to describe the human monitor's detection of additive failures in stationary random processes.

Sheridan and Tulga [7] have modeled the manner in which the human operator allocates his attention among various tasks. They address a situation in which events present themselves unequivocally and use a dynamic programming approach to determine the action sequence which maximizes the operator's earnings. This action sequence is begun, but can be superceded by a new sequence calculated in response to the appearance of additional tasks.

Rouse [8] has investigated the issue of allocation of decision making responsibility between a human operator and an automated decision maker. He presents a mathematical formulation of the multi-task decision making situation appropriate to the modeling of either decision maker. Based on displayed information, the decision maker is assumed to generate probabilities that events have occurred in his tasks. He also generates density functions which characterize his perceptions of what might occur in his tasks while his attention is diverted to a particular task and how long his attention will be diverted should he decide to take a given action. Combining estimates of the probabilities events have occurred with the density functions of time between events in the tasks and action times with respect to the tasks, the decision maker chooses his actions to minimize an appropriate cost criterion. In this paper, we present a model of the human's event detection performance consistent with this mathematical formulation, describe an experimental study of event detection performance in a multiple process monitoring situation, and address the application of the model to the process monitoring situation.

THE EVENT DETECTION MODEL

The event detection model assumes that, in attempting to detect events, the human generates the probabilities that events have occurred. A discriminant analysis approach [9,10] is used to model the human's generation of these probabilities. Our use of discriminant analysis to model the human's generation of event probabilities is motivated by the fact that this approach does not require explicit models of the systems the human is monitoring. An understanding of the systems is certainly helpful in determining the features to extract from the observations. But explicit models of the systems' structures are not required.

For each task i, various features x_{ij}, $j=1,2, \ldots,m_i$, are extracted from the human's task related observations z_i. These features are properties of the observations that characterize (or are believed to characterize) the presence or absence of events related to the task. Following the extraction of a set of features, the value of a linear discriminant function

$$Y_i = v_{i1}x_{i1} + \ldots + v_{im_i}x_{im_i} \quad (1)$$

is calculated. Based on previous experience with the task, estimates are made of the discriminant function coefficients v_{ij}, $j=1,2, \ldots,m_i$, with which to combine the feature values x_{ij} to obtain the discriminant function score Y_i that best differentiates observations of events from the rest of the task related observations. Estimates of the mean and variance of the discriminant function over observations of events and over the rest of the observations are also formed. The a posteriori probability that an event has occurred is generated using the value of the discriminant function score, the estimates of the means and variances of this score over events and "non-events", and an estimate of the a priori probability of the event.

If the human operator is forced to make a yes/no response on the presence of an event, we might assume that he chooses the response which maximizes his expected reward. We can then express his decision in a signal detection manner and state that he should respond "yes, an event related to task i has occurred" if the following inequality holds:

$$\frac{P(e_i/Y_i)}{1 - P(e_i/Y_i)} > \frac{V_{CR_i} + C_{FA_i}}{V_{H_i} + C_{M_i}} \quad (2)$$

$P(e_i/Y_i)$ is the a posteriori probability that an event related to task i has occurred. The value of this probability is generated by the event detection model. V_{CR} is the value of correctly responding "no event" (a correct rejection), C_{FA} is the cost of incorrectly responding "event" (a false alarm), V_H is the value of correctly responding "event" (a hit), and C_M is the cost of incorrectly responding "no event" (a miss).

It is predicted, then, that if the operator is forced to make a yes/no decision on the presence of a task related event, he calculates the likelihood ratio of the event (the left hand side of Eq. (2)). He compares the magnitude of the likelihood ratio with a threshold determined by the values of correct responses and the costs of incorrect responses (the right hand side of Eq. (2)). He responds "event" if the likelihood ratio exceeds the threshold.

THE EVENT DETECTION EXPERIMENT

An experiment has been run employing a situation in which subjects simultaneously monitor several dynamic processes for the occurrence of events and make yes/no decisions on the presence of events in each process. Figure 1 illustrates the display observed by the subjects in the experiment. The static display was generated on a Tektronix 4010 by a time-shared DEC-System 10 and depicts the measured values of the outputs of nine processes over 100 sampling intervals (i.e., 101 points). The processes had identical second order system dynamics with a natural frequency of 0.75 rad/sec and a damping

ORIGINAL PAGE IS
OF POOR QUALITY

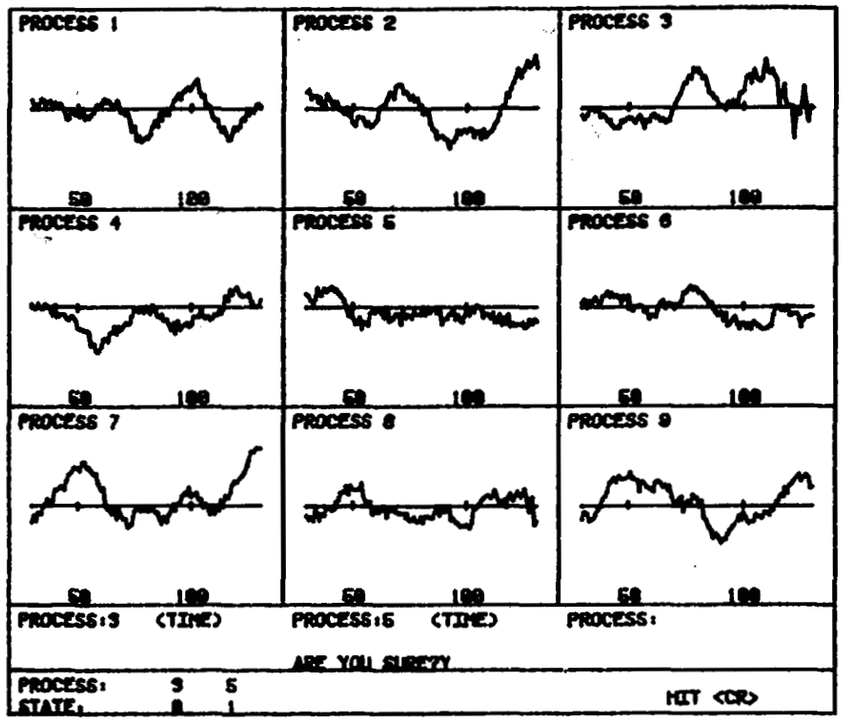

Figure 1. The Multiple Process Monitoring Situation

ratio of 0.5. Samples were taken at 0.2 second intervals. The inputs to the processes were zero-mean Gaussian white noise sequences of identical variance. The displayed measurements were obtained by corrupting the process outputs with additive zero-mean Gaussian white noise sequences which normally had identical variance. The measurement noise variance was normally selected to yield measurements with signal-to-noise ratios of 25.0. An abnormal event in a process was defined by an increase in the measurement noise variance such that the signal-to-noise ratio following an event occurrence was decreased to 95% of the signal-to-noise ratio of the preceding measurement. Thus, abnormal events became more pronounced with each measurement following their occurrence.

After scanning the nine process histories, the subject was given an opportunity to key in the numbers of processes in which he had decided an abnormal event had occurred. He was then given feedback regarding the actual states of the processes he had keyed in ("1" indicating the normal state, "0" indicating the abnormal state). An iteration in a trial was completed by erasing the display, scoring the subject's performance, and returning all abnormal processes detected by the subject to the normal state. Another iteration was then begun by generating a new display depicting the process histories advanced 10 sampling intervals in time as illustrated by Figure 2. (The dashed vertical lines indicated to the subject the point at which he last responded to each process.)

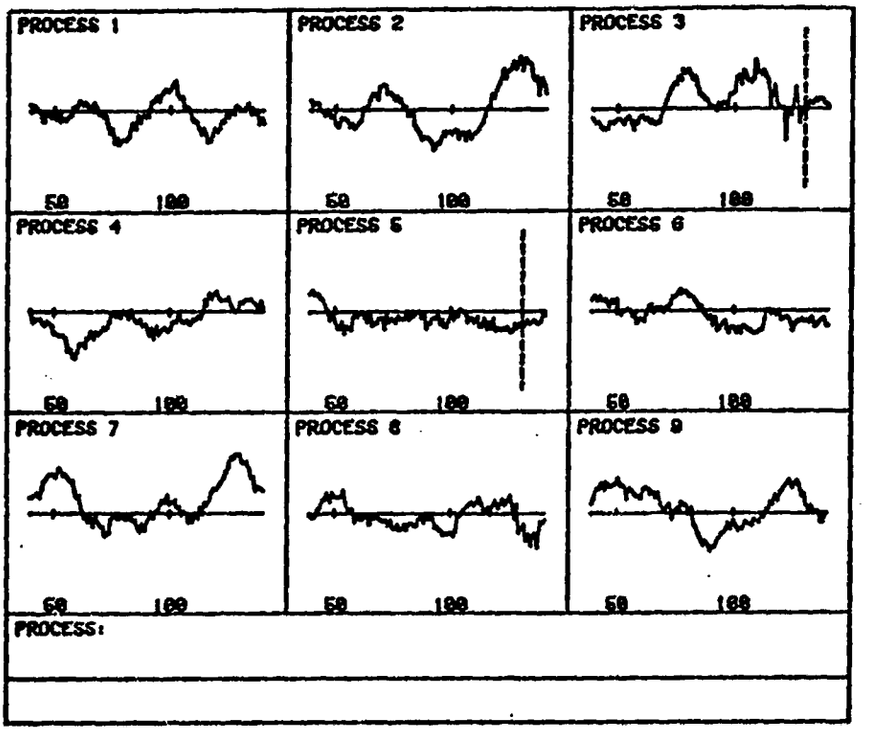

Figure 2. An Updated Display

The subject was allowed to respond to as many events as he thought had occurred. He was awarded points for his hits, receiving high scores for responding to events soon after their occurrence and lower scores for tardier responses. A fixed number of points was deducted for each false alarm. The subject was allowed to study the displays as long as he wished, but any time taken beyond the first minute on each iteration reduced the score awarded for hits made on that iteration.

Eight subjects were given three trials spaced over several days. Each trial was 20 iterations long. The first and third trials given half the subjects were identical, with one event scheduled to occur per iteration. Their second trial scheduled the same events as the first and third trials, but also scheduled an additional event occurrence each iteration. The rest of the subjects were given the same trials in different order so that two events were scheduled to occur per iteration in the first and third trials while one occurrence per iteration was scheduled in the second trial. (Not all scheduled events actually occurred. If an event was scheduled to occur in a process in which a previous event had not yet been detected by the subject, the scheduled event was deleted from the trial.) Events were scheduled to occur uniformly over the nine processes and over the 10 new points displayed for each process on each iteration (the last 10 points on the first iteration, in which all 101 points were new) within the constraint that no two events could occur in a process within 30 sampling intervals of

each other.

Before each trial, the subject was told the average number of new events he could expect to occur per iteration. He was not given any information regarding the dynamics of the processes, but was told that he could expect the processes to exhibit similar characteristics when operating normally. He was also not told what parameter changes defined events, but was told that all events would generally exhibit similar characteristics, and all would become more pronounced as time passed. The subject was given several iterations of training before each trial during which solid vertical lines were included on the process histories to mark exactly when and where events had occurred.

During each trial, the subject was asked to keep a log in which he described his strategies for event detection and noted characteristics of the process measurements he used in his attempts to detect events. After each trial, he was asked to order these characteristics in terms of their usefulness in event detection.

APPLICATION OF THE MODEL TO THE EXPERIMENTAL SITUATION

The event detection model suggests that the human operator in the experimental situation just described extracts various features from his observations of the process measurements. He attempts to select features which characterize the presence or absence of task related events. Through his experience with the processes, the operator has formed estimates of the discriminant function coefficients with which to combine the features to obtain a discriminant function score. He has also formed estimates of the means and variances of this score over observations of events and over the rest of his observations. The operator generates the likelihood ratio that an event has occurred based on the value of the discriminant function score. his estimates of the means and variances of the score, and his estimate of the a priori probability of an event occurrence. He compares the likelihood ratio with a threshold that is based solely on the values of correct responses and the costs of incorrect responses and responds "event" if the likelihood ratio exceeds the threshold.

Four features of the process measurements were selected for use with the event detection model. Selection of these features was guided by the comments of the experimental subjects regarding the characteristics of the process measurements they found useful in event detection. The first feature involves the magnitude changes between successive measurements in a sequence of the most recent measurements. The second feature involves the presence of reversals in direction in this sequence (changes from positive slope to negative, or vice versa, of the line segments connecting the measurements of the sequence). The third feature tests for the simultaneous occurence of large magnitude changes and reversals. The fourth feature, like the first, is a measure of magnitude changes, but it is much more local in that it

involves only the four most recent measurements of the process output.

In extracting these features from the process measurements, the values of the features over recent measurements are weighted more heavily than the values over earlier measurements. The weight decreases exponentially with the age of the measurement and the rate of this decrease is a free parameter. The value of the first feature, for example, a measure of the magnitude changes between successive measurements in a sequence of the n most recent measurements of a process' output, is given by

$$x_1 = \{ \sum_{k=1}^{n-1} |z(k+1)-z(k)| \cdot \exp[-\beta(n-1-k)] \} / \sum_{k=1}^{n-1} \exp[-\beta(n-1-k)] \qquad (3)$$

where z(k) is the k th measurement in the sequence, z(n) is the most recent measurement, and β is the free parameter governing the relative weighting of the feature's value over recent and earlier measurements in the sequence.

In the generation of the likelihood ratio of an event in a process at a given iteration of an experimental trial, the sequence of process measurements over which the features are calculated ends with the last measurement displayed for the process on that iteration. The cutoff length used in extracting the features from the process is a free parameter. Values of the features over process measurements taken earlier than the cutoff are not calculated (or, effectively, are assigned zero weight). If the subject responded "event" to the process at some point following the cutoff, then features are calculated over only those measurements occurring after this response. The information on the state of the process that the subject gains when he responds to the process motivates this constraint. If the process is in the normal state, then on succeeding iterations the subject knows that if an event has occurred, it must have occurred following his last response. If the process is in the abnormal state, then the process is reset to normal when the subject keys in his response. On succeeding iterations the subject knows that if another event has occurred in the process, it must have occurred following his last response. In either case, the subject (and the model) should calculate features only over measurements occurring after the subject's last response.

The estimation of discriminant function coefficients requires a representation of normal and abnormal process measurements. This representation was formed using the process histories displayed to the subject on his third experimental trial. The process histories are separated into two groups of sequences - normal and abnormal. Sequences of measurements beginning when a process was returned to the normal state and ending when an event occurred are defined to be normal. Sequences of measurements beginning when an event occurred and ending when the process was returned to the normal state are defined to be abnormal. The values of the four features were calculated over the entire length of each of the sequences in the two groups. A discriminant analysis was then performed on the resulting two groups of feature values to determine the discriminant function coefficients v_j, j=1,2,...,m, with which to combine the features to best differentiate between the two groups. The mean value and the variance of the

ORIGINAL PAGE IS
OF POOR QUALITY

resulting discriminant function scores for the sequences in each of the two groups was also calculated.

The final requirements for application of the event detection model to the experimental situation are estimates of the a priori probabilities of event occurrences and the selection of a threshold against which likelihood ratios of events can be compared. For experimental trials in which one event was scheduled to occur per update of the display over the nine processes monitored by the subject the a priori probability of an event occurrence in each process was fixed at 1/9. For trials in which two events were scheduled to occur per display update, the a priori probability was fixed at 2/9. The threshold against which the likelihood ratios of events are compared is assumed to remain constant through an experimental trial. The magnitude of this constant is a free parameter.

RESULTS

Figure 3 compares the event detection performance of the model with the actual performance of each of the eight subjects in the third trial of the experiment. In this trial, 20 events were scheduled to occur in the trials given subjects A,B,C, and D, while 40 events were scheduled to occur in the trials given subjects E,F,G, and H. In applying the model to each of these trials, the number of measurements over which features were extracted (cutoff

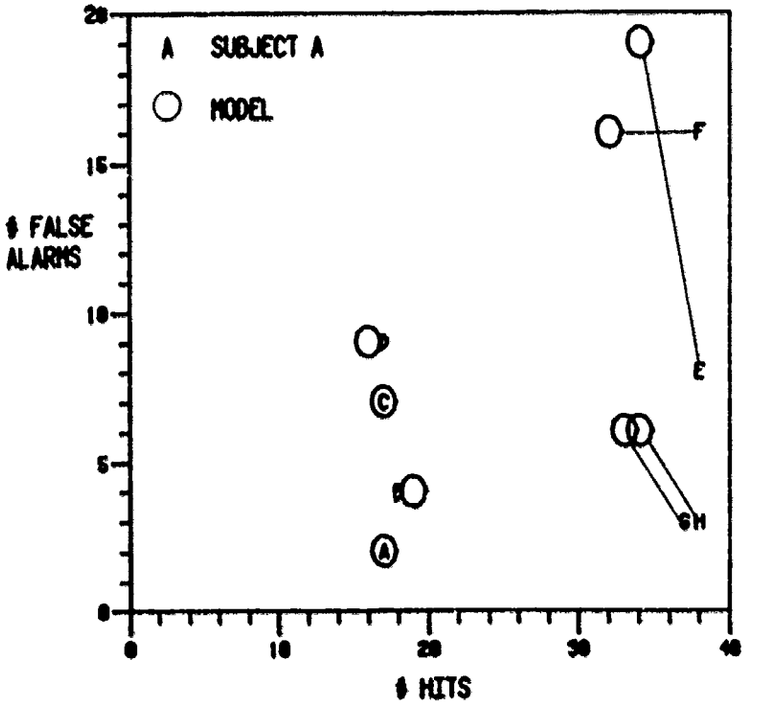

Figure 3. Comparison of Model with Subjects on Third Trial

length) and the relative weighting of recent and older points (β) were adjusted to improve the fit of the model's performance to each subject's performance. The value of the threshold against which likelihood ratios of events were compared was also adjusted to improve the fit. Figure 3 reveals a high degree of correspondence between the model's performance and the performance of most subjects.

Figure 4 compares the event detection performance of the model with the actual performance of the eight subjects in the second trial of the experiment. In this trial, 40 events were scheduled to occur in the trials given subjects A,B,C, and D, while 20 events were scheduled to occur in the trials given subjects E,F,G, and H. In applying the model to each of these trials, none of the parameters of the model were changed from the settings used to obtain the results presented in Figure 3. Despite the fact that the numbers of events scheduled in these trials differ from those in the trials used to assign the values of the parameters, the correspondence between the model's performance and the performance of most subjects is reasonable.

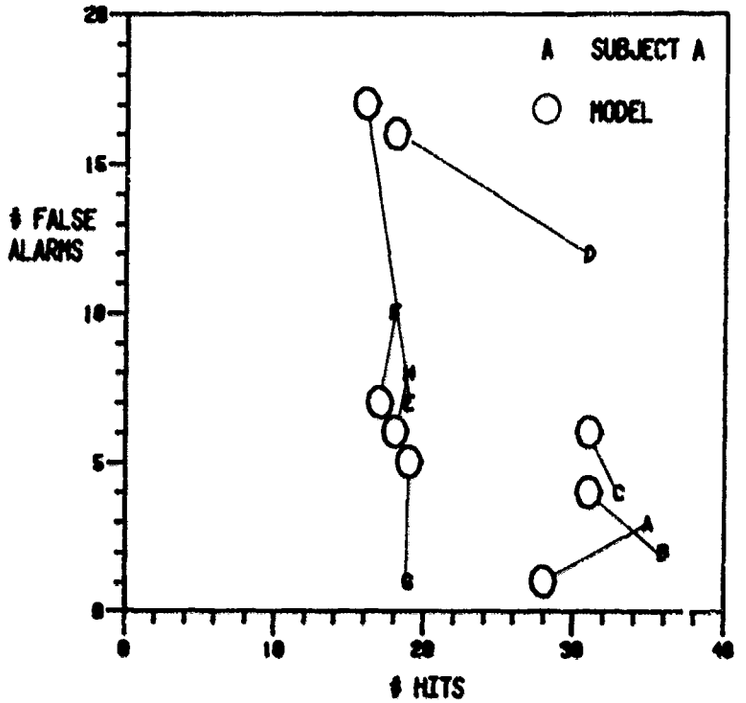

Figure 4. Comparison of Model with Subjects on Second Trial

Table 1 compares the mean detection times (in terms of the number of sampling intervals which elapsed from the occurrence of an event to the time of its detection) for hits common to both subject and model in the trials presented in Figures 3 and 4. It should be noted that the fact that the mean detection times of the model are consistently smaller than those of the subjects is an artifact of the manner in which the model's performance was investigated. The model was tested on the process histories displayed to a subject in his experimental trial. In these trials, a process was returned to the normal state at the point at which the subject detected an event in

ORIGINAL PAGE IS
OF POOR QUALITY

the process. Thus, in going over the process histories the model can never respond to an event later than the subject responded to it. If the model fails to respond to an event by the time of the subject's response, the model is scored as having missed that event.

Table 1. - Comparison of Mean Detection Times

	Trial 1		Trial 2	
Subject Code	Subject	Model	Subject	Model
A	24	19	24	20
B	26	21	25	19
C	28	17	28	17
D	32	21	30	16
E	18	13	22	17
F	17	14	27	16
G	20	17	27	20
H	20	17	22	18

We plan to evaluate the model in the near future using a somewhat different approach. Rather than running the model over the process histories displayed to a subject on an earlier experimental trial (and constraining the timing of the model's responses by the timing of the subject's responses in that trial), we will use the model in place of the subject in the event detection experiment. Processes in which events occur will then remain in the abnormal state until the model responds to the process The only constraint on the model's detection times will be the end of the experimental trial. Because the model's detection time for each event need no longer be less than or equal to the subject's detection time for that event, we expect that, for a given number of hits, the model's threshold can be raised to achieve the longer mean detection times and smaller numbers of false alarms characteristic of the subjects in the experiment.

CONCLUDING REMARKS

In applying the event detection model to the experimental situation described in this paper, we studied a situation in which the subject was forced to respond yes or no to the possibility of an event related to each of nine processes. In general, the human operator is not forced to make such yes/no decisions with respect to each of his tasks. Instead he uses his estimates of the probabilities of task-related events (which the event detection model generates) in deciding how to allocate his attention among his tasks. We plan to run an experiment investigating the human's attention allocation performance in a multiple process monitoring situation similar to

the one employed in the event detection experiment discussed here. Data from this experiment will be used to develop and validate a model of attention allocation performance in multi-task situations. (The modeling of human attention allocation performance in multi-task situations is considered in [11].) This model might be used in conjunction with the event detection model as a part of the design process for, and the implementation of, automated decision making systems.

REFERENCES

1. Senders, J. W.: "The Human Operator as a Monitor and Controller of Multidegree of Freedom Systems," IEEE Trans. Human Factors in Electronics, vol. HFE-5, no.1 pp.2-5, Sept. 1964.

2. Smallwood, R. D.: "Internal Models and the Human Instrument Monitor," IEEE Trans. Human Factors in Electronics, vol. HFE-8, no.3, pp. 181-187, Sept. 1967.

3. Carbonell, J. R : "A Queueing Model of Many-Instrument Visual Sampling," IEEE Trans. Human Factors in Electronics, vol. HFE-7, no.4, pp. 157-164, Dec. 1966.

4. Carbonell, J. R.; Ward, J L.; and Senders, J. W : "A Queueing Model of Visual Sampling: Experimental Validation," IEEE Trans. Man-Machine Systems. vol. MMS-9, no.3, pp.82-87, Sept. 1968.

5. Senders, J. W ; and Posner M. J. M.: "A Queueing Model of Monitoring and Supervisory Behavior," in T. B. Sheridan and G. Johannsen, Eds., Monitoring Behavior and Supervisory Control, New York: Plenum 1976, pp.245-259.

6. Gai E. G.; and Curry, R. E.: " A Model of the Human Observer in Failure Detection Tasks," IEEE Trans. Systems, Man. and Cybernetics, vol. SMC-6, no.2, pp.85-94, Feb. 1976.

7. Sheridan, T. B.; and Tulga, M. K.: 'A Model for Dynamic Allocation of Human Attention Among Multiple Tasks," Proceedings of the Fourteenth Annual Conference on Manual Control, University of Southern California, April 1978.

8. Rouse, W. B.: "human-Computer Interaction in Multitask Situations," IEEE Trans. Systems, Man, and Cybernetics, vol. SMC-7, no.5, pp. 384-392, May 1977.

9. Tatsuoka, M. M.: Multivariate Analysis. New York: Wiley, 1971.

10. Afifi, A. A.; and Azen, S. P.: Statistical Analysis. New York: Academic Press, 1972.

11. Rouse, W. B.; and Greenstein, J. S.: "A Model of Human Decision Making in Multi-Task Situations: Implications for Computer Aiding," Proceedings of the 1976 International Conference on Cybernetics and Society, Washington, Nov. 1976.

D45

N79-15633

PILOT DECISION MAKING IN A COMPUTER-AIDED FLIGHT MANAGEMENT SITUATION*

Yee-yeen Chu and William B. Rouse

Department of Mechanical and Industrial Engineering
Coordinated Science Laboratory
University of Illinois
Urbana, Illinois 61801

SUMMARY

An experimental representation of a computer-aided multi-task flight management situation has been developed. A computer aiding program was implemented to serve as a back-up decision maker. An experiment was conducted with a balanced design of several subject runs for different workload levels. This was achieved using three levels of subsystem event arrival rates, three levels of control task involvement, and three levels of availability of computer aiding. Experimental results compared quite favorably with those from a computer simulation which employed a $(M/E_k/2):(PRP/K/K)$ queueing model. It was shown that the aiding had enhanced system performance as well as subjective ratings, and that the adaptive aiding policy further reduced subsystem delay.

INTRODUCTION

As aircraft become more complicated and greater demands and better performance are being required of pilot, the development of automated airborne systems to share the tasks of piloting an airplane becomes increasing attractive. Advances in electronics and computer technology have made this approach both feasible and promising. Progress in sophisticated cockpit design and growth in avionic computer systems reflect the trend.

Equiped with autopilot and airborne computers performing automatic navigation, guidance, energy calculations, flight planning, information management, etc., the next-generation of aircraft are quite likely to be capable of carrying out all phase of flight automatically. However, the human pilot is likely to reamin a part of the system to cope with unpredicted or failure situations for which automation may be economically or politically infeasible. The pilot's roll then is changing from one of controller to one of supervisor and manager, responsible for monitoring, planning and decision making.

* This research was supported by the National Aeronautics and Space Administration under NASA-Ames Grant NSG-2119.

676

PAGE INTENTIONALLY BLANK

The pilot as the airborne system manager has responsibility to monitor the aircraft subsystems such as navigation, guidance, etc. as well as the autopilot and to detect possible hardware failures and potential hazards. He must constantly respond to action-evoking events such as: to communicate information, to change aircraft configuration and to reduce 4-D accuracy errors. He is also required to respond to unexpected events such as a change in flight plan, to establish the backup mode, and to declare emergencies, etc. [1]. The pilot is in a multi-task situation.

If the pilot perceives an irregularity in one of the subsystems, he may seek more detailed information through either the on-board information system or actual sensor readings. Or, if he considers the irregularity to be minor, he may decide to continue his monitoring for higher priority events. There may also be autopilot malfunctions or sudden changes requiring the pilot to take charge of flight control. A proper representation of information through a flight map display indicating the continuous functioning of automatic control may help to ensure his remaining alert and responding quickly.

As described above, the automated system can normally take charge of the whole system except during critical situations such as when the system is suffering from a malfunction. Or a high-workload situation may develop when the aircraft is close to the ground when a high level of pilot activity is required. In all of these situations, the pilot is more than usually busy and further assistance of a computer would be most useful.

The recent development of fast and intelligent computer systems presents the potential for providing sound, well-evaluated airborne decisions which could reduce system risk, pilot workload and errors. While the computer as a decision maker is basically an implemented set of algorithms, adaptation and learning is possible. It is reasonable to expect that this evolving "intelligent" computer may be employed as the supervisor to the subsystem computers, taking charge of the tasks within its decision capability. The pilot and the computer thus have comparable abilities and overlapping responsibilities in performing these tasks. The problem that arises is how to allocate responsibility between the pilot and the computer for a subset of all tasks.

We have proposed that responsibilities not be strictly assigned to each decision maker. Instead, allocation should adapt to the state of the aircraft and the state of the pilot [2]. Further, to retain a coherent role, the pilot should be given overall responsibility for the whole aircraft while the computer would enable the pilot to avoid having to continually exercise all of these responsibilities. On one hand, it may not be appropriate for the computer to make the vital, final judgement where losses may extend beyond the point of recovery. On the other hand, there may be vigilance problems and the pilot's performance may degrade. This leads to the idea of utilizing the computer as a backup for the pilot. The allocation problem becomes one of deciding when the computer should request and relinquish responsibility.

Given these descriptions, we will explore several issues concerned with pilot decision making in computer-aided flight management situations. Is system performance enhanced by computer aiding? How effective are different aiding policies? How does the pilot feel about aiding? Is his role or performance affected? To investigate the feasibility of the approach, and to predict the effects of numerous system variables and aiding policies, a queueing formulation of multi-task decision making was developed and will be discussed in the next section.

APPROACH

The pilot in the automated flight management system described earlier has a variety of tasks to perform. As the number and variety of tasks increases, the workload of the pilot is increased. It is essential to appropriately allocate his attention and effort among the tasks. He may be in a situation that he wants both to monitor the tasks often enough to reduce growing uncertainty and risk, and to perform a task quickly and accurately to lessen the cost involved in the delay of action. This issue is being investigated by Greenstein and Rouse [3]. To simplify the issue, the pilot is assumed to employ a quasi-optimal decision making strategy for scanning displays and allocating attention. This is based on the assumptions that the tasks are independent and that events unequivocally present themselves. The pilot scans the task display in order of decreasing priority at a given rate. He then performs the first task for which he perceives some action-evoking events. The computer is assumed to adapt the same strategy either by being hard-wired or learning from the pilot. Now we may look at the multi-task decision making as a queueing system with two servers (the pilot and the computer) and K+1 classes of customers (K subsystem events plus control events represented by displayed 4-D errors in manual control mode).

In the queueing model, each server is characterized by his observation of system state, his perceptions of event occurrences, of event arrival rates and of event service rates. Combining the above information and the system cost criteion allows the model to predict system performance measures such as event delay statistics and server occupancy which is fraction of time the server is busy.

A convenient cost criterion, in terms of a stationary expected cost structure, includes waiting cost, service cost, and switching cost. When the computer service cost and switching cost may be negligible, the optimal policy is to have the computer on all the time. However, it is more likely that the human will be better at performing the task but not have sufficient time to do all the tasks. Also evidence of vigilance and warm-up decrements suggests that there is an acceptable workload range that sustains performance on long tasks. Thus we may want to seek a policy for computer aiding such that a minimum waiting cost is achieved while maintaining a specified workload level.

Based on results from literature [4], we will advocate the use of the stationary expected cost policy, subject to minimizing deviation from acceptable pilot workload, for computer on-off of the following form: turn

the computer on at arrival epochs when $N = c_1n_1 + c_2n_2 + \ldots + c_Kn_K > M$, and turn it off when $N < m$, where $c_1, c_2, \ldots, c_K$ are cost rates assessed according to relative priorities and n_k is the number of events waiting in the subsystem k. This policy (i.e., M and m) should vary as the system variables vary. Specific values of M and m have to be determined for various levels of traffic demand (i.e., event arrival rates), server performance and task complexity (i.e., service rates and probabilities of errors). An appropriate approach to implement the adaptive policy is to set up a table of stationary control policies beforehand and to employ a table look-up along with on-borad estimation of system variables.

To obtain the optimal stationary policy, i.e., to determine the values of M and m, a computer simulation was performed. Poison arrivals and Erlang service time distributions for subsystem were assumed. The K subsystem tasks were preempted by the control task whenever it occurred. The system was represented as a preemptive resume priority queueing system: $(M/E_K/2):(PRP/K/K)$ with implemented threshold control.

A simple case was considered in which the model parameters were determined in the following manner. 1) Subsystem arrival rates, service rates, and waiting cost rates were all uniform among the subsystems. 2) Two levels of arrival rates were assumed, i.e., low arrival (at 0.0167 events per second) and high arrival (at 0.0333 events per second). 3) Pilot performance in terms of service rates, service errors and control services were obtained from the experiment discussed in the next section. 4) The computer aiding employed the same service rates as the pilot and automatically went off when no event needed service (i.e., m=0). The results based on the computer simulation of 10,000 events for K=6 and server occupancy for pilot of = 0.7 showed that, without control task, M=7 for low arrival and 3 for high arrival; with control task, M=3 for low and 1 for high arrival. If workload is the primary consideration, these are threshold values which the computer should employ to adapt to both the subsystem arrival rate and the control task involvement.

Prediction of system performance by the model was also obtained through the computer simulation. The results will be discussed in the later section.

THE EXPERIMENT

Two experiments are to be discussed here. A brief review is given of an experiment previously reported by Walden and Rouse [5] investigating pilot decision making in an unaided situation. The second experiment, considering the computer aiding and autopilot malfunction situations, employs basically an outgrowth of the experimental representation used in the previous experiment.

The experimental situation developed earlier [6] used a PDP-11 driven CRT graphic system to represent a cockpit-like display to an experimental subject. The display shown in Figure 1 included standard aircraft instruments such as artificial horizon, altimeter, heading and airspeed indicators. Also displayed was a flight map which indicated the airplane's

position relative to the course to be followed. A small circle moved along the mapped course indicating the position the aircraft should have for it to be on shcedule.

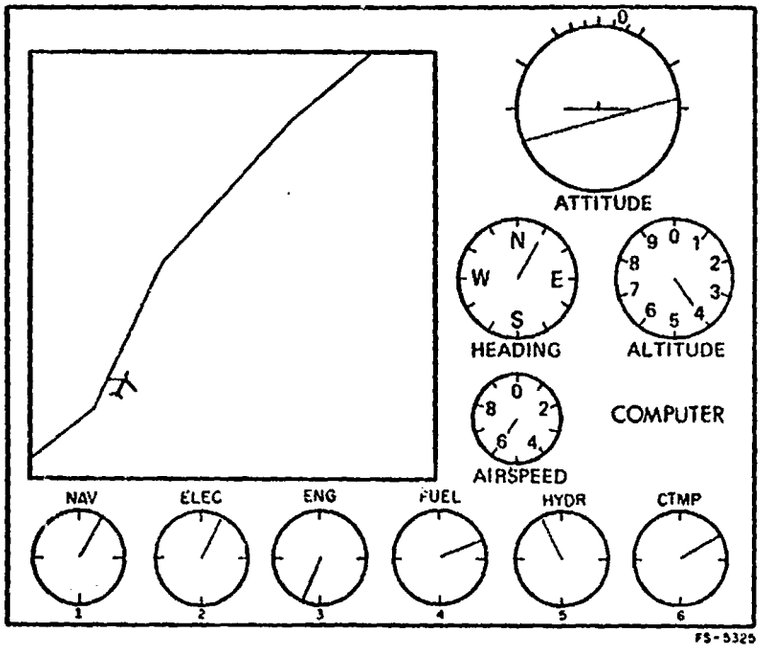

Figure 1. The Flight Management Situation.

In the manual control mode, the pilot controlled the pitch and roll of Boeing 707 aircraft dynamics with a joystick. Another control stick controlled the airspeed. The pilot's control task was to fly the airplane along the mapped route while maintaining a fixed altitude and stable pitch and roll attitude.

Below the map were the subsystem dials that represented the numerous aircraft subsystems which the pilot monitored for possible action-evoking events. Upon detecting an event (represented by the pointer pointing downward as shown for the engine subsystem in Figure 1) to which he wished to respond, the subject selected that subsystem via a 4x3 keyboard. The display shown in Figure 2 then appeared. This represented the first level of a check list-like tree associated with the subsystem of interest. He then searched for a branch labeled with a zero and seleted the branch with his keyboard. After completing the last level of the tree, the action was completed and the display shown in Figure 1 returned, with the subsystem information or diagnostic check complete.

Using the experimental situation, an experiment was performed by Walden [5] to study unaided pilot decision making strategies and the resulting performance. The two independent variables in the experiment were the inter-arrival time of subsystem events and the difficulty of the flight path.

The results showed that, while average waiting time increased with subsystem event arrival rate, the average service time appeared to be independent of subsystem arrival rate. The waiting time was also shown to increase as the control task was added. This effect was only a function of the mere presence of the control task, rather than the control task difficulty. Incorrect actions in servicing subsystems tended to increase with subsystem arrival rate, but showed no consistent variation with control task difficulty. False alarms, however, tended to occur more frequently with the easier control task and lower subsystem arrival rate. This presented evidence of performance degradation under low workload situations.

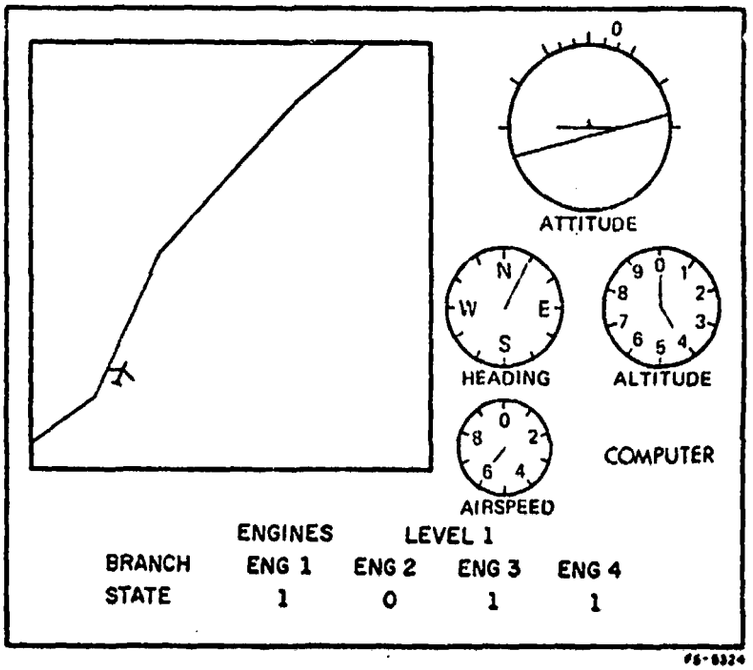

Figure 2. Display When Pilot Had Reacted To an Event in Engine Subsystem.

The data collected was used in the queueing model of pilot decision making in an unaided monitoring and control situation. The model gave a reasonable prediction of pilot performance in performing subsystem tasks, suggesting that it was an adequate description of pilot decision making in the given situation and that a similar model would be useful in the adaptive aiding system.

Based on the experimental representation discussed above, a new experimental situation for adaptive aiding was developed with the aiding program (i.e., the computer decision maker) and the coordinator program (i.e., the on-off algorithm) added to the original system. Issues concerning the capability of the computer to perform the subsystem tasks, the communication linkage between the pilot and the computer, and the activities of the coordinator deserve further discussion.

The computer is assumed to be able to perform monitoring and diagnostic check procedures using information from channels linked with subsystem computers and from the data links. It makes no errors such as false alarms, missed events, or incorrect actions after it gains confidence in performing the task. The detection and service times are assumed constant. As for the service discipline among the subsystems, the computer employs the same priority rule as that used by the pilot. To be consistent in its back-up role, the computer probably adapts itself to the pilot and avoids interference with him. To this end, the pilot is allowed to override any decision the computer has made.

Without knowing what each other is doing, the pilot and the computer may compete for the same task or resource. The prospect of conflict between the two is highly undesirable, since, it simply causes confusion, results in higher workload and degraded performance. The question as to how to design effective communication links without increasing the pilot's workload becomes important.

To inform the pilot of the computer's action, a succinctly displayed computer status indicator on or near the subsystem displays would seem to be satisfactory. Relevant information, if needed by the pilot for further details, may be structured into a hierarchical check-list procedure. In the experimental situation shown in Figure 3, The 'NAV' symbol over the navigation dial flashed, if the computer decided that an event had occurred and was waiting to be serviced in the navigation system. This was to tell the pilot that he could take charge of the navigation system and the computer would take some other responsibility to avoid interference; otherwise, the symbol would continue to flash for a total period of four seconds until the computer started interacting with the navigation system, resulting in a dim indicator showing in the navigation dial. If the pilot was in the middle of performing some other subsystem check procedure, say, within the engine system, he would not see the flashing 'NAV' symbol over the navigation dial. The status of the computer was then shown on the lower right hand corner of the CRT by an 'AIDING NAV' symbol (flashing during the interval of possible pilot preemption), if the computer was awaiting preemption or interacting with the navigation subsystem. This computer status area was blank if the computer was not actively involved in the subsystems.

Airborne pilot-to-computer communication is, in general, more complicated. Problems involved include estimating and processing signals as well as matching or recognizing system status. For the purpose of the experiment reported here, however, the communication channel from the pilot to sybsystems was predefined. For our experimental situation, these included the keyboard input and stick response sampling (through an A/D converter). These channels provided the monitoring computer a way of determining if the pilot was interacting with any portion of the system. If a number had been received through keyboard, and the checklist was being processed then the pilot had to be performing a subsystem task. The deviation of stick from normal position revealed that the pilot was performing the control task.

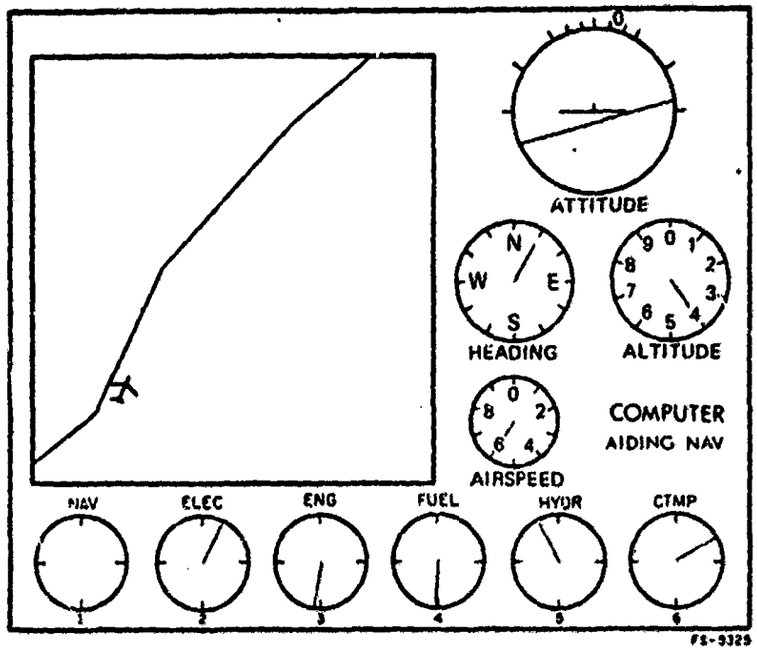

Figure 3. Display When the Computer Is Servicing Navigation System.

While the computer had to constantly check the pilot's action to avoid a conflict, the coordinator had to synchronously check the subsystem states to determine if there was any system change. The decision epoch was when an event arrival or departure occurred. Then the coordinator calculated both the weighted sum of events and the threshold. The criterion discussed earlier was used to determine if the computer was to be turned on at the arrival epoch or to be turned off at completion epoch.

Data, sampled synchronously (twice per second), included subsystem status and states, autopilot status, aircraft dynamic variables, stick and keyboard responses, computer status and the threshold values.

An experiment based on the experimental representation described above was conducted. Eight trained subjects, all of them male students in engineering, participated in a balanced sequence of sixteen experimental runs (see Table 1) with different workload levels. This was achieved by combining three levels of control task involvement (perfect autopilot, manual control, autopilot with possible malfunctions), three levels of subsystem event arrival rates (no arrival, low arrival, high arrival), and three levels of availability of computer aiding (no aiding, aiding with fixed switching policy, and aiding with adaptive policy). For each experimental run, the subject was first told the specific tasks to perform, then a 14-minute trial was given, and a questionare was filled out by the subject.

ORIGINAL PAGE IS
OF POOR QUALITY

Table 1. Design of Experiment.

	Subject 1	Subject 2	Subject 3	Subject 4
Autopilot without Malfunction	(training)	(training)	(training)	(training)
	low arrival with aiding	low arrival without aiding	high arrival with aiding	high arrival without aiding
	low arrival without aiding	low arrival with aiding	high arrival without aiding	high arrival with aiding
	high arrival with aiding	high arrival without aiding	low arrival with aiding	low arrival without aiding
	high arrival without aiding	high arrival with aiding	low arrival without aiding	low arrival with aiding
Manual Control	(training)	(training)	(training)	(training)
	no arrival	no arrival	no arrival	no arrival
	low arrival with aiding	low arrival without aiding	high arrival with aiding	high arrival without aiding
	low arrival without aiding	low arrival with aiding	high arrival without aiding	high arrival with aiding
	high arrival with aiding	high arrival without aiding	low arrival with aiding	low arrival without aiding
	high arrival without aiding	high arrival with aiding	low arrival without aiding	low arrival with aiding
Autopilot with Malfunction	(training)	(training)	(training)	(training)
	no arrival	no arrival	no arrival	no arrival
	low arrival with aiding	low arrival without aiding	high arrival with aiding	high arrival without aiding
	low arrival without aiding	low arrival with aiding	high arrival without aiding	high arrival with aiding
	high arrival with aiding	high arrival without aiding	low arrival with aiding	low arrival without aiding
	high arrival without aiding	high arrival with aiding	low arrival without aiding	low arrival with aiding
	low arrival adaptive aid	low arrival adaptive aid	high arrival adaptive aid	high arrival adaptive aid
	high arrival adaptive aid	high arrival adaptive aid	low arrival adaptive aid	low arrival adaptive aid

For the experiment runs with perfect autopilot, only the subsystem task was considered. An "autopilot" kept the aircraft on course and on schedule. These runs served as baseline performance for the subsystem task. In the manual control runs, the subject had to perform both subsystem and control task. He was told that the control task was more important than the subsystem task. For the runs where autopilot maufunctions were possible, the autopilot was available during most of the experiment such that the subject was not required to fly the airplane except to occasionally check autopilot performance. As soon as he detected an autopilot malfunction, which was characterized by the airplane deviating from the mapped course at a rate of one degree per second, he was required to take over the flight control task, and fly the airplane back to the mapped course. In this case, the airplane would lock on the desired course as soon as it flew within the 800-feet oval of the on-schedule circle, and the autopilot mode was restored. The autopilot malfunction happened relatively infrequently, based on a Poison distribution with mean inter-arrival time of 160 seconds.

After the pilot detected the autopilot malfunction, he would have to devote a major portion of his attention to the control task, leaving subsystem tasks less attended, while risk and uncertainties grew as subsystem event detection and service were further delayed. This is one of many situations in which airborne computer aiding is more valuable. Also, in this period, the pilot's workload suddenly increased. To adapt to this type of change, a lower threshold value can be used to reduce subsystem service delay and pilot workload.

Based on this idea, two experiment runs with adaptive computer aiding were included in the set of runs with autopilot malfunctions possible. Instead of using M=3 all the time as in the fixed threshold policy, the adaptive policy used M=1 whenever the pilot was in manual mode. In total, there were seven experimental runs with autopilot malfunction: one run with no subsystem arrival (serving as a baseline performance for malfunction), two runs with no aiding, two with fixed-threshold aiding, and two with adaptive aiding. This arrangement allowed for the evaluation for the effectiveness of computer aiding and further the benefit of the adaptive policy beyond that of fixed aiding.

Three or more, depending on the task situation, of the following performance measures were evaluated in every experimental run:

1) average delay in response and service for subsystem events,
2) subsystem service errors (e.g., false alarms, incorrect actions, etc.),
3) 3-D RMS and average flight course errors,
4) flight control inputs including aileron, elevator, speed, etc.,
5) detection and service times for autopilot malfunctions,
6) server occupancy in terms of the fraction of time the subject was performing either subsystem or control tasks,
7) subjective ratings of level of effort required for the tasks and the desirability of computer aiding.

All these measures were obtained by analyzing the sampled data. The subsystem event response time was measured from the time of event occurrence to the time at which an action was initiated. The service time was measured from the time of last action initiation to the time of action completion for the event. The waiting time was measured from the time of event occurrence to the time of action completion for the event. Waiting time is equal to the sum of response time and service time only when the event is serviced by one server and no incorrect action is incurred. The results based on the analyses of variance are discussed in the next section.

RESULTS

The subsystem event waiting times averaged across subjects for the various task situations are shown in Figure 4. An analysis of variance conducted showed that among the statistically significant factors (at the .05 level) are the three experiment variables, i.e., the control mode, the subsystem arrival rates, and the computer aiding. As expected, the subsystem waiting time increased as the subsystem arrival rate increased, as the control involvement increased, and when no computer aiding was provided. A

ORIGINAL PAGE IS
OF POOR QUALITY

separate test showed that the adaptive policy was also significant, i.e., the adaptive aiding further reduced the subsystem waiting time beyond the fixed-threshold aiding, even though the adaptive policy was only effective during a small portion of time in the experiment.

The subjective ratings of the level of effort across subjects are shown in Figure 5 Factors of significance include all three experiment variables. As expected, the perceived level of effort increased as control involvement increased, as subsystem arrival increased, and as computer aiding was removed. However, a separate test showed that the effect of the adaptive policy was not significant, probably because the adaptive policy was employed rather infrequently, and when it was being used, the subjects usually were too involved with restoring the autopilot to notice the fact that the computer was helping more often then usual.

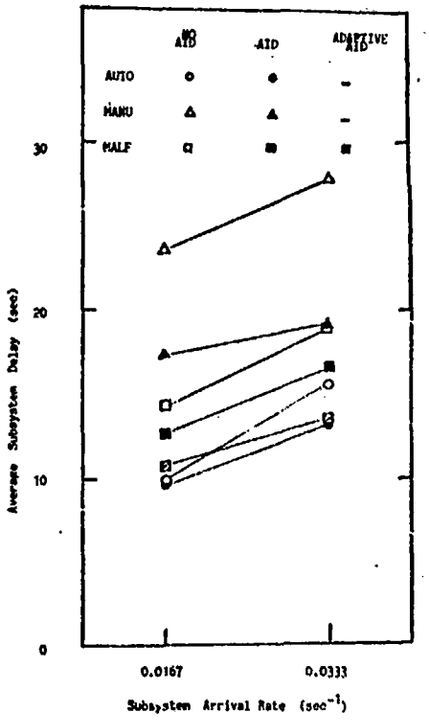

Figure 4 Average Subsystem Delay.

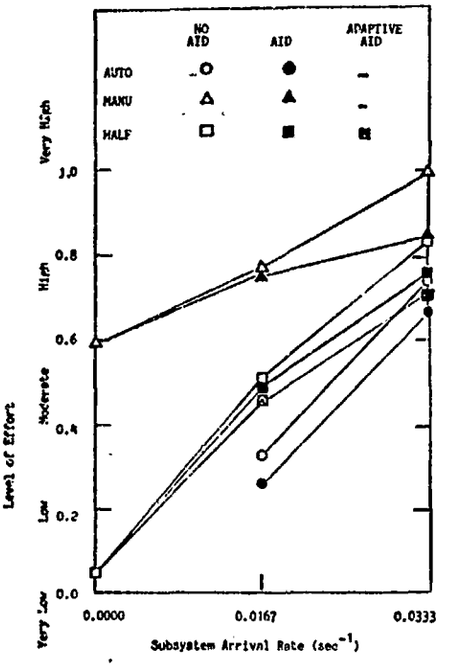

Figure 5 Subjective Ratings of Effort.

The RMS course error across subjects is shown in Figure 6. The analysis of variance showed that only control mode had an effect on the control error. No consistent variation in the course error was shown as subsystem arrival rate or aiding situation varied. The lower course RMS error for the autopilot malfunction mode probably resulted from subject's more intense attention to the control task in the case of malfunction.

The RMS roll angle across subjects is shown in Figure 7. Also, only control mode had a significant effect on the control input. The subjects were found to use more extreme control actions and more attention to fulfill

the malfunction task requirements. Sumarizing the above, systems that are designed to relax control requirements, such as the autopilot, seem to improve both control and subsystem performance, while systems that are designed to relax subsystem requirement, such as computer aiding or highly reliable subsystems, seem to improve only subsystem performance. The possible reason for this is that the control task perempts subsystem tasks, and thus, the control task inefficiency is likely to affect the performance of subsystem tasks; the reverse is not true.

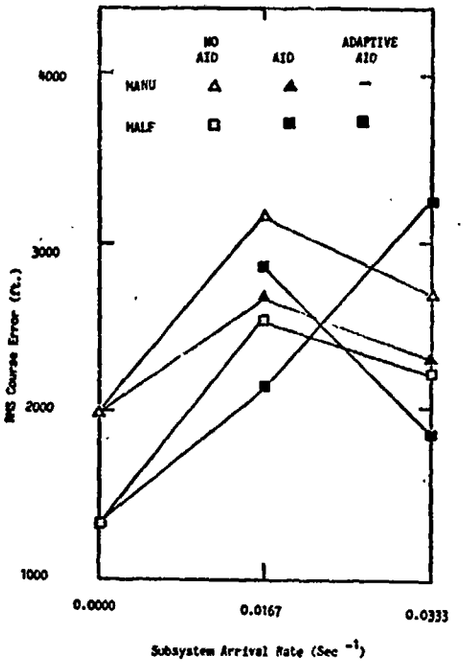

Figure 6. RMS Course Error.

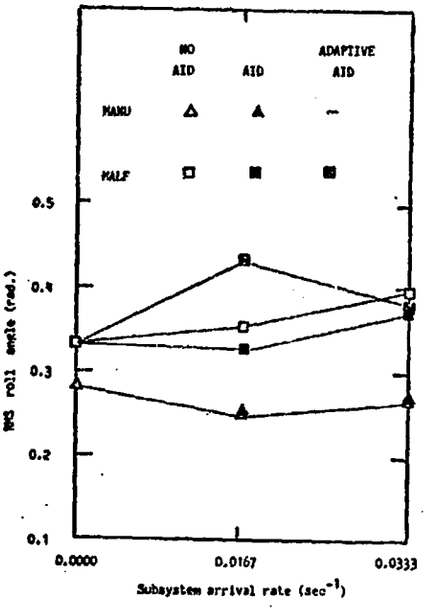

Figure 7. RMS Roll Angle.

Subjective ratings of three aspects of computer aiding were also determined: effectiveness, desirability of the aiding, and ease of interaction with the aiding. The results indicate that the aiding was considered easy to interact with and desirable by the subjects. Its effect on performance improvement was perceived to be from moderate to large. The subjects perceive the aiding to be relatively more effective and more desirable with a high subsystem arrival rate or a high control involvement situation. They, however, did not feel that it was more difficult to interact with the aiding in those situations. In fact, all the subjects were quite in favor of both the aiding scheme used in the experimental situation and the general computer aiding idea. More analyses of performance measures are discussed by Chu in his thesis [7].

The empirical data were compared with simulation results from the queueing model of pilot decision making in computer aided situation discussed earlier. This allowed an evaluation of the model's ability to represent the

ORIGINAL PAGE IS
OF POOR QUALITY

given situation. The comparison of subsystem waiting statistics is shown in Table 2.

Table 2. Comparison of Waiting Time.

Arrival Rate	Aiding Type	Mean		Standard Deviation	
		Model	Data	Model	Data
Autopilot Mode					
Low	No Aiding	9.73	9.71	5.39	6.04
Low	Aiding	9.34	9.82	4.30	5.13
High	No Aiding	14.71	15.79	13.46	14.21
High	Aiding	13.79	13.16	12.00	7.43
Manual Mode					
Low	No Aiding	20.13	23.62	16.24	23.53
Low	Aiding	17.56	17.17	10.26	11.31
High	No Aiding	32.87	27.81	45.51	28.64
High	Aiding	19.58	19.19	11.85	12.17
Autopilot Malfunction Mode					
Low	No Aiding	12.00	14.25	8.85	13.81
Low	Aiding	11.13	12.84	6.79	10.52
Low	Adaptive Aiding	10.25	10.68	4.91	5.52
High	No Aiding	17.47	19.03	18.96	21.16
High	Aiding	13.66	15.52	8.52	11.55
High	Adaptive Aiding	12.32	13.25	7.10	8.33

In the model, a Poison distribution of control event arrivals and an Erlang distribution of control service times with shape parameter $k=2$, were assumed. To generate the results in Table 2, the values of 0.1 sec^{-1} (in manual mode) and 0.16 (in malfunction mode) were used as mean control arrival rates, and 0.47 and 0.34 as mean control service rates. These values were obtained by analyzing subject's aileron control input and, serve as a first approximation.

The results compare reasonably well. All parameters in the model were empirically measured and no adjustments were made. The model predicts performance in autopilot mode very well. A better estimate of control task parameters will surely improve the model accuracy in manual control and autopilot malfunction modes.

CONCLUSION

The experimental results show that all the experimental variables, i.e., the subsystem arrival rates, the control task involvement, and the availability of computer aiding, were statistically significant in terms of affecting the performance measures of interest, mainly, the subsystem delays, and subjective effort ratings. It was shown that the aiding enhanced system

performance in terms of subsystem average delays and subjective effort ratings. The adaptive aiding policy was shown to further reduce subsystem waiting time.

The queueing model fits the experiment result reasonably well. Further exploration of control task preemption is needed to improve model accuracy. The model also provides the capability to predict the server occupancy for different task situations. Included in the future work will be a test of the correlation between this server occupancy measure and the subjective effort ratings to determine if this measure may effectively serve as a workload indicator.

Finally, the computer-aided flight management situation will next be implemented in an aircraft simulator where regular pilots will be used as subjects.

REFERENCES

1. Wempe, T.E., "Flight Management - Pilot Procedures and System Interfaces for the 1980 - 1990's", AIAA Paper No. 74-1297, AIAA Life Science and System Conference, November 1974.

2. Chu, Y. and Rouse, W.B., "Optimal Adaptive Allocation of Decision Making Responsibility between Human and Computer in Multi-task Situations", Proceedings of the International Conference on Cybernetics and Society, pp. 168-175, September 1977.

3. Greenstein, J.S. and Rouse, W.B., "A Model of Event Detection in Multiple Process Monitoring Situations", Proceedings of the Fourteenth Annual Conference on Manual Control, April 1978.

4. Bell, C.E., "Optimal Operation of an M/G/1 Priority Queue with Removable Server", Operations Research, 21-6, 1973, pp. 1281-1290.

5. Walden, R. S. and Rouse, W.B., "A Queueing Model of Pilot Decision Making in a Multi-task Flight Management Situation", Proceedings of the Thirteenth Annual Conference on Manual Control, pp. 222-236, June 1977.

6. Rouse, W.B., Chu, Y., and Walden, R.S., "An Experimental Situation for Study of Pilot Interaction with Automated Airborne Decision Making Systems", Proceedings of the Twelfth Annual Conference on Manual Control, May 1976, NASA TM X-73, 170, pp. 39-44.

7. Chu, Y., Adaptive Allocation of Decision Making Responsibility between Human and Computer in the Multi-task Situations", Ph.D. Thesis in progress, University of Illinois, Urbana, Illinois.

SESSION L: WORKLOAD

Chairman: T. Sheridan

D46

N79-15634

TIME ESTIMATION AS A SECONDARY TASK TO MEASURE WORKLOAD:

SUMMARY OF RESEARCH

Sandra G. Hart*
University of Utah
Salt Lake City, Utah

Duncan McPherson**
University of California
Berkeley, California

Leslie L. Loomis**
San Jose State University
San Jose, California

Abstract

This paper outlines the results of a series of experiments designed to evaluate the utility of time estimation as a secondary measure of piloting workload. Actively produced intervals of time were found to increase in length and variability, whereas retrospectively produced intervals decreased in length although they also increased in variability with the addition of a variety of flight-related tasks. If pilots counted aloud while making a production, however, the impact of concurrent activity was minimized, at least for the moderately demanding primary tasks that were selected. The effects of feedback on estimation accuracy and consistency were greatly enhanced if a counting or tapping production technique was used. This compares with the minimal effect that feedback had when no overt timekeeping technique was used.

Actively made verbal estimates of sessions filled with different activities decreased in length as the amount and complexity of activities performed during the interval were increased. Retrospectively made verbal estimates, however, increased in length as the amount and complexity of activities performed during the interval were increased. These results support the suggestion that time estimation provides a useful index of the workload involved in performing concurrent tasks.

* Supported by NASA Grant NGR-45-003-108 to the University of Utah.
** Supported by NASA Grant NSG 2269 to the San Jose State University Foundation.

692
PAGE INTENTIONALLY BLANK

INTRODUCTION

The workload involved in performing different manual control and decision making tasks is often difficult to measure within a single task or to compare between different tasks. It is difficult to infer an operator's workload from his measurable performance because: 1) individuals may compensate for additional task load by working harder, resulting in little measurable variation in performance and 2) the total workload is composed of a variety of subtasks such that performance on any one may or may not reflect varying degrees of task load in the others. In addition, different measurement techniques may be required to determine subtask-specific variation in workload.

The purpose of this research program was to develop a battery of primary task indices and unobtrusive secondary tasks that would specifically measure the load imposed by different subtasks that make up the total piloting task in order to measure the overall workload in real and simulated flight. Performance on secondary tasks is often used as an index of primary task workload. Secondary tasks that are commonly used often load the operator to determine his remaining capacity to perform additional tasks while performing the primary task. However, it was decided that tasks selected for inclusion in the workload assessment battery should be unobtrusive and measure primary task load with minimal interference. The tasks also should be similar to tasks that are normally performed in flight, easily learned, implemented and scored.

The results of this research have suggested time estimation as one such secondary measure of the cognitive demands of piloting because it has been shown that an individual's ability to estimate intervals of time varies as a function of concurrent task load. Time estimation is a task that is normally performed in flight. It is unobtrusive, easily learned, implemented and scored and is not altered by repeated presentations unless knowledge of results is given.

Intra- and Inter-Subject Variability

Although individuals tend to be consistent in the length of their time estimates, there are large differences among different individuals. For this reason, each subject should be used as his own control: estimates obtained under different conditions of primary task load can be most easily and unambiguously analyzed by comparison with estimates obtained from the same subject in the absence of concurrent task demands. Individual estimation accuracy seems to be a less important measure than are the direction of change in the length of estimates and the increase in variability of estimates with the addition of a primary task.

Estimation Measurement Method

Four methods have been used extensively to measure an individual's ability to estimate or produce specified intervals of clock time. The verbal estimation method requires that individuals vocalize or record their judgement of the duration of an operationally presented interval. The production method requires that subjects physically generate an interval whose duration is specified by the experimenter. The reproduction method, which combines elements of verbal estimation and production, requires the operational production of an interval whose duration was presented operationally. The method of comparison involves a relative judgement between the durations of two or more operationally presented intervals.

Estimation Mode

Rather than being perceived directly, the temporal aspects of experiences are inferred or deduced from the events that occur in time. Man has adopted objective standards and labels to allow quantification of and communication about temporal experiences because of the difficulties involved in dealing with time in the abstract. Individuals represent durations subjectively by correlating personally

Figure 1.

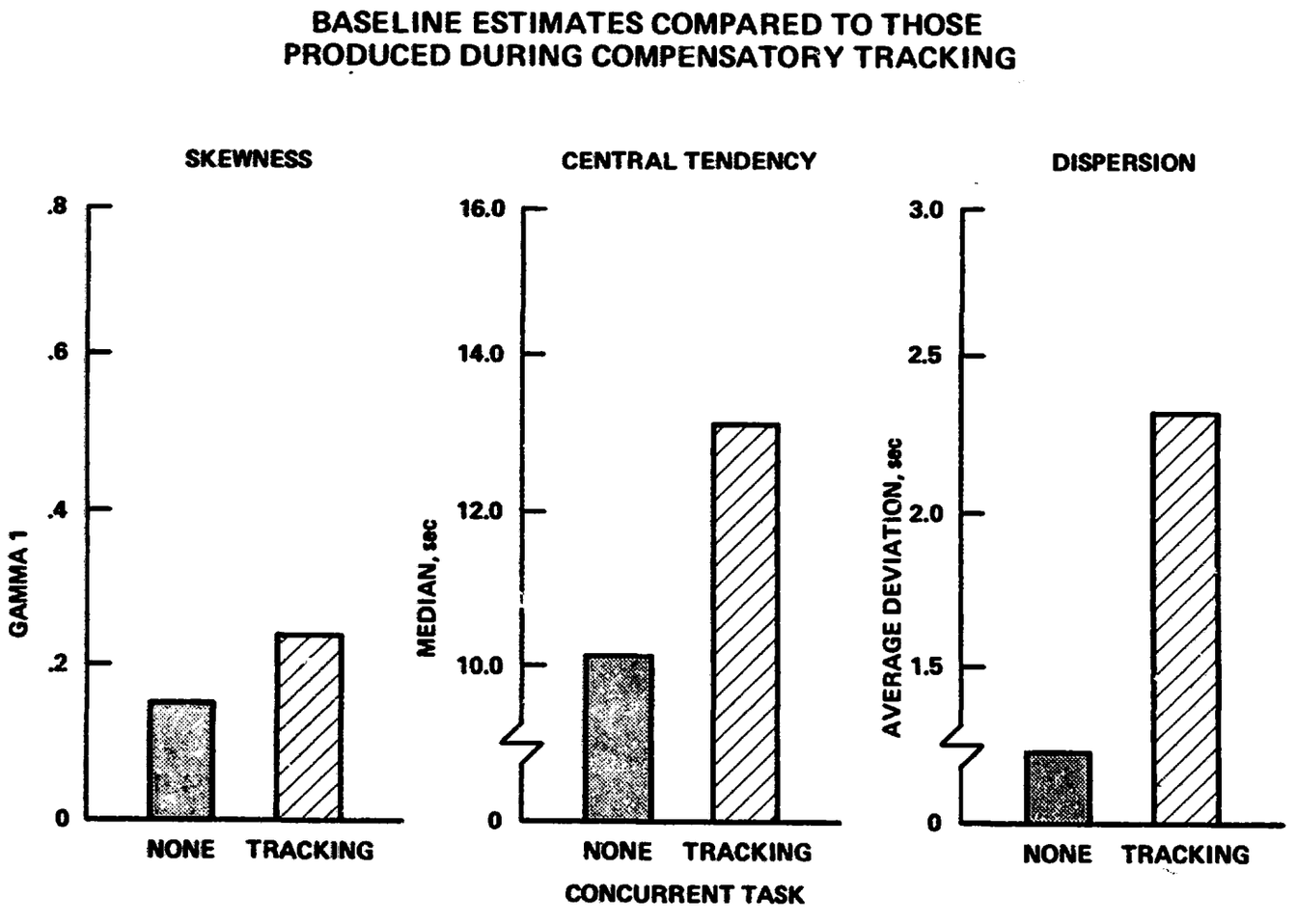

ORIGINAL PAGE IS
OF POOR QUALITY

experienced events with objective temporal standards or rules, such as clocks.

Active Mode

When individuals must produce a specific duration or verbally estimate the length of a presented interval unaided by an objective timing device, they may rely on impressions of past events or mentally or physically replay or generate a sequence of events that is believed to last a specific interval of time in order to make the temporal dimension of the interval concrete. This mode of estimation has been referred to as active estimation (ref. 1).

Retrospective mode

Individuals may also make temporal estimates without attending to time as it passes. They may estimate the duration of an interval at its conclusion by comparing the number and complexity of events that occurred during the interval with remembered durations of intervals similarly filled (ref. 2). This mode of estimation has been referred to as retrospective estimation (ref. 1).

Influence of Concurrent Activity on Active Estimation

The attention demanded by concurrent activity tends to interfere with active estimation. Whenever attention is diverted from active estimation, time passes unnoticed so that individuals may wait too long to terminate a production or verbally underestimate the length of the interval.

Active productions

Hart and McPherson (ref. 3) and Hart and Simpson (ref. 4) have shown that subjects do indeed wait too long to terminate their productions when distracted from active time estimation by competing simple compensatory tracking tasks (fig. 1) or speech recognition. A series of stylized representations of the mean length of 10 sec

Figure 2.

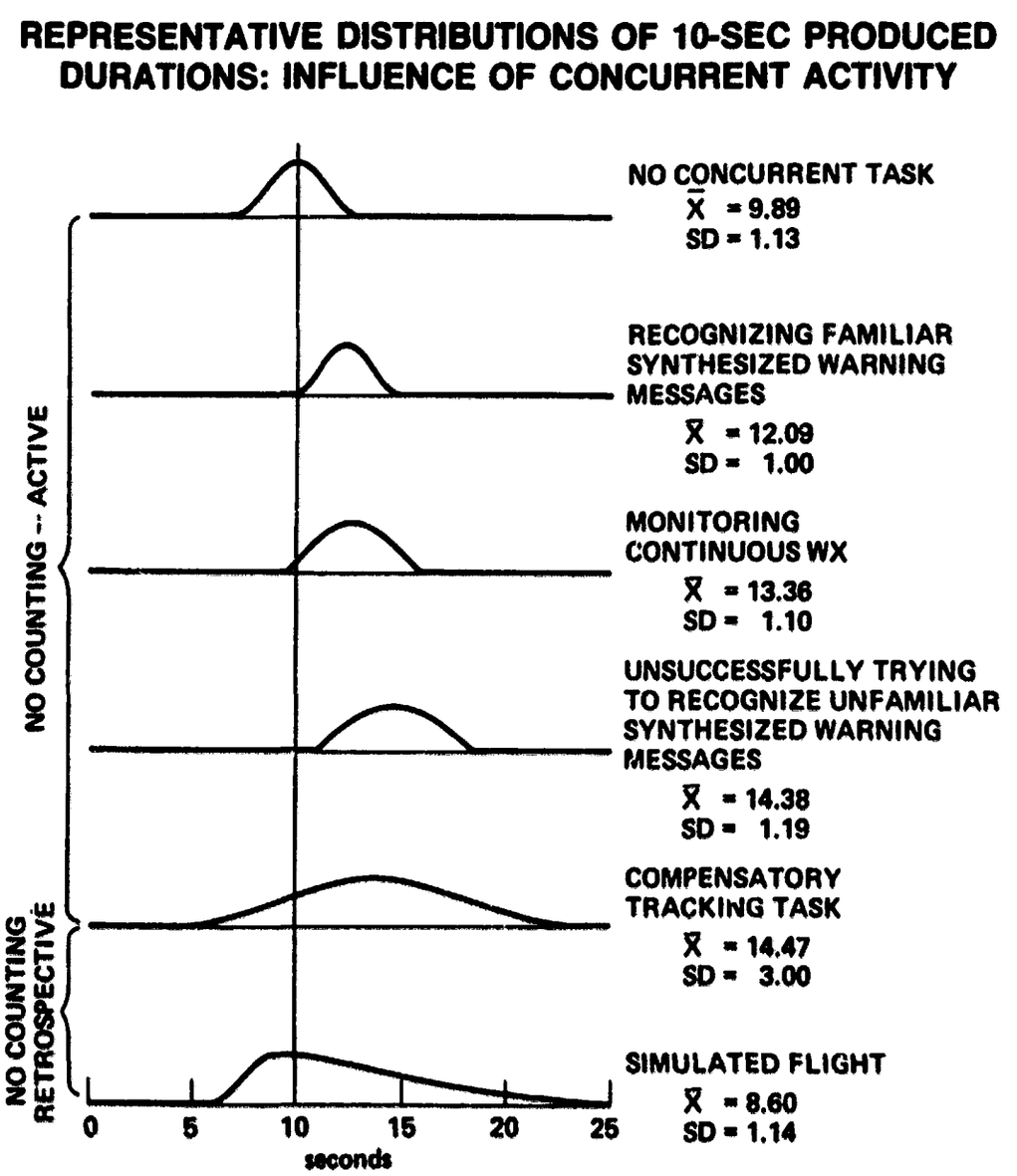
REPRESENTATIVE DISTRIBUTIONS OF 10-SEC PRODUCED DURATIONS: INFLUENCE OF CONCURRENT ACTIVITY
NO CONCURRENT TASK
X̄ = 9.89
SD = 1.13
RECOGNIZING FAMILIAR SYNTHESIZED WARNING MESSAGES
X̄ = 12.09
SD = 1.00
MONITORING CONTINUOUS WX
X̄ = 13.36
SD = 1.10
UNSUCCESSFULLY TRYING TO RECOGNIZE UNFAMILIAR SYNTHESIZED WARNING MESSAGES
X̄ = 14.38
SD = 1.19
COMPENSATORY TRACKING TASK
X̄ = 14.47
SD = 3.00
SIMULATED FLIGHT
X̄ = 8.60
SD = 1.14
NO COUNTING -- ACTIVE
NO COUNTING RETROSPECTIVE
0
5
10
15
20
25
seconds

Figure 3.

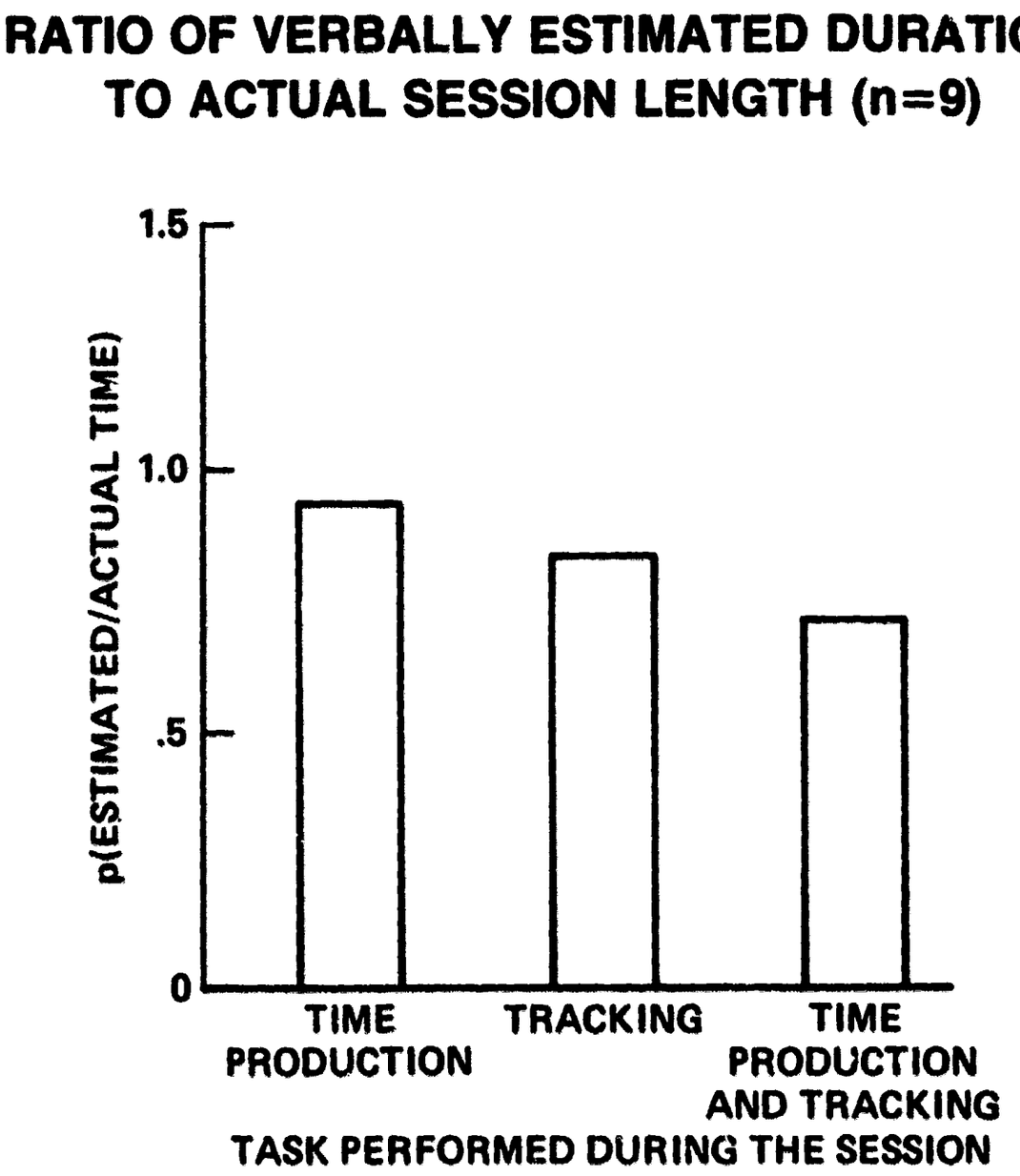
RATIO OF VERBALLY ESTIMATED DURATION TO ACTUAL SESSION LENGTH (n=9)
p(ESTIMATED/ACTUAL TIME)
1.5
1.0
.5
0
TIME PRODUCTION
TRACKING
TIME PRODUCTION AND TRACKING
TASK PERFORMED DURING THE SESSION

productions obtained under different experimental conditions is given in figure 2. Each distribution's shape approximates that of actual data obtained and was drawn to include three standard deviations about the obtained mean. As the demands of the concurrent tracking and recognition tasks were increased, the length of produced durations increased by 4 sec or more and their variability more than doubled. Other, less demanding concurrent tasks, such as monitoring continuous aviation weather broadcasts, were also associated with an increase in the central tendency and variability of estimate distributions, but to a lesser degree, as one would expect from their less demanding nature.

Active verbal estimates

Hart (ref. 5) and Hart, McPherson, Kreifeldt, and Wempe (ref. 6) found that actively made verbal estimates decreased in length with the addition of either a simple compensatory tracking task (fig. 3) or a complex multi-manned flight simulation (fig. 4b). The more difficult levels of each task were associated with the shortest active verbal estimates. This is consistent with the finding that active verbal estimation and active production are reciprocally related, and the observed directions of change in estimated and produced durations are both the consequence of underestimation of the passage of time.

Influence of Concurrent Activity on Retrospective Estimation

As the attention demands of a primary task increase, there is less and less attention available for time estimation. When active estimation becomes impossible the retrospective mode of estimation becomes necessary. Here, one presumably remembers the events that occurred during the interval, compares them to other experiences with known duration, and then verbally estimates the duration of the interval or decides whether or not it is time to terminate a production. As the number and complexity of events

ORIGINAL PAGE IS
OF POOR QUALITY

Figure 4

A. PROPORTION OF VERBAL ESTIMATES OF THE DURATION OF FINAL APPROACHES THAT PILOTS REPORTED MAKING ACTIVELY AND RETROSPECTIVELY (n = 9)

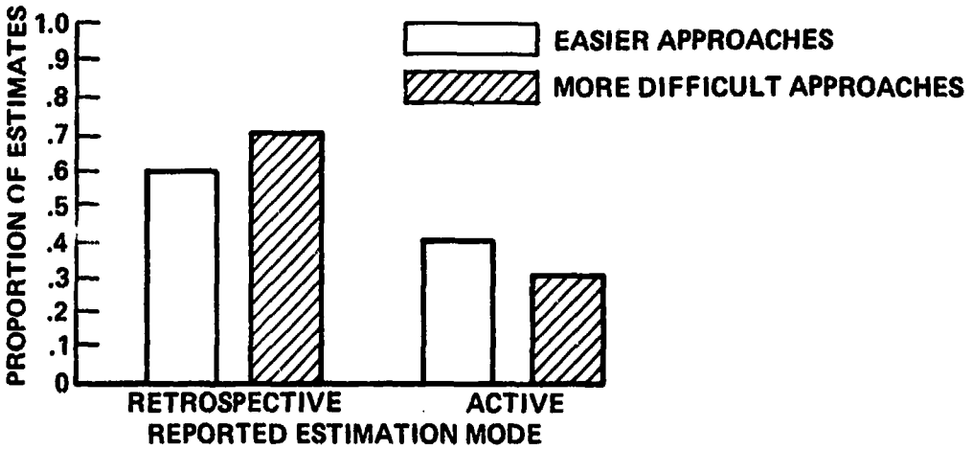

B. AVERAGE RATIO OF ESTIMATED DURATION TO ACTUAL DURATION FOR ACTIVE AND RETROSPECTIVE ESTIMATES

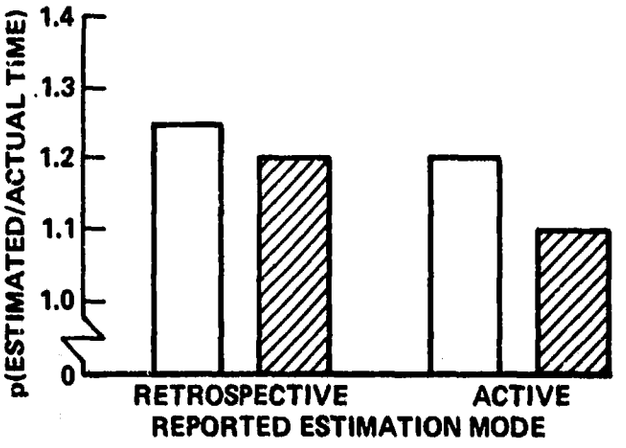

that fill the interval are increased, there is a tendency toward overestimation of the amount of time that has passed resulting in the termination of produced durations too soon or the verbal overestimation of elapsed time. Note that the directions of change in retrospectively verbally estimated and produced durations are the opposite of those obtained with active estimation and production and again the length of verbal estimates and productions are reciprocally related.

Retrospective productions

Hart and McPherson (ref. 3) have shown that the central tendency of 10 sec productions, obtained from pilots during simulated flight, decreased in length, as predicted, and the variability of the produced durations increased in comparison to estimates obtained with no competing activity. (fig. 5) Pilots reported that active estimation was difficult, resulting in their use of the retrospective mode. The distributions of retrospectively made productions were also positively skewed due to a few very long estimates which resulted from the estimation task occasionally being forgotten under conditions of high concurrent task load.

Retrospective verbal estimates

Following a complex multi-manned simulation flight, (ref. 6) pilot indicated that 66% of their estimates of the length of time taken to fly the final two miles of an approach were made retrospectively and that the proportion of retrospectively made estimates increased as the difficulty of the approach increased. (fig. 4a) Retrospectively made estimates were consistently longer than were estimates that pilots reported that they had made actively as predicted. (fig. 4b)

Interaction of Estimation Technique and Concurrent Task

Within the active mode of estimation there are many timekeeping techniques available. A standardized, rhythmic temporal metric (such as

Figure 5.

BASELINE ESTIMATES COMPARED TO THOSE PRODUCED DURING SIMULATED FLIGHT

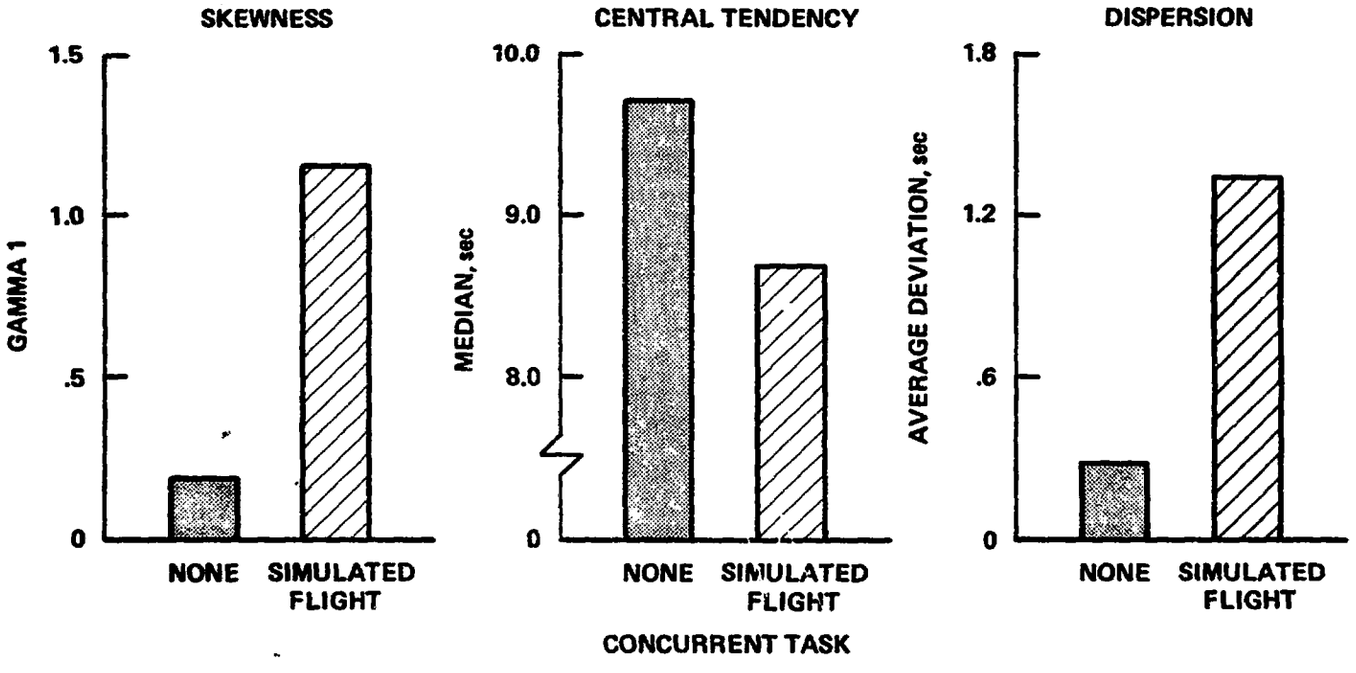

tapping) not only fixes an individual's attention on the time estimation task, which is otherwise difficult to do for a task as abstract and stimulus-deficient as time estimation, but also provides a concrete, repeatable way to keep track of time. Timekeeping techniques that are not externalized, however, are more easily disrupted by additional, more compelling activities and are less stable across time. Some of the estimation techniques that subjects have reported using to keep track of time include counting, tapping, mentally replaying a phrase of music estimated to have the appropriate duration, mentally rehearsing the pre-flight checklist for a helicopter, counting heart beats or breaths, picturing the dial of a clock with a second hand moving around it, or "just waiting" for 10 sec. Of these techniques, those that are externalized, such as counting, provide standard, repeatable units with which to mark off intervals of time resulting in improved estimation stability. Mental rehearsal of remembered experiences judged to have the appropriate duration resulted in less stable productions, because the interval that was repeated may or may not have lasted the appropriate duration. Further, it is difficult to control the rate at which one's mind steps through a memory.

Hart, Loomis and Wempe (ref. 7) found that when attention was focused on a time production task by requiring subjects to rhythmically count aloud 1-sec intervals, production accuracy and consistency were not affected by the addition of a concurrent task. (fig. 6 and fig. 7) With no overt counting, however, the length and variability of produced durations increased significantly with the addition of a tracking task, replicating earlier results (ref. 3). Because performance on the tracking task was the same with both productions techniques, it appears that the shift in attention away from time production found with the no-counting technique was not because subjects could not innately perform both tasks but merely that they in fact did not. When attention was focused on the time production task by the counting technique, production accuracy was not degraded and there was no concomitant degredation of tracking task performance.

ORIGINAL PAGE IS
OF POOR QUALITY

Figure 6.

REPRESENTATIVE DISTRIBUTIONS OF PRODUCED DURATIONS: INTERACTION BETWEEN ESTIMATION TECHNIQUE AND INFLUENCE OF CONCURRENT ACTIVITY

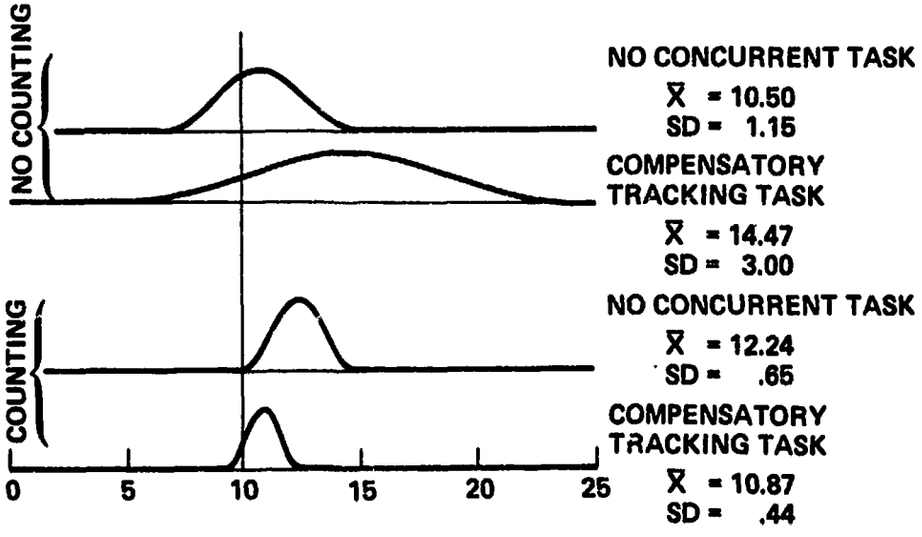

Figure 7.

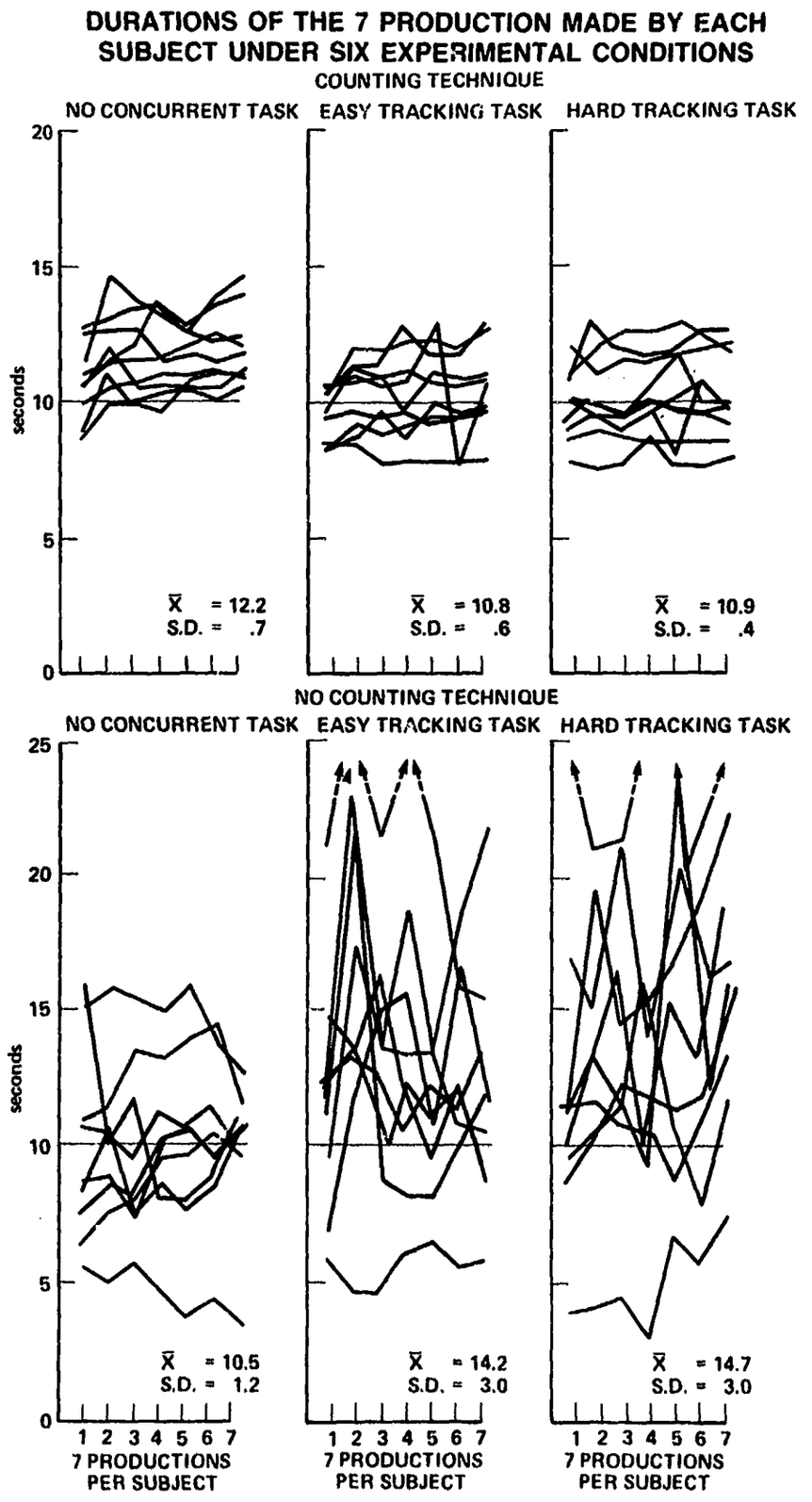
DURATIONS OF THE 7 PRODUCTION MADE BY EACH SUBJECT UNDER SIX EXPERIMENTAL CONDITIONS
COUNTING TECHNIQUE
NO CONCURRENT TASK
EASY TRACKING TASK
HARD TRACKING TASK
seconds
20
15
10
5
0
X̄ = 12.2
S.D. = .7
X̄ = 10.8
S.D. = .6
X̄ = 10.9
S.D. = .4
NO COUNTING TECHNIQUE
NO CONCURRENT TASK
EASY TRACKING TASK
HARD TRACKING TASK
25
20
15
10
5
0
X̄ = 10.5
S.D. = 1.2
X̄ = 14.2
S.D. = 3.0
X̄ = 14.7
S.D. = 3.0
1 2 3 4 5 6 7
7 PRODUCTIONS PER SUBJECT

It is likely that more demanding concurrent activity, such as simulated flight, would also impact the consistency of durations produced with a counting technique. However, no such effects were found with the moderately demanding tracking tasks that were used.

Interaction of Estimation Technique and Feedback

If the ability to estimate and produce intervals of time is learned, then it is likely that knowledge of results (feedback) should enhance timekeeping accuracy and consistency. In addition, the use of estimation techniques that provide rhythmic division of an interval into standard, repeatable units should focus attention on timekeeping and make the temporal dimension of the interval more concrete, thereby enhancing an individual's ability to take advantage of feedback.

In a recent study, Hart, Loomis and Wempe (ref. 8) found that individuals, using estimation techniques that did not involve some sort of overt counting, made less efficient initial use of feedback and did not experience any long term benefits from feedback. Overall accuracy of 10-sec productions, but not variability, was improved significantly by the presentation of feedback, with a rapid return to prefeedback performance levels when feedback was removed. (fig. 8 and fig. 9). During feedback, subjects repeatedly overcorrected. If told that one production was too long, the next production was typically too short and vice versa. Even after 30 trials with feedback following every production, subjects were unable to estimate accurately from trial to trial even though their estimate durations appeared to be accurate overall. If the subjects were instructed to rhythmically tap a button at 1-sec intervals in order to produce a series of 10-sec durations, both accuracy and variability were improved significantly by the addition of feedback. This improvement persisted for at least as long as 30 additional trials after feedback was removed. With this production technique, subjects were able to maintain consistent and accurate estimates from trial to trial, and did not overcorrect as they had

Figure 8.

REPRESENTATIVE DISTRIBUTIONS OF 10-SEC PRODUCED DURATIONS: INFLUENCE OF KNOWLEDGE OF RESULTS (FEEDBACK)

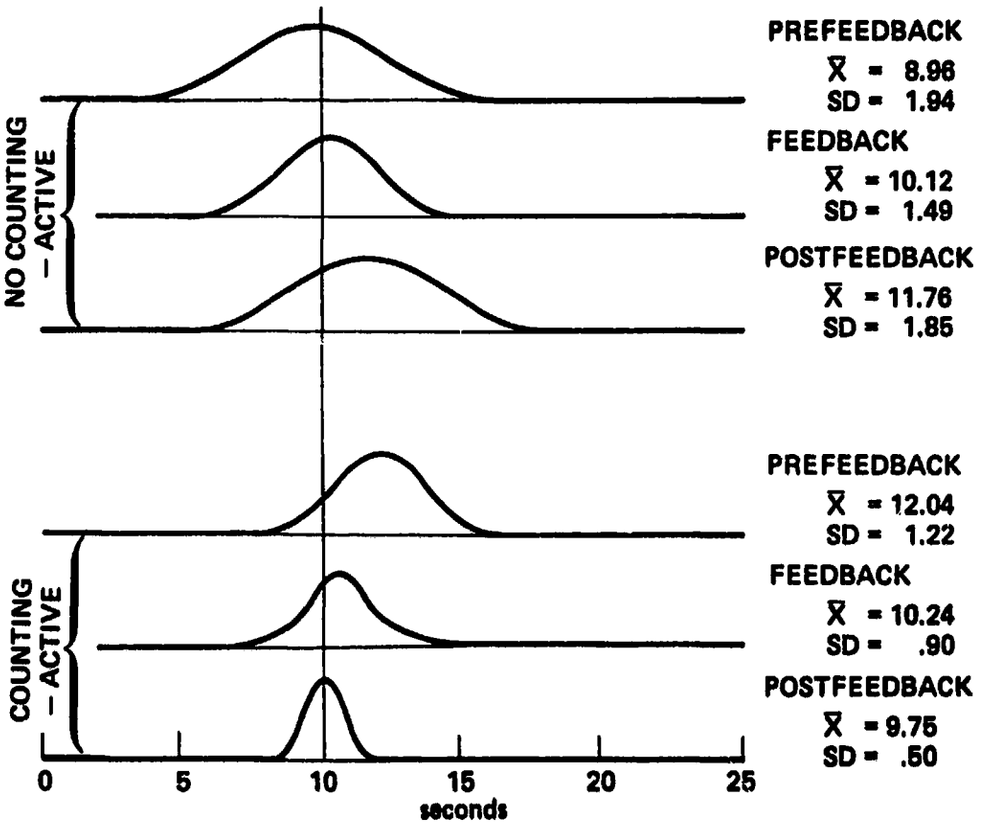

ORIGINAL PAGE IS
OF POOR QUALITY

Figure 9.

COMPOSITE GRAPHS OF RAW SCORES OF 10 SUBJECTS

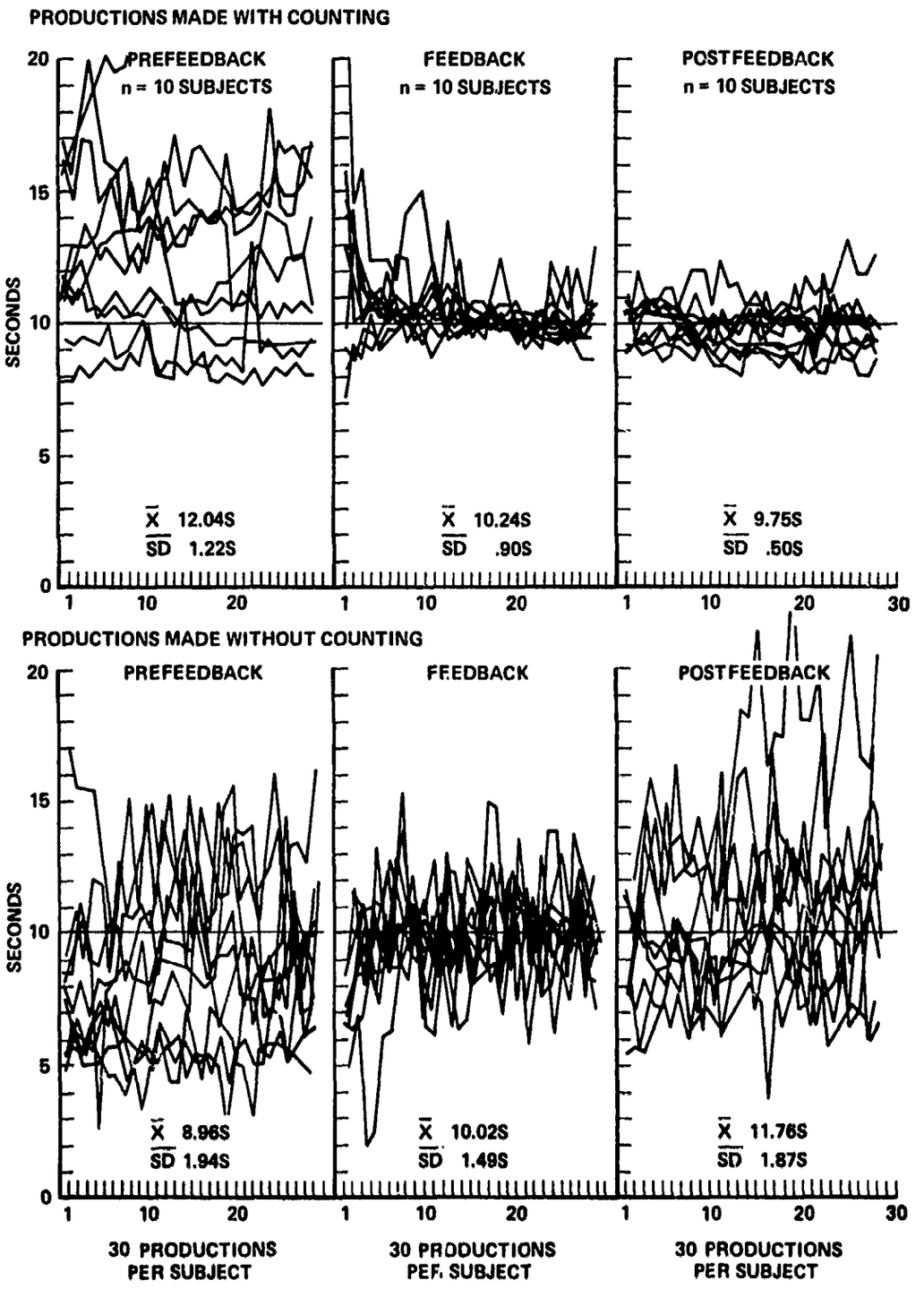

with the no-counting technique. The data suggest that tapping rhythmically not only provides a standardized repeatable temporal metric, but also fixes subject's attention on the time production task, which together combine to enable subjects to use feedback more effectively.

Conclusion

As a result of the foregoing research effort, several recommendations can be made concerning the use of time estimation as a secondary measure of the attention demands of a primary task.

Method

The production of brief intervals of time appears to be the most useful experimental method. The duration and variability of time productions in the range of 1 to 30 sec have been shown to reflect the attention demands of primary manual control, message recognition, and simulated flight tasks. Relatively brief intervals should be used so that the primary task load remains reasonably uniform and describable during the produced interval.

The verbal estimation method also shows some promise as a secondary measure of primary task workload. Its primary advantage over the production method is ease of implementation. Its primary disadvantage is that subjects tend to round off their estimates, thereby losing precision, and their responses tend to become stereotyped if a number of estimates are required. This method appears to have some value, but is less sensitive than the method of production.

Mode

Estimation mode (active or retrospective production or verbal estimation) must also be controlled or identified to obtain reliable and clear results with a time estimation task. Because retrospective productions decrease in length with increasing task load whereas active productions increase in length, care must be taken to identify the mode of production used. If retrospective and active productions are combined in an analysis, their direction of change with the addition of another

task would tend to cancel out masking detailed changes in the underlying processes.

Technique

Timekeeping techniques that are not externalized are most easily disrupted by concurrent task demands and thus provide the most useful measure of primary task demands. Thus, if time production is to be used as a measure of workload, subjects should not be allowed to use any overt time estimation technique such as tapping or counting. If estimation accuracy and consistency are required, however, an overt timekeeping technique should be used. Further research is required to determine at what level of concurrent task load the overt estimation technique would also be disrupted.

Feedback

If an overt timekeeping technique is used, feedback is effective in reducing both error and variability after only two or three repetitions, and the effects of feedback last long after it has been removed. With no overt timekeeping technique, however, estimation error is reduced only on the average, and variability remains high with a rapid return to pre-feedback error levels following removal of feedback.

Data Analysis

Time estimation performance is best evaluated relatively. That is, the amount and direction of change in estimation accuracy and consistency observed in the presence of additional primary tasks should be compared to estimates obtained from the same subject with no additional activity. Care should also be taken to select the appropriate measures of central tendency and variability as distributions of time productions are often positively skewed, particularly when obtained in the presence of competing concurrent activity.